Environmental Estrogens: Assessing Human Gestational Exposure and Interactions with the Estrogen Receptor

A Thesis submitted in partial fulfilment of

the requirements for the degree of

Doctor of Philosophy in Chemistry

at the

The University of Canterbury

Christchurch, New Zealand

by

Lisa Anne Graham

2012

Abstract

Environmental xenoestrogens (EEs) are chemicals that when they enter the body, the body responds to them as it would to endogenous estrogens. Humans are exposed to these chemicals on a daily basis via natural components, additives and contaminants in food and water, through the use of pharmaceuticals and personal care products such as sunscreens, lotions and toothpaste. Exposure to EEs is thought to result in adverse effects on humans such as decreased fertility, increased susceptibility to hormone-sensitive cancers, deformities of the male genitalia and precocious puberty in females. The critical window of exposure is thought to be early fetal development, when tissues are rapidly differentiating under the control of endogenous estrogens. However, there is limited data in the literature on human fetal exposure to EEs. The first objective of this study was to assess human fetal exposure to a suite of 35 EEs by analysis of paired samples of amniotic fluid and maternal urine were collected from 32 New Zealand women between 14 and 20 weeks gestation. The analytical chemistry methods required for this study were developed and validated. The results demonstrate that fetal exposure is highly correlated with maternal exposure. This study is the first to report maternal urine levels of two UV filters and amniotic fluid levels of parabens, UV filters and triclosan. A model based on simple additivity of effect was developed that combined the measured concentrations with literature data on relative estrogenic potency to assess the magnitude of the estrogen signal that may be attributed to the EEs. This model suggests that the fetus may experience an estrogen signal due to the measured EEs that could be as large as the endogenous estrogen signal. A second objective was to use computational docking to study the interactions of the EEs with the human estrogen receptor (hER) protein. The docking studies show that the rigid endogenous ligand, 17β-estradiol (E2) interacts with the hER to produce a single, well-defined complex with the receptor and the flexible EEs produce multiple, distinct energy-equivalent complexes. EEs are not able to interact with the binding cavity to stabilise the rigid hER-E2-like topology of the complex. As a result, the hER-EE complexes can be thought of as more pliable or ‘floppy’ and thus able to respond to the cell context in multiple ways, leading to variations in gene expression in different target tissues. These multiple pathways may explain the range of physiological responses attributed to exposure that depend on the timing of exposure and the sex of the individual exposed.

For Keegan

1996-2011

Acknowledgements

A wise friend told me not too long ago that the PhD is 'about the battle'. To say this PhD has been a battle would be an understatement of grand proportion. For most, the PhD is a logical progression from their undergraduate training, embarked upon early in their career. I came to do my PhD after 18 years in government research in Canada. I followed my (now ex-) husband to New Zealand when he took a position at the University of Canterbury. The opportunity for this project seemed to be just waiting for me, and I could not have planned any better.

Each year of the project brought a different challenge, none of which were related to the research. Half way through the second year, my husband of 19 years walked out. A year to the day later Christchurch was rocked by the first of three major earthquakes. In the final year I lost Keegan.

The research was not without challenges, but with a PhD one expects those challenges.

I'm not sure what my two supervisors, Ian and Sally, expected in taking on a 'mature' student. It's usually the youngsters that have drama in their lives. But through all of this, they have been more than just academic supervisors. They have been solid support, shoulders to cry on, and above all, friends.

Along the way, I've achieved other goals. I ran my first half and full marathons. I competed in several 100+ km road cycling races. And, most of all, I rediscovered the joy of friendship.

There are many people that I wish to thank for their contributions, large and small, to this work:

Ian and David – for fabulous food, wine and company at the Old Schoolhouse, Teddington;

Sally and the Environmental Chemistry group for keeping me on the straight and narrow;

Laura – for all the laughs, tears and for being that wise friend;

Sandra – for the many climbs up Gebbies, Dyers and Evans Passes and for commiseration;

The Christchurch Marathon Clinic for reminding me that I can do pretty much anything I set my mind to;

And my family – Mom and Dad, Kevin and Chris, Lori and John. They're the family that when all the wheels have fallen off your cart, are there to help you put them back on again.

I would like to express my heartfelt thanks to the National Research Centre for Growth and Development, Liggins Institute, University of Auckland for the studentship I received and for their continued support and understanding in coping with the earthquake-related delays.

Finally, this work would not have been possible without the participation of the expectant mothers who generously consented to the use of their samples for this study. Equally important was the collaboration with Dr. Rosemary Reid, Ms. Jeannie Matthews and the Fetal Medicine Unit at the Christchurch Women's Hospital, University of Otago and Ms. Jane Watt of the Canterbury Health Laboratories, who offered valuable advice on the study design and logistics, recruited the study participants and collected the samples for me. I hope I have made all your efforts worthwhile.

Table of Contents

List of Tables

List of Figures

List of Abbreviations

	Abbreviation
percent relative error	%REE
percent relative standard deviation	%RSD
2QTU Ligand	3AS
3-dimensional	3D
3-phenoxybenzoic acid	3PBA
3-phenoxybenzyl alcohol	3PBOH
4-hydroxybenzoic acid	4HBA
4-methyl-benzylidene camphor	4MBC
4-nonylphenol	4NP
3-(4-hydroxyphenoxy)benzoic acid	4OH-3PBA
4-[3-(hydroxymethyl)phenoxy]phenol	4OH-3PBOH
4-tert-octylphenol	4tOP
gene transcription activation function 1	AF-1
gene transcription activation function 2	AF-2
1XPC Ligand	AIT
analysis of variance	ANOVA
androgen receptor	AR
2,4-dihydroxybenzophenone	BP1
2,2',4,4'-tetrahydroxybenzophenone	BP2
2-hydroxy-4-methoxybenzophenone	BP3
Bisphenol A	BPA
Butyl paraben	bPBN
central nervous system	CNS
cytochrome P450	CYP
Daidzein	DAID
DNA binding domain	DBD
Diethylstilbestrol	DES
Estrone	E1
17β-estradiol	E2
Estriol	E3
environmental estrogen	EE
Ethynylestradiol	EE2
Enterolactone (3R,4R)	ENT
Ethyl paraben	ePBN
Equol (R)	EQ-R
Equol (S)	EQ-S
estrogen receptor	ER
estrogen response element	ERE
1L2J Ligand	ETC
2P15 Ligand	EZT
Genistein	GEN
human estrogen receptor	hER
human estrogen receptor alpha	hERα
human estrogen receptor beta	hERβ
Induced-fit docking	IFD
2JJ3 Ligand	JJ3
ligand binding domain	LBD
mono-n-butyl phthalate	mBP
monobenzyl phthalate	mBzP
mono-2-ethylhexyl phthalate	mEHP
monoethyl phthalate	mEP
mouse estrogen receptor	mER
monomethyl phthalate	mMP

	Abbreviation
mono-n-octyl phthalate	mOP
Methyl paraben	mPBN
Methyl triclosan	mTRIC
no observable effect concentration	NOEC
4-hydroxytamoxifen	OHT
Octylmethoxycinnamate	OMC
personal care products	PCP
Protein Data Bank	PDB
Propyl paraben	pPBN
Raloxifene	RAL
rat estrogen receptor	rER
receptor-ligand complex	RL-complex
selective estrogen receptor modulator	SERM
sulfotransferase	SULT
Testosterone	T
Triclosan	TRIC
uridine 5’ diphospho-glucuronosyltransferase	UGT

Glossary

Much of the terminology used in this work may have different meanings to different readers. For clarity, the definitions for key terms are collected in this section. These definitions also include important underlying concepts and are arranged in order to develop these concepts in a logical fashion.

Estrogens: the female sex hormones; refers to a group of 3 compounds (estrone, estradiol and estriol). Estrone (E1) is found in women and men in small amounts. It is produced in the adrenal gland and produced and stored in fatty tissue. Estradiol (E2) is the most active of the three compounds. It is produced by the ovaries in women and by the testes and adrenal glands in men. Estriol (E3) is the major estrogen produced during pregnancy. E3 is produced in large amounts in the placenta and levels in the mother and fetus rise continuously until just before birth.

Androgens: the male sex hormones; refers to a group of 5 compounds, of which testosterone (T) dihydrotestosterone (DHT) are the primary active hormones. DHT is metabolite of T and is a more potent androgen than T because it has a higher affinity for the androgen receptor than T. The other three androgens are intermediates in steroid hormone biosynthesis.

Agonist: a compound that is able to bind to a receptor in a cell and produce the biological response that is controlled or triggered by the receptor. The ability to bind is called ***affinity***. The ability to produce the biological response is called ***efficacy***. An agonist can be an endogenous such as the sex hormones or a foreign substance such as a drug or other chemical. For the sex hormone receptors, the biological response that is of interest is gene transcription. For the sex hormone receptors, agonists activate (initiate, up-regulate) receptor mediated gene transcription.

Antagonist: a compound that is able to bind to a receptor in a cell and blocks or inhibits the biological response that is controlled or triggered by the receptor. An antagonist has *affinity* for the receptor but no *efficacy*. For the sex hormone receptors, antagonists block (inhibit, down-regulate) receptor mediated gene transcription.

Agonist and **antagonist** are also used to describe the 3D conformation of the hER protein ligand binding domain (LBD) on ligand binding, specifically the difference in position of helix 12 (H12) of the LBD that occurs when an agonist or antagonist ligand is bound. Thus, a

ligand can be described as an agonist or antagonist and the hER can be described as taking an agonist or antagonist conformation.

Selective Estrogen Receptor Modulators (SERMs): a class of compounds that interact with the estrogen receptor but unlike pure agonists or antagonists their mode of action depends on the cell type (tissue) they are acting on, resulting in selective inhibition or stimulation of estrogen-like action in the tissue.

Antiestrogen: an antagonist for the estrogen receptor. Functionally, there are three types of antiestrogens: type I or pure antiestrogens oppose estrogen activity in all tissues; type II and III are SERMs and display tissue selective agonist-antagonist activities [1]. Antiestrogens have a range of ***potency*** – the efficiency with which they block hER mediated gene transcription.

Antiandrogen: an antagonist for the androgen receptor.

Environmental Estrogen (EE): a compound that an organism is exposed to via interaction with its environment that promotes or interferes with ER-mediated gene transcription via binding with the ER.

Transcription factor: a cellular protein that binds to a specific DNA sequence, thereby controlling the transcription of genetic information from DNA to mRNA. Transcription factors recruit the RNA polymerase to the specific gene. Transcription factors contain one or more DNA-binding domains which attach to specific sequences of DNA (the target promoter) adjacent to the genes that they regulate. Additional proteins such as coregulators, chromatin remodelers, histone acetylases, deacetylases, kinases, and methylases are also recruited to the transcription factor/RNA polymerase complex to achieve gene transcription.

Target promoter: a region of DNA that facilitates the transcription of a particular gene. Promoters are located near the genes they regulate, on the same strand and typically upstream of the gene. In order for the transcription to take place the RNA polymerase must attach to the DNA near a gene. Promoters contain specific DNA sequences and response elements which provide a secure initial binding site for the RNA polymerase and for proteins called transcription factors that recruit RNA polymerase. These transcription factors have specific activator or repressor sequences of corresponding nucleotides that attach to specific promoters and regulate gene expressions.

Coregulator: a cellular protein that interacts with the ligand bound transcription factor/RNA polymerase complex that enhances or suppresses gene transcription. Coregulators that enhance or increase the rate of gene transcription are called **coactivators** and those that suppress or decrease the rate of gene transcription are called **corepressors**. Coregulator activity is regulated by their absolute and relative expression levels in different cell types. Coregulators allow for cell type and promoter specificity for transcription factors.

Crystal structure refers to the molecular structure of the protein (with or without a co-crystallised ligand) obtained directly from the published atom co-ordinates of the solved and refined molecular structure produced experimentally by x-ray crystallography.

Model refers to the protein structure used for ligand docking obtained after the required processing and preparation of the published crystal structure is completed. The model also still contains the co-crystallised ligand.

Apo describes an empty receptor structure, one without a bound ligand.

In the context of computational docking, **native** is used to identify the ligand that has been co-crystallised with the protein in the crystal structure or the resulting model.

In the context of analytical chemistry, **native** is used to identify the target analyte as distinct from the isotopically labelled analyte identified as the **surrogate**.

To be concise, amino acid residues will be referred to simply as 'residues'. When identifying a particular residue in a protein, the standard 3-letter abbreviation followed by its number in the protein sequence will be used. For example, His524 refers to the 524^{th} residue in the protein sequence, which is a histidine residue.

Small molecules, for example the endogenous hormones or EEs, may be present in bodily fluids in three forms: **free**, **conjugated** and **protein bound**. The free form is the molecule in its original form simply dissolved in the fluid. The conjugated form has a highly water soluble substituent such as sulphate or glucuronate covalently bound to the parent molecule at the site of an active hydrogen such as on a hydroxyl group. These conjugates are products of specific metabolic enzymes. The protein bound form is the parent molecule non-covalently bound to a carrier protein molecule in the blood or amniotic fluid. The free form is readily bioavailable. The protein bound form is sequestered but is readily available in response to a shift in equilibrium in the fluid. The conjugated form is not readily bioavailable and is

normally destined for elimination, unless it meets deconjugation enzymes located on the surfaces of specific cell types in the body.

Nomenclature

The notation for ring designation and numbering substituent positions is illustrated in Figure A. The ring designation is often used in reference to other ligands that do not have this structure to describe the type of interactions with the receptor. Note that the ring designation given in Figure A for GEN does not follow the common convention for flavone ring designation[1], but is used in the ER literature.

The binding cavity of the ERs is also described as having an A-ring end and a D-ring end, in reference to the usual orientation of E2 in the binding cavity. The A-ring end is the Glu/Arg/water molecule end. The D-ring end is the His end and is also described as the entrance channel end.

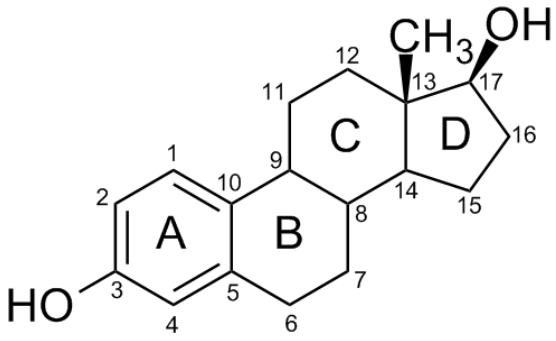

17β-estradiol (E2) | Genistein (GEN)

Figure A. Position numbering and ring notation for ligands, illustrated with 17β-estradiol and genistein.

[1] There is currently no standardised IUPAC convention for flavones nomenclature http://www.iupac.org/web/ins/2009-018-2-800 .The common convention is illustrated at http://www.friedli.com/herbs/phytochem/flavonoids.html#intro

Chapter 1 Introduction

Modern chemistry has brought us many benefits from pharmaceuticals to advanced materials. With these advances comes a responsibility to balance the benefits against undesirable environmental effects. This balance is critical when chemicals interfere with the most fundamental of biological processes – reproduction [2]. Recently, interference of this type was demonstrated on a grand scale when the population of fathead minnows in an isolated Canadian lake was brought to near extinction in just 7 years by exposure to parts per billion concentrations of 17α-ethynylestradiol (EE2, Figure 2.29), the synthetic estrogen used in birth control pills [3]. The exposure dramatically reduced the reproductive capacity of both male and female fish. This is but one example of a larger issue known as *endocrine disruption*: the interference with the synthesis, secretion, transport, binding, action, or elimination of natural hormones in the body that are responsible for the maintenance normal cell metabolism, reproduction, development and behaviour. A similar outcome is possible for humans on exposure to hormonally active chemicals at inappropriate times [4-12].

The Endocrine Society defines an endocrine-disrupting chemical (EDC) as *a compound, either natural or synthetic, which through environmental or inappropriate developmental exposures alters the hormonal and homeostatic systems that enable the organism to communicate with and respond to its environment* [13]. EDCs were originally thought to exert actions primarily through nuclear hormone receptors such as the estrogen receptors (ERs), androgen receptors (ARs) and thyroid receptors (TRs). However, the mechanisms of action are much broader than originally recognized and include non-nuclear steroid hormone receptors (e.g., membrane-bound ERs), nonsteroid receptors such as neurotransmitter receptors and enzymatic pathways involved in steroid biosynthesis and/or metabolism [13].

It has long been accepted that exposure to environmental pollutants can produce mutations in DNA [14]. These DNA mutations can be passed to the individual's offspring. Recently, heritable changes in gene expression *without* DNA mutation have been identified in animals and humans [15, 16]. Such changes in gene expression are described as 'epigenetic' and are mediated by external chemical signals such as hormones or immune status and by environmental pollutants. If undesirable epigenetic changes in an individual occur early in development, they can lead to increased susceptibility to disease or dysfunction later in life and to similar effects in the individual's offspring [16, 17]. At the molecular level, epigenetic mechanisms include chemical modification of the cytosine bases in DNA by methylation; chemical modification of histones (globular proteins that package DNA); and production of

microRNAs (short, single stranded RNAs that down-regulate gene expression by interfering with mRNA function) [15, 17]. These modifications are passed down via cell mitosis [17]. The changes in genome function that result from unintended external influences are insidious and potentially devastating to a species.

In mammalian germ cells and preimplantation embryos, DNA is actively demethylated and remethylated, selectively erasing certain parts of the methylation patterns inherited from the parents and copying others [16]. This process produces cells in the new embryo with the capacity to develop into any of the required tissue types. Methylation is influenced by the external chemical environment of the cell such as the presence of endogenous hormones. Any upset in the reprogramming of the cells at this stage could induce persistent changes in the individual that become heritable in that individual's offspring. For example, gestational exposure of female rats to vinclozolin (a fungicide that acts as an antiandrogen) at the time of gonadal sex determination results in a decrease in fertility of her male offspring. This decrease in fertility was transmitted for at least 3 generations, but only down the male offspring line [18].

In humans, exposure to EDCs is implicated in a wide range of adverse outcomes including uterine fibroids and ovarian tumours [19, 20], hormone related cancers [4, 21, 22], deformities of the male genitalia [7], precocious puberty in girls [23-25], declining male and female fertility [26-28], obesity [29-31], developmental disabilities [32-34] and changes in sexual behaviour [32-34].

The primary focus of this study is human gestational exposure to endocrine active chemicals, specifically environmental estrogens (EEs). The main objective is to assess human fetal exposure to EEs and estimate the increase in estrogenic signal due to this exposure in relation to that due to endogenous estrogens. To achieve this objective, samples of human amniotic fluid with matched maternal urine samples were analysed for a suite of 35 EEs. The EEs of interest were chosen because there is a high probability of exposure through either the diet or use of common products. These compounds are present in personal care products such as toothpaste, antibacterial soaps, deodourants, shampoo, skin lotion and sunscreens; are naturally occurring in soy, legumes and some green vegetables; and potentially present as contaminants in food or drinking water due to contact with plastics. The samples of urine and amniotic fluid were obtained from a cohort of 32 women through collaboration with The University of Otago Christchurch Medical School, the Christchurch Women's Hospital and

the Canterbury Health Laboratories. The study was granted human ethics approval from both the Upper South Regional A Ethics Committee and the University of Canterbury Human Ethics Committee. The required chemical analysis methods were developed and validated and then applied to the samples. Finally, a model was developed to quantify the magnitude of estrogenic signalling that the fetus experiences that can be attributed to the measured levels of EEs and endogenous estrogens.

The secondary focus of this study is an investigation of the interactions, at a molecular level, of the EEs with the human estrogen receptor (hER) protein. This investigation was done using a computational technique widely used in the pharmaceutical industry called ligand-receptor docking. The objective of this part of the study was to consider the biomolecular interaction of the EEs with the hER in an attempt to rationalise the varied and sometimes contradictory observed adverse outcomes that have been hypothesised to result from such exposure.

To achieve the two objectives, several large and diverse bodies of literature have been brought together to find the critical pieces of information that form the foundation of the overarching story. The areas for the literature review presented in Chapter 2 are

- Hormone control of gene expression
- Structure and function of the hER
- Human gestational development
- Adult exposure and metabolic fate of EEs
- The maternal-fetal-placental unit
- Fetal exposure and metabolic fate of EEs
- Sources, activity and potency of EEs

The key findings from the literature review form the basis for the exposure assessment presented in Chapter 6. The computational docking study presented in Chapter 3 provides insight into the molecular interactions between the EEs and the hER which could explain some of the variability in *in vitro* and *in vivo* studies of estrogenicity for these compounds. Chapter 4 presents the development and validation of the methods applied to the analysis of amniotic fluid and maternal urine for the EEs of interest. Chapter 5 presents the study design and the results of the analysis of amniotic fluid and maternal urine. Chapter 6 presents a comparison of the results of this study to the literature. The key findings of the literature review of Chapter 2 are integrated with the results of this study to provide an assessment of fetal exposure. Chapter 7 and Chapter 8 present results of experiments intended to

characterise the kinetics and thermodynamics of binding of EEs to the hER and to develop a relative estrogenicity screening method to characterise biological samples. Finally, Chapter 9 presents overall conclusions of this work and future directions.

Chapter 2 Literature Review

2.1 Hormone Control of Gene Expression

2.1.1 Role of hER

The endocrine system is a collection of glands in the body. Each gland produces and secretes specific hormones (small molecules) directly into the bloodstream to regulate bodily functions. The endocrine system functions as an information signalling network to control critical growth, development and maintenance functions of the body.

In general, endogenous hormones such as estrogens and androgens act via the nuclear receptor proteins, the estrogen receptor (ER) and the androgen receptor (AR), which recognise and specifically respond to their cognate hormones. These nuclear receptor proteins are located in the cytoplasm or nucleus of target cells. They are ligand-inducible transcription factors, meaning that when the endogenous hormone diffuses into the cell, it binds to its specific receptor protein and initiates transcription of the target genes [35-39]. There are two hERs, α and β. They are found in different amounts in different tissues and respond differently to the estrogens.

The uterus, mammary gland, placenta, liver, central nervous system (CNS), cardiovascular system and bone are the classical estrogen target tissues. hERα is the predominant subtype in these tissues and they respond to estrogen challenges with an increase in transcription of estrogen-responsive genes [40-42]. hERα mediates the physiological actions of estrogens in mating behaviour and glucose metabolism. hERβ is primarily expressed in the prostate, testis, ovary, pineal gland, thyroid gland, parathyroids, adrenals, pancreas, gallbladder, skin, urinary tract, lymphoid and erythroid tissues, lung, thymus, spleen and in localised areas of the brain [41, 43]. hERα is either very low or undetected in these tissues. hERβ is essential for normal ovulation efficiency [44] and some aspects of mating behaviour [45] and immune responses [42], but is not essential for female or male sexual differentiation, fertility or lactation [44]. hERβ also acts to regulate expression of hERα, reducing the potency of estrogens acting through hERα [46-48]. According to KBERG: KnowledgeBase for Estrogen Responsive Genes [49], there are 1069 estrogen responsive human genes corresponding to 1051 unique target promoters.

2.1.2 Role of Estrogens

The physiological effects of estrogens in both males and females have been reviewed by Nilsson et al. [37] and Kuiper et al. [50], and are briefly summarised here.

In females, the ovaries are the main producer of E2 and it stimulates pubescent growth and is responsible for female characteristics such as breasts, a wider pelvis and fatty tissues around the buttocks and hips. In adult females, E2 regulates the menstrual cycle, stimulates the development of vaginal secretions and prepares the body for pregnancy by thickening the uterine lining.

In males, most of the E2 is produced in the testes but the adrenal and pituitary glands also produce small amounts. In males, E2 promotes the growth of the penis and the development of testicles and plays an important role in prepubescent boys by stimulating the growth of facial and body hair, deepening the voice and aiding the development of thick masculine muscles. E2 also stimulates the growth and maturation of sperm. Healthy levels of E2 in men also result in higher libidos.

In both males and females, estrogens have a role in the cardiovascular system in response to vascular injury. Estrogens also influence a variety of functions in the central nervous system such as learning, memory, awareness, fine motor skills, temperature regulation, mood and reproductive functions.

In human female fetus, estrogen signalling is critical to the onset and completion of primordial follicle formation (primordial follicles contain immature oocytes) [51]. Androgens are also important but their role is less clear [51].

The role of both estrogens and androgens in early brain development is well recognised. Their influence contributes to the differences in cognition and behaviour between males and females and to individual variations within the sexes [52]. Strong correlations exist between prenatal hormone levels and childhood play behaviour and for sexual orientation and tendencies toward anger [52].

In adults, circulating hormones are bound to plasma-steroid binding proteins and albumin in the blood and are also present as water soluble sulphate and glucuronide conjugates. Only a small fraction of the hormones are free (unbound and unconjugated) in the blood [53]. In humans the human sex-hormone-binding globulin (hSHBG) is the main, specific transport protein for steroid hormones. The steroid hormones bind with high affinity to different sites on the protein and T binds with slightly higher affinity than E2 ($K_D \approx 0.63$ and 1.5 nM respectively). Hormones can also bind to albumin, but the binding is non-specific and of low affinity [54]. Because the amount of albumin in adult blood is much greater than hSHBG,

most of the circulating hormones are bound to albumin. It is the small fraction of free hormone (<2% in adult humans) that is responsible for biological activity. The unbound steroid hormones passively diffuse into and out of the cells. There are no known active transport mechanisms for the free steroid hormones [53].

In contrast, the fetus does not produce a high affinity hormone binding protein and exactly how the levels of steroid hormones are controlled in the fetus in the first and second trimesters while differentiation is occurring is not fully understood [53]. All three estrogens (E1, E2 and E3) are secreted from the placenta into the umbilical vein in the unconjugated form [55]. The fetus sulphates the estrogens for return to the placenta via the umbilical artery [53, 55]. Fetal metabolism is further discussed in Section 2.5.4.

Total serum (free + protein bound) E2 levels vary substantially over the development and lifetime of a human and are different in males (blue bars) and females (pink bars) as shown in Figure 2.1. Note the dramatic increase in E2 levels that occur between mid-gestation and birth and the subsequent rapid decline in the first few days of life. In adults, approximately 1.5% to 3% of the total serum E2 concentration is free E2. No information was found for the %free levels in fetal blood during gestation.

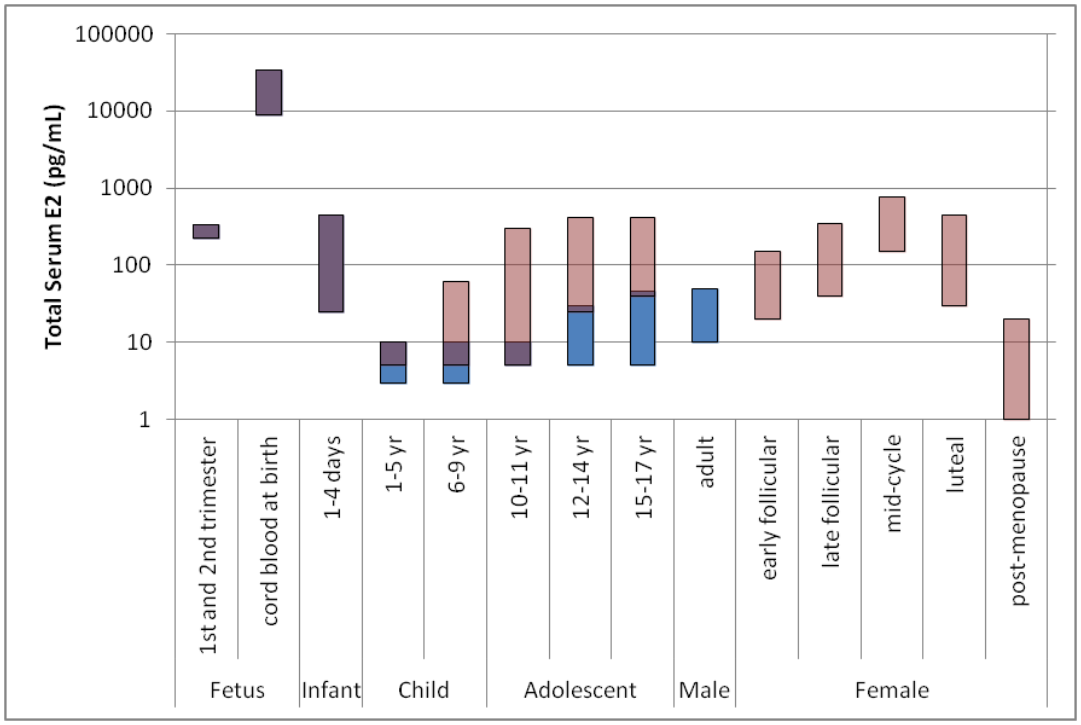

Figure 2.1. Human total (free + protein bound) serum E2 concentrations [51, 55, 56]. Blue bars indicate male levels, pink bars indicate female levels. The overlap of male and female levels appears grey.

2.1.3 Endocrine Disruption

Endocrine disruption is a broad topic that deals with upsetting the balance of the natural hormone levels in an organism [4, 6, 24, 57-59]. Of particular concern is the disruption of the reproductive hormone balance caused by exposure to chemicals. These disruptions have adverse effects not only on the exposed individual but on future generations by permanently altering gene expression via epigenetic mechanisms [60, 61].

There are several mechanisms of disruption that affect hormone signalling. Using the disruption of sex hormone signalling as an example, different mechanisms are illustrated in Figure 2.2. The mechanisms can be categorised as genomic (acting directly through nuclear receptor binding) or non-genomic (influencing the balance of endogenous hormones via other means such as interfering with hormone synthesis or metabolism). In Figure 2.2, the genomic mechanisms are indicated in red and the non-genomic mechanisms are indicated in blue.

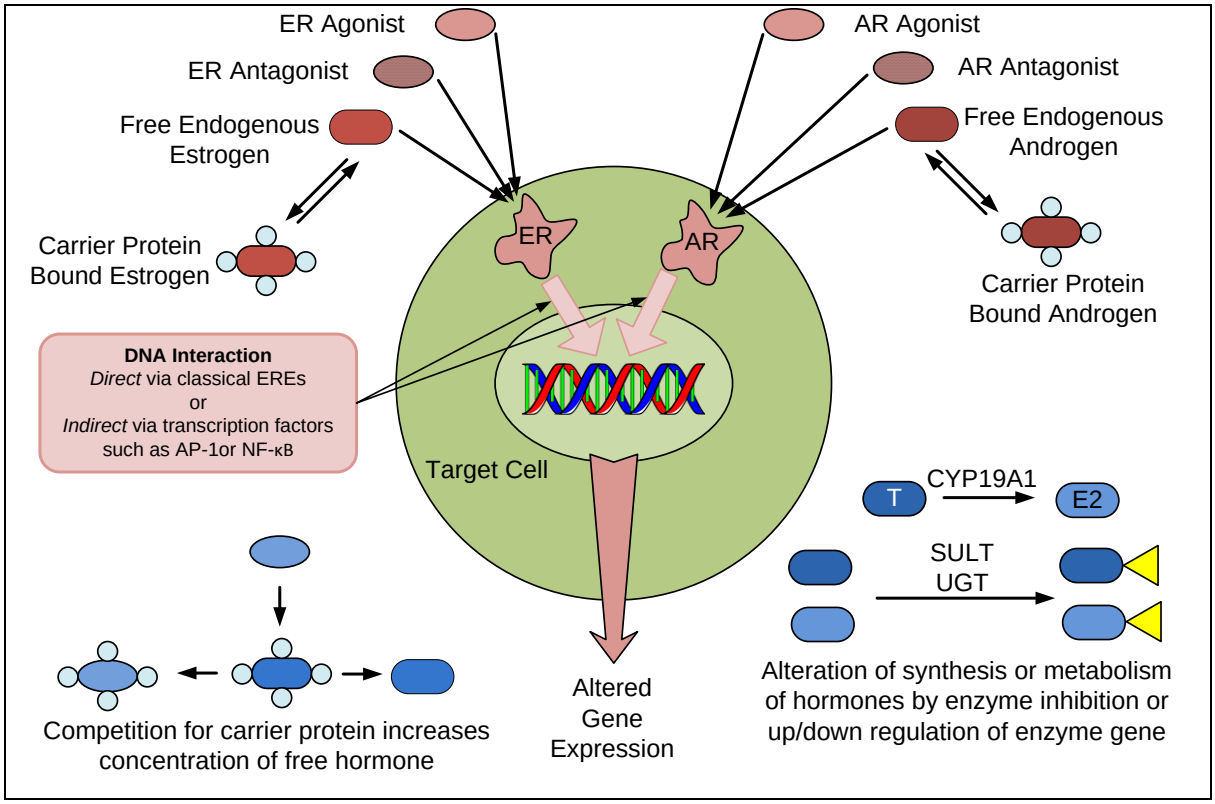

Figure 2.2. Mechanisms of endocrine disruption illustrated using sex hormone signalling as an example. Disruption can occur by interference with receptor mediated gene transcription (red) or by upset of hormone biosynthesis (blue).

EEs are able to bind to the ER and either up-regulate or down-regulate estrogen target gene expression. To further complicate matters, a chemical may simultaneously act on more than one of the pathways or mechanisms shown in Figure 2.2. For example, a chemical may simultaneously be estrogenic (up-regulates estrogen target genes) and antiandrogenic (down-regulates androgen target genes) or act on both genomic and non-genomic pathways, depending on where they are found in the body. For these reasons a phenotypic definition of environmental estrogen is difficult to provide [62].

The focus of this project is the disruption of estrogen signalling in humans. It is important to realise that estrogen signalling disruption does not occur in isolation, but is only one part of the highly complex and poorly understood issue of endocrine disruption [63].

2.2 Human Estrogen Receptor Structure and Function

2.2.1 hER Structure

The ER is a member of the nuclear receptor superfamily of ligand-inducible transcription factors [39]. There are two genetically distinct forms of the hER, referred to as hERα and hERβ. The hERα gene *ESR1* is located on chromosome 6q25.1 and the hERβ gene *ESR2* is located on chromosome 14q23.2 [64, 65]. The hERα consists of 595 amino acids and has a molecular weight of 66 kDa and hERβ consists of 530 amino acids and has a molecular weight of 55 kDa. The hERα was identified in 1958 [35, 66] and cloned in 1986 [67]. The hERβ was first reported in 1996 [68, 69].

As illustrated in Figure 2.3, there are six functional domains (A-F) in the hER proteins [40, 70]. The N-terminus A/B region does not have a well-defined tertiary structure [65]. It is involved in transcriptional activation and holds the activation function AF-1. AF-1 activates target genes by directly interacting with components of the transcriptional machinery and with coregulatory proteins that regulate gene transcription [35]. AF-1 is constitutively active (ligand independent) and regulated by polypeptide growth factors such as *epidermal growth factor* (EGF) and *insulin-like growth factor* (IGF) [70, 71]. The C region or mid-region is the DNA binding domain (DBD) that binds with high affinity to specific DNA sequences in target gene promoter regions called *estrogen response elements* (EREs). This region plays a central role in receptor dimerisation, providing the surfaces necessary for the 'head to head' dimerisation of two receptor molecules. Binding of the dimerised hER at the ERE sites

allows recruitment of transcriptional machinery and specific coregulatory proteins to transcribe the specific ER target gene. The D domain is the hinge domain and has not been well characterized. It is thought to contribute flexibility to the receptor structure as it is located between the two highly structured domains of the receptor molecule: the DBD and the ligand binding domain (LBD). It also influences DNA binding properties of the individual receptors and it may also serve as an anchor for certain corepressor proteins [35, 65]. The E domain is the LBD and holds the ligand binding pocket, the activation function AF-2, sites for coregulatory protein binding and for interactions with heat-shock proteins [40]. The two separate activation functions, AF-1 and AF-2, function co-operatively and synergistically with one another. AF-2 is strictly ligand-dependent [71]. hERα has both AF-1 and AF-2 activation functions. ERβ has only the AF-2 domain [72]. The C-terminus F domain is involved in homo- and hetero-dimerisation of the receptor and is the binding site for chaperone proteins such as the heat-shock proteins Hsp70 and Hsp90. In the unliganded state, the chaperone proteins interact with the receptor protein to open the binding cavity so that it is accessible to the ligand [65].

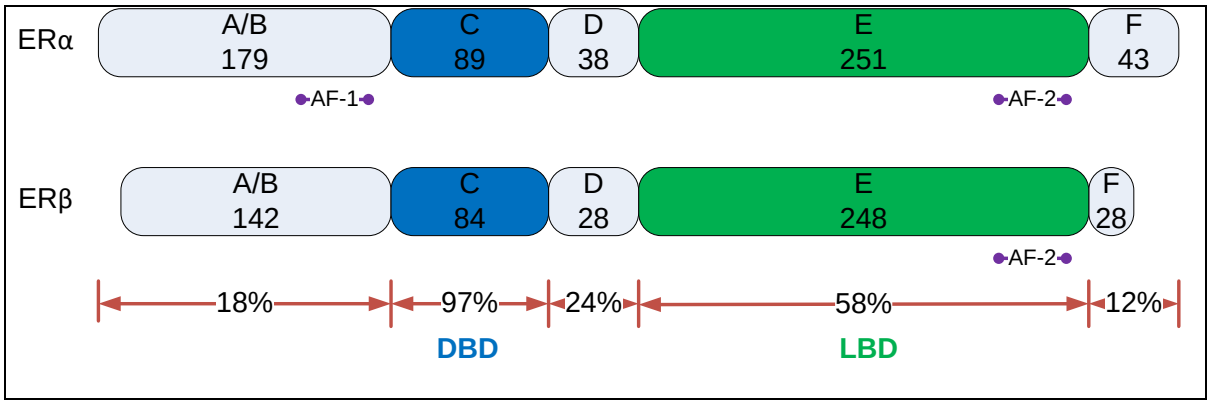

Figure 2.3. Schematic representation of estrogen receptor protein structural domains. Within each segment, the number of amino acid residues is given. The %homology is indicated below each domain.

The two hERs are highly conserved (97%) in the DBD but are less similar in the LBD (58%). This suggests that hERβ would recognize and bind to similar EREs as hERα but that each receptor would have a distinct spectrum of ligands [40]. The DBD contains two zinc fingers which are involved in DNA binding and receptor dimerisation. The balance of the structure is much less similar between the two receptors, around 30% [68, 73], suggesting that proteins interacting with the two receptors for essential function are considerably different, thus directing the two receptors to different specific target genes [40, 74].

All ER ligands bind exclusively to the LBD of the receptor [75]. E2 interacts with hERα via a hydrogen bonding network formed from the 3-OH of the A-ring of E2 interacting with Arg394, Glu353 and a single water molecule. The 17β-OH on the D-ring of E2 forms a hydrogen bond with His524 [76, 77]. The remainder of the molecule participates in a number of hydrophobic contacts at various points around the cavity. The binding interactions for hERα are illustrated in Figure 2.4. The binding mode of E2 with hERβ is identical to that shown for hERα.

The role of the water molecule as a pivot in the ligand recognition mechanism is observed in all published crystal structures of ligand bound hER. It is thought to participate in positioning the ligand into the pocket rather than acting as a bridge for binding [71, 76]. The hER is able to bind a wide range of non-steroidal ligands. A phenolic A-ring is highly favourable but not essential for ligand binding. The remainder of the binding pocket can interact with a number of different hydrophobic groups. This ability to bind a variety of compounds is attributed to the relatively large size of the binding pocket (hERα 450 $Å^3$; hERβ 390 $Å^3$) compared to the volume of E2 (245 $Å^3$) [77, 78]. The LBD is composed of 12 α-helices, of which H3 through H12 form a 'wedge' shaped ligand binding cavity with H12 acting as a 'lid' [77]. This structure is illustrated in Figure 2.5.

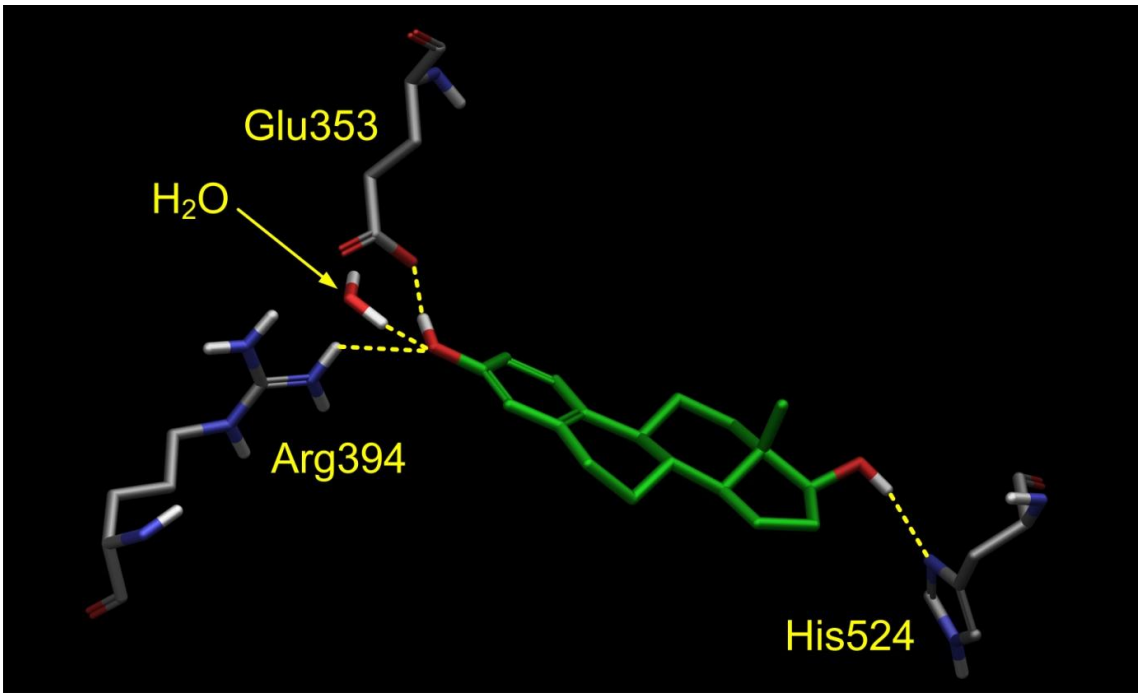

Figure 2.4. Hydrogen bonding network of E2 in hERα. Atom co-ordinates from PDB entry *1ERE*. Image produced in Schrodinger Suite 2010 *Maestro*.

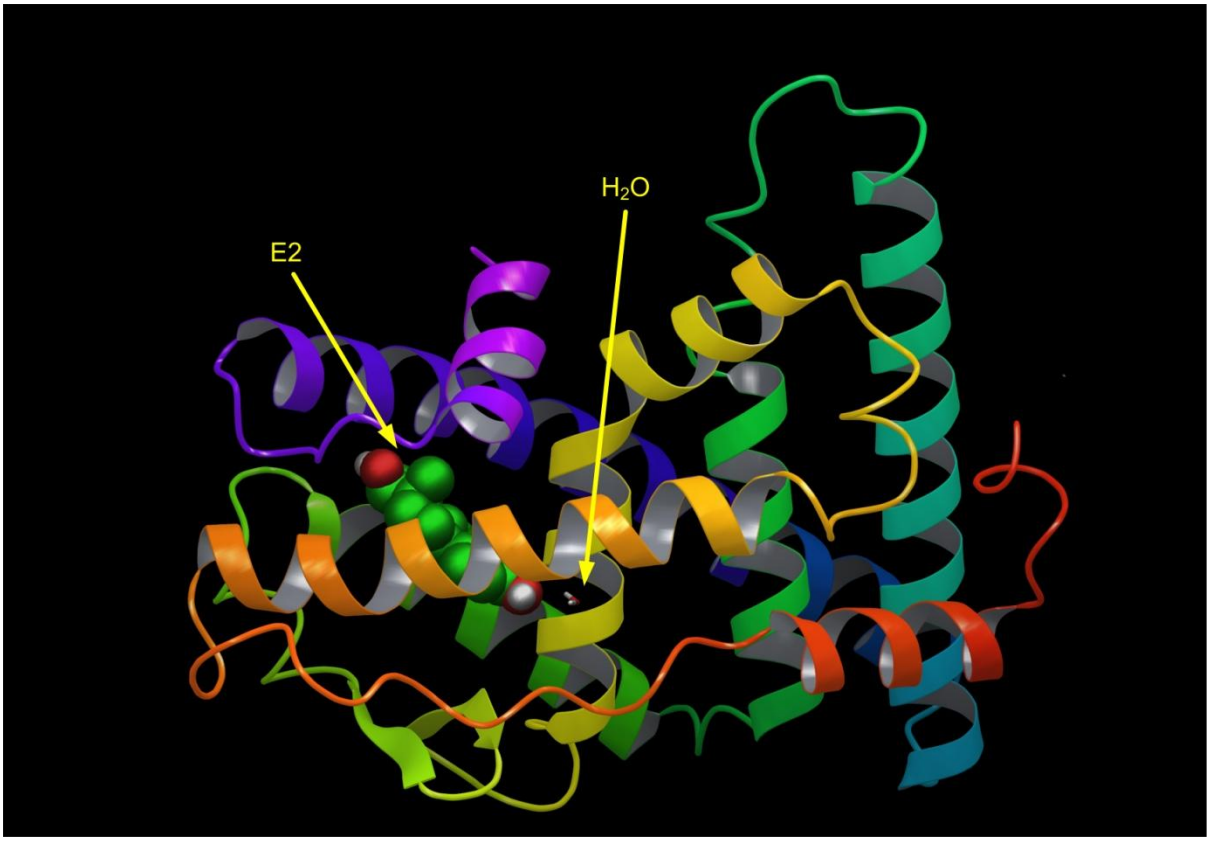

Figure 2.5. Tertiary structure of the hERα LBD with E2 (shown in space-filling representation) and the water molecule (shown in tube representation) in the binding cavity. Ribbons illustrate the α-helix protein structure. Thin lines illustrate flexible loops which are disordered regions connecting two ordered regions. Ribbons with arrows illustrate β-sheet structure. Atom co-ordinates from PDB entry *1ERE*. Image produced in Schrodinger Suite 2010 *Maestro*.

Within the LBDs of hERα and hERβ, there are only two substitutions of residues in close proximity to bound agonists: hERα Leu384 is replaced by hERβ Met336 and hERα Met421 is replaced by hERβ Ile373. The reduction in binding pocket volume in hERβ is due primarily to the replacement of Leu384 with Met366. Given the conservative nature of these substitutions, it is not surprising that E2 is non-selective for hERα and hERβ. Other compounds exhibit a preference for one of the hERs. For example, the phytoestrogen GEN is moderately selective, with a higher affinity for hERβ over hERα [79].

The binding of an agonist such as E2 causes a major reorganisation of the tertiary structure of the receptor LBD. The C-terminal H12 folds against H3, H5/6 and H11, closing the binding pocket. This exposes the functional AF-2, a hydrophobic groove on the surface of the hER

LBD as shown in Figure 2.6(a). The positioning of the H12 helix is critical for recruiting coactivators to the AF-2 site and subsequent initiation of gene transcription and has been proposed as an important mechanism for determining the agonist efficacy of different ligands [75, 80, 81]. Antagonist binding repositions H12 so that it occupies this hydrophobic groove, preventing coregulator recruitment [81] as shown in Figure 2.6(b). The coregulators have a conserved motif (LxxLL; L=leucine, x = any other amino acid) called the NR box that is necessary and sufficient for binding to the AF-2 site of the agonist-bound receptor [75, 82]. As stated earlier in this section, the main surfaces for receptor dimerisation are located in the C region (DBD). The C-terminus F region is also involved in dimerisation. Within the LBD, residues 507-518 in hERα (460-469 in hERβ) are essential for dimerisation [83, 84]. These residues are located upstream of His524, directly under the end of H12 when the receptor is in the agonist conformation. The agonist conformation also places the F region in close proximity to these LBD residues.

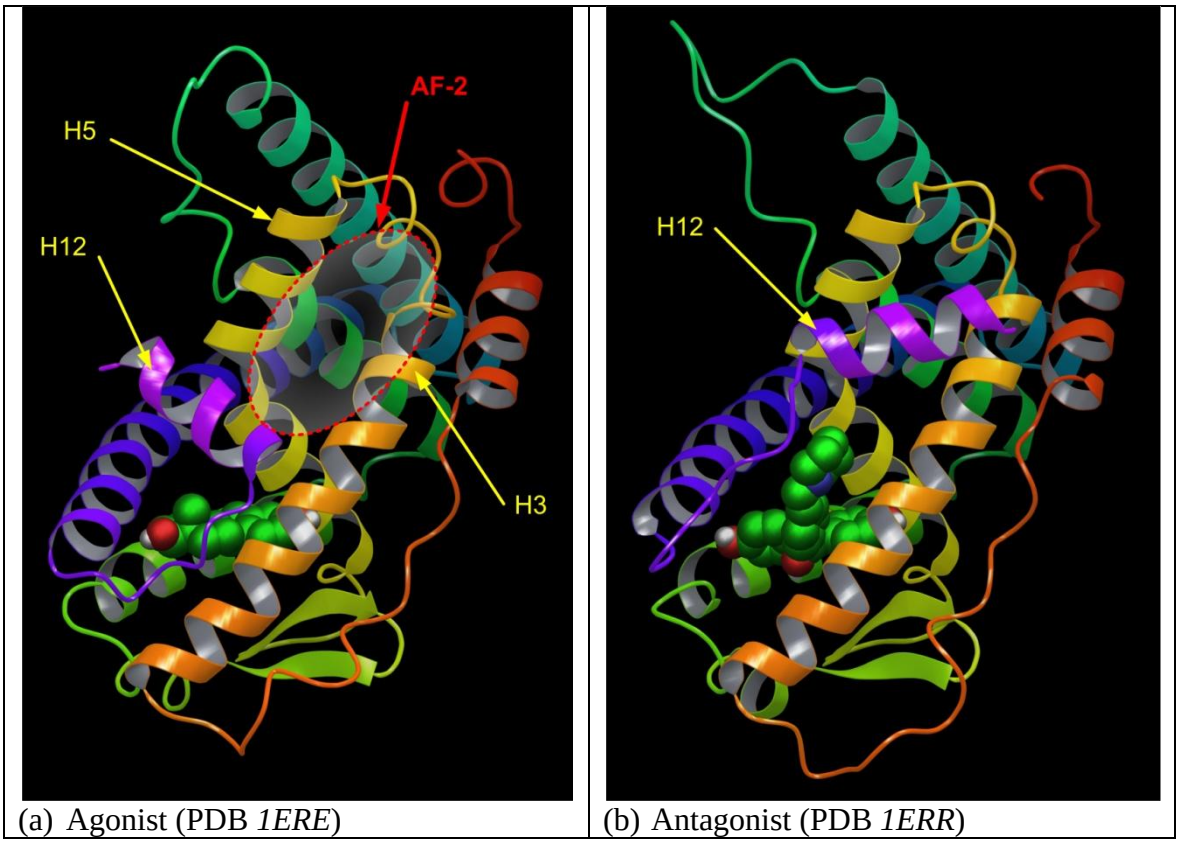

(a) Agonist (PDB *1ERE*) (b) Antagonist (PDB *1ERR*)

Figure 2.6. Positioning of H12 in the agonist and antagonist conformation. The AF-2 site is exposed in the agonist conformation and occupied by H12 in the antagonist

conformation. Atom co-ordinates from PDB entries *1ERE* and *1ERR*. Images produced in Schrodinger Suite 2010 *Maestro*.

The entire ER has never been crystallised, likely because of the large regions of ill-defined tertiary structure (A/B region, D region, F region). The ER LBD also has not been crystallised without a bound ligand. As will be discussed in Chapter 3, a single 'apo' crystal structure of hERα has been solved, but this structure was obtained by crystallising the protein with a ligand, then literally 'soaking' the ligand out of the crystal before collecting x-ray crystallographic data [85].

2.2.2 hER Function

A general review of transcription is provided by Latchman et al. [86]. Three excellent reviews of hER mediated transcription are provided by Hall and McDonnell [70], Ascenzi et al. [65] and Gronemyer et al. [87] and are briefly summarised here.

In the absence of the hormone, the hER is sequestered in a multi-protein inhibitory complex with heat shock proteins (Hsp70 and Hsp90) and other chaperone proteins in either the cytoplasm or the nuclei of target cells. The chaperone proteins hold the ER binding cavity open for ligand entry. Hormone binding induces a conformational change in the receptor that causes dissociation of the chaperone proteins and closing of H12 over the binding cavity. This conformational change promotes dimerisation of the receptor protein followed by high-affinity binding to specific EREs located within the promoter regions of target genes. From the EREs the hER complex recruits RNA polymerase and other coregulatory proteins to positively or negatively regulate gene transcription. In the case of the hER, gene transcription occurs very slowly, at a basal rate, without the recruitment of coregulatory proteins. Coregulatory proteins are classed as coactivators or corepressors that respectively increase or decrease the rate of transcription. The specific suite of coregulatory proteins present in a cell depends on the type of cell and may vary in time or with stages of development.

Receptor dimerisation is required for gene expression through interaction with EREs, but the ligand bound receptor monomer can interact with other transcription factors (e.g. AP-1 and NF-κB) to initiate expression of those target genes [65]. Gene expression regulated via the EREs is described as *direct* and expression regulated through interactions with other transcription factors is described as *indirect*.

Not all tissues respond to ligand-bound hERs. The transcriptional activities of hER ligands are tissue-selective suggesting that the hER requires specific cellular factors for maximum response. Many of these coregulators are used by more than one nuclear receptor. These coregulators are present in limiting quantities in the cells so that ligand bound receptors must compete for the coregulators needed for transcription. The coregulator proteins are recruited at AF-2. There are at least 20 identified coactivators and 6 identified corepressors [70]. The populations of these factors vary by cell type.

2.2.3 Agonism and Antagonism

As was illustrated in Figure 2.6, estrogens function as AF-2 agonists, meaning that they induce a conformational change in the hER that results in the formation of the coactivator binding site (AF-2 site) where coactivator proteins bind. Most antiestrogens function as AF-2 antagonists meaning that the conformational change they induce in the hER prevents the coregulators from binding at the AF-2 site. However, some antiestrogen-hER complexes are able to bind DNA suggesting that they mediate active repression of gene expression by recruiting corepressors to target promoters.

The activity of hER ligands spans a range from full agonist (estrogenic in all tissues) through mixed agonist/antagonistic (SERM) to pure antagonist (antiestrogenic in all tissues). The mechanism of mixed agonism/antagonism may differ depending on the chemical structure of the SERM. For some SERMs the mechanism is related to the ratio of coactivator to corepressor proteins in different cell types and the exact topology of the ER-ligand complex. The topology in turn determines how strongly the ligand-receptor complex recruits coactivators (resulting in an agonist response) relative to corepressors (resulting in an antagonistic response) [88]. This range of possible ligand action and the potential variation depending on the specific target cell in which the ligand is acting results in the wide variety of observed effects obtained in *in vivo* exposure studies.

One example of this variation in observed effects is the difference in action of two breast cancer drugs: RAL and tamoxifen (TAM). The SERM action of TAM is actually produced by its metabolite 4-hydroxytamoxifen (OHT) [89]. The structures of TAM, OHT and RAL are shown in Figure 2.7. TAM (OHT) acts as an antagonist in breast cancer cells and as an agonist in uterine cells [90, 91].

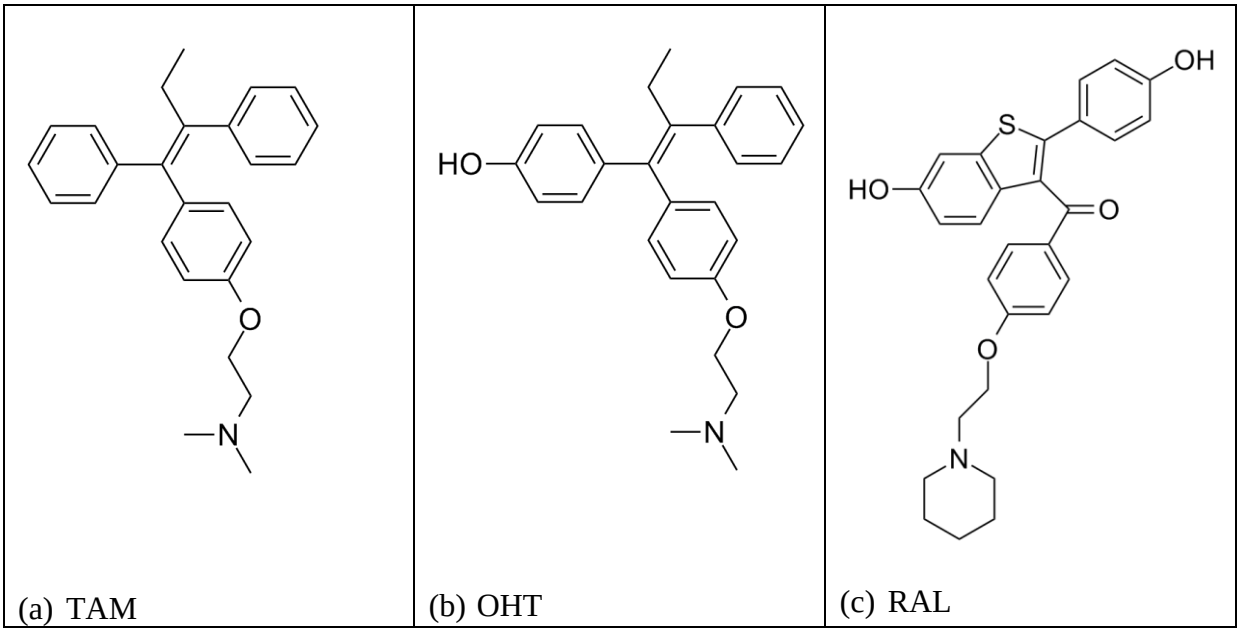

(a) TAM (b) OHT (c) RAL

Figure 2.7. Structures of (a) tamoxifen (TAM), (b) 4-hydroxytamoxifen (OHT) and (c) raloxifene (RAL).

The complexity of effects on gene expression exemplified by TAM and RAL [90, 92, 93] is illustrated in Figure 2.8. The actions of TAM and RAL have been extensively studied *in vitro* using cell lines derived from human breast cancer (MCF-7 cells) and human endometrial cancer (Ishikawa cells). Both TAM and RAL are used in the treatment of hormone-responsive breast cancer. RAL is also used in the treatment of osteoporosis. TAM is associated with an increase in uterine cancer but RAL is not. At the molecular level, both RAL and OHT are hERα and hERβ antagonists. Both compounds bind to the hER and induce the antagonist conformation [77, 81]. However, in the uterus, the two compounds have different effects due to *cell context* and *promoter context*. Even though OHT binds to the hER and induces the antagonist conformation in the receptor, the hER-OHT complex is able to recruit the specific coactivator proteins necessary to up-regulate the genes that lead to the development of uterine cancer. The hER-RAL complex does not. The concentration of one coactivator protein, *steroid receptor coactivator 1* (SRC-1), is higher in the uterus than in the breast. The specific morphology of the hER-OHT complex is able to recruit this coactivator and therefore is more agonistic in the uterus than in the breast. In contrast, the hER-RAL complex more strongly recruits corepressor proteins and consequently is still an antagonist in the uterus, despite the higher concentration of coactivators relative to corepressors.

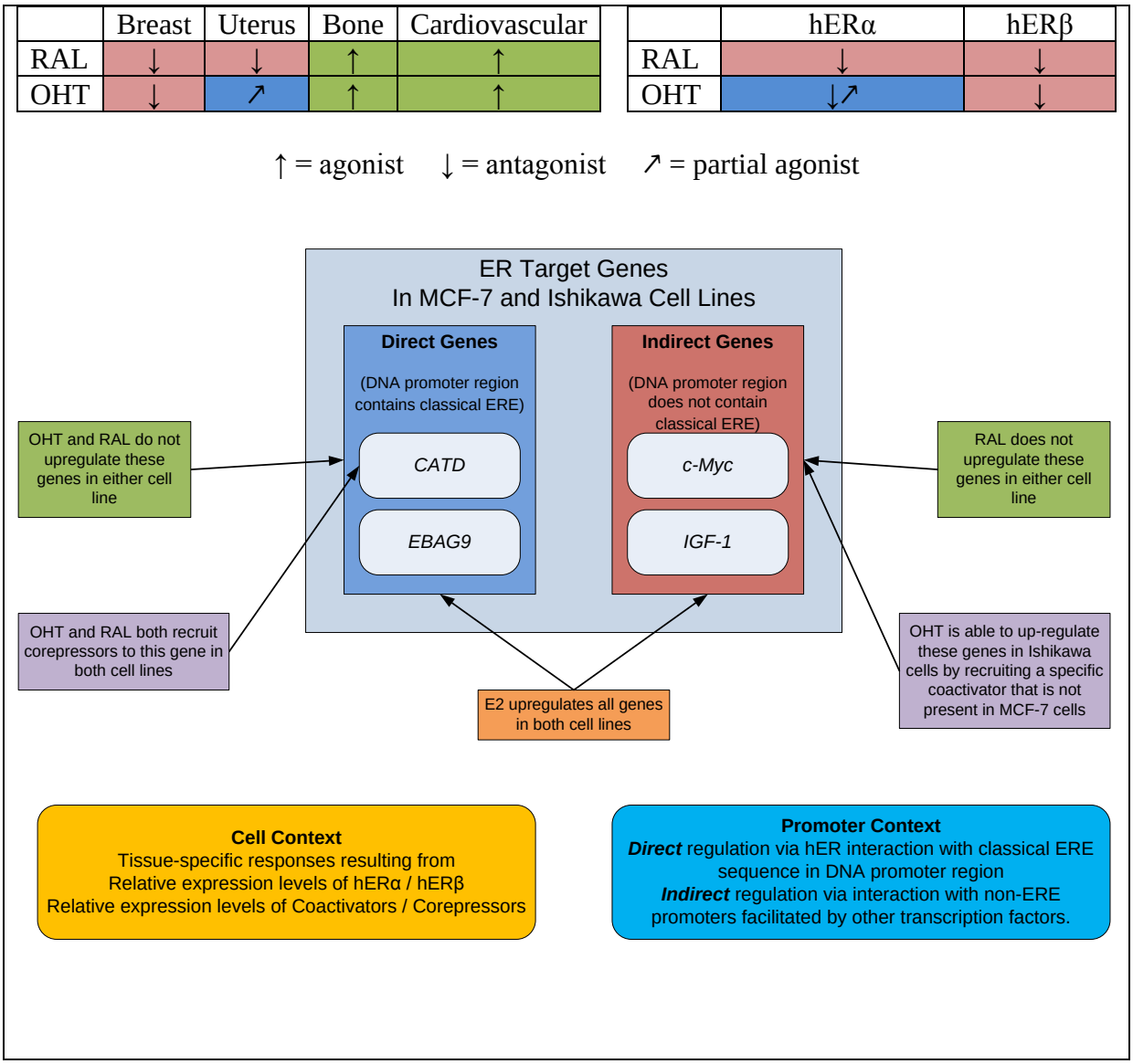

Figure 2.8. Complexity of hER gene expression exemplified by the actions of 4-hydroxytamoxifen (OHT) and raloxifene (RAL) in MCF-7 and Ishikawa cell lines [90, 92, 93]. Different patterns of gene expression are observed in these cell lines. The differences in receptor-ligand complex topology induced by the two different ligands result in different abilities of the hER to recruit the cofactors present in the different cell lines.

The ligand bound hER complex is also able to function as a transcriptional repressor. For example, the activity of the transcription factor NF-κB involved in immune response can be inhibited by hER [94], explaining in part the bone maintenance actions of E2 and the anti-inflammatory actions of E2 observed in brain and the cardiovascular system [95]. Counter-

intuitively, both TAM and RAL are able to mimic the effect of E2 in these tissues. These ligand-receptor complexes remain able to recruit the corepressors needed to achieve this action because the NF-κB pathway is mediated by the AF-1 domain, not the AF-2 domain.

The wide variety of physiological responses to the genomic action of estrogens begins with the same first step – binding of the ligand to the receptor protein. Ligand binding induces a conformational change in the receptor that can be broadly classified as either agonist or antagonist, but it is clear from these examples that small differences in the overall conformation of the ligand-bound receptor strongly influence the degree to which a particular pathway in a particular cell is initiated [85]. But, as demonstrated by OHT and RAL, ligand-bound receptor conformation is not the only determinant of agonist or antagonist action in target cells.

It is known that both the magnitude of exposure to EEs and the timing of this exposure are critical to the observed outcome [23, 96-101]. For example, exposure of a fetus *in utero* early in gestation when tissues are rapidly differentiating can have very different physiological outcomes than exposure as an adult. The sex of the individual exposed is also an important factor since the chemicals interfere with sex hormone signalling. The physiological outcome of exposure to EEs is difficult to predict because not all of the hormone target genes are fully known or understood and because the actions of many chemicals have not been fully investigated. Also, exposure is usually to a mixture of EEs, not just a single chemical. The subtleties of the interaction of EEs with the ER can also lead to situations similar to that seen with OHT and RAL, where cell context is the deciding factor in the observed effect of the molecule. This concept is the topic for Chapter 4.

2.3 Human Gestational Development

In humans, childbirth occurs about 38 weeks after conception and pregnancy begins with implantation of the embryo in the uterus. Implantation occurs approximately 9 days after conception. The term embryo is used to describe the developing offspring during the first 8 weeks following conception, and the term fetus is used from about 2 months of development until birth. Pregnancy is typically broken into three periods, or trimesters, each of about three months.

Human development, as with vertebrate development in general, is described as epigenetic because the genes that regulate development are in turn regulated by the chemical micro-

environment of the differentiating cells [53]. An individual cell has the capacity to develop along different paths. The path that is chosen is determined to a large extent by the cells it neighbours and the chemical (hormonal or immune) signals that are passed from cell to cell. This external influence determines which genes are permanently turned on or off, resulting in the cell developing the functions required of its location [53]. As mentioned earlier, hormonal signalling is vulnerable to interference from external factors such as exposure to environmental pollutants which can result in permanently altered gene expression for the exposed individual and their offspring. In humans, these critical tissue differentiation processes occur early in development, within the first 16 weeks [96].

In humans, organogenesis occurs between days 18 and 60 of gestation and it is during this time that the conceptus is most vulnerable to interference in the development of these organs caused by exposure to chemicals. The CNS, however, is susceptible throughout pregnancy [102].

2.3.1 Sexual Differentiation

From early first trimester through early second trimester (from approximately 4 to 16 weeks gestation) primary and secondary sexual differentiation occurs in humans [96]. For the first few weeks, the male and female genitalia develop along very similar paths and are described as 'indifferent'. From these initial structures, the development of female genitalia is straightforward, but the changes necessary to produce male genitalia are substantial and expression of these genes is controlled by the androgens. The Y chromosome initiates development of the testes. The testes then take control with production of the two main male sex hormones, T and DHT. T suppresses development of oviducts, uterus and vagina which would develop from the Müllerian duct. T is produced by the male fetal testes and interacts with target tissues in the undifferentiated genitals transforming these tissues into the male genitalia. At the same time, T affects the developing brain, programming typical male behaviours and preferences [96].

2.3.2 Estrogen Receptors in the Fetus

The ER has been detected in the human fetal vagina and urogenital sinus as early as the 10^{th} week of gestation [103] and by mid-gestation ERs are present in many human fetal tissues as summarised in Table 2.1 [104]. The relative distribution of hERα and hERβ is indicated by the number of + in Table 2.1.

Table 2.1. Distribution of hERs in human fetal tissues [104]. Relative abundance is indicated by the number of + .

Tissue	hERα	hERβ
Placenta		+
Skin	+	++
Spleen		+++
Kidney		++
Thymus	+	++
Adrenal		++
Uterus	+++	+
Ovary	+	+++
Testis	+	+++
Brain		++

2.3.3 Hormones in the Fetus

The ovaries of the human female fetus secrete estrogens during sexual differentiation [53]. All three estrogens are also synthesised in the placenta from androgens produced in both the maternal and fetal adrenals [53]. In the human male fetus, the aromatase activity required to produce estrogens from androgens is localised in the Leydig and Sertoli cells of the testes, where high levels of hERβ are found. Androgens are also produced in large quantities in the human fetal testis from approximately the 6th week of gestation.

2.4 Maternal Exposure to Environmental Estrogens

Assessing human fetal exposure to EEs requires an understanding of maternal exposure, maternal metabolism, the functions and metabolic pathways of the placenta and the metabolic capacity of the fetus. Differences in drug metabolism between male and female adult humans are well known, as are differences between pregnant and non-pregnant females [105, 106]. These differences may be reasonably well characterised for pharmaceuticals, but they are not well characterised for EEs [107]. In the absence of pregnant female specific data, information on adult humans must be used as a surrogate. While the placenta plays a critical role in the control of endogenous hormones in both the mother and the fetus [108], and it has active transport mechanisms that are specifically dedicated to removal of xenobiotics and toxic endogenous compounds [109], it is now commonly accepted that almost all drugs cross the placenta to some extent [110]. It is therefore not unreasonable to expect EEs to behave in the same way.

2.4.1 Exposure routes

The EEs of interest are components of cosmetics, personal care products and pharmaceuticals and are contaminants in food and water so maternal exposure occurs by several routes including ingestion [111-115], absorption through the skin [114, 116-119] and inhalation [120]. Once EEs reach the bloodstream, they are subject to a variety of metabolic reactions designed to facilitate elimination from the body. Depending on the specific EE and the metabolic reactions it is subjected to, it is possible for the compound to be deactivated by metabolic transformations or conjugation reactions. It is also possible for metabolites to be estrogenic [121].

2.4.2 Metabolic Fate

To be eliminated from the body in either urine or feces, a compound needs to be water soluble. This is accomplished by covalently attaching a highly water-soluble functional group to an otherwise insoluble molecule. In humans, the primary conjugation pathways are glucuronidation and sulphation [122], as illustrated in Figure 2.9.

Glucuronidation via the uridine 5' diphospho-glucuronosyltransferase (UGT) family of enzymes is the major drug detoxification and elimination pathway in humans [123] and this reaction occurs primarily in the liver. The UGT enzyme transfers a glucuronic acid molecule from UDP-glucuronic acid to the target molecule to increase the water solubility of the target molecule, facilitating its elimination. There are 18 known isoforms of the UGT enzyme in humans [124]. Each of the isoforms has a preferred set of substrates on which it acts. For example, morphine (Figure 2.10(a)) is glucuronidated exclusively by the UGT2B7 isoform at both the 3- and 6- positions. Paracetamol (Figure 2.10(b)) is glucuronidated primarily by UGT1A6 and to a lesser extent by UGT1A9 [124]. This type of substrate specificity is likely to hold for the suite of EEs of interest in this study. Substrate specificity of the UGTs has not been extensively studied, and where information is available, the substrates of interest are mainly pharmaceuticals and endogenous hormones.

Sulphation is accomplished by the cytosolic sulfotransferase (SULT) superfamily of enzymes [125]. In humans, 11 isoforms of the SULT enzymes have been identified and represent 3 of the 6 SULT families. The expression of SULT enzymes in humans is carefully regulated, with expression levels differing by tissue type, stage of development. Hormonal influences also affect SULT expression levels [125]. In the adult, SULT1A3 (catecholamine sulfotransferase) is highly expressed in the gastrointestinal tract for the production of

dopamine sulphate. SULT1E1 (estrogen sulfotransferase) is highly expressed in the endometrium and is crucial for controlling levels of estrogen in the endometrium during the menstrual cycle, particularly at the time of potential implantation of an embryo [125]. The endogenous hormones exist in the human circulatory system primarily as sulphate conjugates. Hydroxylated PCBs are well known and potent inhibitors of SULT1E1 giving rise to their endocrine disrupting effects. The 4A family of SULTs are found only in the brain and no natural or xenobiotic substrates have been identified [125]. The human SULTs, with the exception of 1A1, are substrate specific. SULT1A1 is highly efficient in the sulphation of a wide array of xenobiotics [125].

The glucuronidation and sulphation reaction pathways require a nucleophilic site (-OH, -NH_2, -SH, -COOH) on the target molecule to which the glucuronide or sulphate is attached. If the target molecule does not have a suitable site for conjugation, the cytochrome P450 (CYP) superfamily of enzymes or other enzyme metabolic pathways capable of hydrolysis, reduction or oxidation will provide such a site [122].

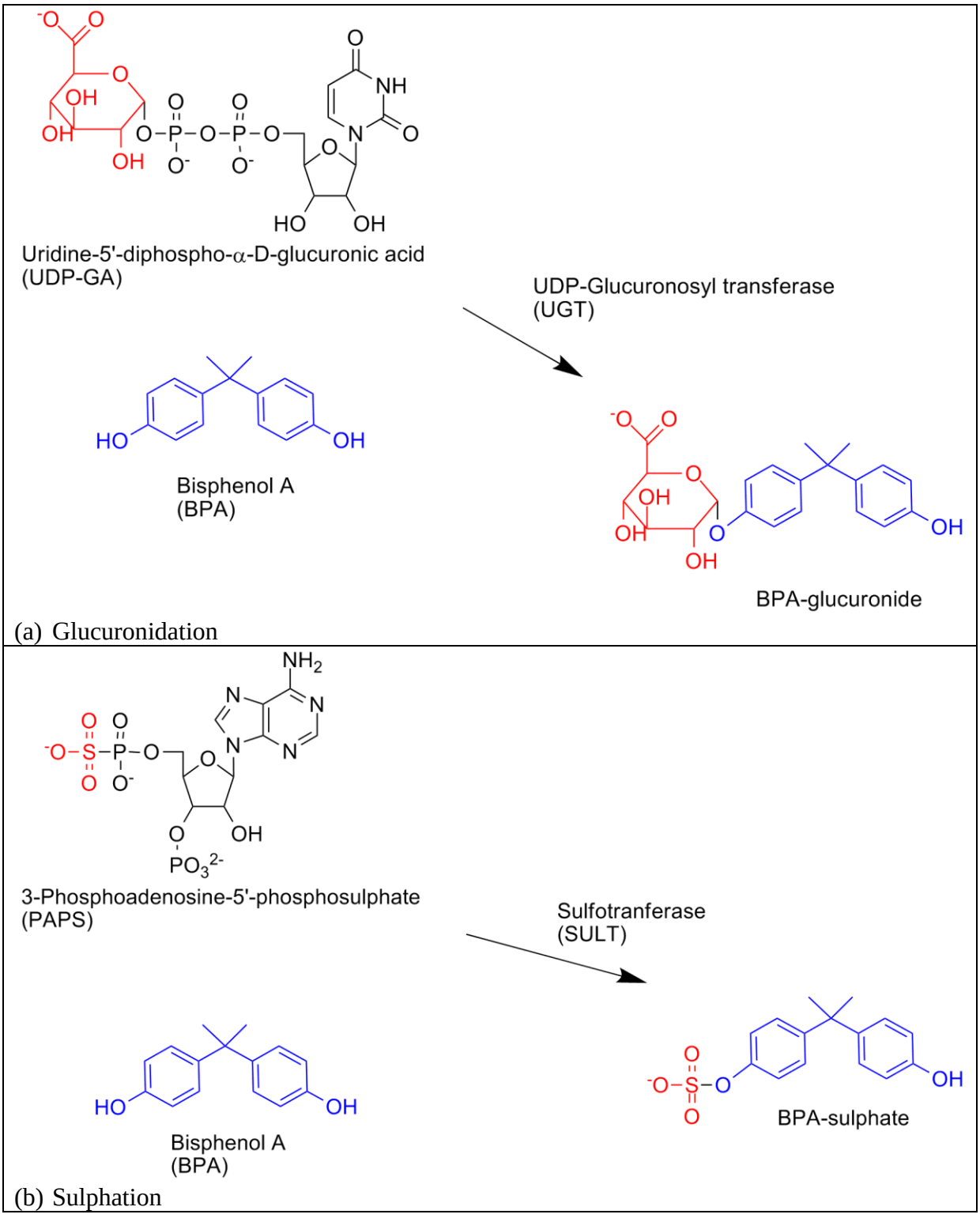

Figure 2.9. Glucuronidation and sulphation conjugation reactions using BPA as an example.

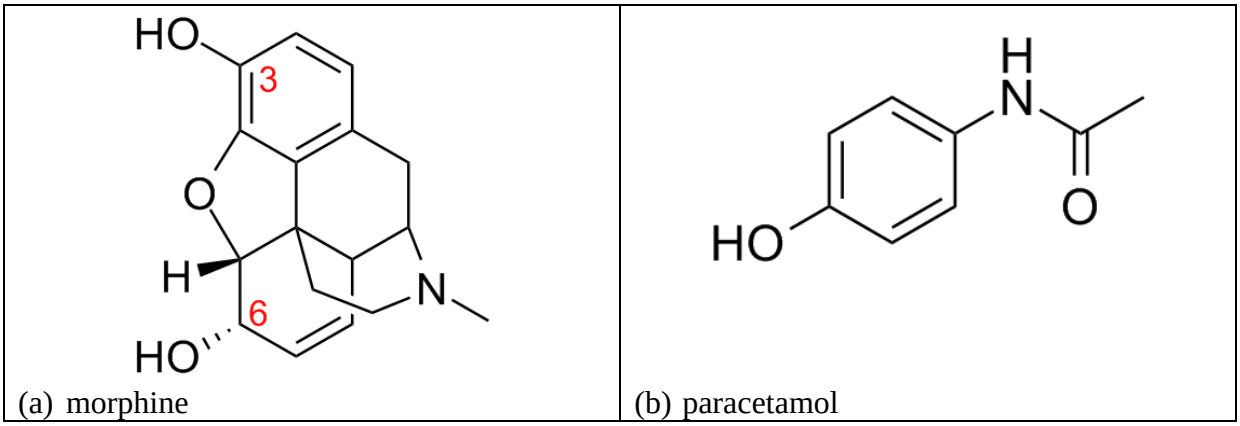

(a) morphine (b) paracetamol

Figure 2.10. Chemical structures of morphine and paracetamol.

The CYP enzymes are a superfamily of heme-containing monooxygenases that use O_2 and electrons to oxidise substrates [102]. There are 14 known families of CYP enzymes in humans. CYP enzymes play a role in fatty acid hydroxylations, steroid biosynthesis and xenobiotic metabolism. Most of the xenobiotic metabolising enzymes are expressed in the liver.

Most of the EEs of interest in this study already have a suitable nucleophilic site, so further transformations are not usually required before the conjugation reaction. This does not mean these reactions do not occur. For some of the EEs of interest, main transformation products have been reported in the literature and are included in the suite of target analytes if the compound is commercially available. For others, their metabolism has not been reported, so the parent compound is the only target analyte. Identifying metabolites is beyond the scope of this project.

The route of exposure determines how quickly a compound can be eliminated. Chemicals that are ingested and pass through the digestive system reach the sites of metabolic reactions very quickly and a large fraction of the ingested amount can be eliminated before it reaches the circulatory system. Exposure through the skin or by inhalation bypasses this 'first-pass' elimination and the chemical can enter the circulatory system directly [122].

Table 2.2 summarises the pertinent information on metabolic clearance, metabolic pathways and identified metabolites for the EEs of interest.

Table 2.2. Metabolites of environmental estrogens

Environmental Estrogen	Parent Compound	Other Metabolites	Glucuronide Conjugate	Sulphate Conjugate
BPA	Serum levels of unconjugated BPA remain in the low ng/mL range 24 h after ingestion [126].		Orally ingested BPA is rapidly but not completely converted to the monoglucuronide [126, 127].	BPA is also sulphated at one or both hydroxyls [128].
Phthalates		Phthalates are rapidly hydrolysed to the monoesters (Figure 2.27) [129, 130]. Higher molecular weight phthalates can undergo additional oxidation of the monoester at the terminal end of the alkyl substituent, forming a secondary alcohol or ketone (ω-1 oxidation) or carboxylic acid (ω-oxidation). The monoesters are also detected in serum, but at much lower levels than in the urine [129, 130].	The monoester is excreted in the urine as both the free molecule and the glucuronide conjugate [129, 130]	
Alkylphenols		Metabolism is complex and occurs by several mechanisms, resulting in many possible metabolites. N-alkylphenols (e.g. NP, Figure 2.24) undergo extensive β-oxidation of the alkyl side chain. The main metabolite found in the urine was 4-hydroxybenzoic acid (free, glucuronidated and sulphated) [121, 131]. Branched alkylphenols (e.g. 4t-OP, Figure 2.25) are more resistant to metabolism. They undergo β-oxidation, but only until the primary carbon atoms in the chain are exhausted [132].	Parent compound and other metabolites are glucuronidated at the phenolic hydroxyl and are excreted in the urine[121, 131, 132]	Parent compound and other metabolites are sulphated at the phenolic hydroxyl and are excreted in the urine [121, 131, 132]

Environmental Estrogen	Parent Compound	Other Metabolites	Glucuronide Conjugate	Sulphate Conjugate
Benzophenones	Unconjugated benzophenones are eliminated in the feces [133].	BP-3 is demethylated to form BP-1 [134]. 2,3,4-trihydroxybenzophenone has also been reported as a metabolite of BP-3 [119].	Benzophenones are glucuronidated and eliminated in the urine [119, 133, 134].	Benzophenones are sulphated and eliminated in the urine [119, 133, 134].
Parabens		The major metabolites of the parabens are 4HBA, p-hydroxyhippuric acid but neither compound is a specific biomarker of paraben exposure.	Glucuronides comprise 28-43% of total concentration in adult urine [135]	Sulphates comprise 55-67% of total concentration in adult urine [135]
Triclosan			Triclosan is assumed to be glucuronidated [136].	
Phytoestrogens			GEN is glucuronidated [137].	GEN is sulphated [137].
Endogenous Estrogens				Sulphate conjugates of estrogens are the main form of circulating estrogens in both the mother and fetus [132, 138].

2.4.3 Concentrations of EEs in Adult Urine

Adult exposure to environmental pollutants is most often characterised by determining the concentration of the compound of interest or its metabolites in urine. The total concentration (free + conjugated) is most often reported. Figure 2.11 illustrates the range of adult urine levels reported in the literature for the compounds of interest in this study. The range of concentrations shown in Figure 2.11 is large because each of the literature studies considered cohorts of different sizes and nationalities and therefore the aggregate data represent diverse lifestyles and levels of maternal exposure as summarised in Table 2.3. To obtain the broadest representation of the literature data, the minimum, median and maximum values reported in each study were used. In the studies where the median value was not reported, the mean value was used. The lowest minimum, highest maximum and the lowest and highest median concentrations for each target analyte in the aggregate data set were determined. The data from individual studies and the corresponding references are given in Table A. 1.

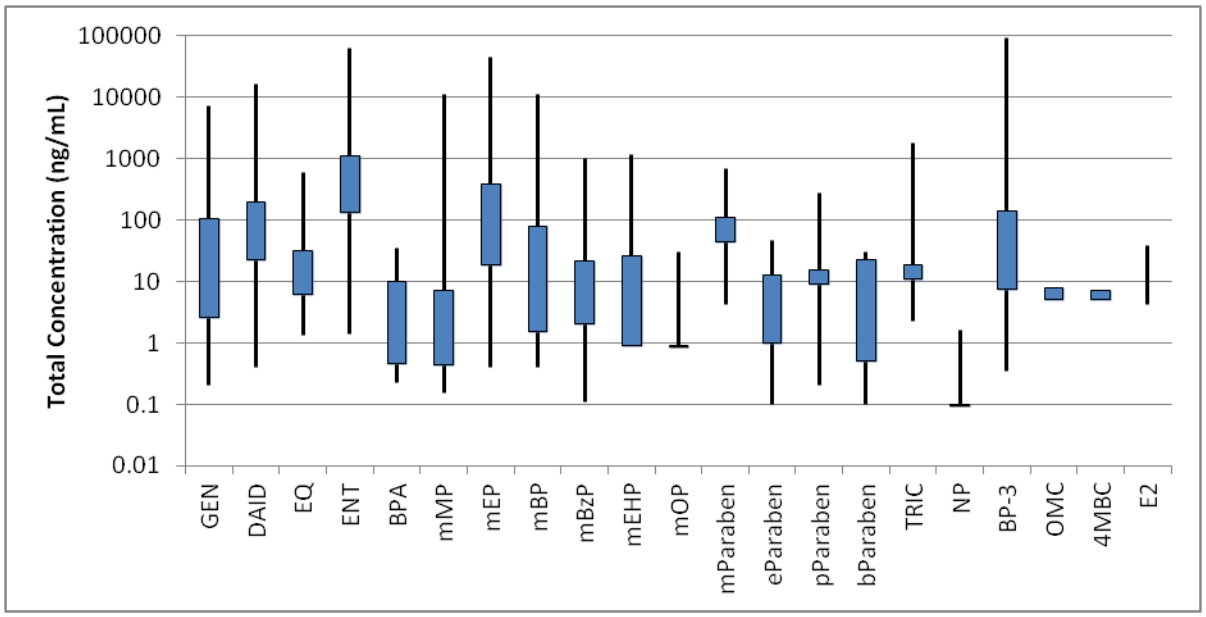

Figure 2.11. Range of reported total EE concentrations in adult human urine. Lines indicate range of reported values, bars indicate lowest and highest median reported values.

Table 2.3. Description of human urine studies included in literature aggregate data set.

Study Name and Reference	Country / Cohort	Target Analytes	Analytical Method	Deconjugation
Huang [139]	Taiwan Maternal, female fetus	mMP, mEP, mBP, mEHP, mBzP	LC-MS/MS	β-glucuronidase only
Huang [139]	Taiwan Maternal, male fetus	mMP, mEP, mBP, mEHP, mBzP	LC-MS/MS	β-glucuronidase only
Ye [135]	USA Adults	mParaben, eParaben, pParaben, bParaben	LC-MS/MS	β-glucuronidase and arylsulphatase
Ye [140]	USA Adults	BPA, TRIC, BP-3, mParaben, eParaben, pParaben, bParaben	LC-MS/MS	β-glucuronidase and arylsulphatase
Calafat [141]	USA Adults	BPA, NP	GC-MS	β-glucuronidase only
Swan [142]	USA Maternal	mMP, mEP, mBP, mEHP, mBzP	LC-MS/MS	β-glucuronidase only
Liu [143]	USA Adults	GEN, DAID, ENT, BPA	HPLC	β-glucuronidase only
Valentin-Blasini [144]	USA Adults	GEN, DAID, EQ, ENT	LC-MS/MS	β-glucuronidase and arylsulphatase
Janjua [116]	Adult males	unknown	unknown	unknown
Janjua [116]	Post-menopausal females	unknown	unknown	unknown
Kato [145]	USA Adults	mMP, mEP, mBP, mEHP, mBzP, mOP	LC-MS/MS	β-glucuronidase only
Blount [146]	USA Adults	mMP, mEP, mBP, mEHP, mBzP, mOP	LC-MS/MS	β-glucuronidase only
Wolff [147]	USA Maternal	BPA, TRIC, BP-3, mMP, mEP, mBP, mEHP, mBzP	LC-MS/MS	β-glucuronidase only
Choi [148]	Korea Adults	GEN, DAID, EQ, ENT, E2	GC-MS	β-glucuronidase and arylsulphatase
Moors [149]	German Adults	GEN, DAID, EQ, BPA	GC-MS	β-glucuronidase only
Grace [150]	UK Women	GEN, DAID, ENT, EQ	GC-MS	β-glucuronidase and arylsulphatase
Wittassek [151]	German Maternal	mBP, mBzP, mEHP	LC-MS/MS	β-glucuronidase

2.5 Maternal-Fetal-Placental Unit

Fetal exposure is usually assessed in the context of the maternal-fetal-placental unit. Exposure of the mother results in a circulating concentration of the compound that is determined by her metabolic clearance of that compound. The compound reaches the placenta via maternal circulation where it must cross a membrane barrier to reach the fetal circulation.

A diagrammatic representation of a 15-week pregnancy is shown in Figure 2.12. As the pregnancy progresses, the chorion and amnion membranes fuse, leaving a small chorion cavity located in close proximity to the placenta. The placenta is a complex structure of blood vessels with membranes separating the maternal and fetal circulations and is the interface between mother and fetus. On the fetal side, the umbilical cord with vein and artery carries blood to and from the fetus. The placenta facilitates nutrient and oxygen exchange and removal of waste products from the fetus [108, 152].

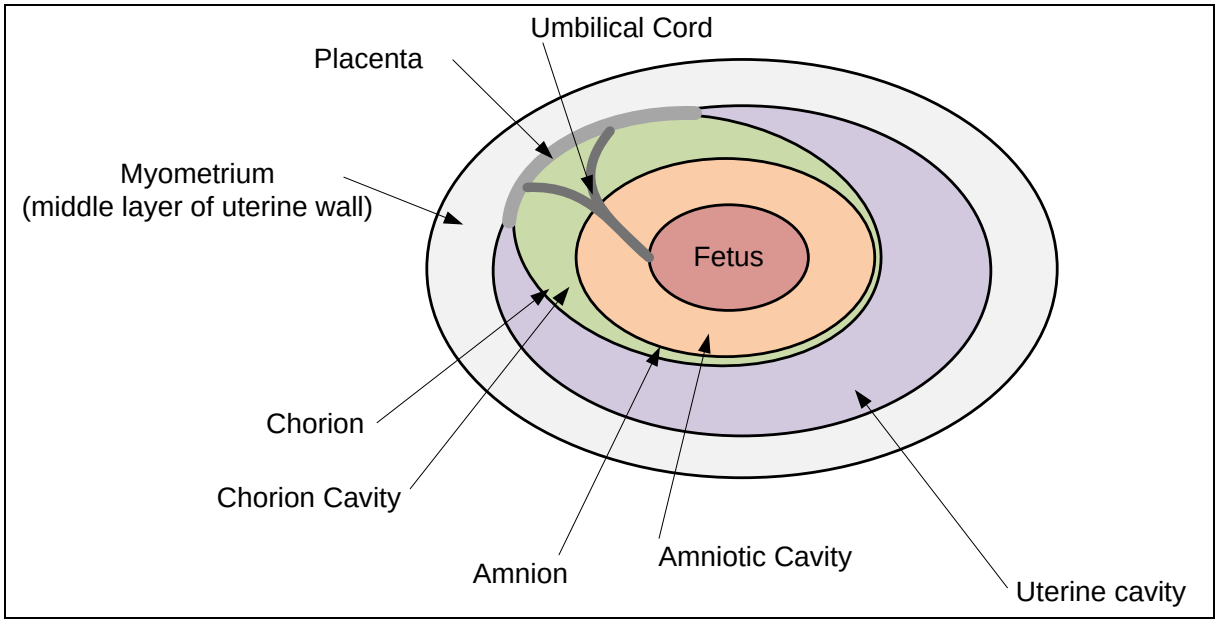

Figure 2.12. Diagrammatic representation of a 16-week pregnancy (adapted from http://media.web.britannica.com/eb-media/31/117431-004-FD591591.jpg).

2.5.1 Placental Metabolism

The placenta also plays a critical role in regulating the levels of endogenous hormones that the fetus is exposed to via blood circulation [108, 153, 154]. Enzymes that conjugate and

deconjugate estrogens (estrogen sulfotransferase and estrone sulphatase respectively) are present in the placenta [132, 138]. The balance in activity between these two enzymes is critical to the control of hormone levels [128]. Several EEs and their conjugates are inhibitors of and/or substrates for the sulphotransferases and sulphatases as summarised in Table 2.4. It is therefore likely that EEs can be both conjugated and deconjugated in the placenta for recirculation to the fetus.

Table 2.4. EEs are inhibitors of and substrates for estrogen metabolism enzymes.

EE	Estrogen Sulfotransferase (SULT1E1)	Estrone Sulphatase (ES)
Triclosan	competitive inhibitor in sheep placenta [155]	
BPA	substrate [128]	BPA sulphate conjugates are substrates [128]
Parabens	inhibitors in the skin [156]	
Alkylphenols	substrates and inhibitors [157]	
Phytoestrogens	GEN, DAID and EQ are inhibitors [158]	DAID sulphate conjugate is an inhibitor [159]

Historically, it was believed that the placenta protected the fetus from 'harmful agents' [153], but it is now known that many of the EEs are able to cross the placenta [152]. Simple passive diffusion, facilitated diffusion and active transport are the primary mechanisms by which chemicals cross the placenta [153]. The placenta has transport protein mechanisms that are active in protecting the fetus by preventing entry of certain classes of toxic substances. The placenta also expresses many of the xenobiotic-metabolising enzymes that are present in the adult liver, though they are not as functionally active as in the liver. These enzymes are also more active in the first trimester than at term [153]. The activity of these enzymes is thought to help limit the transfer of chemicals across the placenta to the fetus [160]. Placental enzyme activity has been shown to increase with maternal lifestyle choices such as smoking and alcohol consumption and with certain medications [153]. Overall, placental metabolism is not a significant factor in limiting the passage of most drugs to the fetus [161].

2.5.2 Placental Transport

Once a compound is within the mother's circulation, the primary pathway for fetal exposure is via the placenta. The maternal and fetal circulations are separated by membranes in the placenta. Hydrophobic, non-ionised molecules less than 600 Da cross the placental

membranes by simple diffusion, provided the concentration in the mother's circulation remains higher than in the fetal circulation.

The placenta also has facilitative transport mechanisms for transport of plasma protein bound molecules and active transport mechanisms for hydrophilic and ionic molecules. Facilitative transport is also driven by a concentration gradient but makes use of a carrier molecule such as a plasma protein to which the small molecule can bind. The transporter protein recognises the carrier molecule for transport across the membrane. Active transport requires energy in the form of ATP and is the dominant pathway for highly hydrophilic and ionic species to cross the placenta.

Simple diffusion is by far the most important transport pathway for chemicals to enter fetal circulation from maternal circulation [102, 161]. The main driving force for diffusion is the concentration gradient across the membrane. So, with continuous maternal exposure, once a chemical has passed through the maternal/placental barrier it may become trapped in the fetal compartment.

The anatomy of the placental villus, the region where the maternal and fetal circulations are in closest proximity is illustrated in Figure 2.13. As gestation advances, the space occupied by fetal connective tissue contracts and at term the fetal capillary epithelium and the basolateral membrane are separated by as little as 2-4 μm [162]. The blood vessels begin to develop in the placenta about 21 days post conception but maternal blood does not begin to flow into the villus space until about 10-12 weeks. Prior to the onset of maternal blood flow in the placenta, the intervillous space is filled with endometrial glandular secretions [162].

The placenta is highly permeable to respiratory gases, but glucose transport across the placenta requires specific facilitative transporters. Transport of lipids and amino acids across the placenta requires specific active transporters but free fatty acids and glycerols can also diffuse.

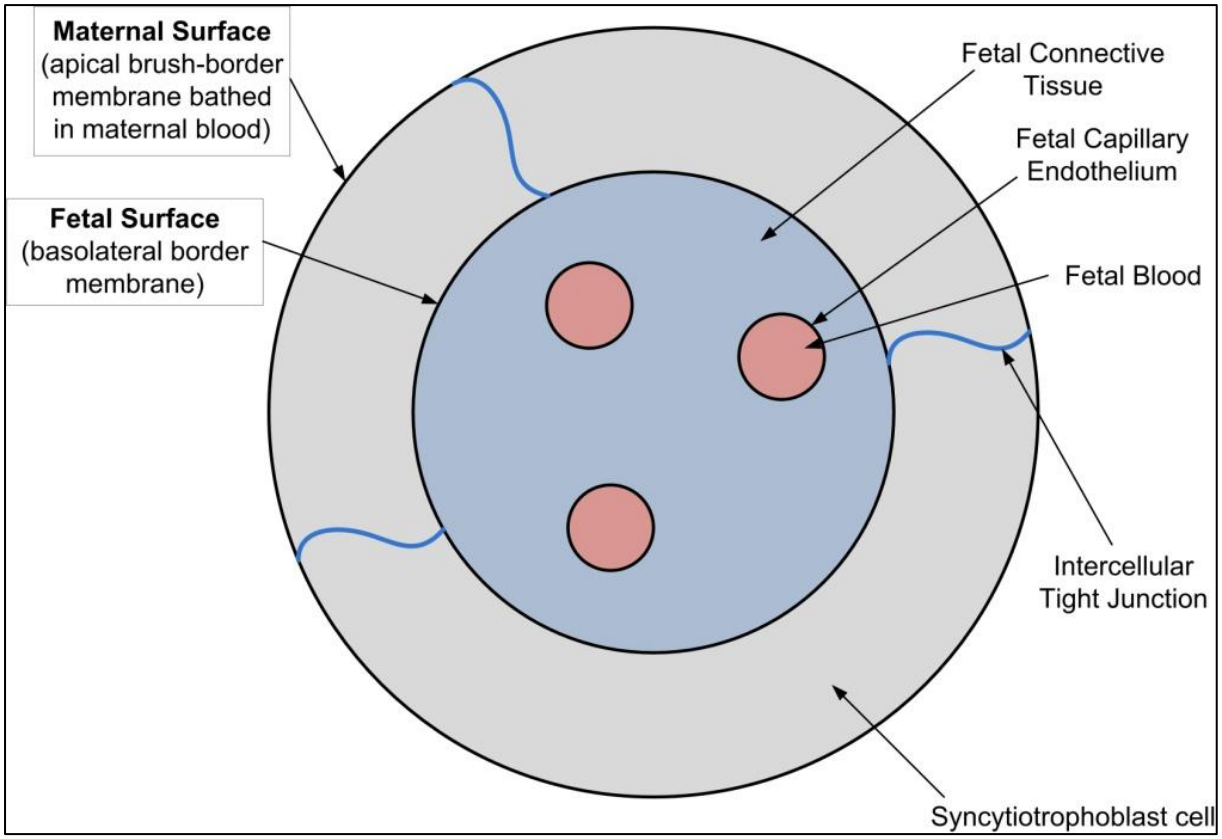

Figure 2.13. Anatomical arrangement of syncytiotrophoblast, cross section of a human placental villus (adapted from [109, 162])

The role of placental transporters in fetal drug exposure is virtually unstudied in humans [163] and what is known comes primarily from animal models or from ex-vivo placental perfusion studies of human term placentae. Several recent reviews of placental transporters have been published [109, 161, 163-166] and are briefly summarised as follows.

The current understanding suggests that facilitative and active transport proteins are located at specific sites within the placental membrane, as illustrated in Figure 2.14. Some transporters are located only on the maternal side of the membrane while others are only found on the fetal side of the membrane. Some transporters are unidirectional. They can either transport molecules that have entered the placenta out to the maternal circulation or the fetal circulation, depending on their location in the membrane or they can transport molecules from the maternal or fetal circulation into the placenta. Other transporters are bidirectional transporters which transport molecules either into or out of the placenta into the maternal or fetal circulation, depending on where they are located. There is evidence that specific groups

of the transporters are located in close proximity to one another and may work co-operatively. The transporters of interest are the P-glycoproteins (P-gp), the Multi-drug Resistance-associated Proteins (MRPs), the Breast Cancer Resistance Protein (BCRP) and the Organic Anion Transporters (OATs).

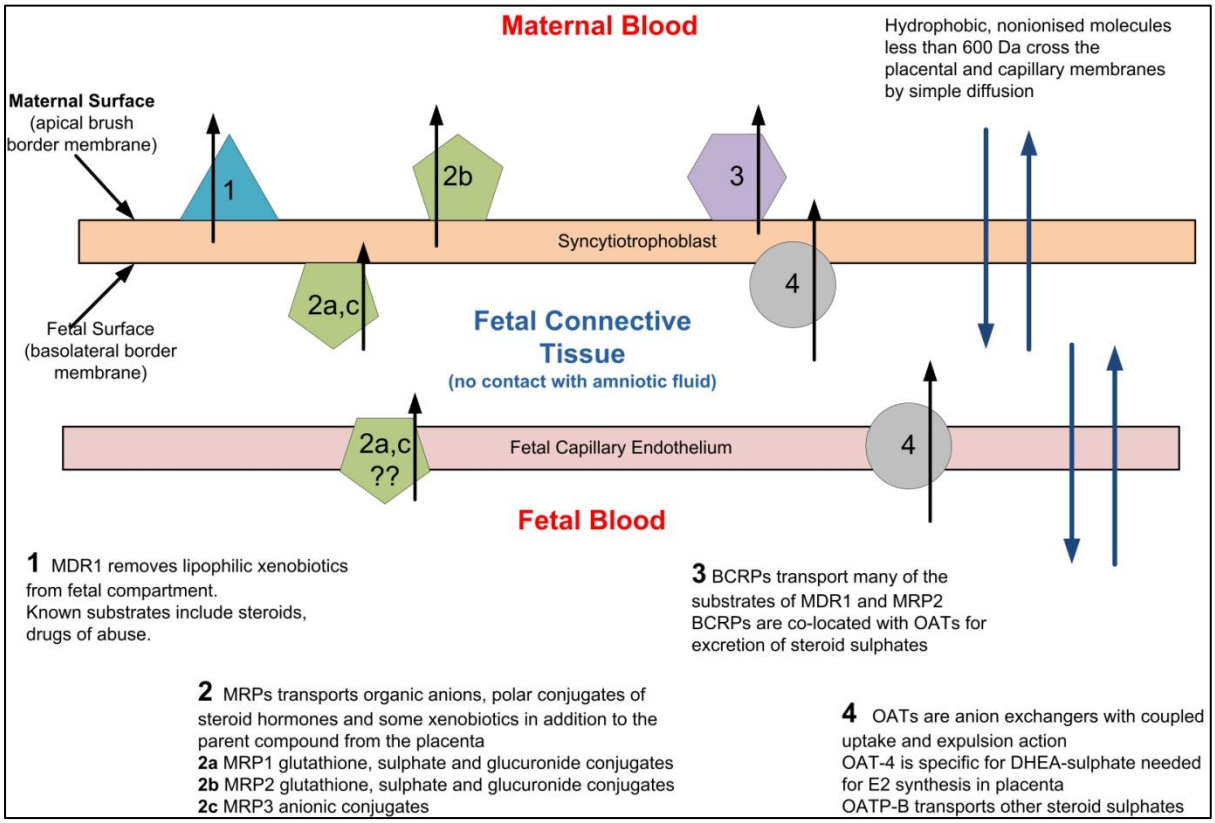

Figure 2.14. Location and directionality of active transport proteins in the placenta (adapted from [163]).

Of the P-gps present in the placenta, only one (MDR1) is involved in xenobiotic transport. MDR1 prevents the entry of hydrophobic molecules into the fetal circulation. It is located on the maternal side of the placental membrane and is a unidirectional transporter actively removing molecules from the placenta to the maternal circulation. MDR1 is able to transport a wide range of lipophilic neutral and cationic drugs. The endogenous steroids are substrates of MDR1. The transport mechanism of P-gps located elsewhere in the body are inhibited by progesterone [167]. Progesterone has been shown to inhibit P-gp transport when present in high concentrations and stimulate transport when present in low concentrations [109] and is being investigated for co-administration with antitumor agents to reverse multi-drug resistance in cancer therapies [109].

The MRPs are able to transport unconjugated amphiphilic anions, the polar conjugates of xenobiotics and endogenous compounds as well as some of the parent compounds. The MRPs are located on both the maternal and fetal sides of the placental membrane and possibly in the fetal capillary endothelium. Growing evidence suggests they work to reduce the accumulation of these compounds in the fetal compartment [109, 161].

The BCRP is located on the maternal side of the placental membrane. It is able to transport many of the same substrates as MDR1 and is thought to act in concert with the OATs in transport of steroid sulphate conjugates.

The OATs of interest (OATP-B and OAT-4) are anion exchangers with a coupled uptake and expulsion mechanism. They simultaneously take up a molecule on one side of the cell and expel a different molecule on the other side of the cell. The substrate for OAT-4 is DHEA-sulphate produced in the fetus and transported to the placenta for synthesis of E2. OATP-B is less specific and is able to transport other steroid sulphates.

BPA [168], NP [169] and GEN [170] all cross the human placenta to different extents intact, as shown by placental perfusion studies. GEN is also conjugated by the placenta, BPA and NP are not [168-170]. The amount of NP on the fetal side of the placenta is much lower than supplied on the maternal side, and the absence of conjugates suggests that NP may be metabolised by the placenta.

Nishikawa et al. [171] demonstrated that glucuronidated BPA is able to cross the rat placenta and that it is subsequently deconjugated in the fetus and amniotic fluid. The rat placenta is used as a model of human placenta because of its structural similarities, but there are some important differences. In rodents, maternal blood and fetal blood vessels are primarily separated by two syncytiotrophoblast layers, but in humans, only a syncytiotrophoblast monolayer separates fetal blood vessels from maternal blood. The authors concluded that it is possible that the human fetus is more sensitive and at greater risk than is the rodent fetus [171].

2.5.3 Composition of Amniotic Fluid

The fetus is suspended in and surrounded by amniotic fluid and it protects the fetus from physical trauma and allows the fetus to move. Amniotic fluid begins to accumulate in the very early stages of embryogenesis [172, 173]. The water in amniotic fluid originally comes from maternal plasma. As development continues, amniotic fluid volume increases and is

thought to be produced, in part, by ultrafiltration of fetal serum through the fetal skin and umbilical cord and by active secretion by the amnion, while the fluid in the chorionic cavity is thought be primarily a transudate of maternal serum produced and secreted by the trophoblast and chorion[174].

Amniotic fluid is composed of water (98-99%) and 1-2% dissolved solids. One half of the dissolved solids are inorganic (electrolytes). One half of the organic solids are proteins and the other half is composed of carbohydrates, amino acids, organic acids, urea, creatinine, lipids and hormones.[173-175]. The urea and creatinine levels in amniotic fluid are higher than in maternal serum and increase as the pregnancy progresses [175]. A number of enzymes are found in amniotic fluid including β-glucuronidase [175]. Estrogens in amniotic fluid are either conjugated or free, not protein bound [52].

Hydrophobic molecules that enter the amniotic fluid are available to the developing embryo/fetus by simple passive diffusion. For example, intra-amniotic injection of cortisol demonstrated that this is an efficient means of supplying glucocorticoids to the human fetus at 11 to 21 weeks gestational age [176]. Around the 11th week of gestation, the fetus begins to produce urine that enters the amniotic fluid. Fluid is also produced within the fetal lungs that is expelled and enters the amniotic fluid. Amniotic fluid is actively swallowed by the fetus, absorbed by the gastrointestinal and recirculated. Free diffusion occurs bidirectionally between the amniotic fluid and the fetus across the fetal skin up to 20 weeks gestation when skin keratinisation begins [173, 177]. Because of this intimate contact, the composition of amniotic fluid is similar to fetal plasma [173] and to fetal extracellular fluid [178] and provides a biologically relevant reflection of fetal exposure up to 20 weeks. Specifically, amniotic fluid obtained between 16 and 20 weeks gestation is accepted as a valid means to assess fetal exposure during the period of development that spans organogenesis [172, 179].

2.5.4 Metabolism in the Fetus

The activity of the UGT family of enzymes is significantly lower in the human fetus as compared to the adult [123, 180-182]. This reduced activity prevents ‘trapping’ of the water soluble metabolites in the fetal compartment and thus their accumulation in the amniotic fluid [123]. Only 2 of the 18 UGT isoforms show appreciable activity in the fetus and both are involved in steroid metabolism. UGT1A3 is the most active at 30% of adult levels and its substrate is E1. UGT2B7 is active at 10-20% of adult levels and androsterone and epitestosterone are the substrates. UGT2B7 is also known to act on a large number of

pharmaceuticals (e.g. morphine) [124]. With the substrate specific activity of UGTs and the low level of activity in the fetus, glucuronidation of EEs reaching the fetus is likely to be low.

In contrast, the activity of SULTs in the fetus is very high, making SULTs the major detoxification pathway in the developing human [125, 182]. Many of the pharmaceuticals that are predominantly glucuronidated in the adult are instead sulphated in the fetus, for example paracetamol [124]. The high activity of SULTs, particularly 1A1, in the fetus compensates to some extent the low UGT activity. The SULT 1C enzymes are exclusively expressed in the fetus and are entirely absent in the adult. SULT1A1 but not SULT1C1 is able to sulphate EEs such as BPA, 4t-OP, NP [183].

CYP activity in the human fetus and even embryo is well developed but is very different from that of the adult human [102]. Enzyme activity is generally lower in the fetus than in the adult. Some enzymes that are present in the fetus are absent in the adult and *vice versa*. CYP3A7 is the most abundant CYP enzyme in the fetus and is present from 50 days of fetal life [184]. Substrates for CYP3A7 hydroxylation include testosterone, cortisol and a number of pharmaceuticals and xenobiotics. The primary function of CYP3A7 is the protection of the fetus from maternal steroid hormones [184]. CYP3A7 function declines rapidly after birth when CYP3A4, the dominant isoform in the adult liver becomes active [184].

The deconjugation enzyme β-glucuronidase is present in cord blood and neonate liver, kidney and intestinal tissue [159]. β-glucuronidase is present in many fetal tissues at 7-17 weeks [185]. The activity level is highest in fetal liver and activity in the small intestine and adrenals is approximately 50% of the liver. Activity is also found in the kidney, heart and lungs. The β-glucuronidase activity in the placenta is about 30% of the liver activity. Sulphatase activity is also present in the fetal liver and small intestine and the placenta at 8-16 weeks [186]. Placental sulphatase activity increases sharply from 10-12 weeks and then declines through gestation.

BPA is the one EE that has been most extensively studied for its effects on the fetus. Schonfelder et al. [127] have demonstrated that as a result of reduced UGT enzyme activity, the rate of clearance of BPA is slower in the fetus than in maternal blood. BPA metabolism to BPA-glucuronide may also be suppressed by testosterone as the expression of UGT enzymes is down-regulated by androgens [187]. BPA may stimulate testosterone production

by suppressing P450 enzymes associated with steroid synthesis and metabolism [188, 189]. These finding may also be true for other EEs.

2.5.5 Measurements of Human Fetal Exposure

Human fetal exposure has been measured for a few of the EEs of interest in this study. Measurements have been made in umbilical vein blood (oxygenated blood enroute to the fetus), placental tissue, meconium and amniotic fluid. For this study, the measurements of interest are those in amniotic fluid collected around 16-20 weeks gestation. Each of the literature studies considered cohorts of different sizes and nationalities and therefore the aggregate data represent diverse lifestyles and levels of maternal exposure as summarised in Table 2.5. To obtain the broadest representation of the literature data, the minimum, median and maximum values reported in each study were used. In the studies where the median value was not reported, the mean value was used. The lowest minimum, highest maximum and the lowest and highest median concentrations for each target analyte in the aggregate data set were determined. If a particular EE was not detected in a study, the reported detection limit for that EE was used. The range of observed concentrations in adult human amniotic fluid is shown in Figure 2.15. The data from individual studies and the corresponding references are given in Table A. 2.

Table 2.5. Description of human amniotic fluid studies included in literature aggregate data set.

Study Name and Reference	Country / Cohort	Target Analytes	Analytical Method	Enzyme Deconjugation
Huang [139]	Taiwan / early 2nd trimester	mMP, mEP, mBP, mEHP, mBzP	LC-MS/MS	β-glucuronidase only
Engel [190]	USA / early 2nd trimester	GEN, DAID, ENT, BPA	HPLC-ELCD	β-glucuronidase only
Silva [130]	USA / early 2nd trimester	mEP, mBP, mEHP	LC-MS/MS	β-glucuronidase only
Ikezuki [191]	Japan / early 2nd trimester	BPA	ELISA	Not required
Yamada [180]	Japan / early 2nd trimester	BPA	ELISA	Not required
Foster [99, 179]	USA / early 2nd trimester	GEN, DAID	GC-MS	β-glucuronidase and arylsulphatase

van de Beek [52]	The Netherlands / early 2nd trimester	E2		None. Free concentration
Chen [192]	USA / early 2nd trimester	BPA	LC/MS	β-glucuronidase and arylsulphatase
Aldercreutz [193]	Japan / at birth	GEN, DAID, EQ,ENT	GC-MS	β-glucuronidase and arylsulphatase
Wittassek [151]	Germany / at birth	mBP, mBzP, mEHP	LC-MS/MS	β-glucuronidase

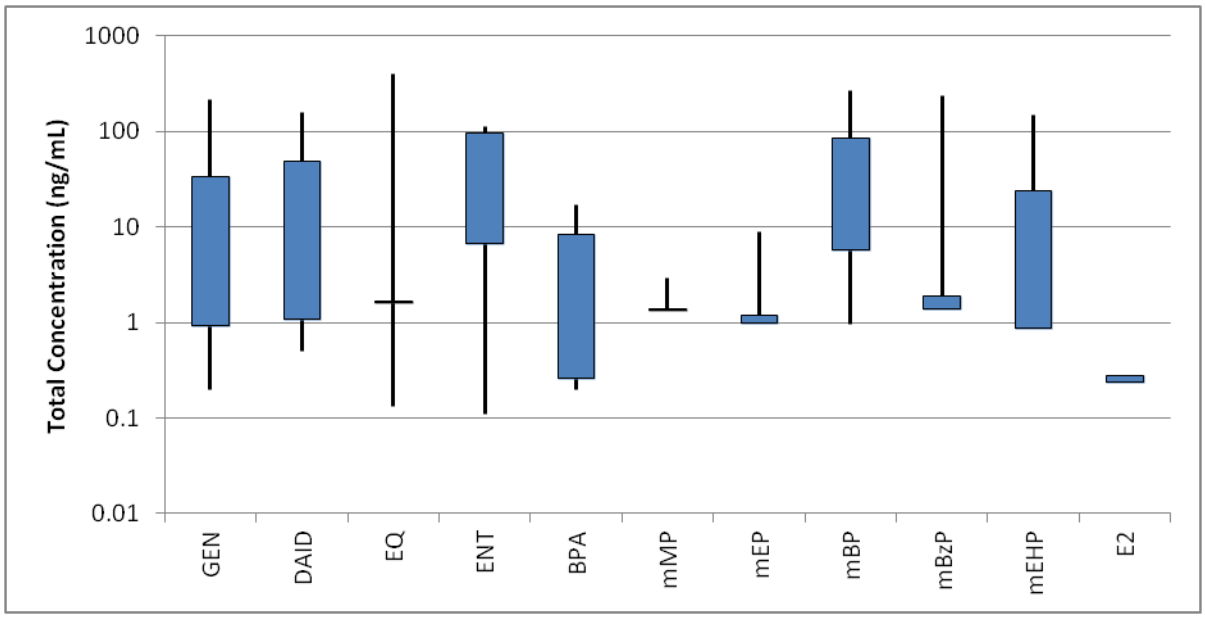

Figure 2.15. Summary of EE concentrations measured in human amniotic fluid reported in the literature. Lines indicate range of reported values, bars indicate lowest and highest median reported values.

2.6 Assessing the Activity of Environmental Estrogens

Environmental estrogens are not as efficient as endogenous estrogens at mediating gene expression; a much higher concentration is required to achieve the same magnitude of response. In some cases, the same magnitude of response is not achieved and the compound is described as a partial agonist.

2.6.1 In vitro Assays

In vitro assays are the first stage in assessing the biological activity of EEs. These assays can be broadly categorised as binding assays, cell proliferation assays and reporter gene assays. The simplest of the assays is the binding assay in which the ability of the test chemical to bind to the receptor protein is quantified. These assays are not able to give any indication of the biological activity of the chemical, but are useful in screening out non-binders from binders. Cell proliferation assays are the next most sophisticated type of assay in which the ability of a chemical to induce cell growth is quantified. The most sophisticated assays are the yeast or mammalian cell based reporter gene assays. The ability of the test chemical to affect

gene transcription is assessed by quantifying a protein produced as a result of gene transcription.

Most cell lines used in *in vitro* bioassays possess some metabolic activity and may lead to false negatives or false positives if metabolism leads to deactivation or activation of the chemical under study. Assays based on mammalian cells are often more sensitive than those based on yeast cells and are considered more relevant to human health [194]. But, the mammalian cell environment is more complex and the levels of receptor expression and composition of coregulators vary among cell lines. Therefore, the response to a particular EDC is different for different cell lines, making interpretation of results difficult [195].

Yeast-based assays are relatively simple and inexpensive to conduct compared to mammalian cell assays. The β-galactosidase reporter gene assays (YES assay) involves cell lysis and takes several days to complete [196] while the yeast based firefly luciferase reporter gene assays can be completed in a day [196]. The permeability of compounds through yeast cell walls may be different than through mammalian cell membranes possibly accounting for some differences in response [197]. Yeast cells BMA64-1A often used in the luciferase reporter gene assay is not able to metabolise TAM to OHT [196] which is the cause of the negative response.

The ER-CALUX assay is a reporter gene assay hosted in the human osteosarcoma cell line (U2-OS). This assay may be able to metabolise some chemicals to give positive results [198] where other assays give negative results.

Mammalian cell lines express endogenous receptor proteins. The MCF-7 and T47-D cell lines are human breast cancer cells and the dominant ER is hERα [199, 200] but they also express androgen, progesterone, glucocorticoid and retinoid receptors [200]. The Ishikawa cell line is a human endometrial carcinoma cell line. This cell line is dominant in hERβ but also has hERα and progesterone receptors [92]. Because of the difference in receptor protein expression, these two cell lines respond differently to some chemicals, as illustrated in Section 2.2.3 with TAM and RAL. These differences in response have been confirmed and validated by comparative profiling of gene expression [201]. Thus, multiple in vitro assays are required to fully characterise the activity of EEs.

An excellent review by Zacharewski [195] presents the advantages and limitations of *in vitro* assays in assessing EEs. The main observations and assessments summarised in Table 2.6.

Table 2.6. Summary of in vitro assays for assessing activity of EEs [195].

Assay Type	Advantages	Disadvantages
Competitive binding	• EEs by definition must bind ER	• cannot distinguish between agonists and antagonists • high concentration of ligand may cause non-competitive displacement • binding is necessary but not sufficient for estrogenicity. The ligand has to be bound long enough to initiate transcription
Cell proliferation assays E-SCREEN (based on either MCF-7 or T47-D human breast cancer cells)	• one of the most sensitive assays (30 pM E2) • agonist behaviour of test chemical is confirmed if proliferation is blocked by the standard reference anti-estrogen drug ICI-182780 • antagonist behaviour is confirmed if E2 proliferation is blocked by the test chemical.	• long incubation time (6 days) • not unequivocal (result can depend on experimental conditions, e.g. cell line clone, culture conditions)
Protein expression assays Vitellogenin (fish hepatocytes) Prolactin (immature rat pituitary cells)	• sensitive (1 nM E2)	• results restricted to specific cell lines, not easy to generalise • labour intensive methods • susceptible to false positives

Endogenous promoter-regulated reporter gene assays reporter genes such as firefly luciferase, β-galactosidase used to provide easily measured and quantified response. ER-CALUX - luciferase reporter gene expression assay based on T47D human breast adenocarcinoma cell line.	• excellent responsiveness and sensitivity • can assess relative potency of EEs • easily measured signal • can obtain a species specific or tissue specific response	• ER has two activation functions, one is constitutively active (AF-1) and the other is ligand induced (AF-2). Need to control for AF-1 activity. • Can be susceptible to non-ER ligand induction effects
Response element regulated reporter gene assays (mammalian cell based systems)	• ensures response is controlled through ERE, not other effects.	• sensitive to serum-borne estrogens (high background activity), so have poor response to test chemical
Yeast-based systems YES =yeast based β-galactosidase reporter gene assay.	• cells do not have endogenous receptor proteins • media is devoid of hormones • highly responsive, very good sensitivity	• function and potency response in yeast not always the same as in mammalian cell lines so results must be confirmed in another assay type

2.6.2 *In vivo* Assays

In vivo assays involve exposing a test organism (e.g. fish, mouse, rat) to the chemical under study, then measuring a change in biological function or phenotype. The studies can look for changes in the exposed individual or the effects of exposure on the offspring. A wide variety of biological end points have been used to monitor effects of exposure to EEs such as changes in expression levels of vitellogenin (egg yolk protein) in male fish or the increase in size and weight of the uteri of immature rodents. These assays are usually applied as a last screening step, once significant positive results have been found in a variety of *in vitro* assays.

One of the disadvantages of *in vitro* assays is that they do not account for metabolic activation of EEs and therefore result in 'false negative' responses (positive *in vivo*, but negative *in vitro*). These assays can also yield false positive responses when chemicals are tested at concentrations orders of magnitude above those seen *in vivo*. With *in vivo* assays,

the effects on the endocrine system are studied in context of other systemic functions such as metabolism and all potential modes of action of a compound are included [202, Van den Belt, 2004 #525].

2.7 Sources, Activity and Potency of Environmental Estrogens

The assessment of human fetal exposure to EEs presented in Chapter 7 is based on measurements of a suite of 35 chemicals in amniotic fluid. This section introduces the chemicals of interest, their use in products relevant to human gestational exposure and summarises the available literature on their estrogenic activity and potency. The compounds and classes of compounds are grouped according to their use.

Relative estrogenic potency (REP) is defined for ER agonists as ratio of concentrations of E2 to test compound required to produce the same level of activity. Usually the relative estrogenic potency is obtained from the ratio of EC_{50} concentrations for E2 and the test compound:

$$\mathrm{REP} = \frac{\mathrm{EC}_{50}\ (\mathrm{E2})}{\mathrm{EC}_{50}\ (\mathrm{Test\ Compound})}$$

The EC_{50} concentration is the concentration at which 50% of the compound's maximal activity is achieved. In some cases, another reference point may be used, such as EC_{10} [203]. The larger the value of the potency ratio, the more estrogenic the compound is. By definition E2 has a relative estrogenic potency of 1. Values of the ratio less than 1 indicate the compound is less estrogenic than E2, values larger than 1 indicate the compound is more estrogenic than E2.

For antagonists, the relative antagonist potency (RAP) is defined as the ratio of the concentration of the test compound needed to affect a 50% inhibition (IC_{50}) of the activity achieved by a reference concentration of a full agonist (RC_A). The reference concentration of the agonist is one that just achieves the maximal activity, but not in a large excess of what is required to achieve the maximal response. Typically, RC_A is chosen as approximately twice the EC_{50}.

$$RAP = \frac{IC_{50}\ (Test\ Compound)}{RC_A}$$

For the ER, the full agonist is usually E2 and for the AR the full agonist is either T or DHT.

A test compound is described as a full ER agonist if it able to produce the same maximal response as E2 and a partial agonist if the maximal response is less than that achieved by E2. In this situation, the fractional activity is reported. A similar distinction is applied to antagonists. A compound is described as a full antagonist if it is able to completely inhibit the maximal response of the reference compound and partial if less than full inhibition is achieved.

The activity results for the compounds of interest are often conflicting as the magnitude of the potency obtained is highly dependent on the assay used. Each of the assays has a different sensitivity to E2 and differences in cell context (endogenous or transfected receptor and ERE, availability of coregulators, etc.). The measured relative estrogenic potencies for the compounds of interest are summarised in Table A. 3 through Table A. 5. For each compound, the minimum, maximum and median potencies obtained by the various assays are shown in Figure 2.16. The data shown in this figure include only reported values. If a compound was reported as inactive in a particular assay, no value was included. When available, antiestrogenic and antiandrogenic potencies are summarised within the subsection for the particular compound.

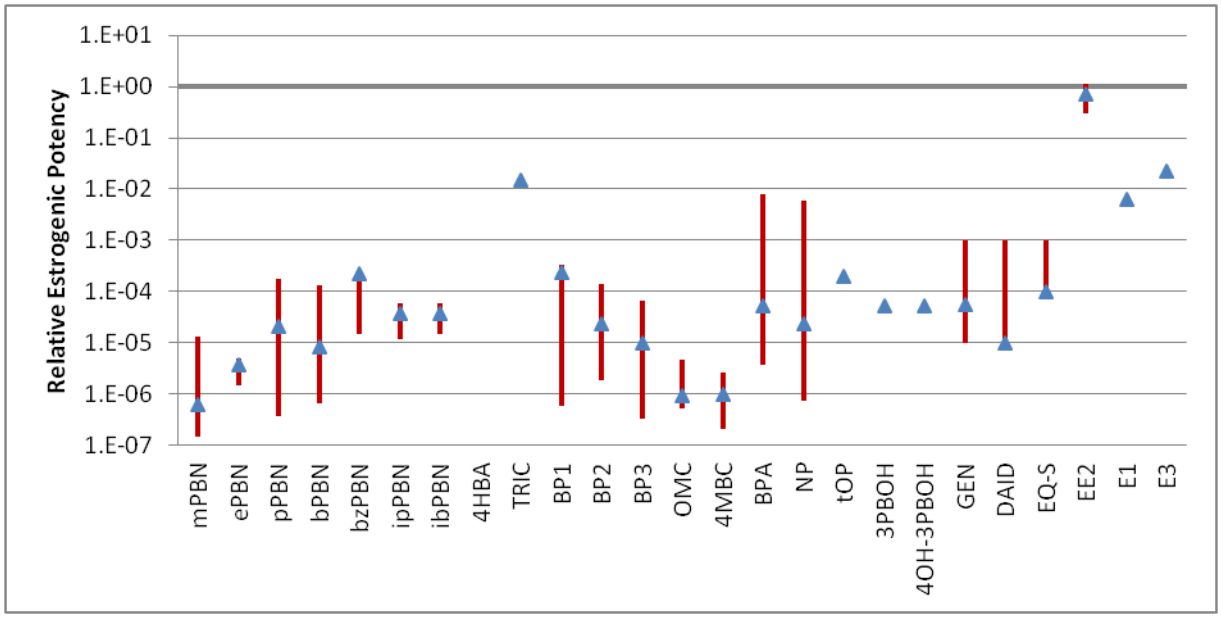

Figure 2.16. Comparison of relative estrogenic potency values for EEs. Median values are indicated with blue triangles, red bars indicate range between maximum and minimum values.

2.7.1 Cosmetics and Personal Care Products

Cosmetics and personal care products (PCPs) include a wide range of consumer products that are used for personal health and/or hygiene or for beautification. These products are often applied to and left on the skin (e.g. lotions) or applied for a short period of time and washed away (e.g. shampoo, hand soap). Some products may enter the body through the mouth (e.g. toothpaste). Some of the chemicals used to preserve PCPs are also found as preservatives in food.

2.7.1.1 Parabens

Parabens (esters of 4-hydroxybenzoic acid, Figure 2.17) are used as preservatives in cosmetics, topical pharmaceuticals and PCPs such as lotions and shampoos and in foods such as jams and baked goods [120]. They prevent bacterial and fungal growth in these products. An excellent review of parabens was published in 2008 by Darbre and Harvey [117].

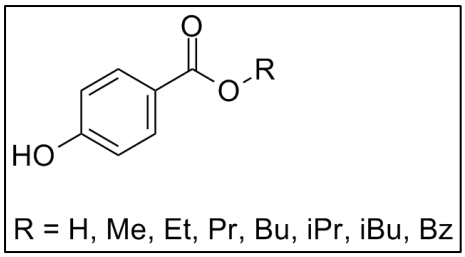

Figure 2.17. Molecular structure of parabens.

Parabens including the major paraben metabolite 4-hydroxybenzoic acid (4HBA) are weakly estrogenic [117, 204-209]. Parabens induce cell proliferation in the E-SCREEN assay [210, 211] and the two studies give different assessments of whether the individual parabens are full or partial agonists. The characterisation of weakly estrogenic is due to the significantly higher concentration of the chemical required to elicit the same response as E2.

Estrogenic potencies relative to E2 were measured for parabens for both hERα and hERβ mediated firefly luciferase reporter gene yeast assays [196] and the YES assay [203]. The results shown in Figure 2.16 indicate parabens are more potent in activating hERβ-mediated gene transcription. The yeast assay results indicate the parabens may be more estrogenic than the E-SCREEN results suggest.

Parabens have also been assessed for androgenicity [212]. At concentrations between 1 nM and 10 µM, 4HBA and the parabens had no direct androgenic activity in a human embryonic kidney (HEK 293) based luciferase reporter gene assays but the parabens were able to inhibit testosterone induced AR transcriptional activity as summarised in Table 2.7. These parabens are described as antiandrogens. 4HBA was unable to inhibit testosterone induced AR transcriptional activity.

As shown in Table 2.8, parabens also inhibit 4-hydroxyandrostenedione induced CYP19A1 (aromatase) activity [210] which indirectly affects endogenous steroid metabolism.

Table 2.7. Antiandrogenic potency of parabens [212].

Paraben	Relative Antiandrogenic Potency	% reduction in AR transcription (at 10 µM)
Methyl	8×10^3	40
Propyl	8×10^3	19
Butyl	8×10^4	33
4HBA	not active	0

Table 2.8. Inhibition of CYP19A1 (aromatase) activity by parabens [210].

Paraben	Relative Antiaromatase Potency	% reduction of aromatase activity (at 100 µM)
Methyl	11.3	55
Ethyl	10.6	55
Propyl	3.5	55
Butyl	26.4	45
Benz	25.8	10
iPropyl	16.2	55
iButyl	No effect observed up to 100 µM	
4HBA	No effect observed up to 100 µM	

2.7.1.2 Triclosan

Triclosan (TRIC, Figure 2.18) is an antibacterial and antifungal agent commonly used in antibacterial hand soaps, underarm deodorants and in one particular toothpaste product [213]. It kills bacteria by inhibiting fatty acid synthesis necessary for building cell membranes and for reproduction [214]. The *in vitro* assay results for TRIC are conflicting as summarised in Table 2.9. TRIC is not androgenic by the hAR-mediated luciferase gene transcription assay but is anti-androgenic in that assay and is able to achieve a 92% reduction in testosterone induced transcription at a concentration of 10 µM [212]. TRIC was also shown to inhibit

testosterone-induced proliferation of androgen-responsive S115 mouse mammary tumour cells at a concentration of 20 μM and was not able to induce cell proliferation in the S115 cells at concentrations up to 100 μM [213]. From these results, TRIC is classified as an antiandrogen.

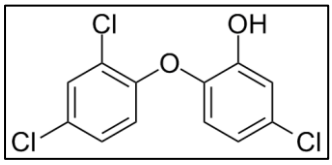

Figure 2.18. Molecular structure of TRIC.

Table 2.9. Relative estrogenic potency results for TRIC in in vitro assays.

Assay	Result
yeast-based hERα mediated firefly luciferase reporter gene assay [215]	inactive
YES assay [215]	agonist
ER-CALUX assay [216]	antagonist
MCF-7 based reporter gene assay [213]	antagonist
MCF-7 assay [210, 217]	inactive possibly cytotoxic [217]
MCF-7 cells [213]	partial agonist in the usual 7-14 day time frame allowed for this assay. Possibly a full agonist if assay was allowed to continue

2.7.1.3 Methyl triclosan

Methyl triclosan (mTRIC, Figure 2.19) is a biodegradation product [218] and possible metabolite [219] of triclosan and has a higher potential to bioaccumulate than the parent compound. No information on its estrogenic activity was found in the literature.

2.7.1.4 2,4-dichlorophenol

2,4-dichlorophenol (24DCP, Figure 2.19) is a possible metabolite of triclosan [219] but no information on its estrogenic activity was found in the literature.

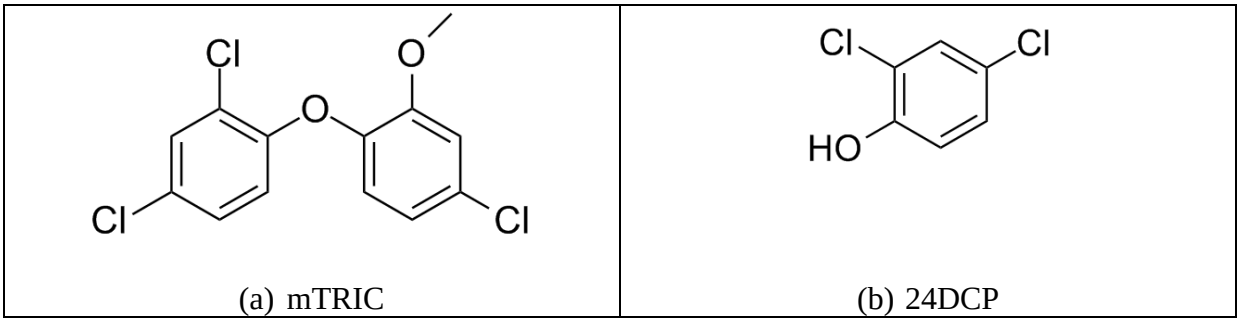

(a) mTRIC (b) 24DCP

Figure 2.19. Possible metabolites of TRIC, (a) mTRIC and (b) 24DCP.

2.7.2 UV Filters

UV filters absorb and dissipate UV radiation and are added to food packaging, cosmetics and personal care products to protect them from degradation. They are the active compounds in topical sunscreens.

2.7.2.1 Benzophenones

Benzophenones (Figure 2.20) are the active ingredients in topical sunscreens and added are to cosmetics including lipsticks and to food container plastics to filter out UV light [220].

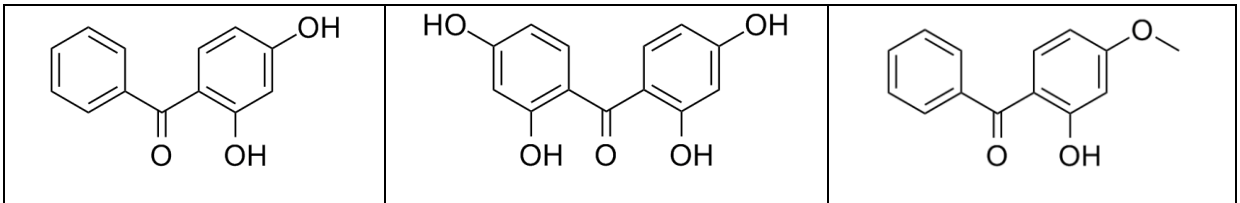

(a) BP-1 (b) BP-2 (c) BP-3

Figure 2.20. Molecular structures of benzophenone UV filters (a) BP-1, (b) BP-2 and (c) BP-3.

BP-3 is estrogenic in both hERα and hERβ mediated HEK293 cell based luciferase reporter gene assays [134], the E-SCREEN assay [221] and the YES assay [203, 222, 223]. BP-3 upregulates pS2 gene transcription in MCF-7 cells [224]. BP-3 is more potent in activating hERα mediated gene transcription. BP-3 did not show any antiestrogenic activity [134] and is not an AR agonist but is an AR antiandrogen with a RAP of 2 x 10^4 for the inhibition of dihydrotestosterone (DHT) induced gene expression in the AR-CALUX assay [198]. The main metabolite of BP-3 is BP-1 and it is a full agonist [134].

BP-1 and BP-2 are estrogenic in the E-SCREEN assay [221] and the YES assay [203, 222]and are able to up-regulate pS2 gene transcription in MCF-7 cells [224].

2.7.2.2 Octyl methoxycinnamate

Octyl methoxycinnamate (OMC, Figure 2.21) is used in topical sunscreens. OMC is an hERα partial agonist in the HEK293 cell based luciferase reporter gene assay, showing 42% of E2 activation at maximum concentration of 100 μM. OMC is not active in the hERβ mediated HEK293 cell based luciferase reporter gene assays and also did not show any antiestrogenic activity [134]. OMC is estrogenic in the MCF-7 cell proliferation assay [221] and is able to up-regulate pS2 gene transcription in MCF-7 cells [224]. OMC is androgen-inactive as it did not activate or inhibit testosterone-induced gene expression in the AR-CALUX assay [198].

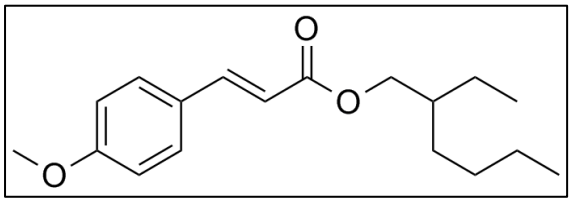

Figure 2.21. Molecular structure of OMC.

2.7.2.3 4-methylbenzylidene camphor

4-methylbenzylidene camphor (4MBC, Figure 2.22) is used in topical sunscreens. 4MBC is estrogenic in the hERα and hERβ mediated HEK293 cell based luciferase reporter gene assays [134], the MCF-7 cell proliferation assay [221] and is able to up-regulate pS2 gene transcription in MCF-7 cells [224]. 4MBC is not an AR agonist but is an AR antiandrogen requiring a concentration ratio of 7 x 10^4 to affect a 50% inhibition DHT induced gene expression in the AR-CALUX assay [198].

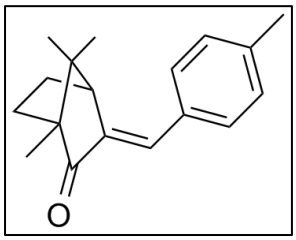

Figure 2.22. Molecular structure of 4MBC.

2.7.3 Industrial Chemicals, Pesticides and Plastics

2.7.3.1 Bisphenol A

Bisphenol A (BPA,Figure 2.23) is used to manufacture polycarbonate plastics and epoxy resins used in protective coatings of food cans and sealants in dentistry [141].

BPA is a full agonist in the hERα and hERβ mediated firefly luciferase reporter gene yeast assays [196], the ER-CALUX assay [197], the YES assay [203], the hERα and hERβ mediated firefly luciferase reporter gene assays in HepG2 cells [225], and the green fluorescent protein (GFP) reporter gene assay established in both MCF-7 and Ishikawa cell lines [226]. In hERα and hERβ mediated firefly luciferase reporter gene assays in U2-OS (human osteoblast) cells, BPA is a full agonist, able to elicit a response 1.2-1.7 times larger than E2 [227]. BPA is estrogenic in MCF-7 cell proliferation exceeding the maximal growth rate of E2 [228]. In the AR-mediated luciferase reporter gene assays in HepG2 cells, BPA has no activity [225] but in the ARhLBD-activating signal cointegrator 1 (ASC1) yeast two-hybrid system, which reflects the androgen-dependent interaction between androgen receptor (AR) and its coactivator, ASC1, BPA acted as potent AR antagonists comparable to a known strong antagonist, cyproterone acetate [229]. BPA is able to reduce the affinity of the ligand bound ER to the co-activator SRC1 [230].

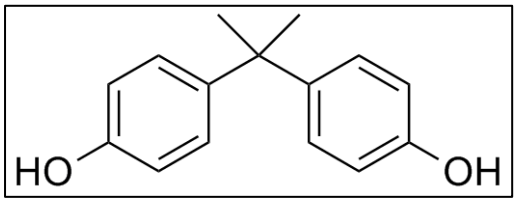

Figure 2.23. Molecular structure of BPA

2.7.3.2 Nonylphenol

Nonylphenol (NP, Figure 2.24) is used to make and is a degradation product of nonylphenol ethoxylates. Ethoxylates are non-ionic surfactants used as dispersants and emulsifiers in a range of consumer products [120, 141].

NP is estrogenic in both hERα [196, 215]and hERβ [196]mediated yeast-based firefly luciferase reporter gene assays. NP is a full agonist in the hERα mediated assay but in the hERβ mediated assay, a full dose-response curve was not obtained in the concentration range

studied, giving an estimated relative potency less than 10^{-5} [196]. NP is also estrogenic in the YES assay [215, 231, 232] and the ER-CALUX assay [197]. In hERα and hERβ mediated firefly luciferase reporter gene assays in U2-OS cells, NP is a full agonist, able to elicit a response 1.2 times larger than E2 [227]. NP is able to reduce the affinity of the ligand bound ER to the co-activator SRC1 [230]. NP is also a potent anti-androgen in the ARhLBD-activating signal cointegrator 1 (ASC1) yeast two-hybrid system [229].

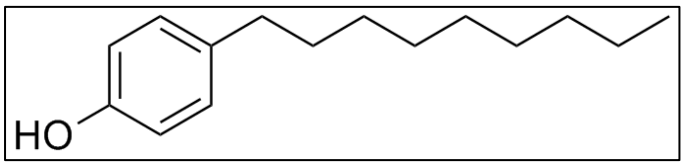

Figure 2.24. Molecular structure of NP.

2.7.3.3 4-tert-octylphenol

4-tert-octylphenol (4t-OP,Figure 2.25) is a surfactant and a degradation product of octylphenol ethoxylates [120]. 4t-OP is a full agonist in the YES assay [203].

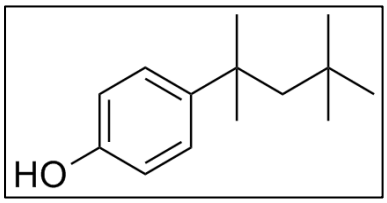

Figure 2.25. Molecular structure of 4t-OP.

2.7.3.4 Pyrethroid metabolites

The pyrethroid compounds cypermethrin and permethrin are commonly used domestic insecticides (aerosols, pet flea treatments) and in agriculture applications. The metabolites of these chemicals are shown in Figure 2.26. The two aliphatic alcohol metabolites (3PBOH and 4OH-3PBOH) are estrogenic in the hERα YES assay [233] while the two acidic metabolites (3PBA and 4OH-3PBA) are not.

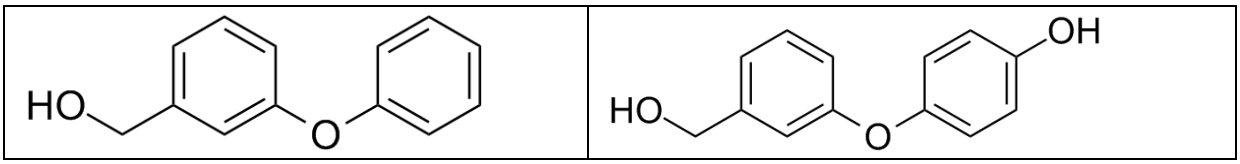

(a) 3PBOH	(b) 4OH-3PBOH
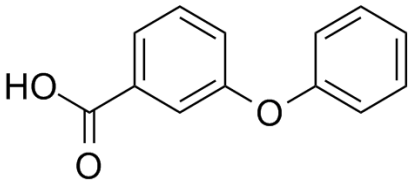	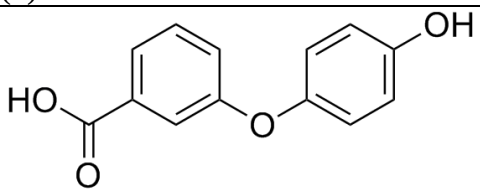
(c) 3PBA	(d) 4OH-3PBA

Figure 2.26. Pyrethroid metabolites.

2.7.3.5 Phthalates

Phthalate diesters (Figure 2.27(a)) are used as plasticizers, as emulsifiers in personal care products and in the coatings on some medications [234]. These compounds are very quickly metabolised to the monoesters (Figure 2.27(b-d)). The monoesters (mBP, mBzP and mEHP) had no activity in the hERα, hERβ or hAR mediated Chinese hamster ovary (CHO-K1) cell based firefly luciferase reporter gene assay [235]. Phthalates act as anti-androgens and the mechanism of action is interference with testosterone biosynthesis and metabolism [236, 237].

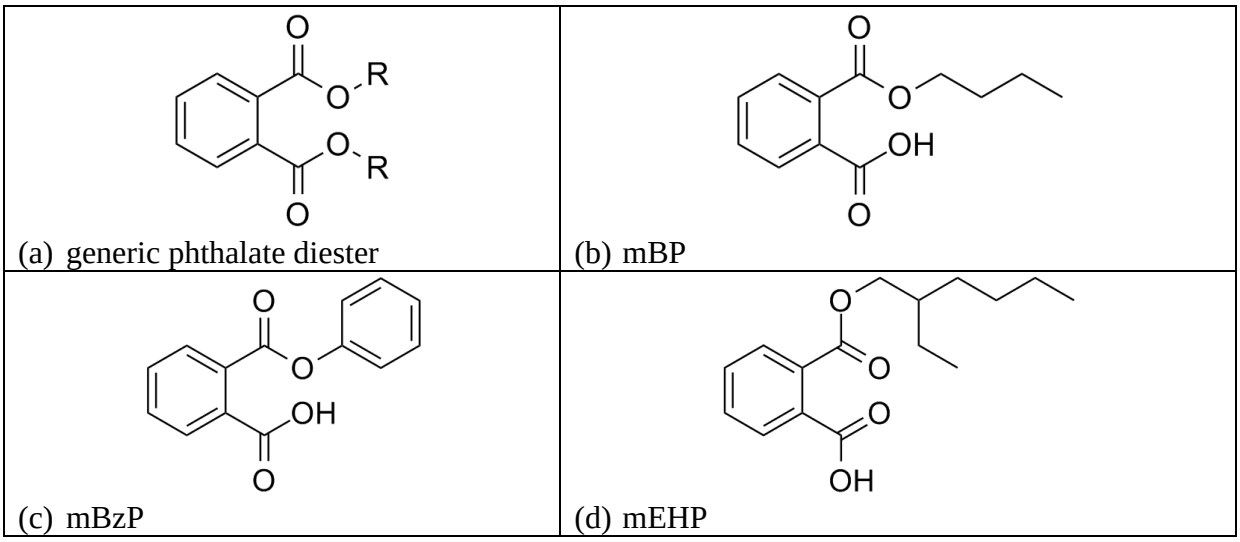

Figure 2.27. Phthalate diester and monoesters.

2.7.4 Phytoestrogens

Phytoestrogens (Figure 2.28) are naturally occurring in foods such as beans and other legumes, grains, green vegetables (e.g. Brussels sprouts and spinach) and coffee. They are present in foods primarily as glycosides (e.g. Figure 2.28(a)), but are hydrolysed in the human gut by enteric bacteria to the aglycones [150] (Figure 2.28 (b)-(d)). The aglycones are estrogenic. There is also some evidence that the glycosides are also weakly estrogenic [238]. The aglycones are then glucuronidated and sulphated by metabolic enzymes in the liver (see Section 2.4.2) and there is some evidence that the glucuronides [239] and sulphates [240] are at least weakly estrogenic. Phytoestrogens have been associated with protective actions against a variety of cancers, cardiovascular disease and osteoporosis. The health benefits and potential adverse effects attributed to phytoestrogens are varied and controversial and have been reviewed [241].

The phytoestrogen content of foods common in the western diet has been determined [242]. Soy products (particularly soy beans and soy nuts) contained the highest concentration of total isoflavones, primarily as daidzein and genistein. Lignans were present in much lower concentrations than the isoflavones. Coumestrol was present in most foods but in much lower concentrations than the lignans. It is relatively rich in very few foods: mung bean

sprouts, flaxseed, and soy nuts. Coumestrol's contribution to total phytoestrogen intake may not be significant unless individuals eat considerable amounts of these foods [242].

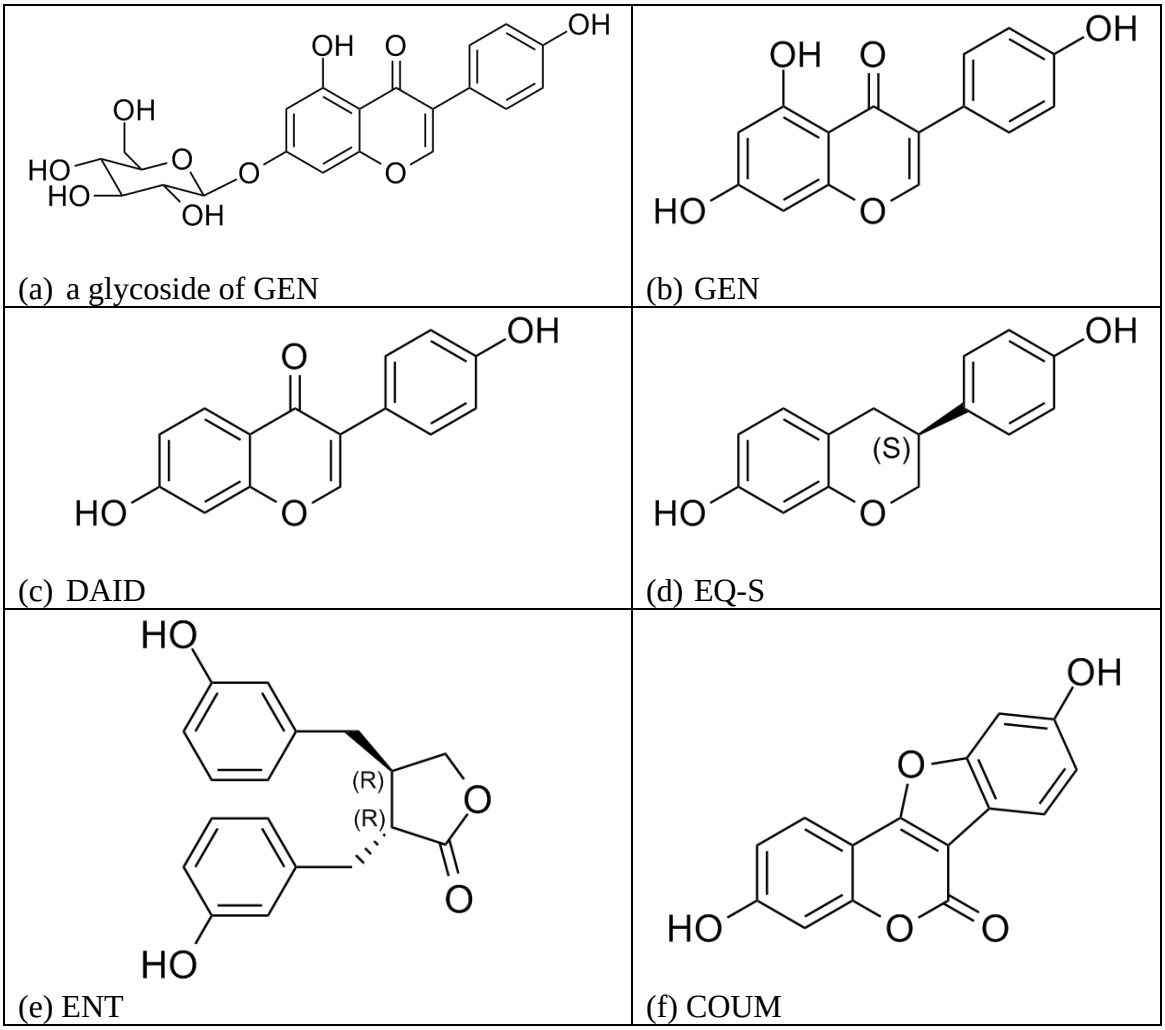

Figure 2.28. Molecular structures of phytoestrogens (a) a genistein glycoside, (b) genistein (c) daidzein and (d) equol (S-isomer) (e) enterolactone (f) coumestrol.

2.7.4.1 Genistein

Genistein (GEN) is a phytoestrogen found in beans such as soy [243] and coffee [244]. GEN is estrogenic in both the hERα and hERβ mediated firefly luciferase reporter gene yeast assays [196], the ER-CALUX assay [197] and in both MCF-7 and Ishikawa cell lines [226]. GEN is a partial agonist, able to induce cell proliferation in human endometrial stromal cells [245], Ishikawa cells [245] and in the E-SCREEN assay [238]. Between 50% and 85% of the proliferation rate of E2 is obtained, depending on the cell line. GEN is a partial agonist in both hERα and hERβ mediated transcription in a yeast-based β-galactosidase reporter gene

assay (not the YES assay) [238]. GEN is more effective in the hERβ assay than the hERα assay. GEN is also able to antagonise E2 induced cell proliferation by up to 20% in both MCF-7 and Ishikawa cell lines when both E2 and GEN are at the same concentration of 10^{-8} M [245]. GEN is able to reduce the affinity of the ligand bound ER to the co-activator SRC1 [230].

2.7.4.2 Daidzein

Daidzein (DAID) is a phytoestrogen found in beans such as soy [243] and coffee [244].

DAID is a partial agonist, able to induce cell proliferation in human endometrial stromal cells [245], Ishikawa cells [245] and in the E-SCREEN assay [238]. Between 50% and 85% of the proliferation rate of E2 is obtained, depending on the cell line. DAID is a partial agonist in both hERα and hERβ mediated transcription in a yeast-based β-galactosidase reporter gene assay (not the YES assay) [238]. DAID is more effective in the hERβ assay than the hERα assay. DAID is also able to antagonise E2 induced cell proliferation by up to 20% in both MCF-7 and Ishikawa cell lines when both E2 and DAID are at the same concentration of 10^{-8} M [245].

2.7.4.3 Equol

Equol (EQ) is a metabolite of DAID produced by bacteria present in the human gut [149]. Two isomers are possible for EQ, but the gut bacteria produce only the S-isomer which is estrogenic.

EQ is a full agonist in the E-SCREEN assay [238] and a partial agonist in both hERα and hERβ mediated transcription in a yeast-based β-galactosidase reporter gene assay (not the YES assay) [238]. In contrast to GEN and DAID, EQ is more effective in the hERα assay than the hERβ assay.

2.7.4.4 Enterolactone

Enterolactone (ENT) is a lignan that occurs as the aglycone and as glycosides in grains and seeds, especially linseed [150]. ENT is also a metabolite of other lignans and is produced in the human gut by microflora [242]. ENT is estrogenic as it is able to stimulate DNA synthesis in MCF-7 cells with an efficacy similar to that of DAID [246].

2.7.5 Pharmaceuticals

2.7.5.1 Ethynylestradiol

Ethynylestradiol (EE2, Figure 2.29) is the main component of oral contraceptives. In The US and Europe, it is estimated that up to 3% of the women taking oral contraceptives become pregnant accidentally due to missed pills and continue taking the pill for weeks to months before the pregnancy is discovered [247]. As a pharmaceutical, EE2 is designed to be a potent estrogen. EE2 is estrogenic in the hERα mediated firefly luciferase reporter gene yeast assay and the YES assay [215].

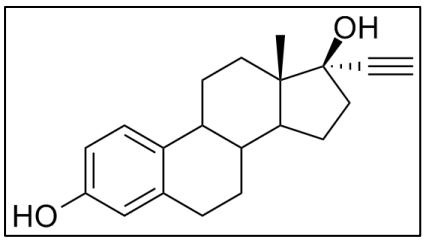

Figure 2.29. Molecular structure of EE2

2.8 Mixtures

Exposure to EEs is an exposure to a mixture of changing composition and concentration. Because the end-point of concern is hormonal signalling, there is no safe threshold below which there is no activity [248]. The simplest approach to assessing the total estrogenic effect of mixtures is the simple additivity model where each component adds to the total in proportion to the concentration weighted by its relative potency. Rajapakse et al [249] *have demonstrated in principle that every xenoestrogen, however weak, may add incrementally to the total estrogenic effect, even at very low concentrations, and even in the presence of potent endogenous steroidal estrogens.*

It is also possible for the mixture to have higher potency than predicted by the simple additivity mode. This behaviour is described as *synergistic*. For example, mixtures of benzophenones, alone or including E2, showed synergistic activity, with substantial increases in observed effect even though each UV filter was present at its NOEC level [222]. Also, BPA, NP and GEN are additive in potency when tested in a mixture with E2 [197]. Unfortunately, these studies were done at a single equipotent mixture composition, so how the synergistic effect changes with mixture composition, concentration level or with E2

concentration is not known. There are mixture effects even with endogenous hormones. E3 is known to behave as an antagonist to E2 when present in equal or up to 10-fold excess concentrations of E2, but as a weak agonist when present in alone or in concentrations 50 fold greater than E2. At a 10-fold excess concentration to E2, E3 is able to reduce E2-dependent transcription by 85% [250].

The complexity of dealing with mixtures in exposure assessment is recognised but methodologies for the assessment of risk due to exposure to mixtures are still hotly debated [249, 251-255]. Nevertheless, some regulatory frameworks are beginning to consider groups of chemicals that act via the same mechanism collectively rather than evaluating the potential risks individually [256].

One approach to simplifying the topic of endocrine disruption is to treat the effects of exposure individually according to the signalling pathway, e.g. estrogen signalling disruption separate from androgen or thyroid disruption. While this approach disregards the potential for the different signalling pathways to interact, e.g. anti-androgenic effects contributing to an overall estrogenic outcome, there is insufficient information available at this time to completely address the problem. It remains sufficient to recognise the shortcomings of the approaches used. Within each signalling pathway, the effects of mixtures can be effectively assessed if the components of a mixture act through a common mechanism or to produce a common effect. Again, it must be recognised that a single component of a mixture may act via different mechanisms within the signalling pathway and that these mechanisms may act in unison or opposition to produce an effect. An example of this complex behaviour was noted with the parabens in section 2.7.1.1. Parabens are simultaneously able to up-regulate hER gene expression, down-regulate hAR gene expression and inhibit aromatase activity thereby suppressing the biosynthesis of estrogens. Parabens can contribute to a common effect (femininisation) via two distinct mechanisms (estrogenicity and anti-androgenicity) and also contribute to a contradicting effect (masculinisation) via suppressing endogenous estrogen biosynthesis. This type of behaviour is likely present with other classes of compounds of interest to estrogenic signalling disruption, but the data is currently lacking.

This study will be limited to assessing whether the human fetus is exposed to a quantity of EEs to significantly up-regulate hER gene expression. This will be done by assuming the individual compounds act additively in this action. The available evidence suggests this is a

valid approach [256]. The contribution of this mixture to anti-androgenic or hormone biosynthesis disruption cannot be addressed at this time.

2.9 Conclusions

Endocrine disruption is a complex topic with co-operating and competing aspects, many of which have received very little attention. Some aspects are likely still not identified. Disruption to estrogen signalling has received the most attention in both environmental exposure research and in health-related areas such as breast cancer research, but the picture is far from clear. The key parts of the puzzle that are currently recognised are summarised as follows.

2.9.1 ER-mediated gene transcription

ER mediated gene transcription is highly complex process and is currently not fully understood. When a ligand binds to the ER, the ligand-receptor complex takes on a specific conformation that is determined to a certain extent by the structure of the ligand. The receptor-ligand complex is not static, but dynamic, and can be considered an equilibrium of multiple favourable conformations. Small variations in the topology of the AF-2 coregulatory protein binding site on the receptor complex influence which of the available coregulatory proteins are recruited, which ER-responsive gene is transcribed and the efficiency with which it is transcribed. Because each of the ER target cell types has a different suite of coregulatory proteins and different expression levels of the two ERs, the same ligand can have very different effects on different cell types. This cell-type specific response to EEs is the first critical factor in determining the biological outcome of exposure.

2.9.2 Maternal Metabolism

Maternal metabolism is effective in clearing a large proportion of most EEs before they reach her circulation. Depending on the route of exposure, the compound will be subject to different metabolic pathways. The clearance rate of the EE from the body will be different for each of the routes of exposure and different tissues will be exposed to different amounts of the compound. However, the parent compounds and/or their conjugates are present in the maternal circulation and in the placenta on the maternal side and thus available to diffuse or be transported across the placental membranes to the fetus.

2.9.3 Placental Transport and Fetal Metabolism

The placental membranes separate maternal and fetal circulations with a barrier similar to the blood-brain barrier. Being hydrophobic, EEs can cross this barrier by simple diffusion. The rate of transport is determined primary by the concentration gradient across the membranes. The placenta has both facilitated and active transport mechanisms that transport protein bound and hydrophilic species in both directions. Some EEs compete with endogenous estrogens for binding sites on plasma binding proteins and may be transported across the placenta by facilitated transport. Conjugates are transported out of the placenta to maternal circulation by active transporters.

Metabolic transformations of EEs by CYP, UGTs and SULTs occur in the human fetus. In contrast to adults, UGT activity in the fetus is low and SULT activity is high. The UGT activity that is present is substrate specific for endogenous hormones, but limited glucuronidation of EEs is possible. Most xenobiotics that are glucuronidated in the adult are sulphated in the fetus. Certain of the CYP enzymes are active in the fetus, mainly those involved in hormone biosynthesis and metabolism. The activity of fetal CYP enzymes to xenobiotics is low in comparison to the adult.

Fetal tissues and the placenta have both β-glucuronidase and arylsulphatase enzymes for deconjugating the conjugates of endogenous steroids. BPA is deconjugated by these enzymes and it is likely that other EEs may be deconjugated as well. This may provide a mechanism whereby EEs are recirculated within the fetal compartment.

The fetus actively expels lung fluid and swallows amniotic fluid. As a result, the respiratory and gastrointestinal tissues are in continuous contact with these fluids. Until skin keratinisation begins around the 20th week of gestation, fetal plasma, extracellular fluid, lung fluid and amniotic fluid compositions are similar because hydrophobic compounds can freely diffuse across fetal skin and other cell membranes. This free movement coupled with the reduced metabolic capacity of the fetal liver means that hydrophobic EEs present in fetal blood have ready access to estrogen sensitive cells.

Clearly, there are competing processes present in both the placenta and in fetal tissues that will have an effect on how easily an EE crosses the placenta into fetal circulation, how effectively and in what form it is metabolised and returned to the placenta for elimination via maternal circulation. The limited quantitative information that is available is primarily for

pharmaceuticals. The literature suggests that EEs enter fetal circulation as the parent compound and may be recirculated to some extent within the fetal compartment in the same way endogenous estrogens and some pharmaceuticals are.

2.9.4 In vitro measurements of estrogenic activity

Several different *in vitro* methods have been used to measure the ability of a compound to induce ER-mediated gene transcription. These methods are hosted in different cell types including yeast and mammalian cells lines. Each method differs in its sensitivity as measured by the EC_{50} for E2. The diversity of host cells also influences the sensitivity of the specific assay for a given ligand for the reasons discussed in Section 2.9.1, and results in the wide variability of estrogenic potencies shown in Figure 2.16. The variability makes it difficult to unambiguously assign a potency value to a ligand and to compare potencies of different ligands.

Estrogenic potency values for the ligands of interest in the study range from 10^{-3} to 10^{-6}, meaning that 3 to 6 orders of magnitude higher concentrations are required to elicit the same effect as E2. Many of the ligands of interest are partial agonists, meaning that their maximum effect is less than that of E2, even at these much higher concentrations. The general conclusions on the activity of the compounds of interest in this study are summarised in Table 2.10.

Table 2.10. Summary of estrogenic and androgenic activity of the compounds of interest in this study.

Compound Class	ER Activity	ER Preference	AR Activity
Parabens	estrogenic	β	antiandrogenic
Triclosan	unclear results indicate antiestrogenic, inactive and estrogenic activity		antiandrogenic
Benzophenones	estrogenic	α	antiandrogenic
OMC	estrogenic	α β inactive	inactive
4MBC	estrogenic	no preference	antiandrogenic
BPA	estrogenic potential super-agonist	no preference	inactive
NP	estrogenic potential super-agonist	α	no information
Pyrethroid Metabolites	estrogenic	no information	no information
Phthalate monoesters	inactive		inactive in *in vitro* tests but antiandrogenic *in vivo*
GEN, DAID	estrogenic when acting alone, antiestrogenic in the presence of E2	β	no information
EQ-S	estrogenic	α	no information
ENT	estrogenic	no information	no information

2.9.5 Other estrogenic modes of action

In addition to ER-mediated estrogenic activity, many of the EEs also have non-genomic estrogenic activity. Non-genomic activity includes interference with hormone biosynthesis and metabolic pathways and competing with endogenous estrogens for binding sites on plasma binding proteins. Some of the EEs also exhibit anti-androgenic activity which has an indirect feminising effect. Very little has been done to quantify these effects.

Chapter 3 Computational Docking

3.1 Introduction

The wide range of adverse outcomes in humans that have been associated with exposure to EEs was presented in Chapter 1; for example, males develop malformed genitalia, females enter puberty earlier, and both males and females exhibit reduced fertility and increased incidence of hormone responsive cancers. As stated in Section 2.2.3, it is thought that these observed outcomes depend on timing, level and route of exposure [23, 96-101]. A specific example of this type of variability of outcome in humans is the SERM behaviour of breast cancer drugs OHT and RAL. These two drugs have different effects on different target tissues (bone and uterus) which is a direct result of the different populations of coregulatory proteins present in the different target cells, i.e. the cell context. The *in vitro* assays for estrogenicity (Section 2.6) also demonstrate this variability in effect. The quantitative measure of estrogenicity obtained from these assays depends on the host cell, the reporter construct and the receptor type, all of which contribute to the variability in measured estrogenicity shown in Figure 2.16.

Strong evidence exists for the molecular basis for this variability. In the case of GEN, the cell context can influence the conformation of the RL-complex [78, 257] [258]. When GEN is co-crystallised with hERβ in the absence of coregulatory peptide, the RL-complex takes the antagonist conformation. When co-crystallised in the presence of a particular coregulatory peptide, the RL-complex is forced to take the agonist conformation because the coregulatory peptide binds to the RL-complex preventing H-12 from occupying the groove.

Combining these two observations, I suggest that that the variability in biological outcomes observed with exposure to EEs is a result of ligand flexibility. The endogenous estrogens are rigid molecules and they are able to engage the receptor protein to produce a stable RL-complex with a well-defined topology. The rigidity of the endogenous estrogens will be discussed in Section 3.3.2. The flexibility inherent in the molecular structures of the EEs do not result in a well-defined RL-complex. Instead, this flexibility allows a multiplicity of energy-equivalent receptor-ligand conformations that are able to differentially recruit coregulatory proteins, thus affecting gene transcription. Ligand flexibility may also contribute to the partial agonist/antagonist nature of many EEs. Ligand flexibility coupled with generally lower binding affinity will result in RL-complexes being more transient and thus less able to interact with DNA and the cellular transcription machinery long enough to complete gene transcription.

In this chapter, two computational docking approaches, rigid receptor docking (RRD) and induced-fit docking (IFD), were used to examine this hypothesis.

3.2 Theoretical Background

3.2.1 Ligand Structure and Transcription

The two hERs (α and β) have different expression levels in different cell types. This differential expression combined with varying types and relative concentrations of coregulatory proteins present in specific cell types provides a complex control mechanism for estrogen target gene transcription.

The molecular structures of the endogenous estrogens are rigid and induce a precise 3D conformation in the hER on binding. This precise conformation is observed in solved protein crystal structures and is described as the agonist conformation. This conformation leads to predictable patterns of gene transcription in target cells. Endogenous estrogens are pure agonists for the hER – they always up-regulate gene transcription in target cells.

Pharmaceuticals have been designed that completely block transcription in all target cells (pure antagonists) and that block transcription in some target cells but not others (selective modulators). These pharmaceuticals also produce predictable effects. The molecular structures of selective modulators are also rigid and have been shown by solved protein crystal structures to induce a radically different conformation (the antagonist conformation, Figure 2.6) in the hER on binding. The selective modulators for hERα (e.g. RAL and OHT, Figure 2.7) have been designed as 'wedges' that actively engage the receptor protein to stabilise this conformation. Selective modulators for hERβ (JJ3, 3AS, ETC, Table A. 7) are also rigid molecules, but in contrast to the hERα SERMS, they do not have and do not require the large 'wedge' feature that the hERα SERMS have to stabilise the antagonist conformation.

Antagonist action is achieved by H12 occupying the coregulatory protein binding site - a structurally conserved cleft on the surface of the ER LBD where the LXXLL motif of the coregulatory molecule binds. The suggested mechanism of antagonism is the competition between the coregulatory proteins and H12 for the binding site [259]. The position of H12 in the agonist conformation is unique but in the antagonist conformation, it is not [259]. Based on study of the hER and other NRs, it has been proposed that "upon ligand binding, H12

would dynamically adopt one of (at least) two stable positions as dictated by the binding characteristics of the ligand" [260].

Experimental evidence suggests that the selective modulator nature of these pharmaceuticals is a result of small variations in the exact topology of the antagonist conformation that are induced by the differences in the 3D shape of the drug molecule. This evidence was produced by *in vitro* binding studies where the ability of the receptor-ligand complex to bind with different peptides that mimic different classes of coregulatory proteins is measured [88, 258]. These *in vitro* assays are complemented by solved crystal structures with the peptide co-crystallised with the receptor-ligand complex.

Crystal structures of endogenous estrogens and pharmaceuticals bound to the two hERs have been solved. Crystal structures can only be obtained when the molecule interacts with the receptor in a well-defined manner. Each of the many millions of receptor-ligand complexes within the crystal must have exactly the same 3-dimensional array of atoms in order to solve the crystal structure. Not all attempts to produce protein crystals with drug candidates as ligands are successful. In many cases, the crystal does not grow large enough or the crystal is not of sufficient quality to allow the structure to be solved [85]. The crystal structure is described as having 'static disorder' in these ill-defined regions. In these cases, the ligand is not able to stabilise the receptor conformation, leading to static disorder in large enough regions of the complex that prevent the structure from being solved.

These small variations in the ligand's molecular structure lead to differences in the ability of the receptor-ligand complex to recruit the cofactors needed to initiate gene transcription. The selective nature of the ligand's action also depends on the selection of cofactors available in the target cell and their relative concentrations. The importance of the ligand's molecular structure in achieving the desired therapeutic effect is well known in medicinal chemistry [259].

One environmental estrogen, GEN, has similar selective modulator properties [261]. GEN is a rigid molecule but has dimensions and overall shape that are different from the estrogens or the pharmaceuticals. hERα has been co-crystallised with GEN and the complex has the agonist conformation [257]. When co-crystallised with GEN, hERβ adopts the antagonist conformation [78], but when GEN and hERβ are co-crystallised in the presence of a peptide designed to mimic a specific coregulatory protein, hERβ adopts the agonist conformation

[257]. The rationale given is that the relative free energies of the two H12 conformations of hERβ-GEN complex are similar, with the antagonist conformation being slightly more stable. This concept is illustrated in Figure 3.1. The presence of the peptide mimic provides additional stabilisation necessary to produce the agonist conformation [257]. Thus, it appears that with GEN, both the receptor type and cell context determine whether it behaves as an agonist or antagonist. While hERβ may have a lower energy barrier between the agonist and antagonist conformations, it has been suggested that the opposite is true for hERα [259, 262]. GEN is not able to induce the antagonist conformation in hERα because it does not have the 'wedge' shape required to stabilise the hERα antagonist conformation.

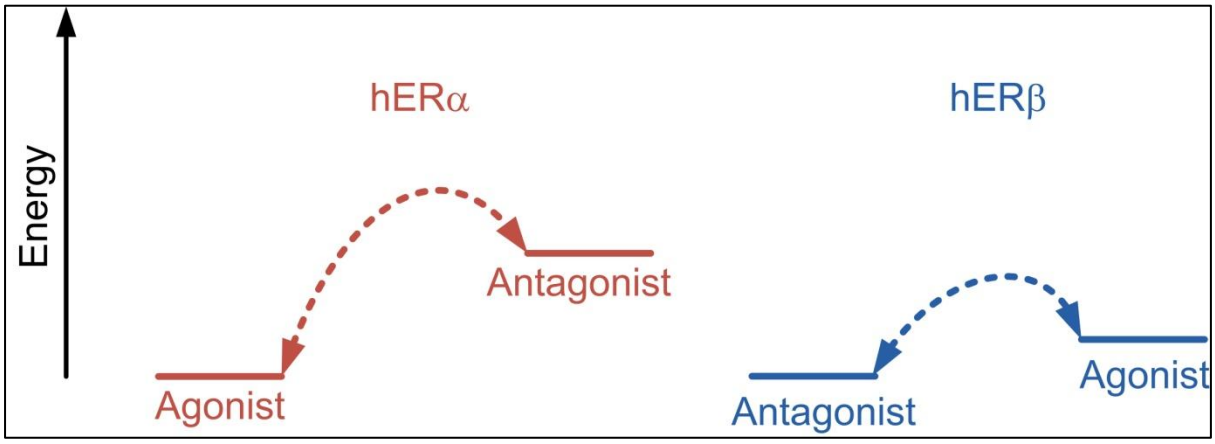

Figure 3.1. Illustration of proposed relative stability of the agonist and antagonist conformations of the two hERs.

Molecular dynamics simulations of the binding of DES with hERα [263] have shown that the hydrogen bond between His524 and the DES ligand hydroxyl is present for 97% of the simulation time. At the other end of the ligand, the hydrogen bond network fluctuates between Glu353, Arg394, a water molecule and the DES ligand hydroxyl and results in the equivalent of 1.5 hydrogen bonds over the simulation time. Since His524 is free to rotate to break and re-form H bonds with the ligand, the authors suggest that hydrogen bonding with His524 is not absolutely required for ligand binding but serves to stabilize the binding mode.

3.2.2 Receptor Protein Structure and Conformation

The agonist and antagonist conformations of the LBD of hERα are shown in Figure 3.2. The helix notation is shown on both conformations. Note the difference in position of H12. In the agonist conformation it is closed over the binding cavity while in the antagonist conformation it is folded back onto the LBD to occupy the cofactor binding site. In Figure

3.3, the agonist and antagonist conformations are shown, highlighting the important regions of the protein structure that are influenced by ligand binding. Note the uncoiling of H11 that results in a lengthening of the loop between H11 and H12 to allow H12 to occupy the cofactor binding site [81]. The three key ligand-residue interactions are shown in Figure 3.4.

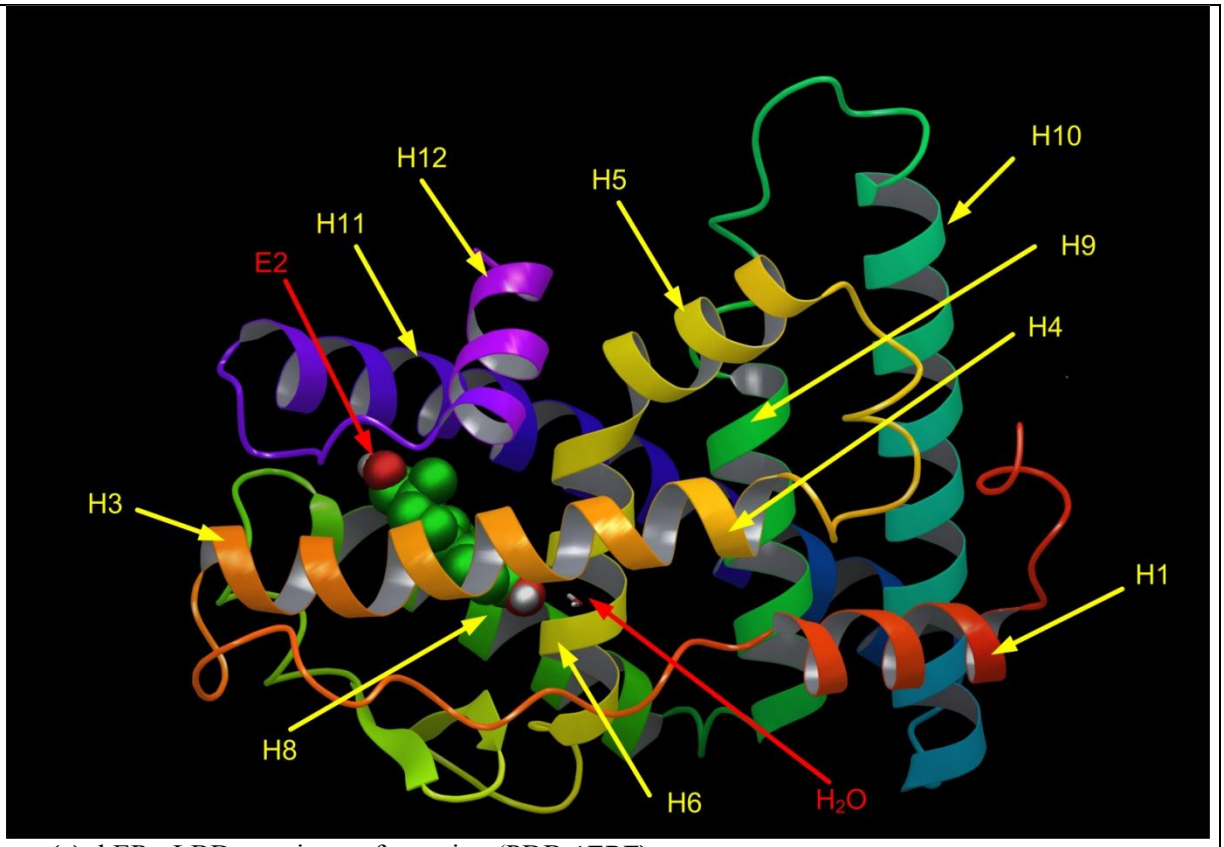

(a) hERα LBD agonist conformation (PDB *1ERE*)

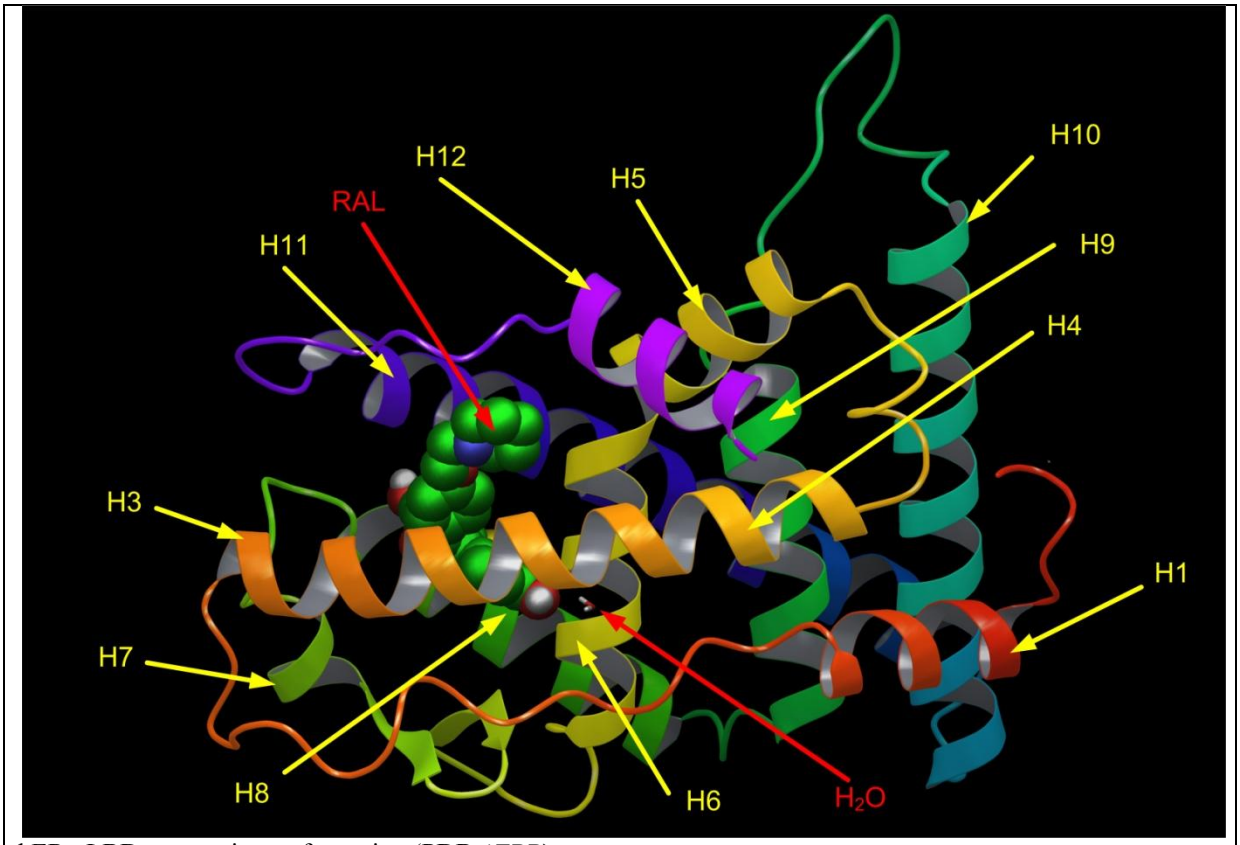

hERα LBD antagonist conformation (PDB *1ERR*)

Figure 3.2. hERα ligand binding domain in the (a) agonist and (b) antagonist conformations. Helices 1-12 are indicated along with the co-crystallised ligand (E2 or RAL) and the binding cavity water molecule.

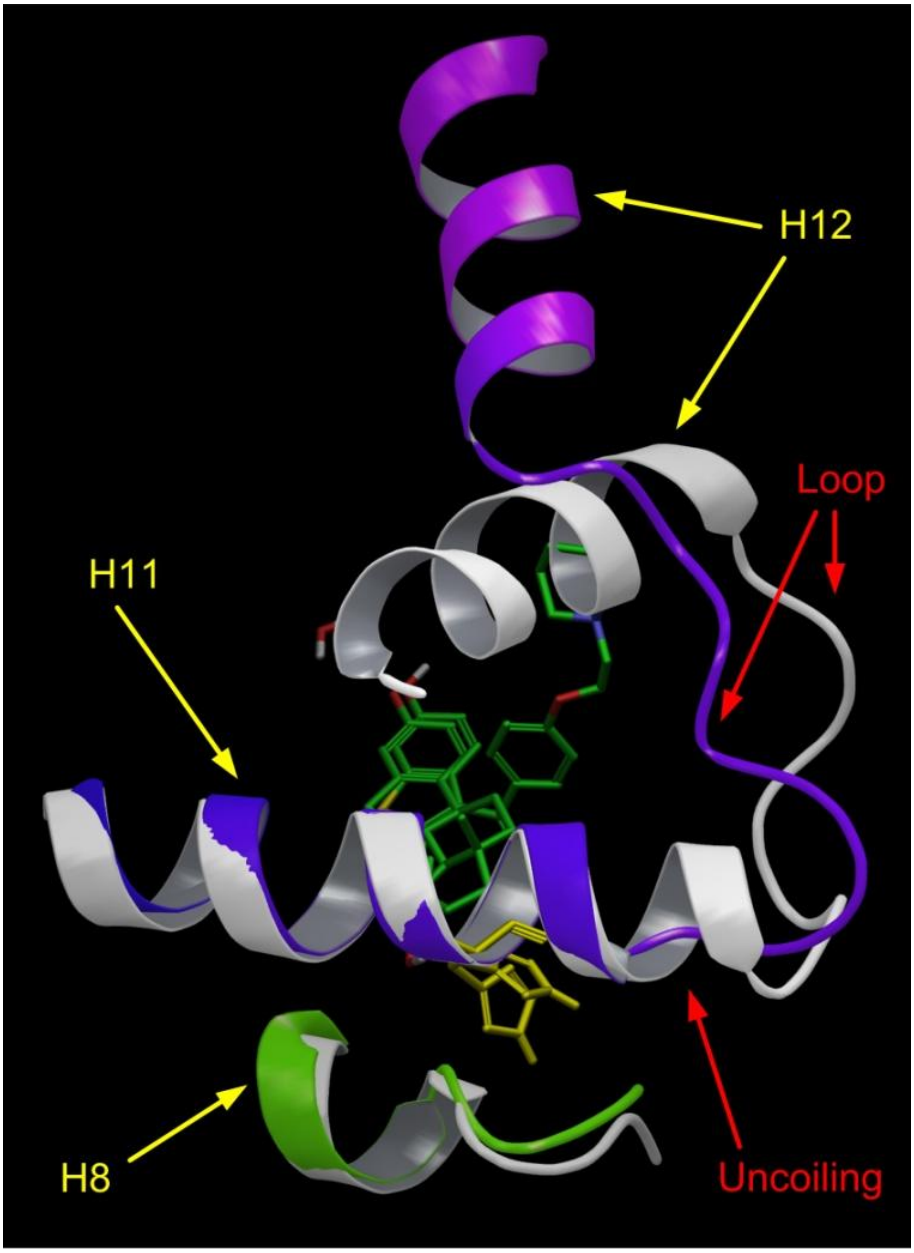

Figure 3.3. Comparison of hERα agonist and antagonist models showing regions of H8 where His524 interacts and regions of H11-H12 that are changed as a result of ligand binding. The agonist protein structure is shown in grey and the antagonist structure is shown in green and blue. The ligands (E2 and RAL) are both shown in green. Note the difference in position of His 524 shown in yellow and the resulting uncoiling of H11. The uncoiling of H11 results in a lengthening of the loop between H11 and H12 to allow H12 to reach the cofactor binding site.

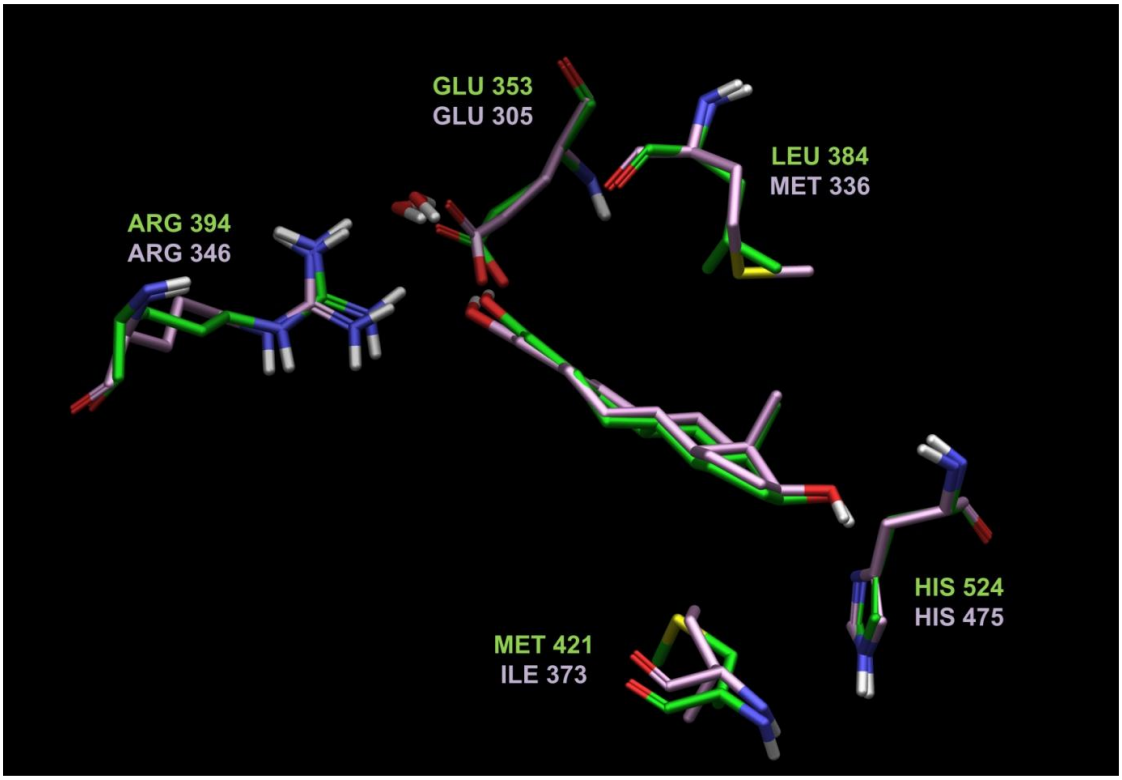

Figure 3.4. Key ligand-reside interactions for E2 with hER. hERα (*1ERE)* is shown in green and hERβ (*3OLS)* is shown in pink. The two residue substitutions between the receptors are also shown (Leu384-Met336 and Met421-Ile373).

3.2.3 Computational Docking

Computational docking is the computer simulation of binding of a ligand to a receptor and is a tool that is routinely used in pharmaceutical research. Docking can be used for the selection of potential drug candidates from a collection or library of possible lead chemicals in a process known as virtual screening or in the design of drug molecules [264-267]. Docking in the form of virtual screening is less frequently used in the study of endocrine disrupting chemicals because the tolerance for false negatives (rejecting a compound that is in fact endocrine active) is much lower than in drug discovery [268]. One study has been reported where computational docking was used in conjunction with additional chemical knowledge to successfully select endocrine disrupting chemicals from a collection of weakly active and inactive compounds [269]. Computational docking has been used in the study of endocrine disrupting chemicals to explore the binding interactions of specific compounds with the ER, for example polybrominated diphenyl ethers [270], polychlorinated biphenyls and dichlorodiphenyltrichloroethane (DDT) and its metabolites [271], phytoestrogens and polyphenols [75] and pesticides [272]. Molecular dynamics simulations have also been used

to study the interaction of both drug targets and endocrine disrupting chemicals with the ER [263, 273-275].

Computational docking is used to predict the preferred orientation of a ligand within the receptor binding cavity and to estimate the binding energy (affinity) for the ligand-receptor complex. Much of the computational docking done with the ER has been for drug development [265, 267] for treatment of breast cancer, osteoporosis and prostate diseases. Currently, a very active area in estrogen receptor drug research is the development of compounds which are SERMs that selectively up- or down-regulate gene transcription controlled by one of the two ERs.

Computational docking requires a collection of computer programs to perform the necessary calculations. There are many tools to choose from depending on the objectives of the study and the degree to which the programs need to be adapted to a particular purpose. Since the objective of this study was to use the tool to study a biological system (rather than to develop computer code to simulate a biological process or to improve the performance of a tool) a commercially available and extensively validated software package with an easy to use graphical interface was chosen. Schrödinger Suite 2010 was used as the primary tool for this work.

The basis of computational docking is the *lock-and-key* model first described by Fischer in 1894 [276]. As the name suggests, the three dimensional structures of the ligand and the receptor are both considered rigid and complement each other like a key fits a lock. It is now recognised that the ligand and receptor structures change during the binding process. The introduction of a ligand to the receptor binding cavity modifies the chemical and structural environment of the binding cavity, for example by formation of salt bridges or expulsion of water molecules, causing the energy landscape of the protein to change. The mutual interaction between receptor and ligand can result in an energy state of the complex that is lower and more stable than the separate receptor and ligand, thus leads to ligand binding. The receptor and ligand undergo a mutual accommodation process that results in small scale adjustments in atom positioning of both the ligand and receptor. The movement in the receptor is usually confined to a region very near the binding cavity and is often not translated or amplified to distant parts of the protein structure. This model, described as *induced fit*, was first presented by Koshland in 1958 [277]. However, long range changes in a protein receptor structure are now known. Recent advances in computational capacity have

led to current efforts to model these larger movements, but it remains difficult to accurately model these larger movements because of the size and complexity of the molecules involved.

Computational docking is based on static models of the receptor and ligand, exploring how the ligand can adopt a shape that best complements and interacts with the binding cavity of the receptor. Small-scale changes in the protein structure in the vicinity of the binding cavity, termed flexibility, are now being considered in docking applications with varying degrees of accuracy and efficiency [264]. Docking is based on static models of the receptor and the minimisation of the potential energy of the receptor-ligand complex. Docking calculations do not consider the kinetic energy of the system, so large-scale movements of the receptor that may occur as a result of ligand binding (e.g. large conformational changes in the protein structure some distance from the binding cavity) cannot be modelled using docking methods. Molecular dynamics models do consider the kinetic energy of the system (e.g. that caused by perturbations to the structure that displace it from a potential energy minimum) and are used to study receptor motion such as these conformational changes. Having said this, docking studies may be able to shed light on the small local changes (triggers) that occur and are then amplified through the protein structure resulting in the large conformational change.

The docking process begins with choosing or developing geometric and chemical descriptions of the separate receptor and small molecule structures. The receptor model is normally derived from an x-ray crystal structure of the receptor, either with a co-crystallised ligand or without (i.e. apo). The ligand model is usually developed using a 3D chemical structure drawing tool. Both the receptor and ligand models are energy minimised before docking begins. Energy minimisation involves finding the position of atoms in a structure such that the total energy of the structure is at a local minimum of potential energy. Then, using search algorithms and force field interactions, the docking process seeks to find optimal placements of the small molecule in the receptor binding cavity. These potential complexes are ranked using a scoring function and the binding affinity for each complex is calculated. From the candidate poses the best pose is chosen. The general steps in the docking process are illustrated in Figure 3.5.

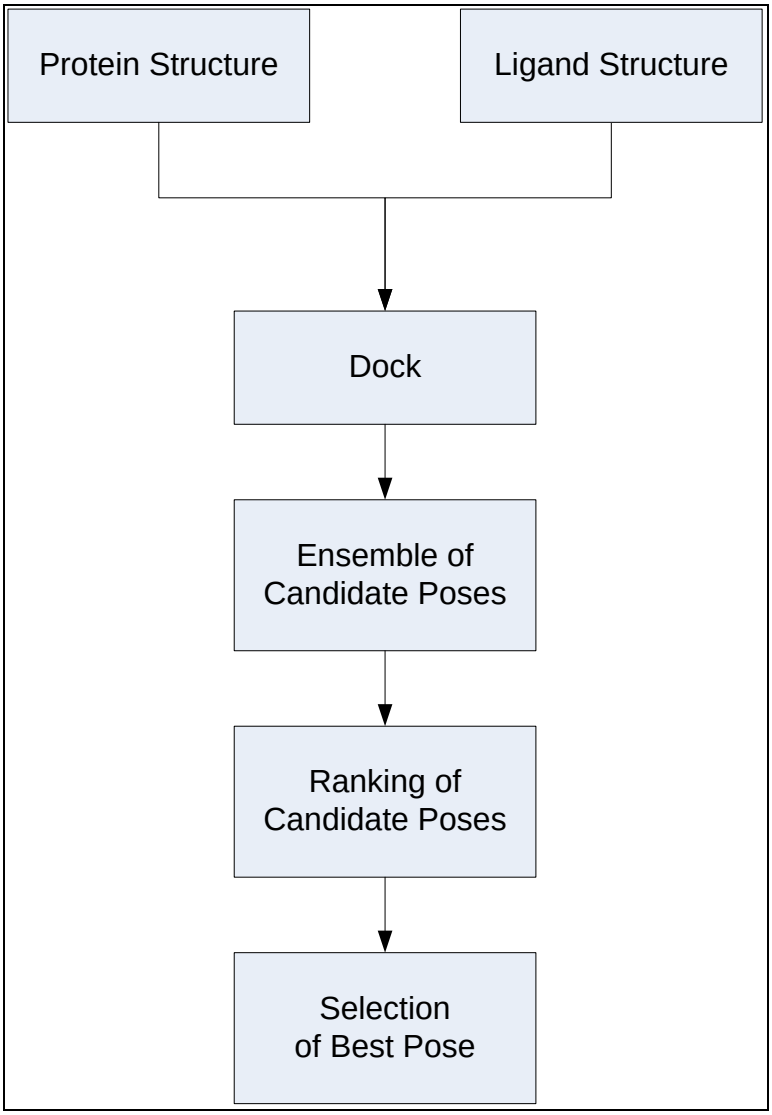

Figure 3.5. Generalised ligand-receptor docking process.

Protein-ligand docking methods generally consist of two components: a *ligand placement algorithm* to enumerate and test possible poses for the ligand in the receptor protein's binding cavity and a *scoring function* to evaluate the energy of each ligand pose and to compare the optimum pose of one candidate ligand to those of other candidate ligands.

The *ligand placement algorithm* is a method to place the ligand in various candidate poses (positions or orientations) in the binding cavity of the receptor. The topography of the binding cavity is represented on a 3-dimensional grid and the ligand is placed in different positions within this grid. Though this could be done randomly or exhaustively, most algorithms use heuristics (rules of thumb based on the chemistry and geometry of the atoms

involved) or standard computer search optimization techniques (strategies to identify and disregard pathways that are not likely to lead to favourable results) to reduce the computational effort needed to identify good candidate poses.

The *scoring function* calculates the energy of the receptor-ligand complex and ranks poses of a given ligand relative to one another to allow the comparison of poses of different ligands. Ideally, the numerical value of the scoring function should correspond directly to the binding affinity of the ligand for the protein, so that the ligands with the best score are the best binders. Current scoring functions have been well validated and generally provide a good approximation for binding affinity, although the degree of accuracy varies with the particular scoring function and receptor under study. If the numerical accuracy of a particular scoring function is not sufficient for the purpose at hand, docked receptor-ligand complexes can be re-scored using one of many different scoring functions available [278-280].

3.2.3.1 Rigid Receptor Docking

The simplest approach to ligand docking is to assume that both the receptor protein structure and ligand are fixed as illustrated in Figure 3.6. The ligand must be an exact lock-and-key fit to the receptor for docking to be successful and the calculated binding affinity to be high.

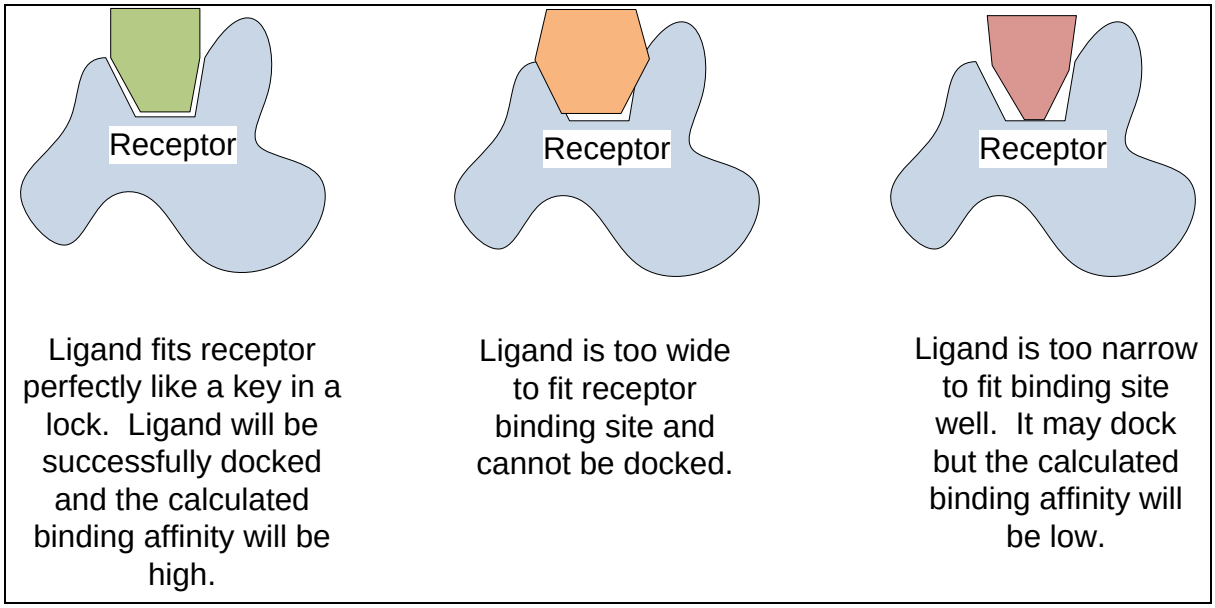

Figure 3.6. Illustration of the limitations of rigid receptor – rigid ligand docking.

This strategy is very restrictive and often results in either unrealistic complexes (e.g. very close positioning of atoms or the ligand interacting unexpectedly or incorrectly with parts of

the receptor) or failure to identify possible valid complexes. This approach is used mostly as screening tool or as part of a filtering step in a complex workflow such as simulating protein structure flexibility. Most often, rigid receptor docking is used with flexible ligands. Because the receptor cannot move, the degrees of freedom of the problem are those of the ligand: three translational, three global-rotational, and one internal dihedral rotation for each rotatable bond. It is generally assumed that bond lengths and the angles formed by adjacent bonds do not change. In this case, the ligand is able to adapt to the binding site to achieve a complex with favourable binding affinity, as illustrated in Figure 3.7.

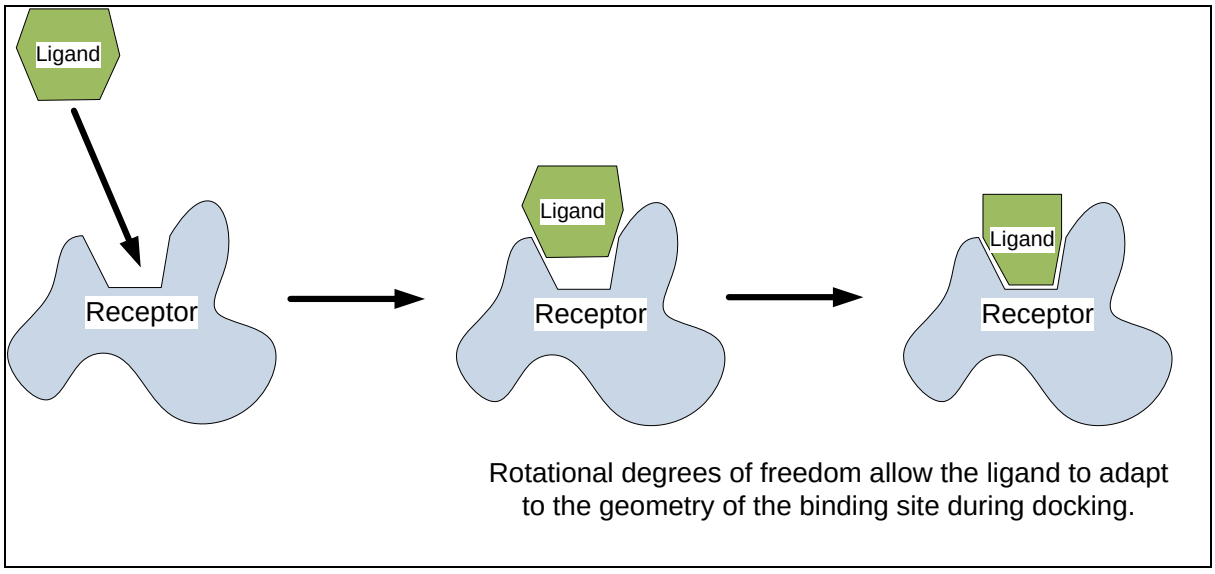

Figure 3.7. Illustration of the rigid receptor-flexible ligand docking concept.

3.2.3.2 Flexible Receptor Docking

Although it is well known that a protein will usually experience some degree of conformational change during the binding process, most docking tools still treat the protein as a rigid structure [281, 282]. The reason for this approximation is the huge increase in computational complexity that is required to fully model protein flexibility. In order to obtain results of docking computations in a realistic time frame, different representations and simplifications of protein flexibility have been implemented that avoid direct generation and search of thousands of potential protein structure conformations.

The simplest approach to representing protein flexibility is the concept of a 'soft' receptor. Soft receptors can be implemented by relaxing the high energy penalty that the system incurs when an atom in the ligand overlaps an atom in the receptor structure. By using a scaling

factor to reduce the van der Waals contributions to the total energy score, the receptor is effectively made softer, allowing, for example, a larger ligand to fit in a binding cavity determined experimentally for a smaller molecule. The rationale behind this approach is that the receptor structure has some inherent plasticity which allows it to adapt to slightly differently shaped ligands through small variations in the orientation of binding cavity residue side chain and backbone positions. If the change in the receptor conformation is small enough, it is assumed that the receptor is capable of adapting to this small change by absorbing and distributing the disruption through the local structure, even though the conformational change itself is not modelled explicitly. It is also assumed that the change in protein conformation does not result in a sufficiently high energy penalty to offset the improved interaction energy between the ligand and the receptor. The main advantages of using soft receptors are that docking algorithms are unchanged and the computational cost of evaluating the scoring function is the same as for the rigid case.

Another approach to representing protein flexibility is an iterative approach of docking with a soft receptor followed by energy minimisation of the entire protein-ligand complex. An ensemble of candidate poses for a ligand within the receptor binding cavity is obtained using soft docking methods. These candidate poses are then ranked and a selection of the top-ranked poses is subjected to energy minimisation which allows the protein structure to 'relax' around the ligand. These minimised receptor-ligand complexes are then re-scored to produce an ensemble of most favourable complexes. This approach requires a significant increase in computational effort, but is still achievable on a desktop computer. For situations where the receptor structure is known to be well defined and retains its integrity on ligand binding, this induced-fit approach is reasonable [283]. However, this approach is not able to model large-scale conformational changes that may be triggered by ligand binding. As suggested earlier, this type of approach could be useful in identifying the small trigger changes in protein structure that are amplified to result in large-scale conformational changes.

3.2.3.3 Scoring Functions

Scoring functions are used to estimate the free energy of binding (binding affinity) of a ligand to a receptor. Scoring functions can be empirical or based directly on force field calculations. Force fields quantify the interaction energy between the receptor and ligand and the internal energy of the ligand by summing energy contributions of non-bonded interactions such as stretching, bending, torsion, van der Waals and electrostatic. Force field scoring functions do

not model individual or specific entropy contributions of solvent effects on binding such as the desolvation energies of the ligand and protein. These effects are taken into account using implicit solvation methods rather than explicit solvation methods. Implicit solvation treats the solvent as a continuum with a dielectric constant that may or may not be uniform through the continuum and the ligand or protein as a particle with some appropriate charge. Explicit solvation models individual water molecules in the vicinity of the ligand and protein. Implicit solvation models are less computationally demanding and have been sufficiently well developed that they are effective for most systems [284]. Empirical scoring functions are weighted sums of independent contributions to binding energy (e.g. hydrogen bonding, van der Waals, hydrophobic, electrostatic, solvent effects). The weighting factors for empirical scoring functions are obtained using statistical methods such as regression analysis using a large and diverse 'training' set of receptor-ligand pairs that represent many different classes of receptor proteins and ligand structures and known experimental binding affinity data. General purpose empirical scoring functions such as those provided by software packages have been 'calibrated' against a diverseset of ligand-receptor pairs and perform well in most circumstances [282, 285, 286]. They are able to indicate which of two ligands has greater affinity but less able to accurately determine which of two poses of a given ligand is preferred, especially with highly flexible ligands [264, 267]. Scoring functions can be developed that are specific to the receptor under study [273]. Such custom scoring functions may be more accurate for prediction of binding energy of new ligands for that particular receptor or for selecting the best pose for a given ligand, but are limited in application to that particular system. The custom scoring function approach is most often used in drug design while the general scoring functions are used for virtual screening applications. For this study, the general scoring function is most appropriate because the objective is to evaluate both multiple poses or clusters of similarity and the differences among ligands, rather than being able to accurately determine which of the resulting poses is the best and using that information to refine the structure of the ligand to improve binding affinity.

3.2.3.4 Molecular Dynamics

To simulate the binding process with as much detail as possible and avoid some of the limitations of soft receptor models, force field based simulation methods such as Monte Carlo or molecular dynamics are used. Molecular dynamics (MD) computations apply the laws of classical mechanics to compute the motion of the atoms in a molecular system. Monte Carlo (MC) methods are based on a random sampling of the conformational space. The main

advantage of these methods is that they are very accurate and can model explicitly all degrees of freedom of the system including the individual solvent molecules if necessary. Unfortunately, the high level of accuracy in the modelling process comes with a prohibitive computational cost. State of the art molecular dynamics protein simulations can only simulate periods ranging from 10 to 100 ns, even when using large parallel computers or clusters. Given that diffusion and binding of ligands takes place over a longer time span, full simulations are often not possible to obtain. MD and MC simulations can be applied to a portion of a protein structure, such as within a specified radius of the ligand binding cavity, or to a pre-minimised structure for a limited sampling period producing informative and useful results [274, 279].

With this computational docking study, the ability of the environmental estrogens to stabilise the estrogen receptor in a particular conformation will be investigated. The molecular structures of the environmental estrogens are more flexible and there are no solved crystal structures of these more flexible molecules bound to the hER in the literature. This could be because no attempts have been made or because crystals of sufficient quality could not be produced to warrant publication.

The key features of the RL-complex to be investigated are

- The existence of multiple distinct energy-equivalent poses for a given ligand and whether they have the potential to result in different effects on gene expression
- The details of the interactions of the ligand with the receptor, particularly with His524/475 and the implications for the ligand's ability to stabilise the RL-complex.

3.3 Materials

3.3.1 Receptor Models

Computational docking relies on models of the receptor protein structure. These models are developed from published x-ray crystal structures. Because the estrogen receptor exists in two forms (α and β) and has two biologically active conformations (agonist and antagonist), a number of different x-ray crystal structures were required to capture this diversity. For this work, the x-ray crystal structures of the human estrogen receptor ligand binding domain listed in Table 3.1 were obtained from the Protein Data Bank (PDB) [287]. The model developed from the crystal structure is identified by the PDB code. Four additional PDB entries were

used as references for orientations of ligands within the binding site but were not used as models for docking as summarised in Table 3.2.

The differences in the models for the key ligand-residue interactions are illustrated in Figure 3.8.

Table 3.1. X-ray crystal structures of the human estrogen receptor ligand binding domain obtained from the Protein Data Bank (PDB) [287].

PDB Code	Receptor (mutations)	Receptor Conformation	Ligand	Resolution (Å)	Chain	Coregulatory Protein Fragment	Reference
1ERE	hERα	Agonist	E2	3.10	A	no	[77]
1A52	hERα	Agonist	E2	2.80	A	no	[288]
1X7R	hERα	Agonist	GEN	2.00	A	yes	[257]
3ERD	hERα	Agonist	DES	2.03	A	yes	[81]
2P15	hERα (S537Y)	Agonist	EZT	1.94	A	no	[289]
2B23	hERα (S537Y)	Agonist	*Apo*	2.10	B	yes	[85]
1ERR	hERα	Antagonist	RAL	2.60	A	no	[77]
3ERT	hERα	Antagonist	OHT	1.90	A	no	[81]
1XPC	hERα	Antagonist	AIT	1.60	A	no	[290]
3OLS	hERβ	Agonist	E2	2.20	A	yes	[291]
1X7J	hERβ	Agonist	GEN	2.30	A	yes	[257]
1L2J	hERβ	Antagonist	ETC	2.95	A	no	[262]
1QKM	hERβ	Antagonist	GEN	1.80	A	no	[78]
2JJ3	hERβ	Antagonist	JJ3	2.28	A	no	[292]
2QTU	hERβ	Antagonist	3AS	2.53	A	no	[293]

Table 3.2. Additional x-ray crystal structures of the estrogen receptor ligand binding domain obtained from the Protein Data Bank (PDB) [287].

PDB Code	Receptor (mutations)	Receptor Conformation	Co-crystallised Ligand	Notes
2QE4	hERα	Agonist	JJ3	Complements model 2JJ3. Does not have a co-crystallised coregulatory protein fragment. The solved structure does not include H12. Whether H12 was not resolved sufficiently to be included in the published co-ordinate file or whether it was not present as part of the protein to begin with was not apparent from the literature reference [292].
1L2I	hERα	Agonist	ETC	Complements model 1L2J [262]. Co-crystallised with coregulatory protein fragment.
1QKN	rat ERβ	Antagonist	RAL	Complements 1ERR. Does not have a co-crystallised coregulatory protein fragment. RAL is in a similar orientation to 1ERR [78]
2FSZ	hERβ	Antagonist	OHT	Complements 3ERT. OHT is in a similar orientation to 3ERT, but H12 is displaced by a second OHT molecule occupying the coregulatory protein binding cleft [294].

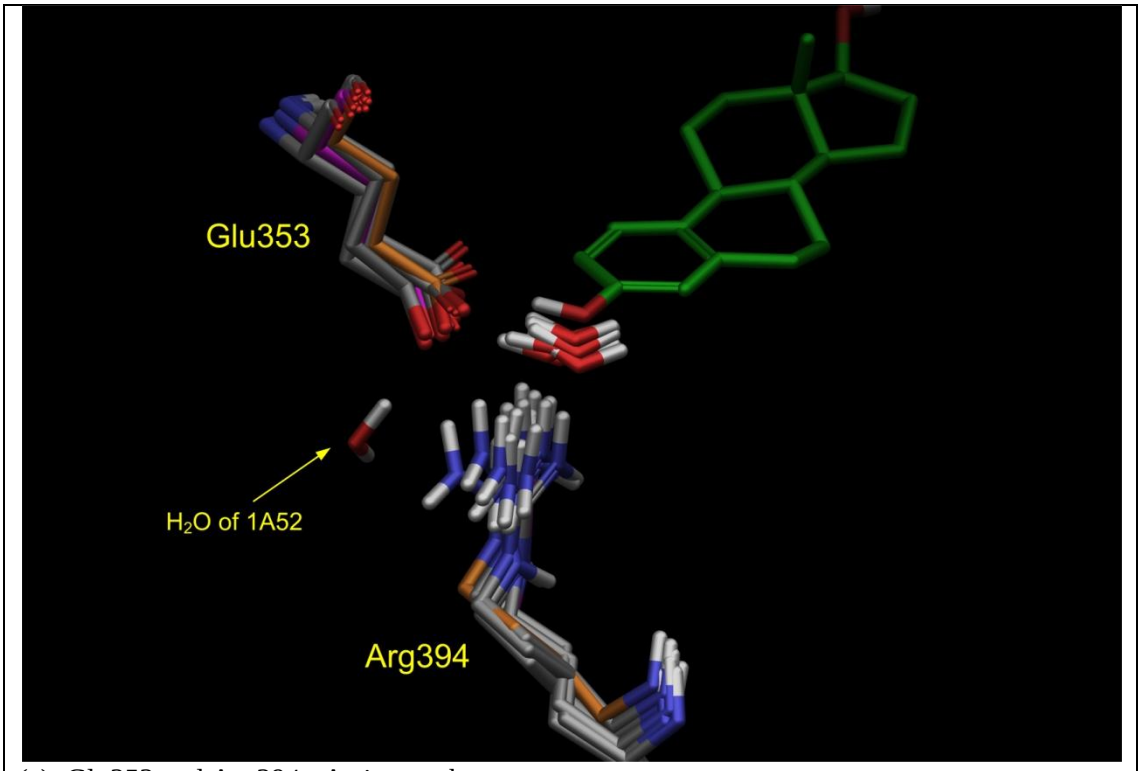

(a) Glu353 and Arg394. A-ring anchor.

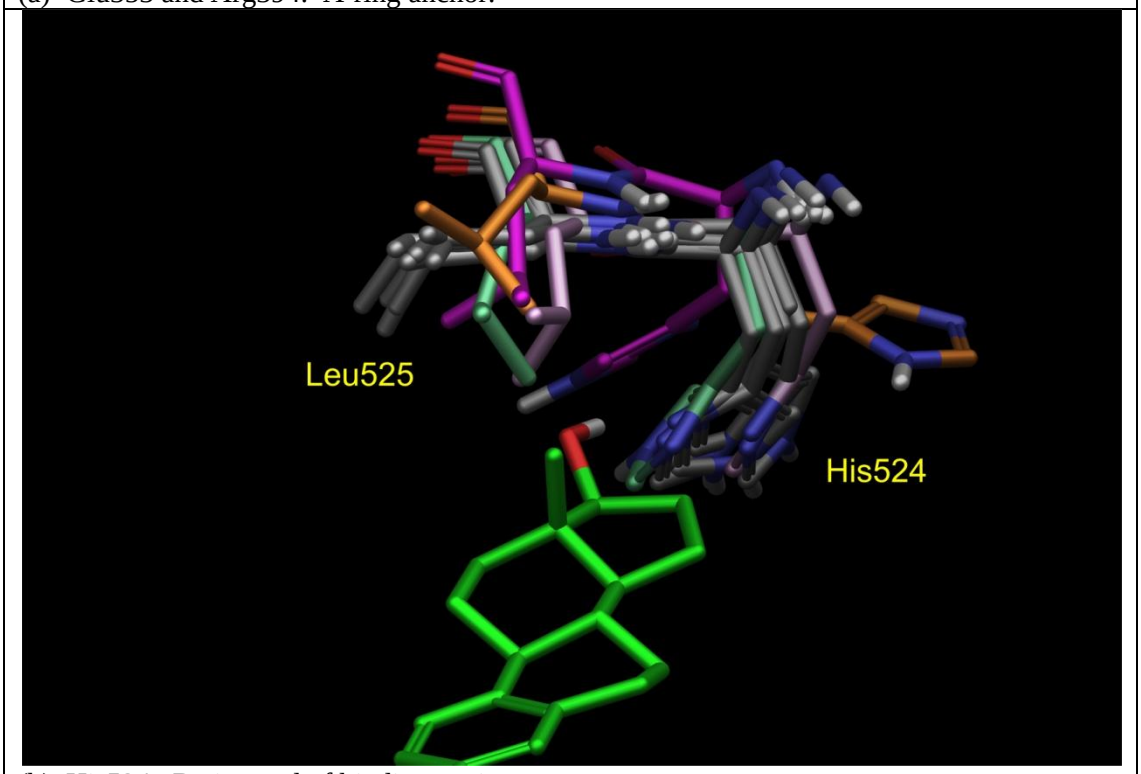

(b) His524. D-ring end of binding cavity.

Figure 3.8. Variation in positions of key ligand binding residues in different hERα models. The grey residues are from the agonist models. The orange residues are from 2B23, purple residues from 3ERT, light green from 1ERR and pink from 1XPC. Note conservation of residue positions in (a) at the A-ring anchor and flexibility in (b) the D-ring end of the binding cavity.

3.3.2 Ligand Structures

Computational docking requires a model for each ligand. This model is developed from the 3D structure of the ligand. The 3D structures for the co-crystallised ligands were extracted from the PDB files. The 3D structures for all other ligands were constructed using the software tools of the Schrödinger Suite. Models for 51 individual molecules representing 47 unique compounds are needed for this study. The 2D structures for these ligands are given in Table A. 7.

All of the ligands were minimised to find the conformation of the ligand that had the lowest internal energy. This calculation searched the entire conformation space of the ligand, including ring conformations (e.g. 6-member ring boat/chair conformations) and rotational degrees of freedom. For the ring conformation search, only those with minimised energy within 50 kJ/mol of the lowest energy conformation were retained. For the steroids (E1, E2, E3 and EE2) and phytoestrogens (COUM, GEN, DAID, EQ) only one conformation was found and it is on this basis that the steroids and phytoestrogens are described as rigid.

3.3.3 Experimental Binding Affinity Data

One of the goals of computational docking is to accurately predict the binding energy of a ligand-receptor complex. To evaluate the accuracy, experimental binding energy data are needed and for this study are obtained from the literature.

Competitive binding assays are the most common method for determining binding affinity for a ligand. The displacement of [^{3}H]-E2 bound to the receptor (ligand binding domain or entire receptor) by the compound under study is measured. A series of samples are prepared, each containing a known but different amount of the compound of interest and a known but a large excess (relative to the receptor concentration) of [^{3}H]-E2. The mixtures are incubated and after a period of time, the protein with bound ligand is separated from solution. The radioactivity due to the protein-bound [^{3}H]-E2 is measured. The concentration of compound required to displace 50% of the [^{3}H]-E2 (IC_{50}) is determined. The relative binding affinity for the compound is calculated as a ratio to the IC_{50} of E2 determined under the same conditions.

In some cases, IC_{50} is reported rather than a relative binding affinity. When this occurs, K_i, the binding affinity for the inhibitor, must be calculated from the experimental data using the equation [295]

$$K_i = \frac{IC_{50}}{\left(1 + \frac{[S]}{K_S}\right)}$$

where [S] is the concentration [^{3}H]-E2 and K_s is the binding affinity of [^{3}H]-E2 to ER. If [S] and K_s are not reported, the data cannot be used.

Experimental ΔG_{bind} values are calculated from experimentally determined values from the equation:

$$\Delta G_{bind} = -RT \ln K_i$$

where R is the gas constant and T is the temperature at which the K_i was determined.

The experimental values for Gibbs free energy of binding from the literature were tabulated for each of the ligands of interest. Table 3.3 summarises for each of the ligands of interest the average ΔG_{bind} and the standard deviation where more than one literature value was found. Also presented in Table 3.3 is the preference ratio which is simply the ratio of binding energies for hERα/hERβ. A preference ratio greater than one indicates the ligand will bind hERα with a greater affinity than hERβ. The literature references are summarised in Table A. 8.

Table 3.3. Experimentally determined ΔG_{bind} (kJ/mol). Values are averages of multiple literature values where a standard deviation is reported. NB = does not bind; NM = not measured. See Appendix for literature references.

	hERα		hERβ		Preference Ratio	Crystal Structure
Ligand	**Avg**	**Stdev**	**Avg**	**Stdev**	**hERα/hERβ**	**Available**
E1	-46.5	3.1	-39.4		1.18	
E2	-52.8	3.1	-51.8	3.3	1.02	x
E3	-46.4	3.4	-46.0		1.01	
T	-18.5		NM			
EE2	-50.3	0.2	-47.1		1.07	
DES	-54.8	4.4	-53.4	4.5	1.03	x
BPA	-36.3	2.4	-38.0	5.2	0.96	
4tOP	-35.4		-36.6		0.97	
4NP	-36.4	6.7	-39.3		0.93	
GEN	-42.3	5.3	-49.3	5.3	0.86	x
DAID	-35.7	4.4	-38.9	4.8	0.92	
COUM	-50.4	3.4	-53.4	4.4	0.94	
R-EQ	-39.2	1.4	-38.4	4.3	1.02	
S-EQ	-39.1	4.2	-43.6	4.2	0.90	
ENT	-40.7		-31.5		1.30	
mParaben	NB		NB			
eParaben	-29.5	1.5	-30.6	1.6	0.96	
pParaben	-32.2	1.1	-34.0	1.5	0.95	
bParaben	-34.0	0.8	-35.9	2.3	0.95	
BP-1	-34.5	11.2	-28.5		1.21	

BP-2	-35.9	8.5	-34.9	0.4	1.03	
BP-3	NB		NB			
OMC	NB		NB			
4MBC	-21.2		-24.6		0.86	
RAL	-51.9	4.1	-45.5	3.9	1.14	x
OHT	-51.1	5.5	-53.8	5.5	0.95	x
EZT	-54.7		NM			x
JJ3	-42.2		-50.7		0.83	x
AIT	-47.3		-42.9		1.10	x
3AS	-39.0		-49.2		0.79	x
ETC	-42.7		-44.8		0.95	x

3.4 Methods

3.4.1 Software Tools

The Schrödinger Suite 2010 is a proprietary software package for studying biomolecular interactions. The various modules and workflows of the suite are accessed through a graphical user interface called *Maestro*. For this work, the applications and workflows listed in Table 3.4 were used. The Schrodinger Suite has been extensively tested and compared to other software tools and its performance is consistently in the top half of the group of tested software tools [286, 296-300] and often one of the top-ranked tools for docking calculations.

Glide is able to correctly redock the cocrystallised ligand with RMS deviations smaller than 1 Å for 132 of the 279 test cases, smaller than 1.5 Å for 168 test cases, and are less than 2.0 Å nearly 70% of the time [301]. The GlideScore values track the experimental binding affinities reasonably well with the overall RMS deviation for 128 testbcases of 3.1 kcal/mol [301].

Table 3.4. Schrödinger Suite 2010 applications used in this work.

Application	**Task**
Maestro (Version 9.1)	Graphical user interface for all Schrödinger applications and workflows.
MacroModel (Version 9.8)	Molecular mechanics toolkit. Combines force fields, accurate effective solvation models, and advanced conformational searching methods to identify the low energy conformation of a single molecule (protein or small molecule) or receptor-ligand complex. Minimisation calculations used by other applications and workflows.
LigPrep (Version 2.4)	Generation of accurate 3D molecular models for ligand molecules, including tautomeric, stereochemical, and ionization variations optimized for further computational analyses. These tools are based on well known bond length, bond angle and atom size parameters and molecular geometry and bonding rules.
Glide (Version 5.6)	An extensively validated ligand placement algorithm and scoring function package to accurately predict binding mode for ligand-receptor complexes.
Prime (Version 2.2)	Protein structure predictions, protein structure refinement and MM-GBSA calculations.
Workflow	**Task**
Protein	Correcting common structural problems (e.g. missing residues or residue side chains) and

Preparation Wizard (2010)	creating reliable, all-atom protein models.
Induced Fit Docking (2009)	A novel method for fast and accurate prediction of ligand induced conformational changes in receptor active cavities. Combines *Glide* and *Prime* to exhaustively consider possible binding modes and the associated conformational changes within the receptor binding cavity.

The process for docking as implemented in the Schrödinger Suite is illustrated in Figure 3.9. The ensemble of poses obtained as output from this process can be further evaluated to obtain information from force field scoring functions.

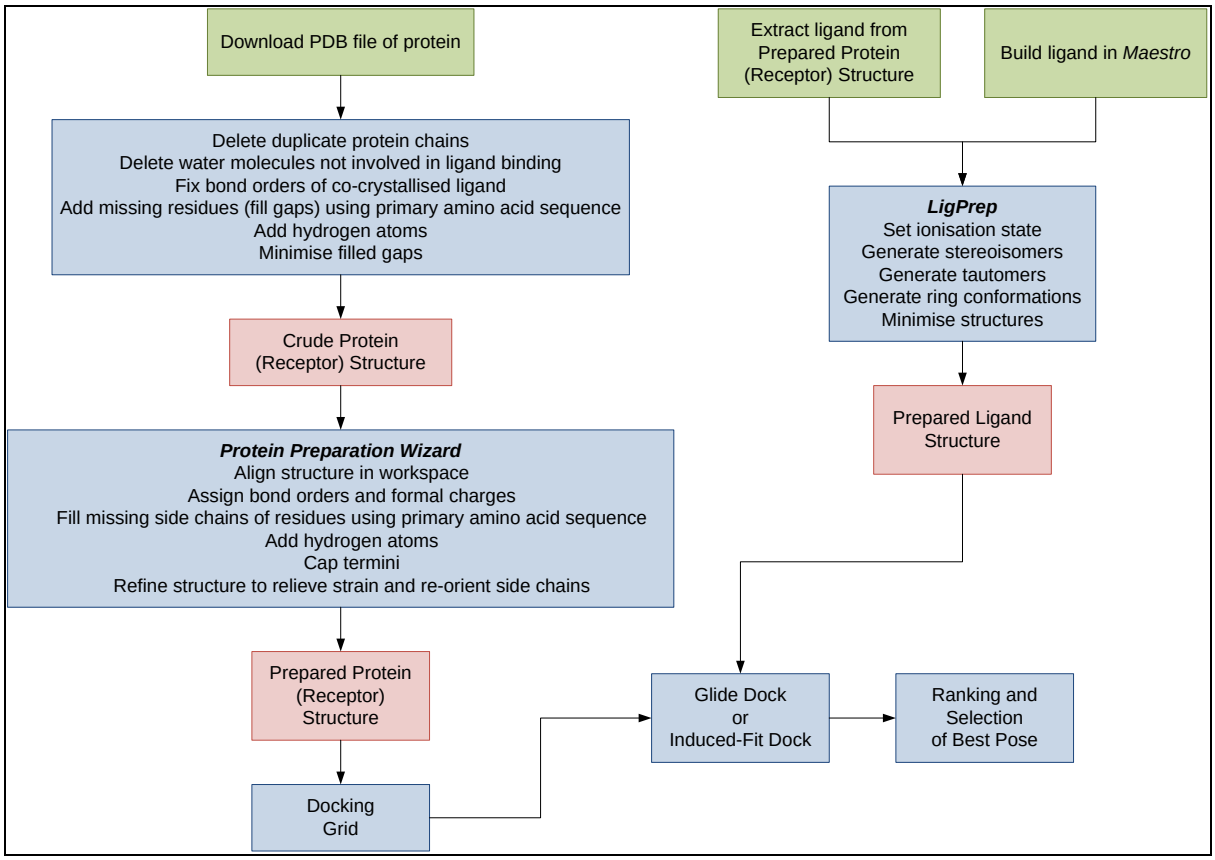

Figure 3.9. Schrödinger Suite ligand docking process.

3.4.2 Receptor Model Development

The x-ray crystal structures of the hER LBD listed in Table 3.1 were used to develop models for docking. Where multiple chains were present in the PDB file, chain A was used except as noted in Table 3.1. The atom co-ordinate files as downloaded from the PDB are not immediately ready for use in computational docking. In some of the crystal structures, small sections of the protein may not be completely resolved due to static disorder of atoms in the crystal. These unresolved segments result in gaps in the atom co-ordinate files. These gaps in the protein structure (missing residues) were filled using the primary amino acid sequence

of the receptor. The gaps were energy minimised in two stages using *MacroModel*. First, only the added residues were allowed to move, with the remainder of the crystal structure frozen. Then, the entire structure was minimised. All minimisations were required to converge to 0.05Å. All water molecules except for the one involved in the hydrogen bond bridge with Glu353 and Arg394 in hERα models and Glu305 and Arg346 in hERβ models were removed. To facilitate visual comparisons, all models were aligned in the *Maestro* workspace to *1ERE*. The PDB atom co-ordinate files do not include hydrogen atoms and include information only on which atoms are to be connected, not bond order. In some cases, as with unresolved segments discussed above, the side chains of individual amino acids are not fully resolved, leading to missing atoms in the residue side chains which requires correction. The N- and C- termini of the protein chain must also be capped or blocked with neutral groups to prevent computational artifacts from the charges at the bare ends of the protein chain. An N-methyl group is normally added to the C-terminus and an acetyl group is added to the N-terminus to provide neutral methyl groups at the ends of the chain. The Protein Preparation Wizard was used to assign bond orders, add hydrogen atoms, fill in missing side chains, cap chain termini, assign hydrogen bonds within the corrected protein structure and to perform a final minimisation of the model.

3.4.3 Ligand Structure Development

The molecular structures of the co-crystallised ligands were extracted from the PDB files. The molecular structures for all other ligands shown in Table A. 7 were constructed in *Maestro*. For each ligand, *LigPrep* was used to determine the ionisation state for carboxylic acids and amines at pH 7 ± 2; generate tautomers (e.g. keto-enol); generate alternate chiralities for all stereocentres; sample ring conformations to find low energy conformations. Finally, the geometry of each structure was optimised which involved allowing the structure to relax in all dimensions to achieve a low energy conformation. Not all possible isomers were produced because of internal filtering to eliminate structures which violate geometric restrictions such as for fused ring systems or conflict with natural product chiralities such as for the steroid framework.

For some ligands *LigPrep* produced more than one stereoisomer (e.g. both 17α- and 17β-estradiol were produced). For those ligands where it was known which stereoisomer was the desired or correct one, only that stereoisomer was used for docking (e.g. only 17β-estradiol was used). For ENT, 4 possible isomers were produced, but only the 3R,4R isomer is found

in vivo [302] and only that isomer was retained for docking. For EQ, 2 possible isomers were produced. Only the S isomer is found *in vivo* [303] and the S isomer is much more estrogenic than the R isomer [303, 304]. For mEHP (see Figure 3.10), the two stereoisomers produced by *LigPrep* were retained because no information could be found indicating which of the two stereoisomers was preferred. Since mEHP is a metabolite of diethylhexyl phthalate (DEHP, CAS 117-81-7), a high volume industrial chemical with unspecified stereochemistry, it is likely that the metabolite is a mixture of the two isomers. A similar situation was found for OMC. The compound must be *trans* at the carbon-carbon double bond (CAS 546-7-3), but the stereochemistry of the 2-ethylhexyl moiety is unspecified, as in mEHP. For 4MBC, there are two chiral centres on the camphor moiety which result in two possible stereoisomers (1R,4S and 1S,4R). 4MBC must also be *trans* at the double bond (CAS 36861-47-9).

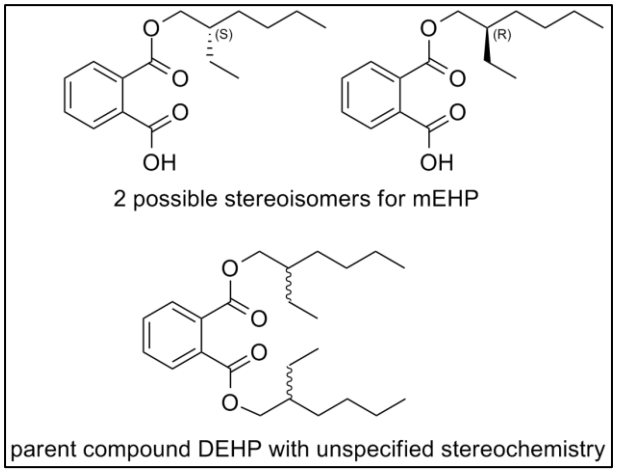

Figure 3.10. Stereoisomers of mEHP derived from the parent compound DEHP.

3.4.4 Rigid Receptor Docking - RRD

RRD was done using *Glide* and was run from within *Maestro* using the applications menu. The first step in *Glide* docking was generating a receptor grid. The binding cavity was defined automatically based on the size, shape and location of the co-crystallised ligand of the particular receptor model. For the hERα apo structure (*2B23*), the centroid of the residues Glu353, Arg394 and His524 was used to define the location of the binding cavity and the size was determined by specifying ligands to be docked were less than 20 Å in length. The receptor grid was kept rigid – with no van der Waals radius or charge scaling of receptor atoms. The ligand was docked flexibly, allowing nitrogen inversions and ring conformations.

No constraints (e.g. required hydrogen bonds or covalent bonds to metal atoms) were specified and all receptor hydroxyl groups were allowed to rotate.

Glide XP was used for docking using default parameters. The core, constraints and similarity options were not used. The core option allows for constraint of ligand poses within the binding cavity based on a reference ligand. The similarity options incorporate a similarity measure between a docked ligand and a reference ligand – a measure of how alike or unlike two molecules are. Both the core and similarity options are useful in virtual screening applications for drug target development to aid in the identification of strong binding ligands from a pool of potential candidates, but not applicable to the task at hand. All of the ligands listed in Table 3.1 were docked with all the receptor models listed in Table 3.1.

For RRD, poses were ranked by XPPoseRank. The calculated binding energy is given by the scoring function XPGlideScore. XPGlideScore was reported in units of kcal/mol and converted to kJ/mol.

3.4.5 Induced-Fit Docking - IFD

IFD was run from within Maestro using the workflow menu. The Glide grid was defined automatically based on the size and orientation of the co-crystallised ligand. Initial Glide docking allows residue side chains to be trimmed (temporarily removed from the protein structure) automatically, based on the B-factor. The B-factor is also called the temperature factor and the higher the value, the more mobile the residue side chain. The more mobile side chains were trimmed as their positions were less certain. The parameters used are summarised in Table 3.5. During the induced fit refinement step, the residues that were allowed to adapt to the placement of the ligand were those within 5 Å of the ligand, plus those residues on H11 where the agonist and antagonist conformations begin to diverge and those residues on H8 in the region where His524/475 H-bonds with the protein structure to either stabilise its interaction with the ligand or to stabilise itself in the absence of a ligand interaction. The refinement regions are shown in Figure 3.11.

For IFD, poses were ranked by IFDScore. IFDScore is defined as the sum of XPGlideScore and 5% of the Prime energy (the total energy of the receptor-ligand complex), so this ranking takes into account the overall energy of the complex, not just a favourable binding energy. The calculated binding energy is given by the scoring function XPGlideScore.

Table 3.5. IFD parameters

Glide Grid Setup	
Box Centre	Centroid of Ligand
Box Size	automatic based on co-crystallised ligand centroid of Glu353,Arg394 and His524 for apo model 2B23. Box is 26 Å long in each direction
Step 1: Initial Glide Docking	
Protein Preparation Constrained Refinement	Yes
Trim Side Chains	Yes, automatic based on B-factor
receptor van der Waals scaling	0.7
ligand van der Waals scaling	0.5
# poses retained per ligand	5
Step 2: Prime induced fit refinement	
Refine residues	within 5Å of ligand additional residues: hERα 418-425, 514-547; hERβ 370-377, 465-501 optimise side chains
Step 3: Glide re-docking	
Glide Docking	XP mode; Redock into structures within 30 kcal/mol of best structure and within the top 5 structures overall

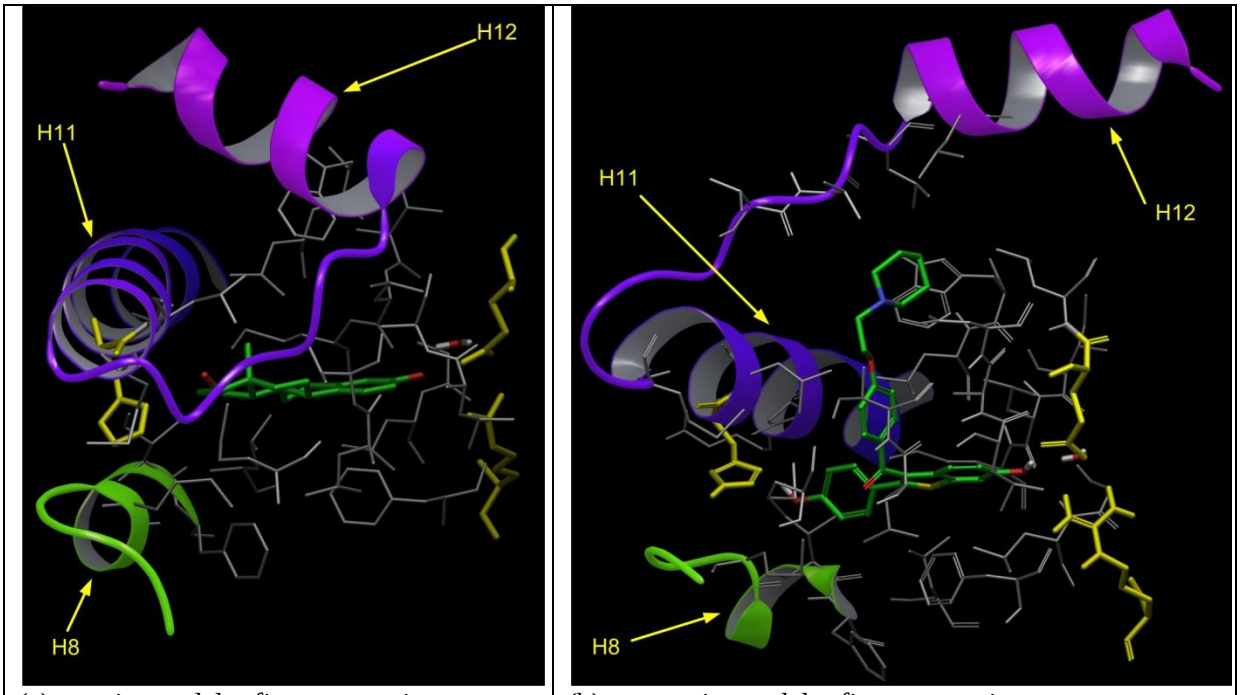

(a) agonist model refinement region (b) antagonist model refinement region

Figure 3.11. Refinement regions for agonist and antagonist models, illustrated with hERα models 1ERE and 1ERR. Residues within 5Å of the ligand are shown in grey, key ligand binding residues (Glu353,Arg394 and His524) are shown in yellow and the additional residues included for refinement are indicated by the ribbon representation. The analogous refinement regions were used for hERβ.

3.4.6 XPGLideScore

XPGlideScore was used in both RRD and IFD to estimate binding energy of the ligand with the receptor. XPGlideScore is optimised to identify and eliminate ligand poses that would have unfavourable energies based on well known principles of physical chemistry (e.g.

inappropriate hydrophobic interactions, poor hydrogen bonding interactions) to weed out false positives. As a result, more precise poses are produced [305] than with standard GlideScore. The cost for this increased precision is computational time. Standard GlideScore is used for ligand database enrichment to quickly identify good candidates for more thorough study using XPGlideScore.

3.4.7 Validation

Validation of the performance of both RRD and IFD examines the accuracy of both ligand placement and binding energy calculation.

The accuracy of ligand placement is quantified by the root mean square distance (RMSD) of the heavy atoms (C, O, N, S) of the ligand in the model and the docked pose. The difference between calculated and experimental binding energy was determined to quantify the accuracy of the binding energy calculation. The number of unique poses within the set of multiple, energy-equivalent poses produced was also determined.

It is commonly accepted that the accuracy of a computation required to make chemical predictions is 1 kcal/mol (= 4.2 kJ/mol) [306, 307]. With this in mind, when multiple poses for a given ligand/model combination are produced by the docking calculation, poses with calculated binding energies within 4.2 kJ/mol of the top-ranked pose are described as *energy equivalent*. Poses with calculated binding energies more than 4.2 kJ/mol from the top ranked pose are therefore disregarded.

The correlation of experimental and calculated binding energies was examined for those ligands that have experimental binding energies as summarised in Table 3.3. The calculated binding energy was considered correct if it was within ±3 kcal/mol (±12.5 kJ/mol) of the experimental value [301].

3.5 Results

Several crystal structures were used for each of the agonist and antagonist α and β receptor conformations in order to capture subtle variations. A total of 15 models were developed, one from each of the 15 crystal structures. Two docking processes were used. Rigid docking holds these models static and IFD allows the models to mutually adapt. With rigid docking, the subtleties among the different models are retained and the docking calculation determines how favourably the particular ligand interacts with a given model. Thus, for less flexible ligands, the ligand will only be docked into models that it fits. Poor fitting will be evident in

less favourable calculated binding energies, or the failure to return a docked pose. The more flexible ligands are better able to adapt to the fixed binding site topology. Flexible ligands may have more poses within the binding site. The calculated binding energies will indicate how 'uncomfortable' a particular binding site is for a particular ligand pose. Among the models that a flexible ligand can fit, the relative difference in calculated binding energies will indicate which of the different receptor-ligand complex conformations are more favourable.

In contrast, IFD allows the receptor model to adapt to a ligand pose and one might expect similar individual models to converge to a common conformation for a given ligand, if the ligand is effective in influencing the receptor conformation.

3.5.1 RRD and IFD validation

3.5.1.1 Native Ligand Re-docking

The first step in validation for both RRD and IFD was native ligand re-docking. The ability of the docking procedure to correctly place the ligand and to correctly predict the binding energy was evaluated for 14 models. Poses are considered energy-equivalent to the top-ranked pose if the difference in calculated binding energies is ≤4.2 kJ/mol. The results for ligand position RMSD, the difference between calculate and experimental binding energy (ΔG_{bind}), the number of energy-equivalent poses and the number of the energy-equivalent poses that are unique are summarised in Table 3.6.

RRD correctly placed the native ligand in all but one model (shaded in red in Table 3.6). The top-ranked pose for E2 in 1A52 was upside-down. The second pose was correct and was energy-equivalent to the top-ranked pose with a 0.02 kJ/mol difference in calculated binding energy. Of the 8 models that had multiple energy-equivalent poses, only 4 had more than one unique energy equivalent pose (1A52, 1ERR, 1XPC and 1QKM). The ligands of both 1ERR and 1XPC have large pendant groups, and the differences in poses were in the location of this pendant group. For model 1QKM, the difference in poses was due to rotation of 30° around the single bond connecting the A and B rings of GEN that inclined the fused flavone ring structure relative to the benzene A-ring.

IFD correctly placed the ligand in all but three models (shaded in red in Table 3.6). However, for these three models, the correct pose was one of the multiple energy-equivalent poses and the details for the correct pose are given in Table 3.6. For GEN in 1X7R, the top-ranked pose was in backwards compared to the correct orientation, but the energy difference

was less than 1kJ/mol. For GEN in 1QKM, the difference in poses is the rotation round the bond connecting the A and B rings, described above for the rigid docking result. The energy difference in this case is 2.3 kJ/mol. For 1L2J, the top-ranked pose is rotated by 180° along the length-wise axis of the ligand as compared to the correct pose. The pose that is closest to the correct orientation of the ligand is still displaced slightly due to the positioning of the ethylene substituents.

For both RRD and IFD, the binding energy was correctly predicted for all but the same two models (shaded in red in Table 3.6). In both cases the predicted binding energies were more favourable than experimental. For model 2P15, the interactions with EZT are different from those of the other receptor-ligand pairs, with the pendant group extending down into the binding cavity rather than out of the cavity. These interactions may not be captured well with the scoring function as this model is likely too new to have been included in the scoring function calibration. Model 1XPC is also a recent addition to the literature and also has different interactions than the other antagonist models (1ERR and 3ERT). The correlation between experimental and calculated binding energies is shown in Figure 3.12.

Table 3.6. Validation of RRD and IFD docking procedures by native ligand re-docking. Red shading indicates results that are outside the validation criteria. See text for details.

				RRD					IFD				
			ΔG_{bind} (kJ/mol)	ΔG_{bind} (kJ/mol)		RMSD (Å)	Distinct /Energy Equivalent Poses	Correct Pose	ΔG_{bind} (kJ/mol)		RMSD (Å)	Distinct /Energy Equivalent Poses	Correct Pose
	Model	Ligand	Expt.	Calc.	Diff				Calc.	Diff			
ERα	*1ERE*	E2	-52.8	-49.0	3.7	0.15	1/1		-51.3	1.4	0.26	2/5	
	1A52	E2	-52.8	-49.8	3.0	upside-down	2/2	2 ΔG = -49.6 kJ/mol RMSD = 0.14 Å	-47.5	5.3	0.25	1/4	
	1X7R	GEN	-42.3	-48.7	-6.3	0.17	1/1		-51.7	-9.4	backwards	3/4	3 ΔG = -50.9 kJ/mol RMSD = 0.39 Å
	3ERD	DES	-54.8	-48.9	5.9	0.39	1/2		-52.0	2.8	0.43	2/5	
	2P15	EZT	-54.7	-68.9	-14.2	0.30	1/3		-87.6	-32.9	0.38	1/2	
	1ERR	RAL	-51.9	-56.3	-4.4	0.77	2/8		-59.1	-7.2	0.52	2/4	
	1XPC	AIT	-47.3	-64.2	-16.9	1.08	2/2		-65.5	-18.2	0.43	2/3	
	3ERT	OHT	-51.1	-59.6	-8.6	0.38	1/3		-59.6	-8.5	0.79	3/4	
ERβ	*3OLS*	E2	-51.8	-42.3	9.5	1.23	1/1		-52.4	-0.6	0.33	1/1	
	1X7J	GEN	-49.3	-45.6	3.7	0.59	1/1		-48.0	1.3	0.32	2/5	
	1QKM	GEN	-49.3	-45.2	4.1	0.28	2/3		-48.6	0.7	0.83	2/4	4 ΔG = -46.3 kJ/mol RMSD = 0.24 Å
	2JJ3	JJ3	-50.7	-45.9	4.8	0.21	1/2		-48.7	2.0	0.85	4/5	
	2QTU	3AS	-49.2	-54.4	-5.2	0.12	1/1		-55.0	-5.8	0.43	1/5	
	1L2J	ETC	-44.8	-51.1	-6.3	0.80	1/1		-53.8	-4.6	rotated 180°	2/4	4 ΔG = -52.3 kJ/mol RMSD = 1.75 Å

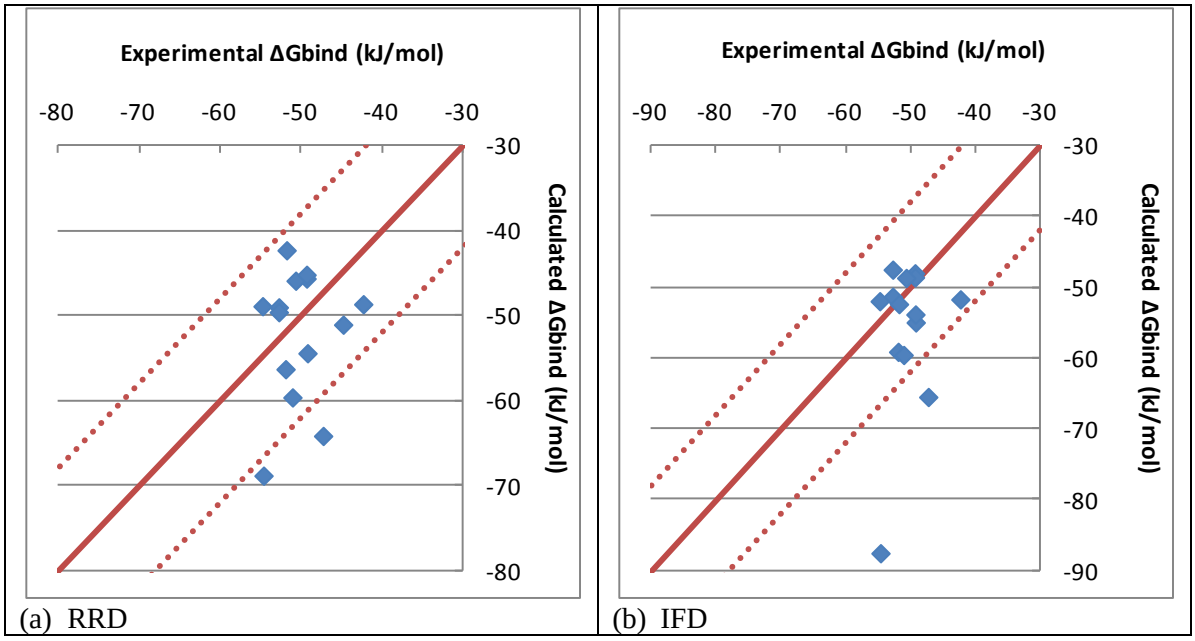

Figure 3.12. Correlation of calculated and experimental ΔG_{bind} for RRD and IFD native ligand re-docking. Solid line is 1:1 correlation and broken lines indicate ±12.5 kJ/mol uncertainty region of calculated binding energy.

3.5.1.2 Co-crystallised Ligand Cross-docking

The second step in the validation was cross-docking of co-crystallised ligands in the other models. The results for RRD and IFD are summarised in Table 3.7 and Table 3.8 respectively. The native docking results are also included for completeness. In both tables, the calculated binding energy for the top-ranked pose is given. Green shading indicates that the top-ranked pose had the ligand in the correct orientation in the receptor model. Yellow shading indicates that the correct pose was energy-equivalent to the top-ranked pose. No shading indicates that none of the energy-equivalent poses were correct. ND indicates the ligand was not docked into the model.

IFD was able to reproduce the correct ligand docking pattern achieved by RRD. RRD was able to correctly dock both E2 and GEN into most α-agonist, β-agonist and β-antagonist models. IFD had similar success for docking GEN, but less success with E2. IFD appears to favour the rotation of Leu524/476 into the binding cavity and this causes a clash with the 13-CH_3 of E2. In these situations, E2 was docked upside-down or backwards. The β-antagonist ligands JJ3 and 3AS were correctly docked into 1X7R in their α-agonist positions. IFD was slightly less successful in docking 3AS than JJ3, likely because the two F atoms of 3AS required more adjustment than the 2 H atoms of JJ3. The third β-antagonist ligand, ETC, was

not correctly docked into any of the other models. The interactions of ETC with the ERs appear to be very subtle. The correct conformation of the C-ring and its ethylene substituent could not be achieved with most models. IFD was able to produce the pocket needed to correctly position EZT into models 1ERE, 1QKM and 1L2J. Neither RRD nor IFD was able to correctly dock any of the ligands into 2B23. In 2B23, the key residues Glu353, Arg394 and His524 are displaced significantly from the positions required for interaction with the ligands. IFD is able to achieve some movement of Glu353 and Arg394 to allow the ligands to be placed within the binding cavity, but IFD is not able to move His524 sufficiently to complete the binding interaction. IFD was also unable to successfully dock the α antagonists (RAL, OHT and AIT) into either the α or β agonist models. In all cases, the large wedge of the ligand was compacted into the binding cavity. The correct docking achieved with 1A52 was a result of the deflected position of H12, allowing the wedge to be positioned in the entrance channel.

The correlation of calculated with experimental ΔG_{bind} is shown in Figure 3.13 for both RRD and IFD cross-docking. Only the results where the ligand is correctly docked are included. Overall, the scoring function performs very well, but IFD tends to result in calculated binding energies that are more favourable than the experimental values for hERα.

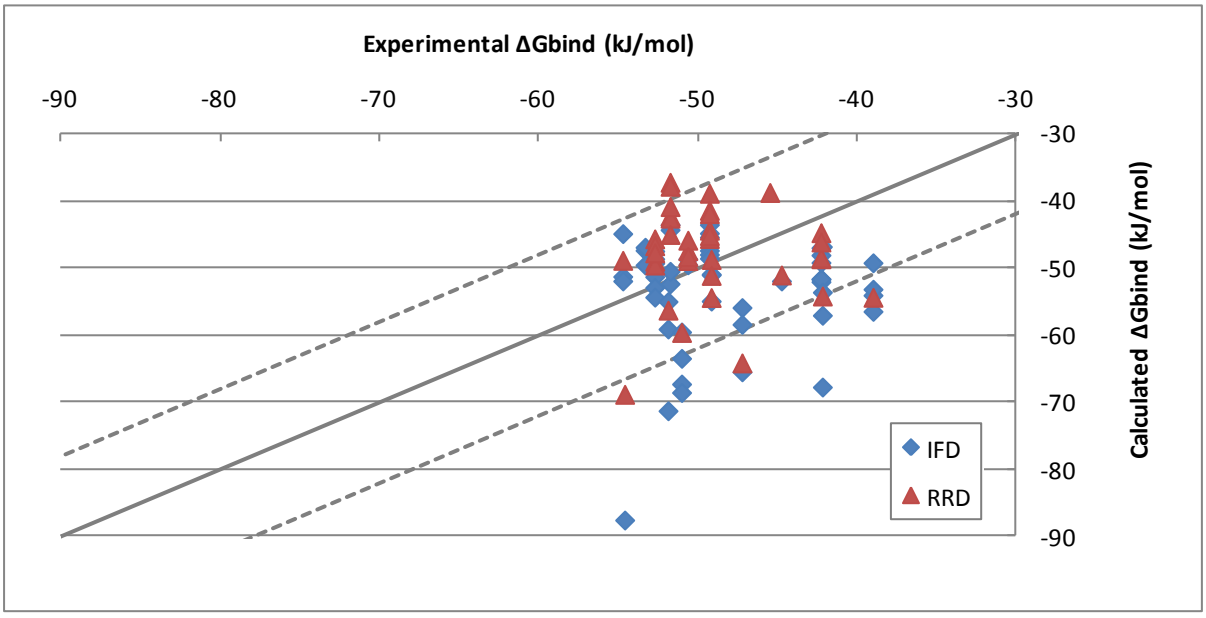

Figure 3.13. Correlation of calculated and experimental ΔG_{bind} for RRD and IFD cross-docking. Solid line is 1:1 correlation and broken lines indicate ±12.5 kJ/mol uncertainty region of calculated binding energy.

Table 3.7. Calculated binding energies (kJ/mol) of the top-ranked pose obtained by RRD cross-docking co-crystallised ligands in the other models. ND indicates the ligand was not docked in the model. Green shading indicates the correct orientation of ligand was achieved. Yellow shading indicates the binding the correct orientation achieved in a pose that was an energy-equivalent to the top-ranked pose.

		E2	GEN	DES	EZT	RAL	AIT	OHT	JJ3	3AS	ETC
ERα Agonist	**1ERE**	-49.0	-45.1	-45.6	ND	ND	ND	ND	-50.4	-49.4	-48.5
	1A52	-49.6	-44.8	-45.5	ND	-39.0	-49.2	-63.5	-52.0	-52.5	-53.6
	1X7R	-45.7	-48.7	-49.1	ND	ND	ND	ND	-54.2	-54.4	-58.7
	3ERD	-46.7	-48.5	-48.5	ND	ND	ND	ND	-53.2	-45.5	-58.6
	2P15	-47.8	-46.2	-46.2	-68.9	-47.6	-39.8	-52.4	-48.9	-51.4	-42.4
ERα Antagonist	**1ERR**	-42.6	-47.0	-45.5	-27.2	-56.3	-39.6	-53.3	-31.8	-33.0	-29.6
	1XPC	-46.7	-47.2	-49.4	ND	-58.1	-64.2	-61.4	-47.6	-31.3	-24.7
	3ERT	-19.9	-43.7	-47.0	-23.5	-51.6	-30.5	-59.6	-28.5	-24.5	-49.8
EBβ Agonist	**3OLS**	-42.3	-44.4	-44.0	ND	ND	ND	ND	-47.8	-49.9	-47.7
	1X7J	-42.6	-45.6	-47.0	ND	ND	ND	-30.2	-50.5	-53.2	-50.1
ERβ Antagonist	**1QKM**	-45.0	-45.2	-43.1	ND	ND	ND	ND	-47.5	-42.5	-48.8
	2JJ3	-37.3	-38.9	-40.1	ND	-38.8	ND	-43.1	-45.9	-48.8	-48.3
	2QTU	-40.9	-41.4	-40.8	ND	ND	-17.8	-27.6	-48.9	-54.4	-50.6
	1L2J	-37.9	-41.9	-42.2	ND	ND	ND	-28.3	-48.3	-51.1	-50.1

Table 3.8. Calculated binding energies (kJ/mol) of the top-ranked pose obtained by IFD cross-docking co-crystallised ligands in the other models. ND indicates the ligand was not docked in the model. Green shading indicates the correct orientation of ligand was achieved. Yellow shading indicates the correct orientation achieved in a pose that was an energy-equivalent to the top-ranked pose.

		E2	GEN	DES	EZT	RAL	AIT	OHT	JJ3	3AS	ETC
ERα Agonist	**1ERE**	-51.3	-52.1	-52.7	-64.7	-52.0	-64.7	-58.7	-53.6	-54.1	-58.0
	1A52	-47.5	-47.4	-44.9	-57.3	-55.0	-55.9	-63.5	-53.1	-49.8	-57.2
	1X7R	-52.9	-51.7	-51.3	-58.8	-63.8	-48.1	-65.1	-57.1	-56.5	-65.9
	3ERD	-57.8	-48.1	-52.0	ND	ND	-69.2	-62.5	-67.8	-55.6	-63.1
	2P15	-54.4	-51.6	-46.0	-87.6	-56.8	-54.0	-61.9	-67.4	-59.3	-61.5
ERα Antagonist	**1ERR**	-49.3	-49.2	-47.7	-49.2	-59.1	-60.2	-67.3	-46.8	-49.3	-52.5
	1XPC	-55.1	-52.6	-53.2	-55.1	-71.3	-65.5	-68.6	-51.1	-54.4	-49.3
	3ERT	-48.7	-47.0	-50.9	-43.0	-53.0	-58.4	-59.6	-51.0	-53.2	-53.8
EBβ Agonist	**3OLS**	-52.4	-47.4	-47.4	-46.7	-39.2	-44.9	-53.6	-47.9	-53.2	-54.5
	1X7J	-50.5	-48.0	-49.6	-58.8	ND	-50.8	-52.8	-53.0	-52.6	-56.7
ERβ Antagonist	**1QKM**	-44.3	-48.6	-46.9	-66.2	-50.0	-51.0	-44.7	-49.6	-51.1	-50.8
	2JJ3	-43.6	-45.4	-48.2	-53.1	-51.1	-52.5	-54.5	-48.7	-51.0	-51.7
	2QTU	-46.5	-43.6	-50.6	-55.7	-58.4	-55.2	-52.8	-48.3	-55.0	-57.9
	1L2J	-42.5	-44.9	-46.6	-58.7	-58.5	-47.0	-42.5	-44.7	-55.4	-52.0

With the results summarised in Table 3.7 and Table 3.8, the models that were best able to capture the known range of interactions of ligands with the receptor were 1ERE, 1X7R, 1ERR, 3OLS, 1X7J, 1QKM and 2JJ3. The remainder of the study will be limited to these models of the hER.

3.5.1.3 Ligands without Crystal Structures

The only validation that is possible for the docking of ligands without crystal structures is the comparison of calculated and experimental binding energies shown in Figure 3.14. Both RRD and IFD predict the experimental binding energies for these ligands within the stated uncertainty of ±12.5 kJ/mol. The results shown in Figure 3.14 are for the ligands identified in Table 3.3 as not having published crystal structures. Their experimental binding energies are also given in Table 3.3.

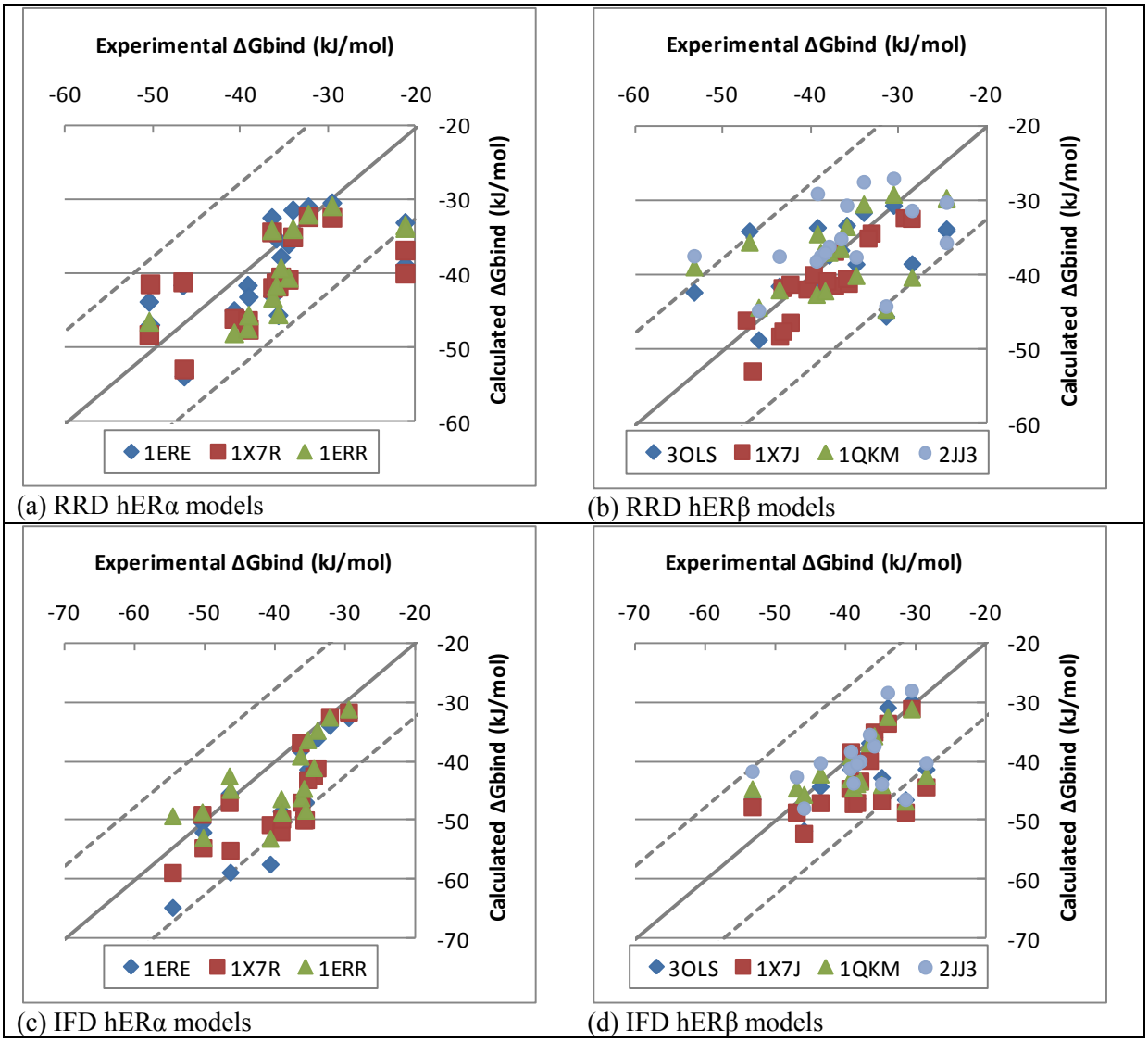

Figure 3.14. Correlation of experimental and calculated binding energies for (a,b) RRD and (c,d) IFD. Solid line indicates 1:1 correlation; broken lines indicate stated uncertainty of ±12.5 kJ/mol.

3.5.2 Calculated Binding Energies

The calculated binding energies for those ligands that do not have literature values for comparison are summarized in Table 3.9. The shaded value is the most favourable binding energy for that ligand. TRIC could not be docked in any of the models. Most of the remaining ligands have the most favourable binding energy when docked in hERα agonist models. Only 4 ligands preferred antagonist models. mTRIC is notable in that it could only be docked in antagonist models and showed a considerable preference for the hERβ antagonist models.

Table 3.9. Calculated binding energies (kJ/mol) for ligands without literature values.

	ERα	ERα	ERβ	ERβ
	Agonist	Antagonist	Agonist	Antagonist
NP-M1	-43.0	-40.9	-36.2	-36.6
NP-M2	-42.3	-36.9	-37.3	-34.8
NP-M3	-31.9	-35.4	-32.9	-32.1
OMC-S	-44.6	-34.3	ND	-39.7
OMC-R	-44.4	-40.4	-40.9	-39.4
BP-3	-43.5	-39.7	-41.7	-41.7
PHBA	-31.0	-28.5	-28.8	-28.4
M-Paraben	-30.9	-30.9	-30.5	-29.5
mTRIC	ND	-26.3	ND	-38.9
TRIC	ND	ND	ND	ND
3PBA	-45.9	-42.3	-46.3	-40.9
3PBOH	-40.7	-39.3	-40.4	-38.7
4OH-3PBA	-40.7	-36.0	-37.1	-36.6
4OH-3PBOH	-41.3	-40.5	-38.6	-39.3
mOP	-44.0	-42.9	-44.5	-39.5
mEHP-S	-43.9	-41.2	-44.9	-46.0
mEHP-R	-44.4	-42.3	-46.4	-44.3
mBzP	-46.7	-37.3	-45.0	-41.6
mBP	-46.5	-44.1	-46.1	-32.5
mEP	-37.0	-36.1	-35.9	-36.1
mMP	-38.6	-39.6	-33.5	-34.6

3.6 Discussion

3.6.1 Challenges and Limitations in Computational Docking

Although there is a theoretical and physical basis for the calculations in computational docking, the complexity of the systems necessitates assumptions and simplifications in order to make the problem tractable and computationally possible with current computer systems. These assumptions and simplifications result in the introduction of errors which can lead to numerical disagreement between computational results (e.g. binding energy) and

experimental data. Minimising the effects of these assumptions and simplifications and improving their quality is an active area of research in computational chemistry.

Defining or calibrating scoring functions to predict binding energies from computational results is one way to minimise the effects of these assumptions. However, in some cases, these calibrated scoring functions may not be the best choice if the system under study behaves very differently from those used in calibrating the scoring function. In such cases, the energy values produced directly by the computations may be a better choice. Alternatively, if the numerical accuracy of a particular scoring function is not sufficient for the purpose at hand, docked receptor-ligand complexes can be re-scored using one of many different scoring functions available [278-280].

For the present study, the scoring function implemented in the Schrödinger Suite is a good choice because hERα is one of the systems used in the calibration of the *GlideScore* scoring function and validation of the *Glide* docking methodology [300, 308, 309]. *Glide* has been shown to perform better than many other docking software packages in both accuracy of predicted binding energies and in accuracy of ligand placement [300, 308, 309]. It is therefore not unreasonable to expect that the calculated binding energies and ligand poses obtained from the Schrödinger Suite for this study of hERα and hERβ to be representative of what may occur *in vivo*. However, for the purposes of the present work, it is still important to recognise that computational results may not always agree numerically with experimental results but should reflect the trends demonstrated by experimental results. For these reasons, validation of the model results using known test scenarios is essential to gain confidence in the computations for predicting behaviour in unknown systems.

One of the characteristics of rigid receptor docking is that the docked ligands tend to be confined to the volume described by the co-crystallised ligand in the receptor model. Since the volume occupied by an agonist is generally smaller than that occupied by an antagonist, all ligands will be docked into both agonist and antagonist models.

With the rigid receptor model, the binding cavity residues are held fixed and the ligand is required to adapt to the binding cavity to find a low energy conformation for the system. As a result, the positions of the key binding cavity residues are important in determining ligand position within the binding cavity. For a given ligand, the differences in key residue

positions may be expected to influence the most favourable conformation of the ligand in the binding site.

It is therefore expected that the known orientation of a given ligand may not be produced by rigid receptor docking in all models, but it is expected that docking the ligand into the model from which it came will produce the correct pose. It is also expected that the alternate poses for a given ligand in some models will have calculated binding energies that are less favourable than that obtained by re-docking the ligand into the model from which it came. It is also possible that rigid receptor docking fails to place the ligand in the binding cavity of a particular model.

When performing IFD, it is reasonable to expect that any given ligand would be docked into any of the models, provided that the adjustment of the models by the induced-fit procedure allows the model to adapt to the ligand. Thus, using multiple models as starting points, it is reasonable to expect most of the models to converge to a common point which is consistent with the crystal structure orientation of the ligand. This convergence should occur if the search space is large enough to include this point and it is a true minimum in energy for the system. Depending on the flexibility of the ligand, multiple distinct and similarly favourable poses may be obtained and convergence to a common point may not be as clean. The interpretation of this scenario is that the ligand is similar to that already observed for GEN; that the ligand may act as a partial agonist or partial antagonist.

3.6.2 Validation Study

The validation study has demonstrated that

- both RRD and IFD can correctly place a native ligand into its model and can correctly place ligands with known orientations in the binding cavity of models that are similar to the native model.
- the scoring function is able to predict the experimental binding energy within the stated uncertainty of ±12.5 kJ/mol.

RRD worked as expected for the validation set of ligands. Both native re-docking and cross-docking gave the correct pose and correct binding energy (Table 3.6, Figure 3.12, Figure 3.13). RRD did not return a pose for ligands that were not supposed to fit into the binding cavity. Specifically, the ligands with large pendant groups RAL, AIT, OHT and EZT were docked only in their native models. For 8 of the 14 models, native re-docking produced

multiple energy equivalent poses. On examination, more than one distinct pose was found for only 4 of the models.

IFD worked as expected for native re-docking. Both the ligand poses and calculated binding energies were correct and were consistent with the RRD results. IFD cross-docking results were not as definitive as those obtained with RRD. Multiple distinct energy equivalent poses were produced for most ligands including the rigid ligands. In contrast to RRD, IFD cross-docking returned poses for the 3 α-antagonist ligands in the agonist models. In these models, the ligand was coiled and folded to fit into the binding cavity. These poses were considered invalid and were disregarded. IFD was not expected to correctly dock these ligands in these models because of the position of H12. This does illustrate the point that just because a pose is returned with a favourable binding energy, doesn't mean it is a valid pose. IFD results have to be carefully evaluated using knowledge of the system under study.

IFD was not able to correctly dock the α-antagonist ligands into the hERβ antagonist models. All three of these ligands are known to bind to hERβ because there are experimental binding energies for all three ligands and because crystal structures for OHT in hERβ (PDB 2FSZ) and RAL in the rat ERβ (PDB 1QKN) are published. In these crystal structures, both ligands take positions in ERβ analogous to their positions in ERα. The failure of IFD to successfully place these ligands in the antagonist hERβ models is a result of the position of H12 and the loop connecting H11 and H12 in these models (Figure). H12 is not displaced as far in the hERβ models as it is in the hERα antagonist models or in 2FSZ. In the case of OHT, the loop at V487 clashes with what would be the position of the terminal amide of OHT, preventing full extension of the side chain. The binding orientation of OHT in 2FSZ may also be aided by binding of a second OHT molecule to the co-activator binding site, radically displacing H12 and its connecting loop.

GEN provides a particular challenge to both RRD and IFD. GEN behaves as an agonist in hERα and as both an agonist and antagonist in hERβ. Gen takes essentially the same position within the binding site in all three situations and the binding affinity is greater for hERβ than for hERα. RRD cross-docking predicted the correct orientation of GEN 4 of 5 hERα agonist models and in all the hERβ models, although the flavone ring was tilted slightly compared to the expected orientation. In the other hERα agonist models GEN was docked backwards. The backwards docking of GEN has been previously reported [273], so was not unexpected.

This validation has also highlighted the limitations of IFD in convergence of different models to a common end point. IFD was unable to reposition the key residues of model 2B23 to correctly position the ligands as found in the other α-agonist models. IFD was also not able to move His524 of model 3ERT to correctly dock RAL or for 1ERR to accommodate AIT. To accurately consider the positioning of EEs in the binding cavity, the models 1ERE, 1X7R, 1ERR, 3OLS, 1X7J, 1QKM and 2JJ3 were deemed most representative of the behaviour of hERα and hERβ as these models had the best success rate in ligand cross-docking. The receptor-ligand interactions represented by the other models were considered too far removed from the convergence point defined by E2 and GEN and possibly only achievable by the specially designed ligands.

3.6.3 Important Receptor-Ligand Interactions

The cross-docking exercise revealed two ligand interactions with the receptor models that are important in understanding the binding behaviour of environmental estrogens. They are the rotation of the binding cavity and how this leads to the uncoiling H11 and the A-ring clamp.

3.6.3.1 Rotation of the binding cavity

The positions of His524/475, Leu525/476 and Ile424/376 are strongly influenced by the bound ligand and differ significantly between the agonist and antagonist models as illustrated in Figure 3.15 with 1ERE and 1ERR and in Figure 3.16 with 1ERE and 3ERT. These differences create a rotation of the binding site as illustrated in Figure 3.17. The residue side chains are able to take up some of the distortion of the binding site caused by the various ligands, but eventually, the distortion is transmitted to the backbone of the protein structure. The relative positions of the carbonyl and amide functionalities of the protein backbone determine whether the hydrogen bonding network that stabilises the α-helix structure remains intact with ligand binding. The antagonist conformation is achieved by uncoiling H11 by one turn, lengthening the loop between H11 and H12 and thus allowing H12 to take up the position characteristic of the antagonist receptor model.

In both *3ERT* and *1ERR*, the backbone hydrogen bond network is broken by the shift in position of Leu525 as shown in Figure 3.18. The carbonyl of Leu525 forms a hydrogen bond with the amide and the side chain hydroxyl of Ser527, one residue earlier than in *1ERE*. This disrupts the subsequent backbone hydrogen bonds allowing the helix to uncoil. In *1XPC*, H11 uncoils one turn earlier. In *1XPC*, the ligand's B-ring is 6-membered whereas in RAL, this ring is 5-membered. The D-ring hydroxyls of the two ligands are in different positions

thus influencing the position of His524. OHT does not have a D-ring hydroxyl so is unable to engage His524. Instead, the side chain of His524 forms a hydrogen bond with the side chain carboxylate of Glu419, aiding the disruption of the backbone hydrogen bond network. These hydrogen bonding networks are summarised in Table 3.10 and are consistent among the α and β models.

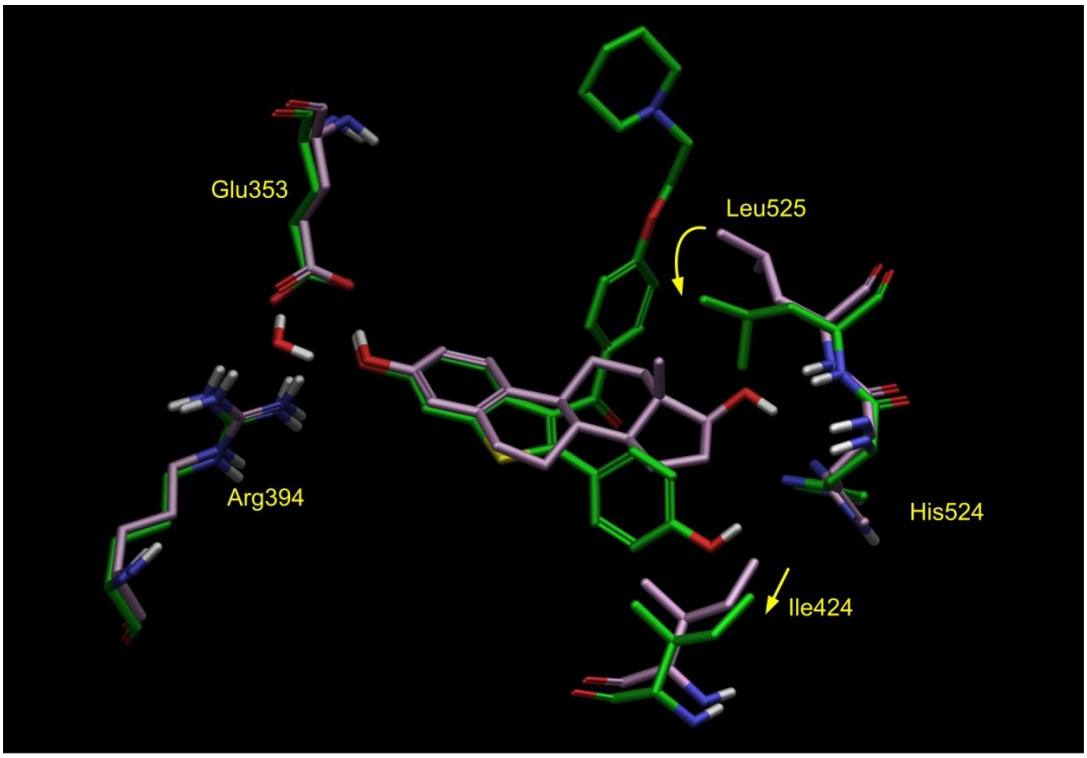

Figure 3.15. Comparison of *1ERR* (green) and *1ERE* (pink) binding cavities. Note shift in D-ring end caused by RAL (green).

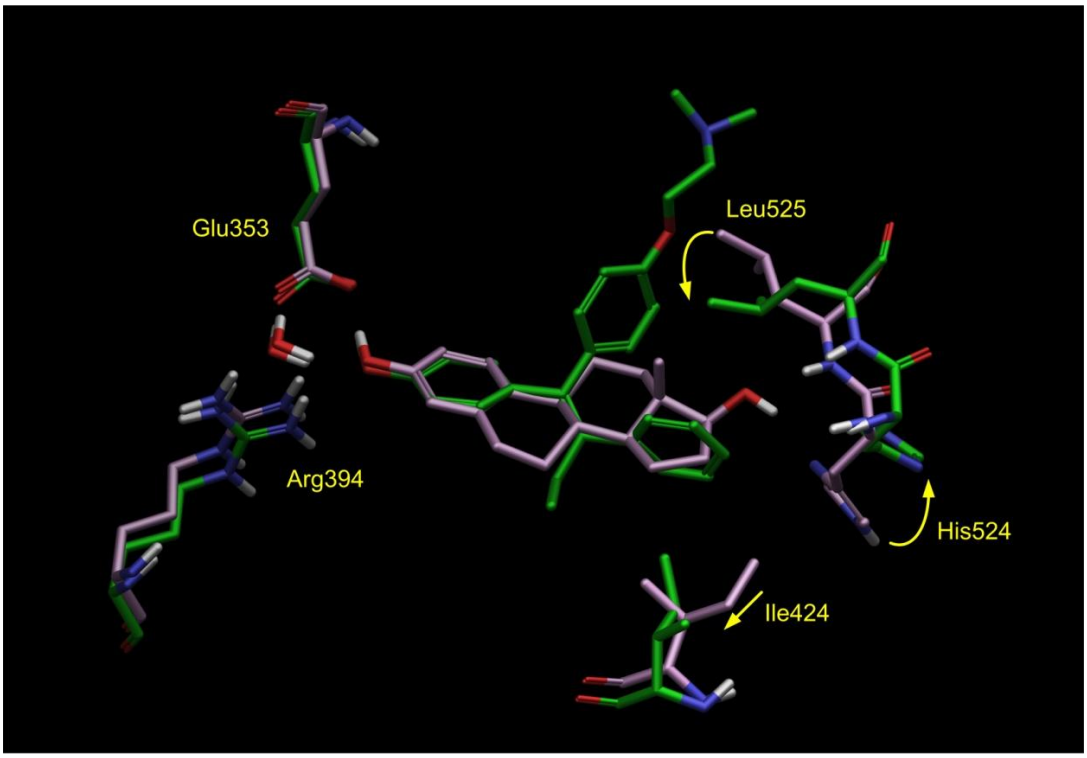

Figure 3.16. Comparison of *3ERT* (green) and *1ERE* (pink) binding cavities. Note shift in D-ring end caused by OHT (green) and deflection of His524 out of binding cavity because OHT does not engage with it.

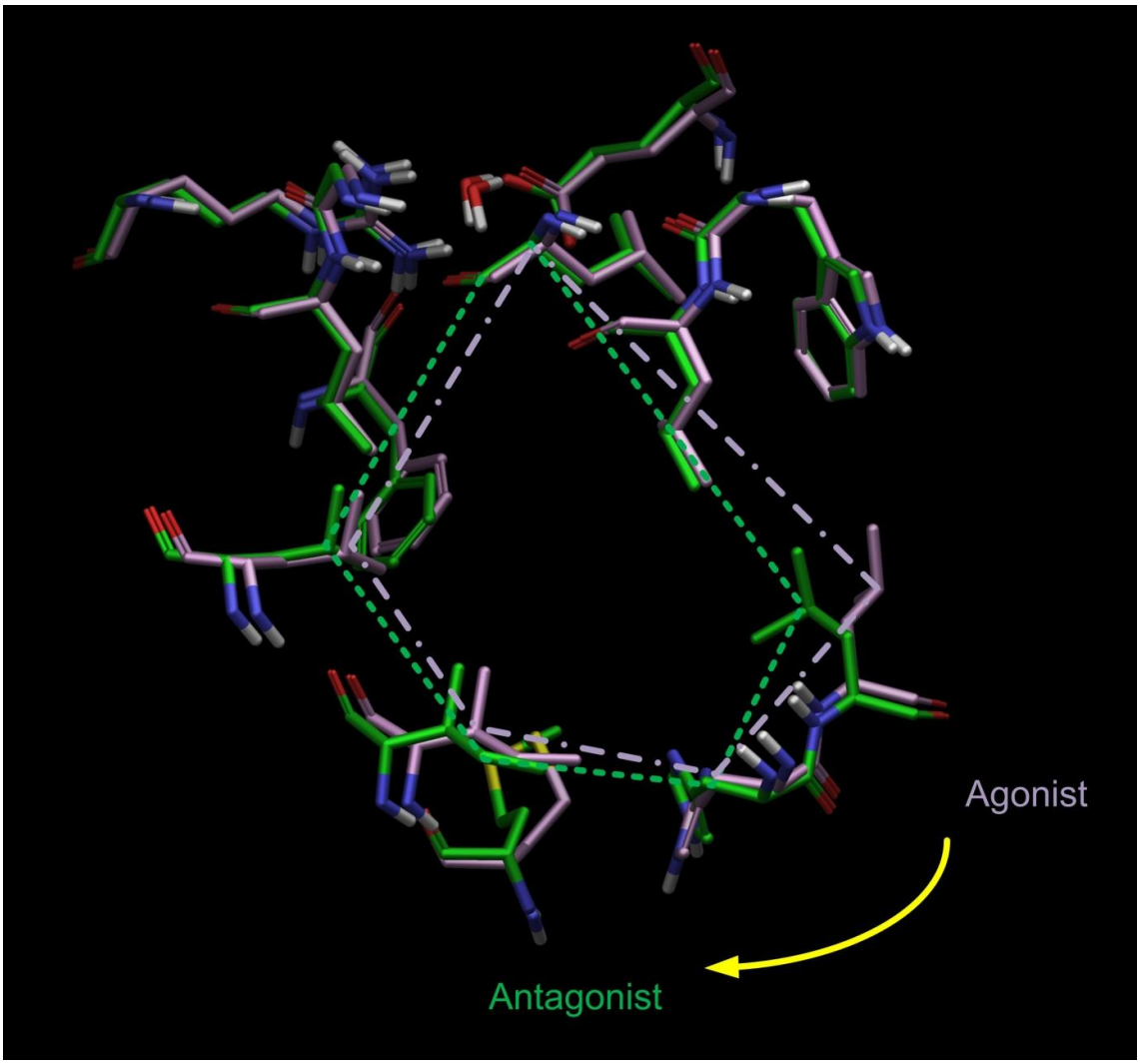

Figure 3.17. Schematic illustration of the rotation of the binding cavity between agonist (*1ERE*, pink) and antagonist (*1ERR*, green) models.

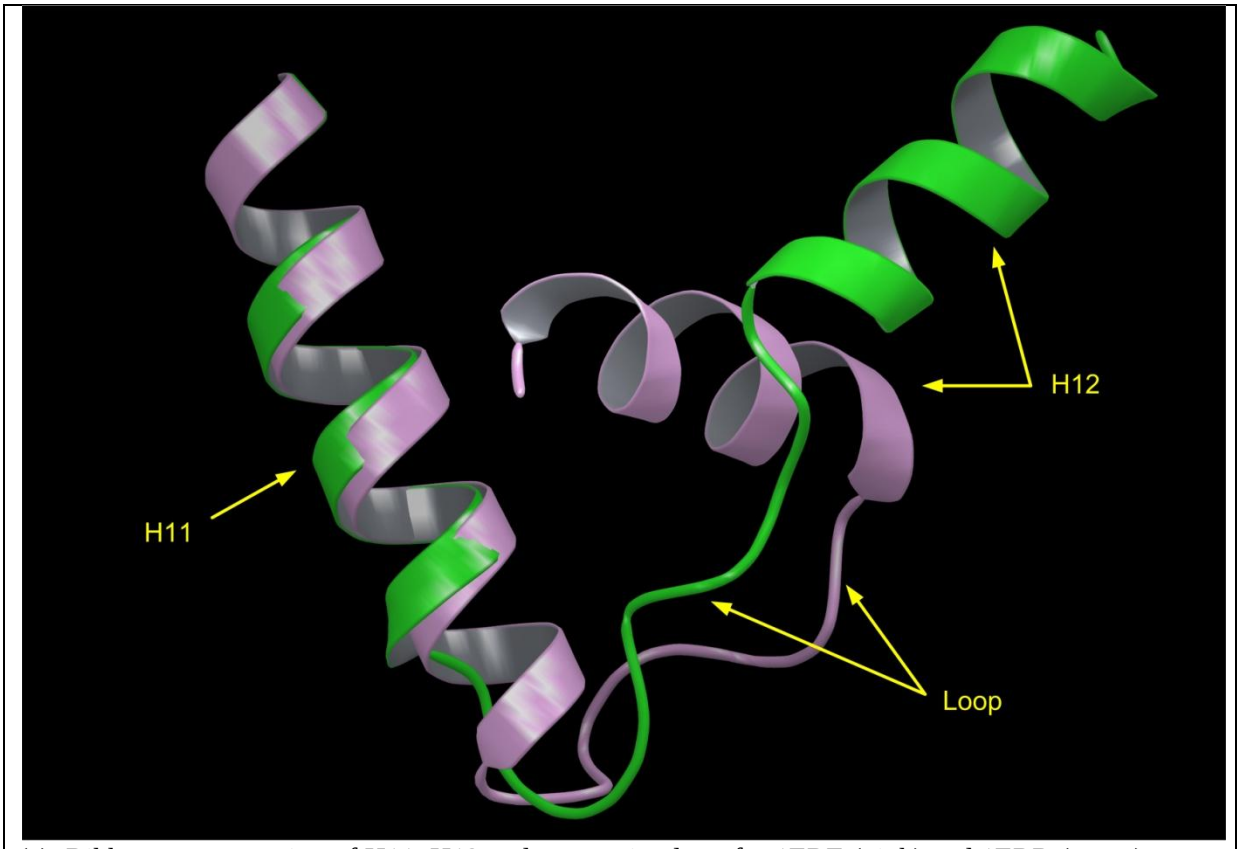

(a) Ribbon representation of H11, H12 and connecting loop for 1ERE (pink) and 1ERR (green)

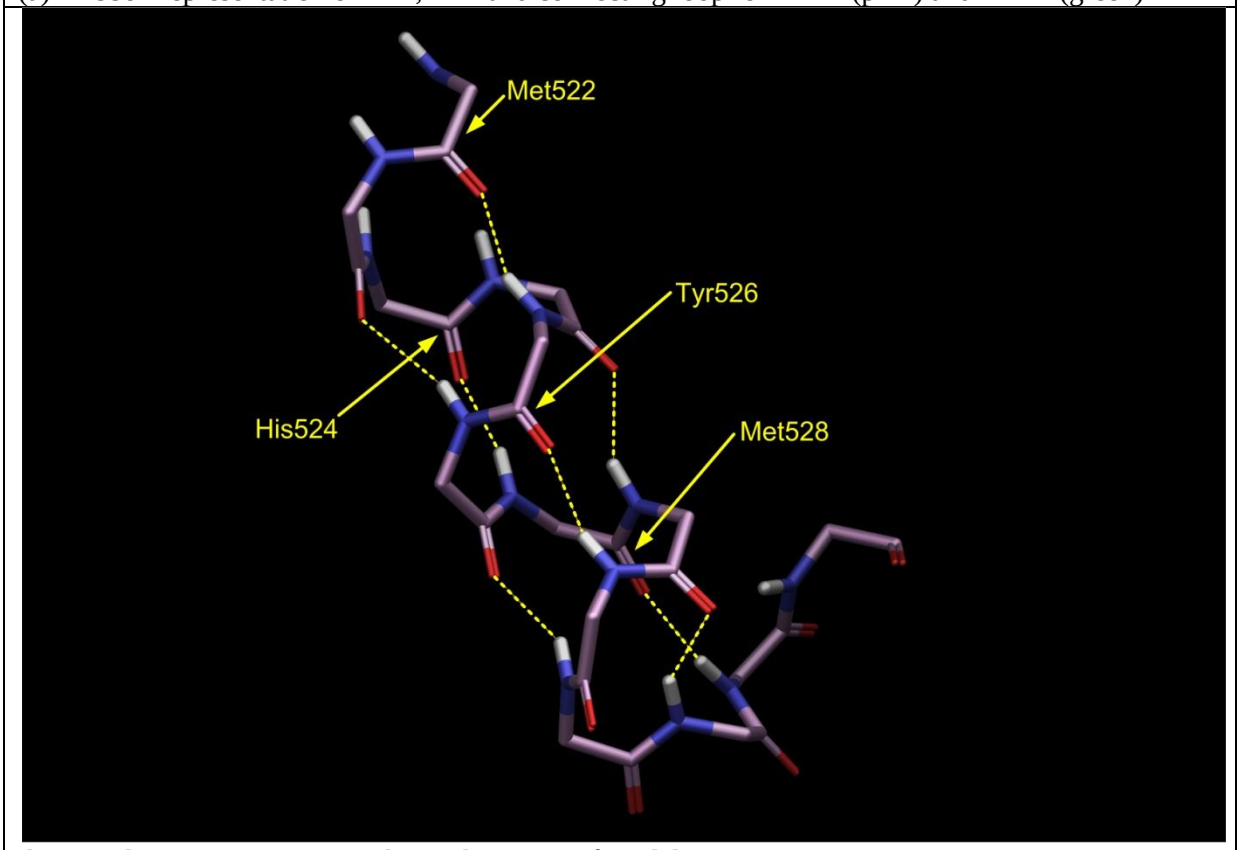

(b) Residues Met522-Lys529 (located in H11) of model 1ERE

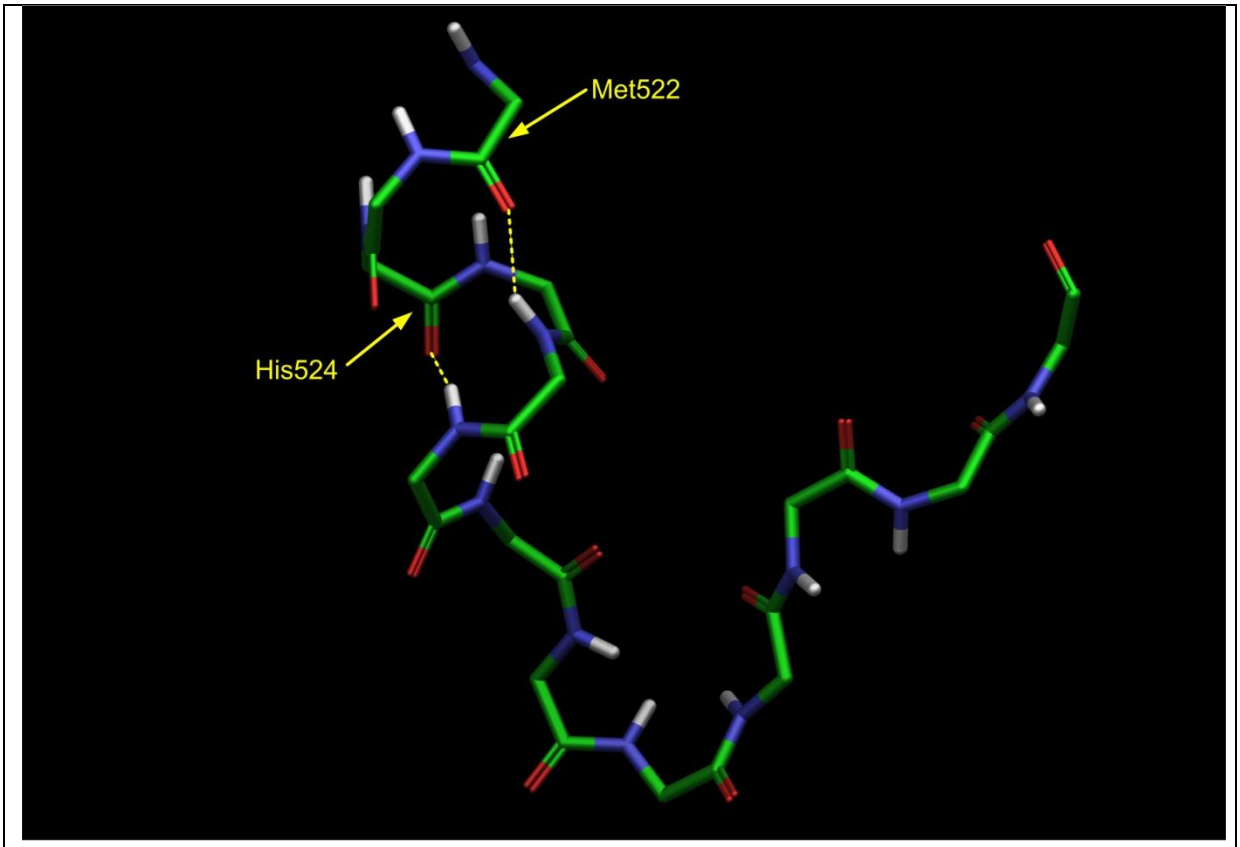

(c) Residues Met522-Lys529 (located in H11) of model 1ERR

Figure 3.18. Mechanism of H11 uncoiling illustrated using hERα models 1ERE (pink) and 1ERR (green).

Table 3.10. Hydrogen bonding pattern (carbonyl → amide). Residue differences between hERα and hERβ are highlighted in red.

hERα		hERβ	
Agonist (1ERE)	**Antagonist (1ERR)**	**Agonist (3OLS)**	**Antagonist (1L2J)**
Met522 → Tyr526	Met522 → Tyr526	Met473 → Leu477	Met473 → Leu477
Glu523 → Ser527	Glu523 →	Glu474 → Asn478	Glu474 →
His524 → Met528	His524 → Ser527	His475 → Met479	His475 → Asn478
Leu525 → Lys529	Leu525 →	Leu476 → Lys480	Leu476 →
Tyr526 → Cys530	Tyr526 →	Leu477 → Cys481	Leu477 →
Ser527 → Lys531	Ser527 →	Asn478 → Lys482	Asn478 →
Met528 → Val533	Met528 →	Met479 → Val484	Met479 → Cys481
Lys529 →	Lys529 →	Lys480 →	Lys480 →

A measure of the disruption of the α-helix structure is the relative angle between the backbone carbonyls between His524/475 and Leu525/476. The positions of His524 and Leu425 of hERα (His475 and Leu476 equivalent in hERβ) of all 7 of the hER receptor models with agonist ligands bound are shown in Figure 3.19. The side chain of His524/475 is able to take up the disruption caused by the variation in length of agonist ligands so as not

to disturb the orientations of the backbone carbonyls that participate in hydrogen bonding in the backbone of H11.

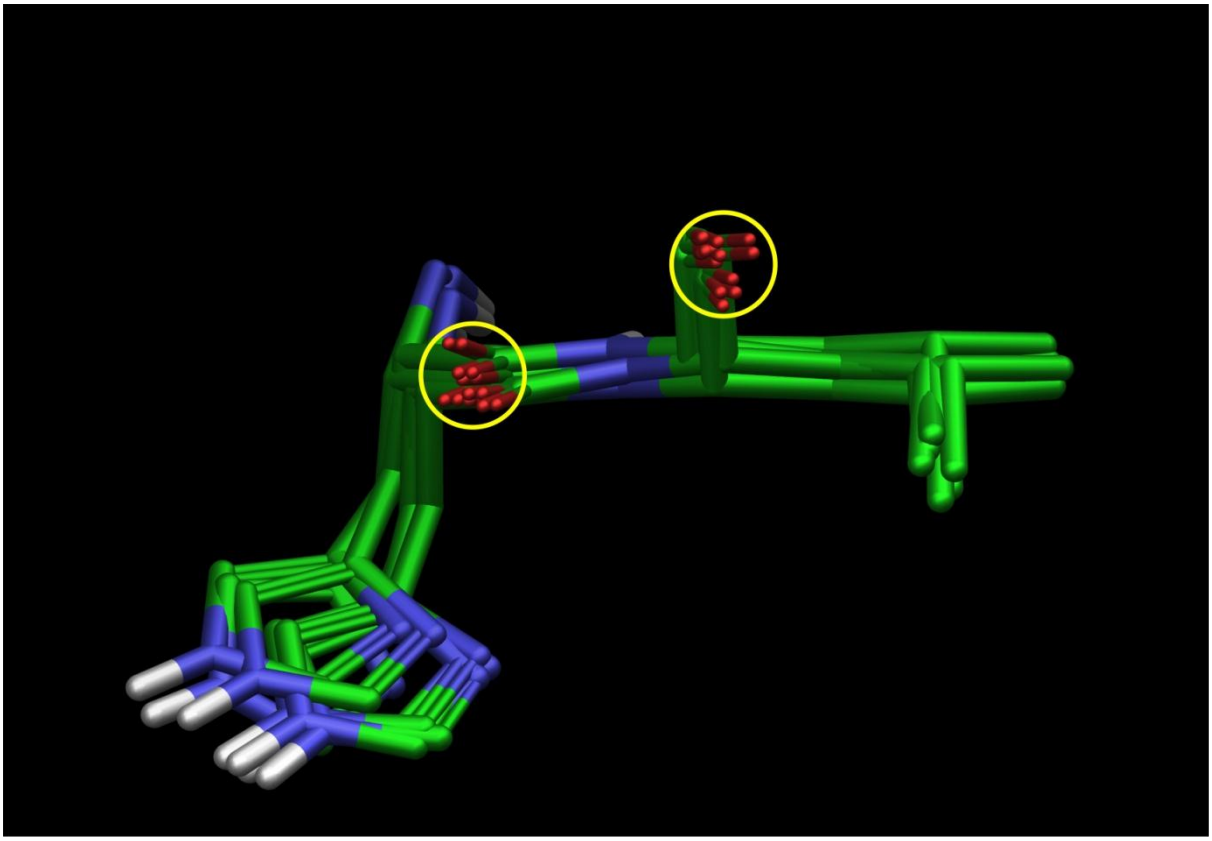

Figure 3.19. The effect of agonist binding on positions of both His524/Leu425 of hERα and His475/Leu476 in hERβ. All hERα and hERβ models are shown. Note conservation of position of protein backbone carbonyls as indicated by yellow circles and position of Leu side chain. The His side chain takes up the ligand-imposed distortion.

A similar view of the hERα antagonist models are shown in Figure 3.20 with model 1ERE (green) included for reference. The circles are in exactly the same position as in Figure 3.19. The effect of antagonist binding on the relative positions of the two backbone carbonyls is clear. The side chains of His524 and Leu525 are significantly shifted and are unable to accommodate the disruption without disturbing the backbone hydrogen bonding of H11. This leads to a breakdown in the α-helix structure of H11, lengthening the loop connecting H11 and H12, allowing H12 to rest in the coregulatory protein binding groove.

In hERβ, the disruption of the protein backbone at His475/Leu476 caused by antagonist binding is more dramatic than that for hERα, as shown in Figure 3.21. As discussed in Section 3.2.1, hERβ antagonist molecules do not require the large 'wedge' substituent to maintain the antagonist conformation of hERβ. For the hERβ antagonist ligands to maintain the antagonist conformation of hERβ, the disruption of the protein backbone at

His475/Leu476 must therefore be more dramatic and extensive. As a result, the hERβ antagonist ligands do not need to be able to physically block the closed position of H12.

The relative positioning of the carbonyls between His524/475 and Leu525/476 in each of the models was measured using the dihedral angle tool in Maestro. The angle is defined in Figure 3.22 and the results are summarised in Table 3.11. This angle is larger for antagonists than for agonists in both models and may be diagnostic of the agonist/antagonist behaviour of EEs.

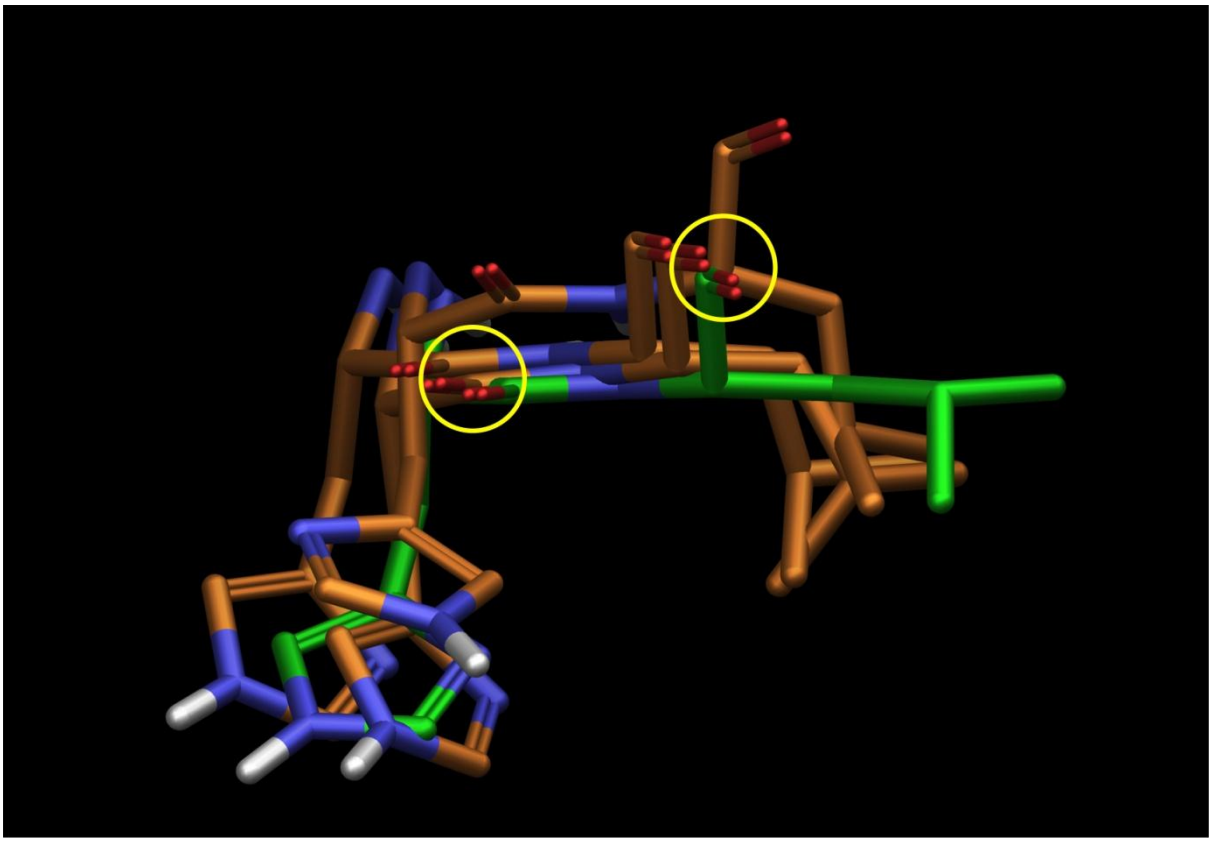

Figure 3.20. The effect of antagonist binding on positions of His524/Leu525 of hERα. Models 1ERR, 1XPC and 3ERT are shown in orange. The yellow circles indicate where the carbonyls are located in the agonist receptor conformation of Figure 3.19. The model 1ERE is shown in green for reference. Note the dislocation of the backbone carbonyls.

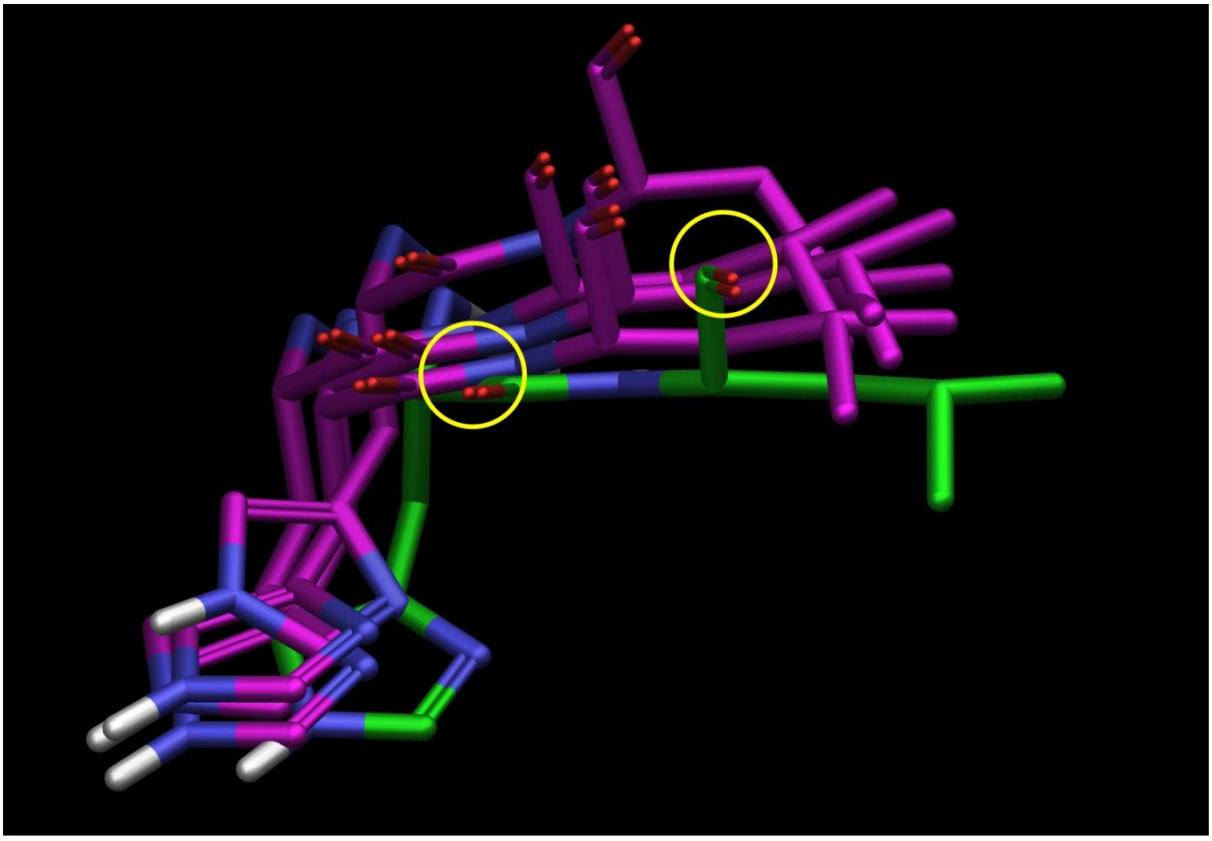

Figure 3.21. The effect of antagonist binding on positions of His475/Leu476 of hERβ. Models 1L2J, 1QKM, 2JJ3 and 2QTU are shown in purple. The yellow circles indicate where the carbonyls are located in the agonist receptor conformation of Figure 3.19. The model 3OLS is shown in green for reference. Note the dislocation of the backbone carbonyls.

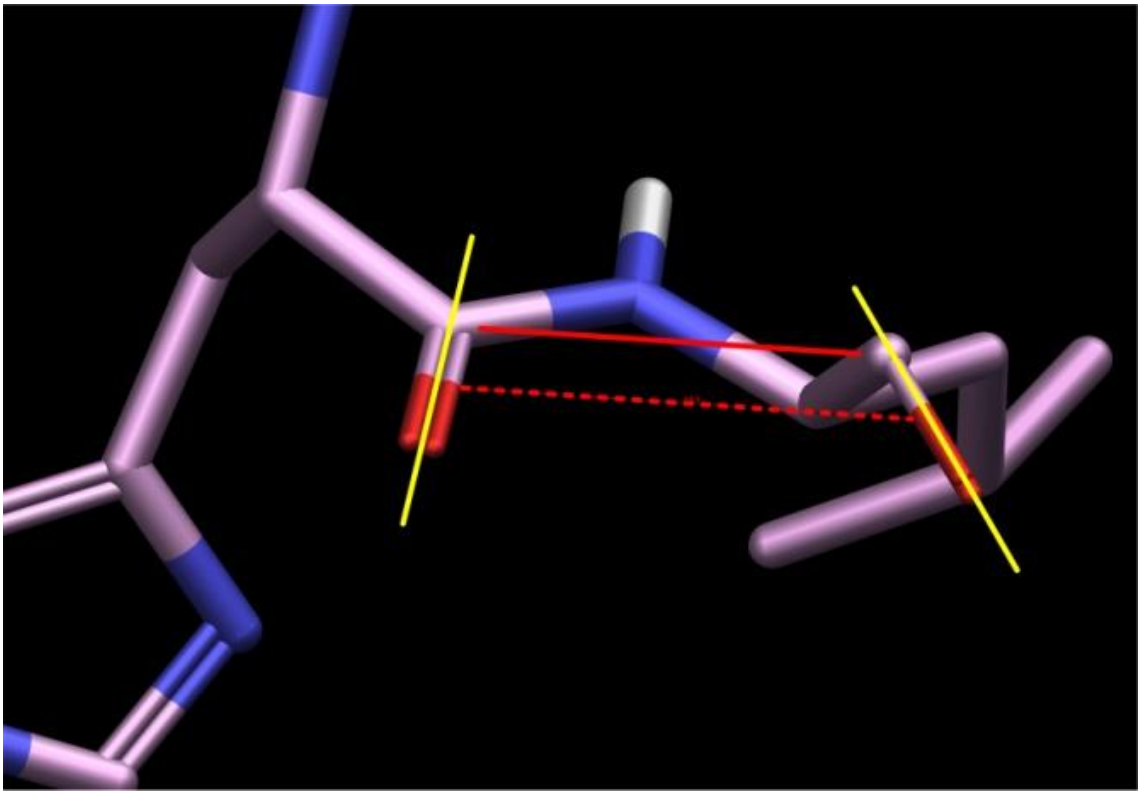

Figure 3.22. Definition of the dihedral angle between the backbone carbonyls of His and Leu.

Table 3.11. Dihedral angle measured for each of the models with the co-crystallised ligand in place. Ligand length as measured between opposing hydroxyl groups is also given.

	Model	Ligand	Dihedral Angle	Ligand Length (Å)
hERα Agonist	3ERD	DES	15.5	12.1
	1X7R	GEN	16.5	12.2
	1L2I	ETC	18.9	12.1
	1ERE	E2	21.1	11.0
	1A52	E2	21.1	11.0
hERα Antagonist	1XPC	AIT	22.9	11.6
	1ERR	RAL	29.3	11.7
	3ERT	OHT	32.4	10.7
hERβ Agonist	3OLS	E2	16.4	11.0
	1X7J	GEN	18.5	12.2
hERβ Antagonist	2JJ3	JJ3	20.1	11.9
	2QTU	3AS	21.8	12.0
	1L2J	ETC	24.1	12.1
	1QKM	GEN	25.0	12.2

The diagnostic ability of the dihedral angle was evaluated with the IFD cross-docking results. When cross-docked in 1ERE, GEN caused the dihedral angle to decrease from 21.1° to 16.4°, the same angle as seen with GEN in 1X7R. In contrast, when cross-docked in 1X7R, E2

results in an opening of the dihedral angle to 18.9°, approaching the angle seen in 1ERE. The longer ligand (GEN) is able to stretch the binding cavity to actively engage both ends of the binding cavity, resulting in a decrease in the dihedral angle, straightening the α-helix structure of H11, possibly producing small changes in the positioning of H12 over the binding cavity. The shorter ligand (E2) is able to contract the binding cavity slightly, but the 13-CH_3 of E2 prevents the binding cavity from collapsing by holding Leu525 in place.

E2 was correctly docked in 1ERR, causing the dihedral angle to decrease slightly from 29.3° to 28.2°. A larger change was not seen because E2 engaged the key residues in a similar manner to RAL. The inability of IFD to model large changes in protein structure may also have attenuated the response. However, when OHT was docked in 1ERR, the dihedral angle decreased to 18.5°. OHT was not able to engage His524 because it does not have a D-ring hydroxyl, thus allowing the His524-Leu525 pair to collapse into the binding site. This collapse was seen because the exact positioning of the wedge of OHT was different in the cross-docking pose of OHT in 1ERR from that of OHT in its native crystal structure.

A similar pattern was seen with hERβ models. GEN resulted in a decrease in the angle when cross-docked in 3OLS and E2 caused an increase in angle when cross-docked in 1X7J.

The most convincing evidence for the dihedral angle to indicate agonist or antagonist behaviour is in model 1A52 where H12 is deflected away exposing the entrance channel for positioning of the antagonist ligand wedge, yet the binding cavity residues are in the agonist conformation. All 3 of the α-antagonists (AIT, OHT and RAL) were correctly docked in 1A52 causing the dihedral angle to increase from 21.1° to 26.0°, 26.1° and 29.7° respectively.

Thus, if the dihedral angle for hERα poses is less than 21.1°, the ligand is most likely to behave as an agonist. For hERβ, a slightly narrower angle of 18.5° differentiates agonists from antagonists.

The ligand's ability to effectively engage both ends of the binding cavity, in addition to having a wedge to physically reposition H12 in hERα determine the ligand's ability to influence the receptor conformation.

3.6.3.2 A-ring Clamp

The second feature of the binding site that plays a key role in ligand positioning is the alignment of Phe404/356 and Leu387/339. These two residues, if they remain vertically

aligned, will capture the aromatic ring of the ligand. If the aromatic ring is phenolic, this capture facilitates hydrogen bond formation with Glu353/303 and Arg394/346 and the water molecule. This behaviour is described herein as the 'A-ring clamp' and is illustrated in Figure 3.23. The deflection of Phe404 in model 3ERT is a result of the position of the ligand OHT.

The A-ring clamp is the primary ligand positioning mechanism within the binding cavity. This clamp will retain a ligand within the binding cavity even the ligand is not able to engage the D-ring end of the binding cavity.

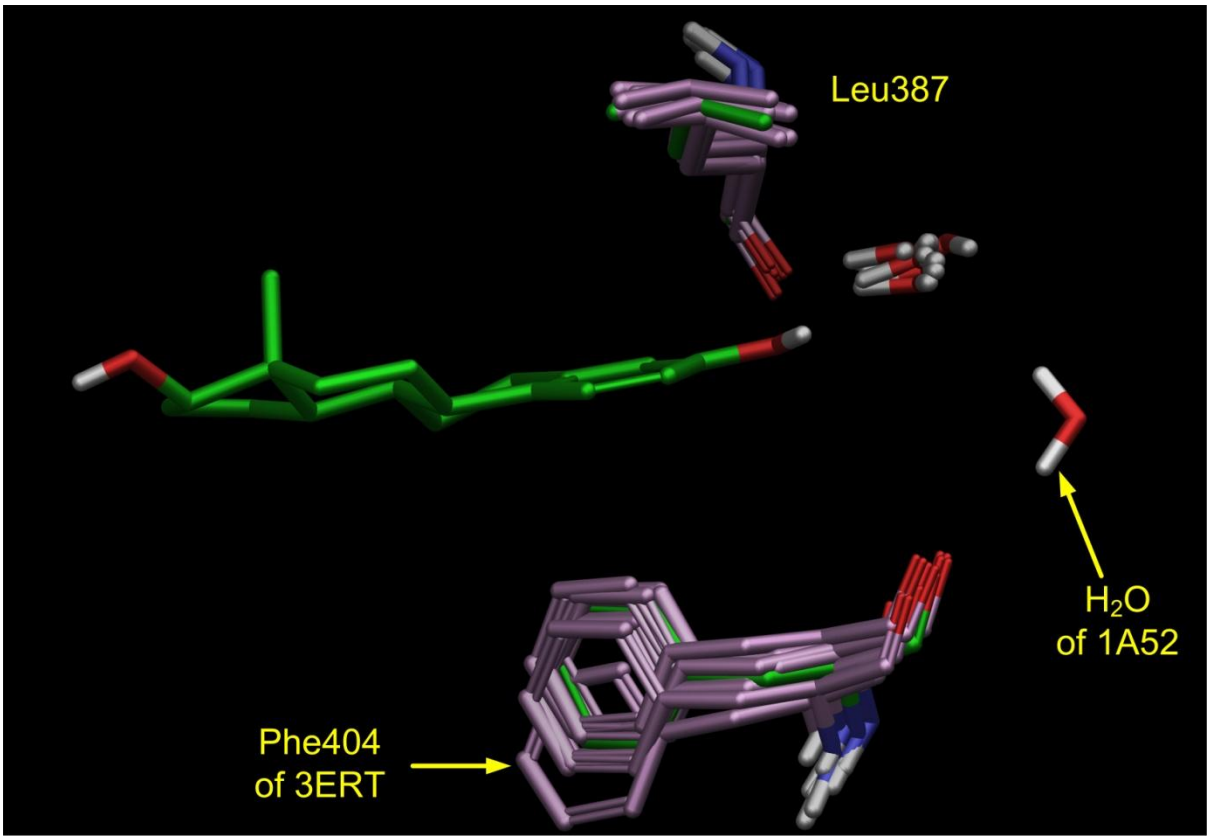

Figure 3.23. A-ring clamp. Note conservation of Leu387 and Phe404 positions in all of the hERα models, both agonist and antagonist conformations. The green residues and the position of E2 are from *1ERE*.

3.6.4 Modelling of EEs

RRD placed all of the EEs within the binding cavity of all models. The resulting poses had many common features. The A-ring clamp recognised the benzene ring of the ligand, regardless of whether it was phenolic (as in the parabens) or not (as in the phthalate monoesters). In all models except 3ERT, the orientation of the ligand benzene ring was coincident with that of the A-ring of E2. In 3ERT the clamp was displaced, allowing the

benzene ring to be inclined relative to that of E2. This positioning of the ligand by the benzene ring allowed the rest of the ligand structure different opportunities to interact with the binding cavity, depending on what parts it could reach.

In contrast, IFD did not dock all of the EEs in all of the models. TRIC and 4MBC were not docked in any of the models. Although these ligands had a benzene ring that could be captured by the A-ring clamp, other features of these ligands including Cl atoms (TRIC) and large bulky hydrophobic substituents (4MBC) resulted in poor interactions with the balance of the binding cavity. The inability to dock TRIC is not surprising given the conflicting estrogenicity data presented in Section 2.7.1.2. 4MBC is estrogenic as indicated in Chapter 2 and does have a published binding energy (Table 3.3). Also, mTRIC was docked only in the α and β antagonist models.

The EEs were grouped according to type of interactions with the binding cavity. The group 1 ligands had sufficient length (>10 Å) and a second hydroxyl functionality to potentially interact with the binding cavity in an E2-like way. Group 1 included the phytoestrogens (COUM, DAID and EQ) and the other steroid ligands (E1, E3 and EE2). These ligands were similarly docked by both RRD and IFD. The phytoestrogens COUM, DAID and EQ are planar molecules of similar structure to GEN and it was not surprising that they were docked in similar positions to GEN. The same was true of the steroid ligands. Their poses were the same as E2. The group 1 ligands are rigid in comparison to the other EEs, with at most, one rotational degree of freedom (DAID, EQ) and are most 'estrogen-like'. The phytoestrogens resulted in dihedral angles in the range of 17.5-18.4, greater than that of GEN (16.5). The steroid ligands had dihedral angles in the range 17.7-19.4, less than the angle of E2 (21.1). The poses for the group 1 compounds obtained with 1ERE are shown in Figure 3.24. Analogous poses for these ligands were obtained in the other models. For the steroid ligands, only one distinct pose was obtained. For the phytoestrogens, both RRD and IFD often returned more than one distinct energy-equivalent pose. These additional poses were backwards or upside-down compared to the first pose, but lying in the same plane. These multiple poses are a direct result of the ligands not having features similar to the steroids (i.e. the 13-CH_3 and both hydroxyl groups are phenolic) to introduce asymmetry to the molecule and to determine a single, best fit position within the binding cavity.

The 13-CH_3 of E2 also positions Leu525/476 to stabilise the α-helix structure of H11. The co-operation between His524/475 and Leu525/476 influences the position of Met528/479,

further stabilising H11. If His524/475 is allowed to hinge open, Leu525/476 can collapse into the binding cavity, pulling Met528/479 with it and disrupting the α-helix structure of H11 as shown in Figure 3.25. This feature was also illustrated earlier as the rotation of the binding site (Figure 3.17). Note that none of the group 1 ligands allows the collapse of Leu525/476.

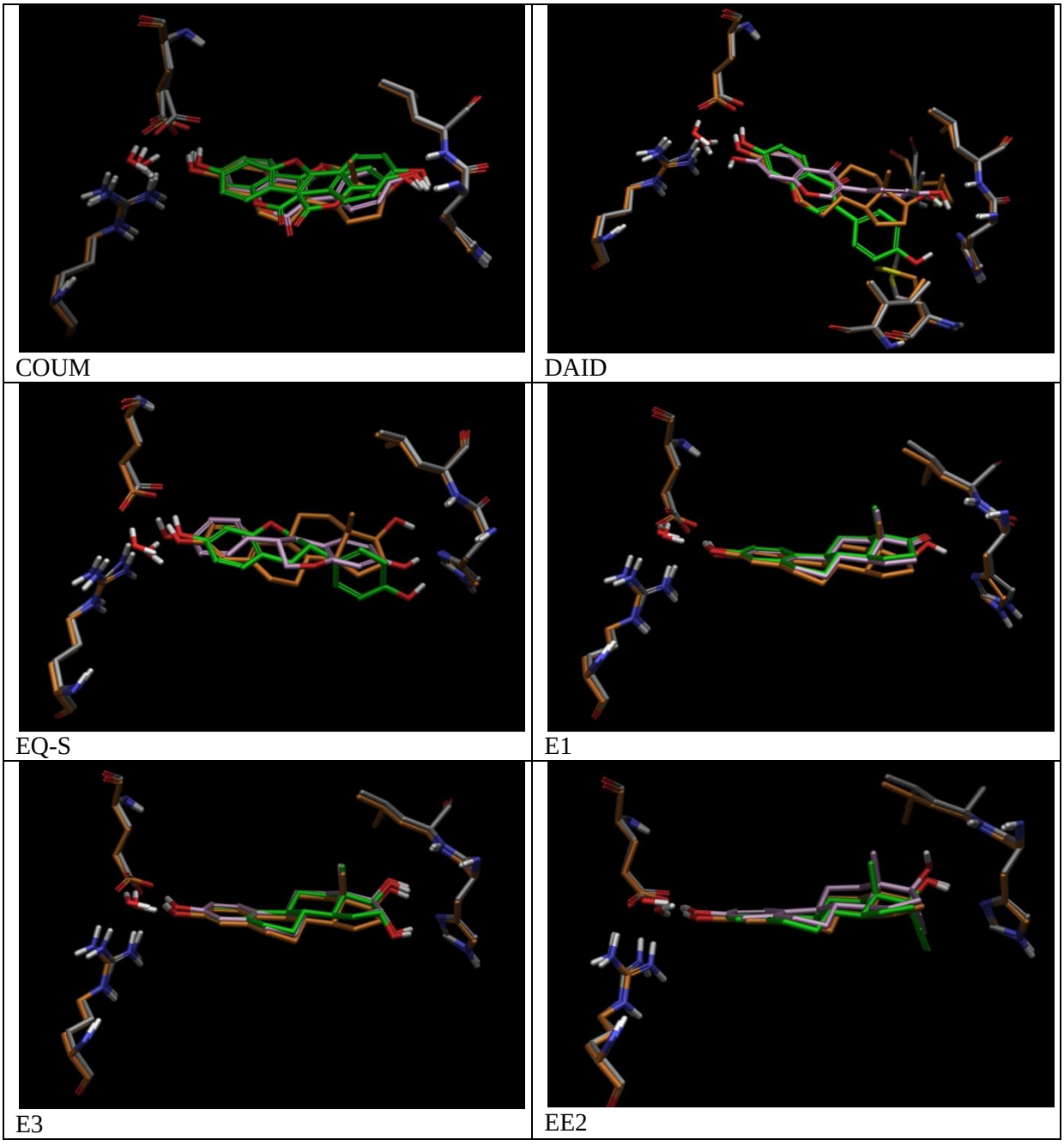

Figure 3.24. RRD (pink) and IFD (green) poses for group 1 ligands obtained with model 1ERE. E2 (orange) is shown in each image for comparison. Residues in orange are from the model and apply to the RRD pose. Residues shown grey show the position refinement obtained with IFD. Note for E1, E3 and EE2 the RRD and IFD ligand poses are nearly identical. For COUM, GEN, DAID and EQ multiple poses are observed.

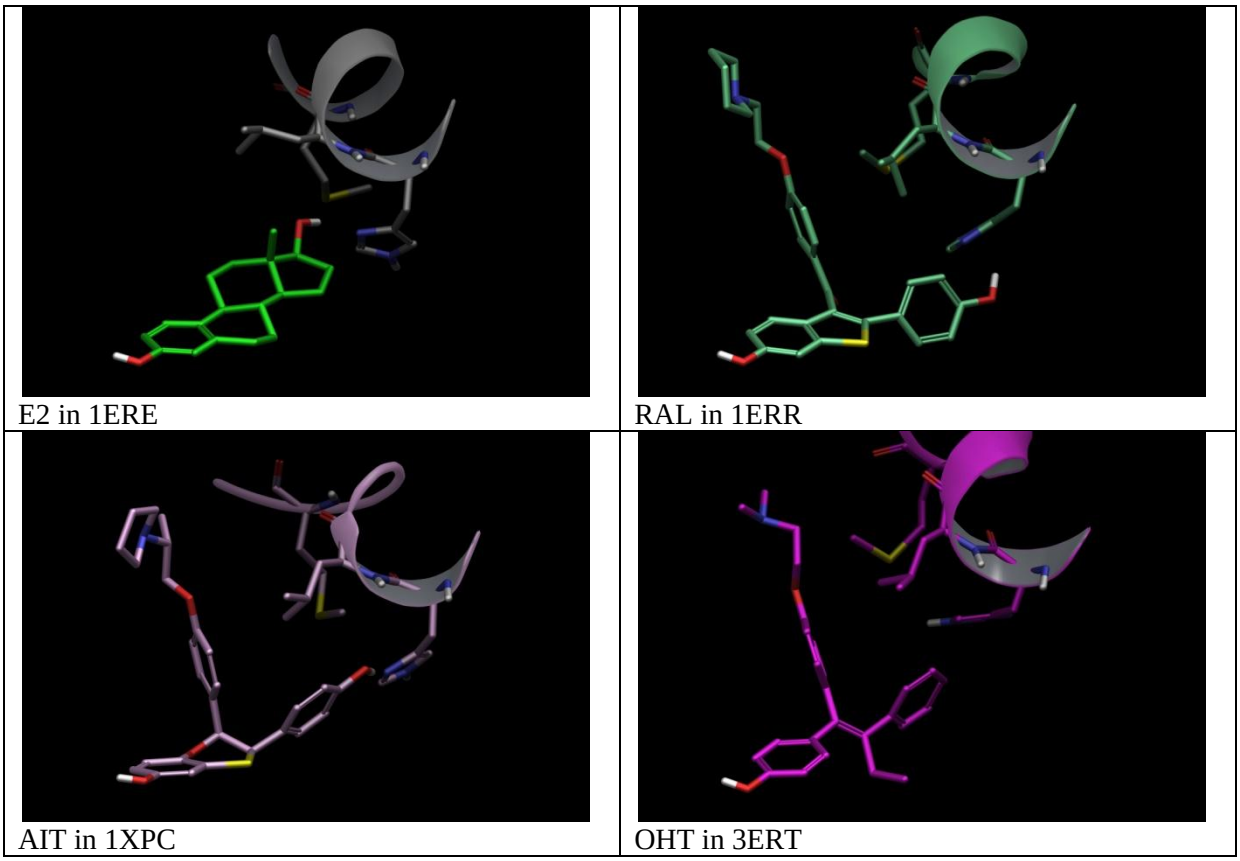

Figure 3.25. Co-operation of His524 and Leu525, acting as a swinging gate to influence the position of Met528 in response to an agonist ligand (E2) and three different antagonist ligands (RAL, AIT and OHT). Note how RAL, AIT and OHT have allowed Leu to collapse into the binding cavity.

The ligands of the second group have a biphenyl-like structure, with 2 degrees of rotational freedom around the central atom (C or O). These ligands generally had more energy equivalent poses, but only 1-3 distinct poses. When free in solution, these ligands are not planar. They adopt various conformations that minimise interactions between the opposing benzene rings, as illustrated with BPA and BP-1 in Figure 3.26. The common feature of this group of ligands is that except for 4OH-3PBOH, they do not span the binding cavity in an E2-like pose. The ligands are captured by the A-ring clamp but the second benzene ring is either oriented up the entrance channel, interacting with Thr347/299 as shown for BPA in Figure 3.27, or oriented downward into the binding cavity as shown for BP-3 in Figure 3.27. These ligands are not large enough to act as a wedge like RAL or OHT, but they are oriented in a similar fashion as shown in Figure 3.27. This orientation leaves His524/475 free to find a stable orientation independent of the ligand. The dihedral angles for these ligands range from 16.0 to 21.1, indicating agonist behaviour.

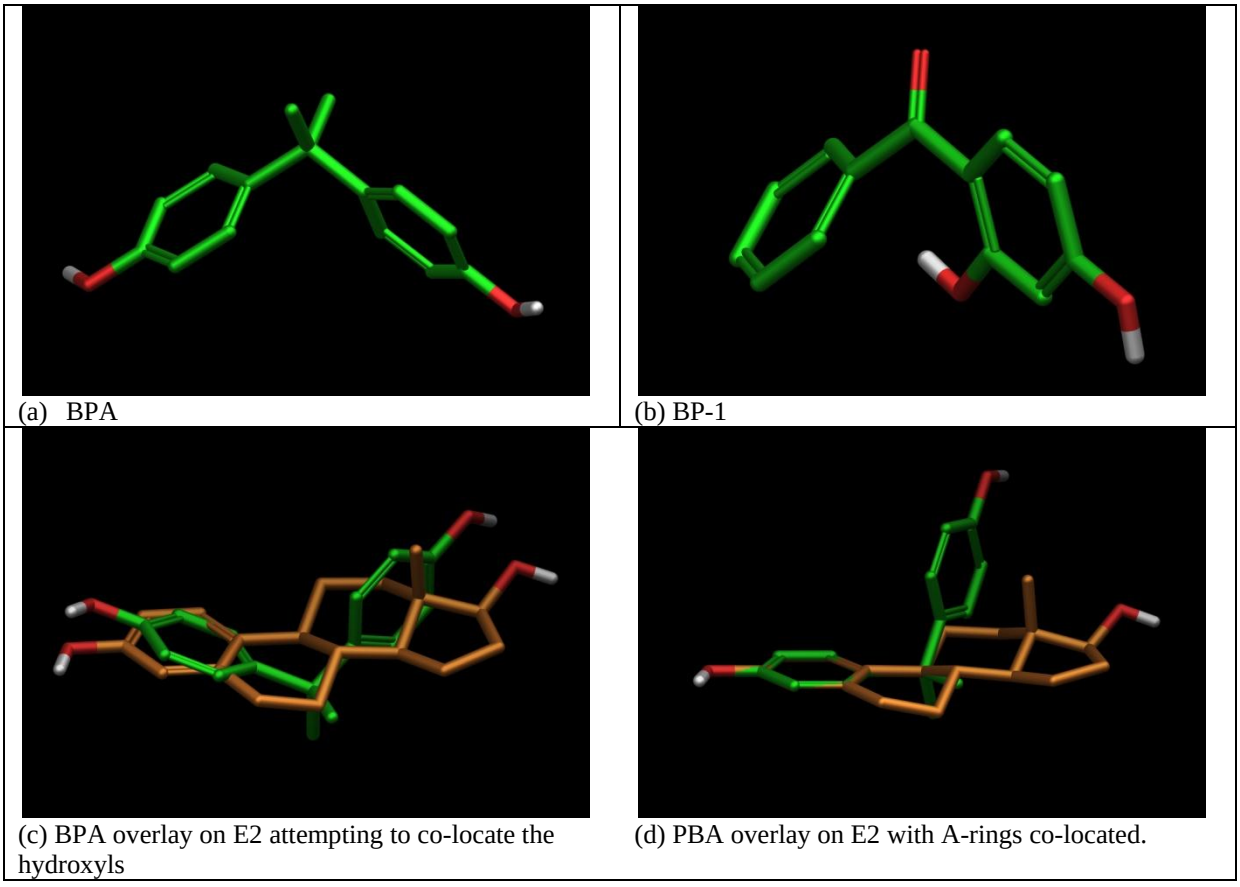

(a) BPA (b) BP-1

(c) BPA overlay on E2 attempting to co-locate the hydroxyls (d) PBA overlay on E2 with A-rings co-located.

Figure 3.26. Energy-minimised conformations of BPA and BP-1 as free ligands in aqueous solution. BPA is also shown overlaid on E2 (shown in orange), contrasting the positions of BPA when attempting to co-locate the hydroxyls with those of E2 and co-locating the A-rings of BPA and E2.

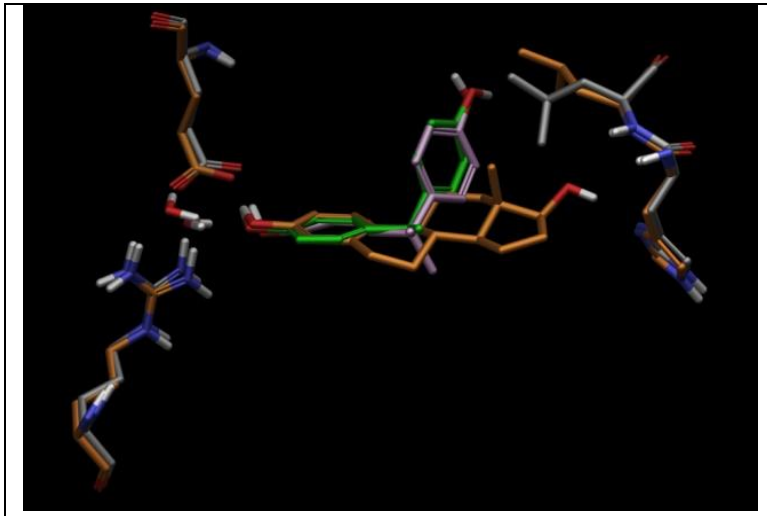

BPA

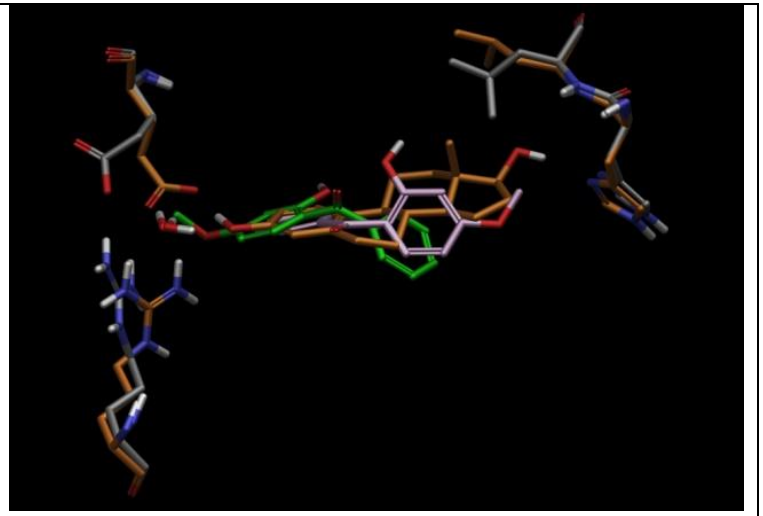

BP-3

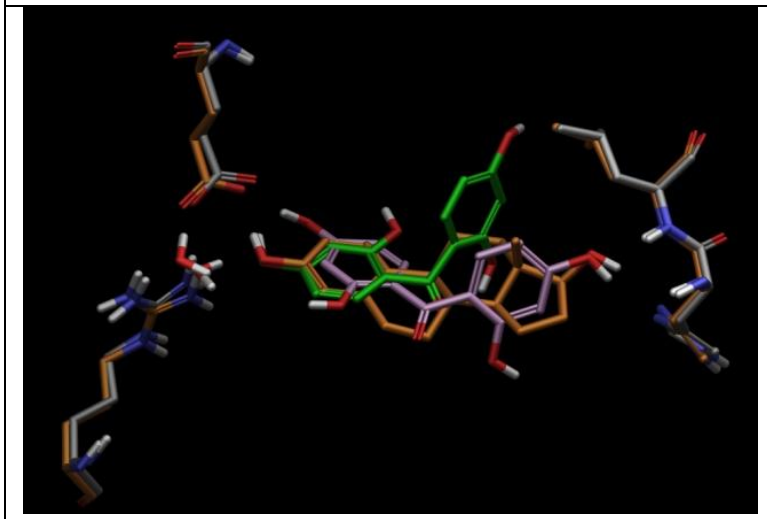

BP-2

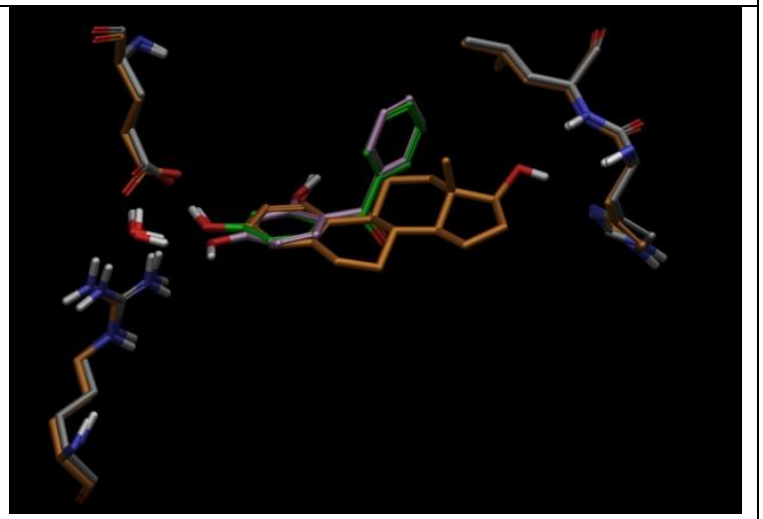

BP-1

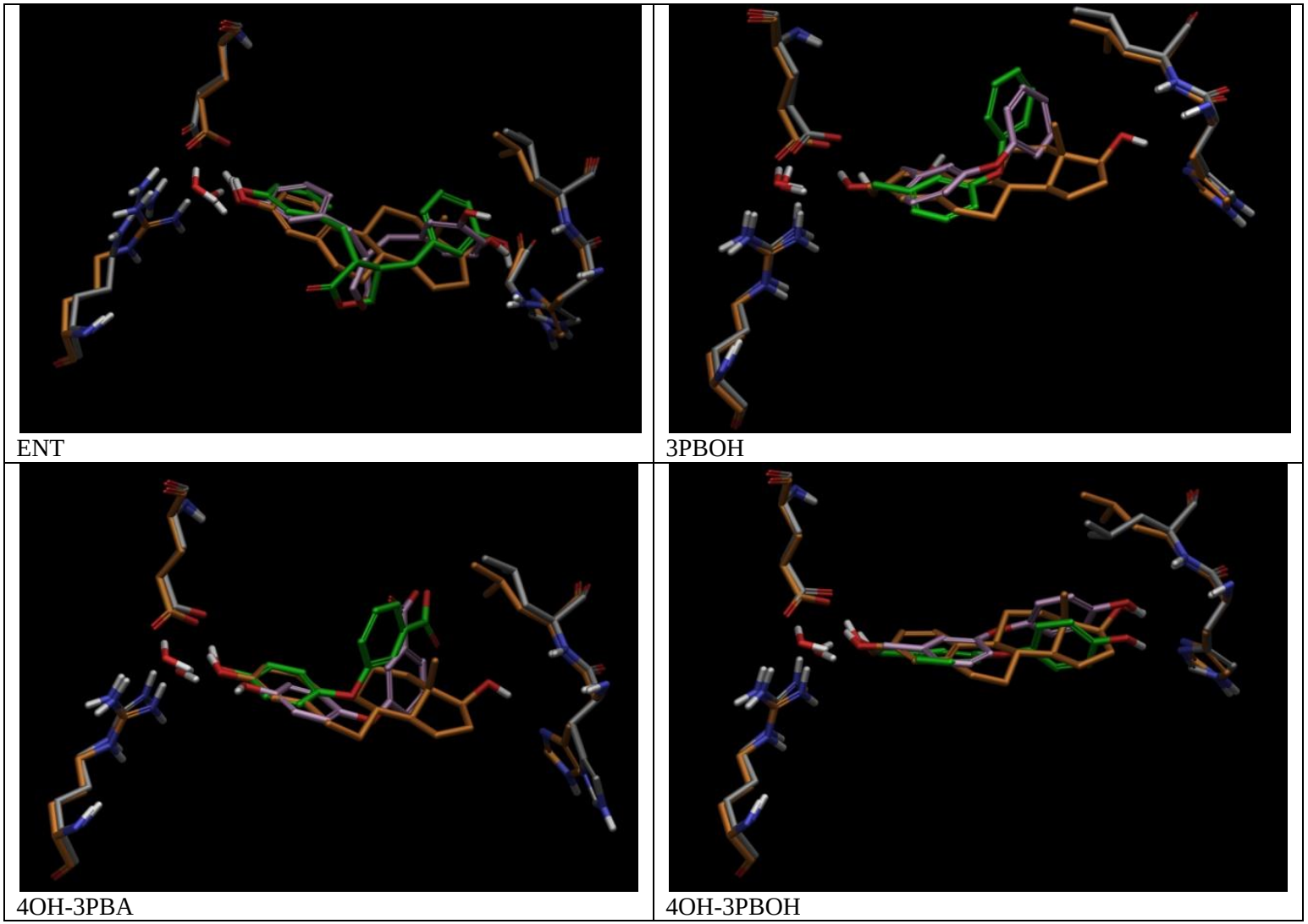

Figure 3.27. RRD (pink) and IFD (green) poses for group 2 ligands obtained with model 1ERE. E2 (orange) is shown in each image for comparison. Residues in orange are from the model and apply to the RRD pose. Residues shown grey show the position refinement obtained with IFD.

The poses obtained for 3PBOH in 1ERE and 1ERR, shown in Figure 3.28, are typical of the multiple energy-equivalent poses obtained for all of the EEs. The difference in binding energy between the most favourable (green) and least favourable (purple) of the three poses in 1ERE is 2.25 kJ/mol. The dihedral angle varies from 14.5 (green) to 20.6 (light blue) to 20.9 (purple), all less than the angle with E2. For the two poses obtained with 1ERR, the difference in binding energy is only 1.1 kJ/mol and the dihedral angle decreases from 33.1 (green) to 26.9 (purple), becoming more agonist-like.

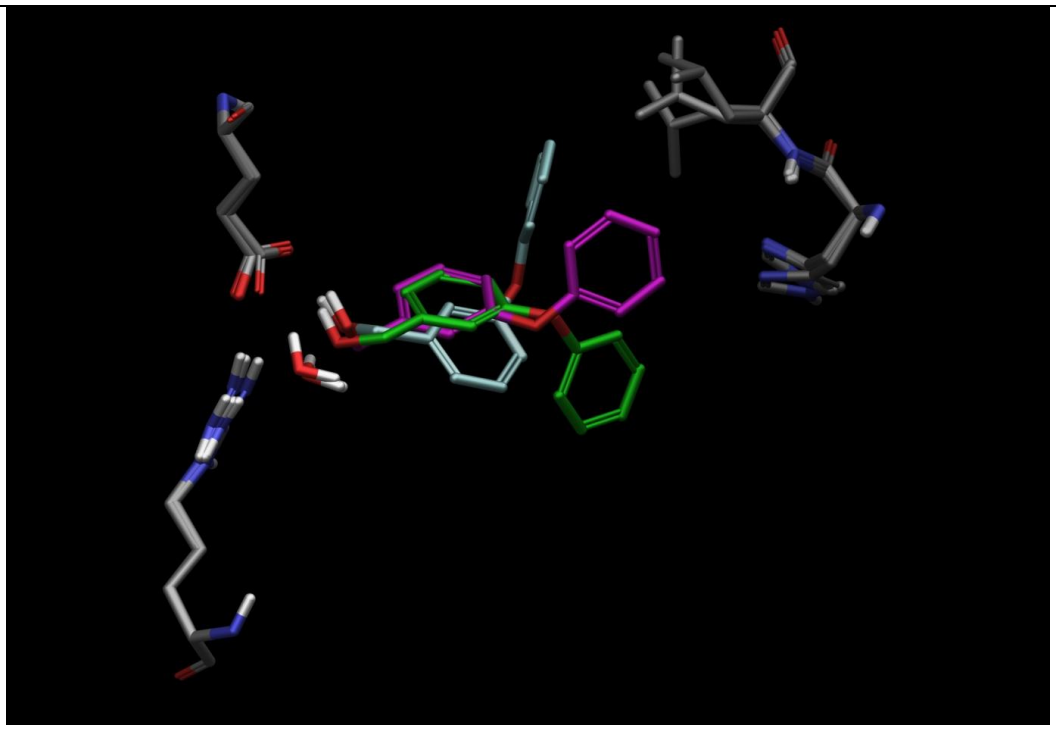

(a) 3PBOH in 1ERE. The difference in binding energy between the most favourable (green) and least favourable (purple) of the three poses is 2.25 kJ/mol. The dihedral angle varies from 14.5 (green) to 20.6 (light blue) to 20.9 (purple).

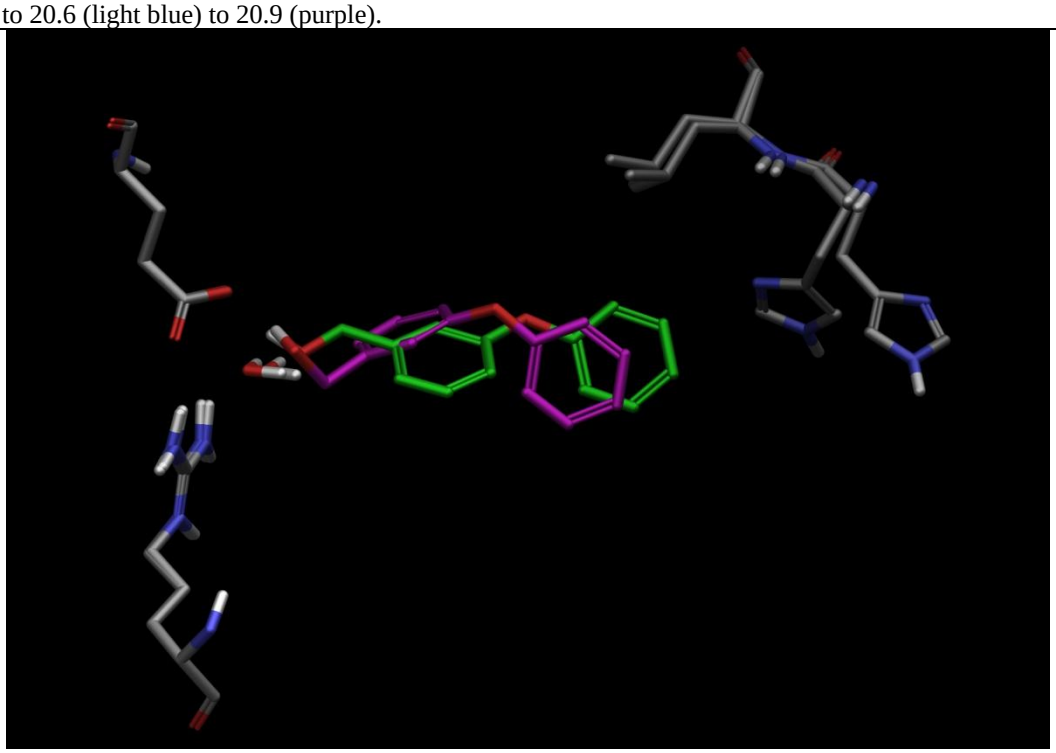

(b) 3PBOH in 1ERR. The difference in binding energy between the most favourable (green) and least favourable (purple) of the two poses is 1.1 kJ/mol. The dihedral angle varies from 33.1 (green) to 26.9 (purple).

Figure 3.28. Multiple distinct energy-equivalent poses obtained for 3PBOH in 1ERE and 1ERR .

The third group of ligands are described as mono-phenolic. They have a single phenolic functionality with a mainly aliphatic tail. All of these ligands are captured by the A-ring clamp and the phenolic ring occupies a position analogous to the A-ring of E2. The smallest of the ligands, 4HBA, is able to rotate by 60° either left or right of the standard E2 orientation as shown in Figure 3.29, because its tails is not long enough to interact with the central part of the binding cavity to maintain the E2-like orientation. Two of the metabolites of NP have terminal aliphatic hydroxyl groups. For NP-M1 and NP-M2, RRD has the aliphatic hydroxyls interacting with His524/475 while IFD shows a variety of other interactions, including NP-M2 oriented backwards with the aliphatic hydroxyl interacting with the Glu/Arg pair and the phenolic ring oriented similar to BPA. The terminal aliphatic carboxylate functional group of NP-M3 is centred within the binding cavity, not interacting with any residues because of its charge. The parabens all occupy similar positions, with the tail following the general trajectory seen with NP. The dihedral angles are smallest for NP and NP-M1 at 8.6 and 11.5 respectively. These two poses also have His524 in a position similar to 2B23. All other ligands have dihedral angles between 16.9 and 20.7 and have His524 in an E2-compatible position. It is not apparent what causes His to take up a position like the apo model with some ligands and not others.

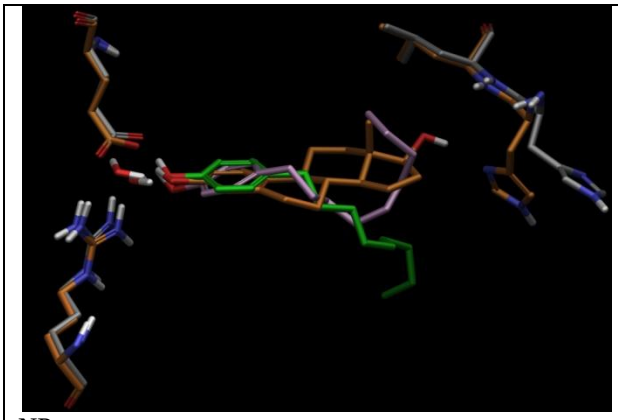

NP

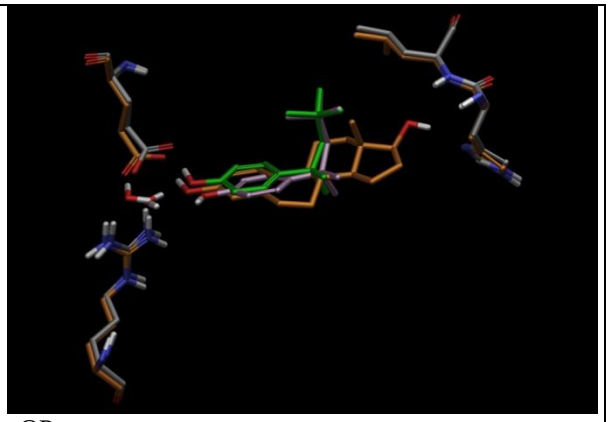

t-OP

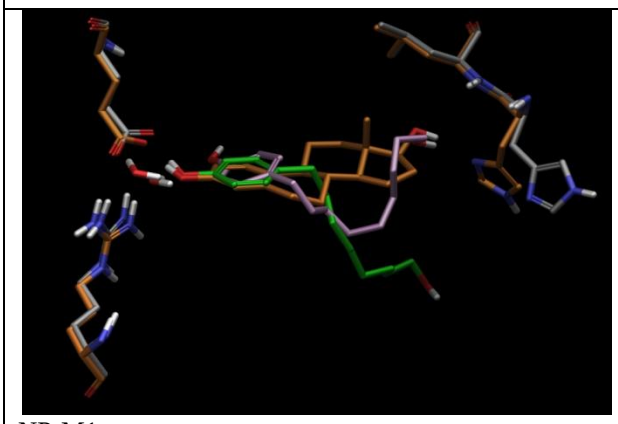

NP-M1

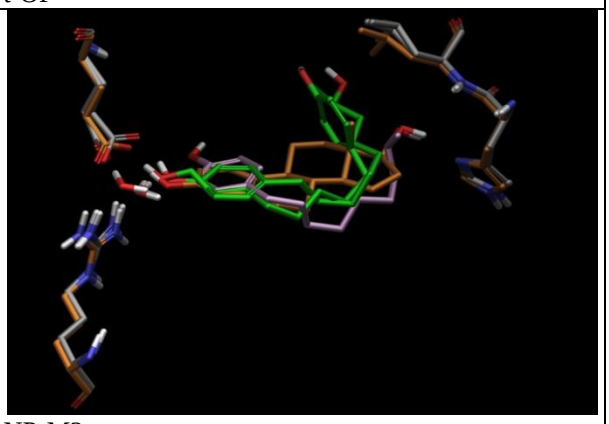

NP-M2

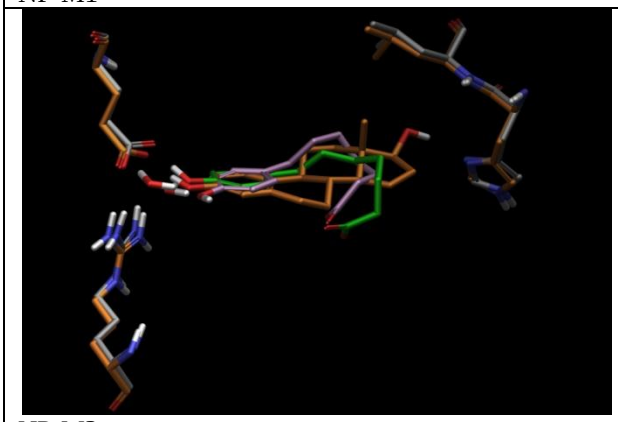

NP-M3

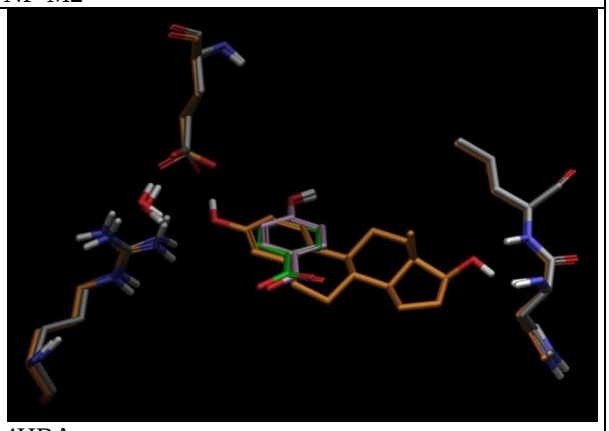

4HBA

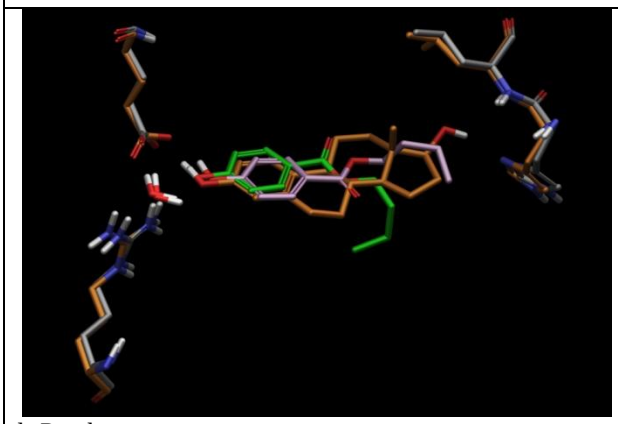

b-Paraben

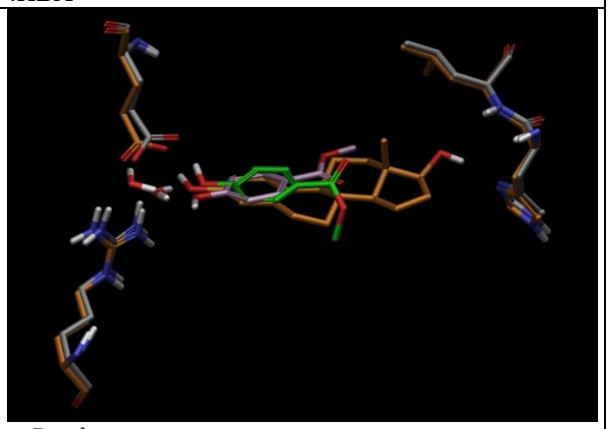

m-Paraben

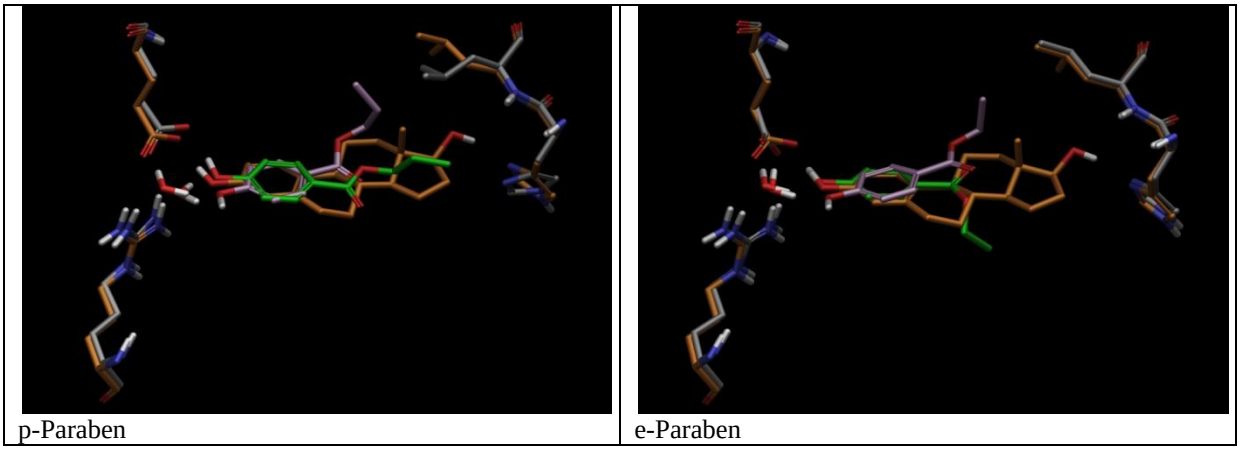

Figure 3.29. RRD (pink) and IFD (green) poses for group 3 ligands obtained with model 1ERE. E2 (orange) is shown in each image for comparison. Residues in orange are from the model and apply to the RRD pose. Residues shown grey show the position refinement obtained with IFD.

The fourth and last group of ligands are described as non-phenolic. They have a benzene ring but no E2-like phenolic hydroxyl. These ligands behave in one of two ways. Either they are captured by the A-ring clamp with the carboxylate interacting with the ARG residue and with the aliphatic tail occupying the central region of the binding cavity; or the benzene ring takes a position similar to the second BPA ring and is oriented up the binding channel with the carboxylate pointing into the centre of the binding cavity. None of the phthalate monoesters had published binding energies and the estrogenicity assays indicated very little if any activity. The calculated binding energies for these compounds indicated moderate affinity, of the same order as BPA and NP ($\Delta G_{bind} \approx$ -40 kJ/mol).

3.6.5 Comparison with Published Docking Studies

Given the importance of the hER in breast cancer, one might expect a large body of computational docking literature. In fact, there is little in the literature for comparison. This could be a result of the proprietary nature of the search for drugs to treat breast cancer. Most of what has been published on docking with hER is in relation to QSAR validation studies where docking has been used to explain or justify predicted binding affinity of drug targets and to evaluate predicted biological activity parameters [279, 310-313]. In all of these studies, only rigid receptor docking was used and the interactions described are in relation to designing a drug target with an effective 'wedge'.

A few studies have considered EEs (e.g. polychlorinated biphenyls [271], COUM [314] and two obscure phytoestrogens [315]). All of these studies used only rigid receptor docking and the focus was calculation of binding energies.

With the docking of PCBs [271], the authors report multiple energy equivalent poses for these flexible ligands. However, these ligands are highly hydrophobic and do not possess a phenolic hydroxyl so do not interact with the ER in an E2-like way, but are instead confined to the highly hydrophobic, large volume space in the centre of the binding cavity.

The docking of COUM [314] also shows multiple positions of the ligand in the binding site, similar to that reported in this work.

Two studies attempt to use docking to identify potential agonist/antagonist behaviour of EEs have been reported.

In the first study [316], the authors use rigid docking to calculate the binding energies of 4NP, 4t-OP and BPA in both agonist and antagonist models and use the difference in calculated binding energies to predict agonist/antagonist behaviour. For these three ligands, they predict agonist behaviour which is consistent with results of biological assays and with the present study. However, it is not clear how they were able to get rigid docking to successfully dock RAL and OHT into the model for 1ERE. This study did not examine the interaction of these ligands with the receptor.

In the second study on polybrominated diphenyl ethers [270], the authors examined the poses obtained by docking these ligands into 4 rigid receptor models. They classified the ligand as an antagonist if more than 50% of the 20 lowest energy poses obtained from the aggregate set of all 4 models demonstrated antagonist features such as the ligand extending up the entrance of the binding cavity. The authors used only antagonist conformation models for this study so it is not known whether the ligands would prefer this 'antagonist-like' pose in an agonist model and could potentially disrupt the agonist conformation.

3.7 Conclusions

The RRD validation study using multiple receptor models demonstrates that the models and software are able to correctly place the ligand in the receptor binding site and correctly predict the corresponding binding energy. This was done in 3 stages: docking the co-crystallised ligand in its native model, cross-docking co-crystallised ligands in the other

models, and docking ligands for which experimental binding energies are available but not crystal structures. Success in all three of these stages strongly supports the credibility of the binding modes and calculated binding energies produced for those ligand-receptor complexes without experimental data. This success also gives confidence that the receptor models are valid for use in modelling receptor flexibility.

The IFD validation study followed the same structure as the RRD validation study and similarly demonstrated that the models and software were able to correctly place the ligand in the receptor binding site and correctly predict the corresponding binding energy at all three stages. This success gives confidence that the predictions of ligand position within the binding site and the calculated binding energies are plausible for the EEs of interest.

The details of the interactions of co-crystallised ligands and the EEs with the binding site were examined and several features were identified that appear to be important and diagnostic in determining whether a ligand will bind with the receptor and whether it will induce the agonist or antagonist conformation of the receptor. First, the positions of the residues 'A-ring' end of the binding cavity described as the 'A-ring anchor' (Figure 3.8) and 'A-ring clamp' (Figure 3.23) are highly conserved among agonist and antagonist conformations of the receptor models with the co-crystallised ligands docked and remain so with the docking of the EEs. This feature recognises the phenolic hydroxyl functionality of the ligand and affects a 'capture' of the ligand in the binding cavity. Second, the 'D-ring' end of the binding cavity (Figure 3.8) is much more responsive to the ligand, provided the ligand is able to engage this end of the binding cavity through a hydrogen bond with the His residue. Third, the interaction (or lack thereof) of the ligand with the His residue propagates back up the protein backbone to cause a disruption between the His and Leu residues which appears to be indicative of the eventual uncoiling of H11 to allow H12 attain the antagonist position covering the AF-2 cofactor binding site. For all agonist models of both hERα and hERβ, the backbone carbonyls have highly conserved positions (Figure 3.19) and a well defined dihedral angle. In contrast, the disruption caused by antagonists leads to an opening of this angle (Figure 3.20 and Figure 3.21) and the disruption is much larger for hERβ than for hERα. This is clearly demonstrated by the measured angles for GEN in hERβ, where in the agonist conformation, the angle is larger than that of E2 (indicating potential antagonist behaviour) and this crystal structure could only be produced by co-crystallising with a peptide designed to mimic the binding of a coregulatory protein in the AF-2 site, preventing

H12 from occupying the site. When hERβ is bound with GEN and crystallised without a coregulatory peptide, the conformation obtained is the antagonist. This is in contrast to GEN in hERα where only the agonist conformation is obtained and the angle obtained is smaller than that for E2 suggesting agonist behaviour.

The IFD results also indicate that when E2 is docked, the dihedral angle converges to a specific value regardless of whether the agonist or antagonist models were used in docking. This demonstrates that there is sufficient flexibility modelled by the IFD approach for the receptor to respond to ligand influences if they exist.

For EEs that most closely resemble the endogenous steroids (Group 1 ligands, Section 3.6.4) even though multiple positions of the ligand within the binding cavity were obtained, they produced the same binding site residue positions as those obtained with E2 and angles less than that of E2 suggesting agonist behaviour.

For EEs that have a biphenyl structure, and for some ligands two hydroxyl groups to potentially interact with both ends of the binding cavity (Group 2 ligands, Section 3.6.4), multiple energy equivalent poses were obtained. These poses resulted in different binding site residue positions from those obtained with E2 and angles less than that of E2 suggesting agonist behaviour. The poses for these ligands indicated they did not engage with the His residue, leaving the D-ring end of the binding site to find a low energy conformation that was not directly influenced by the ligand. As a result, the receptor-ligand complex may be more vulnerable to the external influence of the suite of cofactors present in the particular cell type. This vulnerability is increased with the Group 3 and Group 4 ligands which have progressively more flexibility less ability to directly interact with the D-ring end of the binding cavity. All of the Group 3 and 4 ligands resulted in angles narrower than that for E2, suggesting agonist behaviour. None of the EEs studied demonstrated an ability to open the dihedral angle beyond that for E2 and to suggest antagonist behaviour.

In summary, ligand flexibility reduces the ability of the ligand to stabilise the RL-complex conformation. The RL-complex can be described as ‘floppy’ or pliable as indicated by the large variation in dihedral angles measured for the ligands. Also indicative of the lack of constraint of the RL-complex are the multiple, distinct energy-equivalent complexes proposed by the docking study. These pliable RL-complexes can be influenced by the population of coregulatory proteins present in the target cell. The biological response that is

obtained is therefore a function of both the ligand and the cell context. In addition, flexible ligands can form multiple distinct energy equivalent RL-complexes. Each RL-complex potentially leads to the selection of different genes that are transcribed in a given cell type because a different selection of coregulatory proteins may be recruited.

The flexibility of the ligands and their ability to produce pliable receptor-ligand complexes may explain why exposure to a single compound produces different effects in males and females and produces different effects depending on when during development or life stage the exposure occurs. The adverse effects attributed to fetal exposure (e.g. abnormalities in male genitalia or precocious puberty in females) are very different to those attributed to adult exposure (e.g. reduced fertility, susceptibility to hormone responsive cancers), but it cannot be ruled out that the effects seen in adults do not have a root in fetal exposure.

To further investigate the hypothesis of multiple, distinct, energy equivalent hER-EE complexes, the studies reported in the literature that characterised the behaviour of OHT and RAL in different cell contexts could be undertaken with selected EEs. In particular, the results from such studies obtained for GEN, BPA and NP would be most illuminating, as these ligands represent various points on the spectrum of ligand flexibility.

Chapter 4 Analytical Method Development

4.1 Introduction

The objective of this part of the study was to develop and validate a sample extraction and analysis method for the quantification of EEs in human urine and amniotic fluid. Both gas chromatography-mass spectrometry (GC-MS) and liquid chromatography-mass spectrometry (LC-MS) have the required sensitivity and specificity for the task. While LC-MS has the benefit of not requiring derivatisation, sample-to-sample differences in matrix composition can lead to ionisation suppression and/or enhancement, potentially hindering quantification. GC-MS was chosen because instrumentation was available.

Previous studies of EEs in human fluids (urine, serum and amniotic fluid) have addressed subsets of the target analyte list of this study: phytoestrogens [144, 148-150, 317], phenols only [141, 318, 319], parabens only [320], phenols and parabens [140, 321], benzophenones [322], phthalate monoesters [142, 145, 146, 323]. Even for the reports of multiple subsets of EEs, the analyses were done with separate methods [324]. Of these 16 studies, only 5 used GC-MS and determined phytoestrogens [148-150] and phenols [141, 318]. The remaining studies used LC-MS (for BPA only [319]) or LC-MS/MS.

The target analytes are challenging to determine by GC-MS because they are relatively polar with hydroxyl and/or carboxylic acid functional groups. Because of their ability to form intermolecular hydrogen bonds, these analytes have low volatility. The active hydrogen atom also makes these compounds prone to adsorption onto glass and metal surfaces within the instrument, leading to poor chromatographic peak shape (tailing). In addition, the biological matrix of urine and amniotic fluid poses a challenge with high concentrations of organic acids, amines and sugars. The extraction conditions and cleanup procedures used to achieve very clean extracts of biological samples for a subset of compounds (e.g. steroids and other phenols) will remove the organic acid target analytes. Finally, the small volume of sample requires sensitivity in the ppb range, despite these challenges. Based on the literature reports of EEs in human urine and amniotic fluid presented in Chapter 1, the method will need to have an instrument detection limit less than 2 ng/mL and a method detection limit less than 1 ng/mL after accounting for the sample concentration factor.

4.2 Theoretical Basis

4.2.1 Sample Preparation by Solid Phase Extraction

Solid phase extraction (SPE) is a technique used to isolate and concentrate compounds of interest from a sample. In this case, SPE is used to separate the organic analytes from an aqueous matrix containing inorganic salts and protein. The analytes are retained on the solid adsorbent as the sample flows over the adsorbent. The retained organic analytes are then eluted into an organic solvent for analysis. The adsorbent is packed into a bed sandwiched between two frits in a syringe barrel and a vacuum is used to draw the sample through the cartridge at a constant flow rate. The typical experimental setup is shown in Figure 4.1.

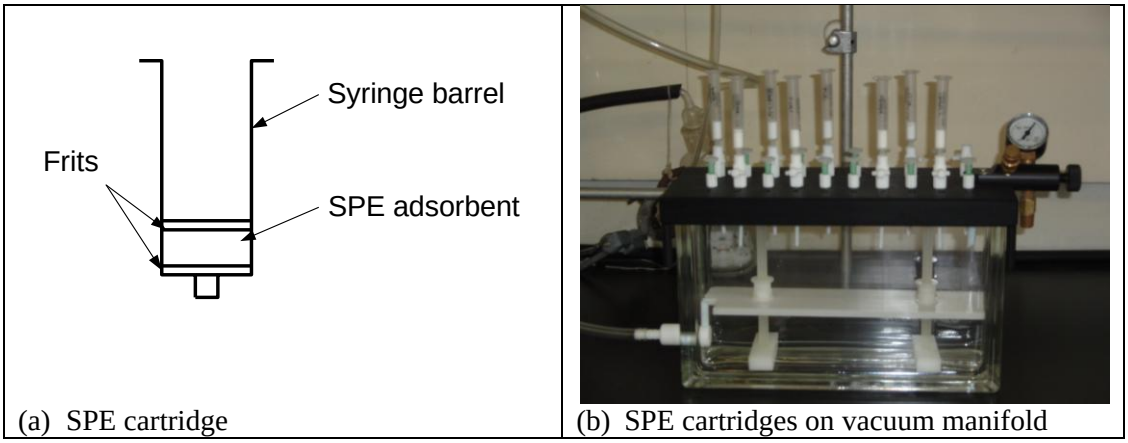

(a) SPE cartridge (b) SPE cartridges on vacuum manifold

Figure 4.1. A typical solid phase extraction (SPE) experimental setup.

Waters Oasis HLB SPE cartridges were used for this work. The adsorbent is a hydrophilic-lipophilic balanced copolymer of divinylbenzene and N-vinylpyrrolidone [325]. The advantages of this material over traditional coated silica phases include no undesirable silanol activity, broader operational pH range, lower breakthrough of polar compounds and improved recoveries of hydrophobic compounds. This material is also tolerant to the bed going dry during the extraction process, making them much easier to use.

4.2.2 Analytical Derivatisation

The reactive hydrogen atom of the hydroxyl and carboxylic acid functional groups must be derivatised for GC-MS analysis [326-329]. There are several different reagents that can be used for analytical derivatisation and some reagents work better for some target analytes than others [330]. The derivatisation strategy of choice for phenols and aromatic acids converts the hydroxyl group to a trimethylsilyl (TMS) ether and the carboxylic acid to a TMS ester as shown in Figure 4.2.

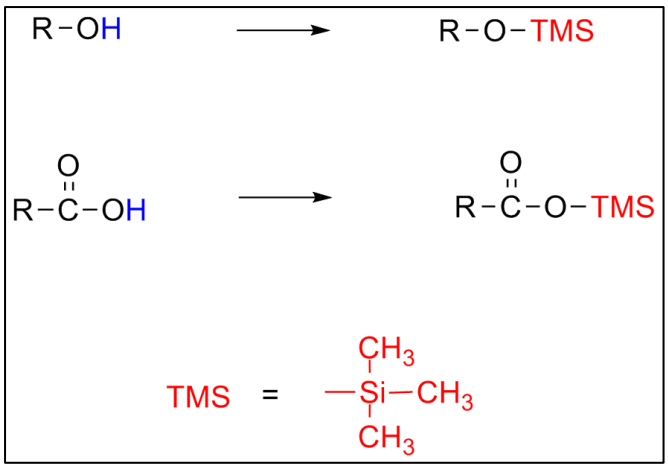

Figure 4.2. Derivatisation of hydroxyl and carboxylic acid functional groups to TMS ether and ester.

While TMS derivatives are more chemically and thermally stable and more volatile than other derivatives [330], they are moisture sensitive and can be readily hydrolysed on exposure to ambient air. The esters are more easily hydrolysed than the ethers [330]. Derivatisation reduces the polarity of the analyte and increases its volatility making GC separation easier, while at the same time, increasing the sensitivity of MS detection [326-329, 331]. The increase in molecular weight that results from derivatisation also moves the MS fragmentation pattern to higher m/z where there is less chance of matrix interference. However, because of its composition, a large fraction of the matrix for these samples will also be derivatised. Several of the target analytes have multiple active hydrogen atoms to derivatise. A few of the target analytes do not require derivatisation as they do not have active hydrogen atoms.

Analytical derivatisation requires optimisation of the reaction conditions (e.g. solvent, derivatisation reagent, catalyst, temperature, time) to ensure the analytes are reproducibly, if not fully derivatised and that undesired products (e.g. structural isomers, degradation products) are not formed. With the derivatisation of steroids, several derivatisation artifacts have been reported such as conversion of EE2 to E1 [332-336] and subsequent derivatisation of the enol form of keto-enol tautomers [337-340] that can then be derivatised. Partial derivatisation of multi-functional analytes can be acceptable if the level of derivatisation is reproducible, such as for GEN [341]. Derivatisation requires the removal of water from the extract and any alcohol solvent used in the extraction. Solvent evaporation must also minimise loss of volatile target analytes.

The reagent chosen for derivatisation was N,O-bis(trimethylsilyl)trifluoroacetamide (BSTFA, Figure 4.3). BSTFA has two main advantages over other reagents. First, the reaction by-products (Figure 4.3) are more volatile than the reaction by-products of other reagents. Second, the fluorine atoms result in less fouling by deposits of silica on heated surfaces such as the ion source. BSTFA is also able to act as its own solvent. BSTFA is strong silylating reagent and is able to derivatise even sterically hindered active hydrogen atoms, such as the 17β-OH of E2 and EE2.

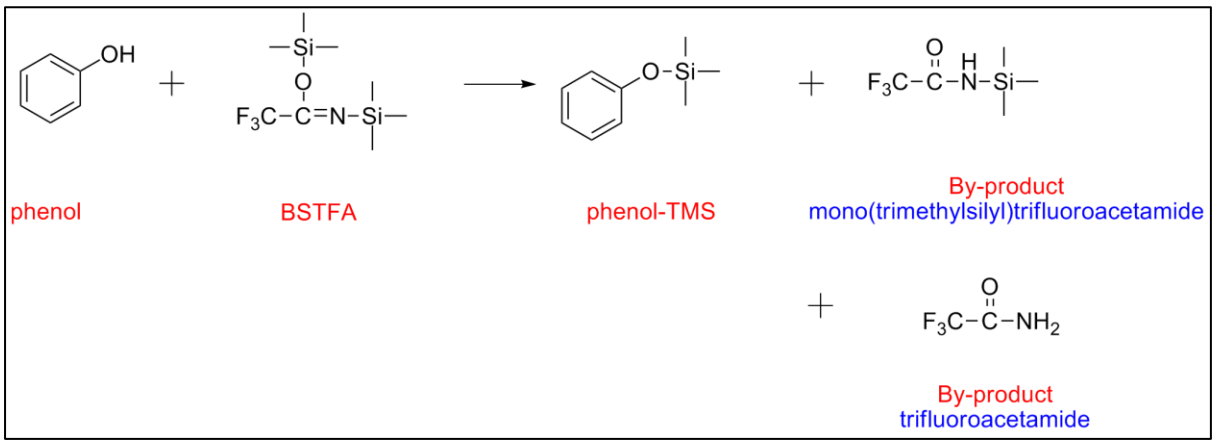

Figure 4.3. Reaction scheme for derivatisation of phenol by BSTFA.

Addition of a second component such as trimethylchlorosilane (TMCS, Figure 4.4(a)) or 1-(trimethylsilyl)imidazole (TMSI, Figure 4.4(b)) in concentrations ranging from 1% to 50% increases the strength of the derivatising reagent [330]. TMSI is advantageous in the current application because it does not react with aliphatic amines and is particularly useful in silylating hindered alcohols such as the 17β-OH of E2 and EE2 [330, 335].

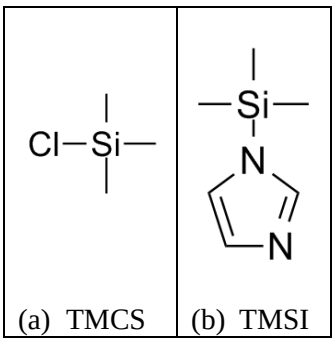

Figure 4.4. Reagents used to increase the derivatisation strength of BSTFA.

Analytical derivatisation can be accomplished using the reagent as solvent or with the addition of a co-solvent to either suppress undesired side reactions or enhance the desired reaction [338, 342, 343]. Three solvents are commonly evaluated: dimethylformamide (DMF), pyridine (PYR) and acetonitrile (ACN). PYR acts as an HCl acceptor and is particularly useful when TMCS is present in the reagent mixture. For BSTFA derivatisation, ACN has been used to prevent derivatisation of carbonyl steroids via keto-enol tautomerisation[338]. Because it is polar and aprotic, ACN can also increase the derivatising strength of the reagent or reagent mixture. Both DMF and PYR have been used to prevent breakdown of di-TMS-EE2 [334, 344] when BSTFA/TMCS mixtures are used. A reaction temperature above 40 °C for at least 30 minutes is normally required to achieve maximum derivatisation yield [338]. Higher temperatures, up to 100 °C and longer times are needed to derivatise more hindered and less reactive hydrogens.

More than 20 individual reports of analytical derivatisation with GC-MS analysis for the determination of phytoestrogens, phenols, steroids, and phthalates in a variety of biological, environmental and food matrices were reviewed. While no common approach was found, several themes were repeated. BSTFA alone did not give complete derivatisation of the target analytes. TMCS (1%) alone or with TMSI (2%) with BSTFA did result in complete derivatisation, especially if the compound had more than one reactive hydrogen and if the reactive hydrogen was sterically hindered. Reaction temperature and time on the order of 70 °C for at least 30 minutes were required. When TMCS was present, PYR was the solvent of choice to scavenge the HCl produced during the reaction. ACN was also advantageous, especially when TMCS was not present.

4.2.3 GC-MS Analysis

The analysis of a sample by GC-MS requires rapid and complete vaporisation of the sample as it is injected onto the GC column. Separation of the components occurs based on differential distribution of the components between the mobile phase (helium carrier gas) and the stationary phase coated on the inside of the column. The components with the highest volatility and that are least able to interact with the stationary phase elute earlier than those of lower volatility and with a higher preference for interacting with the stationary phase. The column is located in an oven that is heated, and the temperature is increased during the analysis to both sharpen the later eluting peaks and to reduce analysis time. Detection by MS can be done in either SCAN or SIM mode. In SCAN mode, a range of mass to charge ratio

(m/z) is scanned providing the complete mass spectrum as each peak elutes from the column. In SIM mode, selected ions (m/z) are monitored. The advantage of SIM mode over SCAN mode is a large increase in sensitivity because only m/z of interest are monitored. This increase in sensitivity is achieved at the expense of obtaining qualitative information that can be used to identify unknowns. The analysis of ppb level components requires the use of SIM mode.

4.2.4 Principles of Analytical Method Validation

With complex matrices such as biological fluids, the analysis of ppb level components requires careful validation of the sample preparation and instrumental analysis methods [345]. The purpose of validation is to ensure the signal attributed to a particular target analyte is due to the presence of that analyte and to nothing else, that the correct result is reported and that the method is reproducible from one day to the next over normal operational conditions [346, 347]. Method validation usually begins with the instrumental analysis and analysis of standards. Once a robust analysis method is available, validation then is then able to consider the sample preparation steps. Method validation also provides an opportunity to quantify the performance criteria of the method. Performance criteria typically include accuracy, precision, reproducibility, selectivity, sensitivity, stability, extraction efficiency and quantification range [345].

Accuracy and precision are fundamental to validation. Accuracy is how close to the 'correct' or true value the analysis result is. Precision is the measure of analysis variability in achieving the correct result on repeated attempts. Accuracy is quantified by the % relative error (%RE) which is defined as the absolute value of the difference between analysis result and target concentration, expressed as a percentage of target concentration. Precision is quantified by the % relative standard deviation (%RSD) of repeated analyses. %RSD is defined as the ratio of the standard deviation to the mean of the analysis result expressed as a percentage. Accuracy and precision are usually determined at the instrumental analysis level by repeated analysis of standards of known composition. Three standards spanning the calibrated range are normally used to assess accuracy and precision.

Variability increases as the concentration of the analyte approaches the limit of detection (LOD) [347]. Guidelines for acceptable limits of analysis accuracy and variability as a function of analyte concentration are given in Table 4.1.

Table 4.1. Guidelines for acceptable levels of analysis variability and % recovery as a function of analyte concentration [345, 347].

Analyte Concentration (ppb)	Accuracy (%RE)	Analysis Variability (%RSD)	% Recovery
100	20	15	80-110
10	20	21	60-115
1	20	30	40-120

Repeatability is how well the entire sample extraction, cleanup and analysis process can be repeated on the same day and on subsequent days and can be assessed by statistical analysis using duplicate samples or blank samples spiked with known amounts of target analytes.

Selectivity is the ability of the method to detect the target analyte in the presence of potential interferences from the sample matrix. SPE is used to remove many of the potential interferences and to get a sample into a solvent amenable to instrumental analysis, but extraction can also take with it compounds that are not of interest but are chemically similar to the target analytes. The instrumental analysis method must then be able to 'see' the target analytes in the presence of these other matrix components. MS detection is highly selective compared to other detection methods (e.g. UV-Vis) but confirmation of selectivity is still required. The selectivity of MS detection in selected ion monitoring (SIM) mode comes from selecting specific ions from the target analyte fragmentation pattern to detect. One ion is used as the quantification ion and others are used as qualifier ions. The ratios of the quantification to qualifier ion intensities must match within a pre-determined range (normally 15%) and the chromatographic peak must be found at a specific retention time for the peak to be identified as the target analyte. It is possible for a co-eluting compound to contribute intensity to one or more of the selected ions, thus upsetting the intensity ratios. In this situation, the peak is not identified automatically by the software. If, after examination of the SIM data, if there is confidence that the interference doesn't affect the quantification ion, the peak can be manually identified as the target analyte.

Sensitivity is defined as the lowest concentration of target analyte that can be measured with an acceptable level of accuracy and precision. Typically, accuracy within 20% [345] with precision depending on analyte concentration as specified in Table 4.1 are set as acceptable limits for determining the lower limit of quantification (LLOQ) for trace bioanalytical methods. The instrumental limit of detection (LOD) differs from the LLOQ in that it is determined based on standards rather than samples and does not include the sample

extraction and cleanup steps of the method. The LOD is often defined as the concentration that corresponds to some factor *k* above the standard deviation of the instrument signal obtained from multiple blank measurements. The value of *k* is normally set at 3 [347]. With chromatographic methods this definition is problematic. The chromatographic signal is peak area and this requires the target analyte to be present at a measurable concentration. Clearly this is not a desirable feature of a blank. In place of a blank measurement, the lowest calibration standard is often used. The standard deviation of multiple measurements of the standard at this level is determined and multiplied by k to obtain an instrument LOD.

Characterisation of stability must be done at several points in the method, for example; storage of stock solutions of calibration standards and other reagents, extracted/prepared samples (as they sit in the autosampler waiting for analysis), freeze-thaw stability, benchtop stability (stability of samples for the length of time it takes to complete sample preparation operations). Ideally, conditions and timing of operations can be controlled to minimise their effects on sample stability.

Extraction efficiency or recovery is a measure of how well the target analyte can be removed from the original sample and presented to the detector. Ideally, recovery should be high to achieve the best sensitivity possible, but at a minimum, recovery should be precise and reproducible [345]. Acceptable limits on recover vary with the concentration of the target analyte as summarised in Table 4.1. In this application, recovery is monitored in each sample by the addition of a known amount of isotopically labelled (^{13}C or ^{2}H) surrogate standards representing each group of target analytes. The recovery of these surrogates is determined and used to correct measured concentrations of the target analytes.

The quantification range is the range of concentrations that can be reliably determined using the method. The lower limit of this range is the LLOQ and the upper limit of quantification (ULOQ) is defined as the highest concentration of the target analyte that can be determined by the method, usually with the same accuracy and precision criteria as the LLOQ. Samples with target analyte concentrations above the ULOQ can be determined by dilution of the sample, provided dilution integrity is demonstrated.

4.2.5 Calibration

The heart of an analytical method is the calibration curve – the equation that relates the measured signal intensity (e.g. peak height or peak area, the dependent variable, y) to the

concentration of a calibration standard (the independent variable, x). Ideally this relationship will be linear and will have a zero intercept, such that the equation of the line is y = mx+0. With MS analyses where the concentration range covers an order of magnitude or more, it is not unusual for the calibration curve to be nonlinear, for example quadratic: $y = ax^2+bx+0$. Regression analysis is used to determine the coefficients for the equation so that the concentration, x, can be obtained for a measured analytical signal, y. Regression analysis assumes the variance of the measured analytical signal is constant across the range of concentration, and often this is not the case [348]. The variance of measurement is often much larger at the higher end of the concentration range than at the lower end. This results in an unintended and undesirable weighting of the regression results leading to a bias toward higher concentrations and a reduction in the accuracy of determining lower concentrations. Weighted regression analysis can be used to counteract this effect, but the choice of weighting factor is not straightforward and must be done by test and evaluation as described by Almeida et al. [348]. The best weighting factor is chosen by calculating the percent relative error (%RE) obtained by comparing the result obtained from the weighted regression with the expected (nominal) concentration for a range of standards spanning the calibration range. A plot of %RE as a function of nominal concentration should appear as a randomly distributed and tightly clustered band around the concentration axis. The smaller the variation in %RE as a function of concentration, without showing any specific trend will indicate the best weighting factor of those evaluated. Typical weighting factors are $1/x^{1/2}$, $1/x$, $1/x^2$, $1/y^{1/2}$, $1/y$, $1/y^2$. If measurement of the analytical signal is the largest source of uncertainty, weightings in y are the best choice. If preparation of calibration standards is the largest source of uncertainty, weightings in x are the best choice [349, 350].

4.3 Materials

4.3.1 Instrumentation

A Shimadzu QP2010s GC-MS system was used for the method development and sample analysis. It was equipped with a split/splitless injection port, electronically controlled carrier gas flow, AOC-20 100 vial autosampler and a quadrupole MS detector with 70 eV electron impact ionisation source (EI positive ion). The MS was tuned using perfluorotributylamine (PFTBA) and the autotune function of the GC-MS workstation software.

4.3.2 Equipment

A Techne sample concentrator equipped with stainless steel needles was used for solvent evaporation under N_2 flow. The needles were solvent cleaned prior to each use. A Techne Dri-Block DB-3D with three 8 position aluminium heating blocks was used for gentle heat during solvent evaporation and for heating the analytical derivatisation reaction. The Dri-Block is digitally controlled, capable of constant temperature heating up to 200 °C with a stability of ± 0.15 °C at 100 °C; ± 1 °C accuracy in temperature set point and position to position variability in temperature of ±0.2 °C at 40 °C

The IST VacMaster 20 position SPE vacuum manifold was used for SPE sample prep. It was equipped with integrated stopcock/needle taps made of Teflon and a vacuum/flow controller to adjust flow rate through the SPE tubes.

4.3.3 Labware

All glassware was silanised to reduce loss of target analytes by adsorption to glass surface. All plasticware (pipette tips, centrifuge tubes) was made of 100% polypropylene to minimise contamination due to leaching of plasticizers from the material [351].

4.3.4 Standard Materials, Reagents and Solvents

Pure compounds, solvents and other reagents were purchased from suppliers as summarised in Table A. 10 and Table A. 11, and were of highest purity available. All solvents were HPLC or GC/LC-MS grade. Aqueous solutions were prepared in reagent grade water (18.3 MΩ) obtained from in-house water purification systems (Milli-Q and Sartorius).

β-glucuronidase (type H-1) and arylsulphatase enzymes, isolated from *Helix pomatia*, were used for deconjugation of glucuronide and sulphate metabolites. The product was purchased from Sigma Aldrich (product number G0751, lot # 068K38091V). The activity of the material was 1.926×10^6 units/g solid for β-glucuronidase and 2.376×10^4 units/g for arylsulphatase. The reaction conditions for this product are 37 °C and pH 5.0.

The buffer used for the enzyme deconjugation reaction (Enzyme Buffer, 1 M NH_4OAc) was prepared by dissolving 33 mL glacial acetic acid and 77 g of ammonium acetate in reagent water, diluting to a final volume of 1L and adjusting pH to 5.0 at 20 °C.

0.1M formic acid solution was prepared by diluting 3.8 mL formic acid (98%) to 1 L with reagent water.

Synthetic urine was prepared as specified in Table A. 12 using available materials and reagent water. Synthetic urine was used as a simulated sample matrix to develop the SPE method. The synthetic urine was stored at room temperature and vacuum filtered through a 0.2 µm membrane filter prior to each use.

4.3.5 Preparation of Quantitative Standards

Individual stock standards of each compound were prepared gravimetrically at a nominal concentration of 400 ppm in HPLC grade ACN. E3 was dissolved in EtOH, GEN and DAID were dissolved in 1:4 DMSO:EtOH as these compounds were not soluble in ACN at 400 ppm. These standards were stored in vials with Teflon-lined silicone septum seals. These standards were stored at the same temperature as the pure compound (room temperature, refrigerated or frozen) as summarised in Table 4.2. Mixtures of native target analytes for qualitative purposes were prepared from these individual standards.

Table 4.2. Storage conditions for stock standards.

Storage Temperature	Target Analytes
Room Temperature (20 °C)	All compounds except those listed below.
Refrigerated (4 °C)	ENT
Freezer (-20 °C)	GEN, DAID, EQ

Mixtures of native target analytes for quantitative purposes were prepared gravimetrically as stock standard mixtures according to compound class at nominal concentration of 400 ppm by dissolving 0.01 g of material in 25.0 mL solvent, as summarised in Table 4.3. The steroids were dissolved in EtOH, and the phytoestrogens were dissolved in 1:5 DMSO:EtOH.

Table 4.3. Stock standard mixtures (400 ppm nominal) for quantitative analysis.

Mixture	Components	Solvent	Storage
Main	TRIC, mTRIC, 4HBA, mPBN, ePBN, pPBN, bPBN, 4NP, 4NC, NP, 4tOP, BPA, 3PBOH, 3PBA	ACN	Room Temperature (20 °C)
Phthalates	mMP, mEP, mBP, mBzP, mEHP		
Steroids	E1, E2, E3, EE2		
UV filters	BP1, BP2, BP3, OMC, 4MBC		
ENT	ENT	EtOH	Refrigerated (4 °C)
Phytoestrogens	GEN, DAID, EQ	1:4 DMSO:EtOH	Freezer (-20 °C)
Internal Standard	BPC	ACN	Room Temperature (20 °C)

The stock mixtures were combined and diluted to a single intermediate mixture at 5 ppm in ACN. The 5 ppm mixture was stored at -20 °C. Working standards at concentrations of 1 ppm or lower were prepared in ACN immediately before use.

The working internal standard was prepared at a concentration of 1 ppm in ACN and was stored at room temperature.

Isotopically labelled recovery surrogates were supplied as solutions at 1000 or 100 ppm or as neat materials. $^{13}C_6$-E2 was supplied as 100 µg quantity of neat material in a vial. To this vial, 1 mL ACN was added to produce a 100 ppm standard. The stock standards were stored at -20 °C. Neat 4NP-D_4 and BP-rec were used to prepare 400 ppm stock standards in ACN and were stored at room temperature. The surrogate mixture was prepared at 1000 ppb in 25 mL ACN by diluting appropriate aliquots of the various solutions. The working surrogate mixture was stored at -20 °C.

The enzyme deconjugation reaction control standard prepared at 400 ppm by dissolving 0.01 g each of 4NP-glucuronide and 4NC-suphate in 25 mL Enzyme Buffer. A working standard at 1 ppm conjugate (0.6 ppm free compound) was prepared by diluting the stock solution with Enzyme Buffer. Both the stock and working standards were stored at 4 °C.

The enzyme solution was prepared fresh immediately before use by dissolving 0.01 g lyophylised powder in 10 mL Enzyme Buffer. The specific activity of this solution was approximately 2000 U/mL β-glucuronidase and 24 U/mL arylsulphatase.

4.4 Methods Development

4.4.1 GC-MS Method Development

The first step in the method development was to establish conditions for GC separation, MS detection and derivatisation conditions.

4.4.1.1 GC Separation

For trace analysis, splitless injection is used as a large fraction of the injected sample reaches the column. Splitless injection without solvent focusing was used because the analytes are significantly less volatile than the solvent and are adequately focused by interaction with the column stationary phase. The sample is in ACN so the initial temperature must be above the boiling point of the solvent (81.6 °C). The GC temperature program is given in Table 4.4. The long final hold time was needed to ensure the least volatile components of the biological

samples were eluted before the next injection. The temperature gradient was optimised to achieve near baseline separation of the target analytes while retaining narrow, sharp peak shape.

Table 4.4. GC temperature program.

Parameter	Value
Injection mode	Splitless, 1 µL injection volume, 1 min sampling time, 5 min vent time
Inlet temperature	250 °C
Inlet pressure program	200 kPa (3 mL/min) for 1 min, then constant flow at 1 mL/min
Transfer line temperature	250 °C
Column oven program	100 °C hold 5 min, 10 °C/min to 300 °C, hold 20 min; 45 min total run time
MS ion source temperature	200 °C

ACN is not a preferred solvent for GC analysis due to its large vapour volume. At 250 °C and an inlet pressure of 200 kPa, a 1 µL injection volume of ACN produces 275 µL of vapour. The inlet liner volume for the instrument is approximately 670 µL. The 1 µL ACN injection fills the inlet liner to approximately 40% capacity. This prohibits the use of larger injection volumes for improving detection limits. The general rule of thumb [352] is to keep the injection vapour volume less than 75% of the inlet liner volume to prevent backflash of the sample out of the inlet which would lead to large injection volume uncertainties. Under the same conditions, a sample dissolved only in the derivatisation reagent, BSTFA, would produce a vapour volume of approximately 54 µL.

4.4.1.2 Analytical Derivatisation

The initial procedure for analytical derivatisation was to pipette an aliquot of the target compound or mixture into a 5 mL reaction vial and evaporate the solvent by gentle heating at 40 °C under a gentle stream of N_2 using the sample concentrator. The vial was removed from the concentrator as soon as the solvent was evaporated to minimise loss of the more volatile target analytes. To the dry residue, 200 µL of derivatisation reagent and 100 µL solvent was added. The reaction vial was sealed with a Teflon lined silicone septum cap and was heated at the desired temperature for the desired length of time in the well of the heating block. However, as calibration check data was acquired, higher than desired variability was found, especially with the more volatile target analytes. The procedure for preparing calibration standards was changed to remove the need for solvent evaporation.

The final calibration standards were prepared by spiking the reaction vial with 100 ng internal standard and evaporating the solvent. To each vial, the native and/or surrogate spikes were added along with a volume of ACN to make the total volume up to 100 µL. To this was

added the 200 µL volume of derivatisation reagent BSTFA/TMSI (98:2) and the mixture heated at 80 °C for 60 minutes. The vials were allowed to cool for 10 minutes. The vials inverted and rolled to ensure the contents were well mixed, then allowed to stand for an additional 5 minutes for the contents to settle. A 200 µL aliquot of the standard was transferred to an amber autosampler vial fitted with a 250 µL glass insert and Teflon-lined silicone septum.

Different reagents mixtures were evaluated by derivatisation of each compound individually and by derivatisation of a 500 ppb mixture of all target analytes. The mixtures tested were: BSTFA, BSTFA/TMCS (99:1), BSTFA/TMCS/TMSI (97:1:2) and BSTFA/TMSI (98:2).

Over time, the use of both BSTFA/TMCS and BSTFA/TMCS/TMSI resulted in a residue building up on the guard column and in the inlet liner which seriously impaired both chromatography and the stability of the derivatives due to active sites on the column. PYR was tried as a HCl scavenger, but impurities in the solvent were substantially higher than observed with ACN when standards analysed in SCAN mode, so this system was not considered any further. These two systems may be acceptable for use with subsets of the target analyte suite, as indicated by literature reports, but was judged as unacceptable for the entire suite of analytes of interest in this study.

The final reagent mixture tested was BSTFA/TMSI with ACN as a co-solvent. This mixture resulted in less fouling of the analytical column, particularly when an inlet liner with glass wool deactivated after assembly was used. Several inlet liners were tested and the Restek SKY technology proved to be the most robust.

4.4.1.3 MS Detection

The MS was operated in two modes – SCAN for qualitative and semi-quantitative analysis during method development and SIM once derivatisation conditions and GC separation parameters were established. The final SIM schedule is summarised in Table x in the Appendix. The ion used for quantification was chosen based on a compromise between relative intensity and the absence of matrix interferences. At least one qualifier ion was used for each compound. Where possible two or three were used. For the compounds with only one qualifier ion, the second or third qualifier ions originally selected had significant matrix interferences rendering them useless.

4.4.2 Calibration and QA/QC Procedures

Once the derivatisation conditions were established, the GC-MS was calibrated. Samples and standards were run as a batch using the autosampler. Calibration standards covering the range of 1 – 100 ppb were prepared along with a reagent blank. Two injections of each standard were made to assess both instrument stability and degradation of the standards over the duration of the batch run. Quantification was done using an internal standard that was added in a known and constant amount (100 ng) to every sample and standard that was analysed. The calibration curve was based on peak area ratio to the internal standard as a function of concentration ratio to the internal standard. Internal standard quantification accounts for injection-to-injection drift in instrument response and sample-to-sample volume differences.

With each batch, three calibration check standards (high, mid and low range), comparatives and other QA/QC samples as needed were analysed. Comparatives were prepared whenever samples were spiked with natives or surrogates. The comparative is an aliquot of the standard of the same volume as delivered to the sample, delivered directly to the reaction vial for derivatisation. It serves as a check on pipette operations and any degradation of the standard. The comparative is not affected by sample extraction losses. Ideally the comparative agrees within the analytical uncertainty of its target concentration.

4.4.3 Calculations

Calibration curves were established within the GC-MS instrument software. The calibration curve for each target analyte was constructed using the ratio of peak areas of target analyte peak and internal standard as the dependent variable (y) and the ratio of concentration of calibration standard to internal standard concentration as the independent variable (x). A quadratic curve with forced intercept was fit to the data using a $1/y^2$ weighting factor.

Two correction factors are needed to correct the reported concentration for the native analytes: the spike volume correction factor (F_V) and the surrogate recovery correction factor (F_{RC}). F_V adjusts for variation in the actual spike volume delivered to the sample and is calculated for the surrogate spike used for all samples and the native spikes used in QC samples. Because the comparatives were subject to solvent evaporation, the more volatile compounds may be affected, so the average F_V obtained for BPA and E2 was used for all compounds. F_{RC} corrects for recovery through the sample extraction process. Thus,

$$F_{V_i} = \frac{C_i(comparative)}{C_i(target)}$$

$$F_V = \frac{F_V(BPA) + F_V(E2)}{2}$$

$$F_{RCi} = \frac{C_{Si}(reported)}{C_{Si}(target) \times F_V}$$

$$C_{RCi} = \frac{C_i(reported)}{F_{RCi}}$$

where C_i(comparative) = reported concentration in comparative for compound i;

C_i(target) = theoretical concentration in standard for compound i;

C_{Si}(reported) = reported concentration for recovery surrogate i in sample

C_{Si}(target) = theoretical concentration for recovery surrogate i;

C_i(reported) = reported concentration for compound i in sample.

C_{RCi} = recovery corrected concentration for compound i in sample.

Because the calibration standards were based on a 1 mL sample volume and the biological sample volumes were larger (2.0 or 2.5 mL), the recovery corrected concentration for each compound then had to be corrected for the sample aliquot volume to standard volume ratio (V_S) to give the concentration in the original sample (C_i):

$$C_i = \frac{C_{RCi}}{V_s}$$

The quantification and qualification ions and the recovery surrogate for each of the target analytes are summarised in Table 4.5.

4.4.4 Sample Extraction Method Development

4.4.4.1 General SPE Method

The general method for SPE is shown in Figure 4.5. The flow rate through the adsorbent bed was 1-2 mL/min. The solvent was evaporated from the SPE eluate and the dry residue taken up in solvent, spiked with 100 ng internal standard, derivatised and analysed by GC-MS.

4.4.4.2 Spiked Water and Synthetic Urine

Initial trials for optimisation of the SPE method, as summarised in Table 4.6, were done with spiked reagent water and synthetic urine. The synthetic urine was filtered before each use as it was prone to going cloudy on storage. 3 mL or 4 mL aliquots (n=2 to 4) were spiked with 100 ng or 10 ng natives and 100 ng surrogates or with 100 ng surrogates only. The surrogate-only spiked samples were used as reagent blanks. For the first trial, the samples were incubated at 37 °C for 60 min to simulate the enzyme deconjugation reaction, acidified by the addition of 500 µL formic acid (98%) and then extracted using the general SPE method outlined above. Trial 2 omitted the incubation and acidification steps.

Table 4.5. Initial and final quantification (Q) and qualification (Q1, Q2, Q3) ions and recovery surrogates for each target analyte.

RT (min)	Target Analyte	Initial m/z			Final m/z				Initial Recovery Surrogate	Final Recovery Surrogate
		Q	Q1	Q2	Q	Q1	Q2	Q3		
12.75	mParaben	209	224		224	209	193		$^{13}C_6$-mParaben	$^{13}C_6$-mParaben
12.94	4NP	196	150		196	211			D_4-4NP	D_4-4NP
13.70	eParaben	193	238		238	193	210		$^{13}C_6$-mParaben	$^{13}C_6$-mParaben
13.87	mMP	89	237	163	237	163	238		$^{13}C_6$-mEP	$^{13}C_6$-mEP
14.45	4HBA	267	223	193	223	193	282		$^{13}C_6$-mParaben	$^{13}C_6$-mParaben
14.66	OP	207	208		208	151	191		$^{13}C_{12}$-Tric	$^{13}C_{12}$-Tric
14.63	mEP	223	251		223	251			$^{13}C_6$-mEP	$^{13}C_6$-mEP
14.92	pParaben	210	193	195	252	237			$^{13}C_6$-bParaben	$^{13}C_6$-bParaben
15.86	4NC	284	299		284	299			D_4-4NP	D_4-4NP
16.12	bParaben	210	195	193	195	266	251		$^{13}C_6$-bParaben	$^{13}C_6$-bParaben
16.67	mBP	223	149	221	223	149	163		$^{13}C_6$-mEP	$^{13}C_6$-mEP
16.99	3PBOH	183	227	272	272	227	257	211	$^{13}C_{12}$-BPA	$^{13}C_{12}$-BPA
17.78	NP	179	180	292	292	180	165		$^{13}C_6$-NP	$^{13}C_6$-NP
18.06	3PBA	271	227		271	227	286	197	$^{13}C_6$-3PBA	$^{13}C_6$-3PBA
19.30	4MBC	254	105		254	239			$^{13}C_{12}$-Tric	$^{13}C_{12}$-Tric
19.42	BP-3	285	286	242	286	242			BP-rec	$^{13}C_{12}$-BPA
19.59	mEHP	221	223	149	223	221	239		$^{13}C_6$-mEHP	$^{13}C_{12}$-BPA
19.85	mTric	302	304		302	254	232		$^{13}C_{12}$-Tric	$^{13}C_{12}$-Tric
19.87	Tric	200	345	347	345	310			$^{13}C_{12}$-Tric	$^{13}C_{12}$-Tric
20.00	BP-1	343	344	105	344	164	271		BP-rec	$^{13}C_{12}$-BPA
20.47	mOP	239	187		239	223	221		$^{13}C_6$-mEHP	$^{13}C_{12}$-BPA
20.50	mBzP	91	179	194	179	222	194		$^{13}C_6$-mEHP	$^{13}C_{12}$-BPA
20.60	BPA	357	358		357	358	372		$^{13}C_{12}$-BPA	$^{13}C_{12}$-BPA
21.53	OMC	178	161		178	161	290		$^{13}C_{12}$-Tric	$^{13}C_{12}$-Tric
23.46	BP-2	519	520		519	520	445		BP-rec	$^{13}C_{12}$-BPA
23.69	Equol	192	177	193	386	267			D_4-Gen	$^{13}C_{12}$-BPA
24.25	E1	342	257	218	342	244	327		$^{13}C_6$-E2	$^{13}C_6$-E2
24.51	E2	285	416	326	326	416	285		$^{13}C_6$-E2	$^{13}C_6$-E2
25.37	EE2	425	285	229	440	425			$^{13}C_6$-E2	$^{13}C_6$-E2
25.57	Ent	180	181		442	165			D_4-Gen	$^{13}C_{12}$-BPA
26.01	E3	297	504		504	414	386		$^{13}C_6$-E2	$^{13}C_6$-E2
26.35	Daid	398	399		398	383	184	355	D_4-Gen	$^{13}C_{12}$-BPA
26.45	Gen-triTMS	471	472		471	472	228		D_4-Gen	not determined
26.78	Gen-diTMS				414	399	415	416		not determined
Recovery Surrogates										
12.75	$^{13}C_6$-mParaben	215	230		230	215	199			
12.92	D_4-4NP	200	154		200	154				
14.63	$^{13}C_6$-mEP	227	255		255	227				
16.12	$^{13}C_6$-bParaben	216	201	199	272	257				
17.78	$^{13}C_6$-NP	185	298	186	298	186	171			
18.06	$^{13}C_6$-3PBA	277	233		277	292	233	203		
18.69	BP-rec	123	288	193	273	288	193			
19.59	$^{13}C_6$-mEHP	225	227	153	227	153	243			
19.86	$^{13}C_{12}$-Tric	206	357	359	359	372	374			
20.59	$^{13}C_{12}$-BPA	369	370		370	369	384			
24.51	$^{13}C_6$-E2	288	422	332	288	422	332			
26.44	D_4-Gen-triTMS	474	475	476	475	476	402			
26.76	D_4-Gen-diTMS				402	417	418			
Internal Standard										

21.20	IS-BPC	385	386		386	385	400			

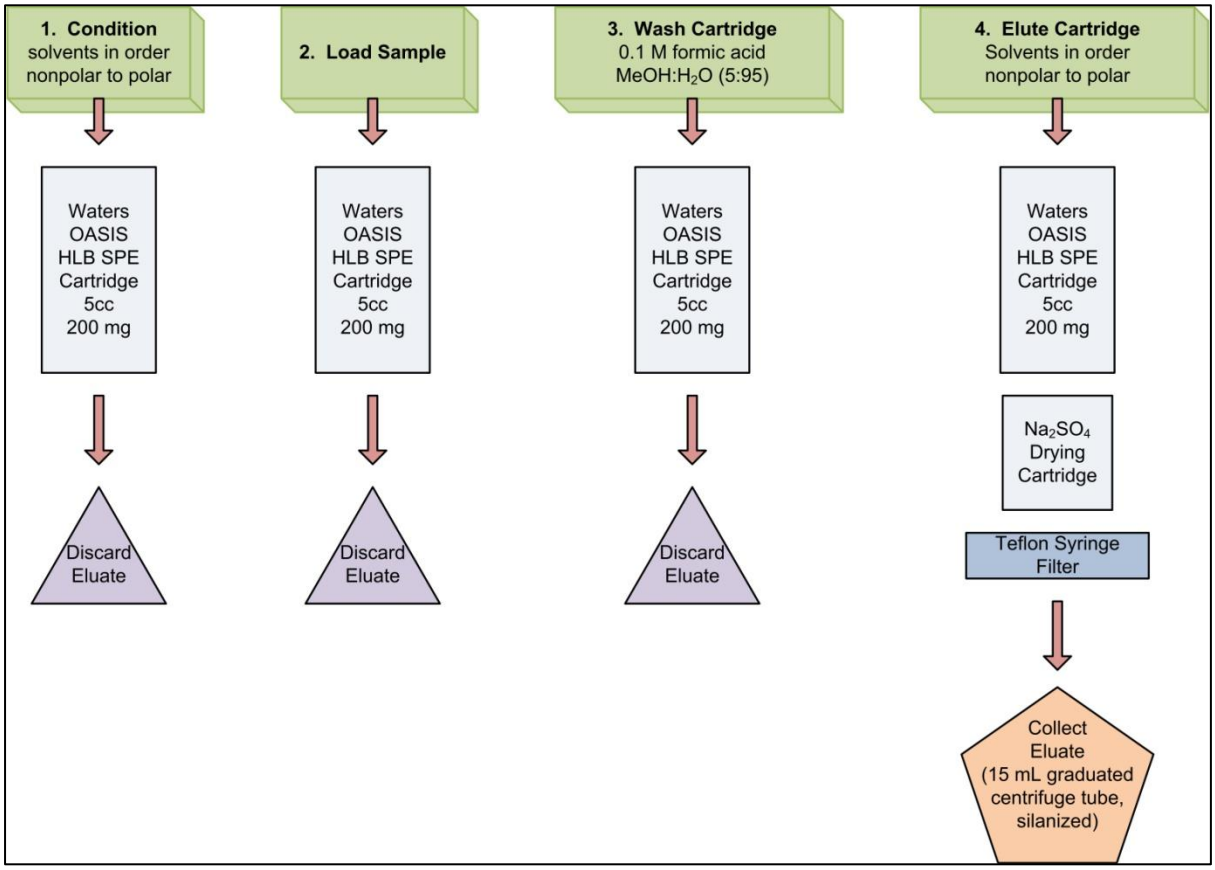

Figure 4.5. General SPE process.

Table 4.6. Solvent combinations, enzyme deconjugation reaction conditions and derivatisation conditions for SPE method validation and enzyme deconjugation reaction trials.

Parameter	Trial 1 (28 Oct 2010)	Trial 2 (8 June 2011)	Trial 3 (7 July 2011)	Trial 4 (8 July 2011)	Trial 5 (9 July 2011)	Trial 6 (12 July 2011)	Trial 7 (15 July 2011)
Matrix	3 mL synthetic urine 3 mL Reagent water (n=2 each)	3 mL synthetic urine (n=2 each)	4 mL synthetic urine diluted with 2 mL Enzyme Buffer (n=3 total)	4 mL synthetic urine diluted with 2 mL Enzyme Buffer (n=2 total)	4 mL synthetic urine diluted with 2 mL Enzyme Buffer (n=3 total)	4 mL synthetic urine diluted with 2 mL Enzyme Buffer (n=4 total)	4 mL synthetic urine diluted with 2 mL Enzyme Buffer (n=2)
Natives Spike	100 ng 0 ng	100 ng 10 ng 0 ng	0 ng	0 ng	0 ng	0 ng	100 ng 0 ng
Surrogate Spike	100 ng	100 ng	100 ng	100 ng	100 ng	100 ng	100 ng
Enzyme Control Spike	no	no	55 ng	55 ng	55 ng	55 ng	55 ng
Enzyme	no	no	0.04 mg	0.08 mg	0.2 mg	0.25 mg	0.25 mg
Incubation	37 °C for 60 min	no	37 °C for 30, 60 and 120 min	37 °C for 60 and 120 min	37 °C for 60, 120, 240 min	37 °C for 30, 60, 120, 240 min	37 °C for 120 min
Acidification/ Buffer	500 µL formic acid (98%) after incubation	no	500 µL formic acid (98%) after incubation	500 µL formic acid (98%) after incubation	500 µL formic acid (98%) after incubation	500 µL formic acid (98%) after incubation	500 µL formic acid (98%) after incubation
Condition	3 mL each MTBE, MeOH, H_2O	3 mL each MTBE, MeOH, H_2O	3 mL each MTBE, MeOH, H_2O	3 mL each MTBE, ACN, MeOH, H_2O	3 mL each MTBE, ACN, MeOH, H_2O	3 mL each Hex, MTBE, ACN, MeOH, H_2O	2 mL each Hex, MTBE, MeOH, H_2O
Load	quantitative transfer 2 x 1 mL 0.1 M formic acid	quantitative transfer 2 x 1 mL 0.1 M formic acid	quantitative transfer 1 mL 0.1 M formic acid	quantitative transfer 1 mL 0.1 M formic acid	quantitative transfer 1 mL 0.1 M formic acid	quantitative transfer 1 mL 0.1 M formic acid	quantitative transfer 1 mL 0.1 M formic acid
Wash	3 mL MeOH/H_2O (40:60) 3 mL 0.1M formic acid 1 mL MeOH/H_2O (40:60)	3 mL 0.1M formic acid 3 mL MeOH/H_2O (5:95)	1 mL MeOH/H_2O (5:95)	1 mL MeOH/H_2O (5:95)	1 mL 0.1 M formic acid 1 mL MeOH/H_2O (5:95)	1 mL MeOH/H_2O (5:95)	1 mL MeOH/H_2O (5:95)

Parameter	**Trial 1 (28 Oct 2010)**	**Trial 2 (8 June 2011)**	**Trial 3 (7 July 2011)**	**Trial 4 (8 July 2011)**	**Trial 5 (9 July 2011)**	**Trial 6 (12 July 2011)**	**Trial 7 (15 July 2011)**
Elute	2 x 3 mL MTBE/MeOH (90:10)	5 mL MTBE/MeOH (90:10)	1 mL MTBE 4 mL MTBE/MeOH (90:10)	1 mL MTBE 4 mL MTBE/ACN (80:20)	1 mL ACN 4 mL MTBE 1 mL ACN	Tube A: 3 mL Hex/MTBE (50:50) + 2 mL ACN/MTBE (20:80) Tube B: 2 mL MTBE/MeOH (90:10)	Tube A: 2 mL Hex/MTBE (50:50) Tube B: 4 mL MTBE/MeOH (60:40) + 1 mL MTBE + 2 mL MeOH
Dry	Na_2SO_4 cartridge	Na_2SO_4 cartridge	Na_2SO_4 in collection tube	$MgSO_4$ in collection tube	$MgSO_4$ in collection tube	acidify aq. layer in Tube A and remove, dry organic layer over $MgSO_4$	acidify aq. layer in Tube A and remove, dry organic layer over $MgSO_4$
Derivatisation Conditions	BSTFA/TMCS/TMSI (97:1:2) 60 °C, 30 min	BSTFA/ TMSI (98:2) 60 °C, 30 min	BSTFA/ TMSI (98:2) 80 °C, 30 min	BSTFA/ TMSI (98:2) 80 °C, 30 min	BSTFA/ TMSI (98:2) 80 °C, 30 min	BSTFA/ TMSI (98:2) 80 °C, 30 min	BSTFA/ TMSI (98:2) 80 °C, 30 min

4.4.5 Metabolite Deconjugation Reaction

The final step in method development was validating reaction conditions for enzyme deconjugation of glucuronide and sulphate metabolites. The reaction conditions were evaluated using 4 mL aliquots of synthetic urine diluted with 2 mL Enzyme Buffer. The enzyme control standard was spiked at 100 µL (equivalent to 55 ng deconjugated compound). 0.5 mL of freshly prepared enzyme solution was added to each sample. Samples were incubated at 37 °C for 30, 60, 90, 120 and 240 minutes. The enzyme reaction was quenched by acidification of the mixture with 500 µL formic acid (98%). After quenching, samples were spiked with 100 ng surrogates, extracted and analysed.

4.4.6 Pooled Amniotic Fluid Sample

A small amount of pooled amniotic fluid (approx. 20 mL) was available for a final test of the extraction methodology and the enzyme deconjugation reaction. For the extraction methodology test, four 2.5 mL aliquots of the pooled fluid were diluted with 4 mL Enzyme Buffer and 2 mL reagent water. Two aliquots were spiked with 100 ng natives and all 4 were spiked with 100 ng surrogates. The samples were extracted following the procedure summarised in Table 4.7 and analysed. For the enzyme deconjugation reaction test, five 2 mL aliquots of the pooled fluid were diluted with 4 mL Enzyme Buffer and 4 mL reagent water. Two of the aliquots were spiked with 100 ng natives, two aliquots were spiked with 55 ng of the Enzyme Control mix and the last aliquot used as a blank. All 5 aliquots had the enzyme solution added and were incubated. All aliquots were processed following the procedure outlined in Table 4.7.

Table 4.7. SPE procedure for pooled amniotic fluid samples.

Parameter	SPE Extraction Trial	Enzyme Deconjugation Trial
Matrix	2.5 mL amniotic fluid diluted with 4 mL Enzyme Buffer and 2 mL reagent water	2 mL amniotic fluid diluted with 4 mL Enzyme Buffer and 4 mL reagent water
Natives Spike	125 ng	0 or 100 ng
Surrogate Spike	100 ng	100 ng
Enzyme Control Spike	no	0 or 55 ng
Enzyme	no	0.5 mg
Incubation	no	37 °C, 2 hours
Acidification	no	500 µL formic acid (98%) after incubation
Condition	2 mL each Hex, MTBE, MeOH, H_2O	2 mL each Hex, MTBE, MeOH, H_2O
Load	quantitative transfer 1 mL 0.1 M formic acid	quantitative transfer 4 mL 0.1 M formic acid
Wash	1 mL MeOH/H_2O (5:95)	4 mL MeOH/H_2O (5:95)
Elute	Tube A: 2 mL Hex + 2 mL Hex/MTBE (50:50)	Tube A: 1 mL MTBE + 2 mL Hex + 2 mL Hex/MTBE (50:50)

	Tube B: 1mL MTBE + 2 mL MTBE/MeOH (60:40) + 4 mL MeOH	Tube B: 2 mL MTBE/MeOH (60:40) + 4 mL MeOH
Dry	acidify aq. layer in Tube A and remove dry organic layer over $MgSO_4$	acidify aq. layer in Tube A and remove dry organic layer over $MgSO_4$
Derivatisation Conditions	BSTFA/ TMSI (98:2) 80 °C, 30 min	BSTFA/ TMSI (98:2) 80 °C, 30 min

4.5 Results

4.5.1 Derivatisation Reagent Evaluation

Three different derivatisation reagent mixtures were evaluated using 500 ng aliquots of the 5 ppm Natives mix and 250 µL of each reagent: BSTFA only, BSTFA/TMCS (99:1) and BSTFA/TMCS/TMSI (97:1:2). The reaction conditions were 60 °C for 30 min. The results are given as ratio of peak area of the target analyte to that of the internal standard and are shown in Figure 4.6. The error bars indicate 1σ on the average of 4 injections over a period of 13 h. The only significant differences between reagents are for EE2 and GEN. The peak monitored for EE2 is that of the di-TMS derivative and it is only present with the 3-part reagent. For GEN, the tri-TMS derivative is monitored and this peak area ratio decreases with the addition of TMCS compared to that obtained with BSTFA only. The addition of TMSI restores the peak area ratio. For the compounds that do not have an active hydrogen (4MBC, mTRIC and OMC) none of the reagents affects the peak area ratio. Based on these results and the difficulties encountered with TMCS, the reagent mixture chosen for further use was BSTFA/TMSI (98:2). The reaction conditions of 60 °C for 30 min were also used as earlier tests with standards indicated longer reaction time and higher temperature did not improve peak area ratio response. A comparison of the two-part and three-part reagent performance under reaction conditions of 60 °C for 30 min is shown in Figure 4.7.

Figure 4.6 also gives an indication of the relative sensitivity of the analysis for the range of analytes. This difference in sensitivity is a direct consequence of the fragmentation patterns of the analytes. NP and 4t-OP produce a single dominant fragment. In contrast, 4MBC fragments extensively. The mass spectra for 4t-OP and 4MBC are shown in Figure 4.8. 4t-OP was quantified using m/z 207 and 4MBC was quantified using m/z 254.

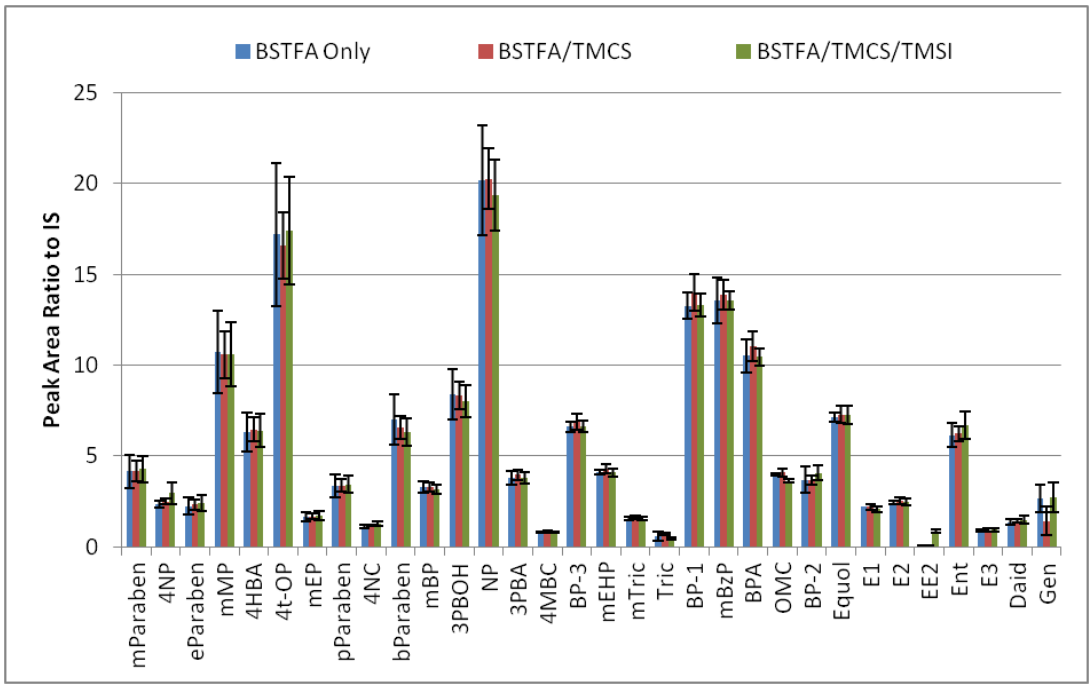

Figure 4.6. Comparison of derivatisation reagents (12 Oct 2010).

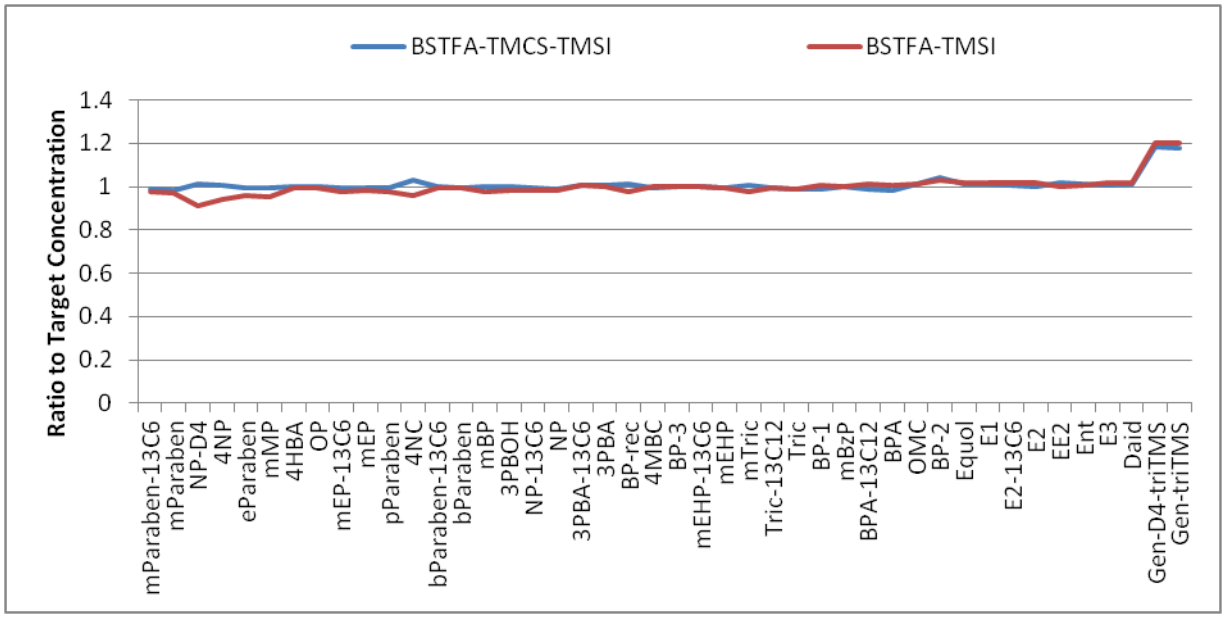

Figure 4.7. Comparison of the performance of two reagent mixtures, BSTFA/TMCS/TMSI (97:1:2) and BSTFA/TMSI (98:2), under reaction conditions of 60 °C and 30 min.

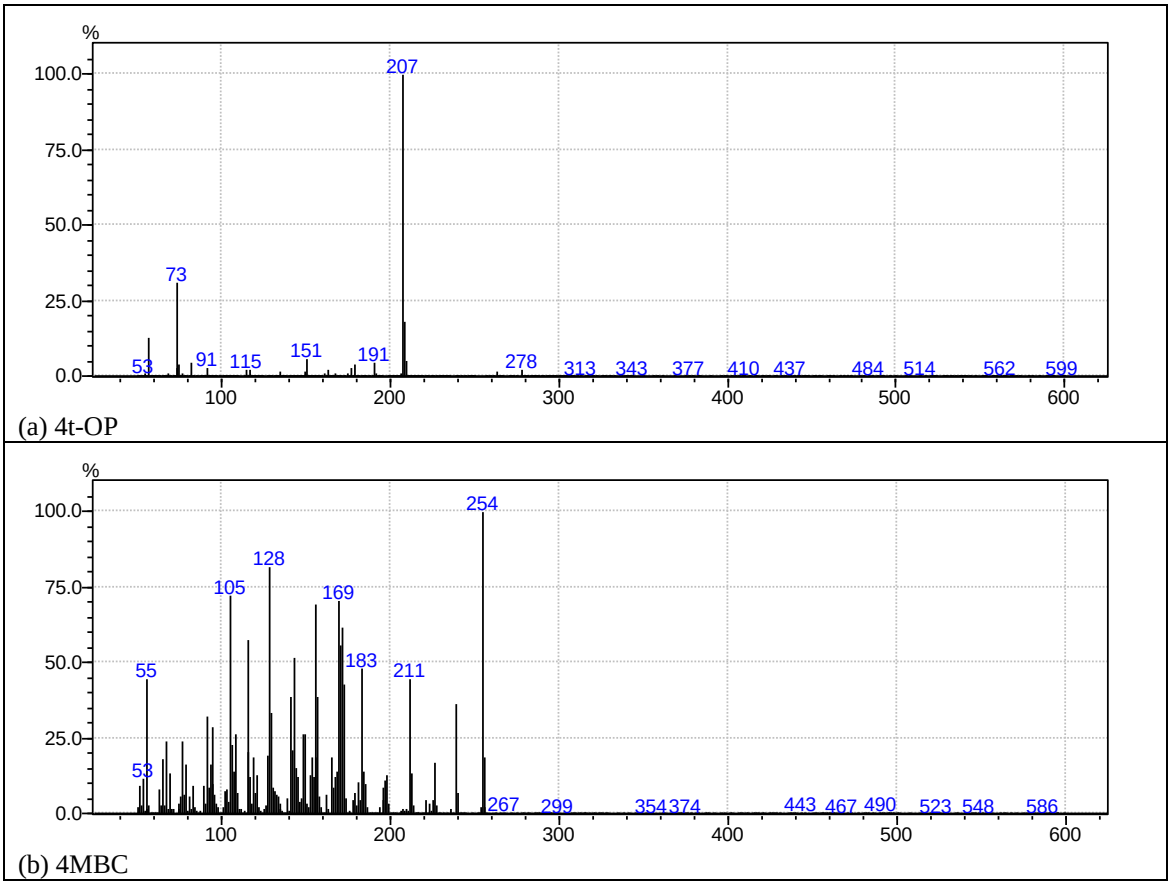

Figure 4.8. Fragmentation patterns for 4t-OP and 4MBC.

4.5.2 Sample Extraction

Establishing a SPE method that achieves high recovery for the diverse set of target analytes involves optimisation of several factors which may work in opposition to one another. The challenges faced included high recovery, reduction or management of co-extracted water and separation of water-soluble matrix components (e.g. sugars, amino acids, salts and protein). The factors optimised included choice of solvent, the order in which the solvents were applied and amounts used and choice of drying agent. Seven separate trials of extraction conditions were completed, as summarised in Table 4.6. The performance of each trial was monitored using labelled surrogate recovery. The surrogate recoveries for each of the trials are compared in Figure 4.12. The recoveries of natives were also monitored as necessary.

The starting point for the optimisation was Trial 1. Surrogate recoveries range from less than 20% for $^{13}C_6$NP to 90% for $^{13}C_6$E2. BP-rec was not included in the surrogate mix used for this trial. The high variability for D4-GEN is due to the difficulties with the derivatisation reaction for this compound.

The native recovery results for SPE trial 1 are shown in Figure 4.9. The recovery corrected results were acceptable at ±20% of target (100 ng), except for 4t-OP, 3PBOH, 4MBC, mTRIC and BP-3. There were no differences in recoveries between synthetic urine and reagent water matrices, except for 3PBOH. The recovery surrogate used for 4t-OP, 4MBC and mTRIC was $^{13}C_{12}$TRIC and was selected based on similarity of partition coefficient (logP, Table A. 13). Using $^{13}C_6$NP as recovery surrogate over-corrected and using $^{13}C_{12}$BPA under-corrected the concentrations for these compounds. For 3PBOH, EQ, ENT and DAID, $^{13}C_{12}$BPA was used as recovery surrogate. This choice could account for the over-correction for EQ and ENT. The blank (unspiked) levels for the target compounds are low as shown in Figure 4.10. For mEHP, mBzP, EQ and GEN, it is possible that either contamination or an interference with the quantification m/z is contributing to the peak area interpreted as the target analyte. No interferences were observed for ENT.

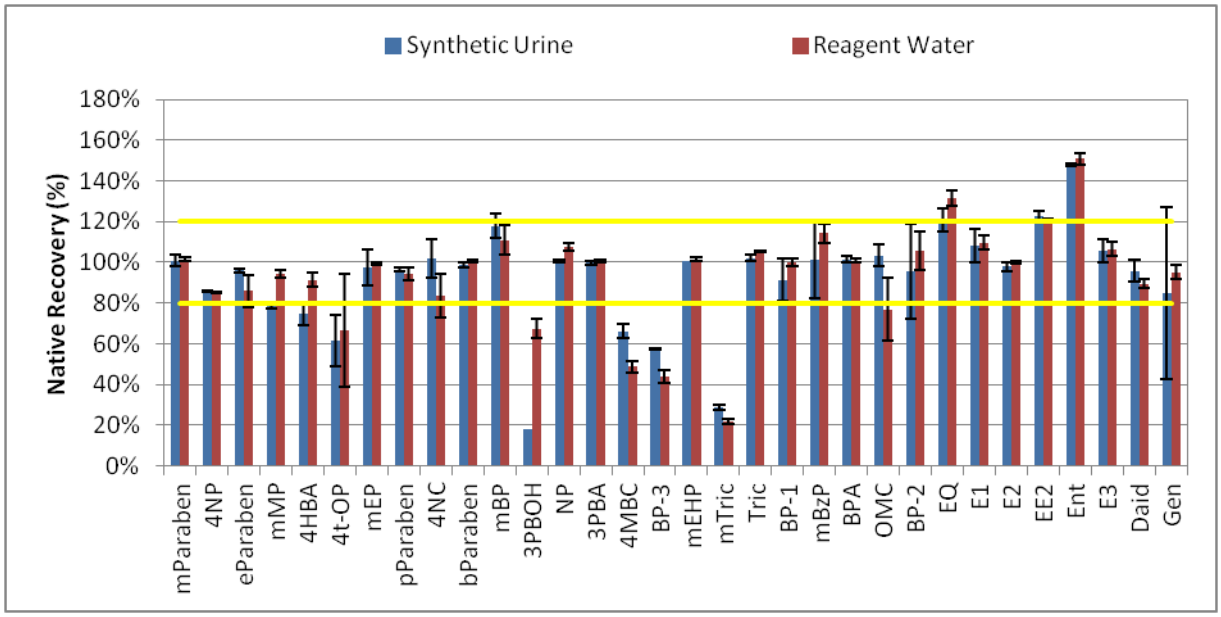

Figure 4.9. SPE trial 1, 100 ng spiked synthetic urine and reagent water results. Recovery corrected concentration as a percentage of the comparative. Error bars indicate ±σ on the average (n=2). Yellow lines indicate ± 20% range on 100% recovery.

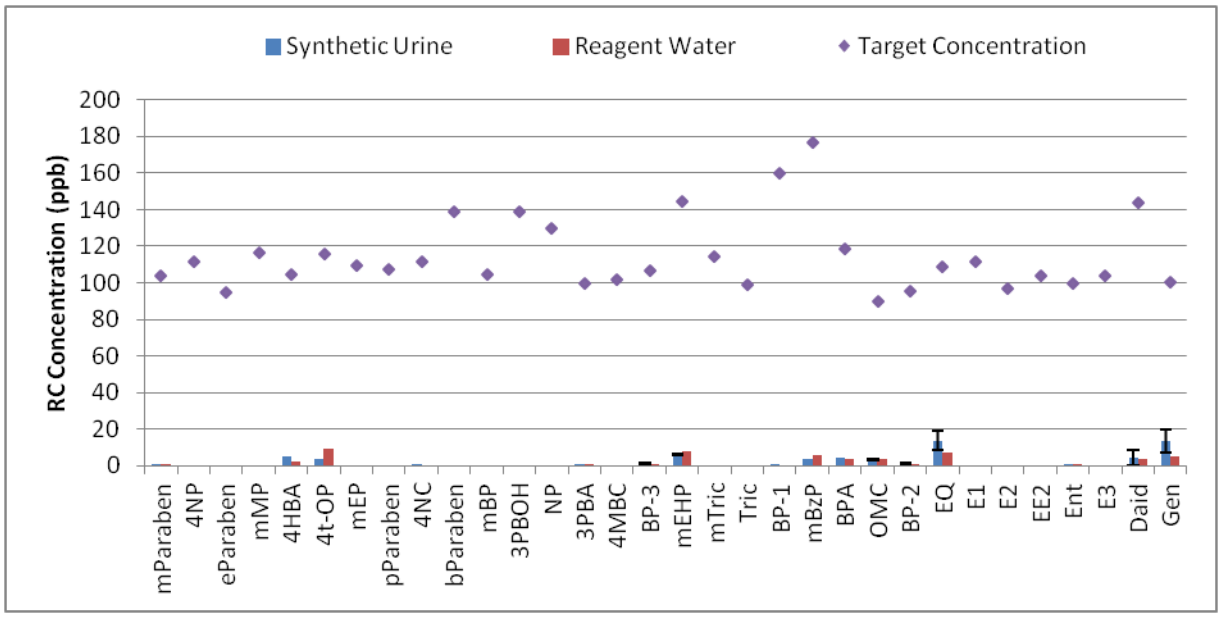

Figure 4.10. Comparison of recovery corrected reagent blank levels to 100 ng spike target concentration. The average of two synthetic urine samples and the single reagent water sample are shown. The error bars indicate ±σ on the average.

These extracts were dried inline with extraction using a second cartridge filled with approximately 1 g Na_2SO_4. The final extract volume of 6 mL took several hours to be reduced to dryness and a white crystalline residue was observed in the reaction vial on dryness. This residue was likely Na_2SO_4 that had been dissolved by residual water and/or methanol in the extract. The water management strategy required improvement to reduce the accumulation of the residue and to reduce evaporation time.

Temporal stability was determined based on the surrogate compounds in the 4 synthetic urine samples and the 3 reagent water samples. Each sample was injected 5 times over a period of 33 hours. Temporal stability was assessed using the variability of repeated injections of the samples in time. Analysis of variance (ANOVA) indicated that the within-sample variability as measured by the mean square error (MSE) was less than between sample variability (differences between the individual synthetic urine or reagent water samples). Temporal stability ranged from 3% to 17% RSD and no clear trend in time was observed. Typical results for $^{13}C_6$-mParaben (most variable) and $^{13}C_{12}$-BPA (least variable) are shown in Figure 4.11.

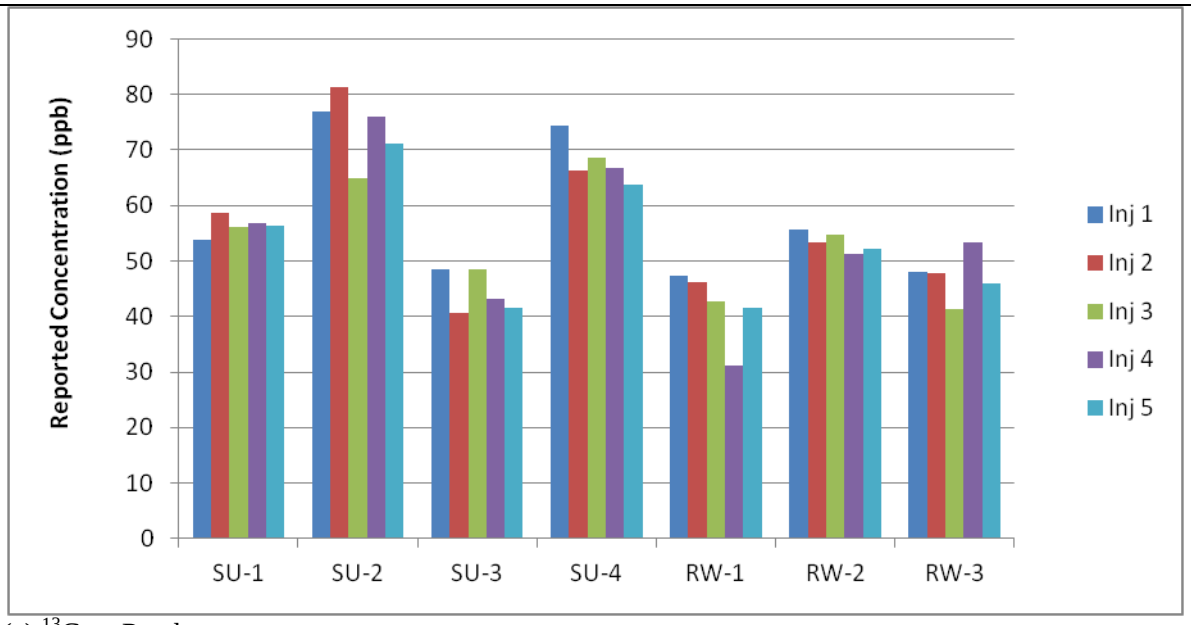

(a) $^{13}C_6$-mParaben
within sample MSE = 20; between sample MSE = 731

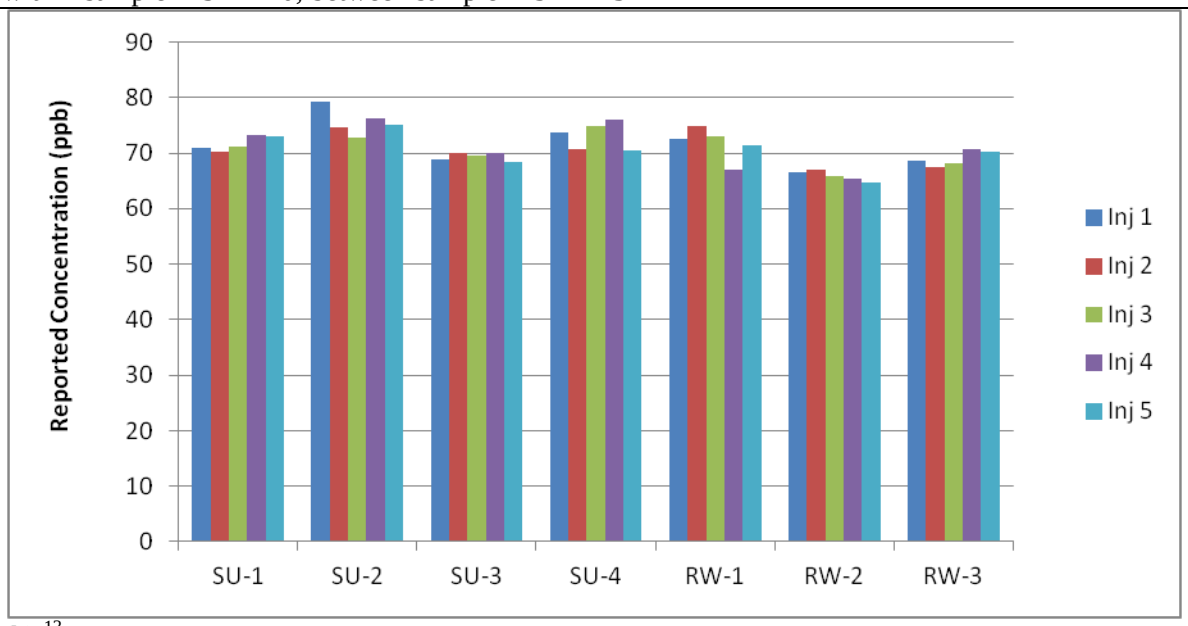

(b) $^{13}C_{12}$-BPA
within sample MSE = 3.6; between sample MSE = 50

Figure 4.11. Comparison of temporal stability and between sample variance for $^{13}C_6$-mParaben and $^{13}C_{12}$-BPA. SU = synthetic urine, RW = reagent water. Time elapsed between Inj 1 and Inj 5 was 33 hours.

Subsequent trials were designed to improve the recovery of the less polar compounds (e.g. NP) without loss of other compounds. Different strategies were also evaluated to better manage the residual water left in the SPE cartridges after loading of the samples. The details

of the trials are summarised in Table 4.6 and the surrogate recovery results are shown in Figure 4.12.

The SPE conditions in Trial 2 improved recoveries slightly for some of the surrogates but the recoveries for others were severely compromised. The major difference was not acidifying the sample prior to extraction which could have resulted in partial ionisation of mEHP and 3PBA. Approximately 8 months had elapsed between Trials 1 and 2 and the synthetic urine had become very cloudy. Although it was filtered prior to use, dissolved proteins may have adsorbed E2 [321, 353], preventing it from being retained by the adsorbent. Acidification would have denatured the protein, freeing E2. Clearly the pH of the samples is a critical factor to control as demonstrated in the results of Trial 3 where the recoveries of mEHP, 3PBA and E2 have been restored. The increase in the amount of MTBE used during extraction may also have contributed to the improved recovery of E2.

The decrease in recovery for mParaben and 4NP in Trial 3 was likely due to volatility. The extracts in Trial 3 again took several hours to dry and a significant amount of Na_2SO_4 was dissolved by the residual water in the samples and transported to the reaction vials.

The increase in GEN in Trial 3 could be due to two factors. First, the installation of a new column and inlet liners with glass wool on the GC-MS. The previous column had been fouled by non-volatile materials resulting in decomposition of GEN in the inlet or on-column. The glass wool in the inlet liner was deactivated *in situ* and is intended to reduce the accumulation of non-volatile material on the column. Second, an increase in the derivatisation reaction temperature from 60 °C to 80 °C may have increased the yield of the reaction. Both the di-TMS and tri-TMS derivatives of GEN were monitored, with the di-TMS derivative present at about 20% of the level of the tri-TMS derivative. The recoveries for the remaining surrogates were unchanged.

Trials 4 and 5 investigated the use of an aprotic polar solvent (ACN) to replace MeOH and the use of MgSO4 as a drying agent in an effort to better manage the residual water content in the extracts. Replacing MeOH with ACN did not change surrogate recoveries compared to Trial 3 as shown in Figure 4.12. The lower variability and slightly improved recoveries for mParaben and 4NP are due to a reduction in solvent evaporation time.

With Trial 5, the samples were left for 24 h at room temperature between quenching the enzyme reaction with formic acid after the specified time and extraction. This is the most

likely reason for the loss of BPA TRIC and GEN and the larger variability observed with the other surrogates in Figure 4.12. From this trial, it was clear that the samples must be extracted immediately after the enzyme reaction is complete.

In Trial 6, hexane was added to the SPE extraction method to increase recovery of the nonpolar compounds and the eluate was collected into 2 tubes. Tube A contained the nonpolar/aprotic fraction and tube B contained the polar/protic fraction. MTBE extracts the residual water content into Tube A but the presence of hexane causes phase separation of the aqueous layer. The aqueous layer was acidified to ensure any organic acids were partitioned into the organic phase. The aqueous layer was then removed and the remaining organic layer was dried over $MgSO_4$. This strategy improved the recovery of mParaben, 4NP, NP, TRIC and GEN and restored BPA recovery, but the recovery of E2 degraded to Trial 2 level. The two extract fractions were analysed separately and the addition of MeOH was responsible for the restoration of BPA and GEN recovery.

With Trial 7, a shift in retention time during the analysis moved the E2 peak so that it was not fully within the SIM window and could not be properly integrated. In comparing the peak height to samples from Trial 5, it appeared that the recovery of E2 had been restored. Removing ACN from the Tube A solvent mix improved the phase separation of the aqueous and organic fractions, shifting the partitioning of E2 back to the organic layer. An interference with the quantification ion for BP-rec resulted in a manually identified peak in the samples approximately 50% larger than in the comparatives, so BP-rec was not reported. As shown in Figure 4.12, recoveries for the other surrogates were similar to those of Trial 6.

4.5.3 Enzyme Deconjugation Reaction

The third SPE trial was also the first test of the enzyme deconjugation reaction. The synthetic urine samples were diluted by 50% with Enzyme Buffer prior to the addition of a 55 ng spike of the enzyme reaction control standard. Incubation times of 30, 60 and 120 minutes at 37 °C were tested with 0.04 mg enzyme. Reaction completion was determined by the ratio of the recovery corrected concentrations of 4NP (β-glucuronidase) and 4NC (arylsulphatase) to the target concentrations of 4NP and 4NC. As shown in Figure 4.13, the arylsulphatase reaction approached completion but the β-glucuronidase reaction was only 55% complete after 120 min.

In Trial 4, the amount of enzyme added was increased, however the solution was 24 h old and had reduced activity. The enzyme solution used in Trial 5 was 48 h old and had significantly lower activity than the fresh solution as seen in Figure 4.13. From this trial, it was clear that the enzyme solution must be freshly prepared before use for full activity. In Trial 6, the quantity of fresh enzyme used resulted in essentially complete hydrolysis of both 4NP-glucuronide and 4NC-sulphate in 120 minutes. With Trial 7, the conditions for the enzyme reaction gave repeatable and stable results as shown in Figure 4.13.

4.5.4 Pooled AF samples

Sufficient pooled amniotic fluid was available to conduct a limited trial of the SPE procedure and the enzyme deconjugation reaction, as summarised in Table 4.7. Surrogate recovery results are illustrated in Figure 4.15 for both tests. For most surrogates, recovery is acceptable and repeatable. The recovery for BP-rec continues to be greater than 100% suggesting a matrix interference with the quantification ion chosen. GEN continues to behave erratically and may not be amenable to quantification by this method. The distribution between di-TMS and tri-TMS derivatives is not stable and appears to be matrix dependent. The recoveries for NP and TRIC remain low, approximately 40-50%.

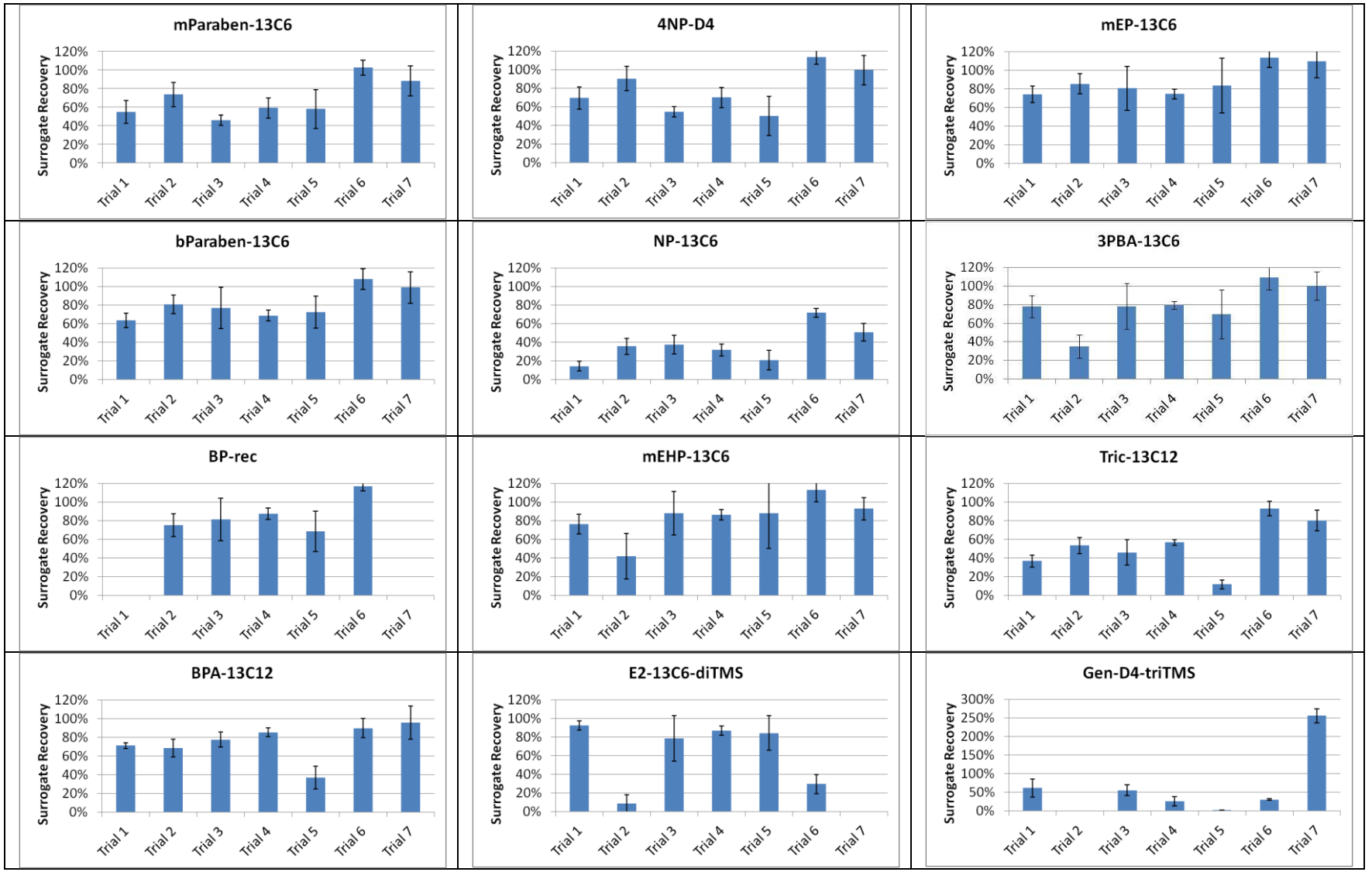

Figure 4.12. Summary of surrogate recoveries for SPE trials 1-7. Error bars indicate ±σ on the average.

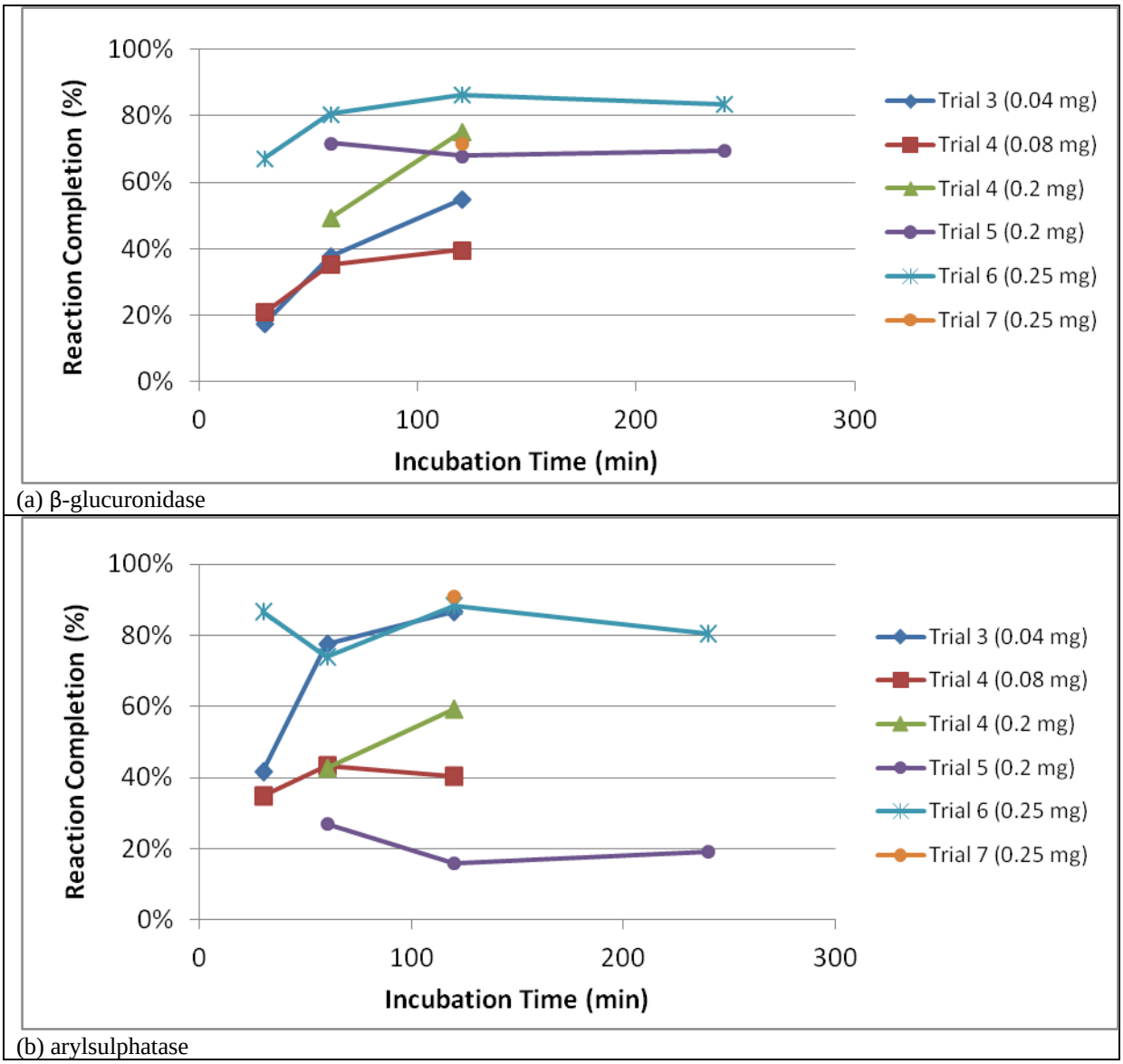

(a) β-glucuronidase

(b) arylsulphatase

Figure 4.13. Enzyme deconjugation reaction completion as a function of time for SPE Trials 3-7.

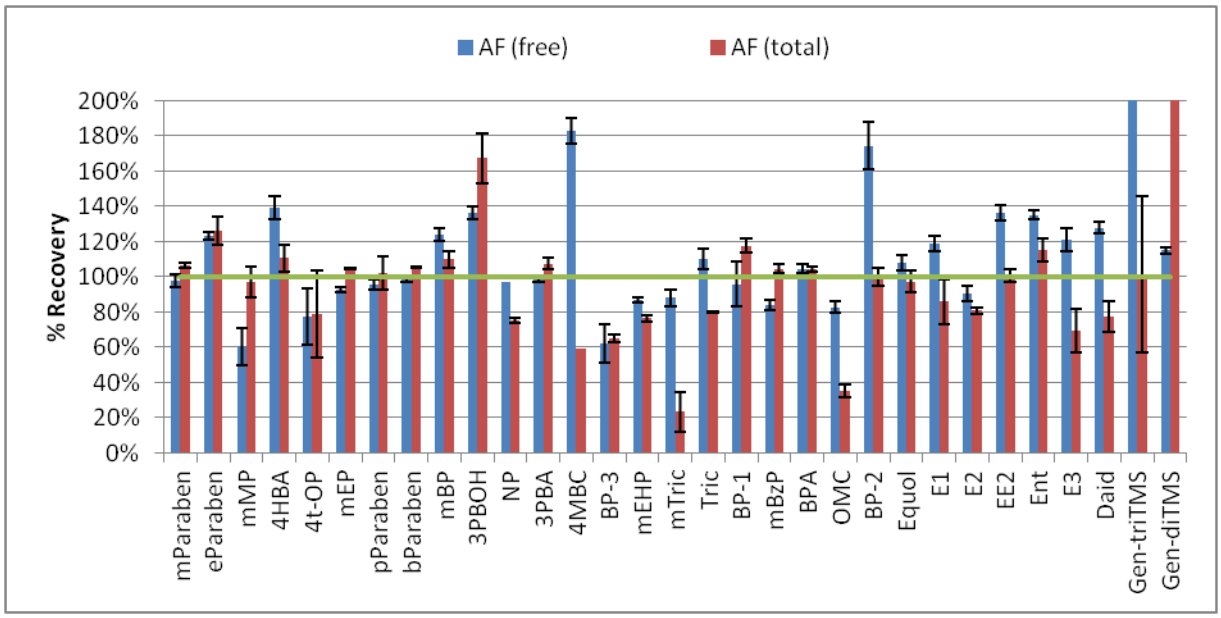

Figure 4.14. %Recovery of native spike in pooled amniotic fluid samples without deconjugation reaction (free) and with deconjugation reaction (total).

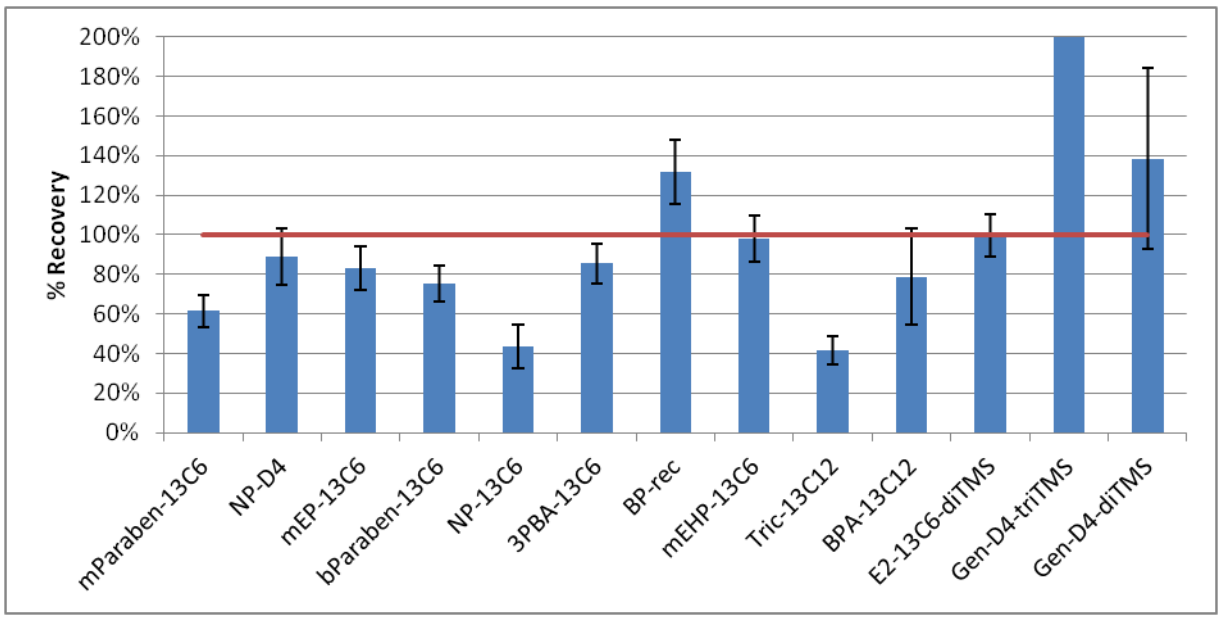

Figure 4.15. %Recovery for surrogates in pooled amniotic fluid samples.

With these results, the changes in quantification and qualification ions indicated in Table 4.5 were made. The method was then applied to the analysis of urine and amniotic fluid samples. Although not ideal, due to time constraints final stages of method validation was done concurrently with sample analysis.

4.5.5 GC-MS Method Validation

4.5.5.1 Analysis Accuracy and Precision

Ideally, accuracy is determined by analysis of a certified reference material or by analysis of standards prepared from materials obtained from a second, independent source. Certified reference materials are not available for the analytes of interest. Cost prohibited the acquisition of materials from a second, independent source. Instead, multiple sets of standards were prepared from the available materials at different times and by different analysts.

Analysis accuracy and precision were assessed using daily calibration check standards at three levels (100, 10 and 1 ppb) representing the lower and mid-range concentration level expected for analytes and one at the upper end of the calibration range. Accuracy was assessed at each level by calculating the %RE for each compound. Precision was assessed at each level by calculating the %RSD for each compound. Each calibration check standard was analysed a minimum of twice on each day, once at the beginning and once at the end of the sample batch and therefore includes contributions from instrument drift and sample instability. The three different calibration standards included in this assessment were prepared from the same materials but by two different analysts on three different days. The results summarised in Table 4.8.

For most analytes, the method performance summarised in Table 4.8 is consistent with the guidelines outlined in Table 4.1. Both GEN and DAID continued to behave erratically, so results for these two compounds are not reported. The %RE for DAID is high, approximately 45% at all levels suggesting an error in calculation, but no evidence was found. At 1 ppb, the %RE for 4HBA is high at 230%, suggesting contamination. EE2 and GEN are not detected at the 1 ppb level. The average instrument accuracy and precision statistics do not vary greatly over the calibration range, indicating that when a compound is detected at 1 ppb, it is reliably detected and quantified. The %RE is often larger at the highest concentration, likely a result of the weighted calibration curve fit to the data. This estimate of analytical precision includes contributions from day-to-day variation in preparing the standards including loss due to volatility of the lighter components, differences among the different calibration standards used and variation in the yield of the analytical derivatisation reaction and therefore represents a realistic estimate of uncertainty.

4.5.5.2 Instrument Limit of Detection

The instrument limit of detection (LOD) is the LOD in the sample as presented to the instrument. It does not include any concentration factors achieved during sample extraction and cleanup. To determine the instrument LOD, the results from the repeated analysis of the 1 ppb calibration standard were used. All of the target analytes except EE2 were reliably detected in the 1 ppb standard. The LOD for EE2 was determined from the 10 ppb standard. As summarised in Table 4.8, the instrument LODs for all target analytes except 4HBA, BPA, BP-2 and EE2 are less than 1 ppb.

Table 4.8. Instrument accuracy (%RE) and precision (%RSD) statistics and instrument LOD (n=11) determined from daily calibration check standards.

	Accuracy (%RE)			Precision (%RSD)			Instrument LOD (ppb)
	100 ppb	**10 ppb**	**1 ppb**	**100 ppb**	**10 ppb**	**1 ppb**	
mParaben-13C6	19	21	10	21	20	20	0.5
mParaben	13	17	13	21	20	20	0.6
eParaben	7	0	5	21	25	21	0.5
mMP	8	9	9	19	20	21	0.8
4HBA	14	26	230	17	17	42	2.4
mEP-13C6	32	19	22	20	18	17	0.5
mEP	40	0	24	27	19	32	0.8
OP	8	1	8	21	22	26	0.7
pParaben	9	15	6	16	19	28	0.8
bParaben-13C6	29	21	5	16	16	25	0.6
bParaben	11	25	12	19	17	23	0.9
mBP	12	5	17	15	18	19	0.5
3PBOH	8	14	4	14	18	29	0.8
NP-13C6	3	7	8	11	11	16	0.4
NP	10	14	1	12	12	20	0.5
3PBA-13C6	13	17	0	15	15	21	0.5
3PBA	21	17	1	17	16	25	0.8
BP-rec	7	9	8	17	20	22	0.6
4MBC	25	6	2	20	25	31	0.9
BP-3	18	15	10	13	21	23	0.8
mEHP-13C6	26	12	4	12	22	22	0.5
mEHP	37	3	7	14	22	29	0.9
mTric	19	16	3	15	21	30	0.8
Tric-13C12	10	15	6	14	18	24	0.5
Tric	21	21	9	15	19	25	0.6
BP-1	7	0	11	10	22	25	0.5
mBzP	27	17	25	13	21	23	0.7
BPA-13C12	1	16	4	9	13	32	0.8
BPA	6	5	10	11	13	33	1.7
OMC	15	12	0	16	24	28	0.7
BP-2	4	1	3	13	21	55	1.4
Equol	17	17	23	9	15	29	0.6
E1	11	10	12	15	19	31	0.7
E2-13C6	11	24	11	15	17	17	0.4
E2	15	2	22	14	18	20	0.3
EE2	17	21	ND	22	21	ND	3.4
Ent	16	20	14	20	27	28	0.7
E3	19	12	12	16	23	38	0.7
Daid	46	49	47	28	33	30	ND
Gen-D4-triTMS	1	5	35	66	65	18	ND
Gen-triTMS	3	9	61	69	76	75	ND
Gen-D4-diTMS	143	427	ND	43	25	ND	ND
Gen-diTMS	116	341	ND	42	27	ND	ND
Min (excluding Daid, Gen)	**1**	**0**	**0**	**9**	**11**	**16**	**0.3**
Max (excluding Daid, Gen)	**40**	**26**	**230**	**28**	**33**	**55**	**3.4**

4.5.5.3 Method Accuracy and Precision

Ideally, method accuracy and precision are determined using matrix blanks. Matrix blanks are by definition identical to samples in every way except that they do not contain the target analytes. For these samples, true matrix blanks were not available. Two approaches were used to estimate method accuracy and precision: spiked reagent blanks and spiked composite urine and amniotic fluid samples.

4.5.5.3.1 Spiked Reagent Blanks

Reagent blanks (0.1 M formic acid and Enzyme Buffer, 5 mL) were spiked with 100 ng and 10 ng natives when the urine and amniotic fluid samples were aliquotted and diluted and returned to the freezer. These spiked reagent blanks were analysed after 4-11 days of storage. The results are summarised in Table 4.9 and illustrated in Figure 4.16.

The 10 ng spike results for 4MBC and OMC are influenced by an interference on the quantification ion that gives high blank levels. For both matrices, the 100 ng spike results are generally within the 40-120% recovery range. There are differences between the two matrices for mMP, NP, 3PBA, BP-3 and mTric, with the recovery from 0.1M formic acid greater than from the Enzyme Buffer. The pH of the matrix during storage is likely the main factor (pH < 3 for 0.1 M formic acid; pH = 5 for the Enzyme Buffer).

The recoveries for the 10 ng spike are higher than for the 100 ng spike. This is due to the high background levels in the extracts as compared to the standards. This issue will be discussed further in section 4.6.1.

Table 4.9. % Recovery of 100 ng and 10 ng native spikes from reagent blanks.

	0.1 M Formic Acid (n=1)		**Enzyme Buffer (n=2)**			
	100 ng	**10 ng**	**100 ng**		**10 ng**	
			avg	**stdev**	**avg**	**stdev**
mParaben	103	123	90	4	147	24
eParaben	92	77	89	2	107	3
mMP	100	102	55	11	81	2
4HBA	102	64	93	5	69	21
mEP	87	76	86	7	97	12
OP	49	69	51	21	83	21
pParaben	103	129	83	4	128	21
bParaben	91	125	80	7	137	20
mBP	119	145	104	5	208	3
3PBOH	90	118	77	8	142	2
NP	92	103	51	28	75	18
3PBA	119	164	90	2	181	9
4MBC	17	0	34	13	14	25
BP-3	115	188	60	16	101	21
mEHP	83	136	83	5	44	54
mTric	100	114	32	24	54	17
Tric	111	142	78	25	127	16
BP-1	111	246	108	9	187	8
mBzP	76	139	103	12	190	27
BPA	81	147	88	1	119	1
OMC	89	20	32	24	6	14
BP-2	102	196	118	24	262	25
Equol	77	126	92	1	223	8
E1	126	228	94	8	251	6
E2	101	173	81	2	174	2
EE2	136	176	109	10	232	43
Ent	103	168	132	31	273	37
E3	127	214	94	3	183	17

Figure 4.16. Comparison of %recovery of 100 ng and 10 ng native spikes in reagent blanks. Error bars indicate ±σ on the average for Enzyme Buffer (n=2). Green lines indicate 40-120% recovery limits Yellow lines indicate recovery limits for spike concentration (80-110% for 100 ng, 60-115% for 10 ng).

4.5.5.3.2 Spiked Composite Samples

Composite urine and amniotic fluid samples were prepared by combining aliquots of individual samples. The composite samples were then aliquotted and spiked at 100 ng, 10 ng and 0 ng of natives, then processed and analysed with the individual samples. The percent recovery of the spiked amount was calculated after recovery correction and blank (unspiked sample) correction. The results are shown in Figure 4.17 and summarised in Table 4.10 for the 100 ng spike and Table 4.11 for the 10 ng spike. For clarity, the 10 ng spiked urine

results are not included in Figure 4.17. GEN and DAID continued to be erratic and the results are not reported.

The overall performance for both matrices is better with the 100 ng spike than the 10 ng spike and is considerably better with amniotic fluid than urine. This is a clear indication of the difficulties with the matrix. With the urine matrix, the results are also better with the total samples than the free samples because the larger, better defined peaks were easier to identify and integrate above the matrix background. Matrix issues will be addressed in the discussion on selectivity and sensitivity in section 4.6.1.

Table 4.10. Average %Recovery and standard deviation for the 100 ng spike of urine and amniotic fluid samples (n=3). NQ indicates analyte not quantified.

	Urine (free)		Urine (Total)		AF (Free)		AF (Total)	
	Average	**Stdev**	**Average**	**Stdev**	**Average**	**Stdev**	**Average**	**Stdev**
mParaben	92	13	123	93	114	12	108	15
eParaben	98	9	115	46	101	8	100	10
mMP	83	8	88	1	95	8	93	10
4HBA	130	69	45	NA	97	12	85	14
mEP	101	44	177	145	101	17	98	21
OP	54	5	79	14	71	9	67	2
pParaben	84	9	125	81	100	11	96	7
bParaben	54	12	69	15	89	2	88	3
mBP	145	34	101	106	105	23	94	28
3PBOH	30	13	22	5	93	6	95	7
NP	109	16	66	17	105	6	91	9
3PBA	95	17	121	17	110	12	105	9
4MBC	71	54	46	17	108	29	38	10
BP-3	65	24	83	104	114	46	80	7
mEHP	125	28	79	3	90	3	91	4
mTric	109	2	28	1	108	25	62	4
Tric	103	14	105	79	99	10	90	7
BP-1	85	9	73	62	122	5	124	13
mBzP	NQ	NA	59	28	90	8	124	13
BPA	68	6	89	13	87	6	92	3
OMC	97	28	18	2	116	14	74	10
BP-2	16	2	5	2	126	23	117	34
Equol	83	11	289	361	102	18	104	14
E1	91	9	65		121	9	107	20
E2	127	11	56	9	96	5	89	9
EE2	232	45	210	50	134	7	128	22
Ent	125	2	NQ	NA	131	19	134	34
E3	80	38	1248	NA	106	12	71	14

Table 4.11. Average %Recovery and standard deviation for the 10 ng spike of urine and amniotic fluid samples (n=3). NQ indicates analyte not quantified.

	Urine (free)		Urine (Total)		AF (Free)		AF (Total)	
	Average	**Stdev**	**Average**	**Stdev**	**Average**	**Stdev**	**Average**	**Stdev**
mParaben	141	59	660	793	138	14	190	35
eParaben	166	41	351	389	98	23	121	3
mMP	108	8	112	NA	120	11	148	21
4HBA	904	1261	571	NA	72	53	119	11
mEP	371	314	1731	NA	86	25	146	66
OP	21	NA	189	92	80	22	110	24
pParaben	109	67	626	747	138	11	159	11
bParaben	NQ	NA	204	NA	135	14	156	13
mBP	464	NA	195	89	175	36	218	66
3PBOH	130	37	NQ	NA	148	7	195	15
NP	NQ	NA	921	NA	162	17	158	23
3PBA	231	28	NQ	NA	201	17	240	33
4MBC	343	NA	NQ	NA	266	183	135	63
BP-3	113	114	612	682	227	75	138	16
mEHP	440	112	76	16	161	8	164	29
mTric	206	23	NQ	NA	184	51	93	4
Tric	517	46	719	911	177	3	153	36
BP-1	305	7	405	455	263	27	265	42
mBzP	110	NA	175	188	201	12	399	131
BPA	115	6	122	6	144	11	141	14
OMC	220	92	45	NA	139	58	86	8
BP-2	111	42	18	21	266	74	332	81
Equol	149	23	5733	NA	185	59	229	28
E1	242	272	171	NA	277	14	175	48
E2	1101	167	128	NA	181	15	188	32
EE2	492	123	584	75	228	34	297	61
Ent	491	305	9	NA	226	87	248	70
E3	219	72	6915	9390	159	9	90	68

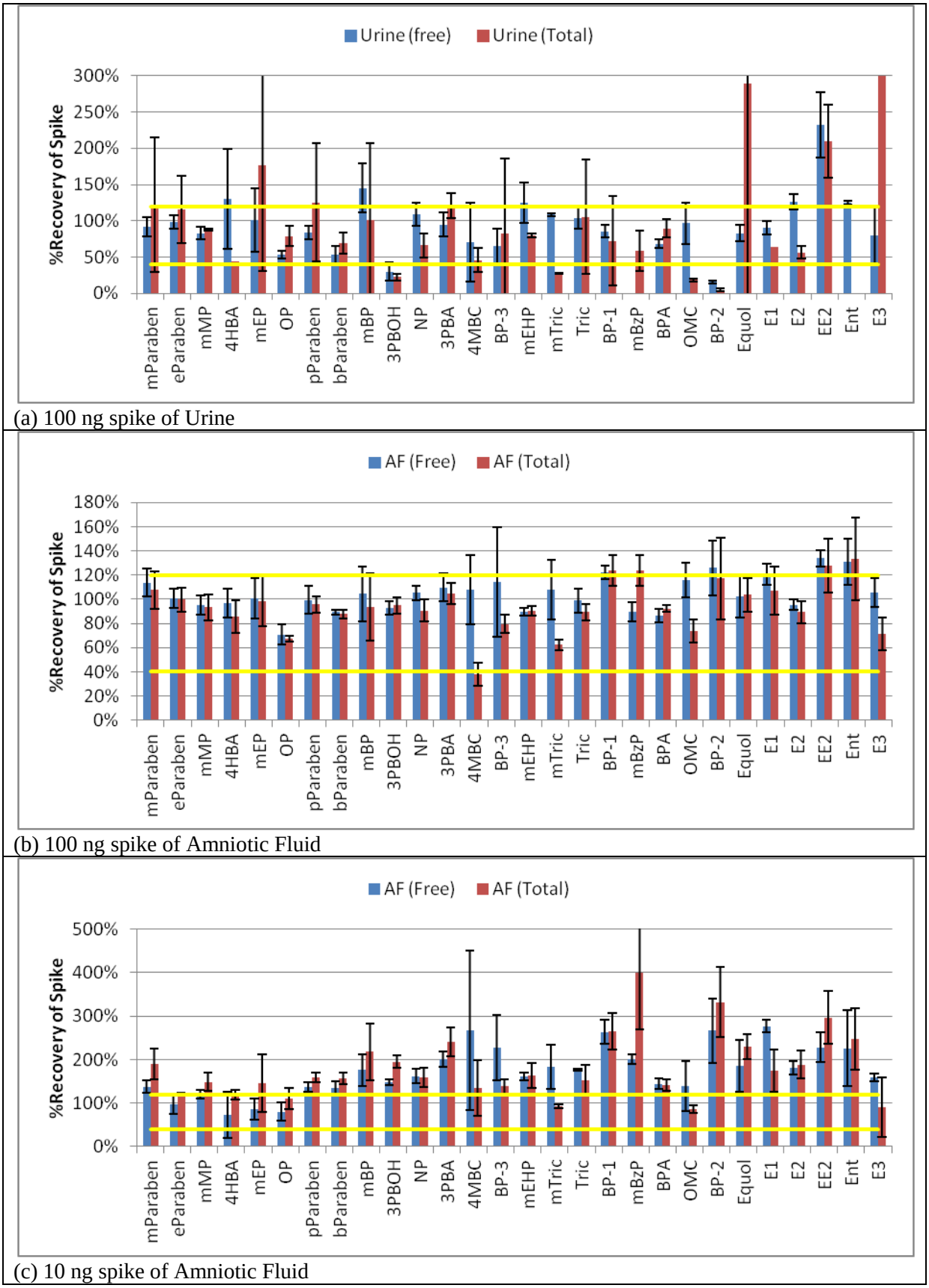

Figure 4.17. Recovery of 100 ng and 10 ng spiked amounts in composite urine and amniotic fluid samples. Yellow lines indicate 40-120% recovery limits.

4.5.5.4 Selectivity and Sensitivity

Selectivity was assessed with both daily calibration check standards and spike recovery samples. The level of interferences present in the daily calibration check standards ought to be low, but if present would be most evident at the lowest concentration level, with %RE increasing dramatically as the concentration of the target analyte decreased. Only 4HBA showed any indication of interferences present in the daily calibration check standards.

The spike recovery results for the reagent blanks and amniotic fluid at 100 ng are generally within the 40-120% recovery limits but at 10 ng, the results indicate the potential for over-estimating analyte concentrations. This is a direct result of forced manual identification as discussed in section 4.6.1. The spike recoveries at both 100 and 10 ng are not particularly instructive for the urine samples due to the high natural concentrations of target analytes. These results are subject to large uncertainties due to the 'small difference between two large numbers' phenomenon.

4.5.5.5 Extension of the Calibration Range

At the completion of sample analysis, additional standards were analysed to extend the calibration range from 100 ppb to 1000 ppb. This was necessary to report the target analytes in the urine samples that were present above 100 ppb. To ensure consistency with the initial calibration, the set of standards used to extend the range overlapped with the existing calibration at 50, 75 and 100 ppb levels. The highest level included in the extended calibration range was 750 ppb because several of the quantification ions were saturated at 1000 ppb. No calibration check data is available above 100 ppb.

4.5.5.6 Method LLOQ

With these challenges, the best estimates of measurement uncertainty and LOQs are obtained from an ad-hoc evaluation of the data. The lowest concentration for each analyte in the sample as presented to the instrument was identified and it represents the smallest peak that could be reliably identified by manual inspection of the chromatogram and examination of the ion ratios of the candidate peak. From this concentration, the reported sample concentration (corrected for surrogate recovery and aliquot volume) was identified. This reported concentration is the best estimate of LLOQ and is given in Table 4.12 for each of the sample matrices. A corrected concentration lower than this level was set to "NQ" for "not quantifiable". With reagent blank subtraction, it is possible to obtain a concentration lower than the LLOQ. If the reagent corrected concentration was less than 1σ of the reagent blank

mean, the blank corrected concentration was set to NQ. The best estimate of ULOQ is the concentration of the highest calibration standard, nominally 100 ppb. Because of the nonlinear calibration curve, uncertainty increases with extrapolation outside the range defined by the calibration standards.

Table 4.12. Best estimate of LLOQ (ng/mL) for target analytes in different matrices.

	Urine n=88		Amniotic Fluid n=70	
	Min	**Detects**	**Min**	**Detects**
mParaben	2	33	0.4	29
eParaben	22	44	1.1	3
mMP	3	37	0.6	24
4HBA	126	38	18	32
mEP	6	32	2.6	65
OP	ND	0	ND	0
pParaben	3	27	1.5	6
bParaben	17	1	2.0	3
mBP	36	7	4.8	22
3PBOH	ND	0	ND	0
NP	ND	0	ND	0
3PBA	ND	0	ND	0
4MBC	53	2	2.8	68
BP-3	5	4	1.2	58
mEHP	46	43	5.8	67
mTric	ND	0	ND	0
Tric	2	26	0.6	44
BP-1	8	5	0.4	53
mOP	ND	0	ND	0
mBzP	5	7	ND	0
BPA	2	44	0.7	68
OMC	ND	0	13	68
BP-2	4	42	0.1	8
Equol	6	23	0.2	13
E1	15	36	6.3	36
E2	7	18	1.5	35
EE2	ND	0	ND	0
Ent	10	23	3.7	49
E3	8	38	4.4	68
Daid	not reliably quantified in any samples			
Gen	not reliably quantified in any samples			

4.5.5.7 Extraction Efficiency

Extraction efficiency was monitored for each sample using labelled surrogates. The average recovery and %RSD for each surrogate by sample type are summarised in Table 4.13. BP-rec was intended to be the recovery surrogate for the benzophenones, but an interference made it useless. An interference also affected the recovery of $^{13}C_6$-mEHP. In both cases, $^{13}C_{12}$BPA was used instead. The recoveries for the remaining surrogates were acceptable,

within the range of 45-99%. The %RSD is a measure of reproducibility of extraction over all samples of a given type and is less than 20%.

4.5.5.8 Method Reproducibility

Method reproducibility is a measure of how well the entire sample extraction and analysis method performs on the same sample on the same day and different days. Reproducibility was assessed using the composite amniotic fluid samples prepared for the matrix spike study. Three unspiked composite samples were processed through the free analysis and three were processed through the total analysis. The results are shown in Figure 4.18. The %RSD on the average of the three samples for each analyte was calculated and plotted as a function of reported concentration, as shown in Figure 4.19. The %RSD on the three repeats ranges from 1% to 86%, with the highest variability generally observed with the lowest reported concentration.

Table 4.13. Extraction efficiency for urine and amniotic fluid samples as measured by %Recovery of surrogates.

Surrogate	Urine				Amniotic Fluid			
	Free		Total		Free		Total	
	Average	%RSD	Average	%RSD	Average	%RSD	Average	%RSD
$^{13}C_6$mParaben	54	17	64	18	66	13	66	10
D_4-4NP	69	12	66	21	81	16	80	11
$^{13}C_6$mEP	60	24	59	29	74	15	80	15
$^{13}C_6$bParaben	68	20	76	26	89	12	86	7
$^{13}C_6$NP	45	20	59	15	76	14	69	10
$^{13}C_6$3PBA	74	10	74	17	88	12	80	8
BP-rec	159	34	194	43	115	6	100	6
$^{13}C_6$mEHP	87	13	104	18	122	12	104	8
$^{13}C_{12}$Tric	52	11	60	20	94	8	85	5
$^{13}C_{12}$BPA	99	9	96	11	99	9	92	5
$^{13}C_6$E2	72	10	76	19	99	8	92	8

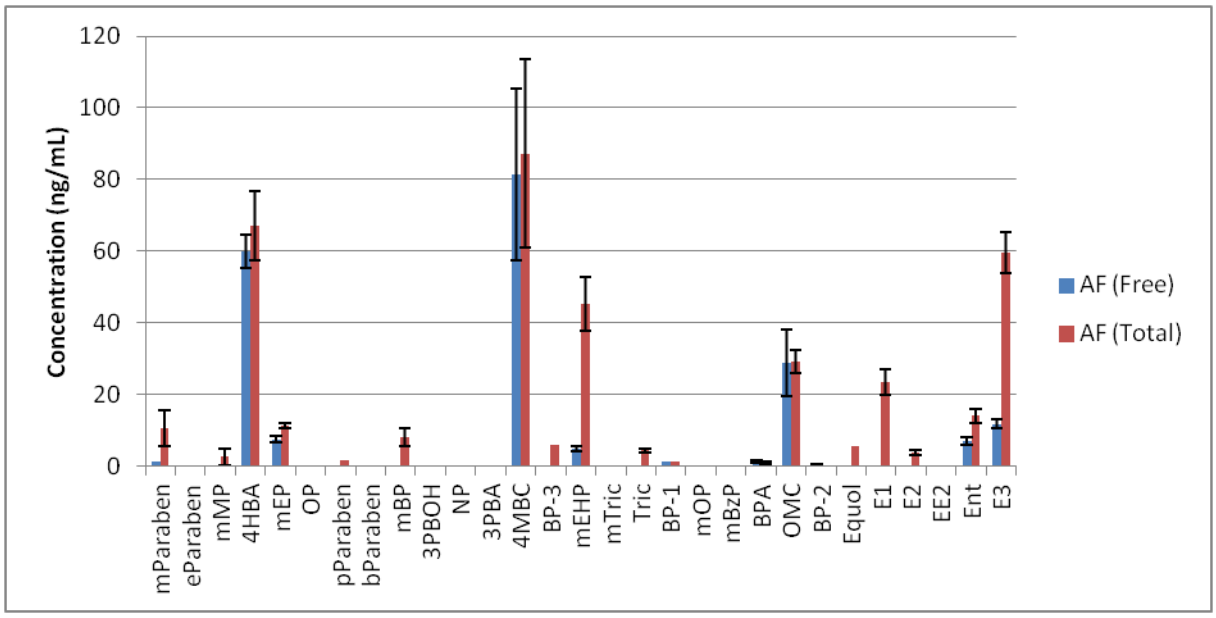

Figure 4.18. Reproducibility of analysis for composite amniotic fluid samples (n=3). Error bars indicate ±σ on the average.

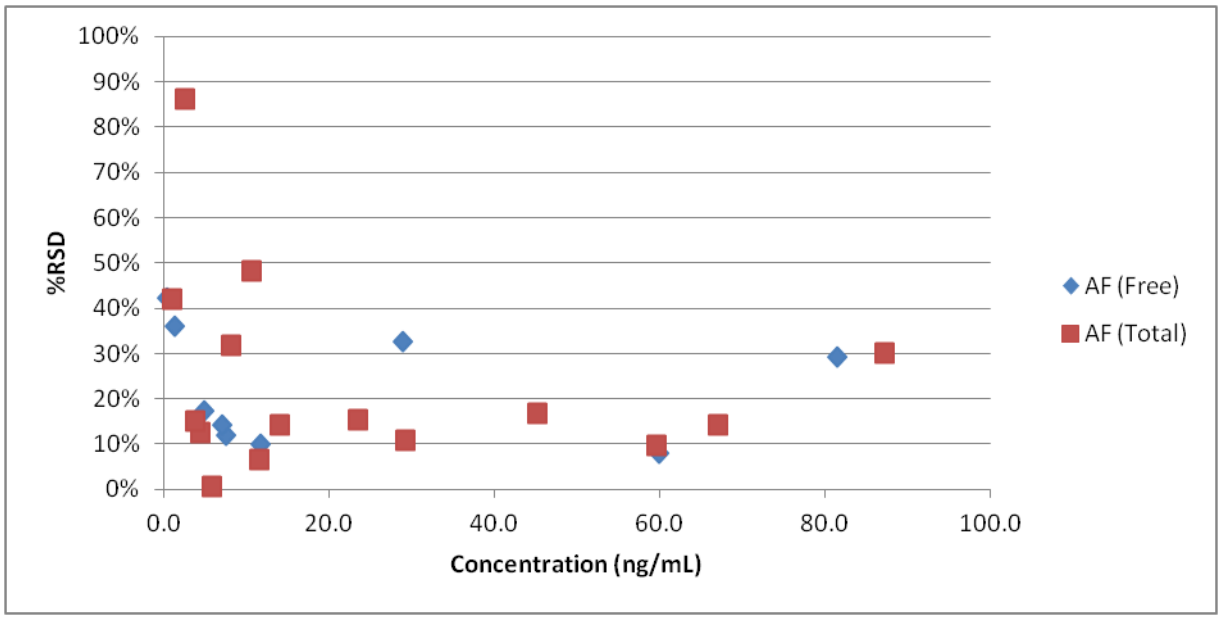

Figure 4.19. Correlation of analysis variability (%RSD, n=3) with reported concentration as determined by the analysis of unspiked composite samples of amniotic fluid for both the free and total analyses.

4.6 Discussion

4.6.1 Selectivity and Sensitivity

Ideally, spike recovery studies are done using matrix blanks. Matrix blanks are by definition identical to samples in every way except that they do not contain the target analytes. Since matrix blanks were not available, spiked reagent blanks and pooled samples were used.

With the spike recovery samples, results were generally within the 40-120% range for both reagent blanks and composite amniotic fluid samples at 100 ng. With the spiked urine samples, some compounds showed good results, others did not. For example, the 4HBA spiked amount was substantially under-reported in urine for two reasons. First, the high natural concentration of this compound in urine was on the order of 1000 ppb. Determining the contribution of a 100 ng spike on top of this large natural concentration is subject to considerable uncertainty due to the small difference between two large values. The extrapolation beyond the calibration range further increases uncertainty. This situation is also present for other compounds, particularly with the total samples. With the urine samples, the signal attributable to the 10 ng spike is well within the measurement uncertainty (nominally ±20% at 100 ppb, Table 4.8) at the natural levels of most of the compounds and therefore not useful.

With the reagent blanks and amniotic fluid samples, the natural levels are much lower and the spike recovery results are much better. There are still a few difficulties with the results. Interferences due to the matrix are a problem as illustrated with the following example for 3PBOH.

To be correctly identified as a target analyte, the peak in the chromatogram must be within a narrow window (±0.1%) of the expected retention time and the ratio of quantification to qualifier ions must be within a specified range (±15%). However, the peaks have width at the base on the order of 0.09 min which is independent of peak height. Thus, peaks at lower concentration are shorter than those at higher concentration and more difficult to detect over the baseline and less certain for assignment of retention time. Figure 4.20 shows 3PBOH in different contexts, a standard, spiked at 10 ng in a reagent blank and amniotic fluid and not present in amniotic fluid. In the 10 ppb standard, the peak is well defined and free of interferences – all ions follow the same Gaussian peak shape. In both the reagent blank (Enzyme Buffer), and the amniotic fluid sample (diluted with Enzyme Buffer), the quantification ion (m/z 272, black trace) is well defined but the three qualifier ions have contributions from nearby peaks. The contribution to m/z 211 (brown trace) makes this ion useless as a qualifier ion. In both the reagent blank and the spiked amniotic fluid sample, the peak had to be manually identified to be included in the report because the ion ratios were not within the specified range. The peak shown in panel (d) is of the unspiked amniotic fluid sample. The peak at RT = 16.964 min is outside the window for identification as 3PBOH and

also does not meet the ion ratio criteria, but this peak will contribute to the area of the 10 ng spike peak as it is within the base width of the 10 ng 3PBOH peak. Although the reported concentration of this peak is only 2.4 ppb, the nonlinear calibration curve results in a much larger apparent contribution to concentration because the area increase occurs on a larger peak at a point in the calibration curve where the slope is greater. This is the main reason for the over-recovery of the 10 ng spike samples. The same situation is present with the 100 ng spike samples, but the relative contribution of the interference peak is much smaller.

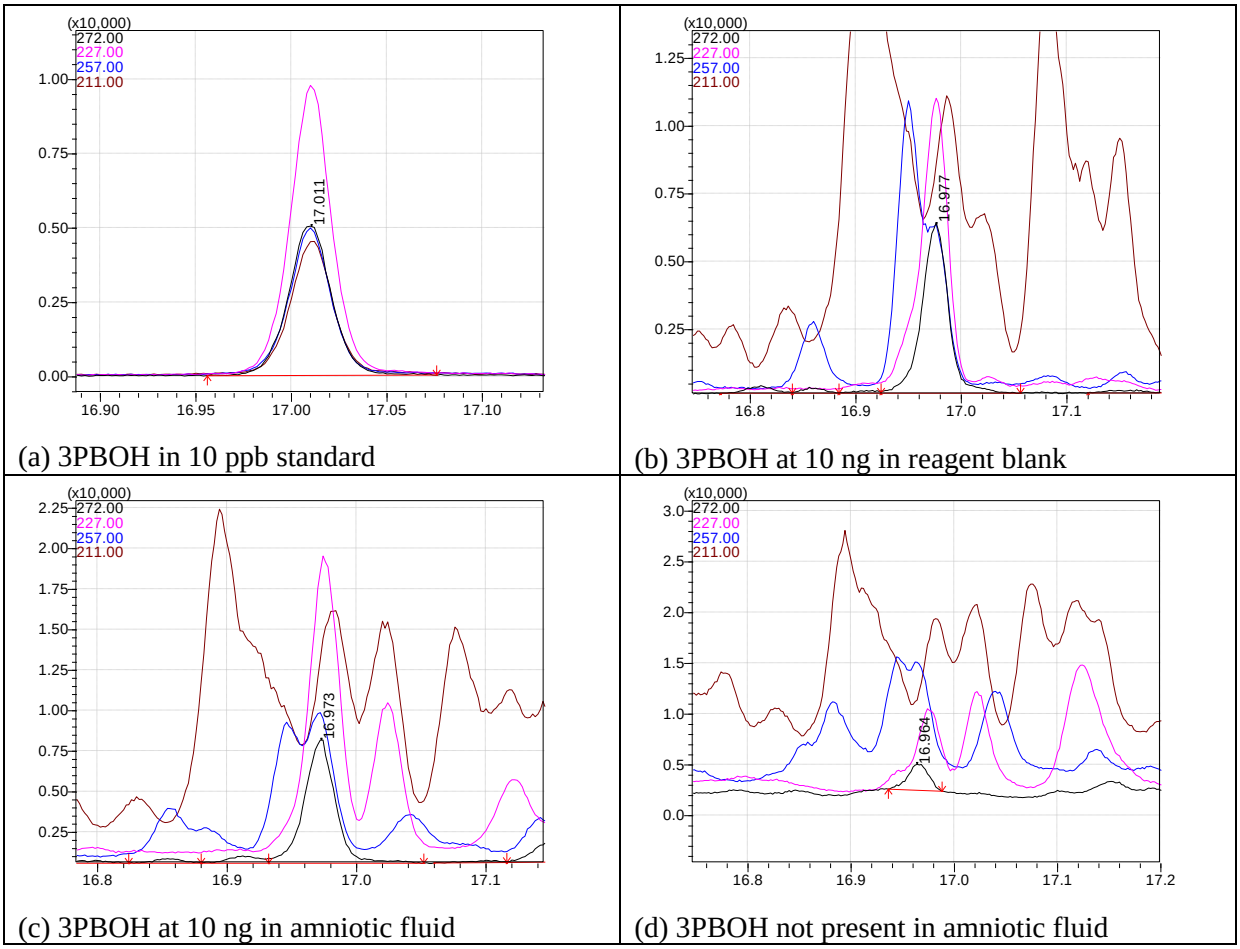

Figure 4.20. SIM chromatograms showing the interference effect on 3PBOH. X-axis is retention time (min), Y-axis is detector signal. See text for explanation.

A similar phenomenon affects 4MBC, but with a different outcome. In this case, the peak size of the spike is relatively small compared to the size of the interference peak. The result of blank subtraction is again a small difference between two large numbers and the large variability in spike recovery. The blank subtraction works well for the 100 ng spike in the free analysis of amniotic fluid where the interference peak is smallest, but rapidly deteriorates as the interference peak grows relative to the spiked amount in the total analysis of amniotic fluid and in both the free and total analyses of urine.

The matrix effect on actual samples is two-fold. First, the target analyte must be present in sufficient quantity to provide both a detectable peak with the correct ion ratios to be identified automatically by the software. A compound by compound review of each sample can lead to confident identification of additional peaks provided the evidence for identification remains strong, as with the case of 3PBOH in the spiked sample given above. If the situation as illustrated with 4MBC is present, only very large concentrations of the target analyte may be detected, and likely only by manual verification. Thus, the complexity of the matrix has negative effects on both selectivity and sensitivity which will be different for each target analyte and each sample type. The effect may also be dependent on the composition of the individual sample, making a general statement about selectivity and sensitivity very difficult to formulate. However, with careful inspection and sound judgement, target analyte identification can be confidently achieved.

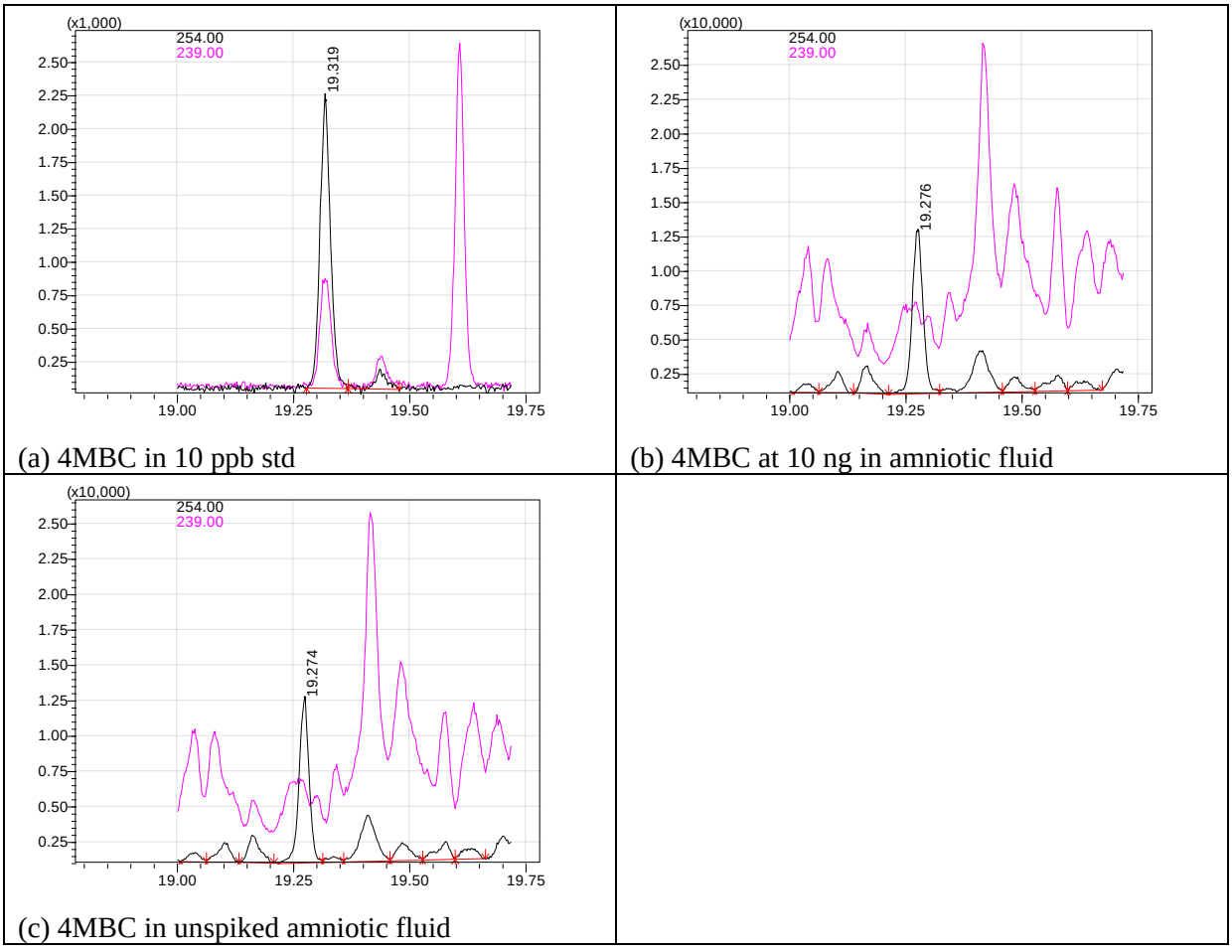

Figure 4.21. SIM chromatograms showing the interference effect on 4MBC. -axis is retention time (min), Y-axis is detector signal. See text for explanation.

4.6.2 Problems with GEN and DAID

The challenges encountered in determining GEN and DAID were due to the complexity of the sample matrix and they were greater for the urine samples than for the amniotic fluid samples. These challenges were a direct result of the scope of the target analyte list which included carboxylic acids as well as phenols.

Initially, the derivatisation reaction performed well for GEN and DAID in the calibration standards, and for extraction of spiked reagent water (Figure 4.9). Matrix related problems began to appear with the spiked synthetic urine samples (Figure 4.9). Subsequent changes to the SPE extraction method intended to improve recovery of the less polar analytes led to the deterioration of the performance of the derivatisation reaction for GEN and DAID as is evident in Figure 4.12. The situation further deteriorates with extraction of real AF samples as seen in Figure 4.14 and Figure 4.15. By the time the urine samples were attempted, the results for GEN and DAID were not useful as the calibration standards were now being affected. Several possible explanations can be offered:

- Incomplete derivatisation, leading to formation of both di- and tri-TMS derivatives. It is also possible that mono-TMS derivative was formed, but it was not determined. The partitioning among the possible derivatives was also not reproducible for either the samples or standards.
- Competition for derivatisation reagent by matrix components leading to interferences with either the kinetics or equilibrium of the reaction for GEN and DAID.
- Decomposition of the derivatives in the GC inlet due to fouling by non-volatile residues. This is quite likely as the previously well-behaved calibration standards began to be affected.
- Non-volatile, insoluble residue left in the reaction vials, even after cleaning, that interfered with the derivatisation reaction for GEN and DAID.

As discussed in Section 4.1, previous studies of EEs in human fluids (urine, serum and amniotic fluid) have addressed subsets of the target analyte list of this study. None of these studies considered both acidic and phenolic analytes in the same extraction and derivatisation method. The published methods for determining phytoestrogens including GEN and DAID by GC-MS with TMS derivatisation [354-359] have two common features in the sample cleanup procedures. First, liquid-liquid extraction of the aqueous samples (pH 3-5) is performed using a nonpolar solvent such as ethyl acetate or diethyl ether. These solvents will

preferentially extract the phenols, and because most aliphatic and aromatic carboxylic acids have pKa values less than 4, they are partially, if not fully ionised in the aqueous phase. This extraction, therefore, leaves the carboxylic acids behind in the aqueous phase. Second, the extract is further cleaned up using gel filtration chromatography to further remove potential interferences to the derivatisation reaction.

4.7 Conclusion

4.7.1 Final Method

With the results from the pooled AF samples, several changes to the quantification and qualification m/z were made (see Table 4.5) in an effort to reduce interferences. This was successful in most cases, but interferences were still present with 4MBC, OMC, BP-rec and $^{13}C_6$-mEHP. Unfortunately, GEN and DAID are not amenable to this method because of the matrix interferences with the derivatisation reaction.

The final SPE method parameters are summarised below.

Table 4.14. SPE procedure for pooled urine and amniotic fluid samples.

Parameter	SPE Extraction Free	SPE Extraction Total
Matrix	2 mL urine or 2.5 mL amniotic fluid diluted with 4 mL 0.1 M formic acid	2 mL urine or 2.5 mL amniotic fluid diluted with 4 mL Enzyme Buffer and 4 mL reagent water
Surrogate Spike	100 ng	100 ng
Enzyme Control Spike	no	55 ng
Enzyme	no	0.5 mg
Incubation	no	37 °C, 2 hours
Acidification	pH <3 on dilution	500 µL formic acid (98%) after incubation pH <4
Condition	2 mL each Hex, MTBE, MeOH, H_2O	2 mL each Hex, MTBE, MeOH, H_2O
Load	quantitative transfer 1 mL 0.1 M formic acid	quantitative transfer 1 mL 0.1 M formic acid
Wash	1 mL 0.1 M formic acid 1 mL MeOH/H_2O (5:95)	1 mL 0.1 M formic acid 4 mL MeOH/H_2O (5:95)
Elute	Tube A: 1 mL Hex/MTBE (50:50) + 2 mL Hex + 2 mL Hex/MTBE (50:50) Tube B: 4 mL MTBE/MeOH (60:40) + 2 mL MeOH	Tube A: 1 mL Hex/MTBE (50:50) + 2 mL Hex + 2 mL Hex/MTBE (50:50) Tube B: 4 mL MTBE/MeOH (60:40) + 2 mL MeOH
Dry	acidify aq. layer in Tube A and remove dry organic layer over $MgSO_4$	acidify aq. layer in Tube A and remove dry organic layer over $MgSO_4$
Derivatisation Conditions	BSTFA/ TMSI (98:2) 80 °C, 60 min	BSTFA/ TMSI (98:2) 80 °C, 60 min

4.7.2 Method Validation

The traditional method performance and validation metrics were at some points difficult to apply to this method because of the matrix challenges. These difficulties affected GEN and DAID to the point that these two analytes could not be reliably determined by the method.

The analysis method performed very well for daily calibration check standards as summarised in Table 4.8. The method was stable over the 4 weeks of sample analysis as illustrated in the control charts in Figure A. 1 and derivatised samples were stable over the typical duration of a batch as illustrated in Figure 4.11. The SPE method performed well for analyte recovery as summarised in Table 4.13.

The instrument LOD was acceptable at less than 1 ppb for all but 4 compounds. The instrument LODs for EE2, 4HBA, BPA and BP-2 were 3.4, 2.4, 1.7 and 1.4 ppb respectively. Attempting to determine LLOQ and ULOQ from spiked samples was difficult due to the matrix interferences and their effects on quantification of the spiked samples as discussed in

section 4.6.1. The ad-hoc evaluation of LLOQ resulted in acceptable overall performance and the method is deemed fit for purpose.

Chapter 5 Gestational Exposure to Environmental Estrogens

5.1 Introduction

Human gestational exposure to EEs can be measured by chemical analysis of amniotic fluid collected early in the second trimester of pregnancy, during diagnostic amniocentesis. This study was granted human ethics approval from both the New Zealand Health and Disability Upper South Regional A Ethics Committee and the University of Canterbury Human Ethics Committee.

A cohort of 32 New Zealand women was recruited for the study after diagnostic amniocentesis at the Christchurch Women's Hospital. The recruitment materials are included in the Appendix. A total of 38 women were invited to participate and the first 32 to give informed consent were included in the study. No specific selection criteria were used. The women were aged 19.6-43.3 years (mean = 31.8, median = 32.7). There were 16 male and 16 female fetuses of gestational age 14.9-20.6 weeks (mean = 17.6, median = 17.0). No other demographic data was collected on the mothers.

Amniotic fluid and matched maternal urine samples were collected from each mother. The maternal urine samples were used to obtain an indication of recent maternal exposure to the EEs of interest in the study.

In this study, it is assumed that maternal exposure is well represented by a single urine sample. Three studies provide evidence to support the assumption that a single urine sample represents an individual's exposure to EEs. In the first study [360], temporal variability and daily reproducibility of urinary measures of seven phthalate monoesters was evaluated in 46 U.S. women on two consecutive days. The daily levels were strongly correlated (Pearson correlation coefficient between the 0.5 and 0.8). The authors suggested that even with the short half-lives of phthalates, women's patterns of exposure may be sufficiently stable to assign an exposure level based on a single first morning void urine measurement. In another study [361], the temporal variability in urinary phthalate metabolite levels over 3 months among 11 U.S. men was evaluated. Up to nine spot urine samples were collected for each man during this time period. Although substantial day-to-day and month-to-month variability in each individual's urinary phthalate metabolite levels were seen, a single urine sample was moderately predictive of each subject's exposure over 3 months. In a third study [324], urine samples from 35 U.S. children aged 6-10 years were analysed for 13 EEs including phthalate metabolites, phytoestrogens and phenols. Six samples were collected from each child over a 6 month period. The authors found that the 6-month average concentration was predicted by

a sample collected at the start of the interval as well as by a sample collected at the end of the interval. They also suggested that an annual urine sample used for exposure assessment in longitudinal studies might be reflective of a participant's year-long exposure for these chemicals.

5.2 Materials

5.2.1 Plastic Labware

Labware as described in Chapter 5 was used. Additional items included

- Sterile polystyrene centrifuge tubes – 15 mL
- Sterile polypropylene centrifuge tubes – 50 mL and 15 mL
- Sterile polypropylene urine specimen containers 60 mL
- Polypropylene pipette tips
- Syringe tip filters, 7.5 mm diameter, 0.22 µm pore, PTFE membrane in polypropylene housing.

5.2.2 Reagents

Reagents as described in Chapter 5 were used.

5.3 Methods

The analytical method described in this chapter has slight modifications from that summarised in Table xxx. These modifications were made to improve the SPE cleanup to reduce matrix effects during analysis, to improve recovery of the nonpolar analytes and to improve water removal from the final extracts. The modifications include increased dilution of the sample, larger quantitative transfer and SPE tube wash volumes and adjustment of the elution solvent volumes. These changes are detailed in Table 5.1.

5.3.1 Sample Collection

Amniotic fluid and maternal urine samples were collected following the hospital's standard procedure using the standard collection vessels. The urine and amniotic fluid samples were delivered to the hospital laboratory within 1 hour of collection and were processed immediately. The urine samples (approximately 20 mL each) were split, with a 5 mL sample sent for creatinine analysis and the remaining sample stored at -20 °C. The amniotic fluid samples (approximately 10 mL) were processed following the hospital laboratory standard procedures for the diagnostic tests. The samples were centrifuged to separate cellular

material from the supernatant fluid. The supernatant fluid was collected into a sterile centrifuge tube and stored at -20 °C. At the completion of sample collection (approximately 3 months), the samples were transported to the analytical chemistry laboratory and stored at -80 °C for approximately 1 year until analysis.

The urine samples were collected in 60 mL polypropylene cups and the amniotic fluid samples were collected in 20 mL polystyrene tubes.

5.3.2 Sample Preparation

Samples were processed in batches of 10-12 with additional QA/QC samples and standards.

Urine samples were thawed at room temperature, transferred to 50 mL sterile polypropylene centrifuge tubes and centrifuged at 5,000 g and 4 °C for 10 minutes to separate insoluble material. Two 15 mL sterile polypropylene centrifuge tubes were prepared for each urine sample, one containing 5 mL 0.1 M formic acid and the other containing 5 mL Enzyme Buffer. A 2 mL aliquot of urine was added to each tube and those not analysed on that day were returned to the -80 C freezer. A composite urine sample were prepared for QA/QC purposes for each batch of urine samples by combining 1mL aliquots of each of the individual urine samples in that batch in a sterile 50 mL centrifuge tube. This composite sample was then aliquotted into formic acid and enzyme buffer in the same way as the individual samples. For each batch, three identical composite urine samples were prepared. For 5 of the 32 urine samples, duplicate aliquots in both formic acid and enzyme buffer were made. Reagent blanks, 3 each of formic acid and enzyme buffer were also made.

Amniotic fluid samples were thawed at room temperature and 3 mL aliquots were added to 5 mL formic acid and 5 mL enzyme buffer, as done with the urine samples. Two composite amniotic fluid samples were made by combining 2 mL aliquots of each sample into two 50 mL centrifuge tubes. These two composite samples were identical and were prepared from 24 of the 32 samples that had sufficient volume. This composite sample was aliquotted into formic acid and enzyme buffer in the same way as the individual amniotic fluid samples. For each batch, three composite samples and one reagent blank were made. The aliqotted and diluted samples were stored in the freezer at -80 °C until analysis.

5.3.3 Sample Extraction

The diluted samples were thawed at room temperature. Samples diluted into 0.1 M formic acid were used for the analysis of free (unconjugated) analytes. The individual urine or

amniotic fluid samples were spiked with 100 ng Recovery Surrogates. Three composite QC samples were used for each batch. One was spiked with 100 ng Natives, the second was spiked with 10 ng Natives and the third was not spiked with Natives. All three were spiked with 100 ng Recovery Surrogates. A reagent blank was spiked with 100 ng Recovery Surrogates. Because of their protein content, the amniotic fluid samples had an additional 3 mL of reagent water added to reduce the viscosity of the samples. All samples were vortex mixed and extracted following the SPE procedure outlined in Table 5.1.

Samples diluted into Enzyme Buffer were used for the analysis of total (free + conjugated) analytes. Three composite QC samples were used for each batch. One was spiked with 100 ng Natives, the second was spiked with 10 ng Natives and the third was not spiked with Natives. A reagent blank was spiked with 100 ng Recovery Surrogates. All samples were spiked with 55 ng Enzyme Control Standard and 500 µL Enzyme and incubated at 37 °C for 90 min. At the end of the incubation time, the reaction was stopped by addition of 500 µL formic acid (98%). All samples were then spiked with 100 ng Recovery surrogates. An additional 3 mL of reagent water was added to the amniotic fluid samples. All samples were vortex mixed and extracted following the SPE procedure outlined in Table 5.1.

Table 5.1. SPE procedure for urine and amniotic fluid samples.

Parameter	Free (unconjugated) Analysis	Total (Free + Conjugated) Analysis
Matrix	2 mL urine or 3 mL amniotic fluid diluted with 5 mL 0.1M formic acid Amniotic fluid diluted with an additional 3 mL reagent water	2 mL urine or 3 mL amniotic fluid diluted with 5 mL 0.1M formic acid Amniotic fluid diluted with an additional 3 mL reagent water
QA/QC Sample Natives Spike	100, 10, 0 ng	100, 10, 0 ng
Surrogate Spike	100 ng	100 ng
Enzyme Control Spike	no	55 ng
Enzyme	no	0.5 mg
Incubation	no	37 °C, 90 min
Acidification	on dilution	500 µL formic acid (98%) after incubation
Condition	2 mL each Hex, MTBE, MeOH, H_2O	2 mL each Hex, MTBE, MeOH, H_2O
Load	quantitative transfer 2 mL 0.1 M formic acid	quantitative transfer 2 mL 0.1 M formic acid
Wash	2 mL 0.1 M formic acid 4 mL MeOH/H_2O (5:95)	2 mL 0.1 M formic acid 4 mL MeOH/H_2O (5:95)
Elute	Tube A: 1 mL Hex/MTBE (50:50) + 4 mL Hex + 2 mL Hex/MTBE (50:50) Tube B: 2 mL MTBE/MeOH (60:40) + 2 mL MeOH	Tube A: 1 mL Hex/MTBE (50:50) + 4 mL Hex + 2 mL Hex/MTBE (50:50) Tube B: 2 mL MTBE/MeOH (60:40) + 2 mL MeOH
Dry	acidify aq. Layer in Tube A and remove dry organic layer over $MgSO_4$	acidify aq. Layer in Tube A and remove dry organic layer over $MgSO_4$
Derivatisation Conditions	BSTFA/ TMSI (98:2) 80 °C, 60 min	BSTFA/ TMSI (98:2) 80 °C, 60 min

5.3.4 Sample Derivatisation

The Tube A fraction was filtered to remove $MgSO_4$ particles using a PTFE syringe tip membrane filter on transfer to the derivatisation reaction vial. The solvent was then evaporated to near dryness. The Tube B fraction was added to the reaction vial and the solvent evaporated to dryness. All solvent evaporations were done with the vials sitting on a surface maintained at 40 °C with a gentle nitrogen stream. The samples were split to retain a portion for future requirements. To the dry residue, a 100 µL aliquot of internal standard solution containing 100 ng of internal standard in ACN and 100 µL of MeOH were added. The samples were allowed to stand for 5 minutes and were vortex mixed to ensure full dissolution. A 100 µL aliquot of the sample was archived in an autosampler vial fitted with a 250 µL insert and stored at -20 C. The remaining sample was evaporated to dryness to remove MeOH, then taken up in 200 µL derivatisation reagent BSTFA/ TMSI (98:2) and 100 µL ACN. The mixture was vortex mixed and then heated at 80 °C for 60 min. The samples

were allowed to cool for 15 minutes, the vials rolled to ensure complete mixing of contents and a 200 µL aliquot was transferred to an autosampler vial fitted with a 250 µL insert ready for GC-MS analysis.

5.3.5 QA/QC

A reagent blank and 3 matrix spike samples (100, 10 and 0 ng Natives) were processed simultaneously with each batch of 10-12 samples. Comparative standards of the 100 and 10 ng Natives spikes and the 100 ng Surrogate spike were prepared and analysed along with daily calibration check standards at 100, 10 and 1 ppb. The comparatives and calibration check standards were prepared directly in reaction vials for solvent evaporation, archive splitting and derivatisation. With the urine samples, individual sample duplicates were prepared for 5 samples because the composite material used to prepare the matrix spike samples was different for each batch. With the amniotic fluid samples, the composite material used for matrix spike samples was the same for all batches and these samples served as replicates. The calibration check standards and comparatives were injected twice, once at the beginning and once at the end of each batch. Two samples were also injected twice during each batch. One randomly selected sample was injected twice sequentially and the first sample of the batch was injected again after the last sample of the batch. These repeat injections were used to monitor sample stability through the duration of the batch analysis.

5.4 Results

5.4.1 Calculations

For each sample, the reported concentration for each target analyte was corrected for surrogate recovery and for aliquot volume as described in Chapter 5. The average concentration of each target analyte was calculated for the reagent blanks (n=6) for the free and total analyses. This concentration was then used to produce separate blank profiles for the urine and amniotic fluid samples that were correctly scaled for the sample aliquot volume. The appropriate average blank profile was then subtracted from the recovery and volume corrected sample profile to give the final concentration result. The complete dataset is given in the Appendix.

5.4.2 QA/QC

Control charts were prepared for the representative compounds from the calibration check standards and duplicate samples and repeat injections of samples were assessed for stability as summarised in Chapter 4.

For the analysis of total (free + conjugates) concentration, the % Completion of reaction was monitored by the enzyme control standards and summarised in Table 5.2. % Completion was calculated with reference to the reagent blank result. For the urine samples, the urine matrix interferences contributed to the peak areas of both 4NP and 4NC in the same manner as described for 3PBOH in Chapter 4. Based on a single composite urine sample that had the enzyme added but not the enzyme control standard, the matrix contribution to these two peaks was on the order of 25 ppb, or about 40% of the total. The larger standard deviation observed with the urine samples is a result of the variable contribution of the matrix composition to the peak area. Through the analysis, two samples were discovered to have had twice the volume of enzyme solution added. The % Completion for these two samples did not differ from the other samples, indicating the enzyme reaction had gone to completion for all samples.

Table 5.2. % Completion of enzyme deconjugation reactions (average ± σ)

Control Standard	Urine (n = 32)	Amniotic Fluid (n = 32)
4NP (β-glucuronidase)	164 ± 60	115 ± 11
4NC (arylsulphatase)	183 ± 63	114 ± 13

Recovery corrected and aliquot volume scaled reagent blanks, an average of 6 samples each for the free and total analyses, are shown in Figure 5.1. The peaks in the blanks identified as 4MBC and OMC are interferences on the quantification ion for those two compounds. Mass spectra for those peaks in the reagent blanks obtained in SCAN mode indicate the peaks are aliphatic hydrocarbons but identification by library search was inconclusive. There was an increase in the blank level of mEHP due to the presence of the deconjugation enzyme, but the other phthalate monoester levels remained constant and low among all blanks. mMP contamination averaged 0.6 ng/mL, approximately 65% of the level found in the free samples and 20% or less of the levels found in the total samples. mEP contamination averaged 2.6 ng/mL and was comparable to the levels found in both the free and total samples. BPA contamination averaged 0.6 ng/mL and was comparable to the levels found in the free samples and about 67% of the levels found in the total samples.

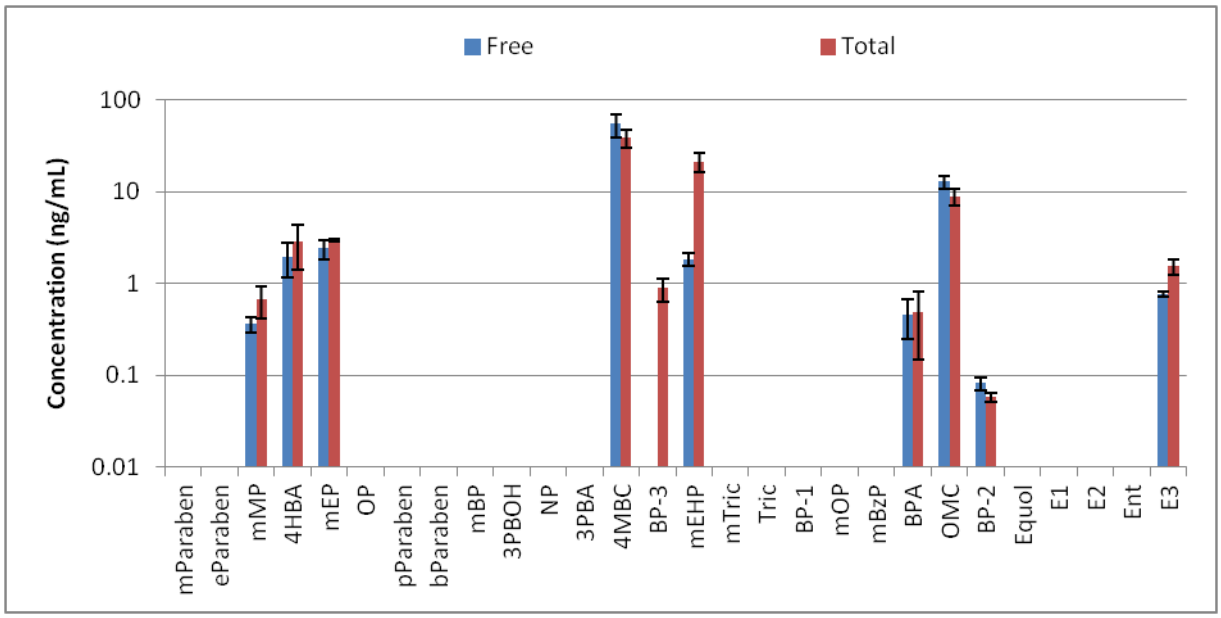

Figure 5.1. Comparison of reagent blanks for the free and total analyses of urine and amniotic fluid. Error bars indicate ±σ on the average (n=6).

5.4.3 Urine Samples

The maximum, minimum and median concentrations for the free analysis are shown in Figure 5.2(a) and for the total (free + conjugated) analysis in Figure 5.2(b). For those compounds quantified in both the free and total analyses, the free concentration accounted for between 15% and 90% of the total concentration. The correlation between free and total concentrations for the urine samples is shown in Figure 5.3 for those compounds detected in both samples. For each analyte, the linear model determined by least squares regression and the coefficient of determination (R^2) are also shown. To measure of the strength of the linear correlation of amniotic fluid concentration with maternal urine concentration, the Pearson correlation coefficient (r) is used. For values of r between 0.5 and 1, the correlation between the two variables is said to be strong and positive. For values of r between 0 and 0.1, there is no correlation. If r is negative, the correlation is negative. The Pearson correlation coefficient for the dependence of the free and total concentrations for each of the analytes of Figure 5.3 is given in Table 5.3.

The linear model that is shown in Figure 5.3 is not intended to be used as a predictive tool for estimating amniotic fluid concentration based on maternal urine concentration, but rather to indicate the linear correlation between the two observed concentrations. For this reason, determining the confidence interval on the regression line is not an appropriate way of assessing the significance of the relationship. Instead, the probability that the observed data are uncorrelated (i.e. r = 0) can be estimated by the following statistic which has a Student's t distribution [362].

$$t = |r| \sqrt{\frac{(N-2)}{(1-r^2)}}$$

Where N = number of paired observations
r = Pearson correlation coefficient

This t-statistic can then be compared to the critical t-value from the Student's t distribution with N-2 degrees of freedom and the probability (p) that the t-statistic is greater than the critical t-value due entirely to chance can be calculated. If the probability, p, is less than 0.05, then the correlation is not statistically significant at the $\alpha = 0.05$ significance level. In other words, there is at most a 1 in 20 chance that the correlation is not statistically

significant. The t-statistics, p-values and classification of the correlation as statistically significant or not are summarised in Table 5.3.

The free and total concentrations 4HBA are very similar and not unexpected given the hydrophilic nature of the compound. In contrast, eParaben does not follow the pattern established by mParaben and pParaben. As indicated by the Pearson correlation coefficient, the dependence is weak. bParaben was not detected in the free analysis of any samples. For TRIC, the correlation shown in Figure 5.3 is not strong and may be negative as suggested in Table 5.3. The correlation of free and total concentrations for BPA is also weak.

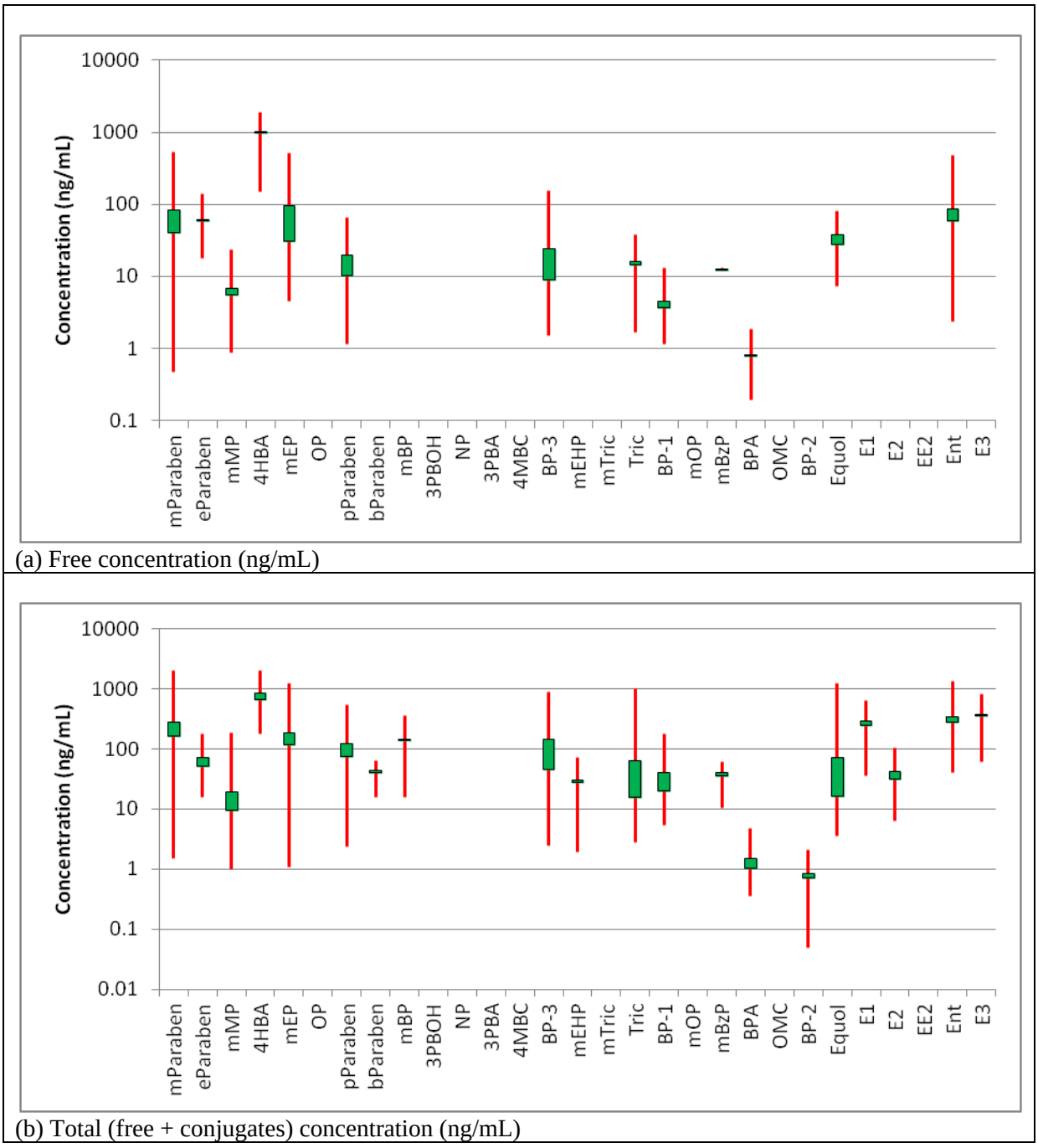

(a) Free concentration (ng/mL)

(b) Total (free + conjugates) concentration (ng/mL)

Figure 5.2. Free concentrations (a) and total concentrations (b) of EEs in maternal urine. Lines indicate maximum and minimum, green boxes indicate the range between the mean and median values.

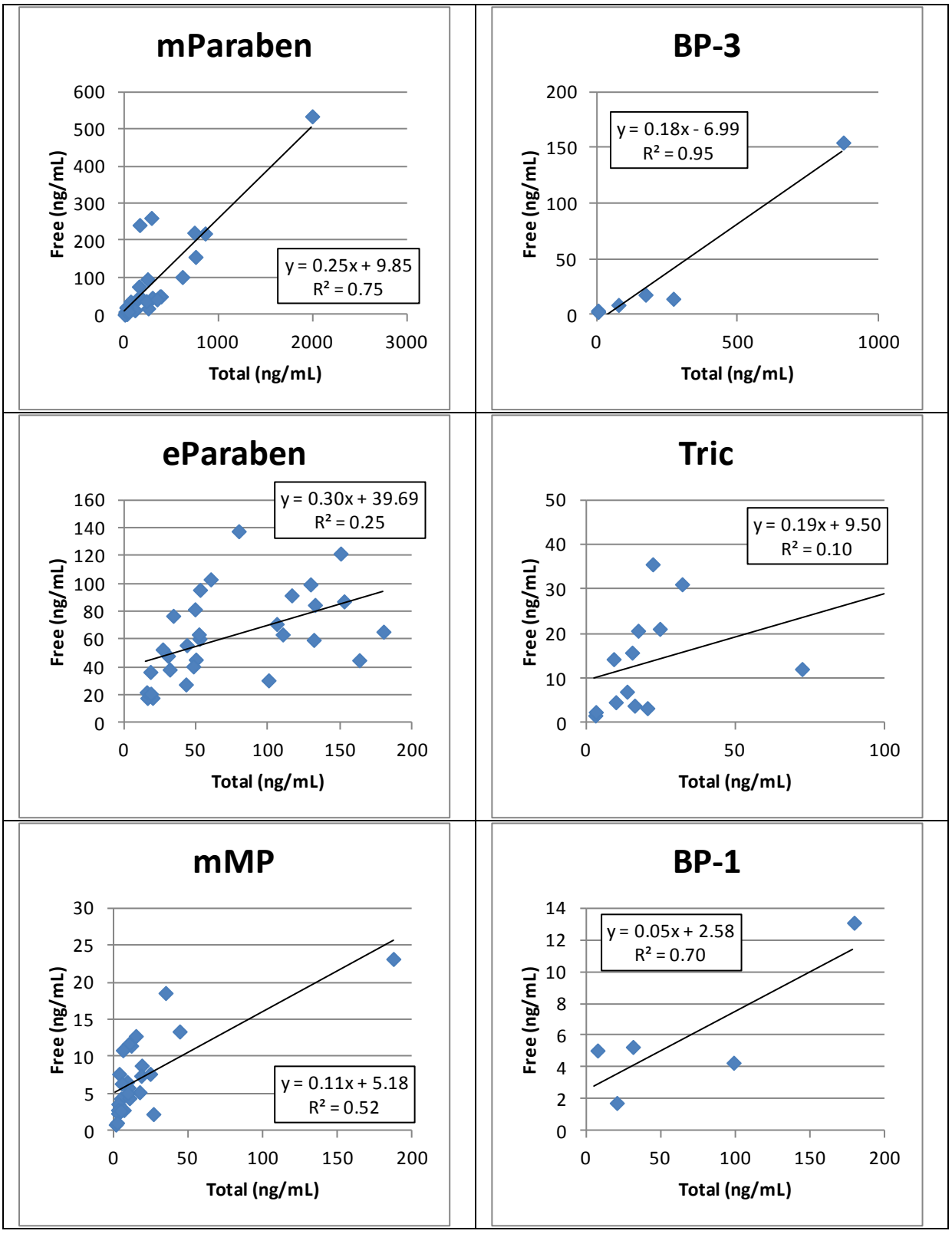
mParaben
Free (ng/mL)
Total (ng/mL)
y = 0.25x + 9.85
R² = 0.75
BP-3
y = 0.18x - 6.99
R² = 0.95
eParaben
y = 0.30x + 39.69
R² = 0.25
Tric
y = 0.19x + 9.50
R² = 0.10
mMP
y = 0.11x + 5.18
R² = 0.52
BP-1
y = 0.05x + 2.58
R² = 0.70

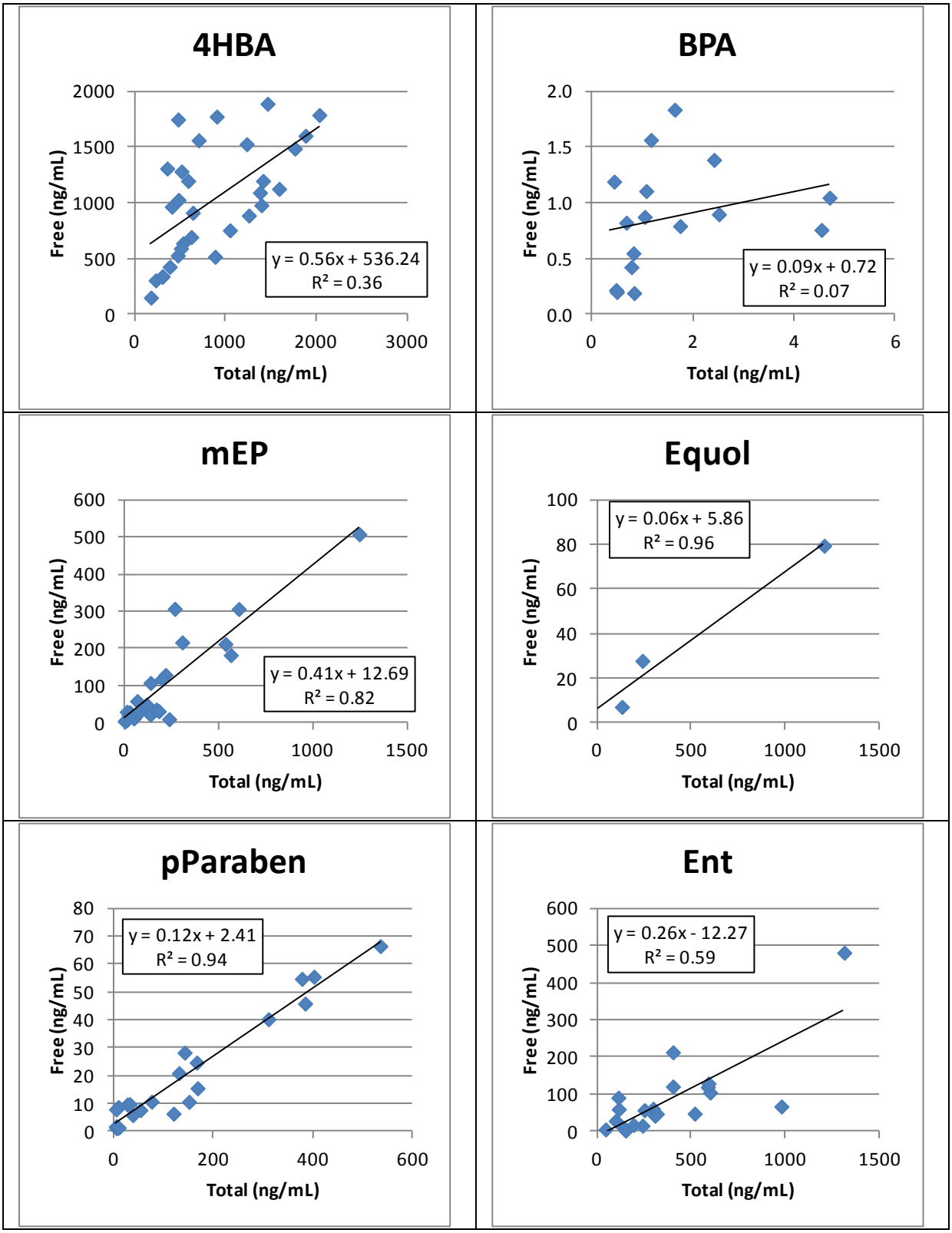

Figure 5.3. Correlation of free and total urine concentrations.

Table 5.3. Pearson correlation coefficient (r) and statistical significance for the correlation of free and total concentration of EEs in maternal urine. (NS = not statistically significant, S = statistically significant)

Compound	Pearson (r)	Description of Correlation	N	t	p (1-tail)	Significance (a=0.05)
Tric	-0.34	medium negative	15	1.29	0.11	NS
eParaben	-0.24	weak negative	30	1.31	0.10	NS
BPA	0.14	weak positive	20	0.58	0.28	NS
4HBA	0.38	medium positive	30	2.19	0.02	S
mMP	0.54	strong positive	28	3.27	1.43E-03	S
mParaben	0.64	strong positive	28	4.27	1.02E-04	S
pParaben	0.66	strong positive	22	3.88	3.99E-04	S
Ent	0.72	strong positive	20	4.39	1.43E-04	S
BP-1	0.76	strong positive	8	2.84	0.01	S
mEP	0.84	strong positive	26	7.49	2.97E-08	S
BP-3	0.94	strong positive	9	7.52	1.80E-05	S
Equol	0.97	strong positive	3	3.70	0.02	S

5.4.4 Amniotic Fluid Samples

The maximum, minimum and median concentrations for the free analysis are shown in Figure 5.4(a) and for the total (free + conjugated) analysis in Figure 5.4(b). In comparison to the urine samples, the free compound accounted for a slightly larger fraction (18% to100%) of the total concentration in amniotic fluid. With few exceptions, there was also no difference between the median concentrations for male and female fetuses as shown in Figure 5.5. In the free analysis, bParaben and EQ were each detected once in male samples and BP-2 was only detected in two female samples. In the total analysis, eParaben was detected only in two male samples while BP-2 was detected only in 5 female samples. The median concentrations of mEP, BPA and OMC were higher in female samples and the median concentration of mMP was higher in the male samples, but by ANOVA, the differences were not statistically significant at the 95% confidence level.

The correlation of free and total concentrations in amniotic fluid are shown in Figure 5.6 for those compounds with sufficient (N>2) data. The Pearson correlation coefficient for these correlations is given in Table 5.4. With the exception of BP-1, the correlation between free and total concentrations is medium to strongly positive.

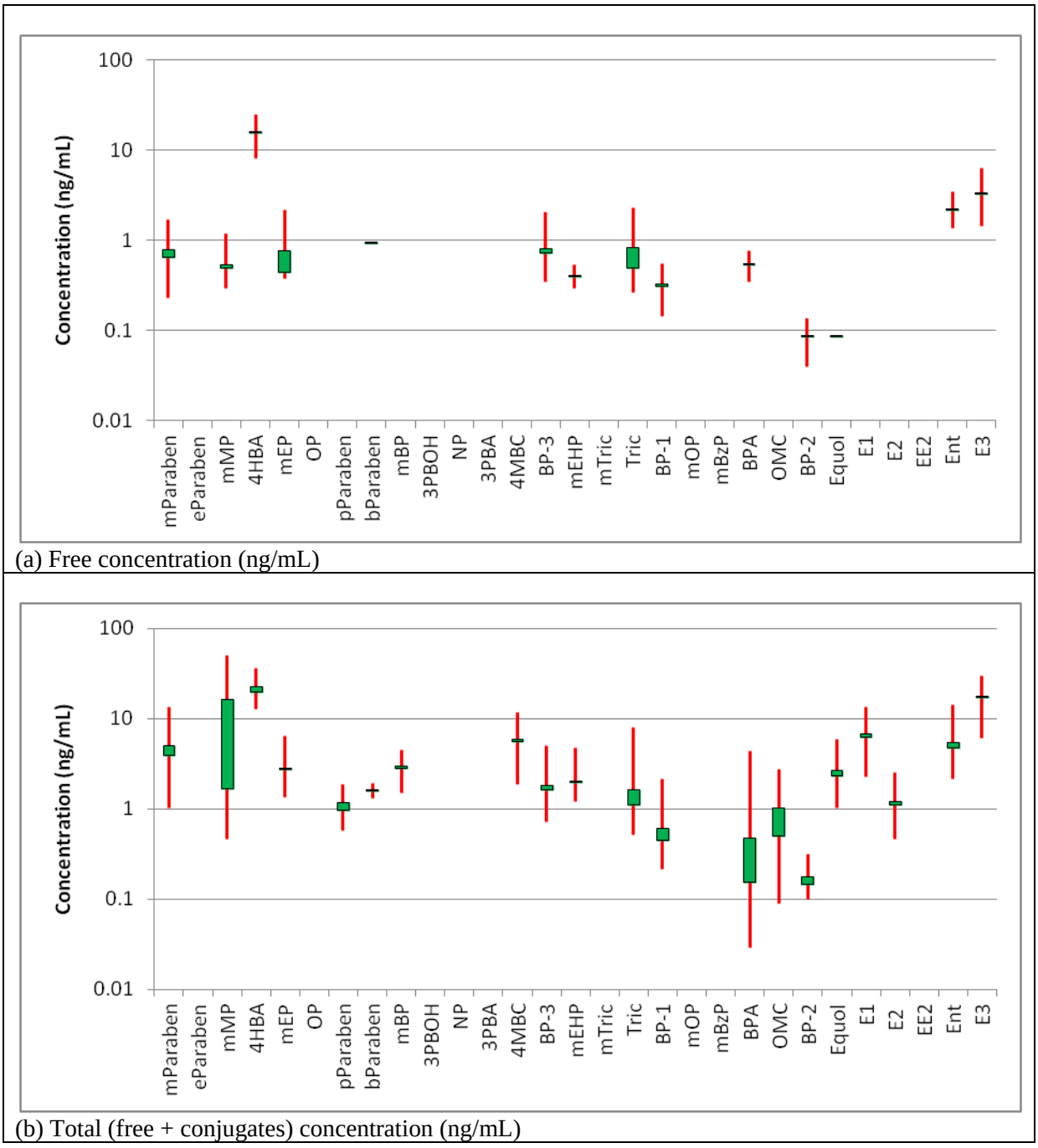

(a) Free concentration (ng/mL)

(b) Total (free + conjugates) concentration (ng/mL)

Figure 5.4. Free concentrations (a) and total concentrations (b) of EEs in amniotic fluid. Lines indicate maximum and minimum, green boxes indicate the range between the mean and median values.

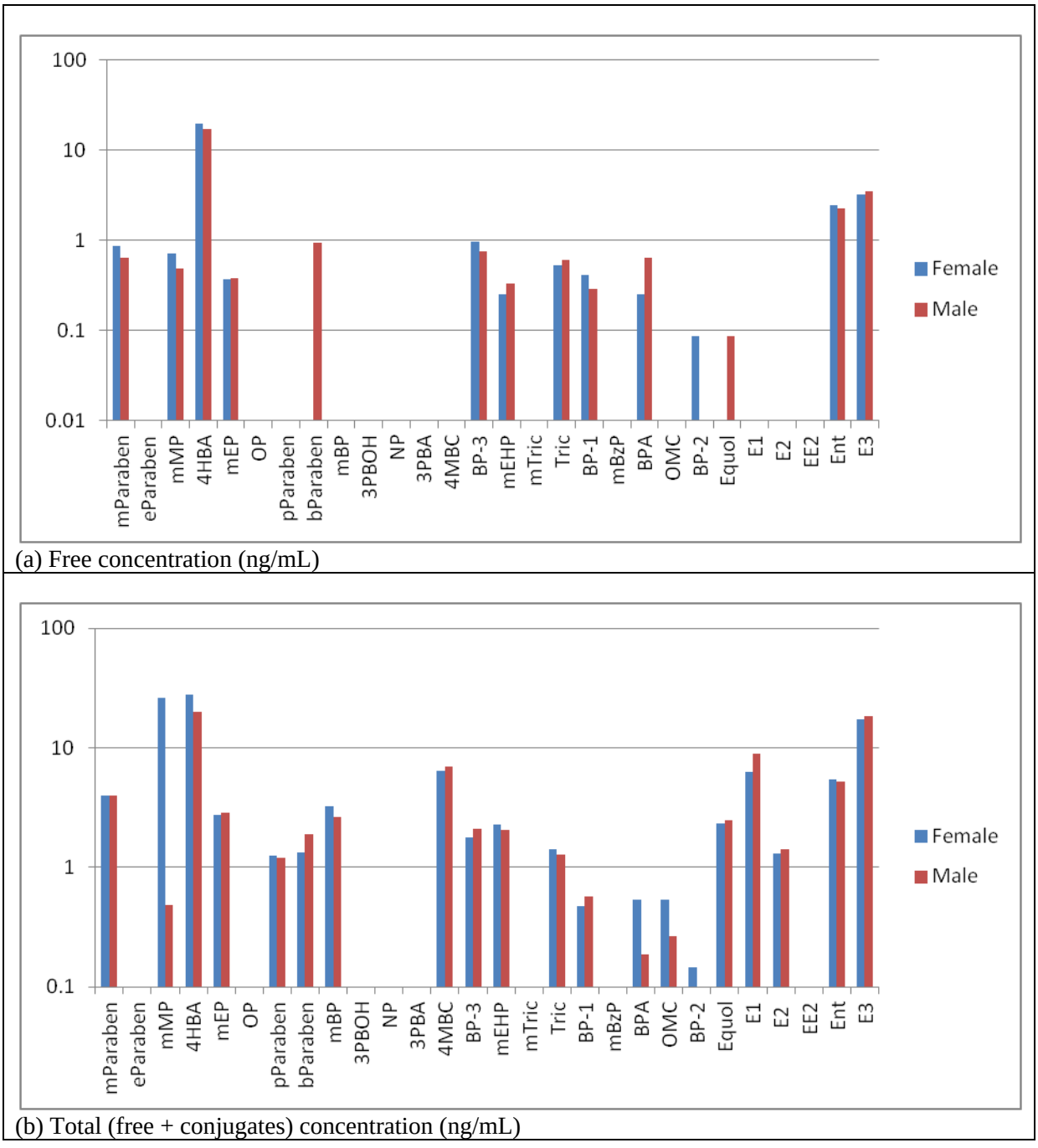

Figure 5.5. Comparison of free and total median concentrations of EEs in amniotic fluid for male and female fetuses.

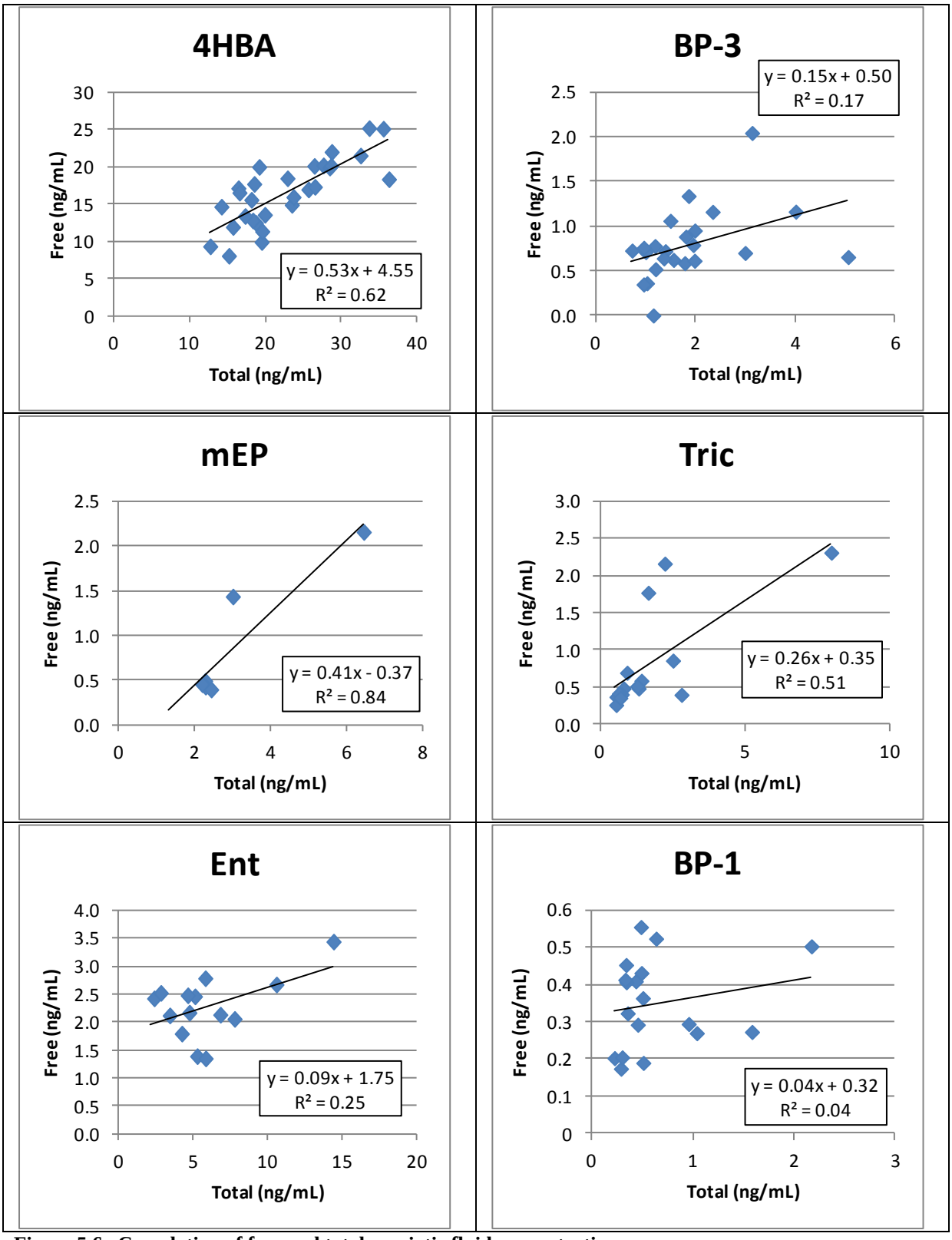

Figure 5.6. Correlation of free and total amniotic fluid concentrations

Table 5.4. Pearson correlation coefficient (r) and statistical significance for the correlation of free and total concentration of EEs in amniotic fluid. (NS = not statistically significant, S = statistically significant)

Compound	Pearson (r)	Description of Correlation	N	t	p (1-tail)	Significance (a=0.05)
BP-1	0.19	weak positive	21	0.85	0.20	NS
BP-3	0.39	medium positive	25	2.01	0.03	S
Ent	0.50	strong positive	19	2.39	0.01	S
Tric	0.71	strong positive	20	4.30	1.7E-04	S
4HBA	0.79	strong positive	29	6.71	1.2E-07	S
mEP	0.92	strong positive	8	5.67	2.3E-04	S

5.5 Discussion

5.5.1 Matrix Challenges

The analysis of urine samples was more difficult than amniotic fluid because of the differences in matrix. Urine has much higher concentrations of organic acids and other species that the SPE method could not remove because the suite of target analytes included organic acids, specifically the phthalate monoesters. All literature reports of phthalate monoesters in urine and amniotic fluid used SPE with LC-MS/MS as the analytical method. LC-MS/MS is much more selective than GC-MS because of the use of tandem mass spectrometers in detection. In MS/MS detection, the ionisation process is gentle, producing only a molecular ion or adduct ion, called the parent ion, of the target analyte. The first MS selects this parent ion for transport to a reaction cell where it is further fragmented. Fragments specific to the target analyte are then selected by the second MS for detection. The two-stage selection process is highly specific for the compound of interest. The first stage greatly reduces the amount of co-eluting material from reaching the detector and the second stage allows specific identification of the parent ion based on its unique fragmentation pattern in comparison to any other possible species that are able to pass the first selection stage. Unfortunately, LC-MS/MS instrumentation was not available for this study.

5.5.2 Correlation of Maternal Urine and Amniotic Fluid Concentrations

The exposure assessment of Chapter 7 is based on the assumption that fetal exposure is directly related to maternal exposure. Maternal exposure was assessed by analysis of urine samples collected at the same time as amniotic fluid samples. The maternal urine samples represent exposure over the previous 6-12 hours while amniotic fluid samples may represent cumulative fetal exposure. Since maternal exposure to the compounds of interest is mainly a function of daily lifestyle and environment, it is not unreasonable to assume that the exposure

chronic rather than acute and results in a reasonably steady level of the target analytes in the body. The rationale is that their normal daily routine whereby exposure to the chemicals of interest occurs is not altered significantly because the participants had no *a priori* knowledge of the study. As discussed in Section 5.1, this assumption is reasonable and the total amniotic fluid concentrations are expected to correlate with total maternal urine concentrations.

The amniocentesis procedure required the mother to have a full bladder, so to account for variable dilution of the urine samples by an increase in water ingestion in the hours before the procedure, the maternal urine concentrations of the target analytes were normalised to the urine creatinine concentration. The biological mechanisms that control amniotic fluid volume are insensitive to short term fluctuations in maternal hydration, so no correction was required. The correlations are shown in Figure 5.7 and the Pearson correlation coefficients are given in Table 5.5. BP-2 was found in only 3 paired samples and at very low concentrations, so there is insufficient data to evaluate a possible correlation. The trendline shown for EQ suggests a negative correlation whereas the Pearson correlation coefficient suggests no correlation. The measured concentrations are low in comparison to other compounds. The very low concentration found in the matching urine sample for the amniotic fluid sample showing ~ 6 ng/mL could be due to the short timeframe of exposure that the maternal urine samples represent. EQ is produced by bacteria in the gut from DAID and it is possible that that mother had not ingested soy products in the previous day but had in the past. A similar explanation could apply to the two amniotic fluid samples showing high concentrations of ENT compared to their matching urine samples. Poor chromatography distorted the peak shape in the amniotic fluid sample matched to the urine sample with mMP at ~300 ng/mg creatinine. The short lifetime of the derivatised samples (less than 24 hours) precluded dilution and re-analysis for samples showing high concentrations.

The lack of correlation observed for mBP is most likely a result of the low concentrations found in comparison to the other phthalate monoesters. Contamination from the enzyme solution is not likely an issue given the absence of mBP in the reagent blanks (Figure 5.1). In contrast, the poor correlation observed for mEHP is likely a result of enzyme contamination.

The lack of correlation observed for E1 and E2 were not unexpected because the placenta controls the levels of E1 and E2 that the fetus is exposed to. The correlation observed for E3

was expected because the placenta excretes E3 into both maternal and fetal circulations. The maternal serum E3 level is actually diagnostically important for Down's Syndrome and intrauterine growth restriction [363].

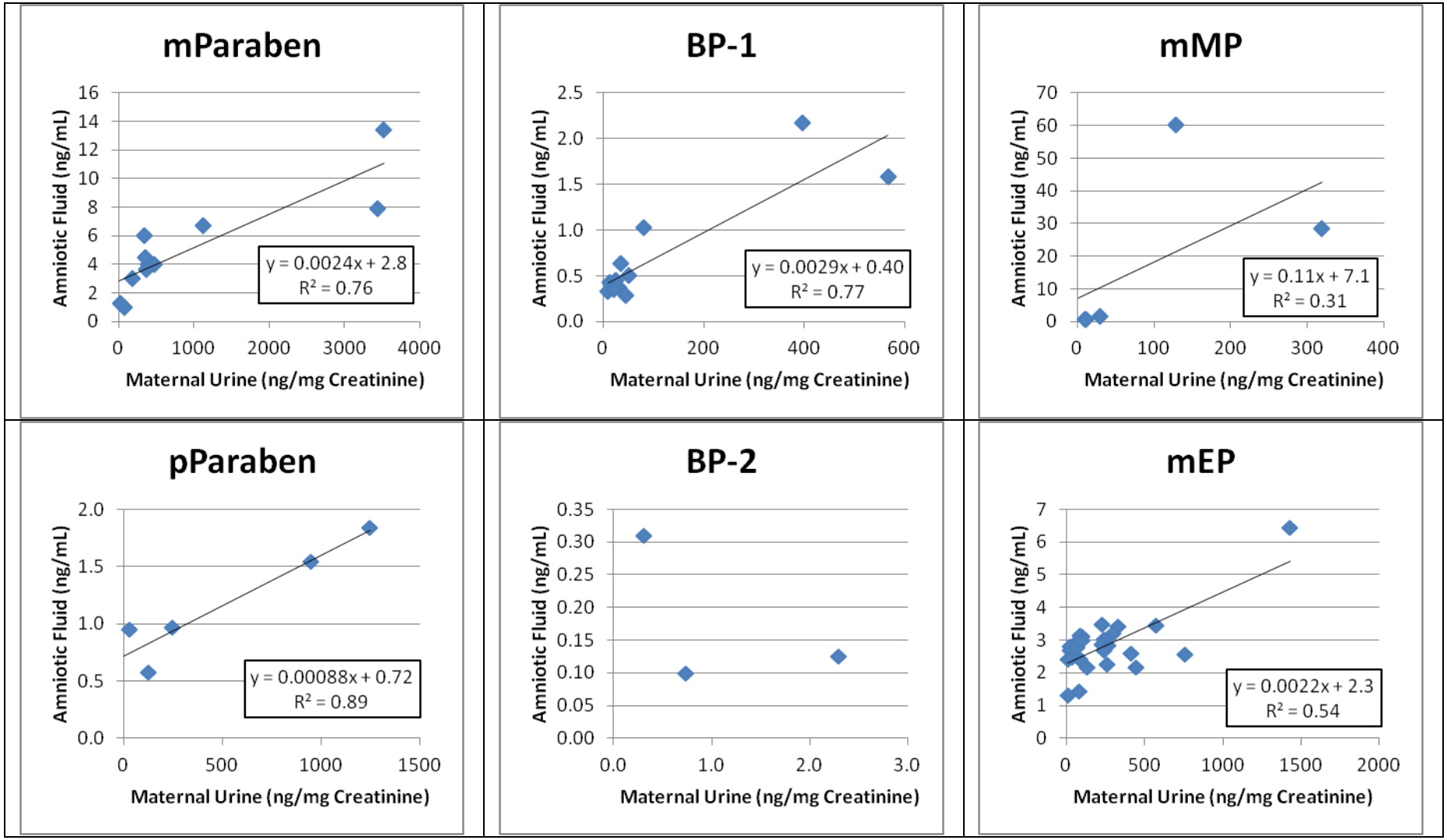
mParaben
Amniotic Fluid (ng/mL)
Maternal Urine (ng/mg Creatinine)
y = 0.0024x + 2.8
R² = 0.76
BP-1
Amniotic Fluid (ng/mL)
Maternal Urine (ng/mg Creatinine)
y = 0.0029x + 0.40
R² = 0.77
mMP
Amniotic Fluid (ng/mL)
Maternal Urine (ng/mg Creatinine)
y = 0.11x + 7.1
R² = 0.31
pParaben
Amniotic Fluid (ng/mL)
Maternal Urine (ng/mg Creatinine)
y = 0.00088x + 0.72
R² = 0.89
BP-2
Amniotic Fluid (ng/mL)
Maternal Urine (ng/mg Creatinine)
mEP
Amniotic Fluid (ng/mL)
Maternal Urine (ng/mg Creatinine)
y = 0.0022x + 2.3
R² = 0.54

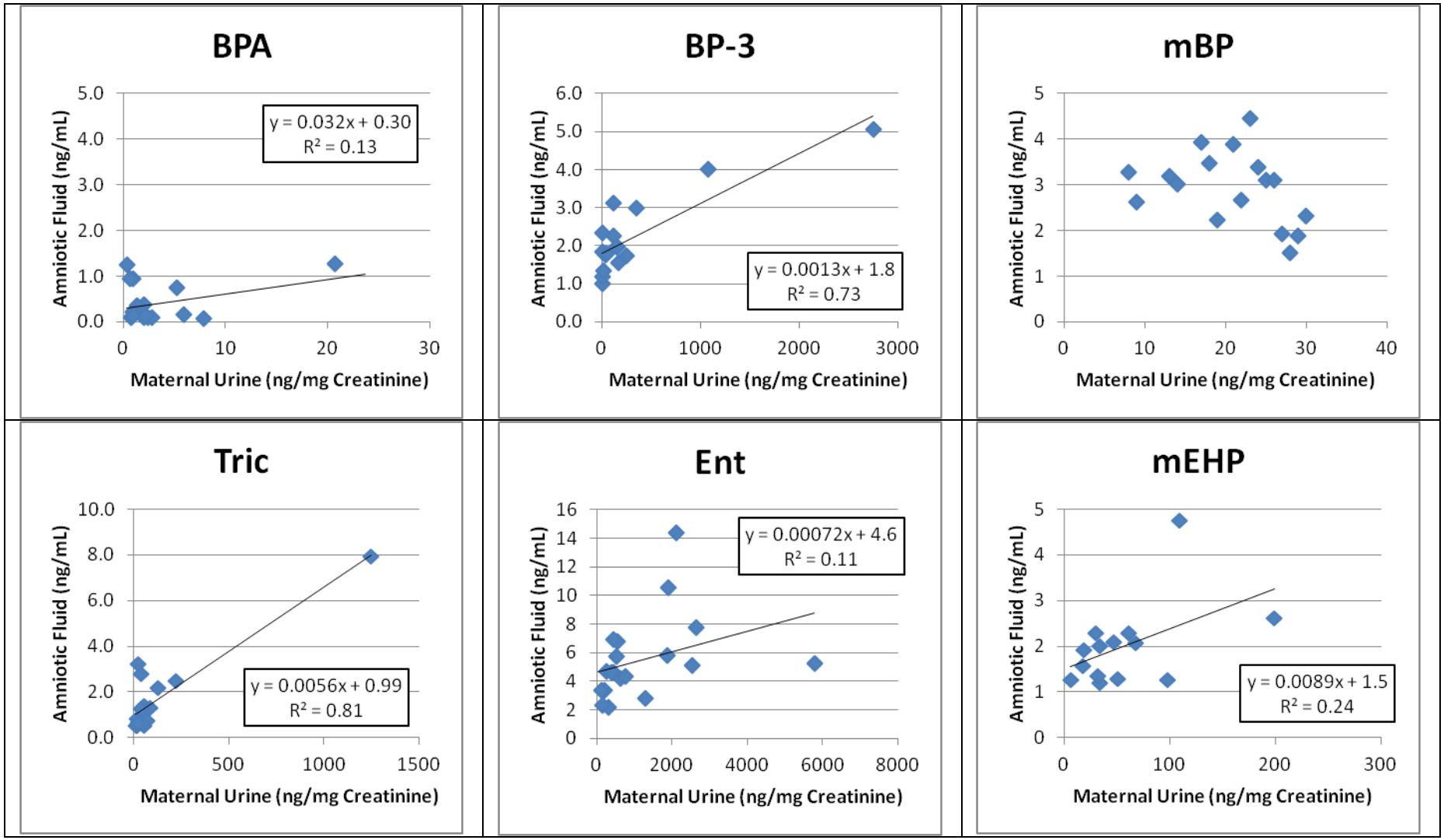
BPA
y = 0.032x + 0.30
R² = 0.13
Amniotic Fluid (ng/mL)
Maternal Urine (ng/mg Creatinine)
BP-3
y = 0.0013x + 1.8
R² = 0.73
Amniotic Fluid (ng/mL)
Maternal Urine (ng/mg Creatinine)
mBP
Amniotic Fluid (ng/mL)
Maternal Urine (ng/mg Creatinine)
Tric
y = 0.0056x + 0.99
R² = 0.81
Amniotic Fluid (ng/mL)
Maternal Urine (ng/mg Creatinine)
Ent
y = 0.00072x + 4.6
R² = 0.11
Amniotic Fluid (ng/mL)
Maternal Urine (ng/mg Creatinine)
mEHP
y = 0.0089x + 1.5
R² = 0.24
Amniotic Fluid (ng/mL)
Maternal Urine (ng/mg Creatinine)

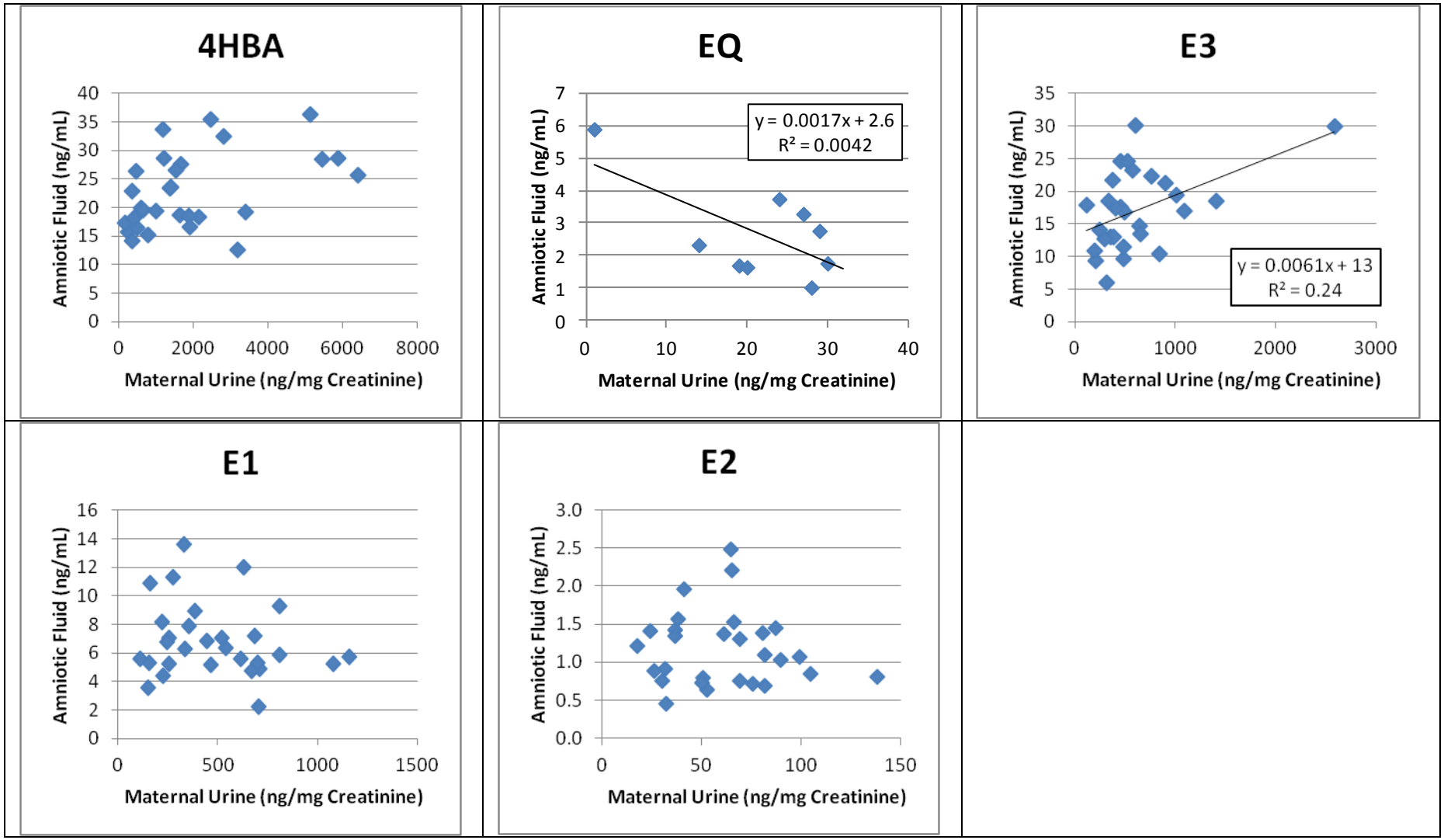

Figure 5.7. Correlation of total amniotic fluid and maternal creatinine-corrected concentrations of the target analytes.

Table 5.5. Pearson correlation coefficient (r) and statistical significance for the correlation of total concentrations of EEs in amniotic fluid and maternal urine. (NS = not statistically significant, S = statistically significant)

Compound	Pearson (r)	Description of Correlation	N	t	p (1-tail)	Significance (a=0.05)
BP-2	-0.58	strong negative	4	1.00	0.19	NS
mBP	-0.38	medium negative	18	1.66	0.06	NS
E1	-0.18	weak negative	29	0.95	0.18	NS
E2	-0.08	not correlated	29	0.41	0.34	NS
EQ	0.06	not correlated	9	0.17	0.43	NS
ENT	0.34	medium positive	19	1.48	0.08	NS
BPA	0.36	medium positive	25	1.85	0.04	S
4HBA	0.45	medium positive	29	2.59	0.01	S
E3	0.49	medium positive	29	2.89	3.6E-03	S
mEHP	0.49	medium positive	14	1.93	0.04	S
mMP	0.56	strong positive	5	1.17	0.15	NS
mEP	0.73	strong positive	28	5.49	3.6E-06	S
BP-3	0.86	strong positive	16	6.17	6.7E-06	S
mParaben	0.87	strong positive	11	5.38	1.1E-04	S
BP-1	0.88	strong positive	16	6.87	1.9E-06	S
Tric	0.90	strong positive	22	9.34	2.1E-09	S
pParaben	0.95	strong positive	5	5.07	1.9E-03	S

5.6 Conclusions and Recommendations

From Figure 5.7 it is clear that a small but measurable quantity of EEs reach the fetus. The correlation between maternal urine and amniotic fluid concentrations is positive and medium to strong (Table 5.5) for those compounds with sufficient data and levels above the quantification limit of the analysis. The correlations are also statistically significant for BPA, 4HBA, E3, mEHP, mEP, BP-3, mParaben, BP-1, Tric and pParaben. The correlations for BP-2, mBP, E1, E2, EQ and ENT are not statistically significant, possibly for the following different reasons:

- Exposure to BP-2 is very low for this cohort. A survey of product composition would confirm whether this ingredient is present in topical sunblock or other products available in Christchurch;
- mBP concentrations are low compared to the other phthalate monoesters;
- E1 and E2 are strictly controlled by the placenta and levels in amniotic fluid are expected to be independent of those in the mother;
- EQ and ENT are present due to naturally occurring components of soy and grains and their presence is highly dependent on maternal diet. As a result, these compounds may show much greater temporal variation in maternal urine than in amniotic fluid.

These correlations are observed despite the difficulties encountered in the analysis of these samples by GC-MS. The results are considered valid and can be used in the exposure assessment of Chapter 6.

GEN and DAID could not be determined by the GC-MS method. This is unfortunate considering the potentially significant contribution these two compounds may make to the estrogenicity of the mixture. Literature data suggest that GEN and DAID concentrations could be in the range of 40 ng/mL (Figure 2.15), much greater than any of the other compounds determined in this study.

It is highly desirable to have the archived sample fractions analysed by LC-MS/MS to confirm the GC-MS results and improve the quality of the dataset for those compounds not amenable to the GC-MS method.

Chapter 6 Exposure Assessment

6.1 Introduction

Fetal exposure to EEs might lead to a number of adverse outcomes as reviewed in Chapter 1. As this exposure is to a mixture of chemicals that can act in unison with or in opposition to one another, predicting the outcome of the exposure is difficult. Further complicating matters is that the same exposure will have different outcomes on the male and female fetus because of differences in sensitivity to estrogen signalling. The objective of this chapter is to bring together the results of the measurements made in this study with those available in the literature to determine whether the potential magnitude of exposure is likely to be of concern. This analysis will address only the estrogenic action of the exposure. However, it must be kept in mind that this estrogenic action does not occur in isolation and that the opposing androgenic action is also present, but at this stage, not quantifiable. The methodology used here is equally applicable to androgenic action once sufficient data are available.

6.1.1 Characterisation of Fetal Exposure

Fetal exposure begins with maternal exposure. Because the exposure of interest is environmental, the most likely pathways are ingestion, dermal and inhalation. Pathways typically associated with therapeutics (e.g. injection) have been disregarded in this study. It is reasonable to assume that maternal exposure to many of these chemicals is chronic and low level, as suggested specifically for BPA [364] rather than acute and of high level because these compounds are present in many of the products used daily, if not multiple times a day and in food and water. Chronic, low level exposure may lead to a pseudo-constant low level of the compounds in the body, rather than the rapid increase and clearance profiles observed in acute dosing studies, and may affect clearance rates (e.g. by induction of metabolic enzymes). For other compounds like GEN and DAID that are found in foods like soy, exposure levels may show more temporal variation, depending on the frequency of exposure. Each of the maternal exposure pathways has different metabolic and elimination pathways associated with it that can either transform or reduce the amount of the compound reaching maternal circulation. The model of fetal exposure is illustrated in Figure 6.1.

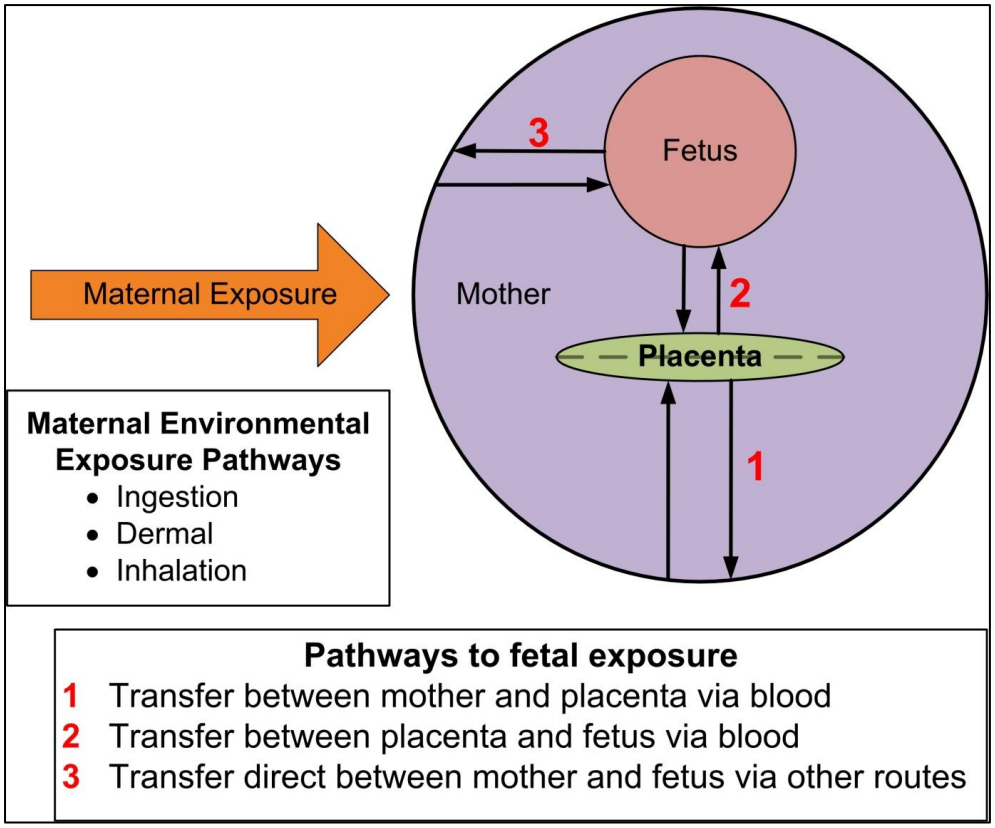

Figure 6.1. Illustration of fetal exposure model.

6.1.2 Role of the Placenta

As discussed in Chapter 1, transport across the placenta occurs by simple diffusion for hydrophobic compounds and by facilitated and active transport for hydrophilic compounds. The EES are hydrophobic and therefore diffuse across the placental membranes from maternal circulation to fetal circulation. As diffusion is driven by a concentration gradient, diffusion back to the mother will only occur if the concentration in the fetal compartment is higher than in the maternal compartment. With a chronic low level exposure scenario for the mother, it is possible that maternal levels will reach a pseudo-steady state and that fetal levels will a reach steady state that is dependent on maternal levels.

The only way out of the fetal compartment for conjugated species is by active transport. The active transporters present in the placenta are both highly substrate specific and nonspecific. Both the placenta and fetal tissues have deconjugation enzymes and this may facilitate recirculation of EEs within the fetal compartment.

Some EEs are known inhibitors of placental conjugation enzymes (Table 2.4). This action will contribute indirectly to the upset of hormone balance within the fetal compartment and possible aggravation or suppression of the genomic response to EEs.

6.1.3 Accumulation in Amniotic Fluid

Once in the fetal circulation, a compound is subject to the metabolic and elimination pathways that are active in the fetus. Fetal xenobiotic metabolism is significantly less active than adult metabolism and exhibits some different pathways than present in the adult. For example, the fetus will preferentially sulphate rather than glucuronidate molecules for excretion in fetal urine. Fetal elimination pathways can deposit metabolites and elimination products in the amniotic fluid, sequester them in meconium, or return them to the mother via circulation. The fetus actively swallows amniotic fluid and expels fluid from the lungs into the amniotic fluid [174, 178, 365-367]. The fluid expelled from the lungs is a transudate of fetal plasma and extracellular fluid which is produced in part from the amniotic fluid. Therefore amniotic fluid makes intimate contact with the respiratory and gastrointestinal tracts of the fetus and diffusion across fetal skin readily occurs until skin keratinisation occurs at approximately 20 weeks. With this intimate contact, the compositions of fetal plasma, interstitial fluid and amniotic fluid are similar, and therefore it is possible for any and all tissue types within the fetus to be exposed to EEs prior to skin keratinisation. After skin keratinisation, compounds eliminated in fetal urine mix with the amniotic fluid. Amniotic fluid is still swallowed and lung fluid is still produced and expelled, but the free diffusion across fetal skin decreases significantly.

The amnion membrane encloses and retains amniotic fluid during pregnancy. The placenta and umbilical cord structures are outside the amniotic membrane and do not come in direct contact with amniotic fluid [363]. In general, fluid flux through the amniotic membrane is regulated by epithelial tissues, which have tight junctions (TJs). TJs prevent the passage of molecules and ions through the space between cells, as in the blood-brain barrier. To be transported across the membrane, materials must actually enter the cells by diffusion or active transport [368]. The active transporters that are present in the placental membrane are also present in the amnion membrane [369], but their localisation and function suggest that their role is to prevent accumulation of xenobiotics and endogenous metabolites within the cells of the amniotic membrane rather than as a fetal protection mechanism.

With samples of amniotic fluid collected prior to 20 weeks, the total concentration of EEs (free + conjugated) increases with time and represents the total exposure of the fetus to these chemicals up until that point in time. The rationale for this is as follows.

1. Transport of free neutral, hydrophobic compounds such as EEs across the placenta is by simple diffusion which is driven by the concentration gradient between maternal and fetal blood.
2. Given that the only exposure route for the fetus is via the placenta, the only way for a hydrophobic compound to enter the fetal circulation is by diffusion across the placenta.
3. Transport of protein bound compounds across the placenta may be possible if progesterone is present in the placenta or maternal circulation at a level high enough to inhibit MDR1 active transport. Some EEs are known to bind to plasma proteins (see section 2.9.5) and thus may end up in the fetal circulation by this mechanism.
4. Sulphate or glucuronide conjugates produced by maternal metabolism and present in maternal blood do not cross the placenta given the localisation and unidirectional function of active transporters such as MRPs, BCRPs and OATs.
5. For chronic maternal exposure to EEs, blood levels of the EEs may remain elevated and may attain a steady state. With diffusion driven transport across the placenta, maternal circulation may serve as a constant supply of EEs to the fetus.
6. The final barrier in the placenta en route from maternal to fetal circulation is the fetal capillary endothelium. Aside from the two steroid-sulphate-specific OATs listed above, it is not known which, if any, of the other active transporters are present at this location. Simple diffusion is the primary mechanism by which molecules can cross, therefore limiting the rate of transport of polar, hydrophilic molecules across the barrier. It is therefore highly likely that once an EE enters the fetal compartment and is conjugated, it remains there until birth.
7. Sulphatase and glucuronidase enzymes are present in fetal tissues and the placenta. They may serve to recirculate EEs within the fetal compartment by cleaving the respective conjugates.

Wittassek et al. have suggested that the 'turnover' of amniotic fluid may facilitate elimination of EEs (phthalate metabolites in their study) via the placenta [151]. This statement is incorrect. In fetal physiology, the turnover of amniotic fluid that is described is the

recirculation of fluids within the fetal compartment through the swallowing of amniotic fluid and expelling fluid from the lungs, not a wholesale volume exchange with the mother. The movement of amniotic fluid (primarily water) into the maternal circulation across the membranes of the uterus has not been directly measured but appears to have little effect on fluid volume [172]. What does cross these membranes is likely to be only water, not solutes, as there are 5 layers of membranes separating the amniotic fluid and the uterine wall. The only exchange between mother and fetus is via the placenta, its active transport mechanisms and passive diffusion.

6.2 Comparison with Literature

6.2.1 Maternal Urine

The results from this study for total concentration of EEs in maternal urine are compared with literature values in Figure 6.2. The results from this study are consistent with other studies representing a range of lifestyles and countries (Table 2.3). This study is the first to report urine levels of BP-1 and BP-2. Six other target analytes (4t-OP, NP, mOP, mTric, 3PBA and 3PBOH) were included in the analysis but were not detected in any of the samples. The levels found in this study are consistent with those reported in the literature. For some compounds, e.g. the parabens, the levels from this study are in the higher range of the literature data. The literature data set was assembled from adult urine results and includes both males and non-pregnant females in addition to pregnant females. It is possible that the levels in male urine for some of the ingredients in personal care products are lower than in female urine, because of the differences in the use of these products.

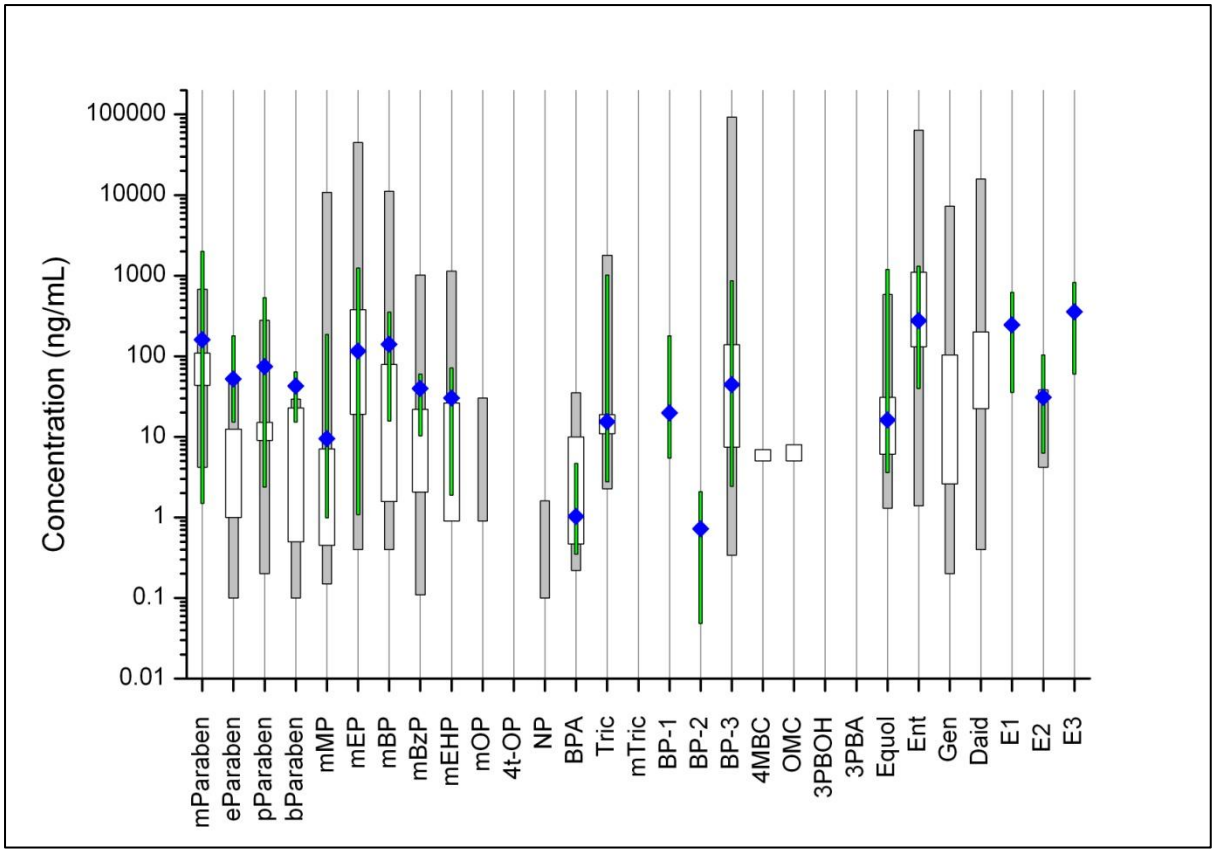

Figure 6.2. Comparison of total (free + conjugated) maternal urine concentrations of EEs obtained in this study with aggregate literature data. White bars indicate the range between lowest and highest literature median values, grey bars indicate range between maximum and minimum literature reported values. Green lines indicate the range between maximum and minimum values reported in this study and the blue diamond indicates the median value for this study.

6.2.2 Amniotic Fluid

The results from this study for total concentration of EEs in amniotic fluid are compared with literature values in Figure 6.3. Literature data are available only for the phthalate monoesters, BPA and the phytoestrogens (Table 2.5). This study is the first to report levels of parabens, UV filters and triclosan in human amniotic fluid. Six other target analytes (OP, NP, mOP, mTric, 3PBA and 3PBOH) were included in the analysis but were not detected in any of the samples. The literature concentrations of the endogenous steroids (E1 and E2) shown in Figure 6.3 are the free concentrations.

The comparison with literature values must be made cautiously because some of the literature studies may underestimate amniotic fluid concentrations, especially with samples collected in the early 2nd trimester. Several studies have used only β-glucuronidase deconjugation. As indicated in Chapter 1, the fetal glucuronidation pathway is much less active than the

sulphation pathway. The glucuronidation pathway does not develop until later in gestation and at term it is only about 30% of the activity of the adult. In contrast, the activity of the fetal sulphation pathway is high during early gestation and decreases in activity as gestation advances. As a result, the majority of the conjugates present in AF collected in the early 2nd trimester are most likely sulphates, not glucuronides. The studies affected are all those that have reported phthalate monoesters and one study reporting BPA and the phytoestrogens as identified in Table 2.5. The reason for the choice of enzyme in the studies identified in Table 2.5 was to avoid potential contamination of their samples by phthalates present in the *Helix pomatia* derived β-glucuronidase / arylsulphatase mixed enzyme. The blank and other control samples of the present study indicated only the mEHP results were affected by contamination of the *Helix pomatia* derived β-glucuronidase / arylsulphatase mixed enzyme. The reagent blank levels for the other phthalate monoesters were low and repeatable or not detected and adequately accounted for any contamination.

The levels reported in this study for a cohort of 32 New Zealand mothers are consistent with, and in some cases, lower than the levels reported in the literature. Median levels of mEP, mBP, BPA and ENT in the New Zealand cohort were lower than the median literature values and mBzP was not detected. The median levels for mEHP and EQ in the New Zealand cohort were similar to those reported in the literature. Unfortunately, the results for GEN and DAID from this study were not reliable enough to be used because of instability of the TMS derivatives during analysis.

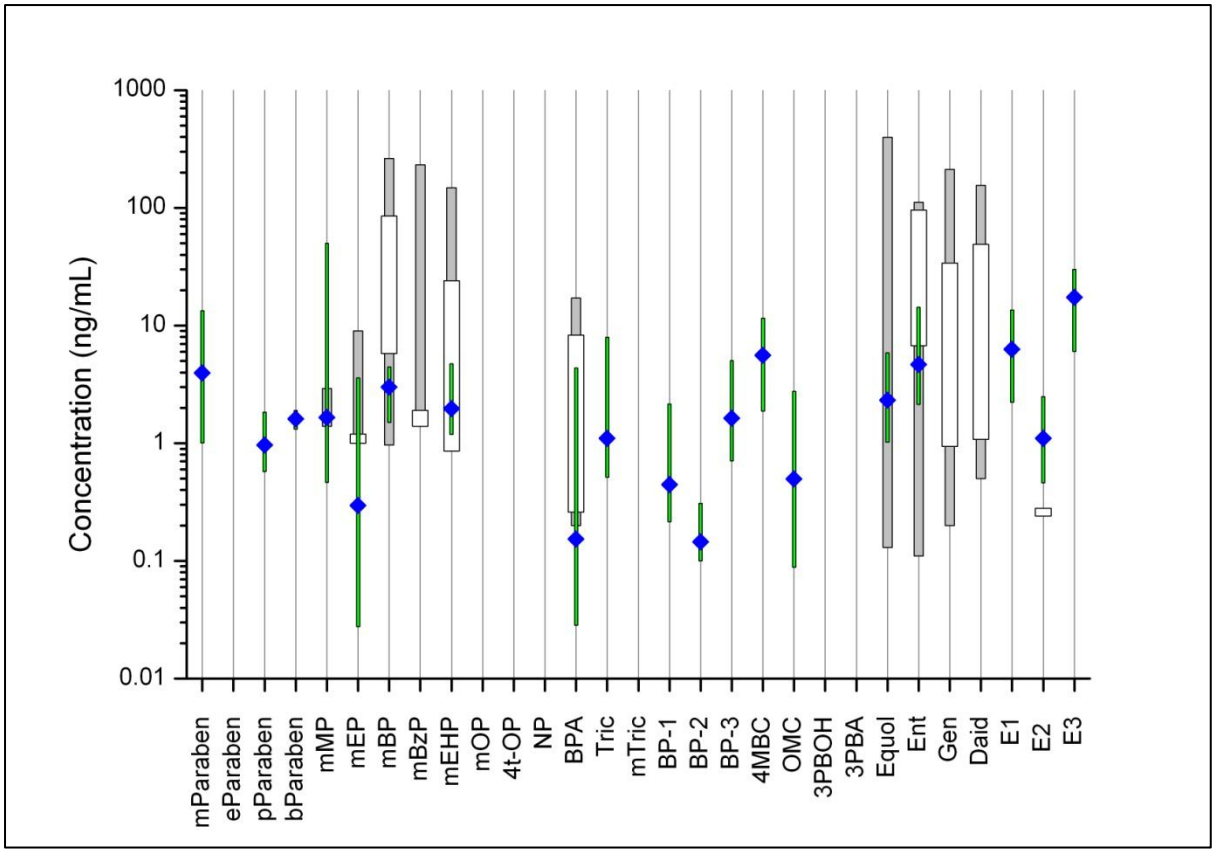

Figure 6.3. Comparison of total (free + conjugated) amniotic fluid concentrations of EEs obtained in this study with aggregate literature data. White bars indicate the range between lowest and highest literature median values, grey bars indicate range between maximum and minimum literature reported values. Green lines indicate the range between maximum and minimum values reported in this study and the blue diamond indicates the median value for this study.

6.3 Relative Estrogenic Load

To estimate the increase in estrogenic load that the fetus is exposed to as a result of these levels of EEs in amniotic fluid, the relative estrogenic potency (Figure 2.16 and Table A. 6) of the compound was used. As there are few data on the relative potency of the compounds of interest for hERβ, this discussion will be limited to hERα.

There is some uncertainty as to how to handle the contribution of E3 to the total estrogen activity. As discussed in section 2.8, E3 is known to behave as an antagonist to E2 when present in equal or up to 10-fold excess concentrations of E2, resulting in an 85% suppression in E2-mediated transcription. But, when E3 is present alone or in concentrations 50 fold greater than E2, it behaves as a weak agonist. In this study, free E2 was not detected, but the literature indicates free E2 concentrations in amniotic fluid are approximately 0.24 ng/mL for male fetuses and 0.28 ng/mL for female fetuses [52]. These levels are below the limit of

quantification of the analytical method used in the current study (1.5 ng/mL, Table 4.12). Free E3 was determined in this study and was approximately 3.2 ng/mL. Therefore, it is possible that E3 behaves as an antiestrogen in amniotic fluid, thus reducing the potency of E2.

A similar behaviour has been reported for both GEN and DAID as discussed in section 2.7.4. Both compounds were able to reduce E2-mediated transcription by 20% when present in equal concentrations to E2, but how this behaviour changed as a function of concentration ratio was not investigated. The concentrations of GEN and DAID in amniotic fluid are expected to be much greater than E2 (see Figure 2.15); however the suppressive effects of GEN and DAID cannot be included in the estimate of relative estrogenicity because the concentration dependence of the suppressive effects has not been characterised.

As discussed in Section 2.8, synergistic effects have also been reported for mixtures of BP-1, BP-2 and BP-3 with or without E2 and for BPA and NP each with E2. These compounds, when present together in mixtures can result in an estrogenic signal that is larger than predicted by the sum of the concentrations, however, no information is available as to how the synergistic effect changes with mixture composition or concentration of E2. Therefore, the effects of such synergism cannot be considered in this study.

There are two possible scenarios, representing conservative and worst-case situations, for the relative estrogenic load experienced by the fetus in response to the levels of endogenous and environmental estrogens in amniotic fluid. In the conservative scenario, the free concentrations of the EEs and endogenous estrogens and their lowest reported estrogenic potencies are used. The potencies of E2 and E3 are set to their independently determined values. In the worst-case scenario, the total (free + conjugated) concentrations of the EEs and the free concentrations of the endogenous estrogens are used. The highest reported estrogenic potencies are used, however to reflect the antiestrogenic behaviour for E3, the potency for E3 is set to zero and the relative potency of E2 is reduced by 85%. The two scenarios are summarised in Table 6.1.

Table 6.1. Comparison of conservative and worst-case scenarios for relative estrogenic load experienced by the fetus up to 20 weeks gestation.

	Conservative Scenario	**Worst-case Scenario**
Concentrations of endogenous estrogens	Use free concentration (Table A. 14 and Table A. 15)	Use free concentration (Table A. 14 and Table A. 15)
Relative estrogenic potency of endogenous estrogens	Use lowest literature potency values (Table A. 6)	Use highest literature potency values (Table A. 6)
Concentrations of environmental estrogens	Use measured free concentrations (Table A. 14 and Table A. 15) but set GEN and DAID concentrations to zero	Use total concentrations (Table A. 16 and Table A. 17)
Relative estrogenic potency of environmental estrogens	Use lowest literature potency values (Table A. 6)	Use highest literature potency values (Table A. 6)
Mixture effects	None considered. Assume simple additivity	Use greatest antiestrogenic effect of E3.

These two scenarios represent the extremes of potential influence of the EEs. The conservative scenario favours the effects of endogenous estrogens while the worst-case scenario favours the effects of the EEs. The total concentration of an EE represents a worst-case scenario of exposure as it assumes the compound enters the fetal circulation via simple diffusion across the placental membrane as the free compound and is subsequently conjugated by the fetus. Because the fetal plasma, extracellular fluid and amniotic fluid compositions are considered similar at this stage of fetal development, the compound is free to diffuse through the fetal tissues and may not necessarily be immediately transported to the kidneys/liver for conjugation. In contrast, endogenous hormone levels are tightly controlled and only the free hormones are active. The concentration of the EE or endogenous estrogen is multiplied by the relative potency and the sum for all compounds calculated. In both scenarios, the literature reported concentrations of free E2 in amniotic fluid for male and female fetuses are used. Because GEN and DAID were not reliably determined in this srudy, the median total (free + conjugate) concentrations from the literature are used in the worst-case scenario (GEN = 1.54 ng/mL and DAID = 5.48 ng/mL). The free concentrations of GEN and DAID are set to zero in the conservative scenario.

The results for each scenario for each individual are shown in Figure 6.4. In the conservative scenario, the EEs account for 0-9% of the relative estrogenic load of the amniotic fluid for female fetuses and 0-10% for male fetuses. In contrast, the EEs account for 14-64% of the relative estrogenic load of the amniotic fluid for female fetuses and 16-78% for male fetuses

in the worst-case scenario. The highest male and female estrogenic loads shown in Figure 6.4(b) arise from higher than average levels of TRIC and BPA in those samples.

The results summarised in Table 6.2 and illustrated in Figure 6.5 are obtained by repeating the calculation using the median free and total concentrations for the male and female fetuses. In this case, there is little difference in the total load of the amniotic fluid of male and female fetuses with either scenario. However, in the worst-case scenario the potential contribution of EEs to the estrogenic load of the amniotic fluid could approach 40% for both male and female fetuses. The major contributor to the differences shown in Figure 6.5 is the anti-estrogenic behaviour of E3 in reducing the transcriptional activity of E2.

Table 6.2. Relative estrogenic load of the amniotic fluid for the conservative and worst-case scenarios using the median amniotic fluid composition.

	Conservative		**Worst-Case**	
	Female	**Male**	**Female**	**Male**
Endogenous	0.346	0.316	0.042	0.039
Environmental	0.007	0.009	0.023	0.026
Total	0.353	0.325	0.065	0.065
%Environmental	2%	3%	36%	40%

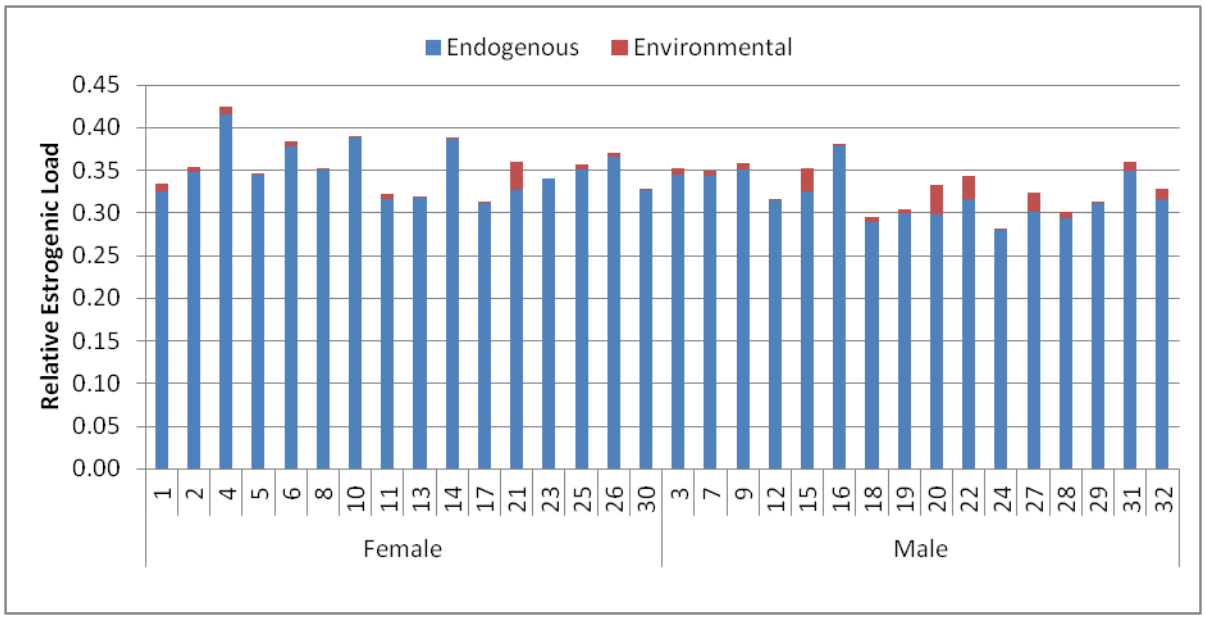

(a) Individual results for the conservative scenario

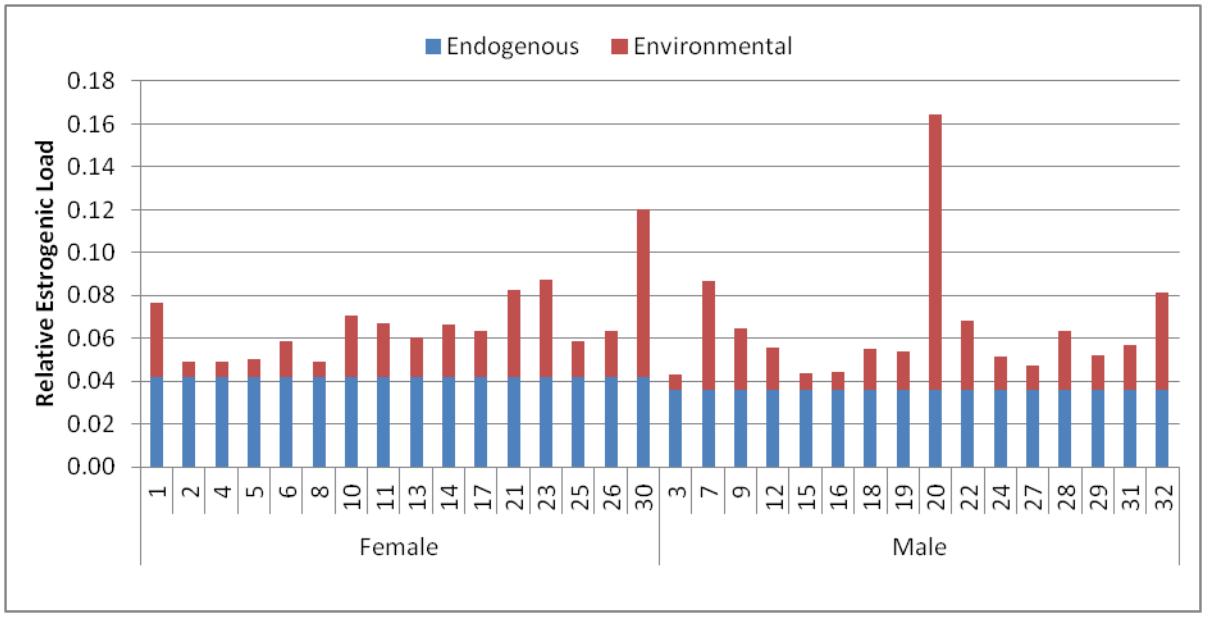

(b) Individual results for the worst-case scenario

Figure 6.4. Relative estrogenic load of amniotic fluid for each individual estimated by the conservative and worst-case scenarios

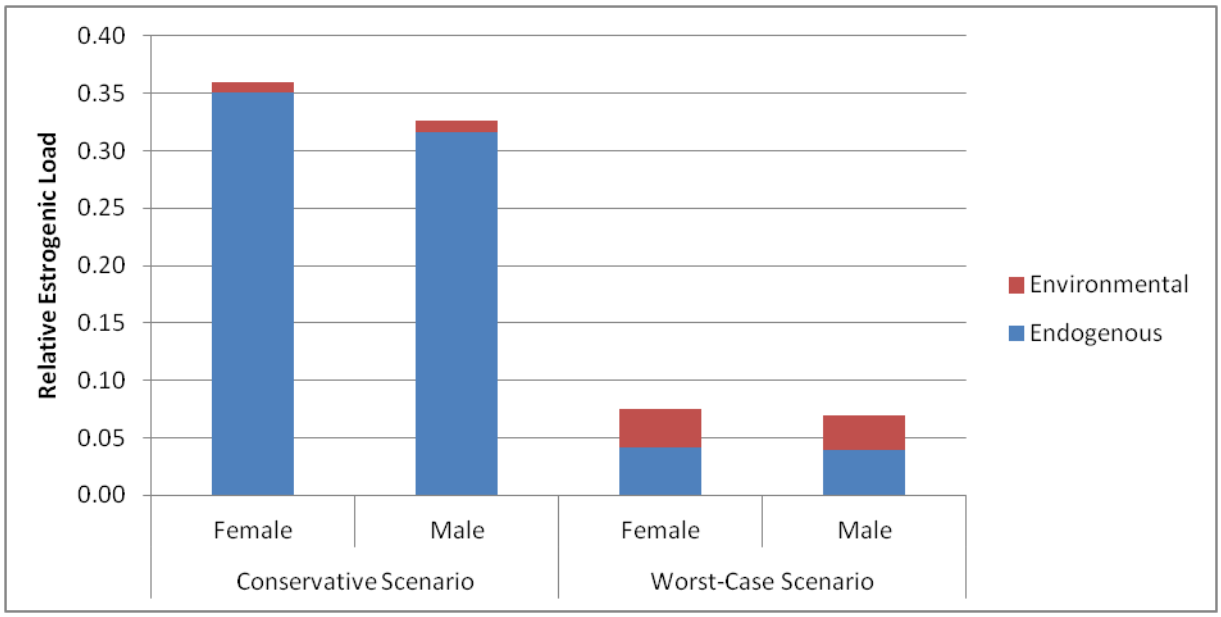

Figure 6.5. Median relative estrogenic load of amniotic fluid for male and female fetuses estimated by the conservative and worst-case scenarios.

6.4 Discussion

This assessment has addressed only the estrogenic potency of amniotic fluid in terms of its potential to up-regulate hER-mediated gene transcription, which is only one small facet of a highly complex and variable situation. There are many co-operating and competing factors at play, especially in attempting to predict the end effects of this type of exposure. Even with the simplifications and assumptions that have been applied to this analysis, it is plausible that fetal exposure to EEs could account for a substantial (40%) increase in the estrogenic potency of the amniotic fluid for both male and female fetuses. With the list of EEs continually growing, this contribution could increase. Androgenic potency is the opposing factor and a similar analysis could be performed if similar data on androgenic potency and amitotic fluid concentrations of environmental androgens were available. At this time, sufficient data are not available in the literature to conduct such a study.

Other competing and co-operating factors have been identified in which the target analytes of this study play a role. Anti-androgenic activity is a co-operating factor exhibited by the parabens, the phthalate monoesters, BP-3 and 4MBC. The parabens also have anti-aromatase activity which inhibits estrogen biosynthesis and competes with their estrogenicity. The phthalate monoesters are not estrogenic or androgenic in any of the *in vitro* assays, but animal studies have repeatedly shown phthalate exposure results in adverse effects on the male reproductive system due to their anti-androgenic activity. Recent monitoring of human

pregnancy and newborns has found indications of similar effects. Triclosan is another compound with conflicting activities. Depending on the assay, it is estrogenic, anti-estrogenic and not estrogenic; not androgenic and androgenic.

GEN, DAID and E3 are antagonists in the presence of E2. Both GEN and DAID are able to reduce E2-mediated transcription by 20% when present at a 1:1 concentration ratio with E2. E3 is able to reduce E2-mediated transcription by 25% at a 1:1 concentration ratio with E2 and by 85% when present at a 10:1 concentration ratio.

The effects of exposure to a mixture of chemicals that are at the same time estrogenic and anti-androgenic have not yet been studied. It is not known whether this type of mixture would amplify one mode of action over the other, resulting in observed effects of both modes of action or result in entirely new observed effects.

6.5 Conclusions

It is abundantly clear that the human fetus is exposed to measurable quantities of EDCs at a critical time in gestation when they have the opportunity to cause the greatest adverse effects. The levels of EEs found in amniotic fluid are strongly correlated with maternal exposure and are reached through normal, daily lifestyle choices that expectant mothers make. The women who participated in this study did not make any changes to their daily routines based on *a priori* knowledge of participation in this study because they were not recruited for the study until after the samples had been obtained for medical diagnostic reasons. The strength of the correlations between maternal urine and amniotic fluid levels obtained in this study for a large number of the target analytes show that maternal urine levels could provide reliable estimates of amniotic fluid levels with a much less invasive method of sample collection.

Even with the simplifications and assumptions that have been applied to this analysis, it is plausible that fetal exposure to EEs could account for a substantial (40%) increase in the estrogenic potency of the amniotic fluid for both male and female fetuses. While there is insufficient information to be able to definitively assess or predict the biological effects of the exposure to EEs on the fetus, should actual conditions be similar to the worst-case scenario presented in this study, there is real potential for EEs to interfere with E2-mediated transcription. The developmental consequences of this interference are difficult to predict because the role of EDCs play in upsetting androgen-mediated transcription and endogenous steroid synthesis and metabolic pathways are even less well understood. The possible

mechanisms and consequences of EE interference with E2-mediated transcription will be discussed in Chapter 9.

Chapter 7 Binding Studies – Surface Plasmon Resonance

7.1 Introduction

The purpose of this work was to obtain experimentally measured binding energies for EEs with the hER. As was found in Chapter 3, the binding energy for many EEs of interest is not known. Endogenous estrogens bind to the receptor with high affinity, but EEs have much lower affinity. Knowledge of the kinetics of binding (i.e. how fast or slowly a ligand associates with and dissociates from the ER) would also be useful in interpreting computational docking results and extending the computational modelling to include molecular dynamics. It is also desirable to have a rapid screening method for determining whether the components in a mixture can bind to the ER before putting the effort into detailed chemical analysis. This chapter presents the development of a method for studying the kinetics of binding of EEs to the ER and for quantifying equivalent estrogenic load of a mixture of EEs. Equivalent estrogenic load is defined as the concentration of E2 that produces the same instrument response as a sample of unknown concentration. This concept will be discussed in more detail later in the chapter.

The method uses the technique of surface plasmon resonance (SPR). Method development begins with establishing a procedure to covalently attach the ER-LBD protein to the SPR sensor chip. Once a functional ER surface is achieved it can be used to study the kinetics of binding of individual EEs to the ER, giving both reaction rate constants and equilibrium binding constants. Then, using the same surface, a method for quantifying the estrogenic load of a mixture of EEs can be developed.

The kinetic studies will provide insight to the ER-ligand binding mechanism, quantifying how quickly or slowly the EEs associate with and dissociate from the ER. Equilibrium studies will provide a consistent set of binding affinity measurements for the suite of EEs. Binding affinity data are needed for model validation in the computational docking study presented in Chapter 4.

This chapter begins with a brief overview of reaction kinetics and equilibrium studies as they pertain to ER-ligand interactions. Next, the fundamentals of the SPR technique are presented. The results of the experimental work follow. The first experiment was a validation of instrument sensitivity. Subsequent experiments were different attempts at immobilising the ER-LBD to the sensor chip. As will be shown, the SPR experiments were only partially successful. The discussion will explain what the difficulties were and how they may be overcome in future work.

7.2 Theoretical Basis

7.2.1 Reaction Kinetics

The first step in the classic genomic mechanism of estrogenic action is the binding of the ligand (L) to the ER (R) to form the receptor-ligand complex (RL).

$$R + L \underset{k_d}{\overset{k_a}{\rightleftharpoons}} RL$$

This type of reaction is described as a 1:1 bimolecular interaction and the reaction rapidly reaches equilibrium. The association reaction rate constant, k_a, is a second-order rate constant and the dissociation reaction rate constant, k_d, is a first-order rate constant. At equilibrium, the strength of ligand binding to the receptor is described by the equilibrium dissociation constant K_D (also called binding affinity) which is defined as

$$K_D = \frac{[R][L]}{[RL]} = \frac{k_d}{k_a}$$

K_D has units of M and decreases with increasing affinity between the ligand and receptor. K_D can also be interpreted as the concentration of ligand L at which 50% of the binding sites of R are occupied.

To determine the association and dissociation rate constants, experimental conditions are established where [L] is in a large excess and thus remains constant. Under these conditions, the binding interaction follows pseudo-first order kinetics [370-372] with an integrated rate equation:

$$[RL]_t = [RL]_{eq}(1 - e^{-k_{obs}t})$$

where

$[RL]_t$ = concentration of receptor-ligand complex at time t

$[RL]_{eq}$ = concentration of receptor-ligand complex at equilibrium

k_{obs} = experimentally determined pseudo-first order reaction rate constant

$[RL]_t$ is measured as a function of t and nonlinear regression is used to fit the integrated rate equation to the experimental data to obtain the value for k_{obs}. For a reversible reaction, k_{obs} is directly proportional to the free ligand concentration [L]:

$$k_{obs} = k_d + k_a[L]$$

The value of k_{obs} is then determined at several ligand concentrations [L] and a plot of k_{obs} as a function of [L] is linear with slope equal to k_a and y-intercept equal to k_d. A simulated example of the data from this type of experiment is shown in Figure 7.1.

The pseudo-first order integrated rate equation is often called the Langmuir model because at equilibrium the Langmuir isotherm can be derived [370]. At equilibrium [RL] is constant, the association and dissociation reaction rates are equal and experimental conditions can be set such that [R] << [L] and that [L]is high enough that it can be considered constant. In this case,

$$[RL] = \frac{[R][L]}{K_D}$$

which can be rewritten, giving the Langmuir isotherm equation

$$[RL] = \frac{[R]}{1 + \frac{K_D}{[L]}}$$

In an experiment where some signal S is measured that is directly proportional to [RL], then [R] is directly proportional to S_{max}, the maximum signal theoretically possible when all receptor sites are occupied by the ligand. A plot of S vs. [L] gives a curve of the form of a square hyperbola and nonlinear least squares regression can be used to obtain values for K_D and S_{max}.

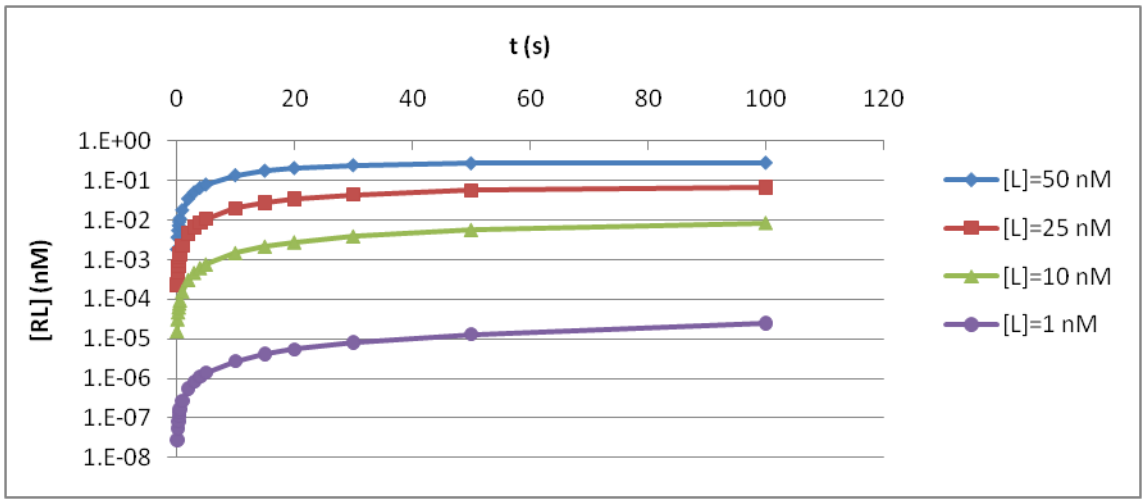

(a) Increase in [RL] as a function of time for constant [R] and different [L].

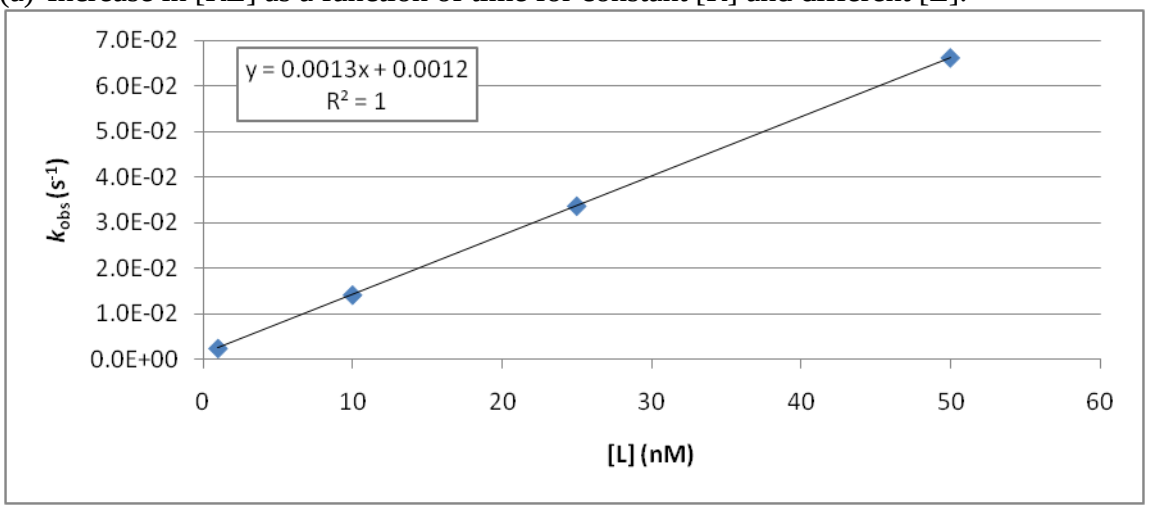

(b) Increase in pseudo-first order rate constant (k_{obs}) as a function of [L] obtained from data shown in panel (a).

Figure 7.1. Simulated data from for a pseudo-first order kinetics experiment. Values for k_a=1.3x10^6 M^{-1}s^{-1}, k_d=1.2x10^{-3} s^{-1} and K_D=0.9 nM are for E2-hERα [373].

7.2.2 Kinetics of ER Ligand Binding

The only study of ER-ligand binding kinetics found in the literature [373], reports association and dissociation reaction rate constants and equilibrium dissociation constants for 6 ligands as illustrated in Figure 7.2.

From Figure 7.2, the association reaction rate constants for the endogenous hormones (E1, E2 and E3) are very similar, but the dissociation reaction rate constants are different resulting in the differences in equilibrium dissociation constants. Of the three endogenous hormones, E2 dissociates the slowest and forms the most stable complex with ER. All of the agonist ligands (E1, E2, E3, BPA, DES) associate quickly, but their dissociation rates vary dramatically. BPA associates and dissociates quickly, resulting in a weak complex. DES

associates very quickly but dissociates slowly thus forms a very stable complex. In contrast, the antagonist, OHT, associates slowly and dissociates slowly, forming a complex with stability similar to E1 and E3. This behaviour is not surprising given the large size of the molecule compared to the endogenous hormones and the precise fit of the pendant group needed to stabilise the antagonist conformation of the receptor.

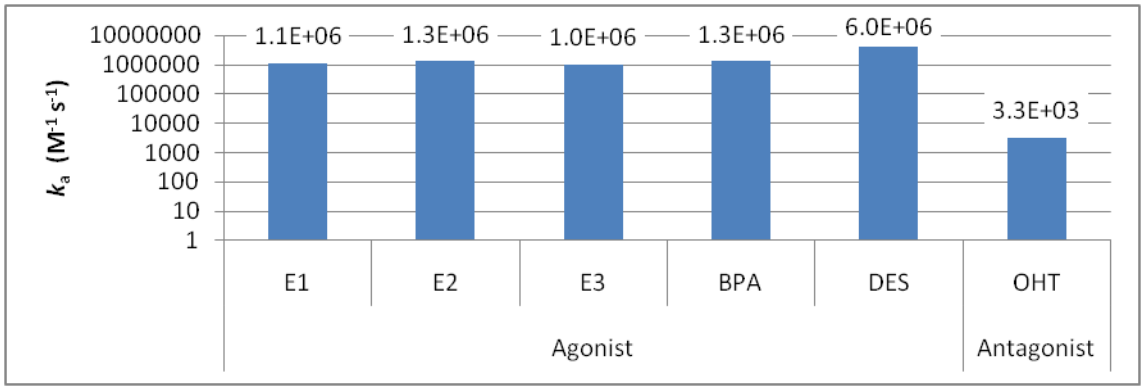

(a) Association reaction rate constant (k_a)

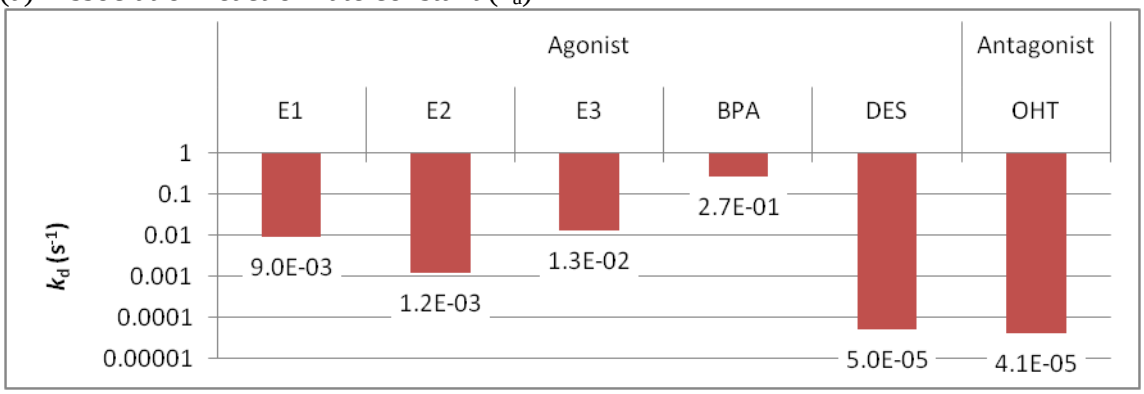

(b) Dissociation reaction rate constant (k_d)

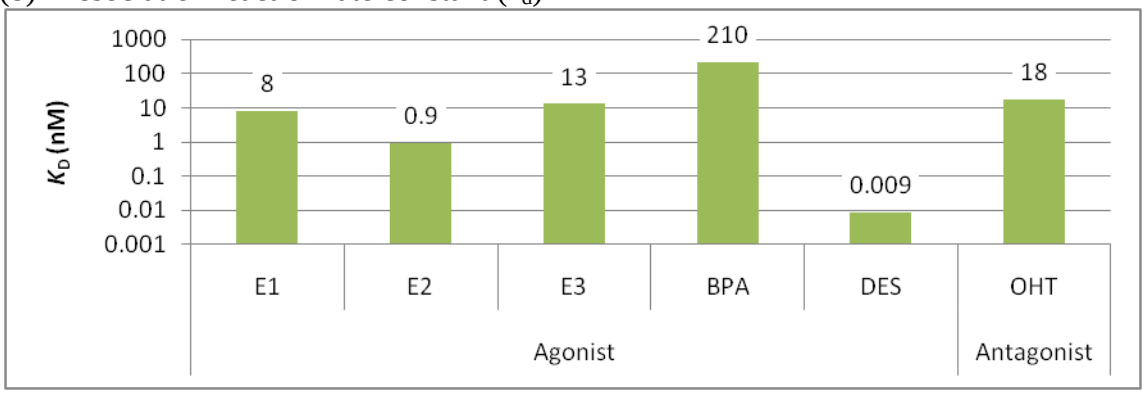

(c) Equilibrium dissociation constant (K_D)

Figure 7.2. Association (k_a) and dissociation (k_d) reaction rate constants and equilibrium dissociation constant (K_D) measured by SPR [373].

7.2.3 Equilibrium Studies

K_D can also be determined directly via equilibrium experiments such as competitive binding assays. For example, the US EPA has adopted a conventional competitive binding assay as their standard method for identifying potentially estrogenic compounds. This assay uses rat uteri as the source of ER [374]. The uteri are taken from Sprague-Dawley rats and the tissue is processed to produce a rat uterine cytosolic (RUC) fraction containing the ER protein. The uterus contains mainly ERα and a small but not insignificant proportion is ERβ [375]. Mixtures of the RUC with [^{3}H]-E2 at a constant concentration plus increasing amounts of the test chemical are incubated with the cytosol preparation at 4 °C for 18 h. The unbound chemicals are removed by adsorption on dextran-charcoal and the residual radioactive concentration of the cytosol preparation is counted by scintillation. The drawbacks to this method include the use of radioactive materials, the tissue extract contains a mixture of both α and β ERs, and of course the sacrifice of animals. Similar assays are available that use expressed proteins instead of those obtained from tissue sources. The purpose of this type of assay is to identify chemicals that have the potential to compete with endogenous estrogens for binding to the ER. This type of assay does not provide any information on whether the chemical tested acts as an agonist or antagonist of gene expression, or how efficiently gene expression is up or down-regulated by the chemical.

The ability to obtain only ERα or ERβ ligand binding domains using cellular expression systems has shown that the two receptors have different binding affinities for all ligands tested (See Table x in Chapter 3). In most cases, the difference is small. But, in some cases the difference is significant, and those ligands are described as selective ER modulators (SERMs). As drug targets, SERMs are important as they are able to treat a disease that involves only one of the two receptors without activating the receptor not involved in the disease (e.g. treating breast cancer without triggering or worsening osteoporosis).

Most of the studies using expressed ERs for binding studies report IC_{50} rather than K_D for the compound of study. In the context of enzyme inhibition, IC_{50} is the concentration at which an inhibitor is able to prevent 50% of the substrate present from binding. For competitive binding studies, IC_{50} is related to the competitive inhibitor K_D by the Cheng-Prusoff equation [295]:

$$K_D = \frac{IC_{50}}{1 + \frac{[S]}{K_M}}$$

where [S] is the concentration of substrate and K_M is the concentration of substrate at which enzyme activity is at half maximal. In the context of enzyme inhibition, K_M is not the K_D of the substrate. However, in the context of hormone-receptor binding inhibition, the activity of the receptor is at half-maximum when it is 50% occupied by the target hormone. For the ER, competitive inhibition studies are done using the target hormone E2. So, in this case $K_M = K_D$ for E2.

Some binding affinity data for EEs are available in the literature however they must be carefully reconciled because they have been produced by varying methodologies, using different sources of ER and under different conditions. There is very little information on the kinetics of the binding of EEs – how quickly the chemicals associate with and dissociate from the ER [373]. Knowledge of the kinetics underlying the binding of EEs to the ER will be useful in explaining the range of biological outcomes of animal exposure studies.

7.2.4 Principles of Surface Plasmon Resonance

SPR is a technique that has been applied to studies of biomolecular interactions with great success [376, 377]. Initially, SPR was used to study protein-protein interactions but recent advances in instrumentation have enabled the study of protein-small molecule interactions such as enzyme-substrate and receptor-ligand. SPR offers the possibility of rapid screening for biological activity that compliments traditional analytical chemistry in the identification of endocrine disrupting chemicals. SPR can be used to quantify total biological activity of a sample of unknown composition and analytical chemistry provides the means to identify and quantify individual components that contribute to the biological activity.

Instruments from two manufacturers, Biacore and Bio-Rad, dominate the SPR literature [378]. The two instruments are based on the same principle but differ in their operation. Much of the published literature is based on the Biacore instrument as it was the first commercially available system. The discussion below relates to the Bio-Rad ProteOn XPR36 instrument that was used for this work.

The principle of SPR is illustrated in Figure 7.3. In this example, the receptor protein is immobilised on the very thin gold surface adhered to the base of an inverted prism. The base

of the prism (the top side) is exposed to a flowing liquid that transports the analyte to the surface to interact with the immobilised receptor protein. Light of a fixed angle of incidence, θ, is directed up through the prism and onto the back of the thin gold film. Light incident on the back of the gold surface is reflected back through the prism to a detector. As a result of the surface plasmon phenomenon (explained below) that occurs at the gold surface, the intensity profile of the reflected light is altered. A minimum in the intensity of the reflected light now occurs at a particular wavelength and angle of reflectance that both depend on the refractive index of what is in contact with top side of the gold surface (n_s) [379-381].

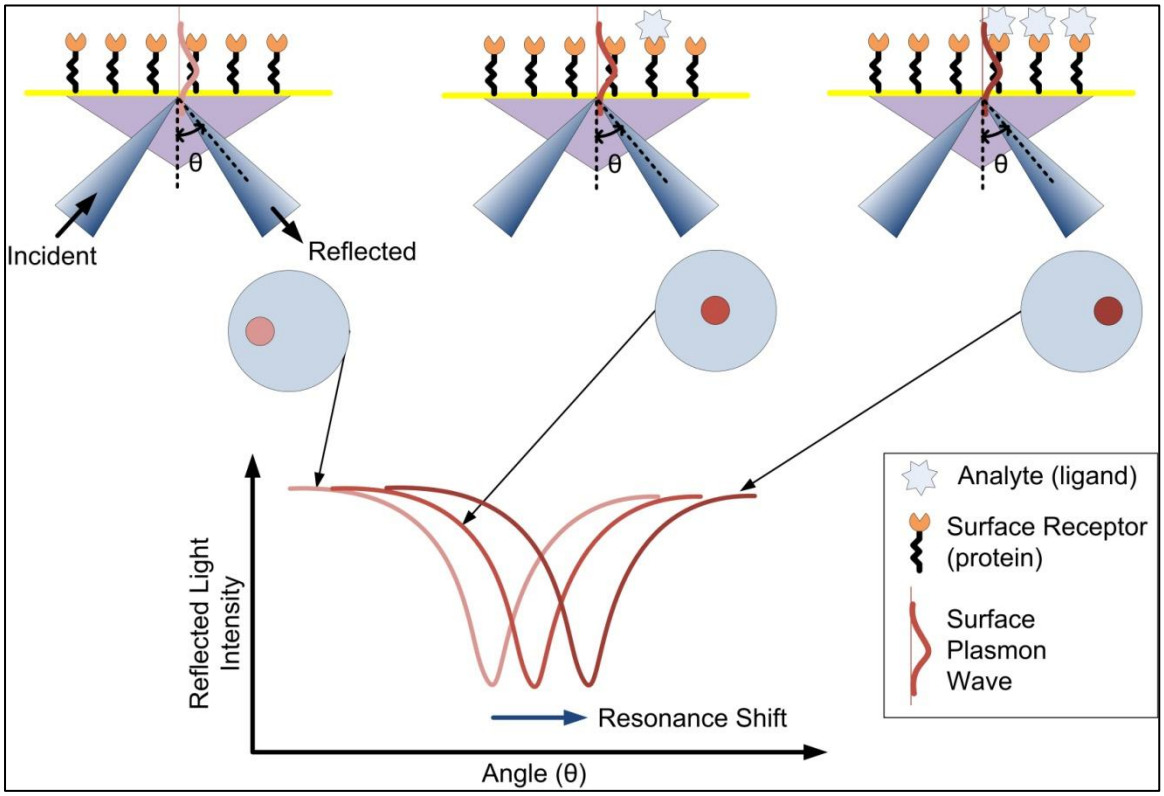

Figure 7.3. The principles of SPR. The magnitude of the shift in angle of reflected light is dependent on the refractive index (mass density) at the surface.

In the Bio-Rad instrument, the incident light is produced by a LED (light emitting diode) and is incident at a fixed angle. The reflected light is directed to a CCD (charge capture device) which captures a 2D image of the reflected light beam. Using this type of detector, the minimum in intensity can be located within the image and the difference in position measured with respect to a reference signal image. This shift in position of the minimum is the 'resonance shift' and is related to the change in refractive index of the sample in contact with the gold surface. The refractive index change is proportional to the change in mass at the

surface caused by the binding and release of the analyte molecule (ligand) by the immobilised receptor protein.

Surface plasmons consist of the collective oscillations of nearly free electrons in the metal film and their associated evanescent electromagnetic waves. A p-polarized lightwave can resonantly couple with a surface plasmon wave propagating at the interface of the metal film and the sample layer. When this resonant coupling occurs (i.e. at the resonance angle), the energy in the incident lightwave is converted into surface plasmon waves and dissipated through ohmic heating; relatively little of the incident light is reflected from the interface to the detector when the metal film thickness is optimized. At other angles or wavelengths, most of the light is reflected off of the sensor surface. The SPR phenomenon creates a minimum in the reflectivity at an angle or wavelength that depends on n_s. The resonance angle for a given wavelength varies as a function of n_s [382]. The signal that is measured is the shift in the minimum of the optical reflectivity curve and is reported in response units (RU). The shift is dependent on both the change in mass and the change in refractive index at the surface of the sensor chip. Careful control and matching of bulk properties of the analyte solutions to the running buffer is necessary to minimize effects of changes in refractive index due to changes in bulk properties of the solutions. 1 RU = 10^{-6} change in refractive index [383].

7.2.5 Coupling to the SPR sensor chip

The active surface of the SPR sensor chip is composed a modified alginate polymer that has exposed carboxylic acid groups. The usual method of binding the selected species to the chip surface is by amine coupling to these carboxylic acid groups. The species to be bound must have a terminal amine group. The carboxylic acid surface is activated by injecting a solution of EDAC (N-ethyl-N'-(3-diethylaminopropyl)carbodiimide) and sulfo-NHS (N-hydroxysulfosuccinimide sodium salt). The species to be bound to the sensor chip surface will displace sulfo-NHS. Any unreacted sites are deactivated with ethanolamine. The reaction scheme is illustrated in Figure 7.4.

For kinetics experiments there is a trade-off between the density of the immobilised species on the surface (i.e. how many immobilised molecules per unit area) and mass transfer. High density increases the signal measured, but if the density is too high, mass transfer of the analyte to a binding site is compromised, thus affecting the results of the kinetics experiment. An important part of method development is finding the optimum ligand density where signal intensity is high but mass transfer issues are minimized.

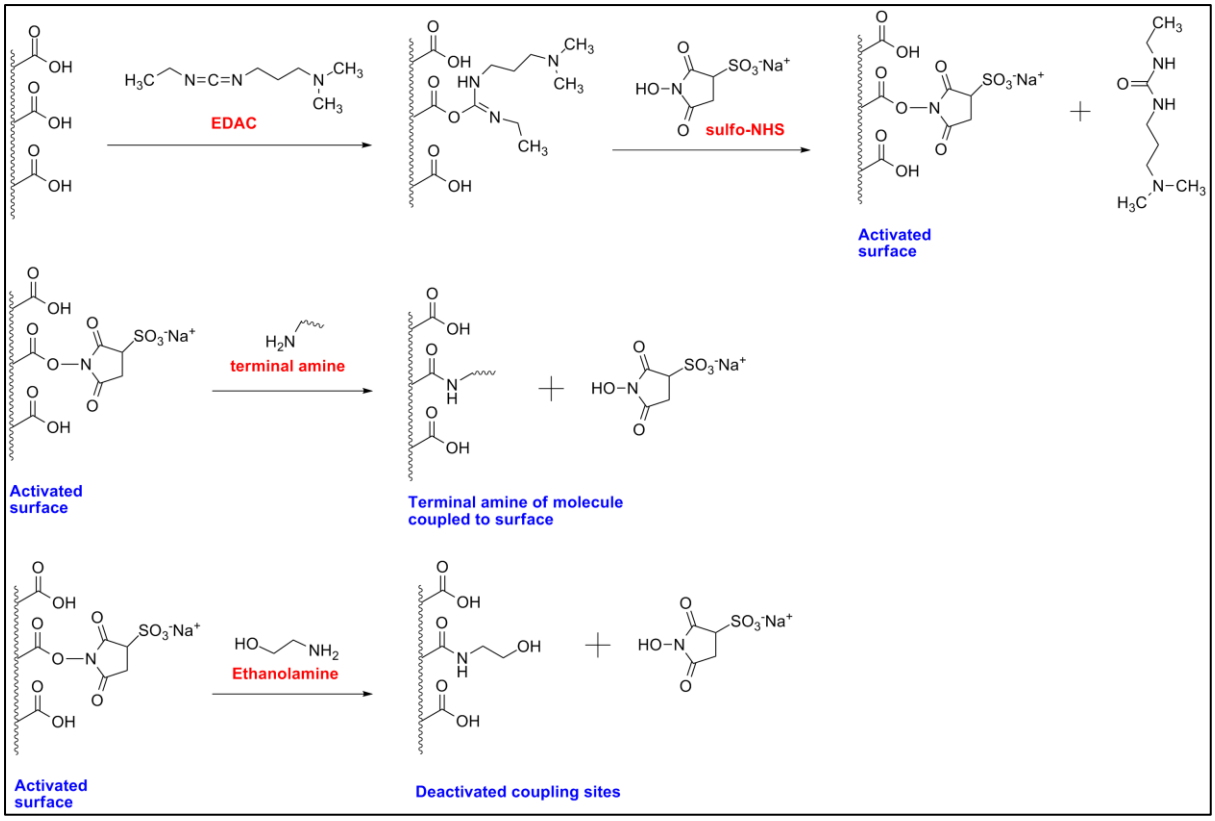

Figure 7.4. The sensor chip surface is activated by EDAC/sulfo-NHS to provide a good leaving group for the subsequent coupling of a molecule with a terminal amine group to the surface. Unused activated binding sites are deactivated using ethanolamine.

7.2.6 Review of SPR-based ER Binding Assays

SPR has been used to study ER-ligand interactions using a traditional competitive binding assay [384-387]. The small molecule ligand (e.g. E2) was immobilised on the SPR sensor chip surface. The ER was incubated with the test chemical and injected, resulting in a competition between the immobilised and free ligands for binding with the receptor. Because the SPR signal is proportional to the mass change that occurs on binding at the chip surface, monitoring the interaction of the high molecular weight receptor protein in solution with the immobilised ligand gives a large signal.

SPR has also been used to study ER-DNA interactions [388-390]. The consensus DNA sequence estrogen response element (ERE) was immobilized onto the sensor chip. The full-length ER was incubated with the ligand of choice. Two receptor-ligand complexes will come together in solution to form a dimer which will bind to the immobilised ERE. However, the unliganded ER monomer can also bind to the ERE, interfering with the desired signal. Careful control of experimental conditions such as incubation time and temperature is necessary to ensure optimal performance.

SPR can also be used to study the interaction of the ligand bound ER with different co-activator proteins [230], providing information on the transcriptional activation of ER by the ligand under study. In this study, the co-activator protein was immobilized onto the sensor chip. The ER was incubated with various estrogenic compounds and injected over the immobilised co-activator protein. The agonist/antagonist behaviour of the ligands was determined since the ligand-bound ER LBD will not bind to the immobilised cofactor if it is in the antagonist conformation.

All three of these strategies work well for studying individual ligands but none of them are applicable to the study of mixtures.

The study by Rich et al. [373] is the only SPR study of ER-ligand interactions to immobilise the receptor on the sensor chip. The ER-LBD was expressed with an N-terminus poly-histidine tag. A His4 monoclonal antibody was produced and immobilized onto the sensor chip. This antibody recognizes and binds to a 4-histidine sequence. The His-tagged ER-LBD was then captured by the immobilized antibody. Because the ER-LBD has only one His tag, this ensures it is bound to the sensor chip surface in an orientation that allows the conformational change to occur on ligand binding. One advantage of this strategy is that the LBD-ligand complex can be easily removed from the antibody after the interaction experiment by washing the surface with a mild acid solution. However, the antibody – His-tag binding affinity is not strong, so careful control of experimental conditions (buffer, pH, etc.) is needed so that the ER-LBD is not removed from the surface during the measurement.

7.2.7 Quantifying Estrogenic Load

One of the objectives of this study was to develop a SPR-based method to screen individual chemicals, known mixtures of chemicals and environmental or biological samples of unknown composition for their ability to bind with the ER. With SPR, the measurements occur under constant flow conditions and a period of time is required for the signal to stabilise at an equilibrium condition. The signal at equilibrium is proportional to the mass change at the surface due to analyte binding. Because the analytes of interest in this study have similar molecular weights (150-300 Da is similar within the resolution of 1 RU in SPR), the method is in effect a counter for molecules that have bound to the immobilised receptor.

For a sample containing a single analyte, the SPR signal obtained under equilibrium conditions is proportional to the analyte concentration as shown in Figure 7.5 for E2 and

BPA. Figure 7.5 was produced using actual experimental data for the interaction of hERα with E2 and BPA extracted from figures in Rich et al. [373].

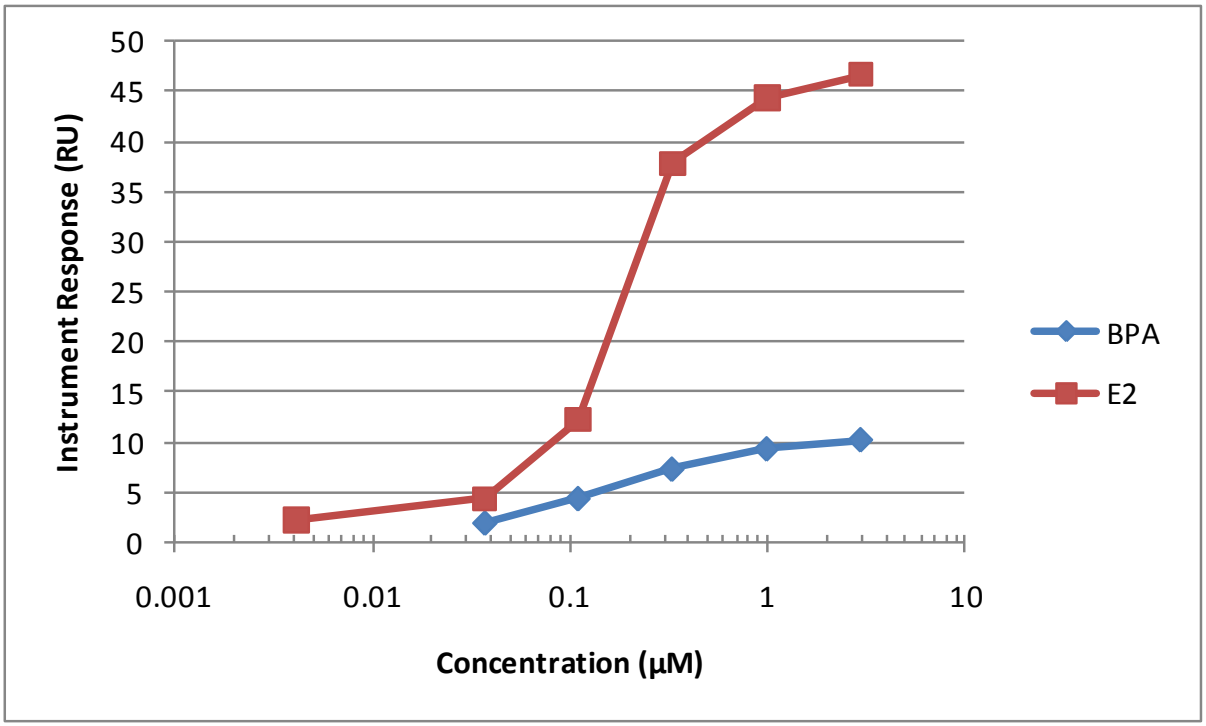

Figure 7.5. SPR signal as a function of ligand concentration for E2 and BPA. (Produced from data taken from Figures in [373]).

The method can be calibrated to quantify an unknown concentration of a single analyte in a sample if and only if it is the only analyte in the sample that will bind to the receptor. Because the measurements are made under equilibrium conditions, the magnitude of the signal obtained is also dependent on the binding affinity of the analyte for the receptor. A lower affinity analyte (BPA, K_D= 210 nM) will produce a smaller signal than a higher affinity analyte (E2, K_D= 0.9 nM) at the same concentration as shown in Figure 7.5. Thus, the signal obtained for a mixture will depend not only on the amount each of the analytes in solution but also on their binding affinities. In this way, the method measures what can be defined as *equivalent estrogenic load* of a mixture. In the context of this SPR method, *equivalent estrogenic load* is defined as the concentration of E2 that produces the same signal as the sample of unknown composition. This measurement of *equivalent estrogenic load* can also be used to compare the relative binding affinities of single chemicals or mixtures to that of a reference compound (e.g. E2). From the example in Figure 7.5, the equivalent estrogenic load of a sample containing 3 µM BPA is approximately 0.08 µM. Stated another way, it takes 3 µM BPA to produce the same receptor occupancy as 0.08 µM E2.

Because the SPR signal is related to the mass gain on binding, other instruments require immobilisation of the small molecule on the sensor chip surface and the receptor protein in the flowing solution if the mass of the small molecule is lower than about 500 Da. However, to be able to handle mixtures of chemicals, the ER protein must be immobilised on the sensor chip. The Bio-Rad instrument used in this study has superior sensitivity compared to its competitors allowing the novel approach to estrogenic load screening.

7.3 Design of a SPR-based Estrogenic Load Biosensor

The ligand binding pocket of the ER is deep in the centre of the receptor and ligand binding is accompanied by a large conformational change in the ER structure that results in the ligand being fully enclosed in the pocket. In contrast, most enzymes (including CAII enzyme used in the instrument validation experiments described later in the chapter) have a readily accessible active site close to the outer surface of the protein. This highly accessible binding site facilitates rapid turnover of substrate to product. These differences are illustrated with the structures of human CAII and hERα shown in Figure 7.6.

Most SPR applications use amine coupling (section xx) to covalently bind one of the two reactants to the sensor chip surface. The protein may be attached via one or more of the surface lysine residues or the N-terminal amine. This arbitrary orientation of the protein on the surface could result in total or partial obstruction of the binding site. For the current application it is critical to ensure that the hER is attached to the sensor chip surface without interfering with ligand access to the binding cavity and the resulting conformational change.

The hER LBD is commercially available as an N-terminus GST-fusion protein. In this construct, the glutathione S-transferase (GST) enzyme is attached to the N-terminus of the hER. The GST enzyme has a very high affinity for reduced glutathione (GSH) which facilitates isolating the fusion protein from the cell lysate of an expression system using affinity chromatography. This high affinity binding can be exploited to immobilise the GST-hER LBD via interaction with GSH that has been covalently bound to the sensor chip.

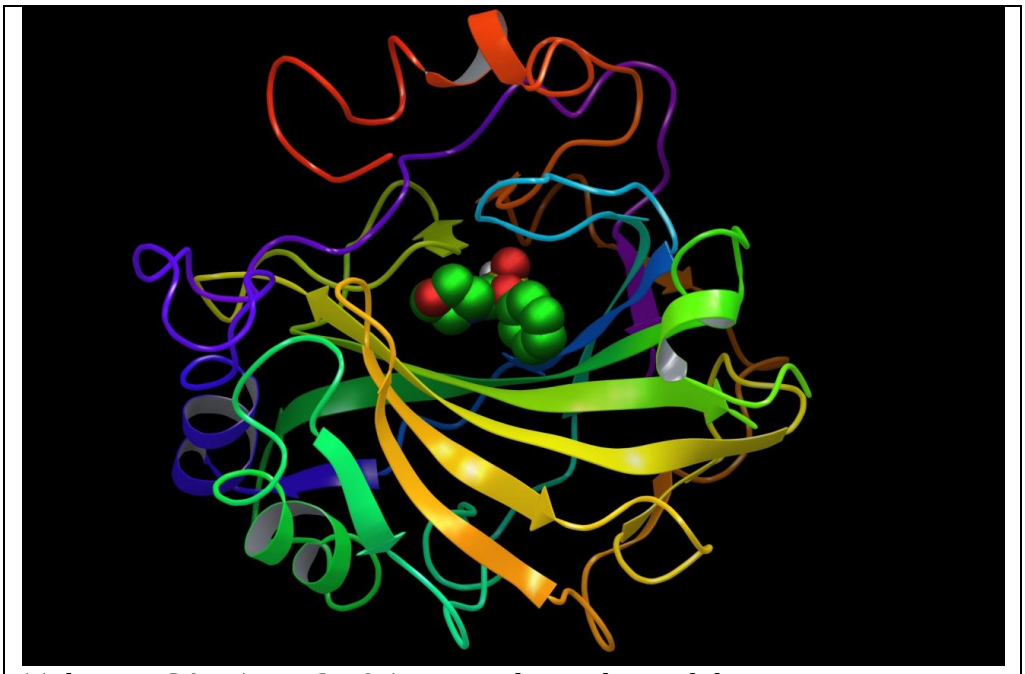

(a) human CAII (PDB 3M04) in complex with an inhibitor

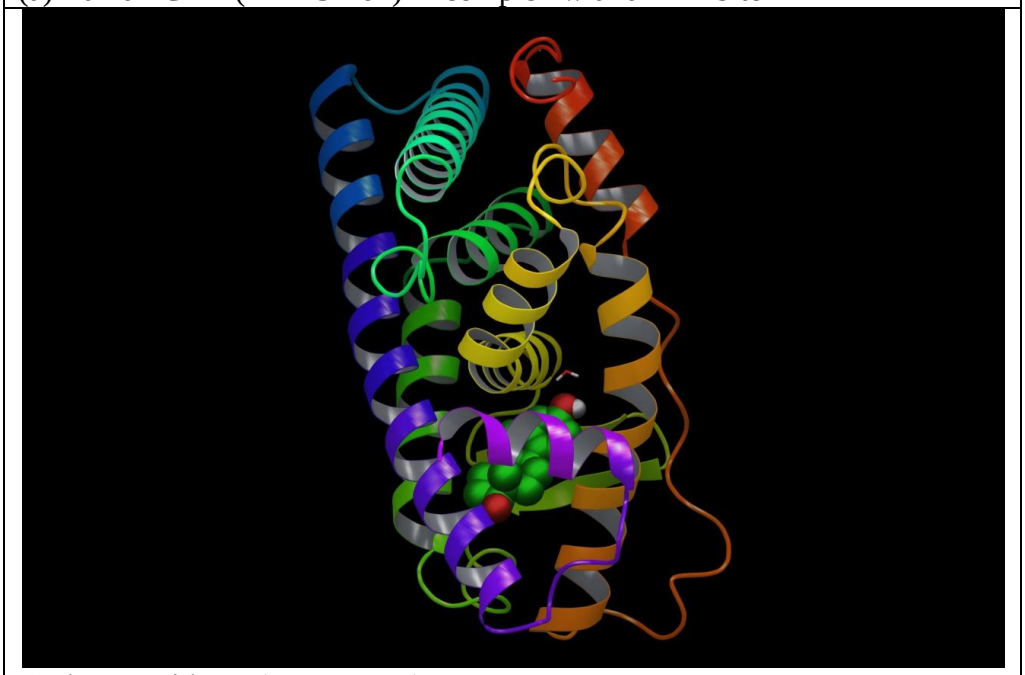

(b) hERα with E2 (PDB 1ERE)

Figure 7.6. Structure of human CAII (PDB 3M04) in complex with an inhibitor showing the readily accessible surface active site, in comparison to the fully enclosed deep ligand binding pocket of hERα with E2 (PDB 1ERE).

7.3.1 GST and Affinity Separations

Glutathione S-transferases (GSTs) are a family of enzymes present in both eukaryotic and prokaryotic cells that play a role in phase II metabolism of xenobiotics [122]. In humans,

GSTs conjugate electrophilic and lipophilic xenobiotics with reduced glutathione (GSH, Figure 7.7) to increase their solubility in the aqueous cellular and extracellular media, facilitating their removal from the body by the kidneys and liver.

The GSTs are large enzymes (23-29 kDa). The GST tag increases the size of the fusion protein quite significantly. For the hER LBDs, the GST tag increases the molecular weight of the protein by 50%. GSTs have a high affinity for GSH (K_D = 80-220 nM [391]) which makes it attractive for affinity purification of expressed proteins.

GST affinity chromatography is used to purify GST-tagged proteins. GSH is covalently bound to agarose or cross-linked agarose beads. The beads can be mixed directly with the crude protein solution or packed in a column through which the crude protein solution is passed. The GST tag binds the immobilised GSH with high affinity. The desired fusion protein is retained on the support while undesired material is washed away. The desired protein is then eluted by flushing with a high concentration solution of GSH. This system is attractive for SPR because it facilitates refreshing the surface of the sensor chip. If the immobilised protein becomes inactive, it can be readily removed by flushing the sensor chip with a high concentration solution of GSH, as done to elute the retained protein in affinity chromatography. If the immobilised GSH becomes oxidised, form glutathione disulphide (GSSH, Figure 7.7), it may be readily reduced by common disulphide bond reducing agents such as dithiothreitol (DTT, Figure 7.7).

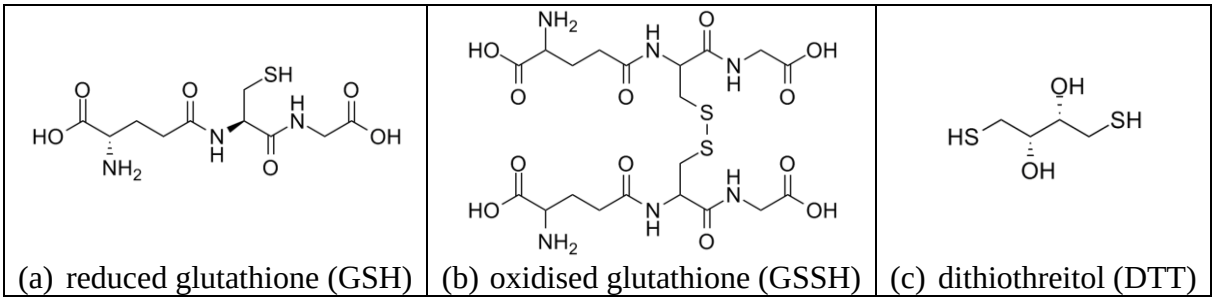

(a) reduced glutathione (GSH) (b) oxidised glutathione (GSSH) (c) dithiothreitol (DTT)

Figure 7.7. Structures for reduced glutathione (GSH), oxidised glutathione (glutathione disulphide, GSSH) and the reducing agent dithiothreitol (DTT).

A number of different affinity media are available. GSH is attached to the support at either the sulfhydryl group or the amine group via a spacer of between 10 and 12 atoms in length. The chemical structure of one medium [392] is shown in Figure 7.8. The spacer arm in this case is described as a hydrophilic spacer.

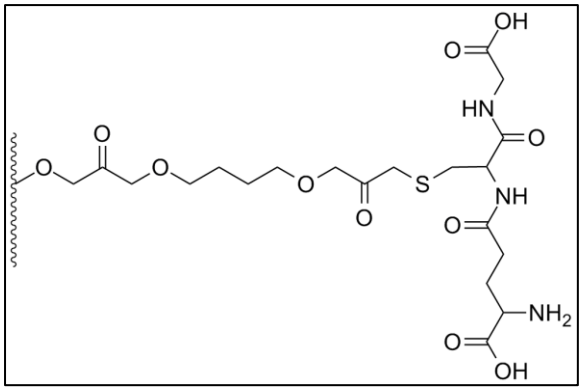

Figure 7.8. Structure of S-linked glutathione (Thermo Scientific [392]).

Spacers are required to relieve steric hindrance between the GSH molecule and the surface of the support and to allow the protein access to the GSH molecule to effectively bind. Even short (4-6 atoms) spacers are effective in relieving the steric hindrance [393, 394]. Initially, hydrophobic spacer arms were used [395] as shown in Figure 7.9. This spacer arm is derived from the amine coupling of 6-aminohexanoic acid to the support surface. The ligand is covalently bound to the terminal carboxylic acid by some appropriate method (e.g. amine coupling as done with the surface).

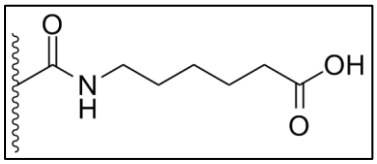

Figure 7.9. An example of a hydrophobic spacer arm.

Previous attempts reported in the literature to make this linkage more hydrophilic resulted in poorer affinity of the protein to the ligand. The hydrophobic interactions between the spacer arm and the protein were discovered to be important and to contribute to the overall affinity of the protein for the tethered ligand [395]. It is also important to have the ligand attached to the support in such a way that it does not interfere with the protein binding process. The efficiency of protein purification was greatly increased by attaching the GSH molecule via the sulfhydryl group with a long tether because the tether allows for hydrophobic interactions with the GST tag which increases the binding affinity between GSH and the GST tag [396].

The success of GST-GSH affinity chromatography relies on not only the correct orientation of GSH on the spacer arm but also interactions of the GST with the spacer arm. These interactions can be understood by examining the 3D structure of GST bound to GSH. The x-ray crystal structure for GST bound to GSH has been solved (PDB *1PKW*, [397]) and is

shown in Figure 7.10. The binding site is broad and open on the surface of the protein. GSH is oriented with the sulfhydryl group pointed into the binding site and the amino group accessible from the top surface. The opening to the binding site is approximately 30 Å in diameter. Another structure of GST with S-hexyl-GSH bound has also been published [398] (PDB *1K3L*) and shows GSH in a similar orientation. The C_6 chain attached to the sulfhydryl group of GSH lies in a groove along the bottom of the binding site. This groove opens to the back surface of the protein. Presumably this is where the substrate to which the enzyme will attach GSH is positioned. It is clear from these structures why a longer tether is required for immobilising GSH via the sulfhydryl group and how the additional protein-tether interactions have the capacity to increase binding affinity.

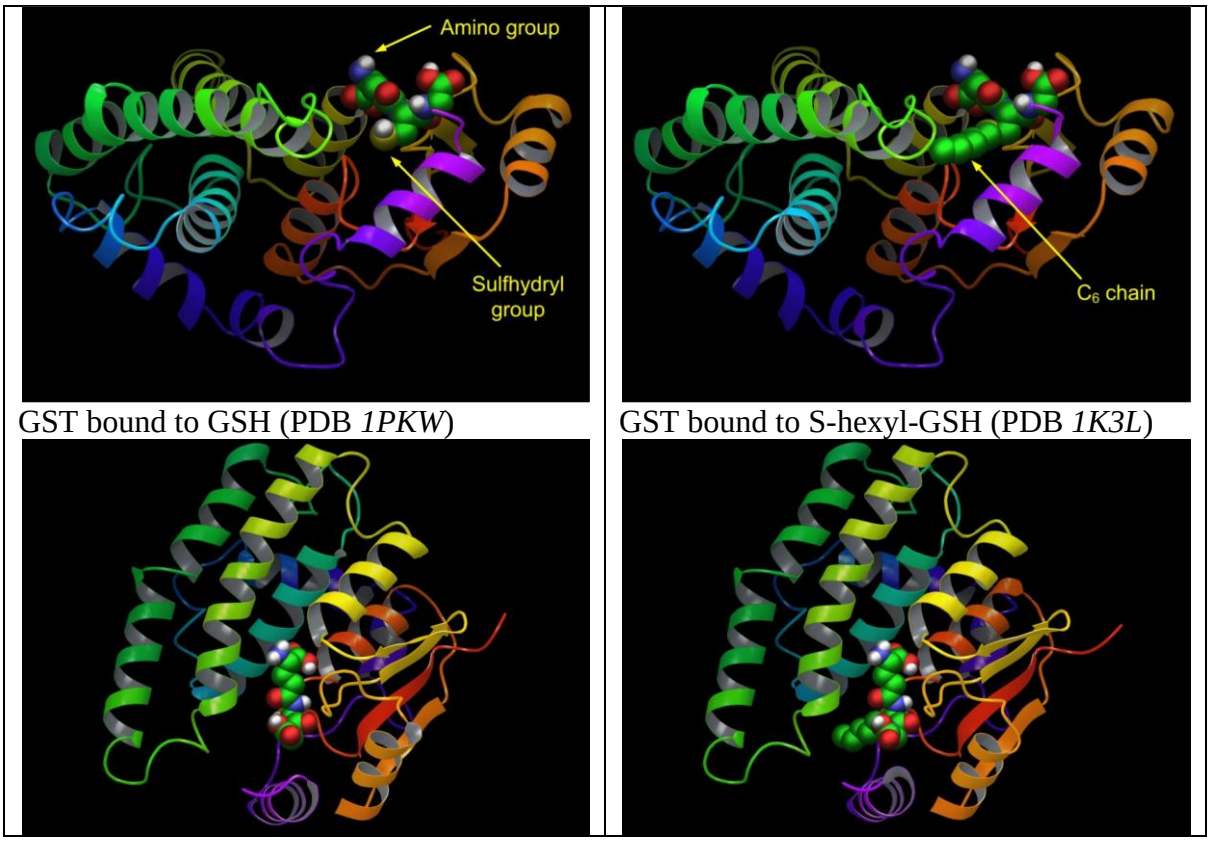

Figure 7.10. Protein structure for GSH bound to GST ([397]) and S-hexyl-GSH bound to GST ([398]) viewed from different angles. Note the surface location of the GSH binding site, how the amino group of GSH is protruding from the top surface of the binding site and how the C6 chain extends back through the protein structure towards an opening on the back surface.

7.3.2 Tethering Options

For the SPR application, a tether needs to be designed that is approximately 12 atoms long that can be amine coupled to the SPR sensor chip and that GSH can be attached to via the sulfhydryl group. A process has been reported for thiol coupling to SPR sensor chips [399, 400]. The scheme is shown in Figure 7.11. The process begins with the standard EDAC/sulfo-NHS activation of the sensor chip. A reactive disulfide group from 2-(2-pryidinyldithio)ethanamine (PDEA) is then introduced. Deactivation of the residual EDAC/sulfo-NHS activated carboxylic acid surface is accomplished with ethanolamine. The sulfhydryl group of the species to be bound to the sensor chip reacts at the disulfide, displacing 2-thiopyridine. Deactivation of the unused disulfide is accomplished using L-cysteine. PDEA is commercially available or can be synthesized following the scheme shown in Figure 7.12 [399, 401, 402]. By replacing 2-cysteamine by 8-amino-1-octanethiol

(Figure 7.13), an analogue of PDEA can be prepared that incorporates a longer tether. The final sensor chip surface with GSH attached is shown in Figure 7.14.

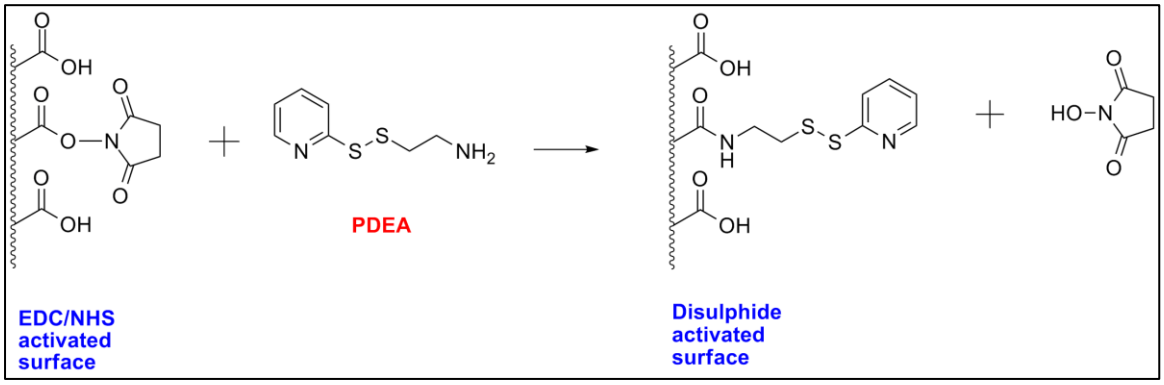

Figure 7.11. Disulphide activation of surface for thiol coupling.

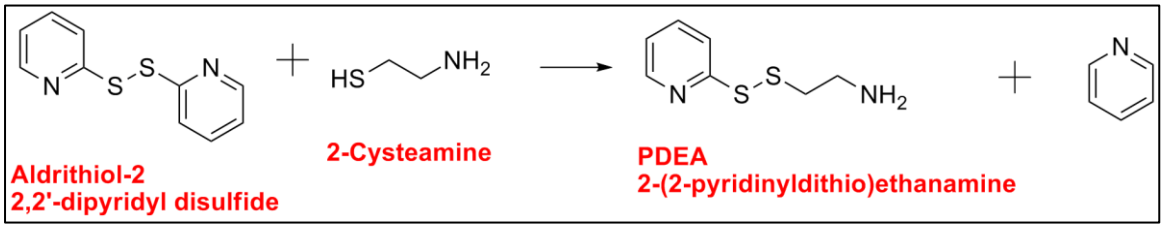

Figure 7.12. Synthesis of PDEA.

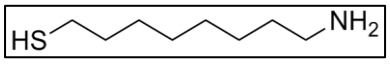

Figure 7.13. 8-amino-1-octanethiol.

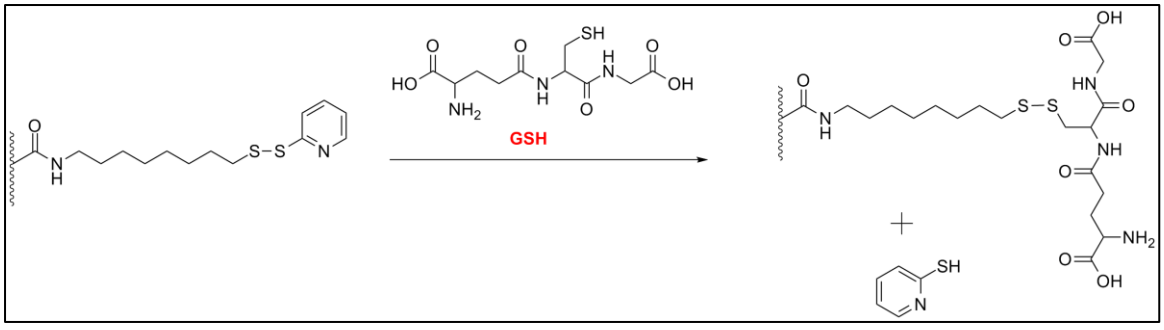

Figure 7.14. Thiol coupling of GSH to sensor chip surface with an alkane tether.

If the alkane tether of Figure 7.14 is too hydrophobic, a polyethylene glycol (PEG) tether could also be used. The carboxy-PEG_4-amine (Figure 7.15) is commercially available, but a slightly different coupling strategy is needed. The PEG_4 is first bound to the sensor chip surface by standard amine coupling. After coupling, the ethanolamine deactivation is performed to deactivate the unused surface groups. Then, the carboxylic acid group on the PEG_4 tether is then activated to bind PDEA and GSH is coupled to the PEG_4 tether. Finally, unused PEG_4 tethers are deactivated by L-cysteine. This scheme is shown in Figure 7.16.

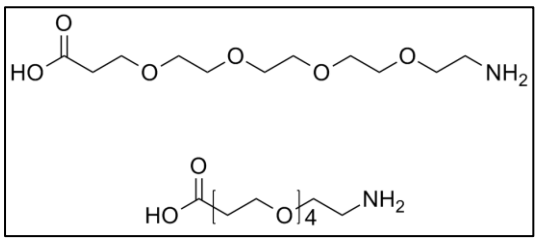

Figure 7.15. Carboxy-PEG_4-amine.

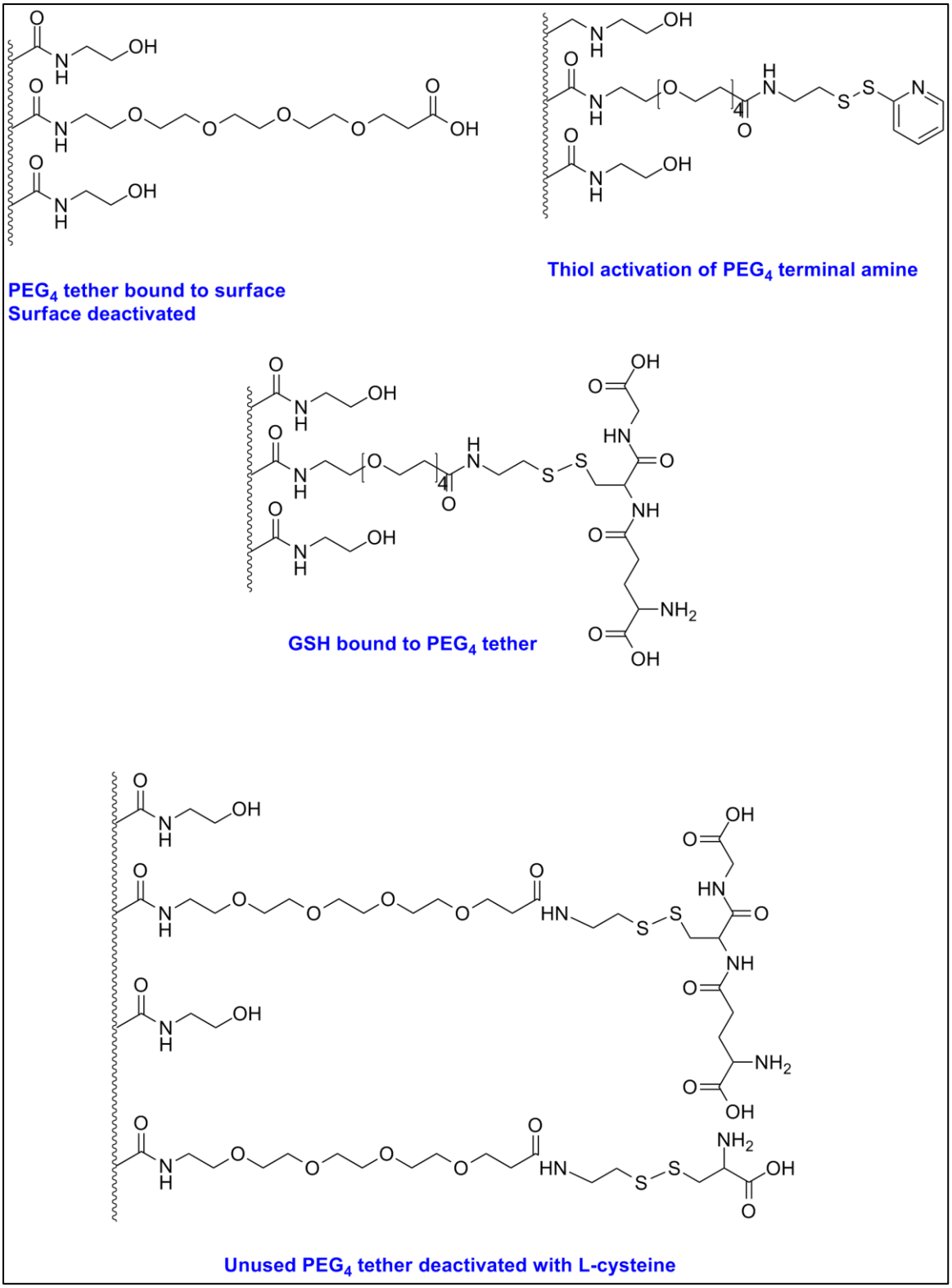

Figure 7.16. Stepwise construction of a PEG_4-tethered GSH surface.

7.4 Methods and Materials

7.4.1 Bio-Rad ProteON XPR36 Instrument

In the Bio-Rad instrument, the sensor chip has a 6x6 matrix of interaction spots, as shown in Figure 7.17. Different protein receptors or protein receptor densities can be immobilized across the 6 'ligand' channels and different analytes or analyte concentrations can be injected across the 6 'analyte' channels allowing for multiple conditions or repeats of the same conditions to be run in a single experiment. The space between the interaction spots are used as reference channels to correct for small differences in bulk refractive index of the solutions injected in each of the channels [383]. The flow direction is described as 'vertical' for the ligand channels and 'horizontal' for the analyte channels.

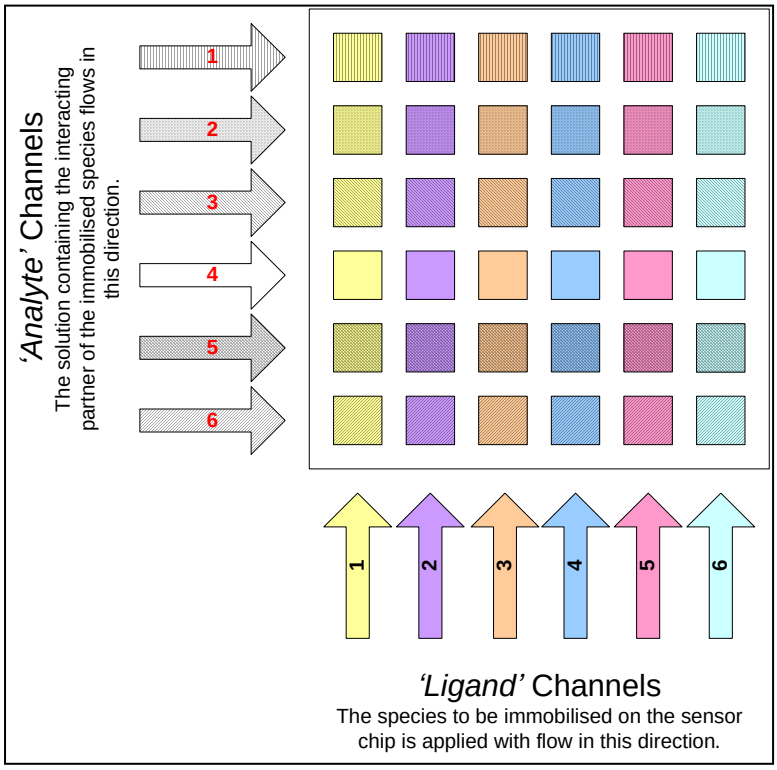

Figure 7.17. Bio-Rad ProteOn XPR36 sensor chip 6x6 matrix.

As the analyte solution flows over the receptor immobilised on the sensor chip surface, the analyte diffuses from the bulk to the surface where it interacts with the immobilised receptor. The signal that is measured in SPR is proportional to the reflective index change which results from the mass increase due to the binding of the analyte species with the receptor. Thus, the signal is proportional to the increase in concentration of the receptor-ligand complex [RL]. The ligand concentration [L] remains constant due to the flow conditions, so

for most receptor-ligand interactions, pseudo-first order kinetics can be assumed and the data analysis presented in Section XX applies [379].

7.4.2 A Typical SPR Experiment

A typical SPR experiment is outlined in Figure 7.18. The basic methodology is the same for both kinetics and equilibrium studies, only the data processing differs. For a kinetics experiment, the shapes of the association and dissociation curves are analysed to give forward and reverse rate constants. For an equilibrium experiment, only the association curve is needed and only the net change in signal is determined.

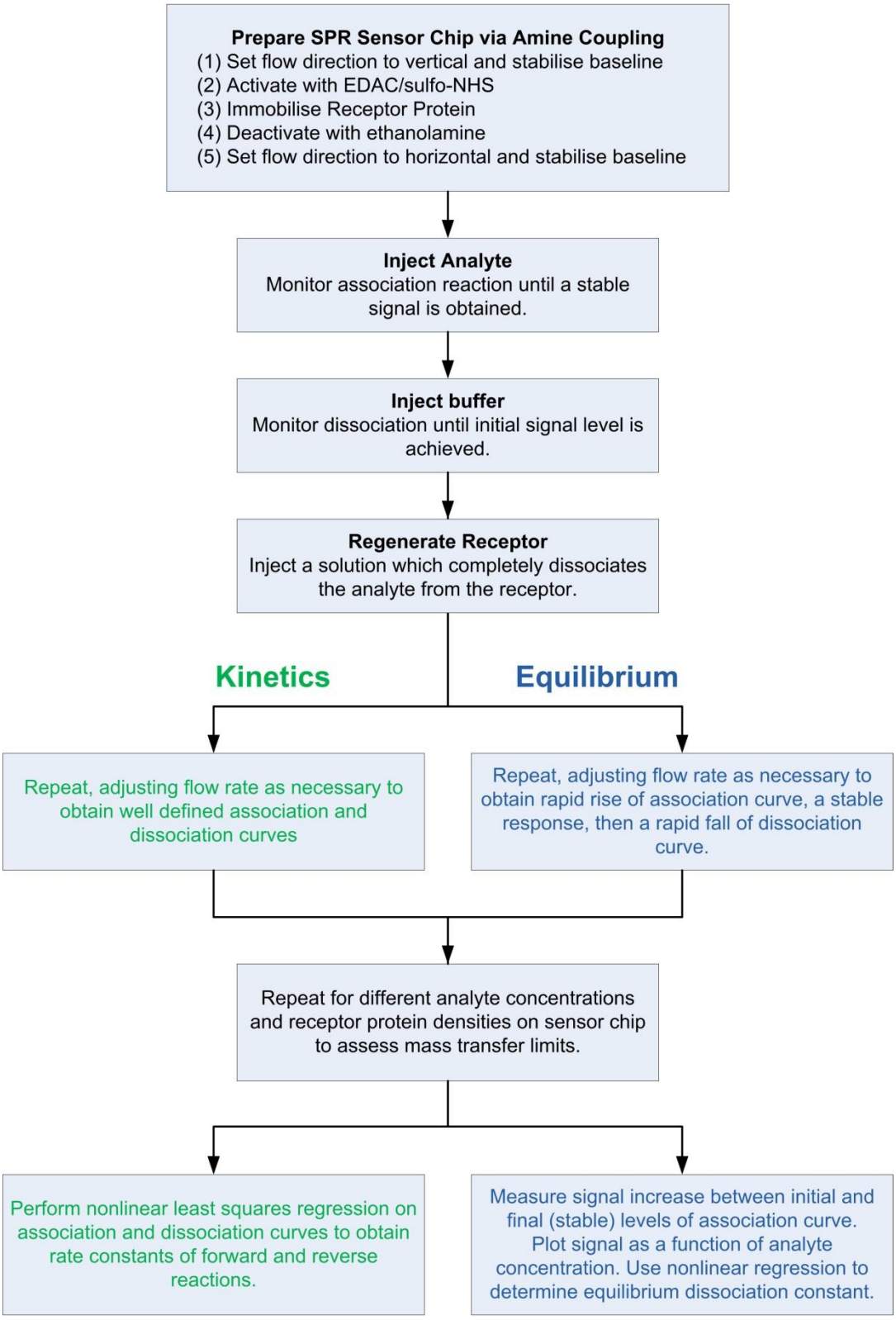

Figure 7.18. Flow chart of typical kinetics and equilibrium SPR experiments.

7.4.3 Validation of Instrument Sensitivity

The first experiment was a validation of instrument sensitivity and used a reagent kit supplied by the instrument manufacturer. The kit is based on the reaction between the enzyme

carbonic anhydrase II (CAII) and its inhibitor carboxybenzene sulfonamide (CBS) and demonstrates the sensitivity of the instrument in detecting the interaction of a small molecule analyte (CBS, MW 201) with a large immobilized enzyme (CAII, MW 31 kDa). Working through this experiment was important for several reasons:

- to become familiar with SPR data processing with a system known to work
- to understand the effects of different instrument parameters (e.g. flow rate, interaction times) on the results
- to demonstrate that the instrument is able to achieve the performance criteria necessary for the ER kinetics studies and for the estrogenic load biosensor application.

7.4.3.1 Materials

The ProteOn Protein-Small Molecule Kit (Bio-Rad product # 176-1030) was purchased from Bio-Rad. The kit includes

- CAII/CBS pair
- ProteOn GLM Sensor Chip (product # 176-5012)
- amine coupling reagents (EDAC, sulfo-NHS and ethanolamine, product # 176-2410)
- sodium acetate buffer pH 5.0
- sodium hydroxide regeneration solution
- instructions

The PBS (phosphate buffer saline) running buffer was prepared from stock reagents. The details of reagent composition are summarised in Table 7.1.

Table 7.1. Buffer and reagent names and compositions.

Buffer/Reagent	**Composition**
PBS Running Buffer (phosphate buffered saline, pH 7.4)	137 mM NaCl 10 mM phosphate (Na_2HPO_4 + KH_2PO_4) 2.7 mM KCl 0.005% Tween-20 3 mM EDTA
Sodium acetate buffer pH 5	10 mM
Sodium hydroxide regeneration solution	50 mM
N-ethyl-N'-(3-diethylaminopropyl)carbodiimide EDAC	400 mM
N-hydroxysulfosuccinimide sodium salt sulfo-NHS	100 mM
Ethanolamine HCl	1M
carbonic anhydrase II CAII	4 μM (0.125 mg/mL) in sodium acetate buffer (pH 5)

carboxybenzene sulfonamide CBS	20 μM

The standard sensor chip activation mixture was prepared by mixing equal volumes of EDAC and sulfo-NHS solutions. The mixture must be prepared immediately before use as it has a half-life of only 60 minutes. The mixture can be diluted with running buffer to achieve different levels of surface activation and thus different densities of protein bound to the surface.

The CBS solution supplied was diluted with running buffer to produce solutions with concentrations of 6.67, 2.22, 0.74, 0.25 and 0.084 μM.

7.4.3.2 Method

The experiment followed the process outlined in Figure 7.18. To achieve different densities of protein bound to the surface, channels L1-L4 were activated with the standard solution and channels L5 and L6 were activated with a 10x dilution of the standard solution. Each analyte channel was exposed to a different analyte concentration as given in Table 7.2. After the dissociation step, any remaining CBS bound to the enzyme was removed by injecting 50 mM NaOH.

Table 7.2. CBS concentrations for the six analyte channels.

Channel	CBS Concentration (μM)
A1	20
A2	6.7
A3	2.2
A4	0.74
A5	0.25
A6	0.084

The instrument was left in standby mode overnight, with running buffer flowing over the sensor chip surface at the minimum flow rate. The following day, additional interactions were performed as summarised in Table 7.3. Interaction 7 was incomplete because there was insufficient volume of analyte in the vials.

Table 7.3. Summary of CAII/CBS interaction parameters.

Interaction	Flow rate (µL/min)	Association Time (s)	Dissociation Time (s)
1†	100	60	600
2	100	60	900
3	50	120	600
4	50	180	600
5	25	240	600
6	150	60	600
7*	200	30	600
8	200	30	600
9	200	45	600

†interactions 2-9 conducted next day with instrument in standby mode overnight.
*invalid result, incomplete injection.

7.4.4 Method Development – Immobilising hER

The first step in developing the estrogenic load biosensor is immobilising the GST-tagged hER LBD on the sensor chip. A number of approaches were tried to attach GSH to the sensor chip:

- Direct amine coupling of GSH to the surface via the amino group
- Thiol coupling at the sulfhydryl group
- Tethering GSH to the chip surface by first amine coupling a polyethylene glycol spacer to the chip surface then amine or thiol coupling GSH to the tether

Method development was limited by the cost of commercially available receptor protein. Facilities were not available in-house to produce protein for this work.

7.4.4.1 Method Development 1 – Direct Amine Coupling of GSH to the Sensor Chip

The simplest way to produce a GSH surface for immobilising the GST-tagged hER-LBD was to directly couple GSH to the sensor chip via standard amine coupling.

7.4.4.1.1 Materials

The reagents and buffer solutions used in the SPR experimental work are summarised in Table 7.4.

Table 7.4. Buffer and reagent names and compositions.

Buffer/Reagent	Composition
PBS Running Buffer (phosphate buffered saline, pH 7.4)	137 nM NaCl 10 mM phosphate (Na_2HPO_4 + KH_2PO_4) 2.7 mM KCl 0.005% Tween-20 3 mM EDTA
N-ethyl-N'-(3-diethylaminopropyl)carbodiimide EDAC	400 mM
N-hydroxysulfosuccinimide sodium salt sulfo-NHS	100 mM
Ethanolamine HCl	1 M
L-Glutathione reduced GSH stock solution	10 mM in running buffer
17β-estradiol E2 stock solution	10 mM in ethanol
GST-tagged hERα	functional receptor concentration was 3407 nM as supplied
GST-tagged hERβ	functional receptor concentration was 11848 nM as supplied

L-Glutathione reduced (GSH) was purchased from Sigma-Aldrich (product # G4251, ≥98.0%). A stock solution of 10 mM was prepared in running buffer. Working solutions at 5 and 0.5 μM were prepared by dilution with running buffer. 17β-estradiol (E2) was purchased from Sigma-Aldrich (product # E8875, ≥98%). A stock solution of 10 mM was prepared in HPLC grade ethanol. Working solutions at 10, 2, 0.1, 0.02 and 0.001 μM were prepared by dilution with running buffer. GST-tagged hERα was purchased from Invitrogen (product # PV4543, 250 pmol). The functional receptor concentration for this product was 3407 nM. Working solutions at 50 nM and 5 nM were prepared by dilution of the supplied solution with running buffer. GST-tagged hERα was purchased from Invitrogen (product # PV4539, 250 pmol). The functional receptor concentration for this product was 11848 nM. Working solution at 37.5 nM was prepared by dilution of the supplied solution with running buffer. The high density sensor chip (Bio-Rad product # 176-5103) was used.

7.4.4.1.2 Methods

The experiment followed the process outlined in Figure 7.18. All 6 sensor chip channels were activated with standard the EDAC/sulfo-NHS solutions. Two different GSH

concentrations were injected to see if a difference in surface density of GSH could be observed. 5 μM GSH was injected in channels L1-L3 and 0.5 μM for channels L4-L6. Next, two different concentrations of GST-tagged hERα-LBD were injected, again to seed if a difference in surface density could be observed. 50 nM GST-tagged hERα-LBD was injected in channels L1 and L2 and 5 nM in channels L5 and L6. Channels L3 and L4 were used as reference channels.

The interaction of the immobilised hER was evaluated twice by injection of E2 in the concentrations listed in Table 7.5. The first injection was performed for 300 s and the second injection was performed for 500 s.

Table 7.5. Concentrations of E2 used for interactions with immobilised hER.

Channel	Concentration (μM)
A1	10
A2	2
A3	0.1
A4	0.02
A5	0.01
A6	0 (running buffer)

The flow direction was then changed back to vertical to attempt to load more hER onto the surface. Two injections of GST-tagged hERα-LBD were performed, using the same parameters as the initial injection.

The flow direction was changed back to horizontal to perform a third interaction E2, using the same parameters as the first two interactions.

The flow was changed to vertical for an attempt to regenerate all 6 channels by injecting 200 μM GSH. This high concentration of GSH was intended to dissociate the GST-tagged hER from surface by competition binding with GSH in solution. Two injections of the regeneration solution were made.

Having exhausted the supply of hERα, a final trial was made using the reference channels and the available hERβ. A total of 3 injections of a 37.5 nM solution of the GST-tagged hERβ were made on channels L3 and L4.

A final interaction with E2 was tried using channels L3 and L4 and the same interaction parameters.

7.4.4.2 Method Development 2 – PEG_4 Tether Coupling of GSH to the Sensor Chip

An attempt was made to couple GSH to the sensor chip using a PEG_4 tether. To simplify the system and to significantly reduce cost, the free GST enzyme was used to test the chip surface instead of the GST-tagged hER.

7.4.4.2.1 Materials

The reagents and buffer solutions used in the SPR experimental work are summarised in Table 7.6.

Table 7.6. Buffer and reagent names and compositions.

Buffer/Reagent	**Composition**
PBS Running Buffer (phosphate buffered saline, pH 7.4)	137 nM NaCl 10 mM phosphate (Na_2HPO_4 + KH_2PO_4) 2.7 mM KCl 0.005% Tween-20 3 mM EDTA
N-ethyl-N'-(3-diethylaminopropyl)carbodiimide EDAC	400 mM
N-hydroxysulfosuccinimide sodium salt sulfo-NHS	100 mM
Ethanolamine HCl	1 M
Carboxy-PEG_4-amine $CA(PEG)_4$	3.8 mM
2-(2-pryidinyldithio)ethanamine PDEA	10 mM in running buffer
L-cysteine	50 mM in running buffer
L-Glutathione reduced GSH stock solution	10 mM in running buffer
Glutathione S-transferase GST	50 μM as supplied

Carboxy-PEG_4-amine ($CA(PEG)_4$) was purchased from ThermoScientific (product # 26120). The stock solution of 1 mg/mL (3.8 mM) was prepared in Milli-Q water. Working solutions were prepared by dilution with running buffer. 2-(2-pryidinyldithio)ethanamine (PDEA) was purchased from GE HealthCare (product # BR-1000-58). The stock solution of 10 mM was prepared in running buffer. L-cysteine was purchased from Sigma-Aldrich (product # 168149, 97%). The stock solution of 50 mM was prepared in running buffer. Glutathione S-transferase was purchased from Sigma-Aldrich (product # G5663, ≥85%). The medium density sensor chip (Bio-Rad product # 176-5012) was used.

7.4.4.2.2 Methods

The method development was undertaken in two stages. First, a single channel on the sensor chip was used to assess the instrument responses to the construction of the surface. Then, the remaining sensor chip channels were used to study the effect of PEG density on the construction of the surface.

The surface was constructed in stages. First, $CA(PEG)_4$ was coupled to the EDAC/sulfo-NHS activated surface and unused activation sites on the surface deactivated with ethanolamine. Then, the terminal acid of the coupled $CA(PEG)_4$ was activated for coupling PDEA using EDAC/sulfo-NHS. Unused activated $CA(PEG)_4$ sites were deactivated using ethanolamine. Next, GSH was coupled to the PDEA activated $CA(PEG)_4$ and unused sites were deactivated using L-cysteine. Finally, GST is bound to the tethered GSH.

For the first test, only channel L1 was activated. Running buffer was injected on the other channels. Two injections of $CA(PEG)_4$ were made using a 0.5 μM solution. A third injection was made using 38 μM. PDEA was injected at a concentration of 50 μM. GSH was injected at a concentration of 5 μM. Multiple additional injections of GSH on channel L1 were done with concentrations increasing from 100 μM to 5 mM to see if GSH binding could be observed. Any unused PDEA activation was then deactivated before injection of GST. Multiple injections of GST were then made at concentrations increasing from 5 μM to 50 μM to see if binding could be observed. Finally, a regeneration solution of 5 mM GSH was injected to see if any bound GST could be displaced.

For the second test, an attempt was made to vary the density of GSH tethered to sensor chip by varying the initial activation level. Channels L2-L5 were activated with different dilutions of the standard EDAC/sulfo-NHS as summarized in Table 7.7. Running buffer was injected on channel L6 for a reference and on previously used channel L1. The concentrations of the different reagents injected to construct and test the surface are summarised in Table 7.8.

Table 7.7. Dilutions of standard EDAC/sulfo-NHS solution used to vary density of GSH on sensor chip.

Channel	Dilution
L2	1:10
L3	1:100
L4	1:200
L5	1:1000

Table 7.8. Reagent concentrations used to construct and test sensor chip surface.

Reagent	Concentration
$CA(PEG)_4$	56 μM
PDEA	100 μM
GSH	5 mM
GST	50 μM

7.5 Results

7.5.1 Validation of Instrument Sensitivity

Instrument sensitivity was validated using the kit supplied by the Bio-Rad. This kit was also used to study the effects of instrument parameters on kinetics and equilibrium experiments. Selected results are presented below to illustrate the type of data produced by the SPR instrument and its interpretation. Understanding and interpreting these features will be important in evaluating the results obtained in the method development experiments.

Figure 7.19 shows the baseline adjusted sensorgrams for channel A1 for the immobilisation of CAII on the sensor chip and an interaction experiment. A sensorgram is a plot of SPR sensor signal (RU) as a function of time (s). The other channels are identical except for regions 8a and 8b. Region 8 is the interaction experiment and for the other channels, the level reached is progressively lower because each channel is exposed to a lower concentration of CBS in the dilution series. The regions numbered 1-9 are described in Table 7.9.

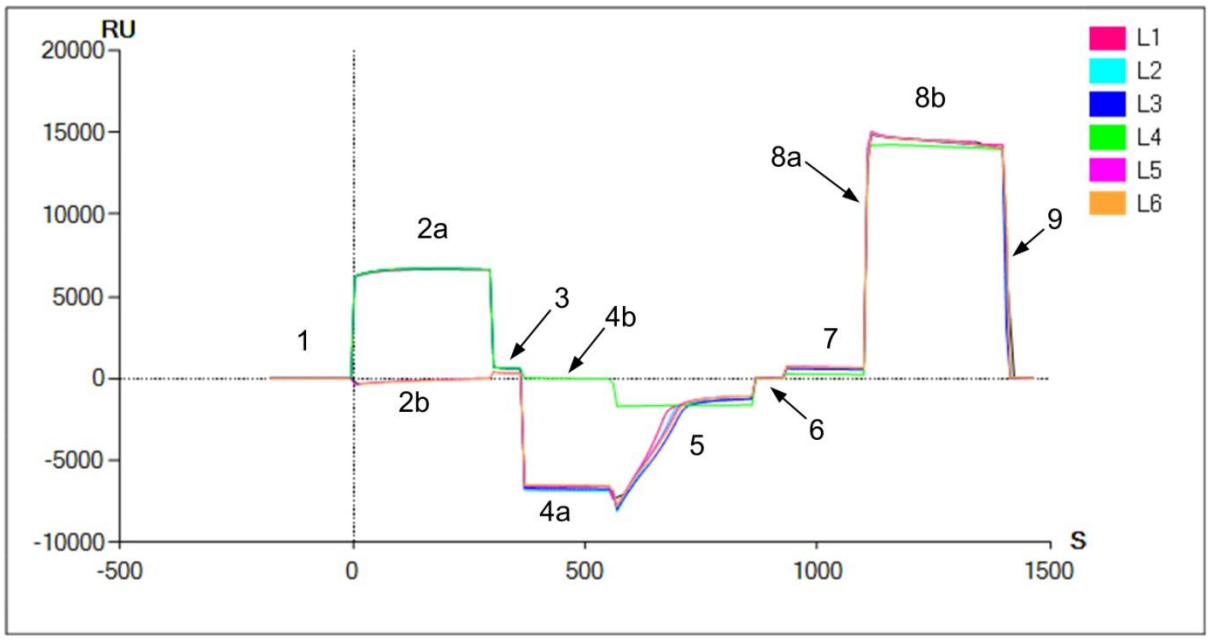

Figure 7.19. Baseline adjusted sensorgram showing surface activation, CAII immobilisation, surface deactivation, followed by analyte association and dissociation reactions. Numbered regions are described in Table 7.9.

Table 7.9. Description of numbered regions of Figure 7.19.

Region	Description
1	Baseline of unmodified sensor chip surface, flow in vertical direction.
2	Activation of sensor chip surface for amine coupling of CAII. Channels L1-L4 follow the higher curve (2a). Channels L5 and L6 follow the lower curve (2b) as they were exposed to a 10x dilution of the standard activation solution.
3	Baseline after activation. Note increase in signal from region 1.
4	CAII enzyme immobilization. The CAII enzyme solution was injected on channels L1-L3, L5-L6 (4a). Channel L4 (4b) is not exposed to the CAII solution.
5	Deactivation of unreacted activation sites.
6	Flush with running buffer followed by rotation of flow to horizontal direction for analyte injection.
7	Baseline of sensor chip with running buffer flowing in horizontal direction prior to analyte injection.
8	Interaction of CBS with CAII. The association reaction occurs for 60 s (8a) while CBS is injected. The dissociation reaction occurs for 600 s while the channels are flushed with running buffer (8b). Each analyte channel was exposed to a different analyte concentration as given in Table 7.2. Channel A1 is shown in Figure 7.19. Channels L1-L6 are exposed to the same concentration. Note difference in response between L4 (green trace, reference channel) and the other channels.
9	Regeneration of surface. Injection of 50 mM NaOH to regenerate CAII, removing any residual bound CBS.

The amount of CAII immobilised on each spot can be quantified using the data of Figure 7.19 and the corresponding data for the other channels. The difference between region 7 and region 3 gives the amount of immobilized ligand in each channel. Using the software region averaging tool, the net changes in RU for each ligand/analyte interaction spot summarized in Table 7.10 were obtained. As can be seen, the 10x dilution of the activation solution resulted in approximately half the amount of ligand bound to ligand channels 5 and 6. The spot to spot variability is very low, on the order of 1%.

Table 7.10. Amount of ligand bound to each ligand/analyte interaction spot as quantified by the net increase in signal (RU).

Ligand Channel	Analyte Channel							
	1	2	3	4	5	6	Avg	%RSD
1	604	594	598	595	585	606	597	1.3%
2	606	604	604	606	607	613	607	0.6%
3	596	600	602	598	598	598	599	0.3%
5	308	309	312	308	307	310	309	0.6%
6	309	309	310	311	308	310	310	0.4%

7.5.1.1 Kinetics Analysis

The reaction between CBS and CAII is a simple 1:1 bimolecular interaction. As the inhibitor interacts with the enzyme bound to the surface of the sensor chip, a complex is formed following first order kinetics. When the analyte solution is washed away from the chip, CBS dissociates from the enzyme. The classic Langmuir adsorption isotherm model without mass transfer was chosen to fit the kinetics data. This assumes that the binding is equivalent and independent for all binding sites and that the reaction is not limited by mass transfer (i.e. analyte diffusion to the surface is faster than the reaction). The validity of this assumption was evaluated in the course of data processing.

For the kinetics experiment, the analyte CBS was injected at a constant flow rate for a specified period of time. The association time is the contact time during which the desired volume of analyte solution is injected and the analyte binds with the immobilised enzyme CAII. Immediately after the injection, running buffer is flowed over the sensor chip for the dissociation time. During this time the analyte dissociates from the ligand. At the conclusion of the dissociation time, the regeneration event injects a solution to remove any undissociated analyte from the enzyme in preparation for the next injection. Nine different interaction

experiments were done at different analyte flow rates and contact times to evaluate the effect of these two parameters determining the reaction rate constants and the equilibrium constant. The interaction parameters are summarised in Table 7.3.

The data processing steps implemented by the software include automated baseline adjustment, automated injection time alignment and automated removal of artifacts from the data (e.g. spikes produced by bubbles in the flow path). The ligand channel L4 was used as a reference to subtract from the other channels to correct for nonspecific binding, drift and bulk refractive index changes. A typical set of association-dissociation curves is shown in Figure 7.20. Each of the 6 curves corresponds to one of the 6 analyte concentrations (A1-A6) listed in Table 7.9. There is a data set similar to this one for each of the 5 ligand channels, and for every interaction experiment.

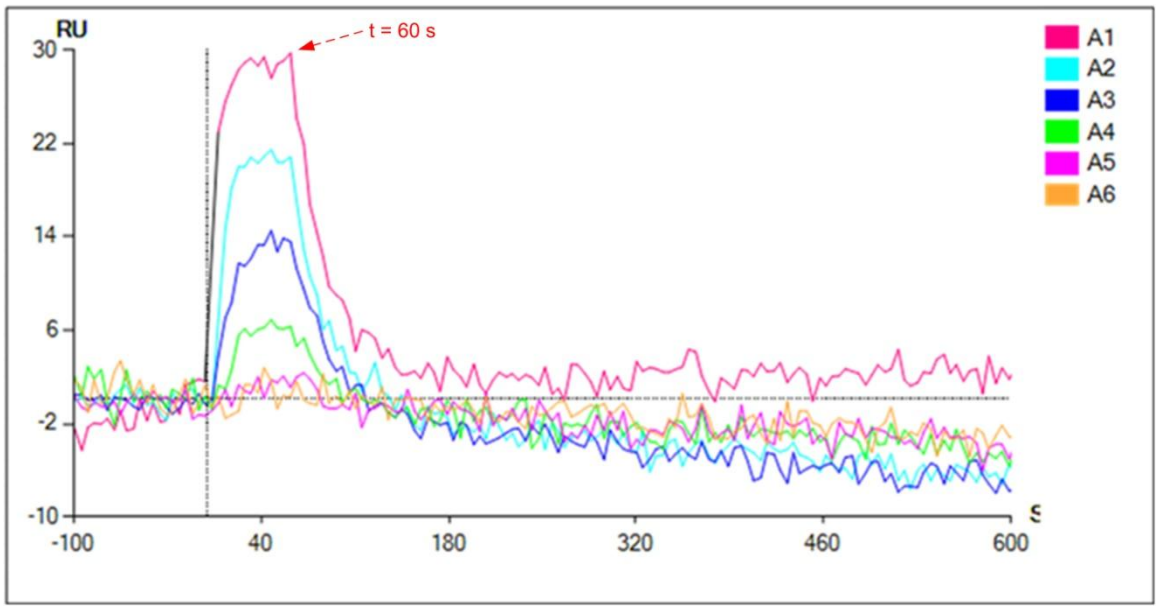

Figure 7.20. Association-dissociation curves after automated processing and reference channel subtraction. (Ligand 1 from Interaction 1)

To analyse the kinetics experiment, the association and dissociation phases of the experiment must be identified. For Figure 7.20, the association phase begins at t=0 and ends at t=60. Within this window the signal increases from zero and gradually reaches a limit value approaching 30 RU for the analyte of the highest concentration. This level indicates the system has reached equilibrium under the conditions present for the concentration of analyte present. The dissociation phase begins at the next data point past t=60 and continues for 600 s.

Nonlinear curve fitting is used to derive estimates of the association rate constant (k_a) and the dissociation rate constant (k_d) from the association and dissociation curves shown in Figure 7.20. The reaction rate constants and the equilibrium constant are determined for each interaction and ligand channel using the series of analyte concentrations. The average values for the three constants for the high ligand density (ligand channels L1-L3) and low ligand density (ligand channels L5 and L6) were calculated for each interaction (set of experimental conditions). The results are shown in Figure 7.21. The equilibrium constant (K_D) shown in Figure 7.21 is determined by the ratio of k_d to k_a. According to the kit instruction booklet, k_a should be in the range 1.6×10^4 to 4.8×10^4 $M^{-1}s^{-1}$ and k_d should be in the range 1.9×10^{-2} to 5.7×10^{-2} s^{-1}. These ranges are indicated by the red lines in Figure 7.21. There is a factor of at least 3 difference between the lowest and highest k_a value predicted by the various interactions. The range of possible results for K_D, as calculated from the range of k_a and k_d values given, is also indicted by red lines in Figure 7.21. The yellow line indicates the most likely value, based on these given values.

For nonlinear regression, the χ^2 test for goodness of fit was used to compare the experimental data to the model chosen to fit the data. If the parameters for the model obtained by the nonlinear procedure produce a good approximation to the true model, χ^2 will be close to 1. Poorer fits will have larger χ^2 values. As can be seen in Table 7.11, the χ^2 values indicate very good fits with the exception of Interaction 1. The curves fit to the data from interaction 4 are shown in Figure 7.22. Clearly, the instrument has no difficulty detecting the refractive index change resulting from the lowest concentration analyte standard, A6.

Table 7.11. Summary of χ^2 values for nonlinear regression.

	Interaction							
Ligand	1	2	3	4	5	6	8	9
1	17.75	1.76	1.54	1.03	1.41	1.17	0.96	1.15
2	7.84	1.75	1.76	0.98	1.41	1.13	0.96	0.99
3	6.8	1.78	1.8	1.08	1.51	1.17	1.19	0.97
5	10.17	1.46	1.61	1.03	1.23	1.18	1.35	0.99
6	10.1	1.52	1.77	1.02	1.16	1.13	1.05	1.06

The shape of the association curve is determined by the flow rate and contact time and has a strong influence on the value of the k_a obtained from the nonlinear regression. The dissociation reactions were all done at a flow rate of 100 μL/min, so the dissociation rate constant obtained should not show much variation. Figure 7.23 shows the interaction curves

for selected flow rates and contact times. Interaction 8 (highest flow rate and shortest contact time) has the lowest values for k_a and highest values for K_D. Interactions 4 and 6 have the highest values for k_a and the lowest values for K_D. The length of time that the association reaction curve has at equilibrium, i.e. approaching a constant value before the dissociation reaction begins, is a critical feature in determining the shape of the curve. Interaction 8 did not reach equilibrium, thus resulting in a higher predicted k_a value. Another factor is the slope of the curve between t=0 and approaching the constant value. The combination of a steep slope and poorly defined equilibrium level will further influence the parameters estimated by the nonlinear regression. Flow rate influences the slope of the curve and both flow rate and contact time influence the length of time at equilibrium.

One concern with choosing the Langmuir model is that it does not account for mass transfer limits on the rate of reaction. If mass transfer was an issue, there would be a significant difference between rate constants and dissociation constants obtained from the low and high ligand density channels. This difference is not observed, suggesting mass transfer is not a limiting factor for this experiment.

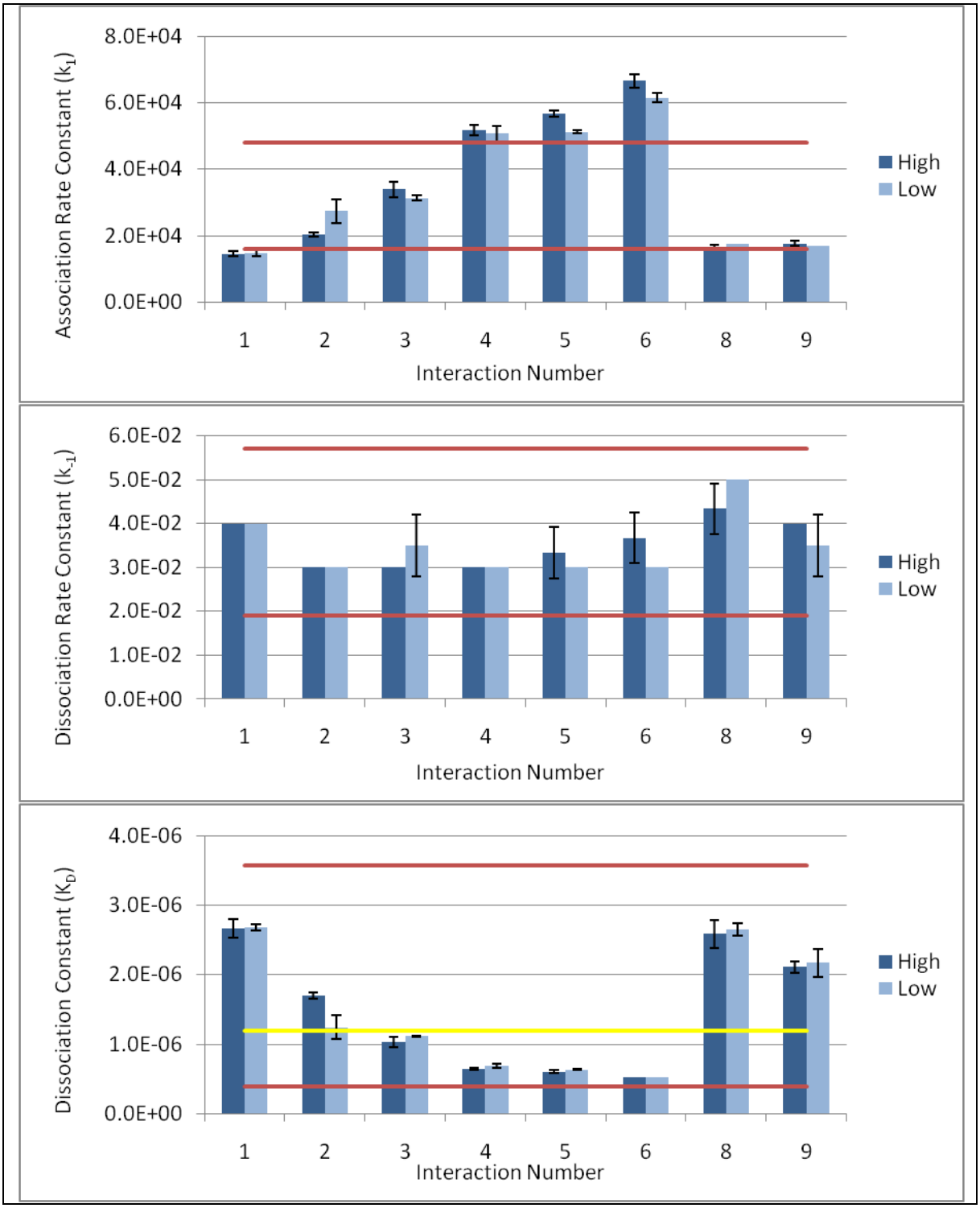

Figure 7.21. Effect of experimental conditions on rate constants and the dissociation constant. Error bars indicate 1σ on the average for experimental data. Red lines indicate range of expected values as provided in kit information. The yellow line indicates the most likely value for K_D based on the given k_a and k_d values.

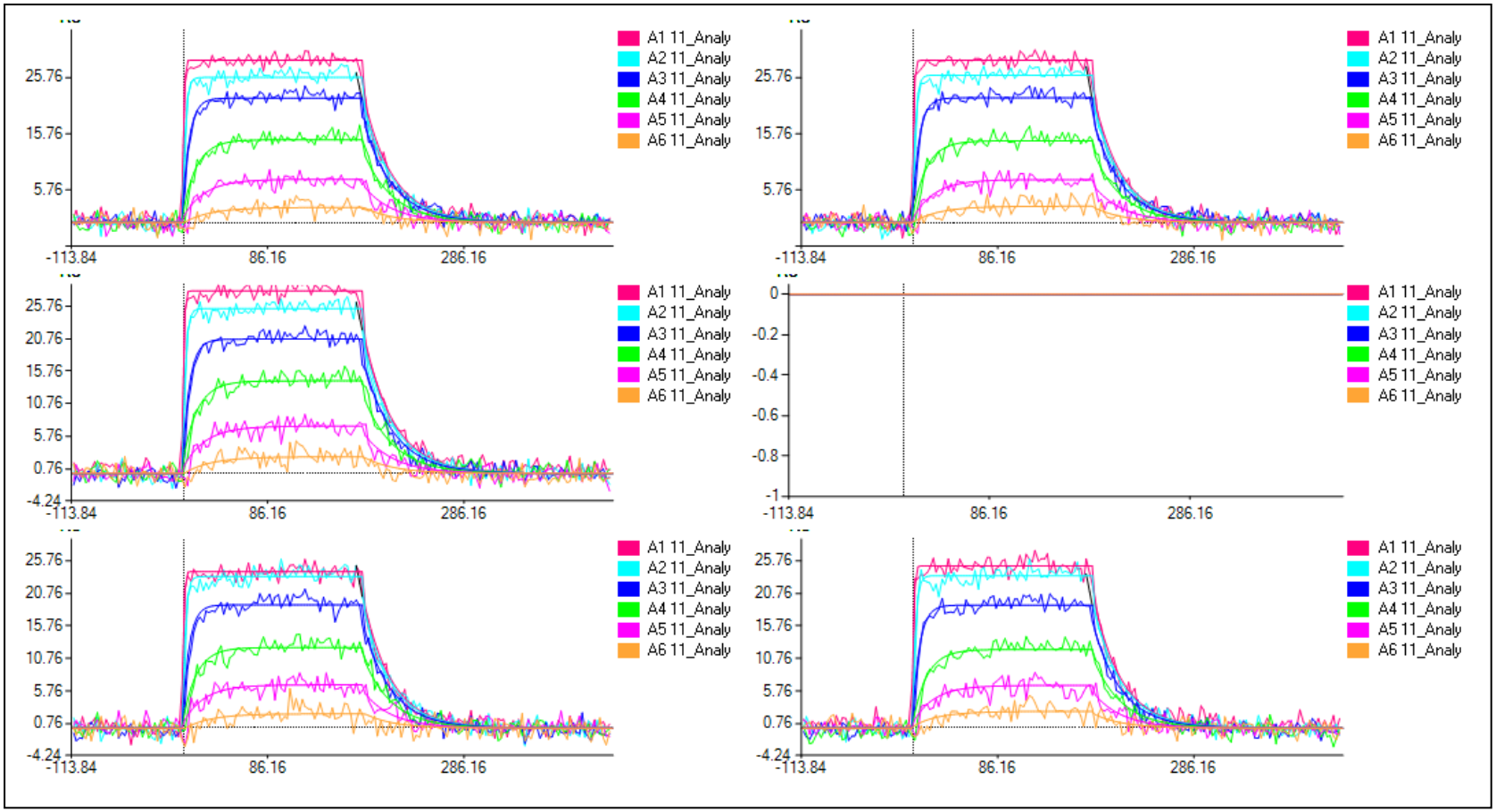

Figure 7.22. Curves fit by nonlinear regression to association and dissociation phases of the experimental data from Interaction 4. All 6 ligand channels are shown.

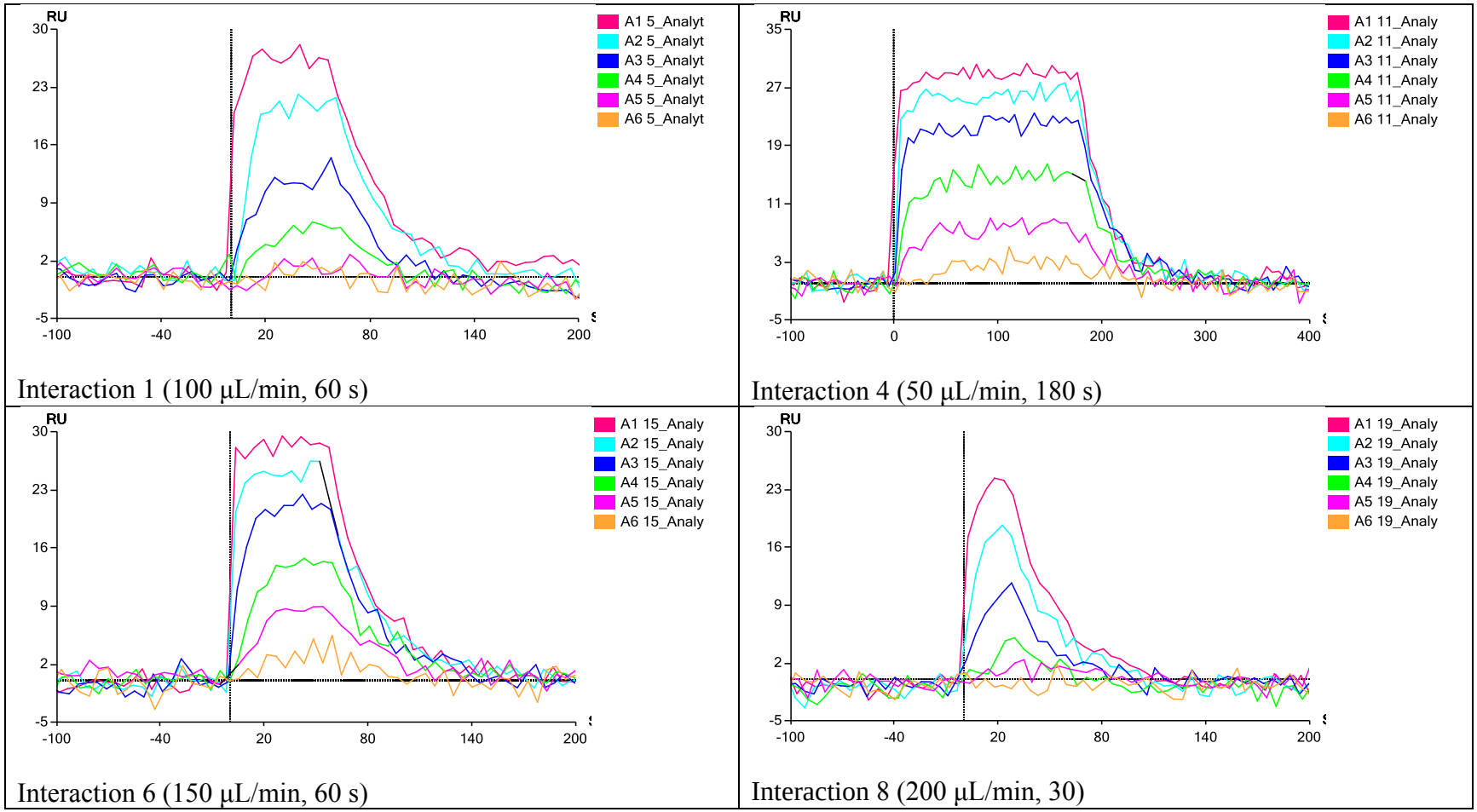

Figure 7.23. The shape of the association reaction curve strongly influences the parameters that are derived by the nonlinear regression. Experimental conditions (flow rate and contact time) influence the shape of the association curve.

7.5.1.1.1 Equilibrium Analysis

If only the equilibrium constant is required, the best way to obtain it is directly by nonlinear least squares regression fitting the Langmuir isotherm model rather than from the kinetics analysis and calculating the ratio $K_D = k_d/k_a$. The results obtained by the equilibrium analysis tool in the instrument software are shown in Figure 7.24.

Interactions 1 and 2 were done under the same flow conditions but interaction 2 was done after the sensor chip was exposed to a low, continuous flow of running buffer overnight while the instrument was in standby mode. This has obviously affected the surface in some way, but since the sensor chip was not used on the third day, it cannot be determined whether the affect was stabilisation (temperature, saturation of surface matrix) or deterioration (e.g. loss of enzyme activity). The effect of flow rate on K_D is apparent from the results for interactions 8 and 9.

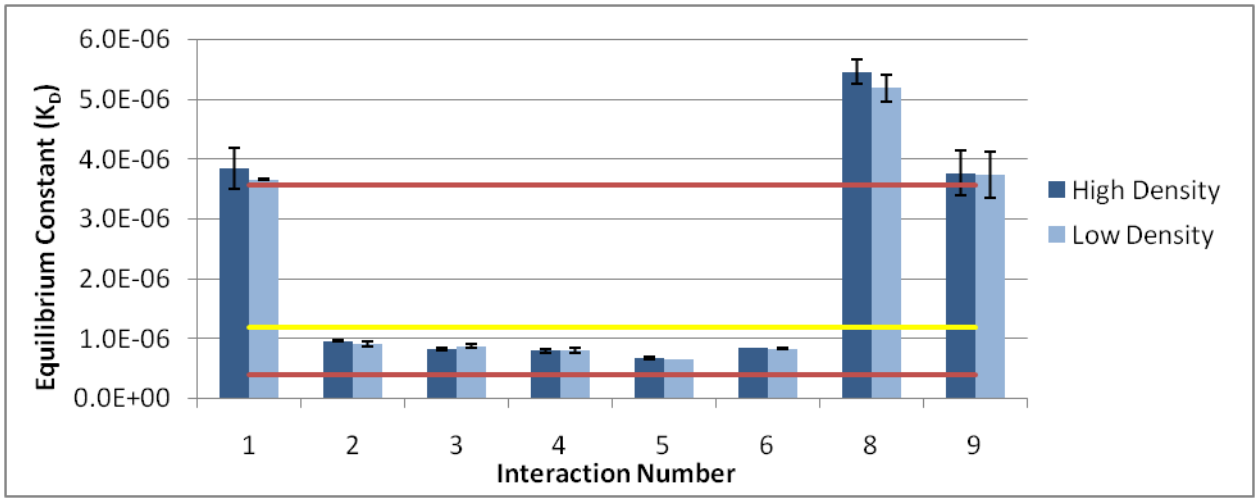

Figure 7.24. Equilibrium constant obtained from equilibrium analysis of the experimental data. Red lines indicate range of expected values as provided in kit information. The yellow line indicates the value for K_D calculated from the given k_a and k_d values. Error bars indicate ±1σ on the average.

Figure 7.25 shows the dependence of K_D on flow rate. As the shape of the association curve becomes distorted at higher flow rates, the calculated K_D increases. As shown in Figure 7.23, the shape of the association curve for interaction 8 has not reached a constant level before the dissociation phase of the interaction was started, indicating equilibrium had not been reached. The nonlinear regression is required to extrapolate where the equilibrium level is located based on the initial portion of the association curve. This is in contrast to interaction 4 where the equilibrium level is well defined.

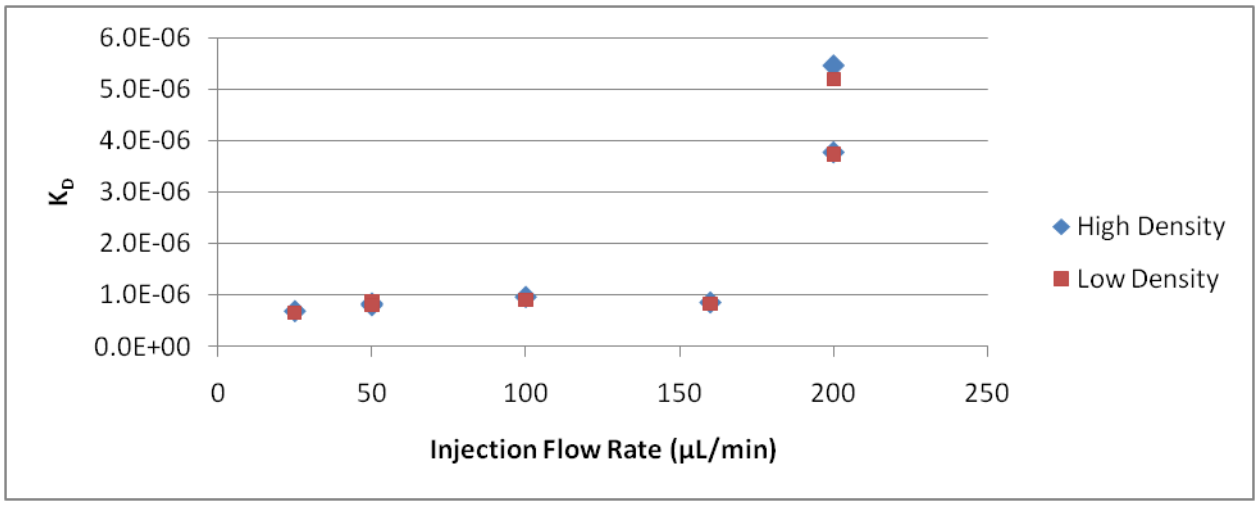

Figure 7.25. Effect of flow rate and contact time during association phase on K_D. The shorter contact time of 30 s at the flow rate of 200 µL/min resulted in a higher value of K_D than the longer contact time of 45 s.

7.5.2 Method Development – Immobilising hER

7.5.2.1 Method Development 1 – Direct Amine Coupling of GSH to the Sensor Chip

In this experiment, an attempt was made to couple GSH directly to the sensor chip and to use the affinity between GSH and the GST-tag to immobilise the GST-hERα fusion protein to the sensor chip in a known orientation.

The sensorgrams obtained for directly coupling GSH to the sensor chip are shown in Figure 7.26. The increase in signal due to GSH injection is relatively small and constant among the 6 channels and is superimposed on a sloping baseline. The sloping baseline is caused by the gradual change in bulk refractive index resulting from gradual removal of residual unreacted activation reagent as the GSH solution flows over the surface. No difference among the channels is observed. This suggested all 6 channels have similar loadings of GSH despite the difference in concentration between channels L1-L3 and L4-L6 and that all 6 channels may be saturated with GSH.

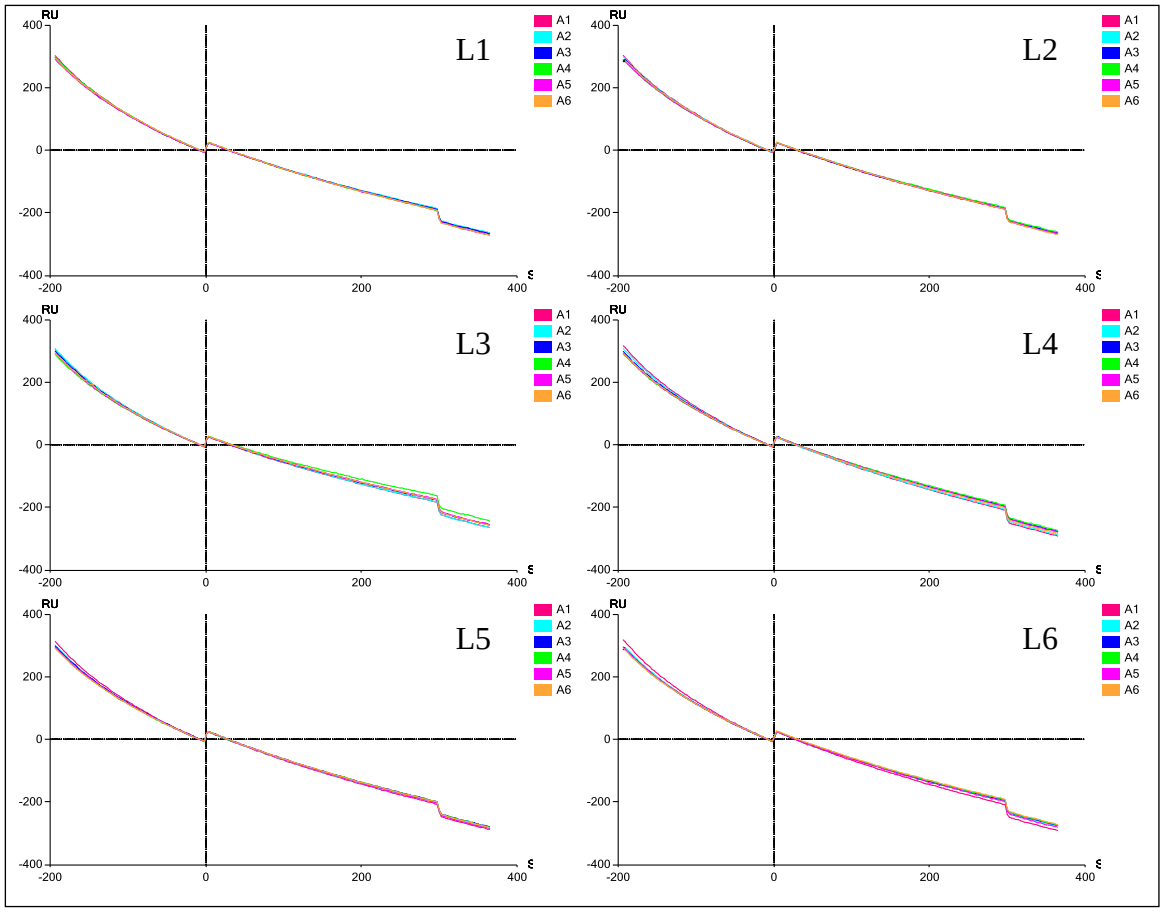

Figure 7.26. Coupling of GSH to sensor chip. The increase in signal due to GSH injection is relatively small and constant among the 6 channels and is superimposed on a sloping baseline. The sloping baseline is caused by the gradual change in bulk refractive index resulting from gradual removal of residual unreacted activation reagent as the GSH solution flows over the surface.

Since the GSH loading appeared to be similar across all 6 ligand channels, the concentration of GST-tagged hERα-LBD was changed to achieve different protein densities. Sensorgrams of channels L1 and L2 with reference channel L3 subtracted are shown in Figure 7.27. The initial increase in signal from t=0 is due to the change in bulk refractive index from running buffer to that of the protein solution. As the solution flows, the slower increase in signal is expected to be due to the association of the GST-tagged hERα-LBD with the immobilised GSH. At the end of 300 s, the running buffer again flows. The difference in signal level with the running buffer flowing after 300 s suggests the GST-tagged hERα-LBD has bound to the chip surface.

The 50 nM hERα solutions for channels L1 and L2 were prepared separately and a dilution error occurred during the preparation of the solution used for channel L2. This is reflected in the differences in responses of channels L1 and L2 observed in Figure 7.27. The 5 nM

solutions used for channels L5 and L6 were prepared by dilution of the 50 nM solutions prepared for channels L1 and L2 and the difference in response is also observed in the sensorgrams for channels L5 and L6 shown Figure 7.28. The amount of ER bound to the sensor chip is determined by difference between pre-injection zero and post injection zero as summarised in Table 7.12. Different amounts of GST-tagged ERα were bound to each channel (L1 > L2 > L5 > L6). The ranking is consistent with the dilution error noted for channel L2 and the propagation of that dilution error into the solution used on channel L6.

In all 4 channels, the signal is still increasing at the end of the 300 s injection interval suggesting additional immobilisation of protein may be possible. The stability of the baseline after injection suggests that there is an affinity capture, not just a non-specific adsorption of the protein to the surface. Non-specific adsorption would appear as a rapidly declining signal after the running buffer flow was started, as seen in Figure 7.26.

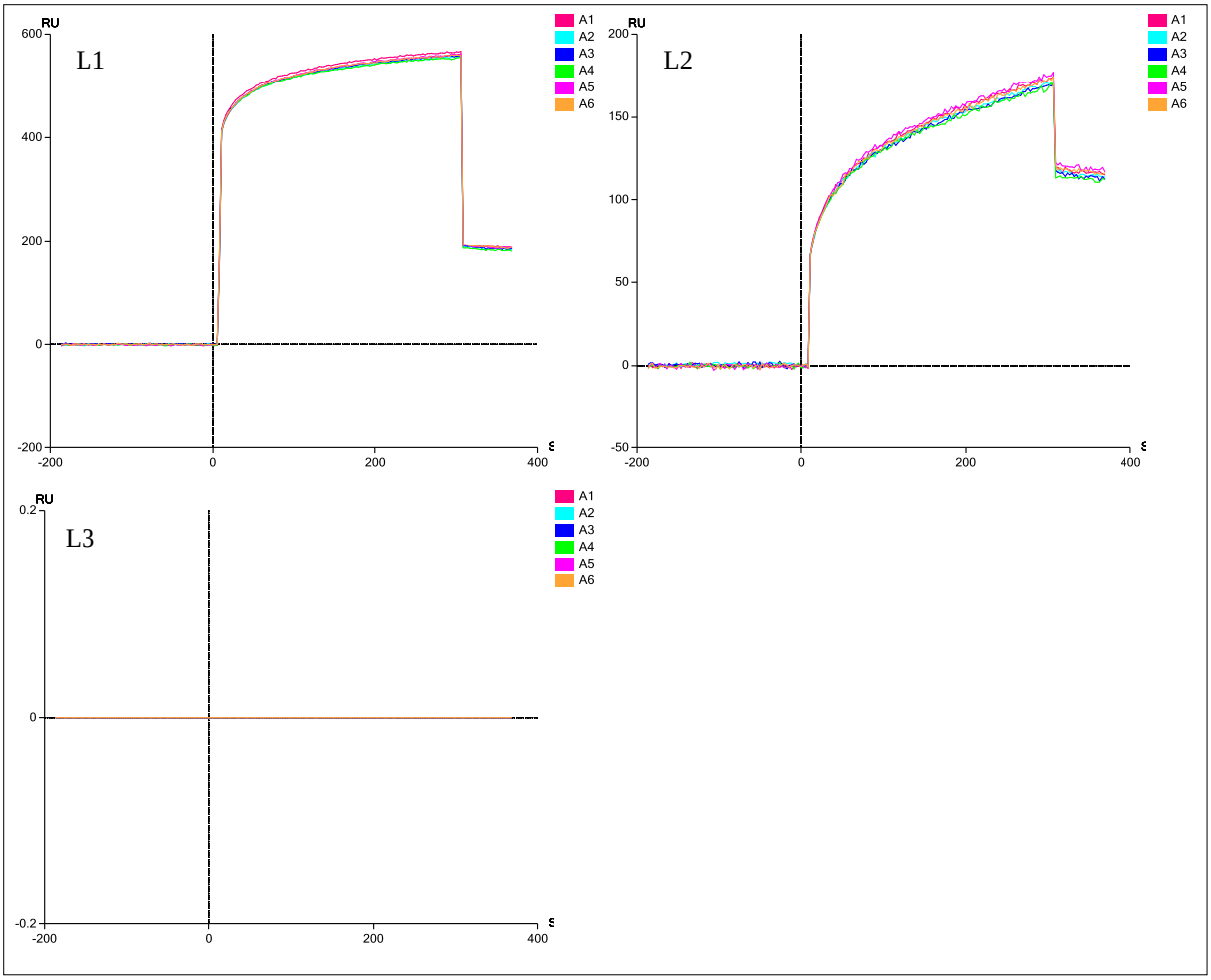

Figure 7.27. Sensorgrams of channels L1 and L2 with reference channel L3 subtracted. The initial increase in signal from t=0 is due to the change in bulk refractive index from

running buffer to that of the protein solution. As the solution flows, the slower increase in signal is the association of the GST-tagged hERα-LBD with the immobilised GSH. At the end of 300 s, the running buffer again flows. The difference in signal level with the running buffer flowing after 300 s suggests the GST-tagged hERα-LBD has bound to the chip surface.

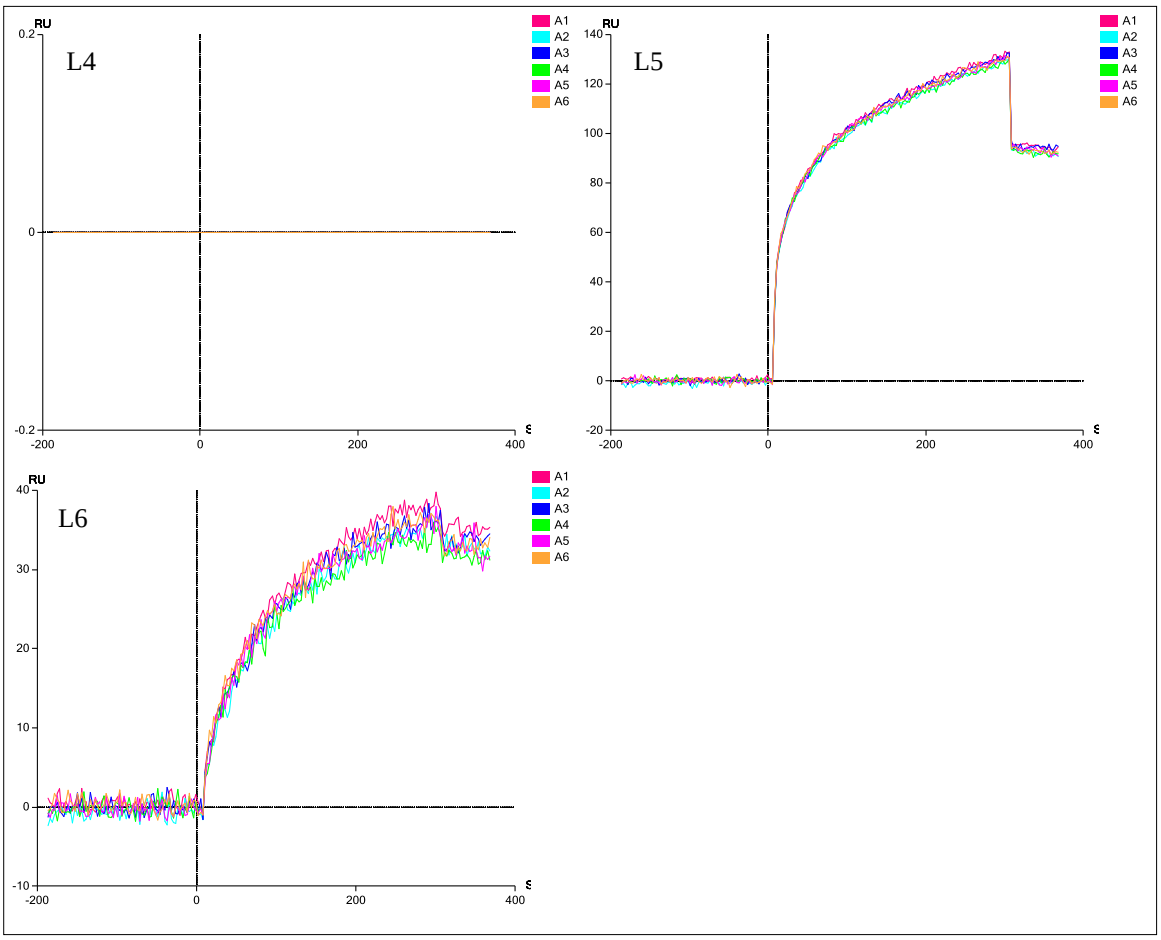

Figure 7.28. Sensorgrams of channels L5 and L6 with reference channel L3 subtracted. Injection of GST-tagged hERα-LBD begins at t=0.

Table 7.12. Pre-injection and post-injection SPR signal values (RU)

	Binding of GST-tagged ERα Average SPR signal (RU)		
Ligand Channel / Analyte Channel	**Pre Injection Zero**	**Post Injection Zero**	**RU Increase**
L1 (A1-A6)	0.01	186	186
L2 (A1-A6)	-0.19	116	116
L5 (A1-A6)	0.06	93	93
L6 (A1-A6)	0.04	33	33

With the apparent success at capturing the GST-tagged hERα-LBD, the flow direction was changed for injection of E2 standards to see if binding of E2 to the immobilised ER could be detected. Five standard solutions of E2 in running buffer were prepared covering a wide range of concentrations as summarized in Table 7.13. The stock E2 solution was prepared at 10 mM in ethanol (EtOH) and then diluted to the desired concentrations with running buffer. These standards were injected at a flow rate of 30 µL/min for 300 s. The dissociation phase was 600 s long with running buffer flowing at 30 µL/min.

Table 7.13. Concentrations of analyte solutions for ERα-E2 interaction.

Solution ID	E2 Concentration (µM)
A1	10
A2	2
A3	0.1
A4	0.02
A5	0.001
A6	0 (buffer blank)

The sensorgrams obtained for the interaction of E2 are shown in Figure 7.29 for channels L1 and L2 and no indication of E2 interacting with the immobilised ER is seen. A second injection of the series of standards was made with no difference in result.

To further investigate, the data from the second injection was viewed by analyte channel (A1-A6) as shown in Figure 7.30. From Figure 7.30, there is a difference in the bulk refractive index of the 5 solutions (A1-A5) as compared to the buffer blank (A6) as summarised in Table 7.14. The bulk refractive index measured at the end of injection is increases with increasing E2 concentration, suggesting the solutions do in fact have E2 present. In neither injection did the association phase reach equilibrium, as indicated by the continuously increasing signal. What might be observed in these interactions is merely non-specific adsorption of E2 to the protein or sensor chip, and is further supported by the declining signal during the dissociation phase. None of the sensorgrams resemble those obtained with the small molecule kit shown in Figure 7.20 and Figure 7.22.

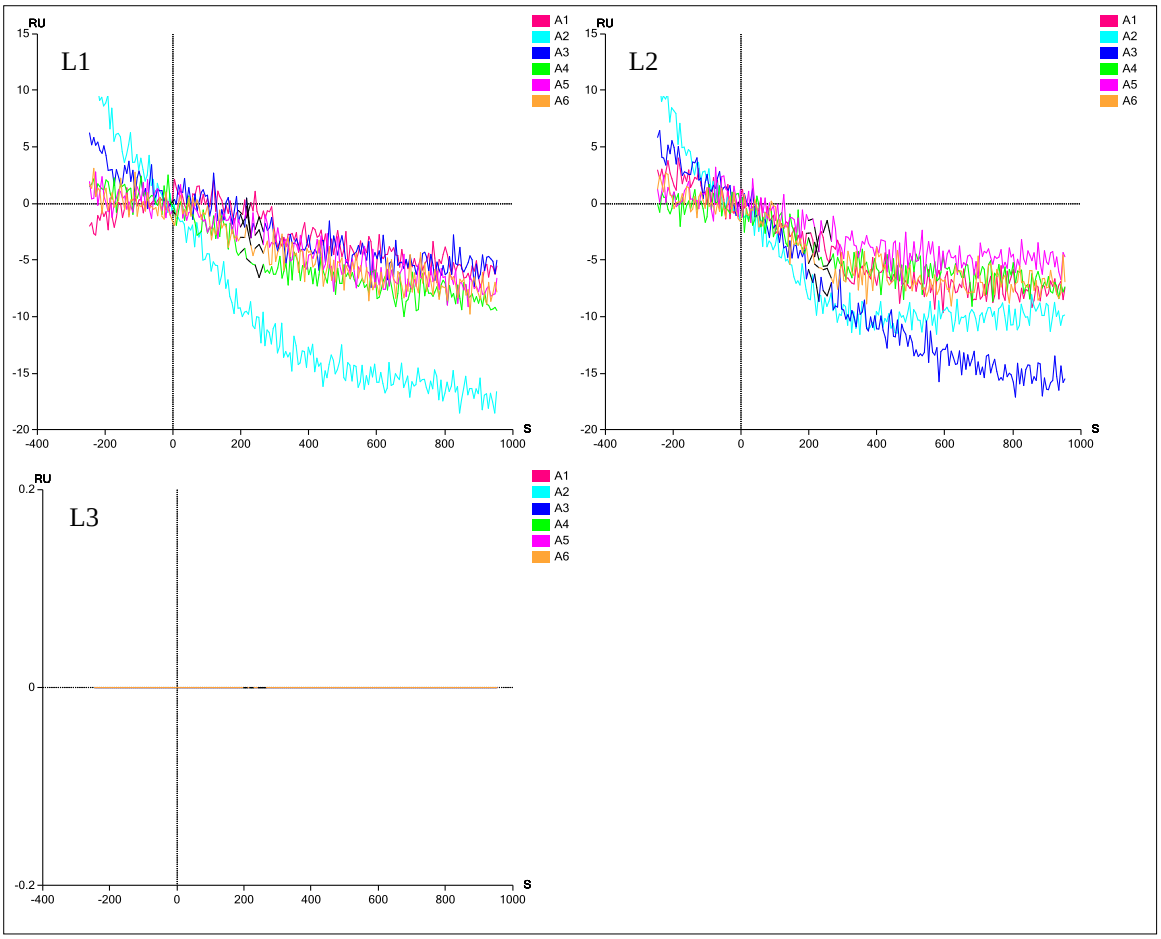

Figure 7.29. Reference channel 3 subtracted from Interaction channels 1 and 2. Curves A1-A6 are E2 concentrations as given in Table 7.13.

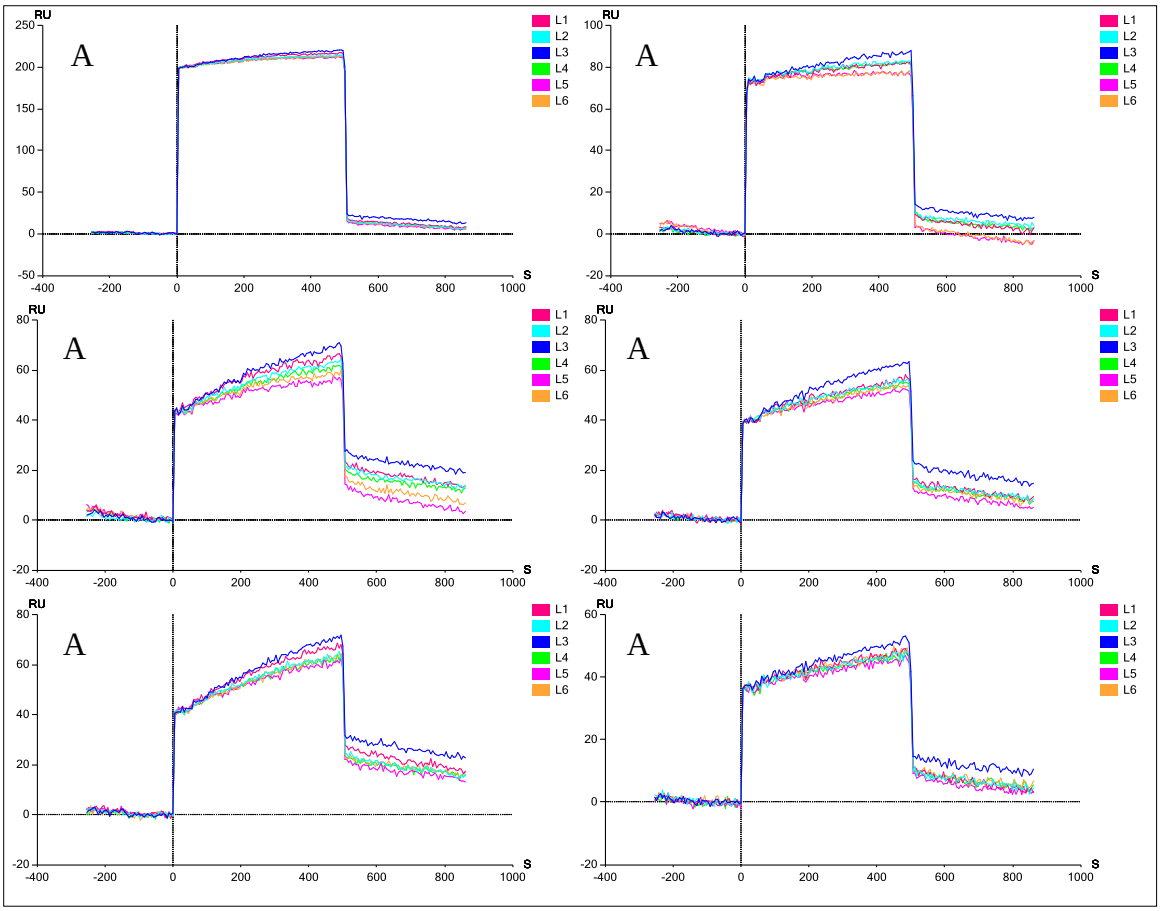

Figure 7.30. View of E2 interaction data by analyte channel. Each panel corresponds to different E2 concentration. Traces are from L1-L6. L3 and L4 are reference channels. No difference between reference channels and channels with GST-tagged ERα is observed.

Table 7.14. RU difference at end of E2 standard injection shown in Figure 7.30.

Analyte Standard	Signal Increase (RU)
A1 (10 µM)	234
A2 (2 µM)	80
A3 (0.1 µM)	50
A4 (0.02 µM)	43
A5 (0.001 µM)	40
A6 (blank)	43

At this stage, a number of different tests were considered to try to understand what was happening. Additional injections of GST-tagged hERα were made, resulting in the incremental increase in SPR signal illustrated in Figure 7.31.

Another attempt to measure the interaction of hERα with E2 was made. No interaction seen and the sensorgrams were no different from those shown in Figure 7.27 and Figure 7.28. The sensor chip was left in the instrument with a low flow of running buffer over the weekend.

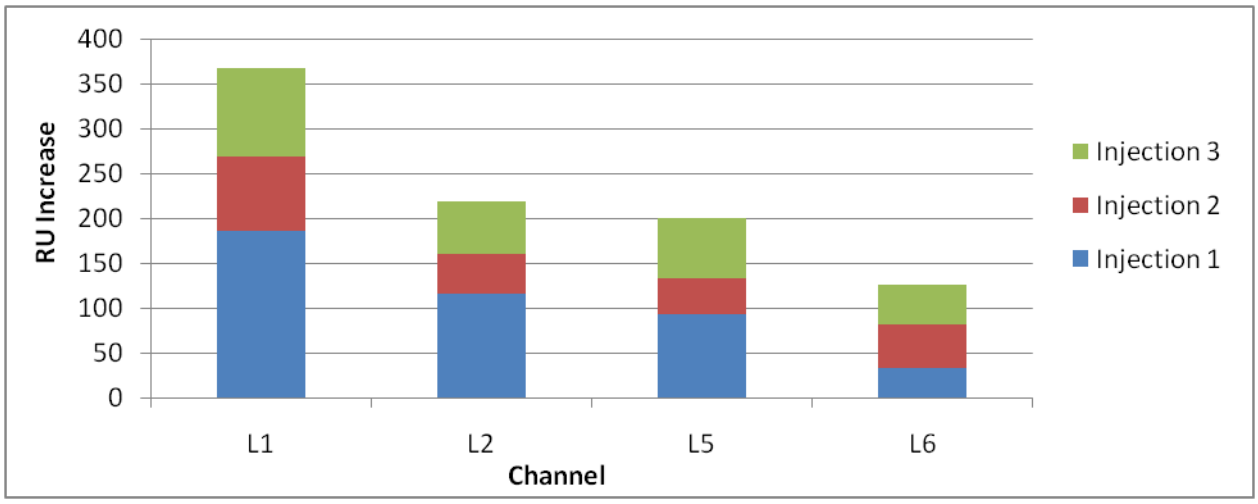

Figure 7.31. Incremental ERα binding measured by the net increase in SPR signal after each injection.

To remove the affinity bound receptor from the sensor chip surface, a regeneration solution of 200 µM GSH in running buffer was used. The first regeneration did not give the expected result. The signal was expected to be lower after the regeneration than before and a difference among the 6 channels was expected as the channels had different amounts of ER were bound. Also expected was a difference between channels 3 and 4 and the other channels as those two channels did not have ER bound. An increase of about 16 RU was observed. A second injection of 300 µL (30 µL/min for 600 s) was made and obtained a similar increase (average 19 RU) in all 6 channels. This suggested an adsorption of GSH to the surface of the sensor chip and that any previously bound ER (if any) may have been removed by the low flow of running buffer over the weekend.

Assuming the results obtained thus far indicate that the sensor chip did not have any ER bound, another attempt was made to bind ER. In their study, Rich et al. [373] used a 2 µM solution of ER injected at 10 µL/min for 5 min. If all ER was captured, the chip would have been loaded with 100 pmol of ER. With the 50 nM GST-tagged hERα solution, the 150 µL injection volume used would give a loading of only 7.5 pmol. The three injections performed

would give a loading of 22.5 pmol. It is possible that insufficient protein was bound to the surface to give a measurable signal with the E2 interaction test.

The vial of GST-tagged ERβ-LBD available contained 250 pmol and was diluted with 1 mL of running buffer to produce a solution is 37.5 nM. Two injections of 150 µL this solution would give a loading of 75 pmol, but there was sufficient quantity of protein to do this for only two of 6 channels. The ERβ solution was injected onto channels L3 and L4 of the sensor chip to ensure no interference from other channels. An average net increase of 57 RU for channels L3 and L4 was observed. An average change for the running buffer injections on the other 4 channels is 2.9 RU. A second injection was done resulting in an average net increase of 58 RU for channels L3 and L4 and an average change for the running buffer injection on the other channels is 1.9 RU. To achieve a third injection of ERβ, 150 µL of running buffer was added to the ERβ vials and mixed. A third injection of 150 µL was done. For this injection a lower net increase in RU was expected since solution was diluted by approximately one third. The average net increase of 14 RU for channels L3 and L4 was observed. The average RU change for the buffer on the other 4 channels was again 1.9 RU.

Assuming that these RU increases on channels L3 and L4 are a result of ERβ capture, the flow direction was changed to the analyte channels and an injection of E2 the standards described in Table 7.13 was done. Sensorgrams similar to those shown in Figure 7.29 were obtained. These results suggest no binding of E2.

7.5.2.2 Method Development 2 – Tether Coupling of GSH to the Sensor Chip

With the failure to capture GST-tagged hER via direct coupling of GSH to the sensor chip, two different tethers were tested. Instead of using the GST-tagged hER, only the GST enzyme was used to test the functionality of the surface.

The carboxy-PEG_4-amine was the first tether evaluated. The PEG was successfully coupled to the sensor chip surface and GSH was successfully coupled to the PEG. But, attempts to capture the GST protein were unsuccessful. The density of the PEG tether was successfully varied but without success in GST capture. The changes in SPR signal observed suggested that the PEG tether may be facilitating a tightly bound water molecule network at the surface of the chip, excluding buffer salts, and causing steric interference with the binding of the protein to the GSH. The evidence of this was an unusual decrease in SPR signal with attachment of the tether.

The second tether evaluated was the aminohexanoic acid. Although shorter, the hydrophobic nature of this tether was reported in the literature to be advantageous in GST-GSH affinity binding as the hydrophobic interactions between the GST protein and the tether tended to stabilize the binding. The SPR signal confirmed a stepwise construction of first the tether to the surface, then GSH to the activated tether. However, binding of the GST protein again was not observed. Variation in density of tether did not result in any capture.

At this point, further investigation was needed before planning additional experiments.

7.6 Discussion

7.6.1 Validation of Instrument Sensitivity

The kit worked as expected. Values for k_a, k_d and K_D were within the ranges expected using both kinetic and equilibrium analysis wizards.

The effects of experimental conditions on the rate constants and equilibrium constant derived from the measurements were examined. The results showed that a well-defined equilibrium level is required for both kinetic and equilibrium analyses. The flow rate and contact time determine the duration of the equilibrium level. A flow rate should be chosen to give an initial slope in the association reaction that is not too steep or too shallow.

Considering all results, the experimental parameters implemented in interactions 2-6 appear optimal for the CAII/CBS system. Increasing the contact time for interactions 8 and 9 may improve the results.

These results also demonstrate that the instrument has the required sensitivity to be able to detect the interaction of a small molecule (MW = 201 Da) with an immobilised enzyme down to a concentration of 0.084 μM (17 ng/mL, 17 ppb). This sensitivity is well within the range of expected concentrations of EEs in biological samples such as urine and amniotic fluid (see Chapter 1). The binding affinity of CBS to CAII is on the order of 1 μM, which is also the same order of magnitude of many EEs (see Chapter 1).

These results demonstrate that the instrument has sufficient sensitivity to proceed with method development for the estrogenic load biosensor.

7.6.2 Kinetics Scuttle an Elegant Idea

With the lack of success of capturing GST via two different approaches to tethering GSH to the sensor chip, the GST affinity chromatography literature was revisited. An unexpected limitation was discovered and it relates to the effect binding kinetics has on the capture efficiency of a GST-tagged protein by immobilized GSH on the sensor chip.

The GST affinity chromatography media technical documentation described that the kinetics of binding for GST was much slower than for other affinity strategies such as polyhistidine tags. The following analysis of the experimental conditions and recommended procedures for GST affinity chromatography and batch purification revealed a potential reason for the lack of success in capture.

The GE Healthcare Affinity Chromatography handbook [403] suggest a maximum linear velocity of 75 cm/h (0.2 mm/s) for small packed columns. Harper and Speicher [404] recommend that for a 2.5-cm-diameter column, a sample-loading flow rate of ≤ 0.1 ml/min is necessary to achieve complete binding of the GST fusion protein to the column at 4 °C. These conditions are equivalent to a linear velocity of 3.4 $x10^{-3}$ mm/s. The geometry of the Bio-Rad SPR flow channel is 450 µm x 100 µm. The minimum flow rate of 25 µL/min in this channel results in a linear velocity of 9.3 mm/s. This flow rate is approximately 46 times higher than the flow rate suggested by GE Healthcare and 2700 times higher than the recommended flow rate suggested by Harper and Speicher.

Tessema et al. [391] determined the dissociation constant, K_D, of a GST fusion of green fluorescent protein (GST-GFP) with immobilized GSH to be 108 nM for high density GSH beads and 190 nM for low GSH density beads in equilibrium binding experiments. They also conducted kinetic experiments to determine binding and dissociation rate constants for the binding of their GST-GFP with immobilized GSH. The association rate constant (k_a) was $2.6x10^3$ $M^{-1}s^{-1}$ for both high and low GSH density beads while the dissociation rate constant (k_d) differed for the high and low GSH density beads ($1.3x10^{-4}$ s^{-1} and $6.4x10^{-4}$ s^{-1} respectively). The dissociation constants determined by the kinetic experiments (50 nM and 250 nM) differed from those determined in the equilibrium experiments.

In comparison to the association and dissociation rate constants shown in Figure 7.2 for hERα ligands, the association reaction for GSH-GST is slow and comparable to that of OHT with hERα. The dissociation reaction is also slow, marginally faster than OHT from hERα but not

as fast as that of E2 from hERα. The experimental conditions used to obtain the results for E2 and OHT [373] are a flow rate of 50 µL/min and a concentration of 1 µM and an interaction time of 30 s and 3 minutes respectively. The simulated association reaction curves for E2 and OHT are shown in Figure 7.32. Indeed, from the shape of the curve, the OHT-hERα association would not have been expected to reach equilibrium until 30 minutes. So, it is not surprising that under the conditions attempted with GST-tagged hER (50 nM at 30 µL/min for 300 s) that very little hERα capture was observed.

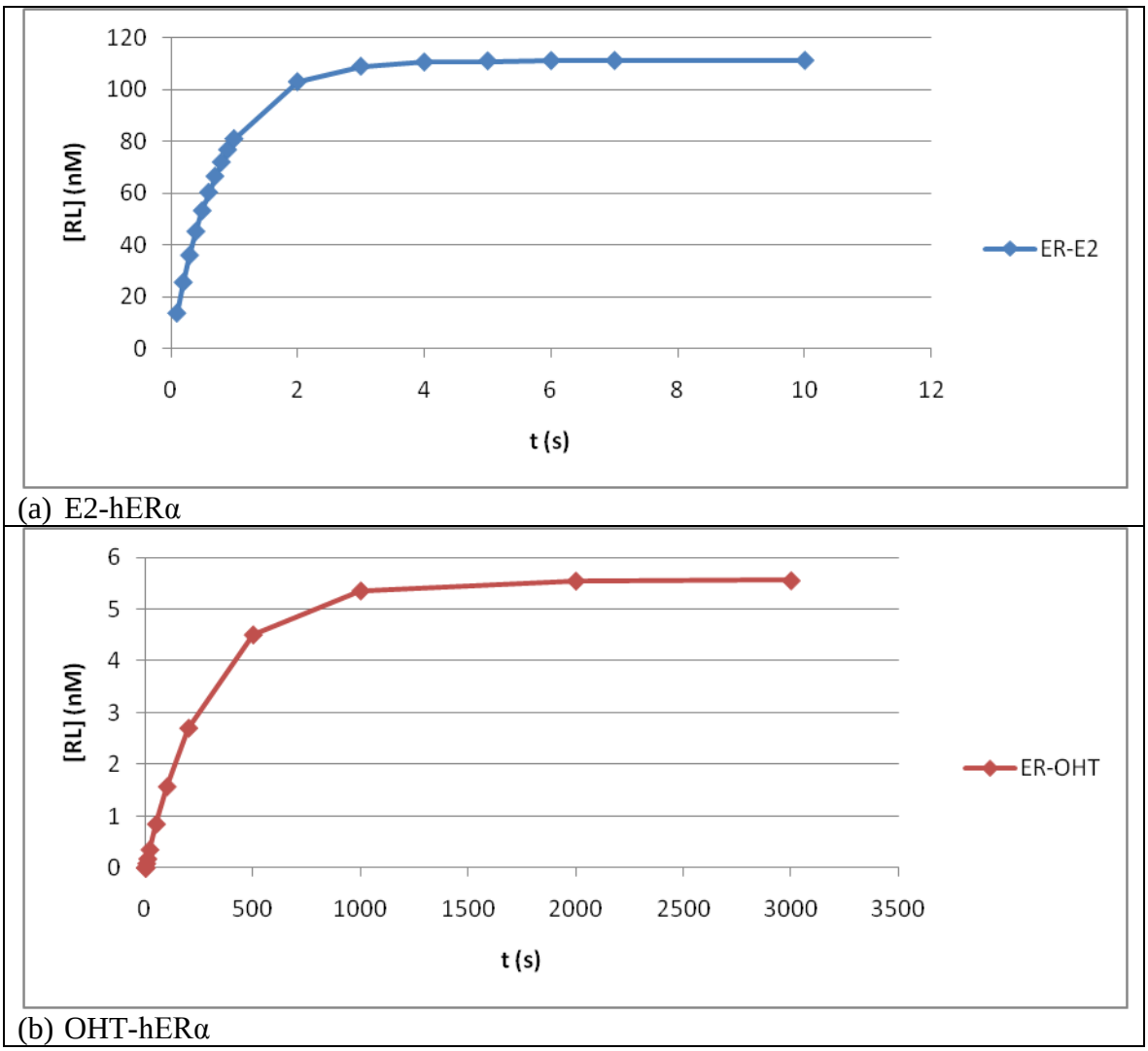

Figure 7.32. Simulated association reaction curves using published rate constant and dissociation constant data for E2-hERα and OHT- hERα. Both curves assume a fractional receptor occupancy of 0.0001 and a concentration of 1 µM of ligand concentration in the injected solution.

7.7 Conclusions

This study demonstrated that although the binding affinity of GST for GSH is high enough to make this system a logical candidate for immobilising GST-tagged proteins to the SPR sensor chip surface, the kinetics of the binding reaction are too slow for this approach to be successful. In order for the GST-GSH strategy to work, a stopped-flow condition is needed to allow the GST-tagged protein to interact with the surface. Incubation times of 30 minutes or more are recommended in affinity chromatography methods to ensure the desired protein is bound before flushing away undesired material. The stopped-flow feature is not available on the Bio-Rad instrument, so the development of the biosensor using the GST-tagged ER was abandoned.

As mentioned earlier, the kinetics of nickel affinity chromatography for purification of His-tagged proteins are much faster, and His-tagged proteins have been used successfully in SPR experiments in the literature [405]. Unfortunately, a commercial source of His-tagged ER was not available and neither was the capacity to produce the protein in-house, so the investigation of this approach must be left for another time.

Chapter 8 Binding Studies – Isothermal Titration Calorimetry

8.1 Introduction

This chapter reports on an attempt to use isothermal titration calorimetry (ITC) to study the thermodynamics of the interaction of endogenous estrogens and environmental estrogens with the hER. An understanding of the relative contributions of enthalpy and entropy to the Gibbs free energy of binding complements the kinetic information on the reaction, leading to a clear picture of the mechanism of interaction of EEs with the hER. This understanding will lead to better predictions of the biological outcomes of exposure to environmental estrogens and to the identification of additional compounds as having estrogenic potential.

This chapter begins with a brief review of the thermodynamics of the receptor-ligand interaction. The principles of ITC and the key factors in designing and ITC experiment are then presented. The results of the experimental work follow. These studies were conducted concurrently with the SPR experiments discussed in Chapter 7. As with the SPR experiments, the ITC experiments were limited by both the cost and format of commercially available hER. The discussion will explain the difficulties encountered and how they may be overcome in future work.

8.2 Theoretical Basis

8.2.1 Reaction Thermodynamics

For the reaction,

$$R + L \underset{k_d}{\overset{k_a}{\rightleftharpoons}} RL$$

where R is the receptor, L is the ligand and RL is the complex formed by non-covalent interaction of R and L, the rate constant for the association (forward) reaction is k_a and the rate constant for the dissociation (reverse) reaction is k_d. At equilibrium, the equilibrium association constant K_A is given by

$$K_A = \frac{k_a}{k_d} = \frac{[RL]}{[R][L]}$$

The dissociation constant, K_D, is simply the inverse of the association constant, $1/K_A$. The standard Gibbs free energy change of the reaction, $\Delta G°$, is given by

$$\Delta G^\circ = -RT \ln K_A$$

or

$$\Delta G^\circ = RT \ln K_D$$

where R is the universal gas constant and T is the temperature in Kelvin. A negative value for ΔG° indicates that the receptor-ligand complex is more stable than the individual isolated receptor and ligand species. ΔG° is related to the enthalpy and entropy of the system by

$$\Delta G^\circ = \Delta H^\circ - T\Delta S^\circ$$

where ΔH° is the standard enthalpy change and ΔS° is the standard entropy change for complex formation. Thus, by measuring ΔH° (observed ΔH corrected for non-specific effects, expressed per mole of substance) and K_A over a range of temperatures, a full thermodynamic characterization of the interaction is obtained:

$$\Delta G^\circ = -RT \ln K_A$$

$$\Delta S^\circ = \frac{(\Delta H^\circ - \Delta G^\circ)}{T}$$

ΔG° provides a concentration independent parameter that allows comparison of the affinities of interactions for different ligands with the receptor. ΔG° has a number of different contributions: intermolecular contacts (non-covalent bonds), conformational changes, hydrophobic interactions, ionisation effects and changes in rotational/translational motion [406].

The change in enthalpy, ΔH°, is a measure of the heat energy associated with going from the free to the bound state and can be thought of as the net heat associated with the making and breaking of non-covalent bonds in forming the biomolecular complex. This value includes not only the bonds associated with ligand binding but also any conformational changes of the components of the interaction. As a result, ΔH° can be complicated to interpret. When coupled with high-resolution structural detail of the interacting molecules (such as computer docking studies), comparison of ΔH° terms for interactions with a given biomolecule and subtly modified ligands can give some insight into the importance of specific, non-covalent bond formation [406, 407]. The ΔH° of interaction is temperature dependent – it varies according to the change in heat capacity (ΔC_p). It may increase or decrease with temperature.

The measured ΔH° may also be dependent on the choice of buffer solution or pH if the interaction is accompanied by a protonation event [408]. The use of a buffer with a high ΔH° of ionization will enhance binding enthalpy. The choice of buffer may have a dramatic effect such that in one buffer, the reaction may be exothermic and in another buffer, the reaction is endothermic. The number of protonation events that occur on binding can be determined from data from experiments in different buffers [406, 407].

The change in entropy term, ΔS, is more difficult to interpret. Entropy is a measure of the tendency of the system to disorder. While the coming together of two molecules imposes some order on the system due to reduction in translational/rotational entropy and reduction in atomic degrees of freedom (configurational entropy), the release of water molecules from the binding site to the bulk solvent results in disorder [406].

Thus, for the receptor-ligand complex to form, ΔG° must be negative and enough heat must be produced (negative ΔH°) to counter any increase in order (negative ΔS°) that is achieved when the two isolated, solvated molecules bind to form a single complex.

8.2.2 Thermodynamics of E2-hER Ligand Binding

At 20 °C, the binding of hER and E2 has a K_D of 0.9 nM [373] and this corresponds to a ΔG° of -50.8 kJ/mol. The binding of E2 to hER is entropy driven at temperatures between 0 °C and 17 °C (ΔH° = 0 at 17 °C) and enthalpy driven at temperatures above 37 °C (TΔS° = 0 at 37 °C) [407]. Between 17 °C and 37 °C the binding is driven by both enthalpy and entropy. At 25 °C, ΔH° accounts for only 37% of ΔG°. The switch to enthalpy driven binding at physiological temperature (37 °C) is interpreted as a minimum in the activation energy needed to disrupt the water molecule cages that shield the hydrophobic portions of the protein from the bulk aqueous solvent. Within the temperature range of 0 °C and 37 °C, the variation in ΔG is small (~6 kJ/mol) [407], but the relative contributions of ΔH° and ΔS° change dramatically.

The binding of E2 to ER also has a large negative molar heat capacity $\Delta C_P°$ of -2.4 kJ mol^{-1} K^{-1} and is typical of protein-ligand interactions. This has been attributed to the large negative vibrational contributions that result from the tightening of the binding cavity around the bound ligand and the repositioning of H12 to close the binding cavity [407].

The ability to describe the binding of environmental estrogens to the hER in this way will be useful in developing a clear picture of the molecular mechanism of action of environmental estrogens and will help to rationalise the varied biological outcomes of exposure.

8.2.3 Isothermal Titration Calorimetry

Isothermal titration calorimetry measures the change in enthalpy (heat) involved in a chemical reaction or physical process. Heat can be taken in from the surroundings (endothermic) or given up to the surroundings (exothermic). The amount of heat is proportional to the amount of reaction that has occurred, the number of moles of material involved and the enthalpy change for the reaction [409]. Enthalpy (ΔH) is measured in kcal/mol or kJ/mol. The rate at which heat is exchanged can also be measured and is equal to the rate of reaction. ITC can be used to simultaneously determine the equilibrium association constant of a reaction (K_A) and ΔH [409]. By measuring the enthalpy, it is possible to quantify the exact enthalpic and entropic contributions to the overall free energy. Thus, for two interactions that have similar affinities and free energies, there can be very different enthalpic and entropic components to the free energies, driven by such factors as changes in protein secondary or tertiary structure and degree of hydration [410].

Observed enthalpies arise largely as a result of changes in interatomic interactions. The most important of these interatomic interactions for biological systems is the hydrogen bond. The magnitude of the interaction enthalpy is dependent on bond lengths and bond angles. The sign of the reaction indicates whether there is a net favourable (negative) or unfavourable (positive) redistribution of the hydrogen bond network between reacting species [410]. Hydrophobic interactions are related to the relative degrees of disorder in the free and bound systems and therefore these interactions are reflected in the entropy change. The release of water molecules from a ‘wet’ surface to the bulk solvent is a common source of favourable entropy. Coupled with the inability of non-polar groups to hydrogen bond with the surrounding water molecules, this is the main reason for the strong energetic influence of hydrophobicity in biology [410]. These types of interactions are typically characterized by a small enthalpy change, either positive or negative, and a favourable (positive) entropy change. A large negative change in heat capacity is thought to arise from the accommodation of non-polar groups by water and is therefore another useful indicator of hydrophobic interactions [410].

Conformational changes are entropically unfavourable. Large unfavourable entropies are often indicative of an 'induced fit' during the interaction and are often seen in receptor binding [410].

Modern ITC instruments can measure heat change rates as small as 0.1 µcal/s (0.4 µJ/s). This sensitivity allows the determination of K_A as large as 10^8 to 10^9 M^{-1} for reactions with rates in the range of 10^{-12} mol/s [409].

Calorimetric measurements can be made in different ways. ITC is based on the power compensation method. The calorimeter cell is controlled at a constant temperature (isothermal). Constant cooling is applied to the cell. The cell is kept at a constant temperature using a temperature controller and heater. As the chemical reaction takes place, heat produced or required by the reaction is compensated for by controlling the power applied through the heater. The raw signal is the power (µcal/s or µJ/s) that is applied through the heater to maintain the cell at a constant temperature.

The experiment is designed so that one component of the reaction is placed in the cell and the second component is titrated into the cell using a syringe injection. Multiple small volumes of titrant are added, with enough time allowed between injections for the calorimeter to return to the constant temperature set point.

Typical ITC data is shown in Figure 8.1. Panel (a) shows the differential power signal recorded in the experiment. Each peak corresponds to the heat released on addition of an aliquot of the titrant. If K_A is large and the molar ratio of ligand to receptor protein at the beginning of the titration is low, then virtually all of the ligand is bound to the receptor and all the peaks are of similar area. As the fractional saturation increases, the amount of heat produced gradually decreases. Eventually all the binding sites are saturated. Small heat changes measured after saturation are caused by the heat of ligand dilution and other nonspecific effects.

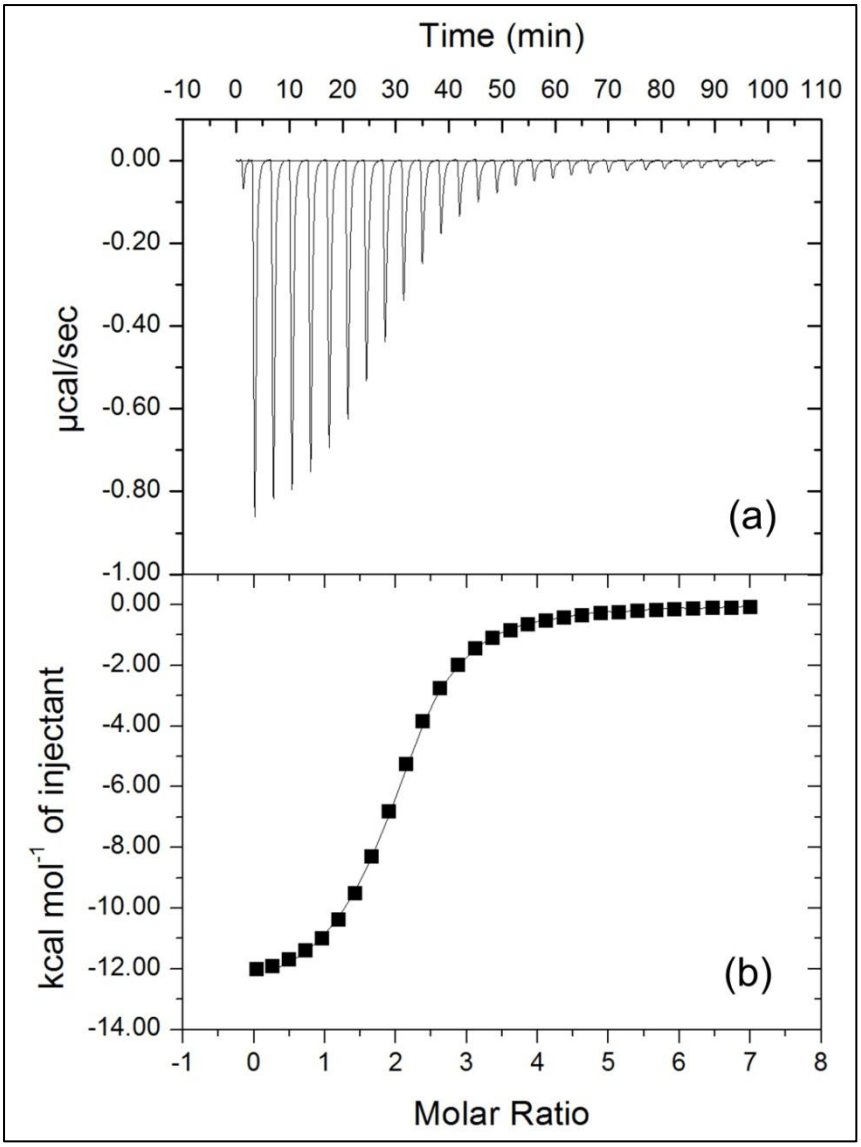

Figure 8.1. Typical ITC data (courtesy Dr. R. Hutton, University of Canterbury).

Integration of each peak individually gives the apparent heat change per addition, $\Delta q_{i,app}$. The apparent heat change has contributions from the binding reaction, dilution and other nonspecific effects:

$$\Delta q_{i,app} = \Delta q_i + \Delta q_{i,dil} + \Delta q_{i,ns}$$

The apparent heat change is proportional to the cell volume, the change in bound ligand concentration and the apparent molar enthalpy of association:

$$\Delta q_{i,app} = \Delta [L_i]_{bound} \times V_{cell} \times \Delta H_{app}$$

After integration with respect to time and normalization per mol of added ligand, ΔH_{app}, K_A and n can be calculated by nonlinear least squares analysis implemented in the software of

the instrument. The integrated data is presented as a sigmoidal plot (panel (b) of Figure 8.1). The ΔH_{app} obtained from this analysis is a global property of the system corrected for nonspecific effects; it reflects the total heat released or absorbed in the calorimetric cell. Other processes such as solvent reorganization, protonation effects or direct, non-covalent bonds also contribute and experiments must be designed to attempt to identify and quantify those contributions.

To obtain reliable binding constants, the concentrations of the interacting species must be in the correct range. If the concentration of binding sites is very much higher than $1/K_A$, all the ligand added will be bound until saturation and the binding isotherm of Figure 8.1(b) will have a rectangular shape with the slope approaching infinity. In the opposite case, the isotherm will be very shallow and full saturation will be difficult to approach. For accurate values of K_A, the concentration of receptor binding sites should not be much higher than $1/K_A$. A dimensionless value, c, is defined as the product of K_A and the total binding site concentration, in this case equal to the active receptor concentration [R]:

$$c = K_A \times [R]$$

As a rule of thumb, c-values between 10 and 100 give accurate K_A values, but sometimes the concentration of R is not useful. Under some conditions, the c-value range may be extended to 1-1000 [411]. For tight binding, the concentration of the receptor may be too low to give measurable heat changes. This places an upper limit on the K_A that can be accurately measured of approximately 10^9 M^{-1} ($\Delta G \sim$-50 kJ mol^{-1}). At the other end, if binding is very weak, the concentration of M may be so high that aggregation of receptor protein molecules can obscure the binding reaction. Often ΔG is dependent on temperature, pH, ionic strength, so experimental conditions can be found to measure it. The E2-hER system, with a $\Delta G°$ of approximately -51 kJ/mol, is at the limit of the operating range of the instrument. Environmental estrogens have much lower affinities for the hER, falling within the operating range of the instrument.

ITC titrations can also be done by titrating a strongly binding ligand into a solution containing the receptor already saturated with a weaker ligand [412]. Free binding energies are obtained from such a displacement experiment if the strong and weak ligands exhibit suitable differences in binding enthalpy.

8.3 Methods and Materials

8.3.1 Methods

8.3.1.1 Isothermal Titration Calorimeter

The instrument available for use is the VP-ITC MicroCalorimeter by MicroCal of Northampton, MA, USA [413]. The instrument has two cells, the reference cell and the sample cell as shown in Figure 8.2.

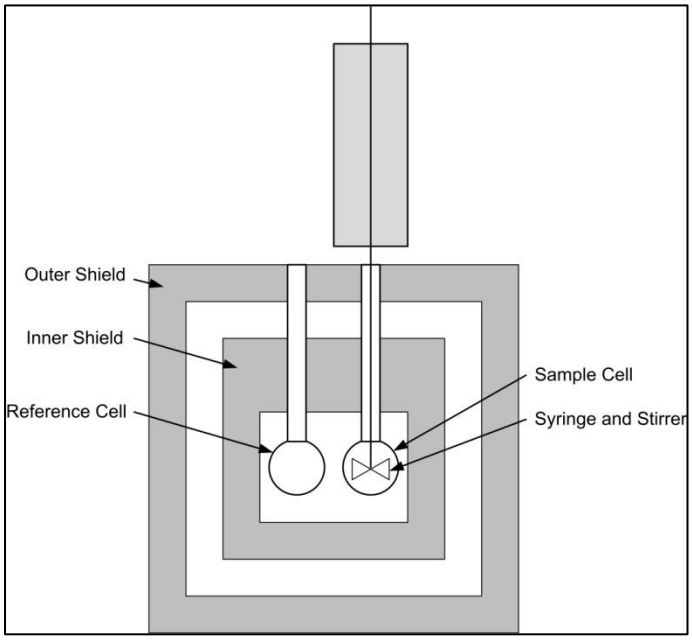

Figure 8.2. Schematic of VP-ITC instrument, adapted from [413].

The sample cell is fitted with a syringe driven by a stepper motor to deliver the titrant to the cell. The temperature difference between the two cells is measured. This temperature difference is used to determine how much power must be applied to the heater to maintain constant temperature. The reference and sample cells are coin-shaped and each have a working volume of 1.4 mL and must be completely filled during operation. The instrument has a sensitivity of 0.1 µcal. Each injection of titrant should produce or require 3-5 µcal of heat to produce good results. Titrant injection volumes are typically 3-15 µL and 10-15 injections are made. Three or four injections should be beyond the saturation of binding sites, giving 'control heat' data within the experiment. The 'control heat' collectively refers to heat produced by dilution, mixing of the titrant with the cell contents and other non-specific heats. Experiments should be done at several different temperatures as the binding constant and heat of binding are usually temperature dependent, while the stoichiometry of

the reaction is not. By conducting experiments at different temperatures, the heat capacity of the reaction can also be determined.

8.3.1.2 Study Design

Documented measurements of the equilibrium dissociation constant (K_D) for the E2-hER interaction are on the order of 0.5 nM, giving K_A in the range of $2x10^9$ M^{-1}. This is near the limit of sensitivity of the instrumentation. The K_A value for BPA is on the order of $2x10^5$ M^{-1}. The large difference in K_A values for E2 and BPA creates two scenarios for designing experiments: tight binding for E2 with hER and weak binding of BPA with hER.

8.3.1.2.1 Tight Binding Scenario – E2

The study of tight binding reactions is limited by the low concentration of receptor required to achieve c-values in the range of 1-1000. The receptor concentrations for the desired c-values are given in Table 8.1. To maximise the heat produced by the reaction, the highest practical hER concentration of 50 nM is chosen for the initial experiments. This concentration is a compromise between sensitivity and having sufficient material to conduct several experiments.

Table 8.1. hER concentrations for a range of c-values for the reaction of E2 with hER.

c-value	hER concentration (nM) Ligand = E2; $K_A = 2x10^9$
1	0.5
10	5
100	50
1000	500

With the concentration of receptor selected, the concentration of the E2 solution injected needs to be determined. It is desirable to achieve a titration ratio of at least 2 when the c-value is in the range of 10-500 [411]. The titration ratio is defined as the ratio [L]/[R] achieved at the end of the experiment. Assuming a cell volume of 1.4 mL, and 10 injections of 10 µL each (100 µL total volume injected), the final concentration of E2 in 1.5 mL will be 100 nM with $150x10^{-12}$ moles of E2 injected in 100 µL. This gives a titrant solution in the syringe with an E2 concentration of 1.5 µM.

8.3.1.2.2 Weak Binding Scenario - BPA

The study of weak binding interactions is limited by the high concentration of receptor required to meet the usual c-value criteria of 1-1000 as shown in Table 8.2. If a c-value of 1 is chosen, approximately 13 vials of ER are required to achieve 2 mL of a 5 μM solution (sufficient for one experiment). This is clearly not feasible or cost effective.

Table 8.2. hER concentrations for a range of c-values for the reaction of BPA with hER.

c-value	hER concentration (μM) Ligand = BPA; K_A = 2x10^5
1	5
10	50
100	500
1000	5000

Successful experiments can be done at c-values down to 10^{-4} if designed correctly [411]. For BPA, a receptor concentration of 50 nM will give a c-value of approximately 0.01, which may be sufficient for a successful experiment. At low c-values, the titrant must be added to great excess to achieve significant binding site population. The range of titration, R_m, is then defined by

$$R_m = \frac{6.4}{c^{0.2}} + \frac{13}{c}$$

Where R_m = [L]/[R] in the cell after the last injection [411].

With c = 0.01, R_m = 1316. As above, with [R] = 50 nM, 10 injections of 10 μL, the total number of moles of BPA injected into the cell will be $1x10^{-7}$, giving a titrant solution in the syringe with BPA concentration of 1 mM. The solubility of BPA is in the range of 120-300 ppm in water at 20 °C, which corresponds to a concentration of 0.5 to 1.3 mM. The desired concentration of BPA may just be achieved in aqueous solution.

8.3.1.2.3 Data Reduction

The question of what experiments to use as controls to correct for other contributions to the measured heat change in the E2 into hERα experiment is now considered. The total heat change observed in the experiment of titrating E2 into hERα ($\Delta H_{T_{E2-hER\alpha}}$) includes components from the heat of interaction of E2 with hERα ($\Delta H_{E2-hER\alpha}$), the heat of dilution

of the E2 solution (ΔH_{E2}), the heat of dilution of the hERα solution ($\Delta H_{hER\alpha}$) and an instrument blank (ΔH_{inst}).

$$\Delta H_{T_{E2-hER\alpha}} = \Delta H_{E2-hER\alpha} + \Delta H_{E2} + \Delta H_{hER\alpha} + \Delta H_{inst}$$

$$\Delta H_{E2-hER\alpha} = \Delta H_{T_{E2-hER\alpha}} - \Delta H_{E2} - \Delta H_{hER\alpha} - \Delta H_{inst}$$

The heat of dilution of the E2 solution is obtained by titrating the E2 solution into the buffer used to dissolve hERα.

$$\Delta H_{T_{E2}} = \Delta H_{E2} + \Delta H_{inst}$$

$$\Delta H_{E2} = \Delta H_{T_{E2}} - \Delta H_{inst}$$

The heat of dilution of the hERα solution is obtained by titrating the reagent blank into the hERα solution.

$$\Delta H_{T_{hER\alpha}} = \Delta H_{hER} + \Delta H_{inst}$$

$$\Delta H_{hER\alpha} = \Delta H_{T_{hER\alpha}} - \Delta H_{inst}$$

An instrument blank is obtained by titrating buffer into buffer. The total heat change for each experiment contains a contribution from the instrument blank. To minimize errors due to subtraction, the following approach is used, where each term in the equation is directly measured:

$$\Delta H_{E2-hER\alpha} = \Delta H_{T_{E2-hER\alpha}} - \Delta H_{T_{E2}} - \Delta H_{T_{hER\alpha}} + \Delta H_{inst}$$

8.3.2 Materials

The full-length receptor proteins hERα and hERβ were purchased from Invitrogen (product # P2187 and P2466 respectively). The ligand binding domains for hER available had the GST tag (as used in the SPR experiments). The effect of the GST tag on ligand binding to the hER in solution was not known, so the full length receptor was chosen for the ITC experiments.

A quantity of 750 pmol active receptor is provided in each vial and the molar concentration of active receptor is on the order of 2.5 – 5 μM. The quantity of protein available is a limiting factor for these experiments.

The supplied hER was buffer exchanged to remove the glycerol and other preservatives from solution. Buffer exchange was done by ultrafiltration using a Vivaspin 500 tube (Sartorius). This device has a capacity of 500 µL and polyethersulfone (PES) membrane of different molecular weight cut-offs. The tube available has a 10 kDa MW cut-off. The hER was buffer exchanged into the ITC buffer described below.

The 750 pmol of hERα was buffer exchanged and diluted into 4 mL ITC buffer to give a concentration of 188 nM. This solution was further diluted to 3 aliquots of 50 nM for the first experiment. The 750 pmol of hERβ was buffer exchanged into 2 mL ITC buffer to give a concentration of 375 nM.

The buffer used for dissolving the receptor protein and preparing titrant solutions (ITC buffer) was 50 mM Tris-HCl, 500 mM KCl, 2 mM DTT, 1 mM EDTA and was prepared from stock reagents.

A stock solution of E2 (Sigma Aldrich product # E8875, ≥98%) was prepared in methanol (MeOH, HPLC grade) at a concentration of 7.3 mM. An aliquot of 3.4 µL of the stock E2 solution was diluted to 25 mL in the ITC buffer to produce a 1.5 µM solution for the hERα experiment. This solution contained 3.36 mM MeOH. The buffer blank solution used for the ITC titration was prepared by adding 3.4 µL MeOH to 25 mL of ITC buffer.

The 375 nM hERβ gives a c-value of 750 for E2 as the titrant. This increase in receptor protein concentration requires a titrant concentration of 10 µM. This E2 solution was prepared by diluting a 32 µL aliquot of the stock E2 solution to 25 mL with ITC buffer. The reagent blank was prepared by diluting a 32 µL aliquot of the MeOH to 25 mL with ITC buffer.

8.3.3 Experiment 1

Prior to starting the series of experiments, the reference cell was filled with degassed Milli-Q water.

The series of experiments described in Table 8.3 was conducted at 20 °C. The initial titrant injection volume of 5 µL was discarded as it often is affected by tiny bubbles and other disruptions caused by inserting the syringe into the measurement cell and starting the stirring. A total of 15 injections of titrant were done. Each experiment takes approximately 1 hour to

complete, after the initial stabilisation time has passed. The instrument operating parameters are summarised in Table 8.4.

The series of experiments described in Table 8.3 was repeated using the 375 nM solution of hERβ instead of the 50 nM hERα solution. Since there was sufficient receptor protein for only one titration, the receptor blank titration was not done and only one interaction titration with E2-hERβ was done.

Table 8.3. Series of ITC experiments with E2 and hERα.

Experiment	Cell Contents	Syringe Contents
Double Blank	ITC Buffer	ITC Buffer
Reagent Blank	ITC Buffer	3.4 mM MeOH in ITC Buffer
Titrant Blank	ITC Buffer	1.5 µM E2 ITC Buffer
Receptor Blank	50 nM hERα	3.4 mM MeOH in ITC Buffer
Interaction	50 nM hERα	1.5 µM E2
Interaction	50 nM hERα	1.5 µM E2

Table 8.4. Experimental conditions for ITC experiments listed in Table 8.3. Series of ITC experiments with E2 and hERα..

Parameter	Value
Cell Temperature	20 °C
Titrant injection volume	10 µL
Initial titrant injection volume	5 µL
Total number of titrant injections	15
Reference power	10 µcal/sec
Initial delay	300 s
Injection duration	20 s 10 s for initial 5 µL injection
Injection spacing	210 s
Filter period	2 s

8.4 Results

8.4.1 First ITC Experiment with hERα

The series of titrations described in Table 8.3 were completed. The double blank titration was repeated twice, the reagent blank titration was repeated three times, the titrant blank was repeated twice and a single titration of E2 into 50 nM hERα was obtained. Examples of the raw data obtained for each titration are shown in Figure 8.3. The software tools were used to integrate the area of each peak and calculate the amount of heat produced on each injection.

The net heat change is normalized to the concentration of the injected titrant (E2) in the cell after each injection. The results are illustrated in Figure 8.4.

The peaks corresponding to heat production with each titrant volume addition shown in Figure 8.3 are very small and show no difference between the various blank and reaction titrations. Overall, the expected trend of decreasing peak area (Figure 8.1) is absent for the reaction titration. There is no difference in the heat of reaction obtained from these data (Figure 8.4), suggesting the concentration of hERα is too low and the quantity of heat produced is below the sensitivity limit of the instrument.

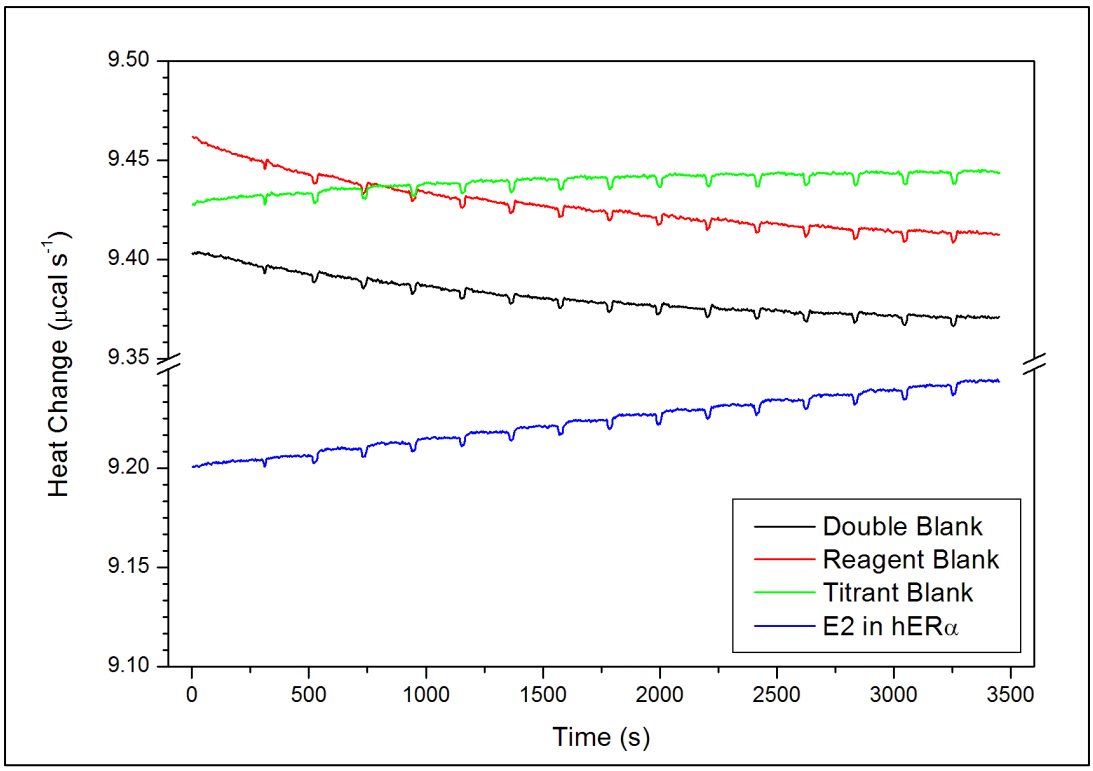

Figure 8.3. The raw ITC data for double blank, reagent blank, titrant blank and the interaction of E2 with hERα.

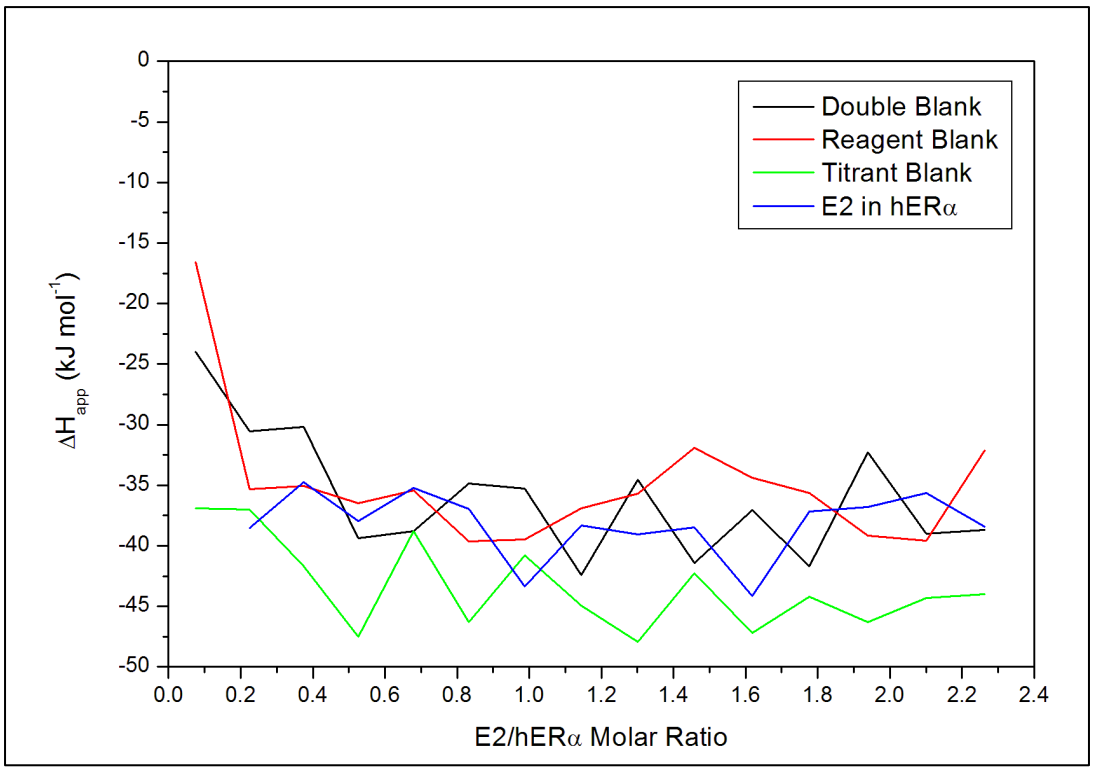

Figure 8.4. Apparent heat change per mol of titrant for double blank, reagent blank, titrant blank and the interaction of E2 with hERα.

8.4.2 Second ITC Experiment with hERβ

Since the initial experiment with the 50 nM hERα solution did not produce a measurable signal, a single experiment at the maximum concentration of receptor protein achievable was attempted using the available supply of hERβ. The double blank and two each of reagent blank and titrant blank titrations described in Table 8.3 were done before the single E2-hERβ interaction was done. Examples of the raw data obtained for each titration are shown in Figure 8.5. The net heat change is normalized to the concentration of the injected titrant (E2) in the cell after each injection. The results are illustrated in Figure 8.4.

There are indications in Figure 8.6 that a signal may be observed. The increase in observed heat production follows the expected trend, with the lowest amount of heat produced with the buffer into buffer titration and the largest amount of heat produced with E2 into hERβ titration. The increase in heat production between the double blank and reagent blank is due to the presence of 31 mM MeOH; the difference between reagent and titrant blank is due to the presence of 10 μM E2, but the expected pattern (Figure 8.1) is still not observed.

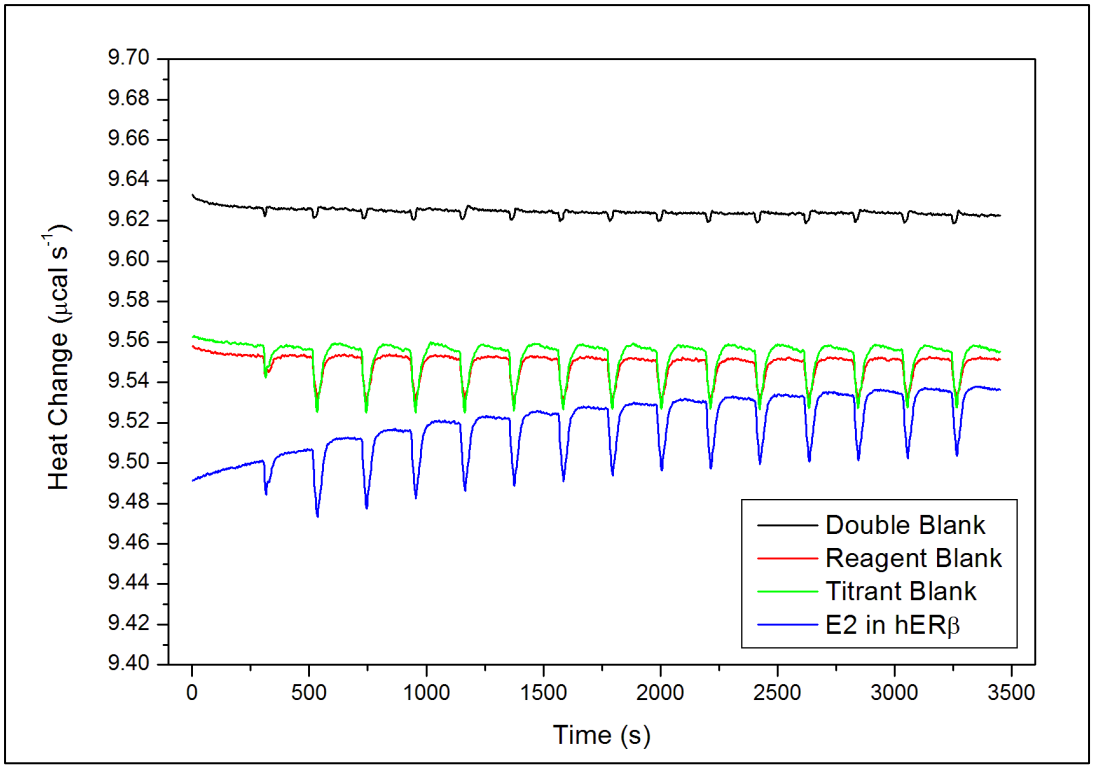

Figure 8.5. The raw ITC data for double blank, reagent blank, titrant blank and the interaction of E2 with hERβ.

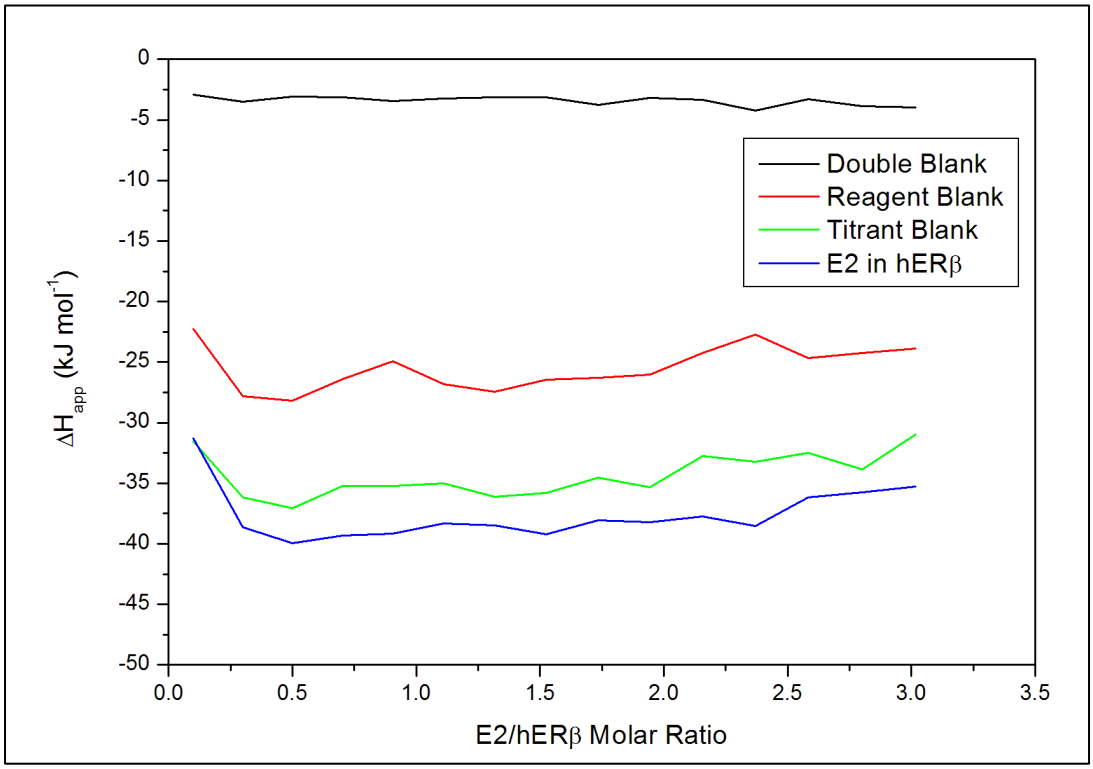

Figure 8.6. Apparent heat change per mol of titrant for double blank, reagent blank, titrant blank and the interaction of E2 with hERα.

8.5 Discussion

ITC is a technique that can be used to measure the heat of reaction such as that evolved or consumed in the binding of a protein and ligand. It was proposed to use this technique to study the heat evolved when E2 or selected environmental estrogens bind with the ER. Initial attempts at measurements with E2 suggested that the heat involved could be quite small. The general methodology suggested in the literature for designing ITC experiments were followed for the initial experiments, but unfortunately these experiments were unsuccessful.

The results suggest that ITC experiments are possible if sufficiently high protein concentration in the reaction cell can be achieved. In contrast to the results shown in Figure 8.4 obtained with a protein concentration of 50 nM, there are measurable differences in the various blank titrations and the interaction titration obtained with a protein concentration of 375 nM and shown in Figure 8.6. The double blank titration gives a very small apparent heat change as would be expected. This difference is mainly due to the temperature difference between the solution in the syringe and the solution in the reaction cell. The increase in apparent heat change for the reagent blank compared to the double blank is due to the MeOH content of the titrant and the heat released on dilution of the MeOH. The small increment between the reagent blank and the titrant blank is due to the presence of E2 and the additional heat released on dilution of E2. The marginal increment in apparent heat change for the titration of E2 into the hERβ solution could be due to any number of factors such as the interaction of MeOH with the protein or binding of E2. Ideally, reagent blank titration into the protein solution would be done to quantify and correct for interactions not due to the binding of E2 and the protein. It is not clear from the results shown in Figure 8.6 whether a curve of the shape shown in Figure 8.1 would emerge with increased protein concentration or whether the molar ratio is not high enough to have reached the point in the curve where the slope increases.

In an effort to identify potential alternate reaction conditions, a simple assessment of the heat expected from the system was undertaken.

For E2 binding with hER, the value for K_A of $2x10^9$ M^{-1} gives a free energy of binding (ΔG_{bind}) of -52 kJ/mol from the equation

$$\Delta G = \Delta H - T\Delta S = -RT \ln K_A$$

Recall from Section 8.2.2 that for E2 binding hER at 25 °C, ΔH accounts for only 37% of ΔG or approximately -20 kJ/mol.

For the first ITC experiment, an active receptor concentration of 50 nM in the measurement cell was achieved. Thus, the amount of protein present in the measurement cell (1.4 mL) is$7x10^{-11}$ mol. This amount of protein would be expected to produce a maximum heat change of 1.4 µJ (-20 kJ/mol x $7x10^{-11}$ mol). This heat change is 10% of the minimum heat change of 15 µJ suggested as a target by the manufacturer. For the second ITC experiment, the protein concentration was 7.5 times greater, producing a maximum heat change of 11 µJ, still below the recommended minimum heat change.

It is possible to do ITC experiments using only the LBD of the ER rather than the full-length protein as demonstrated by Kallen et al.[414].

8.6 Conclusion

These experiments have demonstrated that, for the instrument available, significant quantities of receptor protein are required to study both tight-binding and weak-binding receptor-ligand interactions. The protein concentration is the single most important determinant of the magnitude of the heat signal produced by the reaction and the general methodology presented in the literature can be improved by using what is known about the system (i.e. an estimate of the K_A and either available data or assumptions about the relative contributions of ΔH and ΔS to ΔG) to estimate the magnitude of the heat change produced by the reaction of interest. This estimate of expected heat change could then be compared to the sensitivity of the instrument to determine whether the experiment is likely to be successful under the specific conditions.

The results of the experiments at the highest receptor concentration that was achieved strongly suggest that if sufficient quantities of receptor protein were available, the measurements would be successful.

Chapter 9 Overall Conclusions and Future Directions

9.1 Overall Conclusions

This study had two main objectives:

- Assess human fetal exposure to EEs and estimate the increase in estrogenic load due to this exposure in relation to that from endogenous estrogens
- Consider the biomolecular interaction of the EEs with the hER in an attempt to rationalise the varied and sometimes contradictory observed adverse outcomes that have been hypothesised to result from such exposure.

To achieve the first objective, paired samples of human amniotic fluid and maternal urine were collected from a cohort of 32 New Zealand women following a diagnostic amniocentesis procedure. The required analytical methods were developed and validated for analysis of these samples. The suite of 30 target analytes included 15 compounds determined for the first time in human amniotic fluid and 6 compounds determined for the first time in human urine.

The analytical method developed to determine the EEs in amniotic fluid and urine samples differs from previously published methods (Table 2.3 and Table 2.5) in that it attempts to determine both acidic and phenolic compounds at the same time. This requirement posed several significant challenges that were only partially overcome. The method performed well for determining the acidic phthalate monoesters and phenolic compounds with the exception of the phytoestrogens GEN and DAID. Although the phytoestrogens in urine, amniotic fluid and other matrices have been successfully determined by GC-MS by TMS derivatisation, the published methods [149, 354-359] all employ extensive sample cleanup procedures which would remove both the less polar phenolic analytes as well as the acidic analytes from the sample extract. The method developed in this study worked well for the calibration standards and for the SPE trials with spiked reagent water. The difficulties arose with the analysis of real samples. There are several possible explanations for the poor performance with these analytes. First, incomplete and irreproducible derivatisation of GEN and DAID was observed in the real samples, and to some extent in calibration standards analysed at the same time as the real samples. The sample matrix or even residues remaining adhered to the internal surfaces of the reaction vials after cleaning could be interfering with the derivatisation reaction for these analytes. It is also possible that the derivatives of GEN and DAID were decomposing in the GC inlet due to non-volatile residues deposited in the inlet and at the top of the analytical column.

The results from this study for total concentration of EEs in maternal urine are consistent with other studies representing a range of lifestyles and countries (Figure 6.2). This study is the first to report urine levels of BP-1 and BP-2. Six other target analytes (4t-OP, NP, mOP, mTric, 3PBA and 3PBOH) were included in the analysis but were not detected in any of the samples. For some compounds, e.g. the parabens, the levels from this study are in the higher range of the literature data. The literature data set was assembled from adult urine results and includes both males and non-pregnant females in addition to pregnant females. It is possible that the levels in male urine for some of the ingredients in personal care products are lower than in female urine, because of the differences in the use of these products.

The results from this study for total concentration of EEs in amniotic fluid are consistent with literature values (Figure 6.3). Literature data are available only for the phthalate monoesters, BPA and the phytoestrogens. This study is the first to report levels of parabens, UV filters and triclosan in human amniotic fluid. Six other target analytes (OP, NP, mOP, mTric, 3PBA and 3PBOH) were included in the analysis but were not detected in any of the samples.

The comparison of amniotic fluid levels reported in this study with literature values must be made cautiously. Some of the literature studies may underestimate amniotic fluid concentrations, especially with samples collected in the early 2nd trimester because these results were obtained using only β-glucuronidase deconjugation. As indicated in Chapter 1, the fetal glucuronidation pathway is much less active than the sulphation pathway.

With these results, an assessment methodology was developed to determine whether the levels of EEs found in amniotic fluid were cause for concern. This was done by developing a simple additivity model to estimate relative estrogenic load that included an important interaction mechanism between two endogenous estrogens. This model was used to estimate the proportion of the total estrogenic signal attributable to the EEs and to endogenous estrogens. This model suggested that the estrogenic signal due to EEs could be 36-40% of the total, or in other words, almost as large as the endogenous estrogenic signal. This is definitely a cause for concern, particularly for male fetuses. This assessment was also based on a thorough review of the physiology and metabolism of the maternal-fetal-placental unit, which suggests that once EEs enter the fetal compartment, they become trapped and can be recirculated in the same way as endogenous estrogens. This finding is in contrast to what has previously been assumed [151], that the ‘turnover’ of amniotic fluid facilitates elimination of EEs via the placenta.

The relative estrogenic load model that was developed made use of published information on estrogenic potency of EEs, but was limited in several ways. Ideally, the model would have included the antiestrogenic, androgenic and antiandrogenic potency of the compounds of interest along with their estrogenic potency. This information is not currently available for the enough of the compounds of interest to be included in the model. Additional work is needed to fully characterise the endocrine disrupting potential of these compounds using assays such as those described in Section 2.6.

To achieve the second objective, computational docking was used to investigate the hypothesis put forward in this study that ligand flexibility results in multiple, distinct energy-equivalent receptor-ligand complexes. Should these multiple complexes exist *in vivo*, this would lead to the second hypothesis that these complexes are not be able to interact with the transcription machinery of the target cell in a well-defined and reproducible way to produce a consistent and predictable physiological response in the tissues.

The docking studies of this study show that the rigid endogenous steroid ligands produce a single, well-defined complex with the receptor (hER-E2 complex). This result is well known and demonstrated by published crystal structures of the hER-E2 complex (Table 3.1). The docking studies also show that a single, well-defined hER-ligand complex is formed with ligands that have similar dimensions to E2 but that have limited flexibility such as GEN and DES. Published crystal structures are available for these two ligands (Table 3.1). However, crystal structures have not been published for more flexible ligands such as the EEs. The docking studies show that the flexible EE molecules produce multiple, distinct energy-equivalent complexes (hER-EE complexes). To obtain a solved crystal structure, the individual protein-ligand complexes must be able to come together in a reproducible way to form a crystal. This, in turn, requires each protein-ligand complex in the crystal to have the same 3D orientation of atoms. The inability of the flexible EEs to produce a single, well-defined hER-EE complex was demonstrated with this docking study. These multiple, distinct energy-equivalent complexes, if present in reality, could be the reason published crystal structures do not exist for EEs.

The structural features of the endogenous steroids that are critical in stabilising the hER-E2 complex are the two hydroxyl functionalities (the phenolic A-ring hydroxyl and the aliphatic D-ring hydroxyl) and the 13-CH_3. The role of the two hydroxyl groups has been previously recognised [77], but the importance of the 13-CH_3 in stabilising the topology of the cofactor binding site has not. The two hydroxyls must be separated by a hydrophobic scaffold and

oriented in a specific way to interact effectively with the binding site – to lock it into a well-defined shape. The phenolic A-ring hydroxyl positions the ligand in the binding cavity and serves as the main anchor. The D-ring hydroxyl serves to capture and to orient H11 so that the H12 helix folds over the opening of the ligand binding site, exposing the cofactor binding site. These docking studies have shown that the 13-CH_3 near the D-ring hydroxyl that is oriented in the same direction above the plane of the hydrophobic scaffold as the D-ring hydroxyl serves two subtle but important purposes. This methyl group prevents the binding cavity from collapsing inward onto the ligand as H12 closes over the binding site which in turn stabilises the topology of cofactor binding site located on the external surface of the complex. To quantify the degree of stabilisation, the docking studies demonstrated that the dihedral angle between the backbone carbonyls of the His524/475 and Leu525/476 residues could be used. Because of its well-defined topology, the 'rigid' hER-E2 complex interacts in a predictable way with the cell's transcription machinery. The IFD results indicate that when E2 is docked, this dihedral angle converges to a specific value regardless of the starting conformation of the receptor protein and that this angle is different for hERα and hERβ (21.1° and 16.4° respectively). The degree of convergence decreases with the increase in flexibility of the ligand, suggesting that the hER-EE complexes are more pliable than the hER-E2 complexes; that the flexible ligand is unable to produce a well-defined, rigid complex.

A similar situation was seen with the SERMs, OHT and RAL. These ligands result in rigid, well-defined, but different antagonist conformations of hERα. Slight differences in the topology of the cofactor binding site produced by the specific ligand structures result in the two complexes being able to recruit different cofactors in a given cell type and thus result in different physiological outcomes in the same target tissue. In the uterus, OHT is able to recruit the specific coactivator proteins present in this cell type to achieve gene transcription but RAL is not. In breast cancer cells, both compounds completely block all target gene transcription. This difference in behaviour is attributed to the differences in populations of and the relative concentrations of the cofactors present in the two cell types and the relative ability of the different complexes to recruit these cofactors. This difference in topology is quantified by the different dihedral angles of the complexes: 29.3° for RAL and 32.4° for OHT.

Ligands such as the phytoestrogens (GEN, DAID and COUM) have the two hydroxyl groups but not the 13-CH_3. The absence of the 13-CH_3 along with the fact that both hydroxyls are phenolic allows the ligand to occupy the binding cavity with either phenolic hydroxyl playing the role of

the A-ring. However, the dihedral angles measured for these different ligand poses are quite similar and the calculated binding energies are the same. Thus, some variation in the topology of the cofactor binding site is possible when these ligands are bound. Crystal structures have shown that with hERα, GEN is exclusively an agonist and that with hERβ, GEN can produce complexes with both agonist and antagonist conformations. But, the agonist conformation of hERβ is found only when specific cofactor proteins are present. In other words, the antagonist conformation of the hERβ complex is more energetically favourable than the agonist complex, but the agonist complex can be stabilised in the cell that has the necessary cofactors present in the correct relative abundance. This concept was illustrated in Figure 3.1. These experimental results are reflected in the computational docking results with GEN. The dihedral angle of the hERα-GEN complex is 16.5°, narrower than that of the hERα-E2 complex. The agonist hERβ-GEN complex has a dihedral angle of 18.5°, wider than that of hERβ-E2 and the antagonist conformation hERβ-GEN complex has a dihedral angle of 25.0°, the largest of all hERβ antagonist complexes.

With other, more flexible ligands, computational docking suggests that a larger number of energy-equivalent yet distinct receptor-ligand complexes are possible. These more flexible ligands may or may not have a hydroxyl group capable of playing the role of a D-ring hydroxyl and may or may not have a structure that is capable of supporting the binding cavity in the way the 13-CH_3 does. These ligands are not able to simultaneously interact in all three ways with the binding cavity to stabilise the rigid hER-E2-like topology of the complex. With the hER-EE complexes obtained by IFD, the measured dihedral angles vary significantly while the calculated binding energies are the same. As a result, the hER-EE complexes can be thought of as more pliable or 'floppy' and thus able to respond to the cell context in multiple ways, depending on which of the cofactors are recruited and in what order. The relative abundance of the cofactors may now play a role in how the specific cell responds to the EE. It is therefore possible that the EEs can behave in the same way as pharmaceutical selective modulators, initiating gene transcription in some target cells but not others. It is also possible that the altered topology could influence the selection of which gene is transcribed in a particular target cell by preferentially recruiting one type of cofactor over another.

In addition, for a ligand to be an antagonist in hERα, it requires a large pendant group to act as a wedge to block H12 from closing over the binding site entrance. It also must be able to destabilise the α-helix structure of H11 in the region of His524 and Leu525 to allow the loop and

to extend to permit H12 to occupy the cofactor binding site. In contrast, antagonists of hERβ do not have this wedge feature. Because the antagonist conformation of hERβ may be slightly more energetically favourable than the agonist conformation as illustrated in Figure 3.1, these ligands are able to destabilise H11 sufficiently to spontaneously cause hERβ to adopt the antagonist conformation, without having to also physically block H12 from taking position over the binding cavity. Thus, the docking studies suggest it may be possible for an EE to be either an agonist or antagonist in hERβ but because these ligands do not have a 'wedge' feature, they are only able to act as agonists, albeit weakly, in hERα.

The flexibility of the ligands and their ability to produce pliable receptor-ligand complexes may also explain why exposure to a single compound produces different effects in males and females and produces different effects depending on when during development or life stage the exposure occurs. The adverse effects attributed to fetal exposure (e.g. abnormalities in male genitalia or precocious puberty in females) are very different to those attributed to adult exposure (e.g. reduced fertility, susceptibility to hormone responsive cancers), but it cannot be ruled out that the effects seen in adults do not have a root in fetal exposure.

Finally, combining the range of possible physiological effects of a single EE that are mediated by pliable receptor-ligand complexes, the differential distribution of hERα and hERβ in target tissues and the exposure to changing mixtures of EEs, each of which has a different potential effect profile, it is not surprising that the ability to quantify effects of measured exposures is so elusive.

9.2 Future Directions

Several points that arose during this study remain to be addressed. The first is the importance of completing a confirmation analysis on the urine and amniotic fluid samples. The analytical method developed for this study was not amenable to a few of the compounds, in particular the phytoestrogens genistein and daidzein. These two compounds are expected to contribute a large fraction of the total estrogenicity of the samples. Literature data were used in place of analysis results to complete the exposure assessment and to estimate the relative estrogenic load attributable to EEs. A portion of each sample was archived so that in the event a future opportunity did arise, the dataset could be completed.

Second, the computational docking study required experimental binding energies for comparison. While the data available in the literature was used, the study considered several

ligands that did not have published binding energy data. Two attempts were made to both measure the binding energies for the ligands of interest and to study the kinetics and thermodynamics of ligand binding. The information from these experiments was intended to inform the computational docking study. Although both attempts, one using SPR and the other using ITC, were unsuccessful in producing useful binding data, the SPR and ITC techniques were successfully established and insight was obtained into the approaches needed to make the desired measurements for protein receptors such as hER.

The SPR study was also intended to provide a method to screen biological samples for the total concentration of compounds able to bind to the ER. The results from this study would have been useful in validating the exposure assessment. Both the SPR and ITC experiments would be successful if the capability to produce the required quantities of receptor protein could be established or at least readily accessed.

Third, to further investigate the hypothesis of multiple, distinct, energy equivalent hER-EE complexes, the studies reported in the literature that characterised the behaviour of OHT and RAL in different cell contexts could be undertaken with selected EEs. In particular, the results from such studies obtained for GEN, BPA and NP would be most illuminating, as these ligands represent various points on the spectrum of ligand flexibility.

Finally, the model for estimating relative estrogenic load developed in this study should be extended to complete the assessment of the effects of exposure to environmental estrogenic and androgenic compounds. This will require information on exposure of the fetus to environmental androgens; antiestrogenic, androgenic and antiandrogenic potency data for these compounds; and information on the synergistic or antagonistic effects of simultaneous exposures to environmental estrogens and androgens.

References

1. McDonnell, D.P., et al., *Analysis of estrogen receptor function in vitro reveals three distinct classes of antiestrogens.* Molecular Endocrinology, 1995. **9**(6): p. 659-669.
2. Graham, L.A., *21st Century Chemistry and the Promiscuity of the Sex Hormone Receptors: An Overview*. Chemistry in New Zealand, 2009. **73**(4): p. 143-149.
3. Kidd, K.A., et al., *Collapse of a fish population after exposure to a synthetic estrogen.* Proceedings of the National Academy of Sciences of the United States of America, 2007. **104**(21): p. 8897-8901.
4. Sonnenschein, C. and A.M. Soto, *An updated review of environmental estrogen and androgen mimics and antagonists.* Journal of Steroid Biochemistry and Molecular Biology, 1998. **65**(1-6): p. 143-150.
5. Sharara, F.I., D.B. Seifer, and J.A. Flaws, *Environmental toxicants and female reproduction.* Fertility and Sterility, 1998. **70**(4): p. 613-622.
6. Welshons, W.V., et al., *Large effects from small exposures. I. Mechanisms for endocrine-disrupting chemicals with estrogenic activity.* Environmental Health Perspectives, 2003. **111**(8): p. 994-1006.
7. Vidaeff, A.C. and L.E. Sever, *In utero exposure to environmental estrogens and male reproductive health: a systematic review of biological and epidemiologic evidence.* Reproductive Toxicology, 2005. **20**(1): p. 5-20.
8. Maffini, M.V., et al., *Endocrine disruptors and reproductive health: The case of bisphenol-A.* Molecular and Cellular Endocrinology, 2006. **254-255**: p. 179-186.
9. Welshons, W.V., S.C. Nagel, and F.S. vom Saal, *Large Effects from Small Exposures. III. Endocrine Mechanisms Mediating Effects of Bisphenol A at Levels of Human Exposure.* Endocrinology, 2006. **147**(6): p. s56-69.
10. Fernandez, M.F., et al., *Human exposure to endocrine-disrupting chemicals and prenatal risk factors for cryptorchidism and hypospadias: a nested case-control study.* Environmental Health Perspectives, 2007. **115 Suppl 1**: p. 8-14.
11. Martin, O.V., et al., *Testicular Dysgenesis Syndrome and the Estrogen Hypothesis: A Quantitative Meta-Analysis.* Environ Health Perspect, 2007. **116**(2).
12. Meeker, J.D., *Exposure to environmental endocrine disrupting compounds and men's health.* Maturitas, 2010. **In Press, Corrected Proof**.
13. Diamanti-Kandarakis, E., et al., *Endocrine-Disrupting Chemicals: An Endocrine Society Scientific Statement.* Endocrine Reviews, 2009. **30**(4): p. 293-342.
14. Wogan, G.N., *Molecular epidemiology in cancer risk assessment and prevention: recent progress and avenues for future research.* Environ Health Perspect, 1992. **98**.
15. Baccarelli, A. and V. Bollati, *Epigenetics and environmental chemicals.* Current Opinion in Pediatrics, 2009. **21**(2): p. 243-251 10.1097/MOP.0b013e32832925cc.
16. Perera, F. and J. Herbstman, *Prenatal environmental exposures, epigenetics, and disease.* Reproductive Toxicology, 2011. **31**(3): p. 363-373.
17. Jirtle, R.L. and M.K. Skinner, *Environmental epigenomics and disease susceptibility.* Nature Reviews Genetics, 2007. **8**(4): p. 253-262.
18. Anway, M.D., et al., *Epigenetic Transgenerational Actions of Endocrine Disruptors and Male Fertility.* Science, 2005. **308**(5727): p. 1466-1469.
19. Naz, R.K., ed. *Endocrine Disruptors - Effects on Male and Female Reproductive Systems*. 2nd ed. 2004, CRC Press.
20. McLachlan, J.A., E. Simpson, and M. Martin, *Endocrine disrupters and female reproductive health.* Best Practice & Research Clinical Endocrinology & Metabolism, 2006. **20**(1): p. 63-75.
21. Ariazi, E.A. and V.C. Jordan, *Estrogen-Related Receptors as Emerging Targets in Cancer and Metabolic Disorders.* Current Topics in Medicinal Chemistry, 2006. **6**: p. 203-215.
22. Soto, A.M., et al., *Does breast cancer start in the womb?* Basic & Clinical Pharmacology & Toxicology, 2008. **102**(2): p. 125-133.
23. Den Hond, E., et al., *Endocrine disrupters and human puberty.* International Journal of Andrology, 2006. **29**(1): p. 264-271.
24. Rogan, W.J. and N.B. Ragan, *Evidence of effects of environmental chemicals on the endocrine system in children.* Pediatrics, 2003. **112**(1 Pt 2): p. 247-52.
25. Herman-Giddens, M.E., *Recent data on pubertal milestones in United States children: The secular trend toward earlier development.* International Journal of Andrology, 2006. **29**(1): p. 241-246.
26. Swan, S.H., E.P. Elkin, and L. Fenster, *The question of declining sperm density revisited: an analysis of 101 studies published 1934-1996.* Environmental Health Perspectives, 2000. **108**(10): p. 961-6.
27. Swan, S.H., *Does our environment affect our fertility? Some examples to help reframe the question.* Seminars in Reproductive Medicine, 2006. **24**(3): p. 142-6.

28. Cecconi, S., et al., *The effects of the endocrine disruptors dithiocarbamates on the mammalian ovary with particular regard to mancozeb.* Current Pharmaceutical Design, 2007. **13**(29): p. 2989-3004.
29. Newbold, R.R., et al., *Effects of endocrine disruptors on obesity.* International Journal of Andrology, 2008. **31**(2): p. 201-207.
30. Newbold, R.R., et al., *Perinatal exposure to environmental estrogens and the development of obesity.* Molecular Nutrition and Food Research, 2007. **51**(7): p. 912-917.
31. Grün, F. and B. Blumberg, *Endocrine disrupters as obesogens.* Molecular and Cellular Endocrinology, 2009. **304**(1-2): p. 19-29.
32. Charboneau, J.P. and S.M. Koger, *Plastics, pesticides and PBDEs: Endocrine disruption and developmental disabilities.* Journal of Developmental and Physical Disabilities, 2008. **20**(2): p. 115-128.
33. Gioiosa, L., et al., *Developmental exposure to low-dose estrogenic endocrine disruptors alters sex differences in exploration and emotional responses in mice.* Hormones and Behavior, 2007. **52**(3): p. 307-316.
34. Faass, O., et al., *Female sexual behavior, estrous cycle and gene expression in sexually dimorphic brain regions after pre- and postnatal exposure to endocrine active UV filters.* Neurotoxicology, 2009. **30**(2): p. 249-260.
35. Enmark, E. and J.A. Gustafsson, *Oestrogen receptors - an overview.* Journal of Internal Medicine, 1999. **246**(2): p. 133-138.
36. Jensen, E.V. and E.R. DeSombre, *Estrogen-Receptor Interaction.* Science, 1973. **182**(4108): p. 126-134.
37. Nilsson, S. and J.-Ã.k. Gustafsson, *Biological Role of Estrogen and Estrogen Receptors.* Critical Reviews in Biochemistry and Molecular Biology, 2002. **37**(1): p. 1 - 28.
38. Nilsson, S., et al., *Mechanisms of Estrogen Action.* Physiological Reviews, 2001. **81**(4): p. 1535-1565.
39. Evans, R.M., *The Steroid and Thyroid Hormone Receptor Superfamily.* Science, 1988. **240**(4854): p. 889-895.
40. Weihua, Z., et al., *Update on estrogen signaling.* FEBS Letters, 2003. **546**(1): p. 17-24.
41. Couse, J.F., et al., *Tissue Distribution and Quantitative Analysis of Estrogen Receptor-{alpha} (ER{alpha}) and Estrogen Receptor-{beta} (ER{beta}) Messenger Ribonucleic Acid in the Wild-Type and ER{alpha}-Knockout Mouse.* Endocrinology, 1997. **138**(11): p. 4613-4621.
42. Couse, J.F. and K.S. Korach, *Estrogen Receptor Null Mice: What Have We Learned and Where Will They Lead Us?* Endocrine Reviews, 1999. **20**(3): p. 358-417.
43. Gustafsson, J.A., *Estrogen receptor beta--a new dimension in estrogen mechanism of action.* Journal of Endocrinology, 1999. **163**(3): p. 379-383.
44. Ying, C., et al., *Estrogen receptor is expressed in pig embryos during preimplantation development.* Molecular Reproduction and Development, 2000. **55**(1): p. 83-88.
45. Weiser, M.J., C.D. Foradori, and R.J. Handa, *Estrogen receptor beta in the brain: From form to function.* Brain Research Reviews, 2008. **57**(2): p. 309-320.
46. Henley, D.V. and K.S. Korach, *Endocrine-Disrupting Chemicals Use Distinct Mechanisms of Action to Modulate Endocrine System Function.* Endocrinology, 2006. **147**(6): p. s25-s32.
47. Hall, J.M. and D.P. McDonnell, *The Estrogen Receptor {beta}-Isoform (ER{beta}) of the Human Estrogen Receptor Modulates ER{alpha} Transcriptional Activity and Is a Key Regulator of the Cellular Response to Estrogens and Antiestrogens.* Endocrinology, 1999. **140**(12): p. 5566-5578.
48. Lindberg, M.K., et al., *Estrogen Receptor (ER)-{beta} Reduces ER{alpha}-Regulated Gene Transcription, Supporting a "Ying Yang" Relationship between ER{alpha} and ER{beta} in Mice.* Molecular Endocrinology, 2003. **17**(2): p. 203-208.
49. Tang, S., et al., *KBERG: KnowledgeBase for Estrogen Responsive Genes.* Nucleic Acids Research, 2007. **35**: p. D732–D736.
50. Kuiper, G.G.J.M., et al., *The Estrogen Receptor [beta] Subtype: A Novel Mediator of Estrogen Action in Neuroendocrine Systems.* Frontiers in Neuroendocrinology, 1998. **19**(4): p. 253-286.
51. Fowler, P.A., et al., *Development of Steroid Signaling Pathways during Primordial Follicle Formation in the Human Fetal Ovary.* Journal of Clinical Endocrinology & Metabolism, 2011. **96**(6): p. 1754-1762.
52. van de Beek, C., et al., *Relationships between sex hormones assessed in amniotic fluid, and maternal and umbilical cord serum: What is the best source of information to investigate the effects of fetal hormonal exposure?* Hormones and Behavior, 2004. **46**(5): p. 663-669.
53. Nagel, S.C. and F.S. vom Saal, *Endocrine control of sexual differentiation: effects of the maternal-fetal environment and endocrine disrupting chemicals*, in *Advances in Molecular and Cell Biology*, B. Edward, Editor. 2004, Elsevier. p. 15-37.

54. Déchaud, H., et al., *Xenoestrogen interaction with human sex hormone-binding globulin (hSHBG)1.* Steroids, 1999. **64**(5): p. 328-334.
55. Shutt, D.A., I.D. Smith, and R.P. Shearman, *Oestrone, Oestradiol-17β and Oestriol Levels in Human Foetal Plasma During Gestation and at Term.* Journal of Endocrinology, 1974. **60**(2): p. 333-341.
56. Styne, D.M., *Pediatric Endocrinology*. Core Handbooks in Pediatrics. 2004: Lippincott Williams & Wilkins. 372.
57. Baker, V.A., *Endocrine disrupters -- testing strategies to assess human hazard.* Toxicology in Vitro. **15**(4-5): p. 413-419.
58. Safe, S.H., *Endocrine disruptors and human health - Is there a problem? An update.* Environmental Health Perspectives, 2000. **108**(6): p. 487-493.
59. Witorsch, R.J., *Low-dose in utero effects of xenoestrogens in mice and their relevance to humans: an analytical review of the literature.* Food and Chemical Toxicology, 2002. **40**(7): p. 905-912.
60. Bromer, J.G., et al., *Bisphenol-A exposure in utero leads to epigenetic alterations in the developmental programming of uterine estrogen response.* The FASEB Journal, 2010. **24**(7): p. 2273-2280.
61. Zama, A.M. and M. Uzumcu, *Fetal and Neonatal Exposure to the Endocrine Disruptor Methoxychlor Causes Epigenetic Alterations in Adult Ovarian Genes.* Endocrinology, 2009. **150**(10): p. 4681-4691.
62. Koohi, M.K., N. Walther, and R. Ivell, *A novel molecular assay to discriminate transcriptional effects caused by xenoestrogens.* Molecular and Cellular Endocrinology, 2007. **276**(1-2): p. 45-54.
63. Guillette, L.J., Jr., *Endocrine Disrupting Contaminants—Beyond the Dogma.* Environ Health Perspect, 2005. **114**(S-1).
64. Ariazi, E.A., et al., *Estrogen Receptors as Therapeutic Targets in Breast Cancer.* Current Topics in Medicinal Chemistry, 2006. **6**: p. 181-202.
65. Ascenzi, P., A. Bocedi, and M. Marino, *Structure-function relationship of estrogen receptor [alpha] and [beta]: Impact on human health.* Molecular Aspects of Medicine, 2006. **27**(4): p. 299-402.
66. Jensen, E.V., Proceedings of the Fourth International Congress of Biochemistry, Vienna, 1958. **15**: p. 119.
67. Green, S., et al., *Human oestrogen receptor cDNA: sequence, expression and homology to v-erb-A.* Nature, 1986. **320**(6058): p. 134-139.
68. Mosselman, S., J. Polman, and R. Dijkema, *ER[beta]: Identification and characterization of a novel human estrogen receptor.* FEBS Letters, 1996. **392**(1): p. 49-53.
69. Kuiper, G.G.J.M., et al., *Cloning of a Novel Estrogen Receptor Expressed in Rat Prostate and Ovary.* Proceedings of the National Academy of Sciences of the United States of America, 1996. **93**(12): p. 5925-5930.
70. Hall, J.M. and D.P. McDonnell, *Coregulators in Nuclear Estrogen Receptor Action.* Molecular Interventions, 2005. **5**(6): p. 343-357.
71. Cozzini, P. and T. Dottorini, *Is it possible docking and scoring new ligands with few experimental data? Preliminary results on estrogen receptor as a case study.* European Journal of Medicinal Chemistry, 2004. **39**(7): p. 601-609.
72. Tzukerman, M.T., et al., *Human estrogen receptor transactivational capacity is determined by both cellular and promoter context and mediated by two functionally distinct intramolecular regions.* Molecular Endocrinology, 1994. **8**(1): p. 21-30.
73. Muramatsu, M. and S. Inoue, *Estrogen Receptors: How Do They Control Reproductive and Nonreproductive Functions?* Biochemical and Biophysical Research Communications, 2000. **270**(1): p. 1-10.
74. Paech, K., et al., *Differential Ligand Activation of Estrogen Receptors ER{alpha} and ER at AP1 Sites.* Science, 1997. **277**(5331): p. 1508-1510.
75. Lambrinidis, G., et al., *The estrogen receptor and polyphenols: molecular simulation studies of their interactions, a review.* Environmental Chemistry Letters, 2006. **4**(3): p. 159-174.
76. Jordan, V.C., *Antiestrogens and Selective Estrogen Receptor Modulators as Multifunctional Medicines. 2. Clinical Considerations and New Agents.* Journal of Medicinal Chemistry, 2003. **46**(7): p. 1081-1111.
77. Brzozowski, A.M., et al., *Molecular basis of agonism and antagonism in the oestrogen receptor.* Nature, 1997. **389**(6652): p. 753-758.
78. Pike, A.C., et al., *Structure of the ligand-binding domain of oestrogen receptor beta in the presence of a partial agonist and a full antagonist.* EMBO Journal, 1999. **18**(17): p. 4608-18.
79. Manas, E.S., et al., *Structure-Based Design of Estrogen Receptor-B Selective Ligands.* Journal of the American Chemical Society, 2004. **126**(46): p. 15106-15119.
80. Feng, W., et al., *Hormone-Dependent Coactivator Binding to a Hydrophobic Cleft on Nuclear Receptors.* Science, 1998. **280**(5370): p. 1747-1749.

81. Shiau, A.K., et al., *The Structural Basis of Estrogen Receptor/Coactivator Recognition and the Antagonism of This Interaction by Tamoxifen.* Cell, 1998. **95**(7): p. 927-937.
82. Heery, D.M., et al., *A signature motif in transcriptional co-activators mediates binding to nuclear receptors.* Nature, 1997. **387**(6634): p. 733-736.
83. Fawell, S.E., et al., *Characterization and colocalization of steroid binding and dimerization activities in the mouse estrogen receptor.* Cell, 1990. **60**(6): p. 953.
84. Lees, J.A., et al., *A 22-amino-acid peptide restores DNA-binding activity to dimerization-defective mutants of the estrogen receptor.* Molecular and Cellular Biology, 1990. **10**(10): p. 5529-5531.
85. Nettles, K., et al., *NF-κB selectivity of estrogen receptor ligands revealed by comparative crystallographic analyses.* Nature Chemical Biology, 2008. **4**: p. 241.
86. Latchman, D.S., *Transcription factors: An overview.* The International Journal of Biochemistry & Cell Biology, 1997. **29**(12): p. 1305-1312.
87. Gronemeyer, H., J.-A. Gustafsson, and V. Laudet, *Principles for modulation of the nuclear receptor superfamily.* Nature Reviews Drug Discovery, 2004. **3**(11): p. 950-964.
88. Paige, L.A., et al., *Estrogen receptor (ER) modulators each induce distinct conformational changes in ER α and ER β.* Proceedings of the National Academy of Sciences, 1999. **96**(7): p. 3999-4004.
89. Grainger, D.J. and J.C. Metcalfe, *Tamoxifen: Teaching an old drug new tricks?* Nature Medicine, 1996. **2**(4): p. 381-385.
90. Shang, Y. and M. Brown, *Molecular Determinants for the Tissue Specificity of SERMs.* Science, 2002. **295**(5564): p. 2465-2468.
91. Smith, C.L. and B.W. O'Malley, *Coregulator Function: A Key to Understanding Tissue Specificity of Selective Receptor Modulators.* Endocrine Review, 2004. **25**(1): p. 45-71.
92. Johnson, S.M., et al., *Ishikawa cells exhibit differential gene expression profiles in response to oestradiol or 4-hydroxytamoxifen.* Endocrine-Related Cancer, 2007. **14**(2): p. 337-350.
93. McDonnell, D.P., *The Molecular Pharmacology of SERMs.* Trends in Endocrinology and Metabolism, 1999. **10**(8): p. 301-311.
94. Chadwick, C.C., et al., *Identification of pathway-selective estrogen receptor ligands that inhibit NF-κB transcriptional activity.* Proceedings of the National Academy of Sciences of the United States of America, 2005. **102**(7): p. 2543-2548.
95. Turgeon, J.L., et al., *Hormone Therapy: Physiological Complexity Belies Therapeutic Simplicity.* Science, 2004. **304**(5675): p. 1269-1273.
96. Pryor, J.L., et al., *Critical windows of exposure for children's health: The reproductive system in animals and humans.* Environmental Health Perspectives, 2000. **108**(SUPPL. 3): p. 491-503.
97. Safe, S. and S. Papineni, *The role of xenoestrogenic compounds in the development of breast cancer.* Trends in Pharmacological Sciences, 2006. **27**(8): p. 447-454.
98. Helferich, W.G., J.E. Andrade, and M.S. Hoagland, *Phytoestrogens and breast cancer: A complex story.* Inflammopharmacology, 2008. **16**(5): p. 219-226.
99. Foster, W.G., et al., *Human developmental exposure to endocrine active compounds.* Environmental Toxicology and Pharmacology, 2002. **12**(2): p. 75-81.
100. Iguchi, T., et al., *Developmental toxicity of estrogenic chemicals on rodents and other species.* Congenital Anomalies, 2002. **42**(2): p. 94-105.
101. Weiss, B., *Endocrine Disruptors as a Factor in Mental Retardation.* International Review of Research in Mental Retardation, 2005. **30**: p. 195-223.
102. Hakkola, J., et al., *Xenobiotic-Metabolizing Cytochrome P450 Enzymes in the Human Feto-Placental Unit: Role in Intrauterine Toxicity.* Critical Reviews in Toxicology, 1998. **28**(1): p. 35-72.
103. Taguchi, O., G.R. Cunha, and S.J. Robboy, *Expression of nuclear estrogen-binding sites within developing human fetal vagina and urogenital sinus.* American Journal of Anatomy, 1986. **177**(4): p. 473-480.
104. Brandenberger, A.W., et al., *Tissue Distribution of Estrogen Receptors Alpha (ER-α) and Beta (ER-β) mRNA in the Midgestational Human Fetus.* Journal of Clinical Endocrinology & Metabolism, 1997. **82**(10): p. 3509-3512.
105. Arbuckle, T.E., *Are there sex and gender differences in acute exposure to chemicals in the same setting?* Environmental Research, 2006. **101**(2): p. 195-204.
106. Sakuma, T., et al., *Sex Differences of Drug-metabolizing Enzyme: Female Predominant Expression of Human and Mouse Cytochrome P450 3A Isoforms.* Journal of Health Science, 2009. **55**(3): p. 325-337.
107. Tomicic, C., et al., *Sex differences in urinary levels of several biological indicators of exposure: A human volunteer study.* Toxicology Letters, 2011. **202**(3): p. 218-225.
108. Strauss, J.F., F. Martinez, and M. Kiriakidou, *Placental steroid hormone synthesis: unique features and unanswered questions.* Biology of Reproduction, 1996. **54**(2): p. 303-311.

109. Young, A.M., C.E. Allen, and K.L. Audus, *Efflux transporters of the human placenta.* Advanced Drug Delivery Reviews, 2003. **55**(1): p. 125-132.
110. Garland, M., et al., *Fetal morphine metabolism and clearance are constant during late gestation.* Drug Metabolism and Disposition, 2006. **34**(4): p. 636-646.
111. Müller, S., P. Schmid, and C. Schlatter, *Evaluation of the estrogenic potency of nonylphenol in non-occupationally exposed humans.* Environmental Toxicology and Pharmacology, 1998. **6**(1): p. 27-33.
112. Waring, R.H., et al., *Phytoestrogens and xenoestrogens: The contribution of diet and environment to endocrine disruption.* The Journal of Steroid Biochemistry and Molecular Biology, 2008. **108**(3-5): p. 213-220.
113. Allmyr, M., et al., *The influence of age and gender on triclosan concentrations in Australian human blood serum.* Science of The Total Environment, 2008. **393**(1): p. 162-167.
114. Dayan, A.D., *Risk assessment of triclosan [Irgasan®] in human breast milk.* Food and Chemical Toxicology, 2007. **45**(1): p. 125-129.
115. Allmyr, M., et al., *Triclosan in plasma and milk from Swedish nursing mothers and their exposure via personal care products.* Science of The Total Environment, 2006. **372**(1): p. 87-93.
116. Janjua, N.R., et al., *Systemic Absorption of the Sunscreens Benzophenone-3, Octyl-Methoxycinnamate, and 3-(4-Methyl-Benzylidene) Camphor After Whole-Body Topical Application and Reproductive Hormone Levels in Humans.* J Investig Dermatol, 2004. **123**(1): p. 57-61.
117. Darbre, P.D. and P.W. Harvey, *Paraben esters: review of recent studies of endocrine toxicity, absorption, esterase and human exposure, and discussion of potential human health risks.* Journal of Applied Toxicology, 2008. **28**(5): p. 561-578.
118. Chedgzoy, P., G. Winckle, and C.M. Heard, *Triclosan: release from transdermal adhesive formulations and in vitro permeation across human epidermal membranes.* International Journal of Pharmaceutics, 2002. **235**(1-2): p. 229-236.
119. Hayden, C.G.J., M.S. Roberts, and H.A.E. Benson, *Systemic absorption of sunscreen after topical application.* The Lancet, 1997. **350**(9081): p. 863-864.
120. Rudel, R.A. and L.J. Perovich, *Endocrine disrupting chemicals in indoor and outdoor air.* Atmospheric Environment, 2009. **43**(1): p. 170-181.
121. Zalko, D., et al., *In Vivo Metabolic Fate of the Xeno-Estrogen 4-n-Nonylphenol in Wistar Rats.* Drug Metabolism and Disposition, 2003. **31**(2): p. 168-178.
122. Parkinson, A. and B.W. Olgivie, *Biotransformation of Xenobiotics*, in *Casarett and Doull's Toxicology The Basic Science of Poisons 7th Edition*, C.D. Klaassen, Editor. 2008, McGraw Hill Medical: New York. p. 161-304.
123. Garland, M., et al., *The contribution of fetal metabolism to the disposition of morphine.* Drug Metabolism and Disposition, 2005. **33**(1): p. 68-76.
124. de Wildt, S.N., et al., *Glucuronidation in Humans: Pharmacogenetic and Developmental Aspects.* Clinical Pharmacokinetics, 1999. **36**(6): p. 439-452.
125. Coughtrie, M.W.H., *Sulfation through the looking glass--recent advances in sulfotransferase research for the curious.* The Pharmacogenomics Journal, 2002. **2**(5): p. 297-297-308.
126. Taylor, J.A., et al., *Similarity of Bisphenol A Pharmacokinetics in Rhesus Monkeys and Mice: Relevance for Human Exposure.* Environmental Health Perspectives, 2010. **119**(4).
127. Schonfelder, G., et al., *Parent Bisphenol A Accumulation in the Human Maternal-Fetal-Placental Unit.* Environmental Health Perspectives, 2002. **110**(11): p. A703-A707.
128. Stowell, C.L., et al., *A Role for Sulfation-Desulfation in the Uptake of Bisphenol A into Breast Tumor Cells.* Chemistry and Biology, 2006. **13**(8): p. 891-897.
129. Silva, M.J., et al., *Metabolite profiles of Di-n-butyl phthalate in humans and rats.* Environmental Science and Technology, 2007. **41**(21): p. 7576-7580.
130. Silva, M.J., et al., *Detection of phthalate metabolites in human amniotic fluid.* Bulletin of Environmental Contamination and Toxicology, 2004. **72**(6): p. 1226-1231.
131. Müller, S., P. Schmid, and C. Schlatter, *Pharmacokinetic behavior of 4-nonylphenol in humans.* Environmental Toxicology and Pharmacology, 1998. **5**(4): p. 257-265.
132. Pedersen, R.T. and E.M. Hill, *Identification of novel metabolites of the xenoestrogen 4-tert-octylphenol in primary rat hepatocytes.* Chemico-Biological Interactions, 2000. **128**(3): p. 189-209.
133. *2 Final Report on the Safety Assessment of Benzophenones-1, 3, 4, 5, 9, and 11.* International Journal of Toxicology, 1983. **2**(5): p. 35-77.
134. Schreurs, R., et al., *Estrogenic activity of UV filters determined by an in vitro reporter gene assay and an in vivo transgenic zebrafish assay.* Archives of Toxicology, 2002. **76**(5): p. 257-261.
135. Ye, X., et al., *Parabens as urinary biomarkers of exposure in humans.* Environmental Health Perspectives, 2006. **114**: p. 1843-1846.

136. Sandborgh-Englund, G., et al., *Pharmacokinetics of Triclosan Following Oral Ingestion in Humans.* Journal of Toxicology and Environmental Health, Part A, 2006. **69**(20): p. 1861-1873.
137. Soucy, N.V., et al., *Kinetics of genistein and its conjugated metabolites in pregnant Sprague-Dawley rats following single and repeated genistein administration.* Toxicological Sciences, 2006. **90**(1): p. 230-240.
138. Zhu, B.T. and A.H. Conney, *Functional role of estrogen metabolism in target cells: review and perspectives.* Carcinogenesis, 1998. **19**(1): p. 1-27.
139. Huang, P.-C., et al., *Association between prenatal exposure to phthalates and the health of newborns.* Environment International, 2009. **35**: p. 14-20.
140. Ye, X., et al., *Temporal stability of the conjugated species of bisphenol A, parabens, and other environmental phenols in human urine.* Journal of Exposure Science and Environmental Epidemiology, 2007. **17**(6): p. 567-572.
141. Calafat, A.M., et al., *Urinary concentrations of bisphenol A and 4-Nonylphenol in a human reference population.* Environmental Health Perspectives, 2005. **113**(4): p. 391-395.
142. Swan, S.H., et al., *Decrease in anogenital distance among male infants with prenatal phthalate exposure.* Environmental Health Perspectives, 2005. **113**(8): p. 1056-61.
143. Liu, Z., M.S. Wolff, and J. Moline, *Analysis of environmental biomarkers in urine using an electrochemical detector.* Journal of Chromatography B, 2005. **819**(1): p. 155-159.
144. Valentin-Blasini, L., et al., *Urinary and serum concentrations of seven phytoestrogens in a human reference population subset.* Journal of Exposure Analysis and Environmental Epidemiology, 2003. **13**(4): p. 276.
145. Kato, K., et al., *Determination of 16 Phthalate Metabolites in Urine Using Automated Sample Preparation and On-line Preconcentration/High-Performance Liquid Chromatography/Tandem Mass Spectrometry.* Analytical Chemistry, 2005. **77**(9): p. 2985-2991.
146. Blount, B.C., et al., *Levels of seven urinary phthalate metabolites in a human reference population.* Environmental Health Perspectives, 2000. **108**(10): p. 979-982.
147. Wolff, M.S., et al., *Prenatal phenol and phthalate exposures and birth outcomes.* Environmental Health Perspectives, 2008. **116**(8): p. 1092-1097.
148. Choi, M.H., et al., *Determination of non-steroidal estrogens in breast milk, plasma, urine and hair by gas chromatography/mass spectrometry.* Rapid Communications in Mass Spectrometry, 2002. **16**(24): p. 2221-2228.
149. Moors, S., et al., *Simultaneous determination of daidzein, equol, genistein and bisphenol A in human urine by a fast and simple method using SPE and GC-MS.* Molecular Nutrition and Food Research, 2007. **51**(7): p. 787-798.
150. Grace, P.B., et al., *Quantification of isoflavones and lignans in urine using gas chromatography/mass spectrometry.* Analytical Biochemistry, 2003. **315**(1): p. 114-121.
151. Wittassek, M., et al., *Fetal exposure to phthalates - a pilot study.* International Journal of Hygiene and Environmental Health, 2009. **212**(5): p. 492-498.
152. Barr, D.B., A. Bishop, and L.L. Needham, *Concentrations of xenobiotic chemicals in the maternal-fetal unit.* Reproductive Toxicology, 2007. **23**(3): p. 260-266.
153. Myllynen, P., M. Pasanen, and O. Pelkonen, *Human placenta: a human organ for developmental toxicology research and biomonitoring.* Placenta, 2005. **26**(5): p. 361-371.
154. Collier, A.C., et al., *Assisted reproduction technologies impair placental steroid metabolism.* Journal of Steroid Biochemistry and Molecular Biology, 2009. **116**(1-2): p. 21-28.
155. James, M.O., et al., *Triclosan is a potent inhibitor of estradiol and estrone sulfonation in sheep placenta.* Environment International, 2010. **In Press, Corrected Proof**.
156. Prusakiewicz, J.J., et al., *Parabens inhibit human skin estrogen sulfotransferase activity: Possible link to paraben estrogenic effects.* Toxicology, 2007. **232**(3): p. 248-256.
157. Harris, R.M., et al., *Sulfation of "Estrogenic" Alkylphenols and 17β-Estradiol by Human Platelet Phenol Sulfotransferases.* Journal of Biological Chemistry, 2000. **275**(1): p. 159-166.
158. Harris, R.M., et al., *Phytoestrogens Are Potent Inhibitors of Estrogen Sulfation: Implications for Breast Cancer Risk and Treatment.* Journal of Clinical Endocrinology & Metabolism, 2004. **89**(4): p. 1779-1787.
159. Kunert-Keil, C., et al., *Deconjugating Enzymes; Sulphatases and Glucuronidases*, in *Enzyme Systems that Metabolise Drugs and Other Xenobiotics*. 2002, John Wiley & Sons, Ltd. p. 521-554.
160. Ikeda, Y., et al., *Metabolism of bisphenol A in the rat syncytiotrophoblast cell line, TR-TBT 18d-1.* Journal of Health Science, 2007. **53**(1): p. 146-150.
161. Syme, M.R., J.W. Paxton, and J.A. Keelan, *Drug transfer and metabolism by the human placenta.* Clinical Pharmacokinetics, 2004. **43**(8): p. 487(28).

162. Gude, N.M., et al., *Growth and function of the normal human placenta.* Thrombosis Research, 2004. **114**(5-6): p. 397-407.
163. Vähäkangas, K. and P. Myllynen, *Drug transporters in the human blood-placental barrier.* British Journal of Pharmacology, 2009. **158**(3): p. 665-678.
164. Endres, C.J., et al., *The role of transporters in drug interactions.* European Journal of Pharmaceutical Sciences, 2006. **27**(5): p. 501-517.
165. van der Aa, E.M., et al., *Mechanisms of drug transfer across the human placenta.* Pharmacy World & Science, 1998. **20**(4): p. 139-148.
166. Unadkat, J.D., A. Dahlin, and S. Vijay, *Placental Drug Transporters.* Current Drug Metabolism, 2004. **5**(1): p. 125-131.
167. Ganapathy, V., et al., *Placental Transporters Relevant to Drug Distribution across the Maternal-Fetal Interface.* Journal of Pharmacology and Experimental Therapeutics, 2000. **294**(2): p. 413-420.
168. Balakrishnan, B., et al., *Transfer of bisphenol A across the human placenta.* American Journal of Obstetrics and Gynecology, 2010. **202**(4): p. 393.e1-393.e7.
169. Balakrishnan, B., et al., *Passage of 4-nonylphenol across the human placenta.* Placenta, 2011. **32**(10): p. 788-792.
170. Balakrishnan, B., et al., *Transplacental Transfer and Biotransformation of Genistein in Human Placenta.* Placenta, 2010. **31**(6): p. 506-511.
171. Nishikawa, M., et al., *Placental transfer of conjugated bisphenol A and subsequent reactivation in the rat fetus.* Environmental Health Perspectives, 2010. **118**(9): p. 1196-1203.
172. Underwood, M.A., W.M. Gilbert, and M.P. Sherman, *Amniotic Fluid: Not Just Fetal Urine Anymore.* Journal of Perinatology, 2005. **25**(5): p. 341-341-8.
173. Cho, C.K.J., et al., *Proteomics analysis of human amniotic fluid.* Molecular and Cellular Proteomics, 2007. **6**(8): p. 1406-1415.
174. Campbell, J., et al., *Biochemical composition of amniotic fluid and extraembryonic coelomic fluid in the first trimester of pregnancy.* British Journal of Obstetrics and Gynaecology, 1992. **99**(7): p. 563-565.
175. Bonsnes, R.W., *Composition of amniotic fluid.* Clinical Obstetrics and Gynecology, 1966. **9**(2): p. 440-448.
176. Pearson Murphy, B.E., *The absorption by the human fetus of intra-amniotically injected cortisol.* Journal of Steroid Biochemistry, 1982. **16**(3): p. 415-417.
177. Hardman, M.J., et al., *Barrier Formation in the Human Fetus is Patterned.* Journal of Investigative Dermatology, 1999. **113**(6): p. 1106-1113.
178. Modena, A.B. and S. Fieni, *Amniotic fluid dynamics.* Acta Bio Medica Ateneo Parmense, 2004. **75**(S1): p. 11-13.
179. Foster, W.G., et al., *Detection of phytoestrogens in samples of second trimester human amniotic fluid.* Toxicology Letters, 2002. **129**(3): p. 199-205.
180. Yamada, H., et al., *Maternal serum and amniotic fluid bisphenol A concentrations in the early second trimester.* Reproductive Toxicology, 2002. **16**(6): p. 735-739.
181. Matsumoto, J., H. Yokota, and A. Yuasa, *Developmental Increases in Rat Hepatic Microsomal UDP-Glucuronosyltransferase Activities toward Xenoestrogens and Decreases during Pregnancy.* Environmental Health Perspectives, 2002. **110**(2).
182. Juchau, M.R., S.T. Chao, and C.J. Omiecinski, *Drug Metabolism by the Human Fetus.* Clinical Pharmacokinetics, 1980. **5**(4): p. 320-339.
183. Suiko, M., Y. Sakakibara, and M.-C. Liu, *Sulfation of Environmental Estrogen-like Chemicals by Human Cytosolic Sulfotransferases.* Biochemical and Biophysical Research Communications, 2000. **267**(1): p. 80-84.
184. Oesterheld, J.R., *A review of developmental aspects of cytochrome P450.* Journal of Child and Adolescent Psychopharmacology, 1998. **8**(3): p. 161-174.
185. Jirsová, V., et al., *β-Glucuronidase Activity in Different Organs of Human Fetuses.* Neonatology, 1965. **8**(1): p. 23-29.
186. Heringová, A., et al., *Sulfatase Activity in Placenta, Liver and Small Intestine of Human Fetuses.* Neonatology, 1969. **14**(5-6): p. 265-269.
187. Guillemette, C., et al., *Differential Regulation of Two Uridine Diphospho-Glucuronosyltransferases, UGT2B15 and UGT2B17, in Human Prostate LNCaP Cells.* Endocrinology, 1997. **138**(7): p. 2998-3005.
188. Hanioka, N., et al., *Suppression of male-specific cytochrome P450 isoforms by bisphenol A in rat liver.* Archives of Toxicology, 1998. **72**(7): p. 387-394.
189. Hanioka, N., et al., *Interaction of bisphenol a with rat hepatic cytochrome P450 enzymes.* Chemosphere, 2000. **41**(7): p. 973-978.

190. Engel, S.M., et al., *Xenobiotic phenols in early pregnancy amniotic fluid.* Reproductive Toxicology, 2006. **21**(1): p. 110-112.
191. Ikezuki, Y., et al., *Determination of bisphenol A concentrations in human biological fluids reveals significant early prenatal exposure.* Human Reproduction, 2002. **17**(11): p. 2839-2841.
192. Chen, M., et al., *Determination of bisphenol-A levels in human amniotic fluid samples by liquid chromatography coupled with mass spectrometry.* Journal of Separation Science, 2011. **34**(14): p. 1648-1655.
193. Adlercreutz, H., et al., *Maternal and neonatal phytoestrogens in Japanese women during birth.* American Journal of Obstetrics and Gynecology, 1999. **180**(3 I): p. 737-743.
194. Legler, J., et al., *Detection of estrogenic activity in sediment-associated compounds using in vitro reporter gene assays.* Science of The Total Environment, 2002. **293**(1-3): p. 69-83.
195. Zacharewski, *In Vitro Bioassays for Assessing Estrogenic Substances.* Environmental Science & Technology, 1997. **31**(3): p. 613-623.
196. Leskinen, P., et al., *Bioluminescent yeast assays for detecting estrogenic and androgenic activity in different matrices.* Chemosphere, 2005. **61**(2): p. 259-266.
197. Legler, J., et al., *Development of a stably transfected estrogen receptor-mediated luciferase reporter gene assay in the human T47D breast cancer cell line.* Toxicological Sciences, 1999. **48**(1): p. 55-66.
198. Schreurs, R.H.M.M., et al., *Interaction of Polycyclic Musks and UV Filters with the Estrogen Receptor (ER), Androgen Receptor (AR), and Progesterone Receptor (PR) in Reporter Gene Bioassays.* Toxicological Sciences, 2005. **83**(2): p. 264-272.
199. Shaw, L.E., et al., *Changes in oestrogen receptor-[alpha] and -[beta] during progression to acquired resistance to tamoxifen and fulvestrant (Faslodex, ICI 182,780) in MCF7 human breast cancer cells.* The Journal of Steroid Biochemistry and Molecular Biology, 2006. **99**(1): p. 19-32.
200. Horwitz, K.B., M.E. Costlow, and W.L. McGuire, *MCF-7: A human breast cancer cell line with estrogen, androgen, progesterone, and glucocorticoid receptors.* Steroids, 1975. **26**(6): p. 785-795.
201. Inoue, A., et al., *Comparative profiling of the gene expression for estrogen responsiveness in cultured human cell lines.* Toxicology in Vitro, 2007. **21**(4): p. 741-752.
202. Gray, L.E., et al., *Xenoendocrine disrupters-tiered screening and testing Filling key data gaps.* Toxicology, 2002. **181**: p. 371-382.
203. Miller, D., et al., *Estrogenic Activity of Phenolic Additives Determined By an <italic>In Vitro</italic> Yeast Bioassay.* Environ Health Perspect, 2001. **109**(2).
204. Pugazhendhi, D., G.S. Pope, and P.D. Darbre, *Oestrogenic activity of p-hydroxybenzoic acid (common metabolite of paraben esters) and methylparaben in human breast cancer cell lines.* Journal of Applied Toxicology, 2005. **25**(4): p. 301-309.
205. Pugazhendhi, D., A.J. Sadler, and P.D. Darbre, *Comparison of the global gene expression profiles produced by methylparaben, n-butylparaben and 17β-oestradiol in MCF7 human breast cancer cells.* Journal of Applied Toxicology, 2007. **27**(1): p. 67-77.
206. Byford, J.R., et al., *Oestrogenic activity of parabens in MCF7 human breast cancer cells.* The Journal of Steroid Biochemistry and Molecular Biology, 2002. **80**(1): p. 49-60.
207. Darbre, P.D., *Environmental oestrogens, cosmetics and breast cancer.* Best Practice & Research Clinical Endocrinology & Metabolism, 2006. **20**(1): p. 121-143.
208. Lemini, C., et al., *In vivo and in vitro estrogen bioactivities of alkyl parabens.* Toxicology and Industrial Health, 2003. **19**(2-6): p. 69-79.
209. Routledge, E.J., et al., *Some Alkyl Hydroxy Benzoate Preservatives (Parabens) Are Estrogenic.* Toxicology and Applied Pharmacology, 1998. **153**(1): p. 12-19.
210. van Meeuwen, J.A., et al., *Aromatase inhibiting and combined estrogenic effects of parabens and estrogenic effects of other additives in cosmetics.* Toxicology and Applied Pharmacology, 2008. **230**(3): p. 372-382.
211. Okubo, T., et al., *ER-dependent estrogenic activity of parabens assessed by proliferation of human breast cancer MCF-7 cells and expression of ER[alpha] and PR.* Food and Chemical Toxicology, 2001. **39**(12): p. 1225-1232.
212. Chen, J., et al., *Antiandrogenic properties of parabens and other phenolic containing small molecules in personal care products.* Toxicology and Applied Pharmacology, 2007. **221**(3): p. 278-284.
213. Gee, R.H., et al., *Oestrogenic and androgenic activity of triclosan in breast cancer cells.* Journal of Applied Toxicology, 2008. **28**(1): p. 78-91.
214. Schweizer, H.P., *Triclosan: a widely used biocide and its link to antibiotics.* FEMS Microbiology Letters, 2001. **202**(1): p. 1-7.
215. Svobodová, K., et al., *Estrogenic and androgenic activity of PCBs, their chlorinated metabolites and other endocrine disruptors estimated with two in vitro yeast assays.* Science of The Total Environment, 2009. **407**(22): p. 5921-5925.

216. Ahn, K., et al., *In Vitro Biologic Activities of the Antimicrobials Triclocarban, Its Analogs, and Triclosan in Bioassay Screens: Receptor-Based Bioassay Screens.* Environmental Health Perspectives, 2008. **116**(9): p. 1203.
217. Liu, B., et al., *Triclosan inhibits enoyl-reductase of type I fatty acid synthase in vitro and is cytotoxic to MCF-7 and SKBr-3 breast cancer cells.* Cancer Chemotherapy and Pharmacology, 2002. **49**(3): p. 187-193.
218. DeLorenzo, M.E., et al., *Toxicity of the antimicrobial compound triclosan and formation of the metabolite methyl-triclosan in estuarine systems.* Environmental Toxicology, 2008. **23**(2): p. 224-232.
219. Canosa, P., et al., *Optimization of solid-phase microextraction conditions for the determination of triclosan and possible related compounds in water samples.* Journal of Chromatography A, 2005. **1072**(1): p. 107-115.
220. Hsieh, M.H., et al., *In Utero Exposure to Benzophenone-2 Causes Hypospadias Through an Estrogen Receptor Dependent Mechanism.* Journal of Urology, 2007. **178**(4 SUPPLEMENT): p. 1637-1642.
221. Schlumpf, M., et al., *Endocrine activity and developmental toxicity of cosmetic UV filters--an update.* Toxicology, 2004. **205**(1-2): p. 113-122.
222. Kunz, P.Y. and K. Fent, *Estrogenic activity of UV filter mixtures.* Toxicology and Applied Pharmacology, 2006. **217**(1): p. 86-99.
223. Schultz, T.W., J.R. Seward, and G.D. Sinks, *Estrogenicity of benzophenones evaluated with a recombinant yeast assay: Comparison of experimental and rules-based predicted activity.* Environmental Toxicology and Chemistry, 2000. **19**(2): p. 301-304.
224. Heneweer, M., et al., *Additive estrogenic effects of mixtures of frequently used UV filters on pS2-gene transcription in MCF-7 cells.* Toxicology and Applied Pharmacology, 2005. **208**(2): p. 170-177.
225. Gaido, K.W., et al., *Interaction of Methoxychlor and Related Compounds with Estrogen Receptor α and β, and Androgen Receptor: Structure-Activity Studies.* Molecular Pharmacology, 2000. **58**(4): p. 852-858.
226. Xu, H., W.L. Kraus, and M.L. Shuler, *Development of a stable dual cell-line GFP expression system to study estrogenic endocrine disruptors.* Biotechnology and Bioengineering, 2008. **101**(6): p. 1276-1287.
227. ter Veld, M.G.R., et al., *Estrogenic Potency of Food-Packaging-Associated Plasticizers and Antioxidants As Detected in ERα and ERβ Reporter Gene Cell Lines.* Journal of Agricultural and Food Chemistry, 2006. **54**(12): p. 4407-4416.
228. Olsen, C.M., et al., *Effects of the Environmental Oestrogens Bisphenol A, Tetrachlorobisphenol A, Tetrabromobisphenol A, 4-Hydroxybiphenyl and 4,4â€²-Dihydroxybiphenyl on Oestrogen Receptor Binding, Cell Proliferation and Regulation of Oestrogen Sensitive Proteins.* Pharmacology & Toxicology, 2003. **92**(4): p. 180-188.
229. Lee, H.J., et al., *Antiandrogenic Effects of Bisphenol A and Nonylphenol on the Function of Androgen Receptor.* Toxicological Sciences, 2003. **75**(1): p. 40-46.
230. Nishikawa, J.-i., et al., *New Screening Methods for Chemicals with Hormonal Activities Using Interaction of Nuclear Hormone Receptor with Coactivator.* Toxicology and Applied Pharmacology, 1999. **154**(1): p. 76-83.
231. Folmar, L.C., et al., *A comparison of the estrogenic potencies of estradiol, ethynylestradiol, diethylstilbestrol, nonylphenol and methoxychlor in vivo and in vitro.* Aquatic Toxicology, 2002. **60**(1-2): p. 101-110.
232. Routledge, E.J. and J.P. Sumpter, *Estrogenic Activity of surfactants and some of their degradation products assessed using a recombinant yeast screen.* Environmental Toxicology and Chemistry, 1996. **15**: p. 241-248.
233. McCarthy, A.R., et al., *Estrogenicity of pyrethroid insecticide metabolites.* Journal of Environmental Monitoring, 2006. **8**(1): p. 197-202.
234. Clewell, R.A., et al., *Kinetics of selected di-n-butyl phthalate metabolites and fetal testosterone following repeated and single administration in pregnant rats.* Toxicology, 2009. **255**(1-2): p. 80-90.
235. Takeuchi, S., et al., *Differential effects of phthalate esters on transcriptional activities via human estrogen receptors [alpha] and [beta], and androgen receptor.* Toxicology, 2005. **210**(2-3): p. 223-233.
236. Lottrup, G., et al., *Possible impact of phthalates on infant reproductive health.* International Journal of Andrology, 2006. **29**(1): p. 172-180.
237. Culty, M., et al., *In utero exposure to di-(2-ethylhexyl) phthalate exerts both short-term and long-lasting suppressive effects on testosterone production in the rat.* Biology of Reproduction, 2008. **78**(6): p. 1018-1028.
238. Morito, K., et al., *Interaction of Phytoestrogens with Estrogen Receptors Alpha and Beta.* Biological & Pharmaceutical Bulletin, 2001. **24**(4): p. 351-356.

239. Kinjo, J., et al., *Interactions of Phytoestrogens with Estrogen Receptors Alpha and Beta (III).Estrogenic Activities of Soy Isoflavone Aglycones and Their Metabolites Isolated from Human Urine.* Biological & Pharmaceutical Bulletin, 2004. **27**(2): p. 185-188.
240. Pugazhendhi, D., et al., *Effect of sulphation on the oestrogen agonist activity of the phytoestrogens genistein and daidzein in MCF-7 human breast cancer cells.* Journal of Endocrinology, 2008. **197**(3): p. 503-515.
241. Setchell, K.D., *Phytoestrogens: the biochemistry, physiology, and implications for human health of soy isoflavones.* The American Journal of Clinical Nutrition, 1998. **68**(6): p. 1333S-1346S.
242. Thompson, L.U., et al., *Phytoestrogen Content of Foods Consumed in Canada, Including Isoflavones, Lignans, and Coumestan.* Nutrition and Cancer, 2006. **54**(2): p. 184-201.
243. Coward, L., et al., *Genistein, daidzein, and their .beta.-glycoside conjugates: antitumor isoflavones in soybean foods from American and Asian diets.* Journal of Agricultural and Food Chemistry, 1993. **41**(11): p. 1961-1967.
244. Alves, R.C., et al., *Isoflavones in Coffee: Influence of Species, Roast Degree, and Brewing Method.* Journal of Agricultural and Food Chemistry, 2010. **58**(5): p. 3002-3007.
245. Kayisli, U.A., et al., *Estrogenicity of isoflavones on human endometrial stromal and glandular cells.* Journal of Clinical Endocrinology and Metabolism, 2002. **87**(12): p. 5539-5544.
246. Wang, C. and M.S. Kurzer, *Phytoestrogen concentration determines effects on DNA synthesis in human breast cancer cells.* Nutrition and Cancer, 1997. **28**(3): p. 236 - 247.
247. Timms, B.G., et al., *Estrogenic chemicals in plastic and oral contraceptives disrupt development of the fetal mouse prostate and urethra.* Proceedings of the National Academy of Sciences of the United States of America, 2005. **102**(19): p. 7014-7019.
248. Brucker-Davis, F., K. Thayer, and T. Colborn, *Significant effects of mild endogenous hormonal changes in humans: Considerations for low-dose testing.* Environmental Health Perspectives, 2001. **109**(SUPPL. 1): p. 21-26.
249. Rajapakse, N., E. Silva, and A. Kortenkamp, *Combining xenoestrogens at levels below individual no-observed-effect concentrations dramatically enhances steroid hormone action.* Environmental Health Perspectives, 2002. **110**(9): p. 917-921.
250. Melamed, M., et al., *Molecular and Kinetic Basis for the Mixed Agonist/Antagonist Activity of Estriol.* Molecular Endocrinology, 1997. **11**(12): p. 1868-1878.
251. Filby, A.L., et al., *Health impacts of estrogens in the environment, considering complex mixture effects.* Environmental Health Perspectives, 2007. **115**(12): p. 1704-1710.
252. Kortenkamp, A., *Introduction: endocrine disruptors-exposure assessment, novel end points, and low-dose and mixture effects.* Environmental Health Perspectives, 2007. **115 Suppl 1**: p. 7.
253. Kortenkamp, A., *Low dose mixture effects of endocrine disrupters: Implications for risk assessment and epidemiology.* International Journal of Andrology, 2008. **31**(2): p. 233-237.
254. Kortenkamp, A., et al., *Low-level exposure to multiple chemicals: reason for human health concerns?* Environmental Health Perspectives, 2007. **115 Suppl 1**: p. 106-114.
255. Payne, J., et al., *Prediction and assessment of the effects of mixtures of four xenoestrogens.* Environmental Health Perspectives, 2000. **108**(10): p. 983-987.
256. Kortenkamp, A., *Ten years of mixing cocktails: a review of combination effects of endocrine-disrupting chemicals.* Environmental Health Perspectives, 2007. **115 Suppl 1**: p. 98-105.
257. Manas, E.S., et al., *Understanding the Selectivity of Genistein for Human Estrogen Receptor-[beta] Using X-Ray Crystallography and Computational Methods.* Structure, 2004. **12**(12): p. 2197-2207.
258. Larson, C.J., et al., *Peptide Binding Identifies an ERα Conformation That Generates Selective Activity in Multiple In Vitro Assays.* Journal of Biomolecular Screening, 2005. **10**(6): p. 590-598.
259. Gangloff, M., et al., *Crystal Structure of a Mutant hERα Ligand-binding Domain Reveals Key Structural Features for the Mechanism of Partial Agonism.* Journal of Biological Chemistry, 2001. **276**(18): p. 15059-15065.
260. Moras, D. and H. Gronemeyer, *The nuclear receptor ligand-binding domain: structure and function.* Current Opinion in Cell Biology, 1998. **10**(3): p. 384-391.
261. Barkhem, T., et al., *Differential Response of Estrogen Receptor alpha and Estrogen Receptor beta to Partial Estrogen Agonists/Antagonists.* Molecular Pharmacology, 1998. **54**(1): p. 105-112.
262. Shiau, A.K., et al., *Structural characterization of a subtype-selective ligand reveals a novel mode of estrogen receptor antagonism.* Nature Structural Biology, 2002. **9**(5): p. 359-364.
263. Oostenbrink, B.C., et al., *Simulations of the Estrogen Receptor Ligand-Binding Domain: Affinity of Natural Ligands and Xenoestrogens.* Journal of Medicinal Chemistry, 2000. **43**(24): p. 4594-4605.
264. Sousa, S.F., P.A. Fernandes, and M.J. Ramos, *Protein–ligand docking: Current status and future challenges.* Proteins: Structure, Function, and Bioinformatics, 2006. **65**(1): p. 15-26.

265. Knox, A.J.S., M.J. Meegan, and D.G. Lloyd, *Estrogen Receptors: Molecular Interactions, Virtual Screening and Future Prospects.* Current Topics in Medicinal Chemistry, 2006. **6**: p. 217-243.
266. Knox, A.J.S., et al., *Target specific virtual screening: Optimization of an estrogen receptor screening platform.* Journal of Medicinal Chemistry, 2007. **50**(22): p. 5301-5310.
267. Knox, A.J.S., et al., *Virtual screening of the estrogen receptor.* Expert Opinion on Drug Discovery, 2008. **3**(8): p. 853-866.
268. Roncaglioni, A. and E. Benfenati, *Computer-aided methodologies to predict endocrine-disrupting potency of chemicals*, in *Endocrine Disrupting Chemicals in Food*, I.C. Shaw, Editor. 2009, Woodhead Publishing Ltd.: Cambridge, UK. p. 306-321.
269. Amadasi, A., et al., *Identification of Xenoestrogens in Food Additives by an Integrated in Silico and in Vitro Approach.* Chemical Research in Toxicology, 2008. **22**(1): p. 52-63.
270. Yang, W.H., et al., *Exploring the binding features of polybrominated diphenyl ethers as estrogen receptor antagonists: docking studies.* SAR and QSAR in Environmental Research, 2010. **21**(3): p. 351 - 367.
271. D'Ursi, P., et al., *Modelling the interaction of steroid receptors with endocrine disrupting chemicals.* BMC Bioinformatics, 2005. **6**(SUPPL.4).
272. Celik, L., J.D.D. Lund, and B. SchiÃ¸tt, *Exploring interactions of endocrine-disrupting compounds with different conformations of the human estrogen receptor Î± ligand binding domain: A molecular docking study.* Chemical Research in Toxicology, 2008. **21**(11): p. 2195-2206.
273. van Lipzig, M.M.H., et al., *Prediction of Ligand Binding Affinity and Orientation of Xenoestrogens to the Estrogen Receptor by Molecular Dynamics Simulations and the Linear Interaction Energy Method.* Journal of Medicinal Chemistry, 2004. **47**(4): p. 1018-1030.
274. Sivanesan, D., et al., *In-silico Screening using Flexible Ligand Binding Pockets: A Molecular Dynamics-based Approach.* Journal of Computer-Aided Molecular Design, 2005. **19**(4): p. 213-228.
275. Zeng, J., et al., *Insights into ligand selectivity in estrogen receptor isoforms: Molecular dynamics simulations and binding free energy calculations.* Journal of Physical Chemistry B, 2008. **112**(9): p. 2719-2726.
276. Fischer, E., *Einfluss der Configuration auf die Wirkung der Enzyme.* Berichte der Deutschen Chemischen Gesellschaft, 1894. **27**: p. 2985.
277. Koshland, D.E., *Application of a Theory of Enzyme Specificity to Protein Synthesis.* Proceedings of the National Academy of Sciences of the United States of America, 1958. **44**(2): p. 98-104.
278. Guimarães, C.R.W. and M. Cardozo, *MM-GB/SA Rescoring of Docking Poses in Structure-Based Lead Optimization.* Journal of Chemical Information and Modeling, 2008. **48**(5): p. 958-970.
279. Yoon, S. and W.J. Welsh, *Identification of a Minimal Subset of Receptor Conformations for Improved Multiple Conformation Docking and Two-Step Scoring.* Journal of Chemical Information and Computer Sciences, 2004. **44**(1): p. 88-96.
280. Lyne, P.D., M.L. Lamb, and J.C. Saeh, *Accurate prediction of the relative potencies of members of a series of kinase inhibitors using molecular docking and MM-GBSA scoring.* Journal of Medicinal Chemistry, 2006. **49**(16): p. 4805-4808.
281. Teodoro, M.L. and L.E. Kavraki, *Conformational Flexibility Models for the Receptor in Structure Based Drug Design.* Current Pharmaceutical Design, 2003. **9**: p. 1635.
282. Hattotuwagama, C.K., M.N. Davies, and D.R. Flower, *Receptor-Ligand binding sites and virtual screening.* Current Medicinal Chemistry, 2006. **13**(11): p. 1283-1304.
283. Sherman, W., et al., *Novel Procedure for Modeling Ligand/Receptor Induced Fit Effects.* Journal of Medicinal Chemistry, 2006. **49**(2): p. 534-553.
284. Guimarães, C.R.W. and A.M. Mathiowetz, *Addressing Limitations with the MM-GB/SA Scoring Procedure using the WaterMap Method and Free Energy Perturbation Calculations.* Journal of Chemical Information and Modeling, 2010. **50**(4): p. 547-559.
285. Schulz-Gasch, T. and M. Stahl, *Scoring functions for protein-ligand interactions: A critical perspective.* Drug Discovery Today: Technologies, 2004. **1**(3): p. 231-239.
286. Kellenberger, E., et al., *Comparative evaluation of eight docking tools for docking and virtual screening accuracy.* Proteins: Structure, Function and Genetics, 2004. **57**(2): p. 225-242.
287. www.pdb.org. Berman, H.M., et al., *The Protein Data Bank.* Nucleic Acids Research, 2000. **28**(1): p. 235-242.
288. Tanenbaum, D.M., et al., *Crystallographic comparison of the estrogen and progesterone receptor's ligand binding domains.* Proceedings of the National Academy of Sciences of the United States of America, 1998. **95**(11): p. 5998-6003.
289. Nettles, K.W., et al., *Structural plasticity in the oestrogen receptor ligand-binding domain.* EMBO Reports, 2007. **8**(6): p. 563.

290. Blizzard, T.A., et al., *Estrogen receptor ligands. Part 9: Dihydrobenzoxathiin SERAMs with alkyl substituted pyrrolidine side chains and linkers.* Bioorganic & Medicinal Chemistry Letters, 2005. **15**(1): p. 107-113.
291. Möcklinghoff, S., et al., *Synthesis and Crystal Structure of a Phosphorylated Estrogen Receptor Ligand Binding Domain.* ChemBioChem, 2010. **11**(16): p. 2251-2254.
292. Norman, B.H., et al., *Benzopyrans as selective estrogen receptor [beta] agonists (SERBAs). Part 4: Functionalization of the benzopyran A-ring.* Bioorganic & Medicinal Chemistry Letters, 2007. **17**(18): p. 5082-5085.
293. Richardson, T.I., et al., *Benzopyrans as selective estrogen receptor [beta] agonists (SERBAs). Part 5: Combined A- and C-ring structure-activity relationship studies.* Bioorganic & Medicinal Chemistry Letters, 2007. **17**(20): p. 5563-5566.
294. Wang, Y., et al., *A second binding site for hydroxytamoxifen within the coactivator-binding groove of estrogen receptor β.* Proceedings of the National Academy of Sciences, 2006. **103**(26): p. 9908-9911.
295. Cheng, Y.-C. and W.H. Prusoff, *Relationship between the inhibition constant (KI) and the concentration of inhibitor which causes 50 per cent inhibition (I50) of an enzymatic reaction.* Biochemical Pharmacology, 1973. **22**(23): p. 3099-3108.
296. Englebienne, P. and N. Moitessier, *Docking ligands into flexible and solvated macromolecules. 4. Are popular scoring functions accurate for this class of proteins?* Journal of Chemical Information and Modeling, 2009. **49**(6): p. 1568-1580.
297. Cheng, T., et al., *Comparative assessment of scoring functions on a diverse test set.* Journal of Chemical Information and Modeling, 2009. **49**(4): p. 1079-1093.
298. Repasky, M.P., M. Shelley, and R.A. Friesner, *Flexible ligand docking with Glide.* Current protocols in bioinformatics / editoral board, Andreas D. Baxevanis ... [et al.], 2007. **Chapter 8**.
299. Perola, E., W.P. Walters, and P.S. Charifson, *A detailed comparison of current docking and scoring methods on systems of pharmaceutical relevance.* Proteins: Structure, Function and Genetics, 2004. **56**(2): p. 235-249.
300. Halgren, T.A., et al., *Glide: A New Approach for Rapid, Accurate Docking and Scoring. 2. Enrichment Factors in Database Screening.* Journal of Medicinal Chemistry, 2004. **47**(7): p. 1750-1759.
301. *Glide 3.5 Technical Notes*. 2005: Schrödinger Press.
302. Adlercreutz, H., et al., *Isotope dilution gas chromatographic-mass spectrometric method for the determination of unconjugated lignans and isoflavonoids in human feces, with preliminary results in omnivorous and vegetarian women.* Analytical Biochemistry, 1995. **225**(1): p. 101-108.
303. Setchell, K.D.R., et al., *S-Equol, a potent ligand for estrogen receptor {beta}, is the exclusive enantiomeric form of the soy isoflavone metabolite produced by human intestinal bacterial flora.* American Journal of Clinical Nutrition, 2005. **81**(5): p. 1072-1079.
304. Muthyala, R.S., et al., *Equol, a natural estrogenic metabolite from soy isoflavones: convenient preparation and resolution of R- and S-equols and their differing binding and biological activity through estrogen receptors alpha and beta.* Bioorganic & Medicinal Chemistry, 2004. **12**(6): p. 1559-1567.
305. *Glide 5.0 User Manual*. 2008: Schrodinger Press.
306. Mulholland, A., *Chemical accuracy in QM/MM calculations on enzyme-catalysed reactions.* Chemistry Central Journal, 2007. **1**(1): p. 19.
307. Bash, P.A., et al., *Progress toward chemical accuracy in the computer simulation of condensed phase reactions.* Proceedings of the National Academy of Sciences, 1996. **93**(8): p. 3698-3703.
308. Friesner, R.A., et al., *Glide: A New Approach for Rapid, Accurate Docking and Scoring. 1. Method and Assessment of Docking Accuracy.* Journal of Medicinal Chemistry, 2004. **47**(7): p. 1739-1749.
309. Friesner, R.A., et al., *Extra precision glide: Docking and scoring incorporating a model of hydrophobic enclosure for protein-ligand complexes.* Journal of Medicinal Chemistry, 2006. **49**(21): p. 6177-6196.
310. Kekenes-Huskey, P.M., et al., *A molecular docking study of estrogenically active compounds with 1,2-diarylethane and 1,2-diarylethene pharmacophores.* Bioorganic & Medicinal Chemistry, 2004. **12**(24): p. 6527-6537.
311. Sippl, W., *Binding affinity prediction of novel estrogen receptor ligands using receptor-based 3-D QSAR methods.* Bioorganic & Medicinal Chemistry, 2002. **10**(12): p. 3741-3755.
312. Sippl, W., *Receptor-based 3D QSAR analysis of estrogen receptor ligands - Merging the accuracy of receptor-based alignments with the computational efficiency of ligand-based methods.* Journal of Computer-Aided Molecular Design, 2000. **14**(6): p. 559-572.
313. Zhizhong, W., et al., *In Silico Prediction of Estrogen Receptor Subtype Binding Affinity and Selectivity Using Statistical Methods and Molecular Docking with 2-Arylnaphthalenes and 2-Arylquinolines.* International Journal of Molecular Sciences, 2010. **11**: p. 3434-3458.

314. Vedani, A., M. Dobler, and M.A. Lill, *Combining protein modeling and 6D-QSAR. Simulating the binding of structurally diverse ligands to the estrogen receptor.* Journal of Medicinal Chemistry, 2005. **48**(11): p. 3700-3703.
315. Sugiyama, H., et al., *Insight into estrogenicity of phytoestrogens using in silico simulation.* Biochemical and Biophysical Research Communications, 2009. **379**(1): p. 139-144.
316. Nose, T., T. Tokunaga, and Y. Shimohigashi, *Exploration of endocrine-disrupting chemicals on estrogen receptor Î± by the agonist/antagonist differential-docking screening (AADS) method: 4-(1-Adamantyl)phenol as a potent endocrine disruptor candidate.* Toxicology Letters, 2009. **191**(1): p. 33-39.
317. Valentin-Blasini, L., et al., *HPLC-MS/MS method for the measurement of seven phytoestrogens in human serum and urine.* Journal of Exposure Analysis and Environmental Epidemiology, 2000. **10**(S1): p. 799.
318. Dirtu, A.C., et al., *Simultaneous determination of bisphenol A, triclosan, and tetrabromobisphenol A in human serum using solid-phase extraction and gas chromatography-electron capture negative-ionization mass spectrometry.* Analytical and Bioanalytical Chemistry, 2008. **391**(4): p. 1175-1181.
319. Sajiki, J., K. Takahashi, and J. Yonekubo, *Sensitive method for the determination of bisphenol-A in serum using two systems of high-performance liquid chromatography.* Journal of Chromatography B: Biomedical Sciences and Applications, 1999. **736**(1-2): p. 255-261.
320. Ye, X., et al., *Quantification of the urinary concentrations of parabens in humans by on-line solid phase extraction-high performance liquid chromatography-isotope dilution tandem mass spectrometry.* Journal of Chromatography B, 2006. **844**(1): p. 53-59.
321. Ye, X., et al., *Automated on-line column-switching HPLC-MS/MS method for measuring environmental phenols and parabens in serum.* Talanta, 2008. **76**(4): p. 865-871.
322. León, Z., et al., *Solid-phase extraction liquid chromatography-tandem mass spectrometry analytical method for the determination of 2-hydroxy-4-methoxybenzophenone and its metabolites in both human urine and semen.* Analytical and Bioanalytical Chemistry, 2010. **398**(2): p. 831-843.
323. Blount, B.C., et al., *Quantitative detection of eight phthalate metabolites in human urine using HPLC-APCI-MS/MS.* Analytical Chemistry, 2000. **72**(17): p. 4127-4134.
324. Teitelbaum, S.L., et al., *Temporal variability in urinary concentrations of phthalate metabolites, phytoestrogens and phenols among minority children in the United States.* Environmental Research, 2008. **106**(2): p. 257-269.
325. *Oasis Sample Extraction Products*, Waters Corp., 2011.
326. Chambaz, E.M. and E.C. Horning, *Conversion of steroids to trimethylsilyl derivatives for gas phase analytical studies: Reactions of silylating reagents.* Analytical Biochemistry, 1969. **30**(1): p. 7-24.
327. Knapp, D.R., *Handbook of Analytical Derivatisation Reactions*. 1979, New York: John Wiley & Sons.
328. Little, J.L., *Artifacts in trimethylsilyl derivatization reactions and ways to avoid them.* Journal of Chromatography A, 1999. **844**(1-2): p. 1-22.
329. Halket, J.M. and V.G. Zaikin, *Derivatization in mass spectrometry - 1. Silylation.* European Journal of Mass Spectrometry, 2003. **9**(1): p. 1-21.
330. *Silylating Agents*, Fluka Chemie AG, 1995.
331. Roth, C.A., *Silylation of Organic Chemicals.* Product R&D, 1972. **11**(2): p. 134-139.
332. Shareef, A., et al., *Suitability of N,O-bis(trimethylsilyl)trifluoroacetamide and N-(tert-butyldimethylsilyl)-N-methyltrifluoroacetamide as derivatization reagents for the determination of the estrogens estrone and 17[alpha]-ethinylestradiol by gas chromatography-mass spectrometry.* Journal of Chromatography A, 2004. **1026**(1-2): p. 295-300.
333. Shareef, A., M.J. Angove, and J.D. Wells, *Optimization of silylation using N-methyl-N-(trimethylsilyl)-trifluoroacetamide, N,O-bis-(trimethylsilyl)-trifluoroacetamide and N-(tert-butyldimethylsilyl)-N-methyltrifluoroacetamide for the determination of the estrogens estrone and 17Î±-ethinylestradiol by gas chromatography-mass spectrometry.* Journal of Chromatography A, 2006. **1108**(1): p. 121-128.
334. Zhang, Z.L., A. Hibberd, and J.L. Zhou, *Optimisation of derivatisation for the analysis of estrogenic compounds in water by solid-phase extraction gas chromatography-mass spectrometry.* Analytica Chimica Acta, 2006. **577**(1): p. 52-61.
335. Zhou, Y.-q., Z.-j. Wang, and N. Jia, *Formation of multiple trimethylsilyl derivatives in the derivatization of 17α-ethinylestradiol with BSTFA or MSTFA followed by gas chromatography-mass spectrometry determination.* Journal of Environmental Sciences, 2007. **19**(7): p. 879-884.
336. Huang, B., et al., *New discoveries of heating effect on trimethylsilyl derivatization for simultaneous determination of steroid endocrine disrupting chemicals by GC-MS.* Chromatographia, 2010. **71**(1-2): p. 149-153.
337. Meunier-Solère, V., et al., *Pitfalls in trimethylsilylation of anabolic steroids: New derivatisation approach for residue at ultra-trace level.* Journal of Chromatography B, 2005. **816**(1-2): p. 281-288.

338. Bowden, J.A., et al., *Enhancement of chemical derivatization of steroids by gas chromatography/mass spectrometry (GC/MS).* Journal of Chromatography B, 2009. **877**(27): p. 3237-3242.
339. Marques, M.A.S., et al., *Analysis of synthetic 19-norsteroids trenbolone, tetrahydrogestrinone and gestrinone by gas chromatography-mass spectrometry.* Journal of Chromatography A, 2007. **1150**(1-2): p. 215-225.
340. Fang, K., et al., *Simultaneous Derivatization of Hydroxyl and Ketone Groups for the Analysis of Steroid Hormones by GC–MS.* Chromatographia, 2010. **72**(9): p. 949-956.
341. Kuo, H.-W. and W.-H. Ding, *Trace determination of bisphenol A and phytoestrogens in infant formula powders by gas chromatography-mass spectrometry.* Journal of Chromatography A, 2004. **1027**(1-2): p. 67-74.
342. Gehrke, C.W. and K. Leimer, *Effects of solvents on derivatisation using bis(trimethylsilyl)trifluoroacetamide.* Journal of Chromatography, 1970. **53**: p. 201.
343. Gehrke, C.W. and A.B. Patel, *Gas-liquid chromatography of nucleosides, effects of silylating reagents and solvents.* Journal of chromatography, 1977. **130**: p. 103.
344. Zhang, K. and Y. Zuo, *Pitfalls and solution for simultaneous determination of estrone and 17α-ethinylestradiol by gas chromatography-mass spectrometry after derivatization with N,O-bis(trimethylsilyl)trifluoroacetamide.* Analytica Chimica Acta, 2005. **554**(1-2): p. 190-196.
345. Bansal, S. and A. DeStefano, *Key elements of bioanalytical method validation for small molecules.* The AAPS Journal, 2007. **9**(1): p. E109-E114.
346. Rambla-Alegre, M., J. Esteve-Romero, and S. Carda-Broch, *Is it really necessary to validate an analytical method or not? That is the question.* Journal of Chromatography A, in press(0).
347. Taverniers, I., M. De Loose, and E. Van Bockstaele, *Trends in quality in the analytical laboratory. II. Analytical method validation and quality assurance.* TrAC Trends in Analytical Chemistry, 2004. **23**(8): p. 535-552.
348. Almeida, A.M., M.M. Castel-Branco, and A.C. Falcão, *Linear regression for calibration lines revisited: weighting schemes for bioanalytical methods.* Journal of Chromatography B, 2002. **774**(2): p. 215-222.
349. Kuss, H.-J., *Weighted Least-Squares Regression in Practice: Selection of the Weighting Exponent.* LC-GC Europe, 2003(December): p. 2-5.
350. Jain, R.B., *Comparison of three weighting schemes in weighted regression analysis for use in a chemistry laboratory.* Clinica Chimica Acta, 2010. **411**(3-4): p. 270-279.
351. Barr, D.B., R.Y. Wang, and L.L. Needham, *Biologic Monitoring of Exposure to Environmental Chemicals throughout the Life Stages: Requirements and Issues for Consideration for the National Children's Study.* Environmental Health Perspectives, 2005. **113**(8).
352. *GC Pressure / Flow Calculator Software for PC: Revision 2.05* Agilent Technologies.
353. Kuklenyik, Z., L.L. Needham, and A.M. Calafat, *Measurement of 18 Perfluorinated Organic Acids and Amides in Human Serum Using On-Line Solid-Phase Extraction.* Analytical Chemistry, 2005. **77**(18): p. 6085-6091.
354. Adlercreutz, H., et al., *An isotope dilution gas chromatographic-mass spectrometric method for the simultaneous assay of estrogens and phytoestrogens in urine.* Journal of Steroid Biochemistry and Molecular Biology, 2004. **92**(5): p. 399-411.
355. Heinonen, S.M., K. WÃ¤hÃ¤lÃ¤, and H. Adlercreutz, *Identification of urinary metabolites of the red clover isoflavones formononetin and biochanin A in human subjects.* Journal of Agricultural and Food Chemistry, 2004. **52**(22): p. 6802-6809.
356. Heinonen, S.M., et al., *Metabolism of the soy isoflavones daidzein, genistein and glycitein in human subjects. Identification of new metabolites having an intact isoflavonoid skeleton.* Journal of Steroid Biochemistry and Molecular Biology, 2003. **87**(4-5): p. 285-299.
357. Heinonen, S., K. WÃ¤hÃ¤lÃ¤, and H. Adlercreutz, *Identification of isoflavone metabolites dihydrodaidzein, dihydrogenistein, 6'-OH-O-dma, and cis-4-OH-equol in human urine by gas chromatography-mass spectroscopy using authentic reference compounds.* Analytical Biochemistry, 1999. **274**(2): p. 211-219.
358. Ferrer, I., L.B. Barber, and E.M. Thurman, *Gas chromatographic-mass spectrometric fragmentation study of phytoestrogens as their trimethylsilyl derivatives: Identification in soy milk and wastewater samples.* Journal of Chromatography A, 2009. **1216**(32): p. 6024-6032.
359. Morton, M., et al., *Analysis of phyto-oestrogens by gas chromatography-mass spectrometry.* Environmental Toxicology and Pharmacology, 1999. **7**(3): p. 221-225.
360. Hoppin, J.A., et al., *Reproducibility of Urinary Phthalate Metabolites in First Morning Urine Samples.* Environmental Health Perspectives, 2002. **110**: p. 515-518.
361. Hauser, R., et al., *Temporal Variability of Urinary Phthalate Metabolite Levels in Men of Reproductive Age.* Environmental Health Perspectives, 2004. **112**: p. 1734–1740.

362. *Pearson product-moment correlation coefficient*; [Cited 15 October 2012] Available from: http://en.wikipedia.org/wiki/Pearson%27s_correlation#Inference.
363. Gabbe, S.G., J.R. Niebyl, and J.L. Simpson, eds. *Obstetrics: Normal and Problem Pregnancies*. 5th ed. 2007, Churchill Livingstone Elsevier: Philadelphia, PA.
364. Vandenberg, L.N., et al., *Human exposure to bisphenol A (BPA).* Reproductive Toxicology, 2007. **24**(2): p. 139-177.
365. Michaels, J.E.A., et al., *Comprehensive proteomic analysis of the human amniotic fluid proteome: Gestational age-dependent changes.* Journal of Proteome Research, 2007. **6**(4): p. 1277-1285.
366. Ross, M.G., et al., *Fetal swallowing: Response to systemic hypotension.* American Journal of Physiology - Regulatory Integrative and Comparative Physiology, 1990. **258**(1 27-1): p. R130-R134.
367. Sinha, R. and M. Carlton, *The volume and composition of amniotic fluid in early pregnancy.* Journal of Obstetrics and Gynaecology of the British Commonwealth, 1970. **77**(3): p. 211-214.
368. Kobayashi, K., et al., *Expression and Distribution of Tight Junction Proteins in Human Amnion During Late Pregnancy.* Placenta, 2010. **31**(2): p. 158-162.
369. Aye, I.L.M.H., et al., *Expression, Localisation and Activity of ATP Binding Cassette (ABC) Family of Drug Transporters in Human Amnion Membranes.* Placenta, 2007. **28**(8-9): p. 868-877.
370. Copeland, R.A., *Protein–Ligand Binding Equilibria*, in *Enzymes: A Practical Introduction to Structure, Mechanism, and Data Analysis*. 2002, John Wiley & Sons, Inc. p. 76-108.
371. Morton, T.A., D.G. Myszka, and I.M. Chaiken, *Interpreting complex binding kinetics from optical biosensors: A comparison of analysis by linearization, the integrated rate equation, and numerical integration.* Analytical Biochemistry, 1995. **227**(1): p. 176-185.
372. Oshannessy, D.J., et al., *Determination of Rate and Equilibrium Binding Constants for Macromolecular Interactions Using Surface Plasmon Resonance: Use of Nonlinear Least Squares Analysis Methods.* Analytical Biochemistry, 1993. **212**(2): p. 457-468.
373. Rich, R.L., et al., *Kinetic analysis of estrogen receptor/ligand interactions.* Proceedings of the National Academy of Sciences of the United States of America, 2002. **99**(13): p. 8562-8567.
374. Laws, S.C., et al., *Nature of the binding interaction for 50 structurally diverse chemicals with rat estrogen receptors.* Toxicological Sciences, 2006. **94**(1): p. 46-56.
375. Kuiper, G.G.J.M., et al., *Comparison of the Ligand Binding Specificity and Transcript Tissue Distribution of Estrogen Receptors {alpha} and {beta}.* Endocrinology, 1997. **138**(3): p. 863-870.
376. Homola, J., S.S. Yee, and G. Gauglitz, *Surface plasmon resonance sensors: review.* Sensors and Actuators B: Chemical, 1999. **54**(1-2): p. 3-15.
377. Rich, R.L. and D.G. Myszka, *Advances in surface plasmon resonance biosensor analysis.* Current Opinion in Biotechnology, 2000. **11**(1): p. 54-61.
378. Rich, R.L. and D.G. Myszka, *Grading the commercial optical biosensor literature—Class of 2008: 'The Mighty Binders'.* Journal of Molecular Recognition, 2010. **23**(1): p. 1-64.
379. De Crescenzo, G., et al., *Kinetic Characterization by Surface Plasmon Resonance-Based Biosensors: Principle and Emerging Trends.* Cellular and Molecular Bioengineering, 2008. **1**(4): p. 204-215.
380. Karlsson, R. and A. Larsson, *Affinity Measurement Using Surface Plasmon Resonance*, in *Antibody Engineering*, B.K.C. Lo, Editor. 2004, Humana Press. p. 389-415.
381. Hahnefeld, C., S. Drewianka, and F.W. Herberg, *Determination of Kinetic Data Using Surface Plasmon Resonance Biosensors*, in *Molecular Diagnosis of Infectious Diseases*, J. Decker and U. Reischl, Editors. 2004, Humana Press. p. 299-320.
382. VanWiggeren, G.D., et al., *A novel optical method providing for high-sensitivity and high-throughput biomolecular interaction analysis.* Sensors and Actuators B-Chemical, 2007. **127**(2): p. 341-349.
383. *Analyzing protein interactions with the ProteOn XPR36 protein interaction array system* in BioRadiations, **119**,pp 16-21, Published 2006. Accessed 19 June 2011, http://www.bio-rad.com/webroot/web/pdf/lsr/literature/Bulletin_5538.pdf.
384. Usami, M., K. Mitsunaga, and Y. Ohno, *Estrogen receptor binding assay of chemicals with a surface plasmon resonance biosensor.* Journal of Steroid Biochemistry and Molecular Biology, 2002. **81**(1): p. 47-55.
385. Hock, B., M. Seifert, and K. Kramer, *Engineering receptors and antibodies for biosensors.* Biosensors and Bioelectronics, 2002. **17**(3): p. 239-249.
386. Pearson, J., et al., *A rapid receptor-ligand assay determination of estrogens using surface plasmon resonance.* Sensors and Actuators B: Chemical, 2001. **76**(1-3): p. 1-7.
387. Miyashita, M., et al., *Surface plasmon resonance-based immunoassay for 17 beta-estradiol and its application to the measurement of estrogen receptor-binding activity.* Analytical and Bioanalytical Chemistry, 2005. **381**(3): p. 667-673.
388. Habauzit, D., et al., *Determination of estrogen presence in water by SPR using estrogen receptor dimerization.* Analytical and Bioanalytical Chemistry, 2008. **390**(3): p. 873-883.

389. Asano, K., et al., *Screening of Endocrine Disrupting Chemicals Using a Surface Plasmon Resonance Sensor.* Analytical Sciences, 2004. **20**(4): p. 611-616.
390. Su, X.D., et al., *Combinational application of surface plasmon resonance spectroscopy and quartz crystal microbalance for studying nuclear hormone receptor-response element interactions.* Analytical Chemistry, 2006. **78**(15): p. 5552-5558.
391. Tessema, M., et al., *Glutathione-S-transferase-green fluorescent protein fusion protein reveals slow dissociation from high site density beads and measures free GSH.* Cytometry Part A, 2006. **69**(5): p. 326-334.
392. *Reusable glutathione agarose resin for purifying GST fusion proteins*; Thermo Fisher Scientific Inc. , [Cited 11 June 2009] Available from: http://www.piercenet.com/products/browse.cfm?fldID=01021302.
393. Phillips, T.M., *Spacer Groups for Affinity Chromatography*, in *Encyclopedia of Chromatography*, J. Cazes, Editor. 2005, Taylor and Francis.
394. Hage, D.S., *Affinity Chromatography: An Overview*, in *Encyclopedia of Chromatography*, J. Cazes, Editor. 2005, Taylor and Francis.
395. *Affinity Chromatography, etc. Spring 2002*; Rutgers University, [Cited June 11 2009] Available from: http://www.cook.rutgers.edu/~dbm/affinity.html.
396. *Immobilized Glutathione - Reusable glutathione agarose resin for purifying GST fusion proteins*; Pierce Protein Research Products, Thermo Fisher Scientific Inc., [Cited 30 September 2008] Available from: http://www.piercenet.com/products/browse.cfm?fldID=01021302.
397. Grahn, E., et al., *New crystal structures of human glutathione transferase A1-1 shed light on glutathione binding and the conformation of the C-terminal helix.* Acta Crystallographica Section D-Biological Crystallography, 2006. **62**(Pt 2): p. 197-207. Epub 2006 Jan 18.
398. Le Trong, I., et al., *1.3-A resolution structure of human glutathione S-transferase with S-hexyl glutathione bound reveals possible extended ligandin binding site.* Proteins., 2002. **48**(4): p. 618-27.
399. Li, X., C. Abell, and M.A. Cooper, *Single-step biocompatible coating for sulfhydryl coupling of receptors using 2-(pyridinyldithio)ethylcarbamoyl dextran.* Colloids and Surfaces B: Biointerfaces, 2008. **61**(1): p. 113-117.
400. Marquart, J.A., *Immobilization Techniques* in Published 28 January 2004. Accessed 25 August 2009, http://www.sprpages.nl/Downloads/PDFfiles/Immobilization.pdf.
401. Ebright, Y.W., et al., *Incorporation of an EDTA-metal complex at a rationally selected site within a protein: application to EDTA-iron DNA affinity cleaving with catabolite gene activator protein (CAP) and Cro.* Biochemistry, 1992. **31**(44): p. 10664-10670.
402. Zugates, G.T., et al., *Synthesis of Poly(beta-amino ester)s with Thiol-Reactive Side Chains for DNA Delivery.* Journal of the American Chemical Society, 2006. **128**(39): p. 12726-12734.
403. *Affinity Chromatography Principles and Methods*. 2007: GE Healthcare. 155.
404. Harper, S. and D.W. Speicher, *Expression and Purification of GST Fusion Proteins* in Current Protocols in Protein Science, **52**,pp 6.6.1-6.6.26., Published Accessed 2 November 2009,
405. Knecht, S., et al., *Oligohis-tags: Mechanisms of binding to Ni^{2+}-NTA surfaces.* Journal of Molecular Recognition, 2009. **22**(4): p. 270-279.
406. Thomson, J.A. and J.E. Ladbury, *Isothermal Titration Calorimetry: a Tutorial*, in *Biocalorimetry 2 Applications of Calorimetry in the Biological Sciences*, J.E. Ladbury and M.L. Doyle, Editors. 2004, John Wiley & Sons. p. 37-58.
407. Gilli, P., et al., *Binding thermodynamics as a tool to investigate the mechanisms of drug-receptor interactions: Thermodynamics of cytoplasmic steroid/nuclear receptors in comparison with membrane receptors.* Journal of Medicinal Chemistry, 2005. **48**(6): p. 2026-2035.
408. Fukada, H. and K. Takahashi, *Enthalpy and heat capacity changes for the proton dissociation of various buffer components in 0.1 M potassium chloride.* Proteins: Structure, Function, and Genetics, 1998. **33**(2): p. 159-166.
409. Freyer, M.W. and E.A. Lewis, *Isothermal Titration Calorimetry: Experimental Design, Data Analysis, and Probing Macromolecule/Ligand Binding and Kinetic Interactions*, in *Biophysical Tools for Biologists: Volume 1 In Vitro Techniques*, J.J. Correia and H.W.I. Detrich, Editors. 2008, Elsevier.
410. O'Brien, R. and I. Haq, *Applications of Biocalorimetry: Binding, Stability and Enzyme Kinetics*, in *Biocalorimetry 2 Applications of Calorimetry in the Biological Sciences*, J.E. Ladbury and M.L. Doyle, Editors. 2004, John Wiley & Sons, Ltd. p. 3-34.
411. Tellinghuisen, J., *Isothermal titration calorimetry at very low c.* Analytical Biochemistry, 2008. **373**(2): p. 395-397.
412. Zhang, Y.-L. and Z.-Y. Zhang, *Low-Affinity Binding Determined by Titration Calorimetry Using a High-Affinity Coupling Ligand: A Thermodynamic Study of Ligand Binding to Protein Tyrosine Phosphatase 1B.* Analytical Biochemistry, 1998. **261**(2): p. 139-148.

413. MicroCal, *VP-ITC Microcalorimeter User's Manual*.
414. Kallen, J., et al., *Crystal structure of human estrogen-related receptor α in complex with a synthetic inverse agonist reveals its novel molecular mechanism.* Journal of Biological Chemistry, 2007. **282**(32): p. 23231-23239.
415. Silva, E., M. Scholze, and A. Kortenkamp, *Activity of xenoestrogens at nanomolar concentrations in the E-Screen assay.* Environmental Health Perspectives, 2007. **115 Suppl 1**: p. 91-97.
416. Silva, E., N. Rajapakse, and A. Kortenkamp, *Something from "Nothing" - Eight Weak Estrogenic Chemicals Combined at Concentrations below NOECs Produce Significant Mixture Effects.* Environmental Science and Technology, 2002. **36**(8): p. 1751-1756.
417. Anstead, G.M., K.E. Carlson, and J.A. Katzenellenbogen, *The estradiol pharmacophore: Ligand structure-estrogen receptor binding affinity relationships and a model for the receptor binding site.* Steroids, 1997. **62**(3): p. 268-303.
418. Kuiper, G.G.J.M., et al., *Interaction of Estrogenic Chemicals and Phytoestrogens with Estrogen Receptor {beta}.* Endocrinology, 1998. **139**(10): p. 4252-4263.
419. Waller, C.L., et al., *Ligand-Based Identification of Environmental Estrogens.* Chemical Research in Toxicology, 1996. **9**(8): p. 1240-1248.
420. Kwon, J.-H., L.E. Katz, and H.M. Liljestrand, *Modeling binding equilibrium in a competitive estrogen receptor binding assay.* Chemosphere, 2007. **69**(7): p. 1025-1031.
421. Mueller, S.O., et al., *Phytoestrogens and their human metabolites show distinct agonistic and antagonistic properties on estrogen receptor α (ERα) and ERβ in human cells.* Toxicological Sciences, 2004. **80**(1): p. 14-25.
422. Mueller, S.O., et al., *Molecular Determinants of the Stereoselectivity of Agonist Activity of Estrogen Receptors (ER) α and β.* Journal of Biological Chemistry, 2003. **278**(14): p. 12255-12262.
423. Blair, R.M., et al., *The Estrogen Receptor Relative Binding Affinities of 188 Natural and Xenochemicals: Structural Diversity of Ligands.* Toxicological Sciences, 2000. **54**(1): p. 138-153.
424. Molina-Molina, J.-M., et al., *Profiling of benzophenone derivatives using fish and human estrogen receptor-specific in vitro bioassays.* Toxicology and Applied Pharmacology, 2008. **232**(3): p. 384-395.
425. Morohoshi, K., et al., *Estrogenic activity of 37 components of commercial sunscreen lotions evaluated by in vitro assays.* Toxicology in Vitro, 2005. **19**(4): p. 457-469.
426. Zhu, B.T., et al., *Quantitative Structure-Activity Relationship of Various Endogenous Estrogen Metabolites for Human Estrogen Receptor α and β Subtypes: Insights into the Structural Determinants Favoring a Differential Subtype Binding.* Endocrinology, 2006. **147**(9): p. 4132-4150.
427. Wolohan, P. and D.E. Reichert, *Use of binding energy in comparative molecular field analysis of isoform selective estrogen receptor ligands.* Journal of Molecular Graphics and Modelling, 2004. **23**(1): p. 23-38.
428. Chen, Z., et al., *Directed evolution of human estrogen receptor variants with significantly enhanced androgen specificity and affinity.* Journal of Biological Chemistry, 2004. **279**(32): p. 33855-33864.
429. Branham, W.S., et al., *Phytoestrogens and mycoestrogens bind to the rat uterine estrogen receptor.* Journal of Nutrition, 2002. **132**(4): p. 658-664.
430. Murk, A.J., et al., *Detection of estrogenic potency in wastewater and surface water with three in vitro bioassays.* Environmental Toxicology and Chemistry, 2002. **21**(1): p. 16-23.
431. Zacharewski, T.R., et al., *Examination of the in Vitro and in VitroEstrogenic Activities of Eight Commercial Phthalate Esters.* Toxicological Sciences, 1998. **46**(2): p. 282-293.
432. Schreurs, R.H.M.M., et al., *Transcriptional Activation of Estrogen Receptor ER[alpha] and ER[beta] by Polycyclic Musks Is Cell Type Dependent.* Toxicology and Applied Pharmacology, 2002. **183**(1): p. 1-9.
433. Satoh, K., et al., *Competitive binding of some alkyl p-hydroxybenzoates to human estrogen receptor α and β.* Yakugaku Zasshi

2000. **120**: p. 1429-1433.
434. Pfitscher, A., E. Reiter, and A. Jungbauer, *Receptor binding and transactivation activities of red clover isoflavones and their metabolites.* Journal of Steroid Biochemistry and Molecular Biology, 2008. **112**(1-3): p. 87-94.
435. Mueller, S.O., et al., *Activation of estrogen receptor [alpha] and ER[beta] by 4-methylbenzylidene-camphor in human and rat cells: comparison with phyto- and xenoestrogens.* Toxicology Letters, 2003. **142**(1-2): p. 89-101.
436. Satoh, K., F. Nagai, and N. Aoki, *Several environmental pollutants have binding affinities for both androgen receptor and estrogen receptor α.* Journal of Health Science, 2001. **47**(5): p. 495-501.

437. Sun, J., et al., *Novel Ligands that Function as Selective Estrogens or Antiestrogens for Estrogen Receptor-{alpha} or Estrogen Receptor-{beta}.* Endocrinology, 1999. **140**(2): p. 800-804.

Appendix

Table A. 1. Summary of total EE concentrations measured in human adult urine (ng/mL).

Reference	[139]	[139]	[135]	[140]	[141]	[142]	[143]	[144]	[116]	[116]	[145]	[146]	[147]	[148]	[148]	[149]	[149]	[150]
Cohort	**mothers, female fetus**	**mothers, male fetus**	**male and female adult**	**male and female adult**	**human**	**mother**	**adults**	**human**	**male (23-29 yr)**	**female (54-86 yr)**	**adult**	**adult**	**mother**	**adults (Korean)**	**adults (Korean)**	**adult males (German) normal diet**	**adult males (German) normal diet**	**adult women (UK)**
GEN							2.6	35						5.7	49.8	104	64	102.5
DAID							22.5	74						9.1	442	196	98	200.1
EQ														3.3	16.4	14	31	6.1
ENT							131	209						1.4	17			1104.5
BPA				0.9	1.28		0.47						1.3			10	9	
MBP	78	79.6				13.5					1.57	41	36					
MEHP	24.6	26.3				3.3					0.9	2.7	6					
MEP	22.2	19.1				128.4					42.9	305	380					
MBzP	3	2.5				8.3					2.06	21.2	22					
MMP	7.1	6.8				0.7					0.45		1.6					
MOP												0.9						
mParaben			43.9	110														
eParaben			1	12.5														
pParaben			9.1	15.1														
bParaben			0.5	22.9														
TRIC				19									11					
2,4-DCP													2.1					
NP					0.1													
BP-3				12.3					140	60			7.5					
OMC									8	5								
4MBC									7	5								
E2														4.2	38.5			

Table A. 2. Summary of total EE concentrations measured in human amniotic fluid (ng/mL).

Reference	[139]	[139]	[190]	[130]	[191]	[180]	[179]	[99]
Cohort	female fetus	male fetus						
GEN			1.38				1.69	0.94
DAID			9.52				1.44	1.08
ENT			95.9					
BPA			0.5		8.3	0.26		
MBP	85.5	81.3		5.8				
MEHP	24	22.1		0.86				
MEP	1	1		1.2				
MBzP	1.4	1.4						
MMP	1.4	1.4						

Table A. 3. Summary of estrogenic potencies of selected EDCs obtained from the E-SCREEN, YES and ER-CALUX assays. Unless otherwise indicated (%efficacy), the potency is for full agonist activity. Literature references are given in square brackets.

Test Name	E-SCREEN	YES	ER-CALUX
Reporter	**Cell Proliferation**	**β-galactosidase**	**Luciferase**
Host cell	**MCF-7**	**Yeast**	**T47D**
Receptor	**hERα dominant**	**hERα**	**hERα dominant**
m-Paraben	7.1×10^{-7} (45%) [210] 1.5×10^{-7} (82%) [211]	3.3×10^{-7} [203]	
e-Paraben	3.7×10^{-6} [210] 1.5×10^{-6} (87%) [211]	5×10^{-6} [203]	
p-Paraben	7.5×10^{-6} [210] 1.5×10^{-6} [211] 3.6×10^{-7} [415]	3.3×10^{-5} [203]	
b-Paraben	1.5×10^{-5} [210] 1.5×10^{-6} (79%) [211] 6.7×10^{-7} [415]	1.3×10^{-4} [203]	
bz-Paraben	1.5×10^{-5} [210]	2.5×10^{-4} [203] 2.2×10^{-4} [416]	
ip-Paraben	1.2×10^{-5} [210] 6×10^{-5} [211]		
ib-Paraben	1.5×10^{-5} [210] 6×10^{-5} (95%) [211]		
4HBA	not active [210]		
Triclosan	not active [210, 217] agonist [213]	1.5×10^{-2} [215]	antagonist [216]
BP-1	5.9×10^{-7} [221]	2.2×10^{-4} (96%) [222] 3.3×10^{-4} [203] 2.5×10^{-4} [416]	
BP-2	1.8×10^{-6} [221]	2.4×10^{-5} (91%) [222] 1.4×10^{-4} [203]	
BP-3	3.3×10^{-7} [221]	1.4×10^{-5} (18%) [222] 6.8×10^{-5} [223] 1×10^{-5} (50%) [203]	
OMC	5.1×10^{-7} [221] 8.3×10^{-7} [415]		
4MBC	4.0×10^{-7} [221] 2.1×10^{-7} [415]		
BPA	1.6×10^{-5} [228] 3.8×10^{-6} [415]	1×10^{-4} [203] 6.2×10^{-5} [416]	7.8×10^{-6} [197]
NP		8.1×10^{-4} [215] 7.2×10^{-7} [231] 1.4×10^{-4} [232]	2.3×10^{-5} [197]
4t-OP		2×10^{-4} [203]	
3PBA		not active [233]	
4OH-3PBA		not active [233]	
3PBOH		5.2×10^{-5} [233]	
4OH-3PBOH		5.2×10^{-5} [233]	
GEN	$\sim 10^{-3}$ (50%) [238] 1.2×10^{-5} [415]	2.9×10^{-4} [416]	6×10^{-5} [197]
DAID	$\sim 10^{-3}$ (50%) [238]		
Equol	$\sim 10^{-3}$ [238]		
EE2		0.3 [215]	
E1	6.3×10^{-3} [415]		
E3	2.2×10^{-2} [415]		

Table A. 4. Summary of estrogenic potencies of selected EDCs obtained from firefly luciferase reporter gene assays hosted in a variety of different cell types. Unless otherwise indicated (%efficacy), the potency is for full agonist activity. Literature references are given in square brackets.

Host cell	Yeast		HepG2		CHO-K1		HEK293		U2-OS	
Receptor	hERα	hERβ	hERα	hERβ	hERα	hERβ	hERα	hERβ	hERα	hERβ
m-Paraben	6 x 10-7 [196]	1.3 x 10-5 [196]								
p-Paraben	5 x 10-5 [196]	1.8 x 10-4 [196]								
Triclosan	not active [215]									
BP-1							3 x 10-4 [134]			
BP-3							1 x 10-5 [134]	1 x 10-6 (80%) [134]		
OMC							<10-6 (42%) [134]	not active [134]		
4MBC							<10-6 (60%) [134]	<10-6 (80%) [134]		
BPA	4 x 10-5 [196]	6 x 10-3 [196]	4.7 x 10-3 [225]	7.9 x 10-3 [225]					5.3 x 10-5 [227]	8.3 x 10-4 [227]
NP	2 x 10-5 [196] 5.8 x 10-3 [215]	< 10-5 [196]								
mBP					not active [235]	not active [235]				
mBzP					not active [235]	not active [235]				
mEHP					not active [235]	not active [235]				
GEN	5 x 10-5 [196]	7 x 10-5 [196]							~10-5 (30%) [238]	~10-5 (50%) [238]
DAID									~10-5 (20%) [238]	~10-5 (50%) [238]

Host cell	Yeast		HepG2		CHO-K1		HEK293		U2-OS	
Receptor	hERα	hERβ	hERα	hERβ	hERα	hERβ	hERα	hERβ	hERα	hERβ
Equol									~10-4 (80%) [238]	~10-4 (50%) [238]
EE2	1.15 [215]									

Table A. 5. Summary of estrogenic potencies of selected EDCs obtained from *in vitro* assays using unique reporter constructs. Unless otherwise indicated (%efficacy), the potency is for full agonist activity. Literature references are given in square brackets.

Reporter	**pS2 mRNA**	**Green Fluorescent Protein**	
Host cell	**MCF-7**	**MCF-7**	**Ishikawa**
Receptor	**hERα dominant**	**hERα dominant**	**hERβ dominant**
BP-1	3.9×10^{-5} [224]		
BP-3	9.6×10^{-6} [224]		
OMC	4.6×10^{-6} [224]		
4MBC	2.6×10^{-6} [224]		
BPA		2×10^{-5} [226]	9×10^{-6} [226]
GEN		2×10^{-5} [226]	9×10^{-5} [226]

Table A. 6. Statistical summary of estrogenic potencies of selected EDCs (low, median and high) for hERα and hERβ, as illustrated in Figure 2.16. Missing values indicate data not available.

	hERα			**hERβ**		
	High	**Low**	**Median**	**High**	**Low**	**Median**
mParaben	7.10E-07	1.50E-07	4.65E-07	1.3E-05	1.3E-05	1.3E-05
eParaben	5.00E-06	1.50E-06	3.70E-06			
pParaben	5.00E-05	3.60E-07	7.50E-06	1.8E-04	1.8E-04	1.8E-04
bParaben	1.30E-04	6.70E-07	8.25E-06			
tOP	4.90E-04	2.00E-04	3.45E-04			
NP	5.80E-03	7.20E-07	1.20E-04	1.0E-05	1.0E-05	1.0E-05
3PBOH	5.20E-05	5.20E-05	5.20E-05			
4MBC	2.60E-06	2.10E-07	7.00E-07	1.0E-06	1.0E-06	1.0E-06
OMC	4.60E-06	5.10E-07	9.15E-07			
BP-1	3.30E-04	5.90E-07	2.35E-04			
BP-2	1.40E-04	1.80E-06	2.40E-05			
BP-3	6.80E-05	3.30E-07	1.00E-05	1.0E-06	1.0E-06	1.0E-06
Tric	1.50E-02	1.50E-02	1.50E-02			
BPA	4.70E-03	3.80E-06	4.65E-05	7.9E-03	7.9E-03	7.9E-03
Equol	1.00E-03	1.00E-04	5.50E-04	1.0E-04	1.0E-04	1.0E-04
Daid	1.00E-03	1.00E-05	5.05E-04	1.0E-05	1.0E-05	1.0E-05
Gen	1.00E-03	1.00E-05	5.00E-05	9.0E-05	9.0E-05	9.0E-05
E1	3.92E-01	6.30E-03	1.40E-01			
E2	1.00E+00	1.00E+00	1.00E+00	1.0E+00	1.0E+00	1.0E+00
E3	3.70E-02	2.20E-02	2.95E-02			
EE2	1.15E+00	3.00E-01	9.20E-01			
mTric						
3PBA						
Ent						
mMP						
mEP						
mBP						
mEHP						
mOP						
mBzP						

Table A. 7. Structures of ligands used in docking.

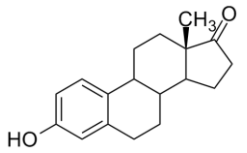	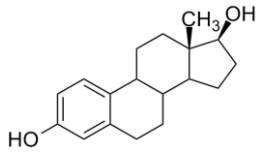	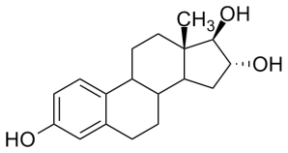	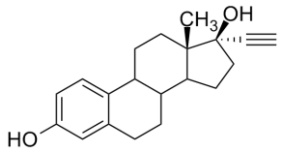	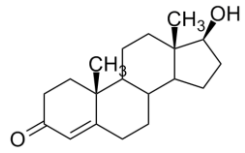	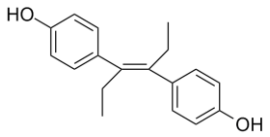
E1	E2	E3	EE2	T	DES
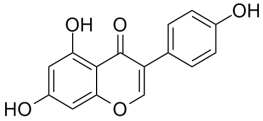	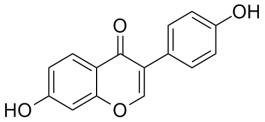	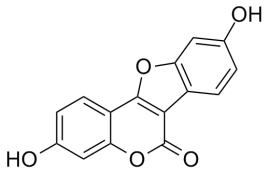	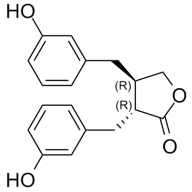	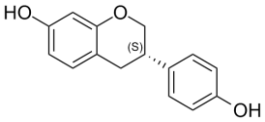	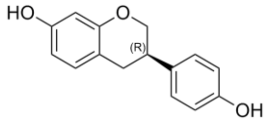
GEN	DAID	COUM	ENT	EQ-S	EQ-R
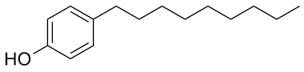	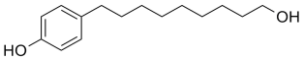	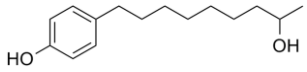	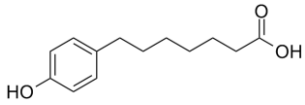	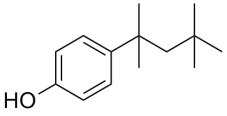	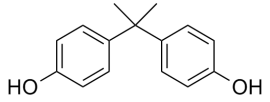
4NP	4NP-M1	4NP-M2	4NP-M3	4tOP	BPA
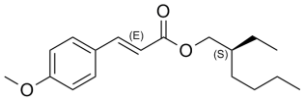	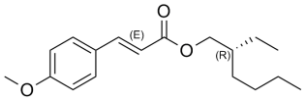	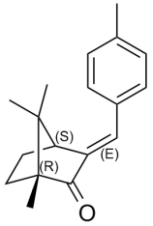	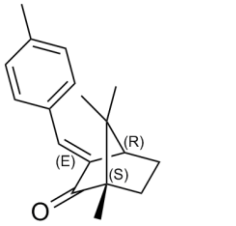	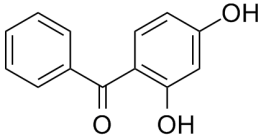	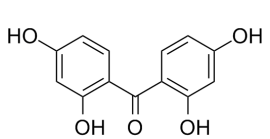
OMC-S	OMC-R	4MBC-1R4S	4MBC-1S4R	BP-1	BP-2
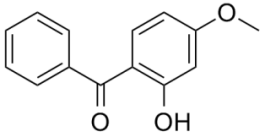	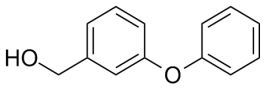	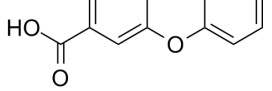	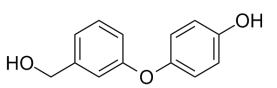	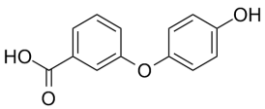	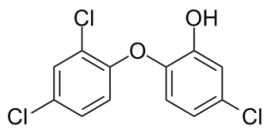
BP-3	3PBOH	3PBA	4OH-3PBOH	4OH-3PBA	TRIC

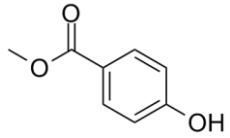 mPBN	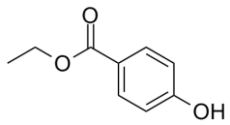 ePBN	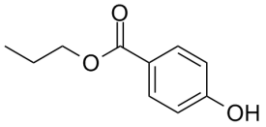 pPBN	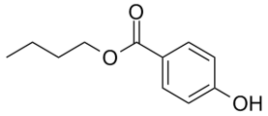 bPBN	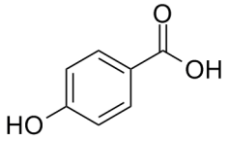 4HBA	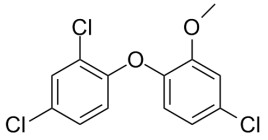 mTRIC
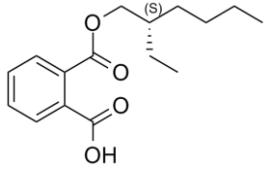 mEHP-S	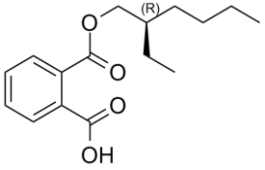 mEHP-R	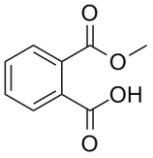 mMP	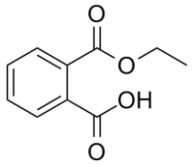 mEP	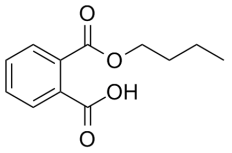 mBP	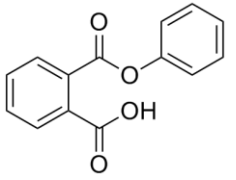 mBzP
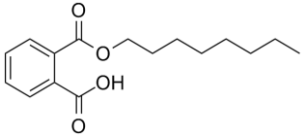 mOP	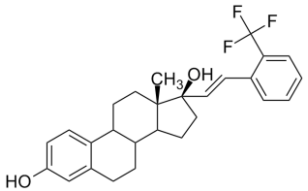 EZT	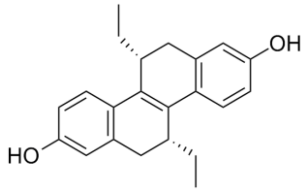 ETC	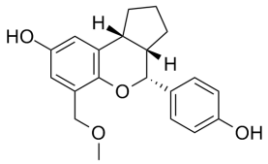 JJ3	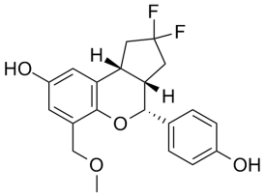 3AS	
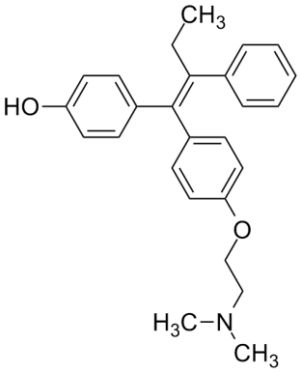 OHT	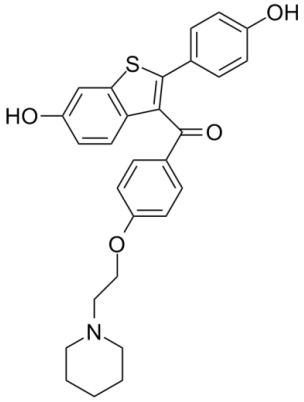 RAL	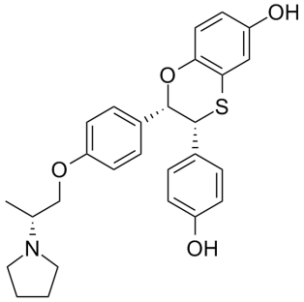 AIT			

Table A. 8. List of references for experimental binding energy measurements given in Table 3.3.

Author	Reference
Anstead et al. (Table 1)	[417]
Kuiper et al. (Table 1 & Table 2)	[418]
Waller et al.	[419]
Kwon et al.	[420]
Mueller et al.	[421]
Rich et al.	[373]
Usami et al.	[384]
Lambrinidis et al.	[75]
van Lipzig et al.	[273]
Laws et al.	[374]
Mueller et al.	[422]
Muthyala et al.	[304]
Blair et al.	[423]
Molina-Molina et al.	[424]
Okubo et al.	[211]
Morohoshi et al.	[425]
Zhu et al.	[426]
Wolohan	[427]
Gangloff, M.	[259]
Chen, Z.	[428]
Branham,W.	[429]
Sippl, W.	[311]
Murk, A.	[430]
Zacharewski, T.,	[431]
Schreurs, R.,	[432]
Lemini, C.,	[208]
Satoh, K.,	[433]
Kuiper et al.	[375]
Pfitscher et al.	[434]
Mueller,	[435]
Satoh,	[436]
Nettles et al.	[289]
Norman et al.	[292]
Blizzard et al.	[290]
Richardson	[293]
Sun et al.	[437]
Setchell et al.	[303]

Table A. 9. Ligand length (Å) for the energy minimized free ligand in water. Length is measured between opposing hydroxyls (or carbonyl or carboxylic acid if the ligand has only one hydroxyl).

Ligand	Length (Å)
E1	10.91
E2	11.03
E3	11.03 (17β-OH) 11.16 (16α-OH)
T	10.80
EE2	11.04
DES	12.08
BPA	9.40
GEN	12.15
DAID	12.16
COUM	11.37
R-EQ	11.99
S-EQ	11.99
ENT	11.79
BP-2	9.62
4NP-M1	15.52
4NP-M2	12.09
4NP-M3	10.50
4OH-3PBOH	10.57
4OH-3PBA	10.97
RAL	11.74
EZT	11.01
JJ3	11.93
AIT	11.57
3AS	11.91
ETC	12.12

Table A. 10. Suppliers for chemicals used in the study.

Sigma-Aldrich	**CAS**	**Cat #**
p-n-nonylphenol	104-40-5	46405-100MG
p-tert-octylphenol	140-66-9	442858
3-phenoxybenzyl alcohol	13826-35-2	190284-25G
3-phenoxybenzoic acid	3739-38-6	190276-5G
2,4-dihydroxybenzophenone	131-56-6	126217-100G
2,2',4,4'-tetrahydroxybenzophenone	131-55-5	T16403-25G
estrone	53-16-7	E9750-1G
estriol	50-27-1	E1253-500MG
ethynylestradiol	57-63-6	E4876-100MG
4-fluoro-4'-hydroxybenzophenone	25913-05-7	274224-50G
2,2-bis-(4-hydroxy-3-methylphenyl)propane	79-97-0	423300-1G
β-Glucuronidase from Helix pomatia	9001-45-0	G0751-500KU
4-Nitrocatechol sulfate dipotassium salt	14528-64-4	N7251-500MG
4-Nitrocatechol	3316-09-4	N15553-1G
4-Nitrophenyl-β-glucuronide	10344-94-2	73677-250MG
4-Nitrophenol	100-02-7	35836-1G
2,4-Dichlorophenol	120-83-2	35811-1G
formic acid	64-18-6	06440-100ML
Phenomenex (AccuStandard)		
monomethyl phthalate	4376-18-5	ALR-139N
monoethyl phthalate	2306-33-4	ALR-137N
monobenzyl phthalate	2528-16-7	ALR-134N
mono-n-butyl phthalate	131-70-4	ALR-135N
mono-2-ethylhexyl phthalate	4376-20-9	ALR-138N
p-hydroxybenzoic acid methyl ester	99-76-3	ALR-130N
p-hydroxybenzoic acid ethyl ester	120-47-8	ALR-113N
p-hydroxybenzoic acid propyl ester	94-13-3	ALR-153N
p-hydroxybenzoic acid butyl ester	94-26-8	ALR-085N
p-hydroxybenzoic acid	99-96-7	ALR-069N
2-hydroxy-4-methoxybenzophenone	131-57-7	ALR-081N
2-ethylhexyl-p-methoxycinnamate	5466-77-3	ALR-144N
4-methyl-benzylidene camphor	36861-47-9	ALR-073N
triclosan	3380-34-5	PCC-0015-10x
enterolactone		ASB-00005455-010
Novachem (Cambridge Isotope Laboratory)		
mono-n-octyl phthalate	5393-19-1	ULM-4593-1.2
triclosan	3380-34-5	C 17803000
methyl triclosan	4640-01-1	C 17803300
mono-2-ethylhexyl phthalate ($^{13}C_4$, 99%)	NA	CLM-4584-1.2
monoethyl phthalate ($^{13}C_4$, 99%)	NA	CLM-4586-1.2
p-n-Nonylphenol ($^{13}C_6$, 99%)	NA	CLM-4306-1.2
Genistein (D_4, 94%)	NA	DLM-4460-1.2
3-Phenoxybenzoic Acid ($^{13}C_6$, 99%)	NA	CLM-4542-SA-1.2
Triclosan (2',4,4'-trichloro-2-hydroxydiphenyl ether) ($^{13}C_{12}$, 99%)	NA	CLM-6779-1.2
p-hydroxybenzoic acid methyl ester (ring $^{13}C_6$, 99%)	NA	CLM-8249-1.2
p-hydroxybenzoic acid butyl ester (ring $^{13}C_6$, 99%)	NA	CLM-8285-1.2
17β-estradiol ($^{13}C_2$, 99%)	NA	CLM-803-1.2
Bisphenol A ($^{13}C_{12}$, 99%)	NA	CLM-4325-1.2
4-Nitrophenol (D_4, 98%)	93951-79-2	DLM-296-0.25
Sapphire Bioscience (Alexis)		
genistein	446-72-0	ALX-350-006-M100
daidzein	486-66-8	ALX-350-009-M050
equol (R+S isomers)	94105-90-5	ALX-385-032-M025

Table A. 11. Suppliers of solvents and other reagents.

Supplier	**Product**
Fisher Scientific	MeOH, EtOH
Merck	ACN
Mallinckrodt	Iso-octane, Hexanes, MTBE
Fluka	formic acid

Table A. 12. Synthetic urine recipe (McCurdy, 2005)

Component	**g/L H_2O**
Urea	16
Sodium Chloride	2.32
Potassium Chloride	3.43
Creatinine	1.1
Anhydrous Sodium Sulfate	4.31
Ammonium Chloride	1.06
Citric Acid	0.54
Anhydrous Magnesium Sulfate	0.46
Anhydrous Sodium Dihydrogen Phosphate	2.73
Anhydrous Calcium Chloride	0.63
Oxalic Acid	0.02
Glucose	0.48
Anhydrous Sodium Silicate (7 mg Si/kg urine)	0.071

Table A. 13. Physical properties of target analytes, recovery surrogates, enzyme reaction controls and the internal standard.

	CAS	MW	MP (°C)	BP (°C)	ACD logP	ACD logD (@ pH 5.5)
Target Analyte						
bisphenol A	80-05-7	228.29	158-159	220 / 4 mmHg	3.43	3.43
monomethyl phthalate	4376-18-5	180.16	82-82	329	1.13	-1.01
monoethyl phthalate	2306-33-4	194.18		340	1.66	-0.48
monobenzyl phthalate	2528-16-7	256.25		441	2.9	0.81
mono-n-butyl phthalate	131-70-4	222.24		363	2.72	0.64
mono-2-ethylhexyl phthalate	4376-20-6	278.34		409	4.67	2.57
mono-n-octyl phthalate	5393-19-1	278.34			4.58	2.76
p-n-nonylphenol	104-40-5	220.35	43-46	127-130 / 27 mmHg	6.19	6.19
p-tert-octylphenol	140-66-9	206.32	79-82	175 / 30 mmHg	4.93	4.93
3-(4-hydroxy-3-phenoxy)benzyl alcohol	63987-19-9	216.23			2.17	2.17
3-(4-hydroxy-3-phenoxy)benzoic acid	35065-12-4	230.22			3.05	1.51
3-phenoxybenzyl alcohol	13826-35-2	200.32	10	135-140 / 0.1 mmHg	3.03	3.03
3-phenoxybenzoic acid	3739-38-6	214.22	147-149	373	3.91	2.36
triclosan	3380-34-5	289.54	56-60	345	5.17	5.17
methyl triclosan	4640-01-1	303.57		359	4.74	4.74
p-hydroxybenzoic acid methyl ester	99-76-3	152.15	125-128	275	1.87	1.87
p-hydroxybenzoic acid ethyl ester	120-47-8	166.18	114-117	297-298	2.4	2.4
p-hydroxybenzoic acid propyl ester	94-13-3	180.2	95-98	156-157 / 3.5 mmHg	2.93	2.93
p-hydroxybenzoic acid butyl ester	94-26-8	194.23	67-70	309	3.46	3.46
p-hydroxybenzoic acid	99-96-7	138.12	213-217	336	1.42	0.33
2,4-dihydroxybenzophenone	131-56-6	214.22	144-147	194 / 1 mmHg	3.17	3.17
2-hydroxy-4-methoxybenzophenone	131-57-7	228.24	62-64	150-160 / 5 mmHg	3.64	3.64
2,2',4,4'-tetrahydroxybenzophenone	131-55-5	246.22	198-200	531	3.16	3.16
2-ethylhexyl-p-methoxycinnamate	5466-77-3	290.4		405	5.66	5.66
genistein	446-72-0	270.24		555	2.96	2.96
daidzein	486-66-8	254.24		512	2.78	2.78
equol (S isomer)	94105-90-5	242.27		442	2.98	2.98
enterolactone	78473-71-9	298.33		479	2.29	2.29
17b-estradiol	50-28-2	272.38	176-180	446	4.13	4.13
estrone	53-16-7	270.37	258-260	445	3.69	3.69
estriol	50-27-1	288.38	280-282	469	2.94	2.94
ethynylestradiol	57-63-6	296.4	182-163	457	4.52	4.52

	CAS	MW	MP (°C)	BP (°C)	ACD logP	ACD logD (@ pH 5.5)
Recovery Surrogates						
Bisphenol A (D_{16}, 98%)	96210-87-6	244.29				
Mono-2-ethylhexyl phthalate ($^{13}C_4$, 99%)	NA	282.34				
Monoethyl phthalate ($^{13}C_4$, 99%)	NA	198.18				
p-n-Nonylphenol ($^{13}C_6$, 99%)	NA	226.35				
17β-estradiol (D_4, 95-97%)	NA	276.38				
Genistein (D_4, 94%)	NA	274.24				
3-Phenoxybenzoic Acid ($^{13}C_6$, 99%)	NA	220.22				
Triclosan (2',4,4'-trichloro-2-hydroxydiphenyl ether) ($^{13}C_{12}$, 99%)	NA	315.57				
p-hydroxybenzoic acid methyl ester (ring $^{13}C_6$, 99%)	NA	158.15				
p-hydroxybenzoic acid butyl ester (ring $^{13}C_6$, 99%)	NA	200.23				
4-fluoro 4'-hydroxybenzophenone	25913-05-7	216.21	164-167		3.09	3.08
4-Nitrophenol (D_4, 98%)	93951-79-2	143.13	113-115			
Enzyme Reaction Control Standards						
4-Nitrophenyl-β-glucuronide	10344-94-2	315.23		644	-0.75	-3.68
4-Nitrophenol	100-02-7	139.11	110-115	279	1.57	1.56
Internal Standard						
2,2-bis-(4-hydroxy-3-methylphenyl)propane	79-97-0	256.34	138-140	238-240 / 12 mmHg	4.35	4.35

Table A. 14. Free concentrations (ng/mL) of target analytes in amniotic fluid samples of female fetuses.

Sample ID	1	2	4	5	6	8	10	11	13	14	17	21	23	25	26	30
mParaben	0.58	1.52	ND	NQ	ND	1.69	0.63	ND	ND	ND	ND	0.96	0.75	ND	NQ	ND
eParaben	ND	ND	ND	ND	ND	ND	ND	ND	ND	ND	ND	ND	ND	ND	ND	ND
mMP	ND	0.72	ND	NQ	ND	ND	0.84	ND	ND	ND	0.31	1.20	ND	NQ	0.72	ND
4HBA	25.08	11.91	NQ	20.07	20.15	NQ	NQ	19.86	18.29	NQ	NQ	21.47	15.90	NQ	NQ	16.49
mEP	0.49	0.37	NQ	NQ	0.19	NQ	NQ	NQ	0.21	2.15	NQ	ND	0.17	ND	NQ	0.39
OP	ND	ND	ND	ND	ND	ND	ND	ND	ND	ND	ND	ND	ND	ND	ND	ND
pParaben	ND	ND	ND	ND	ND	ND	ND	ND	ND	ND	ND	ND	ND	ND	ND	ND
bParaben	ND	ND	ND	ND	ND	ND	ND	ND	ND	ND	ND	ND	ND	ND	ND	ND
mBP	ND	ND	ND	ND	ND	ND	ND	ND	ND	ND	ND	ND	ND	ND	ND	ND
3PBOH	ND	ND	ND	ND	ND	ND	ND	ND	ND	ND	ND	ND	ND	ND	ND	ND
NP	ND	ND	ND	ND	ND	ND	ND	ND	ND	ND	ND	ND	ND	ND	ND	ND
3PBA	ND	ND	ND	ND	ND	ND	ND	ND	ND	ND	ND	ND	ND	ND	ND	ND
4MBC	NQ	NQ	NQ	NQ	NQ	NQ	NQ	NQ	NQ	NQ	NQ	NQ	NQ	NQ	NQ	NQ
BP-3	1.06	0.46	NQ	1.34	1.16	NQ	ND	2.04	0.78	NQ	NQ	0.72	ND	0.88	ND	NQ
mEHP	NQ	0.35	0.25	NQ	0.27	0.18	NQ	NQ	0.42	0.22	NQ	NQ	0.19	0.18	0.27	NQ
mTric	ND	ND	ND	ND	ND	ND	ND	ND	ND	ND	ND	ND	ND	ND	ND	ND
Tric	0.59	0.34	0.63	ND	NQ	ND	ND	0.48	ND	ND	ND	2.16	ND	NQ	0.36	ND
BP-1	0.36	0.37	0.46	0.41	0.55	0.41	NQ	0.53	0.43	ND	NQ	0.20	ND	ND	0.14	0.29
mBzP	ND	ND	ND	ND	ND	ND	ND	ND	ND	ND	ND	ND	ND	ND	ND	ND
BPA	NQ	0.18	0.07	0.37	0.25	NQ	NQ	0.28	NQ	NQ	NQ	NQ	NQ	0.26	0.12	NQ
OMC	NQ	NQ	NQ	NQ	NQ	NQ	NQ	NQ	NQ	NQ	NQ	NQ	NQ	NQ	NQ	NQ
BP-2	ND	ND	ND	0.04	ND	ND	ND	ND	0.14	ND	ND	ND	ND	ND	ND	ND
Equol	ND	ND	ND	ND	ND	ND	ND	ND	ND	ND	ND	ND	ND	ND	ND	ND
E1	ND	ND	ND	ND	ND	ND	ND	ND	ND	ND	ND	ND	ND	ND	ND	ND
E2	ND	ND	ND	ND	ND	ND	ND	ND	ND	ND	ND	ND	ND	ND	ND	ND
EE2	ND	ND	ND	ND	ND	ND	ND	ND	ND	ND	ND	ND	ND	ND	ND	ND
Ent	2.05	2.60	ND	ND	3.43	ND	NQ	1.38	2.45	2.41	NQ	2.47	2.78	ND	ND	ND
E3	2.08	3.09	6.13	NQ	NQ	3.24	4.94	NQ	NQ	4.86	1.44	NQ	2.70	3.22	3.89	NQ

Table A. 15. Free concentrations (ng/mL) of target analytes in amniotic fluid samples of male fetuses.

Sample ID	3	7	9	12	15	16	18	19	20	22	24	27	28	29	31	32
mParaben	ND	ND	0.61	ND	NQ	0.38	0.67	ND	NQ	ND	0.73	1.59	ND	ND	ND	0.61
eParaben	ND	ND	ND	ND	ND	ND	ND	ND	ND	ND	ND	ND	ND	ND	ND	ND
mMP	ND	0.34	0.53	0.40	NQ	0.48	ND	NQ	0.29	0.51	0.57	ND	ND	ND	ND	ND
4HBA	14.57	NQ	21.96	13.52	NQ	NQ	25.15	16.92	NQ	NQ	20.08	17.08	NQ	NQ	15.53	19.94
mEP	0.38	NQ	NQ	NQ	NQ	0.01	NQ	NQ	NQ	NQ	0.14	0.42	NQ	0.45	0.21	1.43
OP	ND	ND	ND	ND	ND	ND	ND	ND	ND	ND	ND	ND	ND	ND	ND	ND
pParaben	ND	ND	ND	ND	ND	ND	ND	ND	ND	ND	ND	ND	ND	ND	ND	ND
bParaben	ND	ND	ND	ND	ND	ND	ND	ND	ND	ND	ND	0.95	ND	ND	ND	ND
mBP	ND	ND	ND	ND	ND	ND	ND	ND	ND	ND	ND	ND	ND	ND	ND	ND
3PBOH	ND	ND	ND	ND	ND	ND	ND	ND	ND	ND	ND	ND	ND	ND	ND	ND
NP	ND	ND	ND	ND	ND	ND	ND	ND	ND	ND	ND	ND	ND	ND	ND	ND
3PBA	ND	ND	ND	ND	ND	ND	ND	ND	ND	ND	ND	ND	ND	ND	ND	ND
4MBC	NQ	NQ	NQ	NQ	NQ	NQ	NQ	NQ	NQ	NQ	NQ	NQ	NQ	NQ	NQ	NQ
BP-3	ND	ND	1.16	ND	NQ	ND	0.95	0.65	NQ	NQ	0.61	0.76	NQ	NQ	0.35	0.79
mEHP	NQ	NQ	NQ	0.27	0.29	NQ	0.53	0.26	NQ	0.45	0.38	NQ	NQ	NQ	NQ	NQ
mTric	ND	ND	ND	ND	ND	ND	ND	ND	ND	ND	ND	ND	ND	ND	ND	ND
Tric	0.46	0.40	0.48	ND	1.75	ND	NQ	0.26	2.31	1.77	ND	NQ	0.51	ND	0.69	0.86
BP-1	0.44	0.41	0.50	0.52	ND	NQ	0.22	0.27	0.29	NQ	NQ	0.32	0.17	NQ	0.20	0.20
mBzP	ND	ND	ND	ND	ND	ND	ND	ND	ND	ND	ND	ND	ND	ND	ND	ND
BPA	0.77	0.34	NQ	0.67	NQ	NQ	NQ	NQ	0.14	NQ	NQ	NQ	NQ	0.65	NQ	NQ
OMC	NQ	NQ	NQ	NQ	NQ	NQ	NQ	NQ	NQ	NQ	NQ	NQ	NQ	NQ	NQ	NQ
BP-2	ND	ND	ND	ND	ND	ND	ND	ND	ND	ND	ND	ND	ND	ND	ND	ND
Equol	ND	ND	ND	ND	ND	ND	ND	ND	ND	0.09	ND	ND	ND	ND	ND	ND
E1	ND	ND	ND	ND	ND	ND	ND	ND	ND	ND	ND	ND	ND	ND	ND	ND
E2	ND	ND	ND	ND	ND	ND	ND	ND	ND	ND	ND	ND	ND	ND	ND	ND
EE2	ND	ND	ND	ND	ND	ND	ND	ND	ND	ND	ND	ND	ND	ND	ND	ND
Ent	2.24	1.79	3.13	ND	NQ	1.53	2.13	NQ	NQ	2.11	2.67	ND	NQ	ND	2.42	2.52
E3	4.76	4.68	5.04	NQ	NQ	6.33	2.21	NQ	2.62	3.48	NQ	NQ	2.46	3.25	4.94	3.45

Table A. 16. Total concentrations (ng/mL) of target analytes in amniotic fluid samples of female fetuses.

Sample ID	1	2	4	5	6	8	10	11	13	14	17	21	23	25	26	30
mParaben	ND	NA	NA	ND	ND	2.98	ND	ND	ND	ND	3.96	13.37	ND	NQ	ND	ND
eParaben	ND	NA	NA	ND	ND	ND	ND	ND	ND	ND	ND	ND	ND	ND	ND	ND
mMP	ND	NA	NA	ND	ND	ND	ND	ND	60.21	ND	NQ	1.66	NQ	NQ	ND	ND
4HBA	35.47	NA	NA	26.37	27.57	NQ	NQ	28.38	36.21	NQ	NQ	32.47	23.63	NQ	NQ	16.50
mEP	2.26	NA	NA	2.67	2.56	NQ	NQ	1.44	3.44	6.44	NQ	NQ	3.46	2.78	NQ	NQ
OP	ND	NA	NA	ND	ND	ND	ND	ND	ND	ND	ND	ND	ND	ND	ND	ND
pParaben	ND	NA	NA	ND	ND	ND	ND	ND	ND	ND	ND	1.54	ND	NQ	ND	0.95
bParaben	ND	NA	NA	ND	ND	ND	ND	ND	ND	ND	ND	ND	ND	ND	ND	1.32
mBP	ND	NA	NA	ND	ND	3.27	ND	ND	3.18	3.01	3.92	3.88	4.45	NQ	NQ	2.32
3PBOH	ND	NA	NA	ND	ND	ND	ND	ND	ND	ND	ND	ND	ND	ND	ND	ND
NP	ND	NA	NA	ND	ND	ND	ND	ND	ND	ND	ND	ND	ND	ND	ND	ND
3PBA	ND	NA	NA	ND	ND	ND	ND	ND	ND	ND	ND	ND	ND	ND	ND	ND
4MBC	NQ	NA	NA	NQ	NQ	NQ	NQ	NQ	4.53	NQ	6.20	9.61	6.55	NQ	NQ	NQ
BP-3	1.48	NA	NA	1.84	2.32	NQ	NQ	3.12	1.17	ND	NQ	1.38	1.73	1.79	NQ	NQ
mEHP	NQ	NA	NA	NQ	NQ	NQ	NQ	NQ	2.62	2.29	4.75	NQ	NQ	1.36	1.26	NQ
mTric	ND	NA	NA	ND	ND	ND	ND	ND	ND	ND	ND	ND	ND	ND	ND	ND
Tric	1.40	NA	NA	ND	0.54	ND	1.40	0.79	NQ	0.95	0.84	2.21	2.20	NQ	NQ	3.22
BP-1	0.50	NA	NA	0.43	0.48	NQ	NQ	ND	0.48	0.43	ND	ND	ND	0.45	ND	0.95
mBzP	ND	NA	NA	ND	ND	ND	ND	ND	ND	ND	ND	ND	ND	ND	ND	ND
BPA	0.09	NA	NA	0.21	0.33	NQ	NQ	1.26	0.75	NQ	NQ	0.08	1.16	NQ	NQ	4.36
OMC	NQ	NA	NA	0.42	0.46	NQ	NQ	NQ	0.42	1.31	2.35	2.42	NQ	NQ	0.53	NQ
BP-2	ND	NA	NA	ND	ND	ND	ND	0.17	0.10	ND	0.13	ND	ND	ND	ND	0.31
Equol	5.88	NA	NA	ND	ND	ND	ND	ND	ND	2.33	ND	ND	ND	ND	ND	1.76
E1	5.22	NA	NA	6.36	4.87	NQ	7.04	4.72	NQ	5.13	2.24	6.29	7.01	7.91	10.86	NQ
E2	1.08	NA	NA	1.38	0.76	NQ	0.92	1.46	NQ	NQ	0.85	1.42	NQ	NQ	1.42	1.30
EE2	ND	NA	NA	ND	ND	ND	ND	ND	ND	ND	ND	ND	ND	ND	ND	ND
Ent	7.72	NA	NA	ND	14.36	3.36	NQ	5.21	5.06	ND	ND	4.58	5.75	NQ	ND	6.90
E3	14.59	NA	NA	17.51	19.40	NQ	24.59	13.40	NQ	16.79	6.03	21.66	23.25	NQ	NQ	11.44

Table A. 17. Total concentrations (ng/mL) of target analytes in amniotic fluid samples of male fetuses.

Sample ID	**3**	**7**	**9**	**12**	**15**	**16**	**18**	**19**	**20**	**22**	**24**	**27**	**28**	**29**	**31**	**32**
mParaben	NA	ND	7.90	ND	ND	ND	4.44	ND	ND	6.03	3.96	ND	ND	1.01	1.23	3.60
eParaben	NA	ND	ND	ND	ND	ND	ND	ND	ND	ND	ND	ND	ND	ND	ND	ND
mMP	NA	0.46	0.50	ND	ND	ND	ND	ND	ND	ND	ND	ND	NQ	ND	ND	NQ
4HBA	NA	18.66	28.66	19.84	NQ	NQ	33.60	25.59	NQ	NQ	28.59	16.35	NQ	NQ	18.07	19.10
mEP	NA	2.52	2.83	3.02	2.87	3.43	2.88	ND	3.10	3.13	NQ	NQ	1.32	2.18	2.17	2.99
OP	NA	ND	ND	ND	ND	ND	ND	ND	ND	ND	ND	ND	ND	ND	ND	ND
pParaben	NA	ND	1.84	ND	ND	ND	0.57	ND	ND	ND	ND	ND	ND	ND	ND	ND
bParaben	NA	ND	ND	ND	ND	ND	ND	ND	ND	ND	ND	1.90	ND	ND	ND	ND
mBP	NA	ND	2.62	ND	ND	ND	3.47	2.23	ND	2.67	3.37	NQ	NQ	1.87	1.86	NQ
3PBOH	NA	ND	ND	ND	ND	ND	ND	ND	ND	ND	ND	ND	ND	ND	ND	ND
NP	NA	ND	ND	ND	ND	ND	ND	ND	ND	ND	ND	ND	ND	ND	ND	ND
3PBA	NA	ND	ND	ND	ND	ND	ND	ND	ND	ND	ND	ND	ND	ND	ND	ND
4MBC	NA	NQ	NQ	NQ	5.02	11.57	6.75	NQ	NQ	NQ	7.19	NQ	NQ	NQ	NQ	NQ
BP-3	NA	ND	3.99	2.24	NQ	ND	1.97	5.04	NQ	NQ	1.96	0.94	NQ	2.98	0.94	NQ
mEHP	NA	NQ	NQ	NQ	2.30	2.02	NQ	NQ	2.09	1.19	NQ	NQ	NQ	NQ	NQ	NQ
mTric	NA	ND	ND	ND	ND	ND	ND	ND	ND	ND	ND	ND	ND	ND	ND	ND
Tric	NA	NQ	1.31	0.80	ND	ND	0.73	0.53	7.95	1.64	ND	ND	1.26	ND	NQ	2.49
BP-1	NA	NQ	2.16	0.63	NQ	ND	ND	1.58	0.45	ND	0.50	0.35	NQ	1.03	0.22	NQ
mBzP	NA	ND	ND	ND	ND	ND	ND	ND	ND	ND	ND	ND	ND	ND	ND	ND
BPA	NA	NQ	0.18	0.08	NQ	0.23	0.20	NQ	NQ	0.13	0.94	NQ	NQ	1.25	0.03	NQ
OMC	NA	0.16	NQ	NQ	NQ	0.27	0.21	0.66	0.43	NQ	2.77	0.09	NQ	NQ	NQ	NQ
BP-2	NA	ND	ND	ND	ND	ND	ND	ND	ND	ND	ND	ND	ND	ND	ND	ND
Equol	NA	ND	ND	ND	ND	ND	ND	1.70	1.64	ND	3.74	3.28	NQ	NQ	ND	ND
E1	NA	11.97	9.25	NQ	NQ	11.31	8.95	NQ	NQ	8.15	5.24	NQ	NQ	3.58	13.57	7.17
E2	NA	2.49	1.03	NQ	NQ	1.38	1.54	1.42	1.57	1.96	NQ	NQ	0.71	0.46	2.21	1.10
EE2	NA	ND	ND	ND	ND	ND	ND	ND	ND	ND	ND	ND	ND	ND	ND	ND
Ent	NA	NQ	ND	ND	ND	ND	6.76	5.78	ND	NQ	10.53	2.15	ND	4.59	2.32	NQ
E3	NA	21.24	29.96	30.08	NQ	NQ	17.39	18.45	NQ	NQ	12.99	10.88	NQ	12.72	24.54	NQ

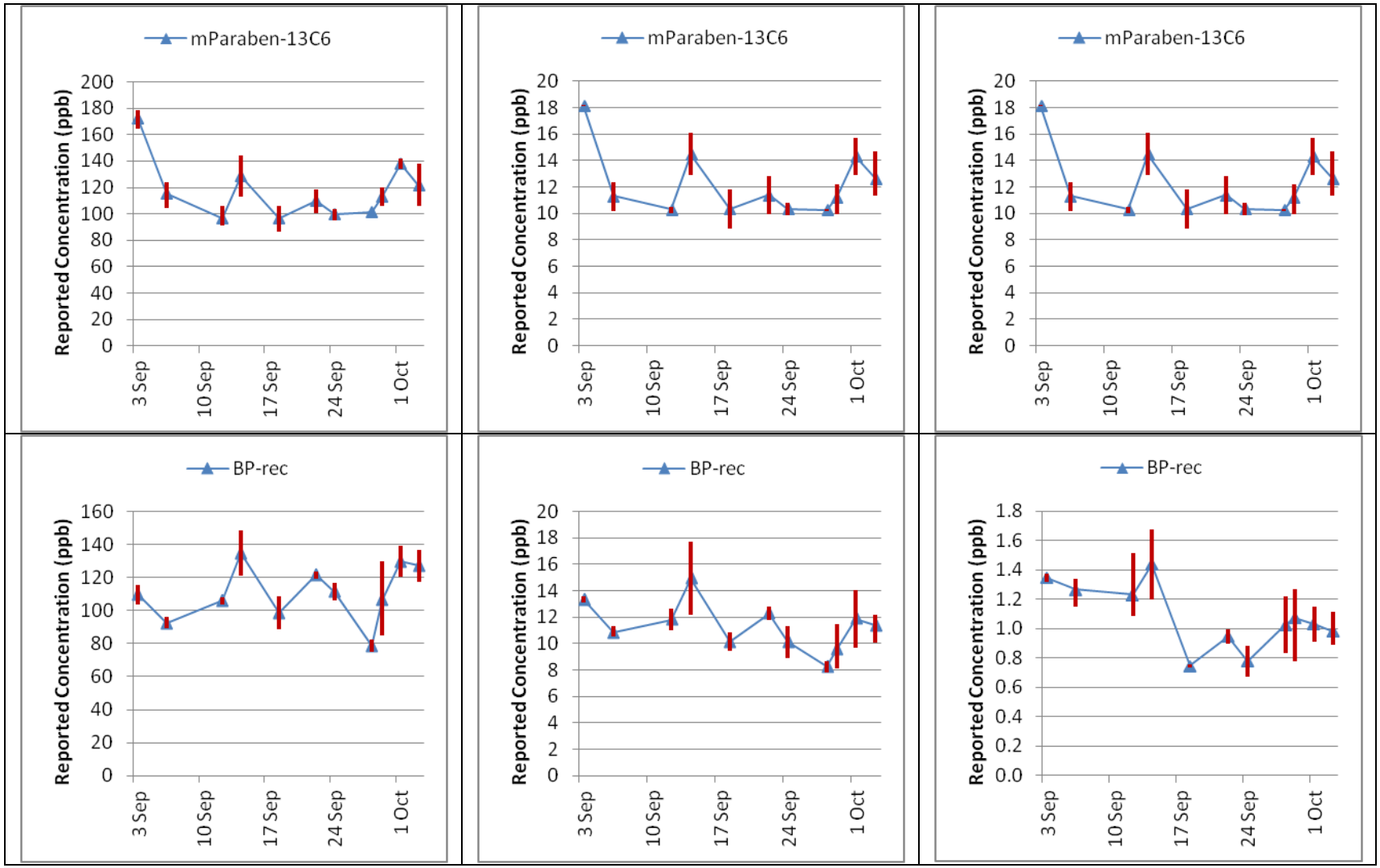
mParaben-13C6
Reported Concentration (ppb)
200
180
160
140
120
100
80
60
40
20
0
3 Sep
10 Sep
17 Sep
24 Sep
1 Oct
mParaben-13C6
Reported Concentration (ppb)
20
18
16
14
12
10
8
6
4
2
0
3 Sep
10 Sep
17 Sep
24 Sep
1 Oct
mParaben-13C6
Reported Concentration (ppb)
20
18
16
14
12
10
8
6
4
2
0
3 Sep
10 Sep
17 Sep
24 Sep
1 Oct
BP-rec
Reported Concentration (ppb)
160
140
120
100
80
60
40
20
0
3 Sep
10 Sep
17 Sep
24 Sep
1 Oct
BP-rec
Reported Concentration (ppb)
20
18
16
14
12
10
8
6
4
2
0
3 Sep
10 Sep
17 Sep
24 Sep
1 Oct
BP-rec
Reported Concentration (ppb)
1.8
1.6
1.4
1.2
1.0
0.8
0.6
0.4
0.2
0.0
3 Sep
10 Sep
17 Sep
24 Sep
1 Oct

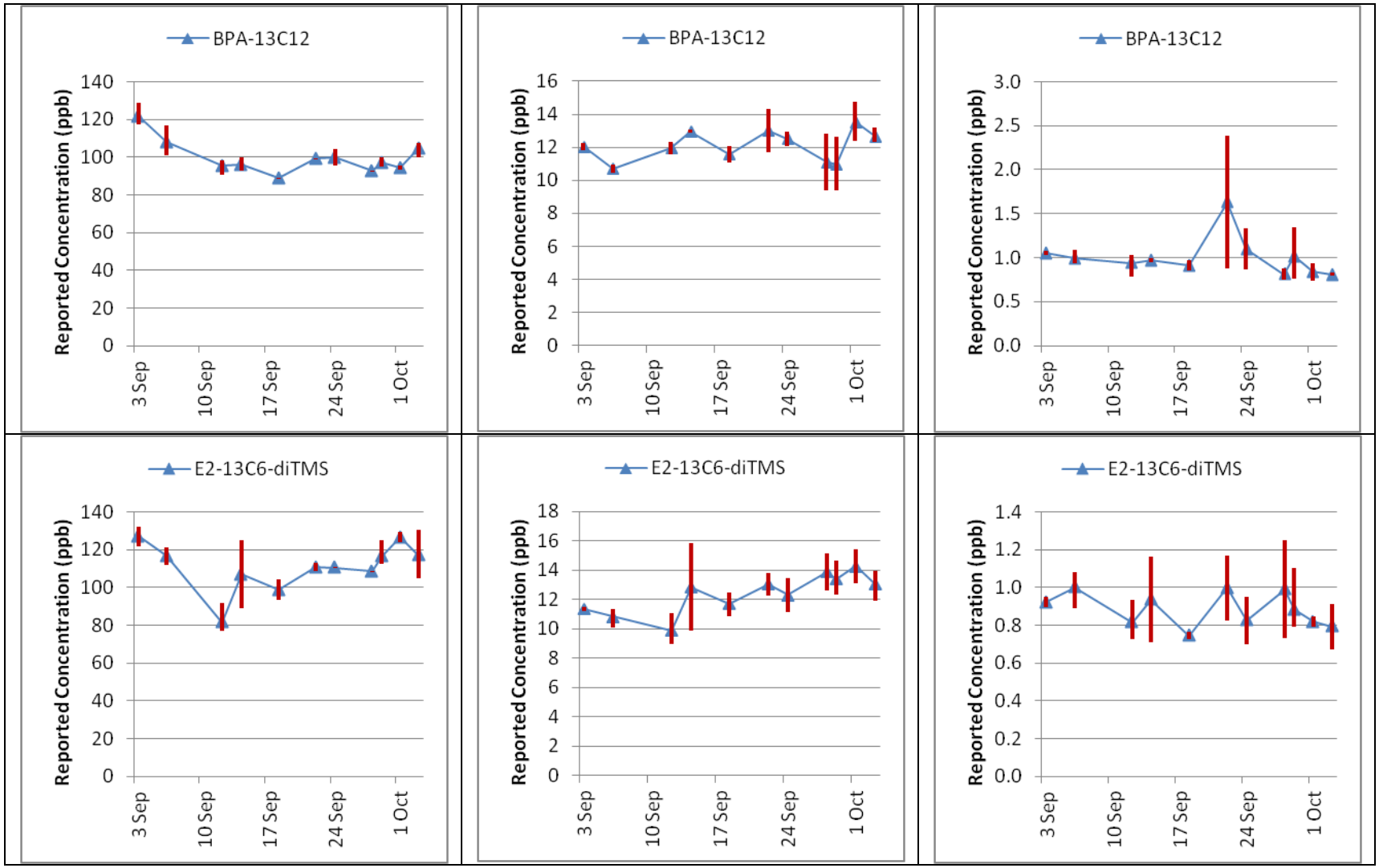

Figure A. 1. Representative control charts for 3 levels of calibration check samples. Symbols indicate the average result for the day, red bars indicate the range of results. A change in standard mix occurred between Sept 12 and 14 which changed the concentration of some of the target analytes.

Department of Chemistry

College of Science
Tel: +64 3 364 2100, Fax: +64 3 364 2110
Email: chemistry@canterbury.ac.nz, www.chem.canterbury.ac.nz

UNIVERSITY OF CANTERBURY
Te Whare Wānanga o Waitaha
CHRISTCHURCH NEW ZEALAND

A Research Study on Environmental Estrogens

You are invited to participate in a research study looking at exposure during pregnancy to chemicals called environmental estrogens. Your participation is entirely voluntary (your choice). You do not have to take part in this study. If you choose not to take part, this in no way will affect your future or continuing health care. If you require an interpreter, one will be provided. You may have a friend, family or whānau support to help you understand the risks and/or benefits of this study and any other explanation you may require.

Motivation for the Study

Environmental estrogens are chemicals which mimic natural estrogen hormones when they enter the human body. We are exposed to low levels of these chemicals on a daily basis. They are found in certain plastics and find their way into food stored and cooked in these plastic containers. They are also in cosmetics, toothpaste, shampoo, antibacterial soaps and sunscreens and can enter the body through the skin or by swallowing. These chemicals can interfere with normal growth and development of humans, affecting behaviour and the reproductive system. Research is just now suggesting that the critical time of human exposure is as a fetus during the first 20 weeks of pregnancy. There is very little known about fetal exposure to these chemicals. Fetal exposure is assessed by measuring the concentration of these chemicals in amniotic fluid. This study will provide the first measurements of fetal exposure in New Zealand and only one of a few studies worldwide. In this preliminary study, we are trying to determine if exposure in New Zealand is potentially significant and deserves further action.

Your Participation

You have consented to an amniocentesis for medical diagnostic purposes. The amniotic fluid sample that was collected consists of two parts – cells and fluid. The laboratory separates the cells from the fluid. Only the cell material will be used for your diagnostic test. As part of this research study, the fluid portion of the sample would be analysed for the chemicals we are interested in. The urine sample that was also collected will be analysed for the same chemicals and used to compare mother's and baby's exposures. The information we need for each sample is the mother's age, the number of weeks pregnant and the sex of the baby. You do not need to learn the sex of your baby at this time unless you wish to. No information identifying you will be included in the study reports.

We would appreciate it if you would complete the consent form attached to this information sheet if you are willing to participate in the study. You may keep this information sheet for future reference.

The Study

This study is being conducted by the University of Canterbury, Department of Chemistry with the co-operation of the University of Otago, Christchurch Women's Hospital and the Canterbury Health Laboratories. The study is funded by the National Research Centre for Growth and Development, Liggins Institute, University of Auckland.

The results of this study will form one part of a PhD thesis and will also be useful to government regulators in New Zealand and around the world in understanding the importance of prenatal exposure to environmental estrogens. Progress reports on the project are sent to the National Research Centre for Growth and Development (NRGCD) which is operated from the Liggins Institute. The results will also be published in the scientific literature, but you may be assured of complete confidentiality of information gathered during the study. Names of participants will never be included in any publication or reporting of results of the study. The study will be complete and published by April 2011. If you are participating and wish to receive a copy of the published report, please tick the box on the consent form.

This study has been reviewed and **approved** by the University of Canterbury Human Ethics Committee and the New Zealand Health and Disability Upper South A Regional Ethics Committee (Ethics Reference Number URA/10/03/019).

If you have questions about the study, please contact:
Lisa Graham (PhD student) on 021 0226 2133 or by e-mail lag46@uclive.ac.nz or Prof. Ian Shaw (PhD supervisor) on 03 364 3105 or by e-mail ian.shaw@canterbury.ac.nz or Dr. Rosemary Reid, Christchurch Women's Hospital on 03 3644 699 or by e-mail Rosemary.Reid@cdhb.govt.nz .

If you have any queries or concerns regarding your rights as a participant in this study, you may wish to contact an independent health and disability advocate:
Free phone 0800 555 050
Free fax: 0800 2 SUPPORT (0800 2787 7678)
Email: advocacy@hdc.org.nz

NATIONAL RESEARCH CENTRE FOR GROWTH AND DEVELOPMENT

UNIVERSITY of OTAGO
Te Whare Wānanga o Otāgo
NEW ZEALAND